Towards retinal repair: analysis of photoreceptor precursor cells and their cell surface molecules

Ya-Ting Han

University College London

Institute of Child Health

A thesis submitted for the degree of

Philosophiae Doctor

For the incredible cells that drive me here.

Acknowledgements

I would like to firstly thank my supervisor Prof. Jane Sowden for her consistent support, encouragement and advice throughout my PhD. I still remember when I just started my PhD and wanted some dendritic cells in a control experiment for some even not so exciting markers, Jane instantly contacted her colleagues to provide me these cells. Cases as such are countless. I have been encouraged to develop my own research ideas and Jane has always been supporting. It is through all these that I confidently and happily conducted my studies here. I am very happy that I chose the right supervisor. Thank you, Jane!

I would also like to thank my secondary supervisor Prof. Robin Ali for his encouragements throughout, Dr. Janny Morgan for her advice during my PhD upgrade, Prof. Andy Copp, Prof. David Muller, Dr. Kenth Gustafsson, Dr. Andy Stoker, Dr. Juan-Pedro Martinez-Barbera, and Dr. Patrizia Ferretti for helpful discussion and advices. Thanks to Dr. Kevin Mills and Dr. Wendy Heywood for their supports with mass spectrometry, especially Wendy for her unlimited kind and generous help during all my time with mass spectrometry. Thanks to Dan who helped and advised me in molecular cloning. Thanks to Rachael who performed all the injections for cell transplantation. Thanks to Jorn who showed me the techniques when I just entered the lab and helped me with my first cell transplantation. The NrlGFP cell transplantation with cell surface markers was also performed together with him. Thanks to Tassos who advised and helped a lot regarding the shRNA. Thanks to Aoife for sharing with me her cilia antibodies. Thanks to Dr. Siobhan Burns and Dr. Gerben Bouma for providing me the dendritic cells. Thanks to Bertrand and Ayad for training me in confocal imaging and flow cytometry respectively.

Friends in the office have made my PhD life much more fun and colourful. Many thanks go to Sara G, Sarah D, Mike, Lily, KP, Vic, Suganthi, Nicola, Barbara, Giulia, Sherry, Sophie, Su, Veronika, and all the people past and present in BDRC.

Special thanks go to Meng who has always been beside me: not only for the lovely meals he cooked, but also for the scripts he wrote for me to run microarray analysis and all the discussions he contributed toward my puzzles in research. And special thanks to Leyo who helped nothing but making my life busier…… and merrier...

Thanks to Child Health Research Appeal Trust from ICH UCL and Overseas Research Scholarship from UCL for funding my study and life.

I, Yating Han confirm that the work presented in this thesis is my own. Where information has been derived from other sources, I confirm that this has been indicated in the thesis.

Towards retinal repair: analysis of photoreceptor precursor cells and their cell surface molecules

Ya-Ting Han

UCL, Institute of Child Health

Abstract

Photoreceptor cells are the sensory cells of the retina, responsible for detecting light and conducting the signals to secondary neurons. Because they cannot be regenerated, loss of photoreceptor cells leads to irreversible blindness. Cell transplantation with postmitotic photoreceptor precursor cells has been shown as a feasible approach to rescue vision in animal models, but the molecular properties of these transplantation-competent cells are not understood. The aims of this thesis are to 1) determine the properties of photoreceptor precursor cells by transcriptome and proteome analysis; 2) identify cell surface molecules that can be used to isolate these cells from cell mixtures and/or that are important for their migration and correct integration in development and in a transplantation context. Nrl/CrxGFP transgene-labelled photoreceptor precursor cells were separated from other retinal cells by flow cytometry and subjected to microarray and mass spectrometry analysis. Bioinformatics analysis showed that the photoreceptor precursor cells were enriched in expression of genes encoding cell projection proteins. Over 200 cell surface molecule candidates were identified and 32 genes encoding confirmed extracellular domains were expressed > 5-fold higher in photoreceptor precursors than other retinal cells. These included the stem cell marker Prom1 (CD133), which was specifically expressed in photoreceptor cells (particularly on their cilia) throughout development as well as on transplanted photoreceptors. Together with CD73 and CD24, it serves as a specific marker to isolate photoreceptor cells for transplantation. An axon guidance molecule Sema7a was shown to be highly expressed in photoreceptor cells. It co-labels with PlxnC1, rather than the expected receptor Itgb1, in developing retina, as well as transplanted migrating photoreceptor cells. Knockout of Sema7a resulted in retinal holes and abnormal photoreceptor synapse projection indicating a role of Sema7a in outer retina lamination. This study sets the foundation for future work on photoreceptor cell surface molecules in development and retinal repair.

Table of Contents

Abbreviation

AAV	adeno-associated virus
Ab	antibody
AcTub	Acetylated α-tubulin
AMD	age-related macular degeneration
ANOVA	analysis of variance
APC	Allophycocyanin
Atp5b	ATP synthase subunit beta mitochondrial
BAC	bacterial artificial chromosome
Basp1	Brain acid soluble protein 1
BBS	Bardet–Biedl syndrome
BCA assay	bicinchoninic acid assay
BH	biocytin hydrazide
bHLH	basic helix-loop-helix
BMP	bone morphogenetic protein
BP	biological process
BSA	Bovine serum albumin
cAMP	cyclic adenosine monophosphate
CC	connecting cilium

CD	cluster of differentiation
Cdhr1/ Pcdh21	cadherin-related family member 1
CenpF	centromere protein F
Cep290	centrosomal protein 290kDa
cGMP	cyclic guanosine monophosphate
Chrna5	cholinergic receptor, nicotinic, alpha polypeptide 5
Chrnb4	cholinergic receptor, nicotinic, beta polypeptide 4
Chx10	ceh-10 homeo domain containing homolog (C. elegans)
CNG	cyclic nucleotide-gated
Cngb3	cyclic nucleotide-gated channel beta 3
Crx	cone-rod homeobox
DAPI	4',6-diamidino-2-phenylindole
DAVID	Database for Annotation, Visualization and Integrated Discovery
DIC	Differential interference contrast
EBSS	Earle's Balanced Salt Solution
Eno1	Alpha enolase
Eno2	Gamma-enolase
ERG	electroretinogram
ES cells	embryonic stem cells
ESI-QTOF	ElectroSpray Ionisation-Quadrupole – Time-of-Flight
ET/ Tbx3	Eye T-box
Fabp7	brain Fatty acid-binding protein
FACS	Fluorescence-activated cell sorting
FAM	6-carboxy-fluorescein
FBS	fetal bovine serum
FCM	Flow cytometry
FDR	False discovery rate
FGF	fibroblast growth factor
FSC	Forward side scatter
Fwk	foetal week
Gabrr3	gamma-aminobutyric acid (GABA) receptor, rho 3
GCL	ganglion cell layer
GEO	Gene Expression Omnibus
GFP	green fluorescent protein
Gnat1	guanine nucleotide binding protein, alpha transducing 1
Gnat2	guanine nucleotide binding protein, alpha transducing 2

GO	Gene ontology
Gpcr	G protein-coupled receptor
GPI anchor	glycosylphosphatidylinositol anchor
GTP	guanosine triphosphate
HEK 293 cells	Human Embryonic Kidney 293 cells
Hnrnpa2b1	heterogeneous nuclear ribonucleoproteins A2/B1
IFT	intraflagellar transport
IHC	immunohistochemistry
IMS	Industrial methylated spirit
INBL	inner nuclear blastic layer
INL	inner nuclear layer
IPL	inner plexiform layer
ipRGCs	intrinsically photosensitive retinal ganglion cells
iPS cells	induced pluripotent stem cells
IS	inner segments
Itga3/CD49c	Integrin alpha 3
Itgb1	integrin beta 1
Jag1/CD339	jagged 1
Jam2/CD322	junction adhesion molecule 2
KO	knock out
LB	Lysogeny broth
LC/MSe	liquid chromatography / mass spectrometry analysis using ESI-QTOF mass spectrometers
LCA	Leber'S congenital amaurosis
Lhx2	Lin 11 Isl 1 Mec 3 homeobox-2
Lifr/CD118	leukemia inhibitory factor receptor
Lmnb1	lamin B1
LPS	lipopolysaccharide
MACS	magnetic automated cell sorting
Marcks	Myristoylated alanine rich C kinase substrate
MC3T3 cell line	Mouse osteoblastic precursor cell line
MDCK cells	Madin-Darby Canine Kidney Epithelial cells
Meis2	myeloid ecotropic viral integration site 1 homolog 2
MF	molecular function
MGB	minor groove binder
MGI	Mouse Genome Informatics
mGluR6	metabotropic glutamate receptor 6

MS	Mass spectrometry
Myo7a	myosin VIIa
NFQ	non-fluorescent quencher
NOS	nitric oxide synthase
Nr2e3	nuclear receptor subfamily 2, group E, member 3
Nr2f2	nuclear receptor subfamily 2, group F, member 2
Nrl	neural retina leucine zipper
Nt5e/CD73	5'-nucleotidase, ecto
Ntng2	netrin G2
Ntsr1	Neurotensin receptor type 1
OCT	optimal cutting temperature
ONBL	outer nuclear blast layer
Onecut1	one cut domain, family member 1
ONL	outer nuclear layer
OPL	outer plexiform layer
Opn1mw	opsin 1 (cone pigments), medium-wave-sensitive
Opn1sw	opsin 1 (cone pigments), short-wave-sensitive
Optx2/ Six6	Optic Six gene 2
OS	outer segments
OSN	olfactory sensory neurons
Otd	orthodenticle
Otx2	orthodenticle homeobox 2
Pax6	Paired homeobox-6
PBS	Phosphate Buffered Saline
Pcdh15	protocadherin 15
PCP	planar cell polarity
PCR	polymerase chain reaction
Pdc	phosducin
Pdeb	phosphodiesterase 6B, cGMP, rod receptor, beta polypeptide
Pdgfr	platelet-derived growth factor receptor
PE	Phycoerythrin
PFA	paraformaldehyde
Pkc	protein kinase C
PlxnC1	plexin C1
Pna	peanut agglutinin
Podxl	podocalyxin-like

PR	Photoreceptor cell
Prnp/ CD230	prion protein
Prom1/CD133	prominin 1
qPCR	quantitative polymerase chain reaction
RetGC	retinal guanylate cyclise
RGCs	retinal ganglion cells
RGD motif	arginine-glycine-aspartic acid motif
Rho	rhodopsin
RMA	Robust Multichip Average
Rom1	retinal outer segment membrane protein 1
Rorβ	retinoid-related orphan receptor-beta
RP	Retinitis pigmentosa
RPCs	retinal progenitor cells
RPE	retinal pigment epithelium
Rpgr	retinitis pigmentosa GTPase regulator
Rpgrip1	retinitis pigmentosa GTPase regulator interacting protein 1
rpm	revolutions per minute
Rx1/ Rax	Retina homeobox-1
Rxrγ	retinoid X receptor-γ
Sag	S-antigen; retina and pineal gland (arrestin)
SAGE	serial analysis of gene expression
sema	semaphorin
Sema7a/CD108	semaphorin 7A, GPI membrane anchor
Serpina3k	Serine protease inhibitor A3K
SHH	sonic hedgehog
shRNAs	short hairpin RNAs
Sirpa/CD172a	signal-regulatory protein alpha
Six3	Sine oculis-related homeobox-3
Slc17a7	solute carrier family 17 (sodium-dependent inorganic phosphate cotransporter), member 7
Slc2a1	Solute carrier family 2 facilitated glucose transporter member 1
SRS	subretinal space
Stxbp1	Syntaxin binding protein 1
Sv2b	synaptic vesicle glycoprotein 2 b
Syn1	Synapsin 1
Tcfap2a	transcription factor AP-2 alpha
Tcfap2b	transcription factor AP-2 beta

TFs	transcription factors
TH	tyrosine hydroxylase
tll/ Tlx	Tailless
Tm	melting temperature
TMHs	transmembrane helixes
Trβ2	Thyroid hormone receptor beta 2
TSAA	translation state array analysis
Tspan	tetraspanin
Tubb2c	Tubulin beta 2C chain
Tubb5	Tubulin beta 5 chain
USH	Usher syndrome
V2Rp5	Vomeronasal 2 receptors
Vdac1	Voltage dependent anion selective channel protein 1
Wnt	Wingless-Int
Zranb1	zinc finger, RAN-binding domain containing 1

List of figures

List of tables

1 Introduction

1.1 Eye structure, retinal structure, photoreceptor structure

Vision is one of the most important sensory inputs to the human brain. It is perceived by the eye in which light signals are guided onto the retina (Figure 1.1 A), a 0.2-mm-thick nervous tissue which receives light signals and processes images. The retina is an orderly laminated structure composed of six types of neurons and one type of glia cells (Figure 1.1 B). Photoreceptor cells lie in the outer nuclear layer (ONL) and are the detectors and processors of light signals. They absorb and convert the photons into electrical responses and pass them to interneurons such as bipolar cells, horizontal cells and amacrine cells. These interneurons, located in the inner nuclear layer (INL), relay the signals from photoreceptors to ganglion cells which will eventually transmit the signals to brain. There are two types of photoreceptor cells: rods for dim light vision and cones for bright light and coloured vision. Both are elegantly structured containing the outer segments (OS), the inner segments (IS), the cell body, and the synapses (Fig 1.1 C). The OS are essentially the factory of phototransduction and are full of membrane disks rich in light-sensing proteins (opsins). Rod OS are longer and feature closed individual membrane disks, with a few basal disks open and connected with the ciliary axoneme (the inner core microtubule-based cytoskeleton structure of cilia). Cone OS are shorter and are formed with open disks that are all connected with the ciliary axoneme. Through the connecting cilium the OS are connected with the IS which is responsible for metabolism and providing the energy for phototransduction. The connecting cilium is the path for opsins and many other shuttle molecules. The IS are connected with the cell bodies which contain transcription machinery in the nucleus at the ONL. The cell bodies further project synapses which transmit signals to interneurons at the outer plexiform layer (OPL).

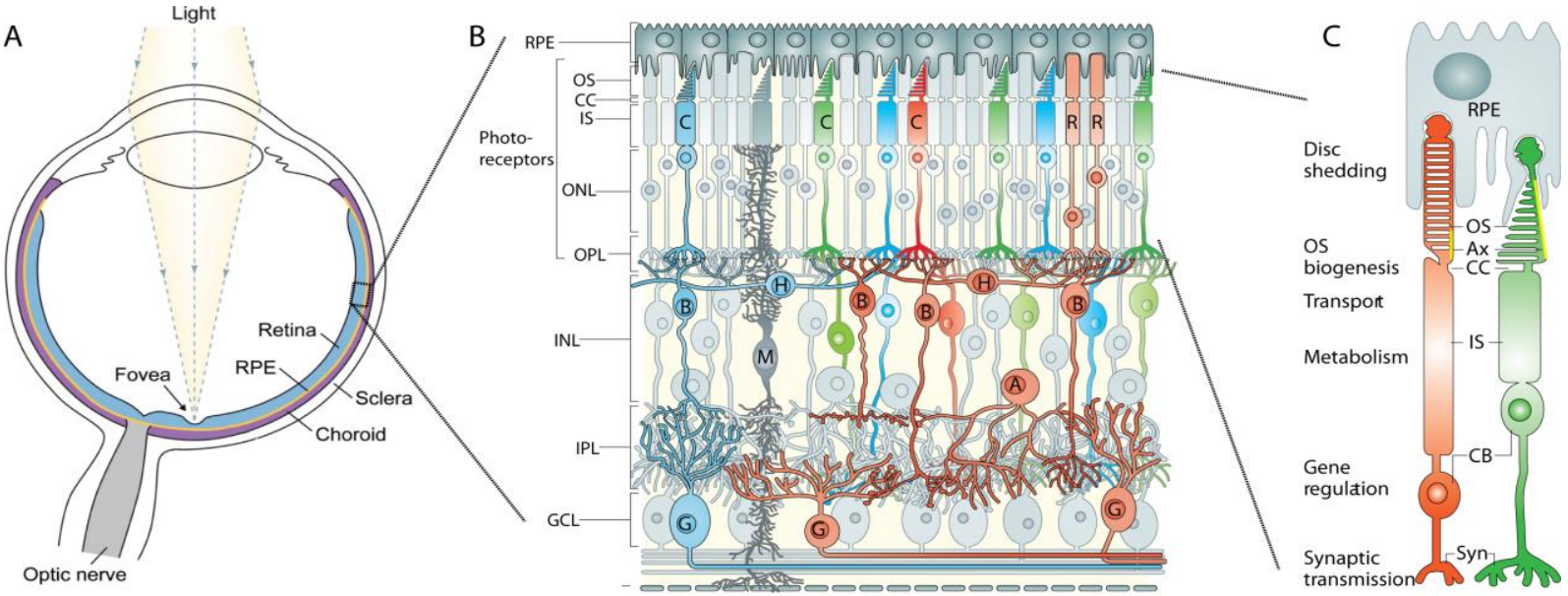

Figure 1.1 Structures of the eye, retina and photoreceptors. (A) **Structure of a human eye. Light goes through the pupil, lens, vitreous humour, retina, and hits the interphase between the retinal pigment epithelium (RPE) and the retina, where the photoreceptors detect the light signal and convert it into neuronal signal.** (B) **Structure of the retina. Cone and rod photoreceptors have outer segments (OS) which associate with RPE, connecting cilium (CC) which connects the OS and the inner segments (IS), cell bodies which are in the outer nuclear layer (ONL), and synaptic terminus (Syn) at the outer plexiform layer (OPL). The photoreceptors detect light signal with their OS and pass neuronal signal to bipolar cells and horizontal cells. The cell bodies of bipolar cells and horizontal cells are in the inner nuclear layer (INL), along with that of Müller glial and amacrine cells. Bipolar cells relay the signals from photoreceptors to amacrine and ganglion cells through synaptic contacts at the inner plexiform layer (IPL). Ganglion cells further convey the signal to the brain via their long axons toward and along the optic nerve. OPL, outer plexiform layer; INL, inner nuclear layer; IPL, inner plexiform layer; GCL, ganglion cell layer; C, cones; R, rods; B, bipolar cell; H, horizontal cell; M, Müller cell; A, amacrine cell; G, ganglion cell.** (C) **Structure of the rod and cone photoreceptors. The photoreceptor OS is composed of stacked membrane disks which are shed daily and phagocytoed by RPE. OS in rod contain closed individual disks with a few basal disks connected to the ciliary axoneme (Ax, shown in yellow), while cone OS are open structures from the plasma membrane with the axoneme extends to the entire length of the OS. Connecting cilium and the structures around the apical surface of IS are important for OS biogenesis and opsin transport. The IS contains metabolic machinery which provides the energy that photoreceptors highly demand. The cellular body contain transcription machinery that regulates gene expression. The synaptic terminus transmit signals to interneurons. (A) and (B) are modified from (Sung and Chuang 2010; Swaroop, Kim et al. 2010).**

1.2 Eye formation and development, eye field TFs

The vertebrate eye originates from the anterior region of the neural plate which is a single field of neuroectodermal cells called the eye field. In Xenopus embryos the eye field originates from a subset of blastomeres at the 32-cell-stage (Moore and Moody 1999). These blastomeres are competent but not destined to form retina, possibly through inhibition of the bone morphogenetic protein (BMP) signaling (Moore and Moody 1999). The eventual fate of retinogenic cells is established in the neural plate stage when precise levels of Wingless-Int (Wnt) signaling are crucial to pattern the presumptive forebrain from which the eyes are derived (Cavodeassi, Carreira-Barbosa et al. 2005; Maurus, Heligon et al. 2005). Specification of the eye field is synchronized with a confined expression of a group of transcription factors within this region, termed the eye field transcription factors (TFs). These TFs include ET (Eye T-box, or Tbx3), Rx1 (Retina homeobox-1 or Rax), Pax6 (Paired homeobox-6), Six3 (Sine oculis-related homeobox-3), Lhx2 (Lin 11 Isl 1 Mec 3 homeobox-2), tll (Tailless or Tlx) and Optx2 (Optic Six gene 2 or Six6).

Mutations or deletions of *Pax6*, *Six3*, *Optx2*, *Rx1*, *Lhx2*, *tll* result in abnormal or no eye formation in many vertebrate species ranging from frog to human (reviewed in (Wawersik and Maas 2000)). Haploinsuficiency of *PAX6* in human cause aniridia and congenital cataracts (Glaser, Jepeal et al. 1994) and mutations in mouse *Pax6* results in small eye defects (Hill, Favor et al. 1991). On the other hand, Pax6 gain of function results in ectopic lens and retina formation in *Xenopus* (Altmann, Chow et al. 1997; Chow, Altmann et al. 1999). The expanded or induced eyes also appear when other eye field TFs like Six3, Rx and Optx2 are over expressed in the vertebrate nervous system (reviewed in (Sernagor, Eglen et al. 2006)). Interestingly, expression of these eye field TFs are coordinated among themselves in that activation of one activates expression of the others and inactivation reduces expression of the others. It is therefore proposed in *Drosophila* (Kumar and Moses 2001) and also been demonstrated later in *Xenopus* (Zuber, Gestri et al. 2003) that it is the coordinated expression of these eye field TFs that drives the specification of the eye field. In this model, ET induces expression of Rx1 which then induces expression of Pax6. Pax6 then cross talks with Six3 and Lhx2 which interactively regulate the expression of each other. Optx2 and tll joined in later to cement eye field formation. This model is conserved in mouse as shown by the similar gene expression patterns in mice and frogs and morphological defects in all the *Rx*, *Pax6*, *Lhx2*, *Six3*, *Six6* and *tll* knock out (KO) mice (reviewed in (Sernagor, Eglen et al. 2006)). Discrepancies remain, however, as the ET homologue in mouse – Tbx3 – does not show abnormalities in the

knock out model, whereas knock out of its highly related family member Tbx2 does ((Behesti, Papaioannou et al. 2009), and reviewed in (Sernagor, Eglen et al. 2006)).

Formation of the vertebrate eye cup starts from the neural plate. As the neural plate folds to form the neural tube, both sides of the rostral neural plate bulge outwards and form the optic vesicles. Once the lips of the neural folds are sealed, the neural ectoderm where the optic vesicles are derived from and the surface ectoderm (epithelium) are established. A series of interactions between the optic vesicles, the surface ectoderm and the surrounding mesenchyme will eventually give rise to the eyes. As the optic vesicles contact the surface ectoderm the lens placode is induced. While the lens placode pushes into the optic vesicle, invaginates and eventually forms the lens, the optic vesicles folds inwards and forms the bilayered optic cup. The outer layer of the optic cup grows into the RPE while the inner layer forms the retina.

1.3 Retinal development

While the anterior section of the optic cup gradually forms the structures for iris and ciliary body, the posterior section continues to develop the neural retina. Cells in this neuroepithelium layer are the early multipotential retinal progenitor cells (RPCs) which undergo rounds of mitotic division and will eventually exit the cell cycle "giving birth to" the different types of retinal cells. The number of mitotic division for RPCs is limited but not fixed, and varies according to data from early labeling experiments. Clonal labeling before the onset of differentiation showed that the clone size varies from 1 – 16 cells per clone in frog (Holt, Bertsch et al. 1988) and 1 – 200 cells in mice (Turner, Snyder et al. 1990). The fate of the RPCs is also variable in that a single clone can produce any type of retinal cells (Wetts and Fraser 1988; Wong and Rapaport 2009).

Despite this, there is a highly conserved order of cell birth across vertebrate species: retinal ganglion cells (RGCs) are always born first, followed by horizontal cells and cones, then amacrine cells, rods, and bipolar cells, and Müller glia are born last (Figure 1.2). This was shown in mice (Carter-Dawson and LaVail 1979b; Young 1985a), wallaby (Harman and Beazley 1989), chick (Prada, Puga et al. 1991), monkey (La Vail, Rapaport et al. 1991) and rat (Rapaport, Wong et al. 2004). In frog, other than that the birth of rods is shifted before amacrine cells the above order remains (Wong and Rapaport 2009). In ferret, rods are born before bipolar cells, and Müller cells are born before rods (Dreher and Robinson 1988) (reviewed in (Lamb, Collin et al. 2007)). In whichever case, the birth sequence of RGCs followed by horizontal cells followed by cones is not changed.

In addition, there seem to be two conserved waves of cell birth. Birth of RGCs, horizontal cells and cones is the first wave, followed by a period when there is no or very low cell birth. This period varies from 4 to 7 days in rat (Rapaport, Wong et al. 2004), 10 to 20 days in monkey (La Vail, Rapaport et al. 1991), to 2 to 3 weeks in wallaby (Harman and Beazley 1989). After this period, the second wave of cell birth (amacrine cells, rods, bipolar cells, and Müller glia in most species, and Müller cells, rods, bipolar cells, and amacrine cells in ferret (Dreher and Robinson 1988)) appear.

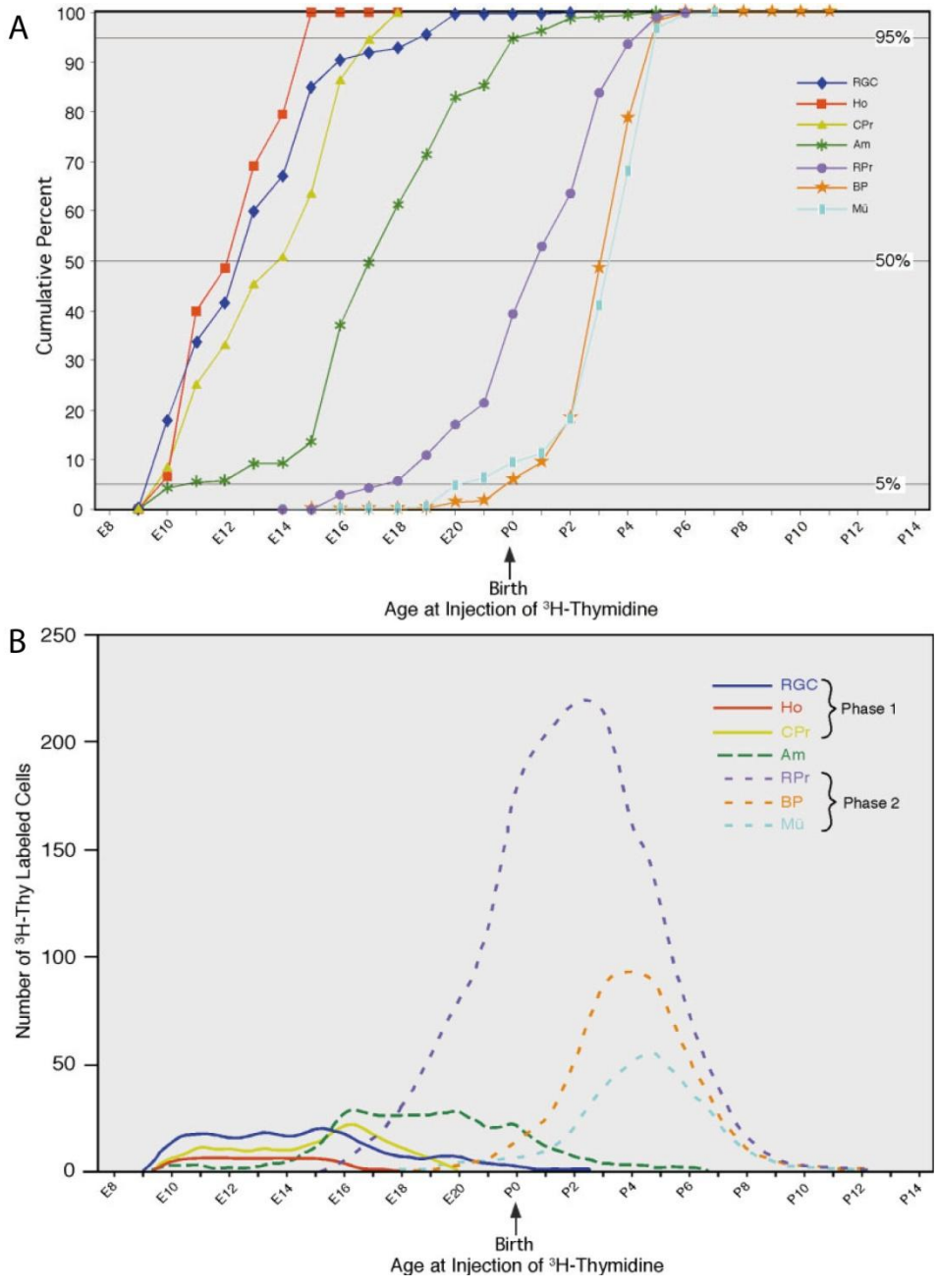

Figure 1.2 Retinal cell birth curves of rat. (A) Cumulative percentage of cells in each class heavily labelled with ^{3}H-TdR along development. (B) Absolute numbers of cells in each class heavily labelled in the mature rat after ^{3}H-TdR administration each day between E8 and P14. Two phases of cell genesis are apparent, phase 1 (solid lines) and phase 2 (short dashed lines) except amacrine cells (long dashed line) exhibit intermediate properties. RGC, retinal ganglion cells; Ho, horizontal cells; Cpr, cone photoreceptor cells; Am, amacrine cells; RPr, rod photoreceptor cells; BP, bipolar cells; MG, muller cells; E, embryonic day; P, postnatal day. Adapted from (Rapaport, Wong et al. 2004)

1.4 Photoreceptor development

Like other retinal cells, photoreceptor cells are derived from the RPCs. Upon their final mitotic division, some RPCs "give birth to" RPC daughter cells that are committed to a photoreceptor fate. These postmitotic photoreceptor precursors continue to grow and mature into fully differentiated photoreceptor cells.

1.4.1 From progenitors to precursors

Although it is not very clear how progenitors are exactly regulated to exit cell cycles and commit to photoreceptor precursors, several signalling pathways (eg. Wnt, Hedgehog, Notch, and FGF) and many homeodomain and basic Helix Loop Helix (bHLH) TFs are known to play in part (reviewed in (Agathocleous and Harris 2009)). The Notch-Delta signalling pathway is probably the most well-studied mechanism (reviewed in (Perron and Harris 2000)). Delta is a ligand for Notch, and is under the control of bHLH proneural proteins (NEUROD1, NEUROD4/MATH3, Neurogenin 2, ATOH7/MATH5, ASCL1/MASH1). Notch promotes RPC maintenance via signalling to the bHLH TFs HES1 and HES5 which downregulate the proneural proteins. Cells with initial higher levels of Delta enhance Notch signalling in their neighboring cells. The neighboring cell therefore has lower level of proneural proteins and Delta. This lower Delta signals back to the original cell to produce lower Notch, but even higher proneural proteins and Delta. Through this amplification, the cells with high Delta and proneural activity will differentiate into photoreceptors. However, the roles of the proneural proteins are still largely undefined.

The progenitor has a moving cell body during the cell cycle (Baye and Link 2007; Del Bene, Wehman et al. 2008). In G1 interphase, the cell body moves towards the vitread surface where the cell undergoes S phase. After DNA replication, the cell body migrates back towards the ventricular surface and undergoes M phase there. This process is termed as interkinetic nuclear migration because it is mainly the nucleus, the main part of the cell body, which migrates within the cytoplasm of the elongated neuroepithelial progenitor cells (Frade 2002; Baye and Link 2008). The daughter cells will either continue the cycle if born as progenitors or exit the cell cycle if born as precursors. In the latter situation, the cell body will migrate towards its final position during the maturation process.

1.4.2 From precursors to mature photoreceptors

1.4.2.1 The development steps towards maturation

The newly born photoreceptor precursor is in a bipolar form pointing to the vitread and ventricular side respectively (Figure 1.3). The ventricular side projects a short process linking

the soma of the precursors to the future outer limiting membrane (OLM) which is formed from adherent junctions between Müller cells and photoreceptor IS. Even at embryonic stages, some of the processes began to protrude from the ONL and show enlargement at the ends in mice (Hinds and Hinds 1979). Ribosomes, mitochondria, even centriole could be found in these bulbous protrusions (Figure 1.3). The soma of the precursors are quite adjacent to the OLM, with that of cone precursors even nearer (Figure 1.4 (Reviewed in (Lamb, Collin et al. 2007))).

It was found in ferret that the other side of the young precursors projects a longer process linking them directly to the IPL, and passing through the OPL without connecting initially (Johnson, Williams et al. 1999). The OPL at this time begins to form with horizontal cells located in the vicinity. Although the photoreceptors will eventually connect with the horizontal cells, initial terminals of photoreceptors are at the two discrete sub-layers of IPL, probably contacting with amacrine or ganglion cells (Figure 1.4). The terminals are morphologically similar to functional synapses and express synaptophysin (Figure 1.4) and synaptotagmin (Johnson, Williams et al. 1999). After about two postnatal weeks in ferret, with continued maturation of horizontal cells and OPL, the vitread process of photoreceptors retracts from the IPL and begins to make synaptic contacts with the horizontal cells at OPL (Johnson, Williams et al. 1999). Bipolar cells, whose maturation coincide with the retraction of the photoreceptor terminal processes, joined in the contacts slightly later (Figure 1.4, and reviewed in (Lamb, Collin et al. 2007)). This phenomenon of connection with the IPL from photoreceptors before they retract to contact OPL did not seem to be well noticed in the literature.

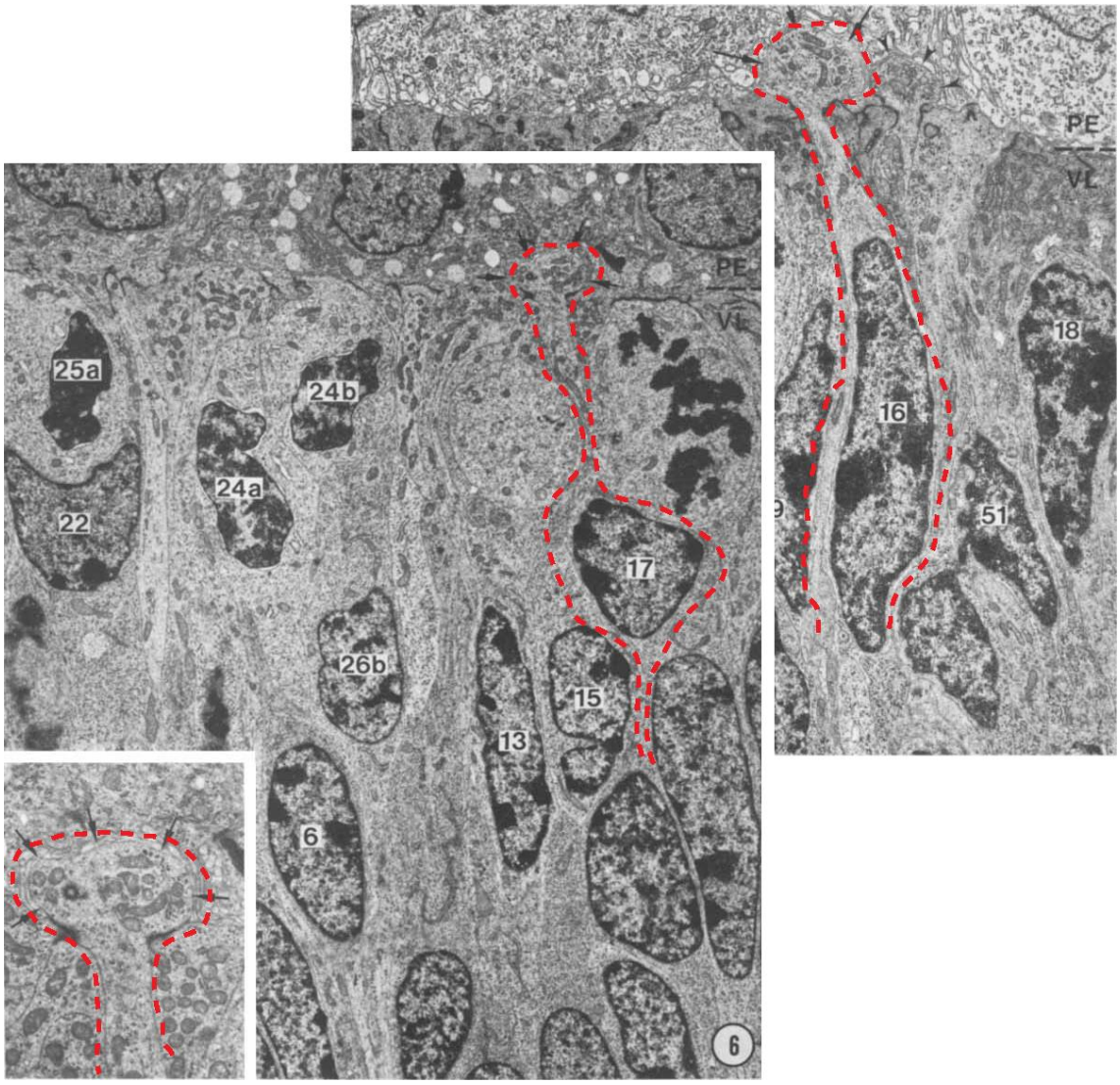

Figure 1.3 Electron micrograph of embryonic mouse retina. (Right) E17 retina shows ventricular process and an enlarged bulbous protrusion of a future photoreceptor cell (cell 16, delineated with dashed red line). The protrusion (arrows) contains ribosomes and mitochondria and is surrounded by future villous processes from the pigment epithelial cells. x6,000; (Middle) E15 retina shows a ventricular process and protrusion of a future photoreceptor cell (cell 17). x4,700; (Left) Higher magnification of the protrusion of cell 17. x14,000. The protrusion contains mitochondria, ribosomes, granular endoplasmic reticulum, and a centriole, and is surrounded by a few layers of membrane from adjacent pigment epithelial cells. PE, pigment epithelium; VL, ventricular layer. Modified from (Hinds and Hinds 1979).

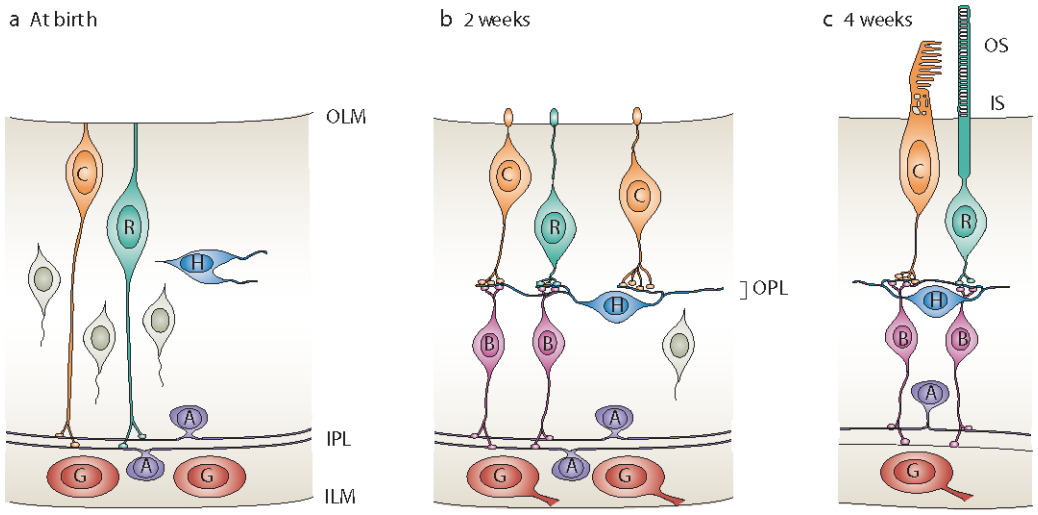

Figure 1.4 Ferret photoreceptor maturation stages (a) Around birth, photoreceptors project a vitread process to the inner plexiform layer (IPL); (b) Two weeks later, the vitread process retract and bipolar cells form between photoreceptors and the IPL; (c) Four weeks later, photoreceptors develop inner segments (IS) and outer segments (OS). A, amacrine cell; B, bipolar cell; C, cone photoreceptor cell; G, ganglion cell; H, horizontal cell; ILM, inner limiting membrane; OLM, outer limiting membrane; OPL, outer plexiform layer; R, rod photoreceptor cell. Adapted from (Lamb, Collin et al. 2007).

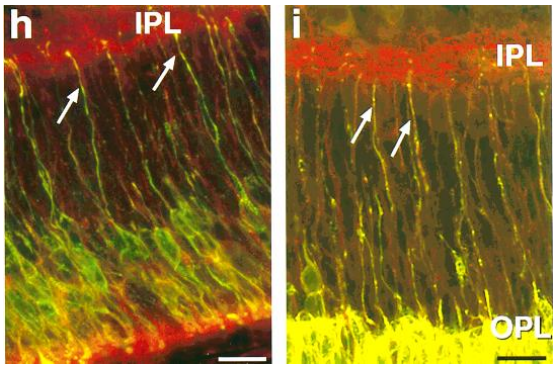

Figure 1.5 Ferret rods project to the IPL. Rod opsin: green; synaptophysin: red.(h) P1, (i) P15. Adapted from (Johnson, Williams et al. 1999).

While the vitread process is synapsing with OPL, the ventricular process of photoreceptors extends and elaborates the inner and outer segment (Figure 1.4). Other than the single study in ferret, the developmental process of photoreceptor maturation after their birth is largely undefined and needs clear investigation. Morphogenesis of mice OS is not fully synchronized to reach maturation until around 3 weeks after birth (LaVail 1973). During this period, the primitive cilium buds out of the plasma membrane and extends with its apical end ballooning

along as visualized by EM (Olney 1968). At P8 – 10, long and highly disorganized disks formed (De Robertis 1960), which will stack perpendicularly to the ciliary stalk eventually. The rod disk stack increases nearly linear to the length of the OS (LaVail 1973). At around P23, the final complete number of photoreceptors (around 70 % of total number of retinal cells) yields 30 times more rods than cones in the mouse (18 – 20 times in human).

The photoreceptor cells begin to express some phototransduction genes and photoreceptor-morphogenesis genes around one week after birth. In ferret, expression of recoverin, vGluT1, and rhodopsin proteins has been detected within the first postnatal week (Johnson, Williams et al. 1999). In human, S opsin begins to be transcribed around foetal week (Fwk) 12 followed by rhodopsin, M opsin and L opsin transcripts at Fwk15 (reviewed in (Swaroop, Kim et al. 2010)). In mouse, mRNA of S opsin begins to express around E13 (Chen, Tucker et al. 1994), followed by the transcription of rhodopsin around P2 and M opsin around P6 (Akimoto, Cheng et al. 2006). Protein of rhodopsin and S-opin are not expressed until around P6 (Morrow, Belliveau et al. 1998) and P5 (Szel, van Veen et al. 1994) in rat.

1.4.2.2 The transcriptional networks regulating the development of precursors

A complex transcription factor network is involved in regulating the development from RPC to precursors to mature photoreceptors. Six key regulators show master roles during this process. The mammalian ortholog of the *Drosophila* paired-type homeodomain orthodenticle (*Otd*), *Otx2*, is probably the earliest regulator of photoreceptor lineage. Conditional knock out of *Otx2* in retinal progenitors converts rods and cones into amacrine-like cells while ectopic expression of Otx2 leads to increased production of rods (Nishida, Furukawa et al. 2003). Although necessary for photoreceptor commitment, postnatal bipolar-cell-specific knock out of *Otx2* shows severe bipolar cell impairment (Koike, Nishida et al. 2007) demonstrating the multi functional role of Otx2.

Specification of the photoreceptor lineage by Otx2 is probably executed via its activation of another *Otd* ortholog, the cone-rod homeobox protein Crx (Furukawa, Morrow et al. 1997). Different from Otx2, Crx expression starts in post-mitotic cells which have just exited the cell cycle (Garelli, Rotstein et al. 2006) rendering it the earliest photoreceptor marker. During mouse retinal development, Crx mRNA expression starts at E12.5 and peaks at P6 (Furukawa, Morrow et al. 1997), coinciding with the onset of cone cell birth and rod maturation respectively (Chen, Wang et al. 1997; Furukawa, Morrow et al. 1997). Crx binds and transactivates the conserved TAATCC/A sequence of photoreceptor-specific genes *rhodopsin*, cone opsin, arrestin, and interphotoreceptor retinoid-binding protein (Furukawa, Morrow et al.

1997). Retrovirus infection of Crx into P0 rat retina significantly increased the frequency of photoreceptor clones and decreased the frequency of amacrine and Müller glial clones (Furukawa, Morrow et al. 1997). A similar approach blocking Crx transactivation activity at P0 showed that the photoreceptors did not form outer segments (Furukawa, Morrow et al. 1997). This is further confirmed by *Crx*$^{-/-}$ mice which lack photoreceptor OS and an electroretinogram (ERG) response (Furukawa, Morrow et al. 1999). Northern blot at P10 of the *Crx*$^{-/-}$ mouse retina showed a great reduction of both rod and cone opsins (rod: *rhodopsin*, cone: *Opn1sw* (or *Blue Cone Pigment*) and *Opn1mw* (green/red)), transducin (rod: *Gnat1*, cone: *Gnat2*), phosphodiesterase (rod: *Pdeb*, cone: *Pdebc*), cGMP – gated channel (rod: *Cncg*), arrestin (rod: *Sag*, cone arrestin), and recoverin transcript levels. These are genes involved in the phototransduction pathway and are essential for proper function of photoreceptors. Requirement of Crx for their expression demonstrates the indispensible role of Crx in the maturation of photoreceptors from precursors. It should be noted that Crx is also expressed in retinal bipolar cells (Liu, Shen et al. 2001) and the pineal gland (Furukawa, Morrow et al. 1999). However, either forced expression of Crx or blockage of Crx transactivation activity did not seem to change the number of bipolar cells when compared with controls (Furukawa, Morrow et al. 1997) indicating Crx action is more specific to photoreceptors than Otx2.

Crx interacts with the neural retina leucine zipper protein Nrl, a member of the Maf family. Through interacting with other TFs, Nrl activates rod-specific genes and specifies the fate of a photoreceptor to become a rod. *Nrl*$^{-/-}$ mice retina show excessive cone-like photoreceptors at the expense of no rods at all (Mears, Kondo et al. 2001), whereas ectopic expression of Nrl in either wild-type or *Nrl*$^{-/-}$ mice transforms all cones into functional rods (Oh, Khan et al. 2007). The *Nrl*$^{-/-}$ mice do not express rod-specific genes (*Rho*, *Gnat1*, *Nr2e3*, *Pdeb*), express low levels of *Rom1*, *Sag* and *Recoverin*, but high levels of cone-specific opsin (*Opn1sw*, *Opn1mw*), transducin (*Gnat2*) and arrestin (Mears, Kondo et al. 2001). *Nrl* transcript can be detected as early as E12.5 and stays on into adulthood (Akimoto, Cheng et al. 2006). Prominent phosphorylation of NRL protein is observed at the peak of rod differentiation (Kanda, Friedman et al. 2007). Reduced phosphorylation is observed in the hot spot mutation (S50 and P51) form of Nrl, accompanied by hyperactivity of Nrl for the rhodopsin promoter with Crx (Kanda, Friedman et al. 2007), indicating a fine tuning of the transcriptional activity by phosphorylation.

Besides the homeodomain and leucine zipper TFs, three ligand-regulated TFs i.e. nuclear receptors also play key roles during photoreceptor fate determination process – Nr2e3, Rorβ and Trβ2. Nr2e3 and Rorβ are retinoid-related orphan receptors whose physiological ligands are still unknown. Directly regulated by Nrl, Nr2e3 suppresses cone gene expression (Chen,

Rattner et al. 2005; Cheng, Aleman et al. 2006), and can also co-activate some rod genes through additional cooperation with Crx (Cheng, Khanna et al. 2004; Cheng, Aleman et al. 2006), hence irreversibly pushing rod precursors into rods. *Rorβ*$^{-/-}$ mice retina are similar to *Nrl*$^{-/-}$ mice but the cones do not have outer segments (Jia, Oh et al. 2009). This indicates Rorβ is involved in rod development, but is also critical for cone development. Indeed, Rorβ synergizes with Crx to initiate S opsin expression (Srinivas, Ng et al. 2006). In response to thyroid hormone, Trβ2 regulates M opsin patterning during cone development (Ng, Hurley et al. 2001).

1.5 Rod photoreceptor cells vs Cone photoreceptor cells

Constituting the majority of retinal cells, rod photoreceptor cells are very sensitive and can respond to single light quanta under dim light (http://webvision.med.utah.edu/). These cells are generated over a long time window (E12 to P10) with a birth peak around mouse birth (Figure 1.2) (Carter-Dawson and LaVail 1979b; Young 1985a; Rapaport, Wong et al. 2004). Cone photoreceptor cells, on the other hand, function under bright light, permit high resolution of visual images and mediate colour vision (http://webvision.med.utah.edu/). There are fewer cones than rods in retina with a ratio of 1:30 in mice (Carter-Dawson and LaVail 1979a). Mouse cone cells are generated in a short embryonic period with a birth peak at E13 – E14 (Figure 1.2) (Carter-Dawson and LaVail 1979b; Rapaport, Wong et al. 2004). Morphologically, mouse rods and cones share a lot of common features yet each type has its own characteristics. The cones have conical-shaped shorter outer segments (hence the name cones) and stubby inner segments whereas the rods have cylindrically shaped long outer segments and slim inner segments (Figure 1.6). With multiple heterochromatin loci, nuclei of cones lie in a single row only in the ventricular/outer side of the ONL, whereas the single chromocentered rod nuclei stack throughout the ONL in rodents. Synapses of cones, known as cone pedicles, are large (8-10 µm diameter), conical, flat end-feet of the cone axons. Synapses of rods are small round enlargements of the axons or cell body, called spherules (3-5 µm diameter).

All retinal cells, including the rods and cones, are derived from proliferating RPCs. Marked by the expression of Pax6 and Chx10, the RPCs in the mammalian retina have a finite capacity to self-renew (Figure 1.7). Although the self-renewal ability of mammalian RPCs is limited (e.g. all cells in the mouse neural retina are post mitotic by around postnatal day 11 (Young 1985a)), a population of RPCs in lower vertebrates, continue to reside in the ciliary marginal zone (CMZ), and have the capacity to generate new retinal neurons throughout life (Hollyfield 1971; Raymond 1991; Reh and Levine 1998). Upon expression of Otx2 during mammalian retinal development, some progenitor cells are beginning to differentiate toward photoreceptor cells

and bipolar cells (Nishida, Furukawa et al. 2003; Zuber, Gestri et al. 2003; Koike, Nishida et al. 2007). Once Crx expression begins, most of the cells will commit to the photoreceptor cell fate and exit the cell cycle, making Crx the earliest marker for photoreceptor cells (Chen, Wang et al. 1997; Furukawa, Morrow et al. 1997). Required to maintain their fate, both the rod and cone photoreceptor cells will maintain Crx expression throughout their lives (Furukawa, Morrow et al. 1997). With the expression of Nrl and its downstream Nr2e3, some of the photoreceptor cells will become rod precursor cells, which will develop into rods eventually. Others will develop into cone precursor cells which will develop into S-cones or M-cones under the regulation of Rxrγ and Trβ2 (Hennig, Peng et al. 2008). The current hypothesis is that unless a particular set of regulatory factors gain dominance to guide precursors to gain a rod or an M-cone identity, the precursors will differentiate into S-cones as a default pathway (Figure 1.7) (Hennig, Peng et al. 2008; Swaroop, Kim et al. 2010). To support this model, human mutations within NR2E3 and mouse Nrl mutations showed enchanced S cone syndrome (reviewed in (Swaroop, Kim et al. 2010)). Further the Trβ2 knockout mice selectively lost M-cones and showed increased S-opsin expression (Ng, Hurley et al. 2001).

Although these regulators are generally regarded as markers for photoreceptor cells of different stages or types, cells, especially the precursor cells may retain the potential to differentiate into any photoreceptor cell types. For example, it was found that the embryonic precursor cells which are Nrl-positively selected (ie. rod precursor cells) express mRNA of S-opsin (Oh, Khan et al. 2007). Therefore, depending on if S-opsin is turned off or not, these cells could become either rods or S-cones. On the other hand, Nr2e3 was found to be expressed in Trβ2-positive cells indicating even mature cones and cone precursor cells express the rod marker Nr2e3 (Haider, Demarco et al. 2006). These raise the questions of if the precursors for rods and cones are same or not and/or at which developmental stage is plasticity lost.

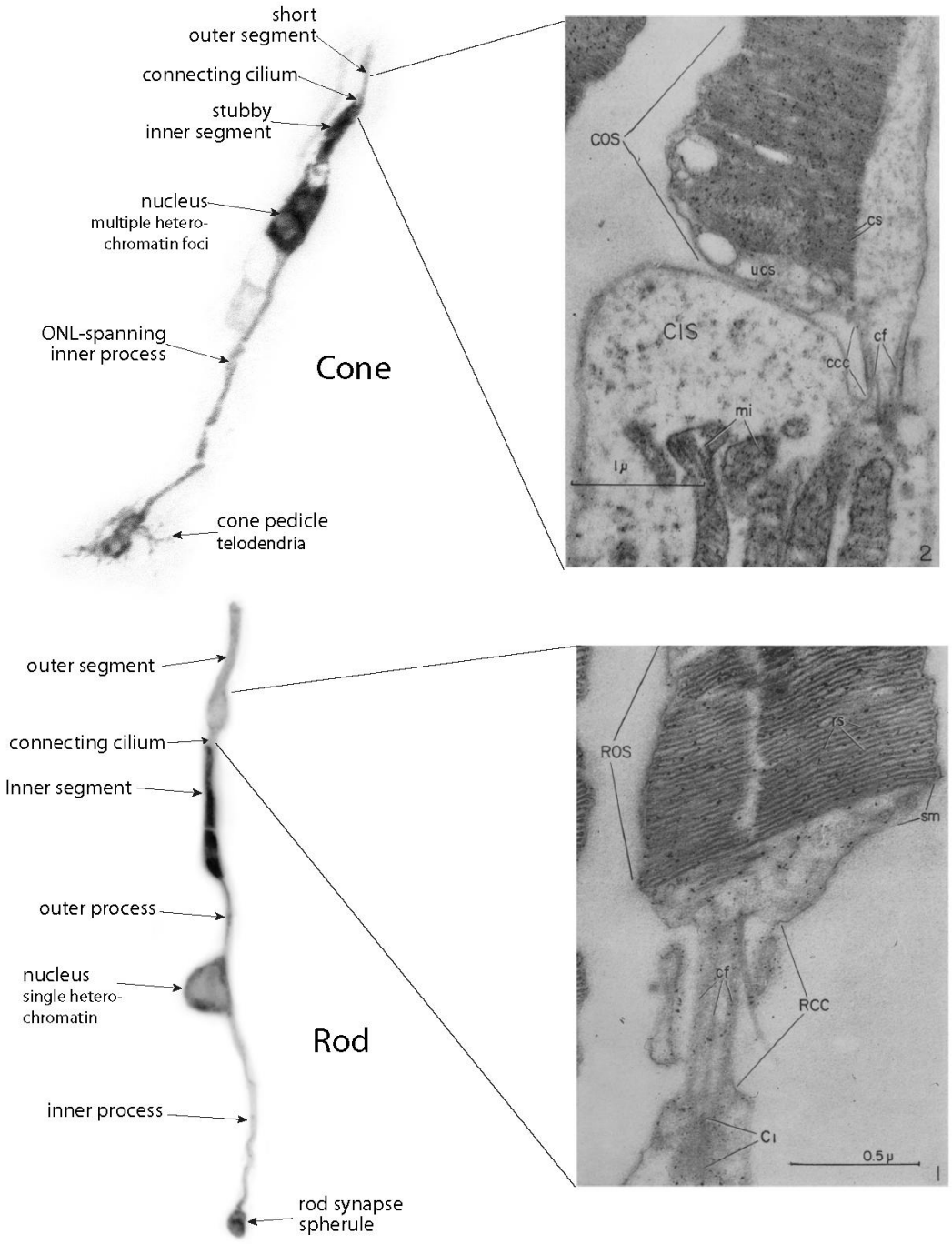

Figure 1.6 Cone and rod morphology. Confocal (Left) and electronic microscope (Right) images of cone (Top) and rod (Bottom) photoreceptor cells. COS, cone outer segment; cs, cone sacs; ucs, unoriented cone sacs; ccc, cone connecting cilium; cf, ciliary filament; CIS, cone inner segment; mi, mitochondria; ROS, rod outer segment; rs, rod sacs; sm, surface membrane; RCC, rod connecting cilium; C1, centriole connected with the connecting ciliumyt0426. EM images of rabbit photoreceptor cells from Robertis (1960); Confocal images using transplanted CrxGFP labeled mouse photoreceptor cells from Baron, M.

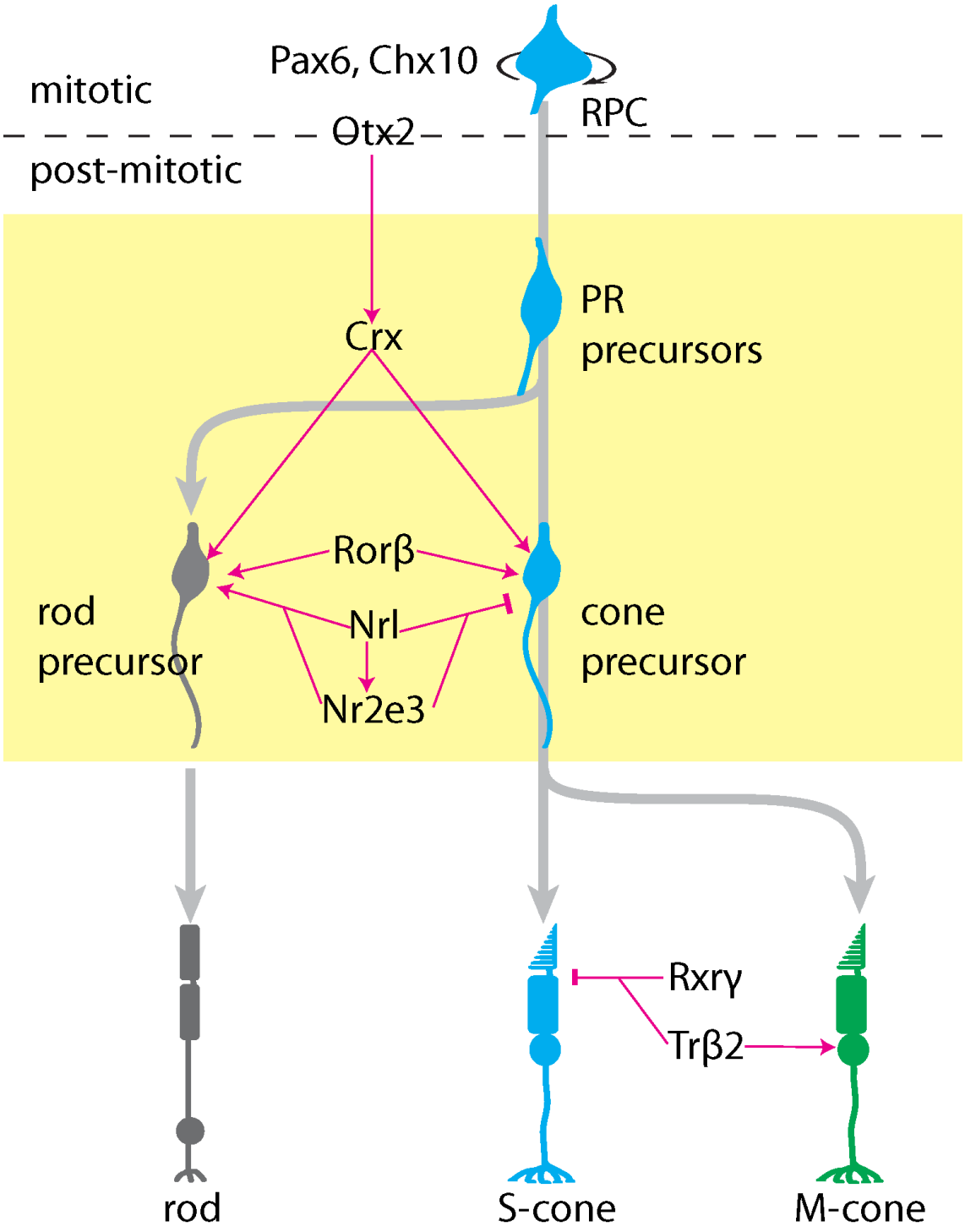

Figure 1.7 Cone and rod markers. Key markers for RPCs are Pax6 and Chx10. The photoreceptor precursors (PR precursors), including both cone and rod precursors, express Otx2, Crx (regulated by Otx2), and Rorβ. Expression of Nrl and Nr2e3, key markers for rod photoreceptor cells, divert the precursors into rod lineage. Expressed in cones, Rxrγ and Trβ2 divert the fate of S-cones into M-cones. Dashed line divides the mitotic RPC which are self-renewable from the remaining postmitotic cells. Yellow area indicate the stage of immature photoreceptor precursor cells. RPC, retinal progenitor cell; PR, photoreceptor.

1.6 Retinal degeneration and cell transplantation therapy

285 million people are estimated to be visually impaired worldwide among which 39 million are blind and 246 million have low vision. Of these, 1.4 million children below age 15 are irreversibly blind for the rest of their lives (World Health Organization website: update June 2012 http://www.who.int/mediacentre/factsheets/fs282/en/index.html). The leading causes of blindness are cataract and various forms of retinal degeneration. Other than glaucoma (the 2nd leading cause of blindness worldwide) and some forms of vitreoretinal degenerations where ganglion cells and the inner retina were affected first, most retinal degenerations are characterized by defects in the outer retina where photoreceptor cells or RPE cells are affected initially. Retinal degenerations can be inherited, acquired and complex. Inherited retinal degenerations are caused by mutations in one or more genes. 203 genes have been identified so far (Retina International: update February 5, 2013 http://www.retina-international.org/sci-news/databases/disease-database/) giving rise to around 27 types of inherited X-linked or autosomal dominant or recessive retinal degenerations (RetNet: update February 4, 2013 https://sph.uth.edu/retnet/sum-dis.htm). Acquired retinal degenerations such as diabetic retinopathy are caused by infection, nutrition, injury and other environmental factors. Complex retinal degenerations such as age-related macular degeneration (AMD) are caused by both genetic and environmental factors.

Retinitis pigmentosa (RP) is the most common form of inherited retinal degeneration, affecting more than 1 million people worldwide with a prevalence of around 1 in 4000 (Hartong, Berson et al. 2006). Starting with night blindness, patients with RP gradually lose peripheral vision to central vision by middle age and some will eventually suffer complete blindness. This is because of the progressive degeneration from the rod-rich peripheral regions to the cone-rich central regions. Nearly one third of RP patients also suffer from Usher's syndrome, Bardet-Biedl syndrome, and other syndromes in which their non-ocular tissues were also affected (Hartong, Berson et al. 2006). 56 genes have been identified so far to cause RP upon mutations (Table 1.1). Among these genes, *RHO* mutations account for 30 to 40% of autosomal dominant RP, *RPGR* mutations account for at least 15% of male sporadic (isolated) RP cases and *USH2A* for 10 to 15% of recessive RP (Retnet: update February 4, 2013 https://sph.uth.edu/Retnet/sum-dis.htm).

Table 1.1 Genes for retinal diseases

Retinitis pigmentosa (56)			Usher	Bardet-Biedl					LCA/RP
ad (23)	ar (36)	x-linked (3)	syndrome	syndrome	ALMS (1)	SLSN (5)	JATD(5)	JBTS(13)	(20)
BEST1	ABCA4	OFD1	ABHD12	ARL6	ALMS1	CEP290	TTC21B	CEP290	CRX
CA4	BEST1	RP2	CDH23	BBS1		NPHP1	WDR19	TMEM67	IMPDH1
CRX	C2ORF71	RPGR	CIB2	BBS2		SDCCAG8	ATD1	RPGRIP1L	OTX2
FSCN2	C8ORF37		CLRN1	BBS4		NPHP4	IFT80	CC2D2A	AIPL1
GUCA1B	CERKL		DFNB31	BBS5		ICCB1	DYNC2H1	TMEM216	CABP4
IMPDH1	CLRN1		GPR98	BBS7				NPHP1	CEP290
KLHL7	CNGA1		HARS	BBS9				TTC21B	CRB1
NR2E3	CNGB1		MYO7A	BBS10				ARL13B	DTHD1
NRL	CRB1		PCDH15	BBS12				INPP5E	GUCY2D
PRPF3	DHDDS		USH1C	CEP290				AHI1	IQCB1
PRPF6	EYS		USH1G	INPP5E				KIF7	KCNJ13
PRPF8	FAM161A		USH2A	LZTFL1				TCTN1	LCA5
PRPF31	IDH3B			MKKS				OFD1	LRAT
PRPH2	IMPG2			MKS1					NMNAT1
RDH12	LRAT			SDCCAG8					RD3
RHO	MAK			TRIM32					RDH12
ROM1	MERTK			TTC8					RPE65
RP1	NR2E3								RPGRIP1
RP9	NRL								SPATA7
RPE65	PDE6A								TULP1
SEMA4A	PDE6B								
SNRNP200	PDE6G								
TOPORS	PRCD								
	PROM1								
	RBP3								
	RGR								
	RHO								
	RLBP1								
	RP1								
	RPE65								
	SAG								
	SPATA7								
	TTC8								
	TULP1								
	USH2A								
	ZNF513								

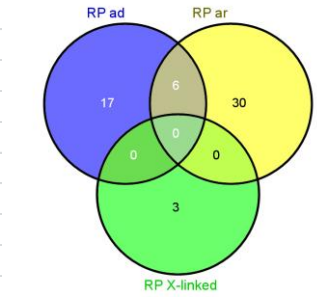

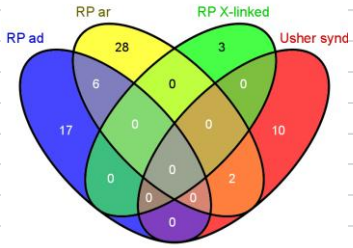

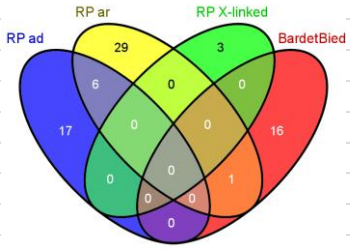

This table only illustrates the major diseases and genetic heterogeneity and is not an exhaustive gene list. ad, autosomal dominant; ar, autosomal recessive; ALMS, Alstrom syndrome; SLSN, Senior–Løken syndrome; JATD, Jeune asphyxiating thoracic dystrophy; JBTS, Joubert syndrome; LCA/RP, Leber congenital amaurosis/retinitis pigmentosa. Numbers in brackets indicating number of genes in this category. Venn diagrams showing the number of common and different genes among RP ad, RP ar and RP x-linked (left), RP ad, RP ar, RP x-linked and Usher syndrome (top right), and RP ad, RP ar, RP x-linked and Bardet-Biedl syndrome (bottom right). Gene data obtained from Retnet: https://sph.uth.edu/Retnet/sum-dis.htm updated on Feb 04, 2013 except ALMS, SLSN, JATD and JBTS which are obtained from (Rachel, Li and Swaroop 2012)

Other inherited retinal degenerations are less common, but could be more severe. Leber'S Congential Amaurosis (LCA) probably represents the most severe retinal disorder. Infants with LCA are born blind and lack functional photoreceptor cells. Most common mutations for LCA lie in *GUCY2D* (retinal guanylyl cyclase 1), *RPE65* (retinoid isomerohydrolase), *CRX* (a transcription factor), *CRB1* (Protein crumbs homolog 1), *RPGRIP1* and *CEP290*. Both RPGRIP1

and CEP290 are cilium proteins involved in retinitis pigmentosa GTPase regulation and ciliogenesis and ciliary transport process respectively. GUCY2D protein is involved in resynthesis of cGMP for dark state recovery after phototransduction. CRB1 protein is expressed in the apical membrane of the adherent junctions in the ONL of the retina playing a role in photoreceptor morphogenesis. RPE65 protein catalyzes production of 11-cis retinal and is involved in retinal pigment regeneration. Other inherited disorders that mark macular degeneration and loss of central vision include Stargardt disease (mutations found in *ABCA4* (Allikmets, Singh et al. 1997; Jonsson, Burstedt et al. 2013), *ELOVL4* (Zhang, Kniazeva et al. 2001; Vasireddy, Wong et al. 2010)), Best macular degeneration (mutations in *VMD2* (Petrukhin, Koisti et al. 1998; Atchaneeyasakul, Jinda et al. 2008)) and Sorsby fundus dystrophy (mutations in *TIMP3* (Jacobson, Cideciyan et al. 2002)).

Usually affecting older adults, AMD is the primary cause of visual impairment in developed countries and ranks the 3rd cause of global blindness with a prevalence of 8.7% (World Health Organization: http://www.who.int/blindness/causes/priority/en/index.html). In advanced AMD patients, the retina detaches from the RPE because of accumulation of drusen – extracellular materials that contain proteins and lipids – between Bruch's membrane and the RPE (dry AMD) or because further blood vessels grow up from the choroid behind the retina (wet AMD). Other than genes that may contribute to AMD such as *ABCA4* (Allikmets, Shroyer et al. 1997), complement system proteins factor H (CFH), factor B (CFB) and factor 3 (C3) (Sivaprasad and Chong 2006), HtrA serine peptidase 1 (HTRA1) (Dewan, Liu et al. 2006; Yang, Camp et al. 2006), age-related maculopathy susceptibility 2 (ARMS2) (Rivera, Fisher et al. 2005; Kanda, Chen et al. 2007), aging, smoking (Thornton, Edwards et al. 2005), obesity (Adams, Simpson et al. 2012), light exposure (Sui, Liu et al. 2013) and oxidative stress (Ugurlu, Asik et al. 2013) have all been associated with AMD.

Photoreceptor cells require a large supply of energy and relevant proteins to be transported to the OS for phototransduction and produce lots of metabolic wastes which are transported back to the IS or phagocytized by RPE along with the shedded disks. Disturbance of this balanced system or defects in photoreceptor morphogenesis will lead to photoreceptor death and consequently retinal degenerations. These retinal degenerations are usually irreversible and effective treatments are few. With advances in our understanding of the etiology and technology innovation, some therapies begin to offer promise in slowing down the degeneration or even restoring vision to some degree (Table 1.2). Implantation of a retinal prosthesis which transmit light stimuli to the brain through optic nerve showed improved vision in three RP patients (Yanai, Weiland et al. 2007), or further showed improved vision as

well as long term safety in 30 blind patients with end-stage outer retina degeneration (Humayun, Dorn et al. 2012). Vitreoretinal surgery (Heussen, Fawzy et al. 2008) and radiation therapy (Kishan, Modjtahedi et al. 2013) also showed some effects in treating wet/neovascular AMD. Many pharmaceutical drugs have been used to slow down the process of AMD via neuroprotective pathway, inhibiting angiogenisis, visual cycle and complement pathways with anti-angiogenic drugs currently the most effective (Zhang, Zhang et al. 2012). For inherited disorders where the genes are mutated, gene therapy can effectively cure the disease by delivering a correct therapeutic gene into the affected tissue (Thrasher, Casimir et al. 1995). In retinal disorders, administration of adeno-associated virus (AAV) construct expressing *RPE65* in LCA2 patients showed significant improvement in visual function (Bainbridge, Smith et al. 2008; Maguire, Simonelli et al. 2008). Although the currently safest viral vectors (AAV) were used in clinic, their long term immunotoxicity remains to be monitored. Indeed there was a mild increase in serum neutralizing antibodies to AAV2 two weeks to three months after injection in two subjects although the levels returned to baseline levels after a year (Simonelli, Maguire et al. 2010). Three years follow up showed that the patients retained the visual function that had been achieved a few months after injection and did not experience serious adverse events related to the vector (Testa, Maguire et al. 2013). For genes too large for viral vectors such as *ABCA4*, DNA nanoparticle package showed successful delivery and improvement of the dark adaption recovery and reduced lipofuscin granules in a Stargardt mouse model (Han, Conley et al. 2012).

Despite these advances, none of the above therapies can provide new functional RPE or photoreceptors cells, which are the key issue for outer retinal degeneration. In addition, these therapies are disease-specific and cannot be used in all the outer-retinal degenerations, except the retinal prosthesis implant which only provides artificial vision. Cell transplantation, on the other hand, supplements the recipients with new correct functional cells and could potentially be used in any of the above retinal degenerations. The question is, can the transplanted cells **integrate** (the process in which the donor cells correctly mature and stabilize their position in the ONL (for photoreceptor cells) or the RPE layer (for RPE) of the retina and make appropriate connections with recipient neural circuits) and properly function after transplantation. For degeneration related to RPE loss/dysfunction, the first clinical trial of human ES cell derived RPE showed positive results in treating dry AMD and Stargardt disease (Schwartz, Hubschman et al. 2012). For degeneration due to photoreceptor loss, a long journey was made and only findings in recent years are promising.

Table 1.2 Therapies for outer (RPE, ONL, OPL) retinal disorders

Therapeutic approach	Subtype	disease	Reference
Pharma-ceutical	complement pathway inhibitors: POT-4, ARC1905, Eculizumab, FCFD4514S	AMD	Zhang, Zhang, and Weinreb 2012*
	visual cycle inhibitors: Fenretinide, ACU-4429	AMD	Zhang, Zhang, and Weinreb 2012*
	anti-angiogenic agents: rapamycin/sirolimus, pigment epithelium-derived factor, …	wet AMD	Zhang, Zhang, and Weinreb 2012*
	neuroprotective agents: brain-derived neurotrophic factor, ciliary neurotrophic factor, glial cell-derived neurotrophic factor, AL-8309B	AMD	Zhang, Zhang, and Weinreb 2012*
	FGF		
	anti-VEGF agents	wet AMD	Ambati and Fowler, 2012*
Gene therapy	RNAi (suppress mutant *RHO* expression while introduce a resistant *Rho* gene)	RP (*RHO*)	Rossmiller, Mao, and Lewin 2012*
	viral vectors:lenti, AAV	RP (*RHO*), Neovascular AMD (*PEDF*), LCA (*RPE65*)	Rossmiller, Mao, and Lewin 2012*; Campochiaro, Nguyen, Shah et al. 2006; Bainbridge, Smith et al. 2008
	DNA nanoparticle	Stargardt disease (ABCA4)	Han, Conley et al. 2012
Cell therapy	RPE	AMD, Stargardt disease,	Lu, Malcuit et al. 2009
	PR	blindness due to PR loss	MacLaren, Pearson et al. 2006
Vitreoretinal surgery		wet AMD	Heussen, Fawzy et al. 2008
Radiation therapy		wet AMD	Kishan, Modjtahedi, Morse, and Lee 2013
Retinal prosthesis implant	Functional electrical stimulation	RP	Yanai et al. 2007
	Argus II Retinal Prosthesis System (microchip)	end-stage outer retinal degeneration	Humayun, Dorn, et al. 2012

*A review. RP: retinitis pigmentosa; AMD: age-related macular degeneration. PR:photoreceptor; RPE:retinal pigment epithelium; RHO: rhodopsin; PEDF:pigment epithelium- derived factor; RPE65:Retinal pigment epithelium-specific 65 kDa protein; ABCA4: ATP-binding cassette sub-family A member 4

The earliest effort was made 50 years ago in which whole fetal rat retinas were transplanted into the anterior chamber of the maternal parent recipients (Royo and Quay 1959). Although they survived for months, the donor retina did not show any connections with the host environment. Similarly, transplanted rat embryonic retinal sheets or aggregates of embryonic retinal neurons were unable to interact properly with the host rat retinas (Zhang, Arner et al. 2003), although they were able to express some markers for retinal cells such as calbindin (for horizontal and amacrine cells), neuronal nitric oxide synthase (NOS, for a subpopulation of amacrine cells), and protein kinase C (PKC, for bipolar cells) (Zhang, Arner et al. 2003). The embryonic tissues or aggregates were then dissociated into single cells and injected into the subretinal space or vitreous cavity of the host animal eye. Transplanted human or mouse retinal progenitor cells (Coles, Angenieux et al. 2004; Klassen, Ng et al. 2004) or brain-derived rat neural progenitor cells (Takahashi, Palmer et al. 1998) showed better interaction with the host mouse or rat retina in that they migrated into all retina layers and developed morphological similarities to various retinal cell types. But expression of photoreceptor-only genes and specific migration into the ONL after transplantation into adult recipients was very inefficient (Takahashi, Palmer et al. 1998; Van Hoffelen, Young et al. 2003; Sakaguchi, Van Hoffelen et al. 2004). Similarly transplantation using mature retinal cells also showed very low integration. The integration efficiency, however, was significantly increased when the postnatal retinal cells were transplanted (MacLaren, Pearson et al. 2006). Furthermore the integrated mouse retinal cells were able to respond to light in the recipient mouse eyes after transplantation (MacLaren, Pearson et al. 2006). Using different stages of retinal cells from an NrlGFP transgenic line which labels only photoreceptor cells that have exited the cell cycle, it was concluded that it is the immature postmitotic photoreceptor precursor cells that have the highest integration efficiency (MacLaren, Pearson et al. 2006).

Due to the nature of mouse retina genesis, the birth peak of rods and cones are in postnatal period (~P0) and embryonic period (~E14) respectively. Despite their much higher integration rate, the postnatal mouse photoreceptor precursors mainly give rise to rods and rarely give rise to cones (Lakowski, Baron et al. 2010). The embryonic mouse photoreceptor precursors on the other hand, labeled with a CrxGFP transgenic reporter give rise to significantly more cones, with a cone/rod ratio similar to the *in vivo* situation after transplantation (Lakowski, Baron et al. 2010). However, the integration efficiency is around 10 fold lower than that of postnatal precursors (Lakowski, Baron et al. 2010). These populations (postnatal and embryonic) both have attributes of a desired transplantable cell population, i.e. high integration and production of both cones and rods. To enrich cell populations which have these desirable attributes, it is

important to elucidate and understand the molecular properties of both early and late precursor cells which can then be used as criteria to screen for ideal cell populations. Specifically, ideal cell populations need to be identified that achieve high level in rod, or cone, or rod and cone integration.

Regarding the sources of donor cells, current research in mouse models uses directly dissociated cells from retinal tissues at a confined period of developmental time such as the peak of precursor generation. This is not a viable option for clinical cell transplantation as unlike blood, which the donors can regenerate after donation, people do not have the ability to form a new retina after donation of their retina. In addition, the majority of both rods and cones in human development are born during foetal week 12 to 32 which is not a feasible period to obtain donor cells. However, recent studies show that it is possible to obtain photoreceptor-like cells (Lamba, Karl et al. 2006; Osakada, Ikeda et al. 2008; Osakada, Ikeda et al. 2009; West, Gonzalez-Cordero et al. 2012) or even the whole optic-cup (Eiraku, Takata et al. 2011) or retina-like structures (Aoki, Hara et al. 2009) from embryonic stem (ES) cells or induced-pluripotent stem (iPS) cells with certain induction protocols. After transplantation, the human ES cell-derived "photoreceptors" express photoreceptor markers and show visual responses in ERG analysis (Lamba, Gust et al. 2009). However, both the retina and the induced cell cultures contain cells of different types and stages. For effective and safe cell transplantation it will be important to select only the transplantation-competent photoreceptor precursors and eliminate cells of other types and stages.

1.7 Why surface molecules of photoreceptor cells

Two research questions emerged along with the concept that cells at the precursor stage integrate best: one is WHY do cells of this stage rather than other stages integrate better; the other is HOW to isolate this population of cells from a cell mixture. While the former question is important for our understanding of these cells, the latter is a practical issue for cell transplantation. Both need to be clearly addressed for cell therapy.

Imagining the integration process of a single cell, it is highly likely that this is an interaction process between the migrating cell and its neighbouring cells and the environment. Hence physical stimuli, chemicals, secreted as well as cell surface proteins from neighbouring cells and the environment will influence the migration process (such as Reelin which guides migration of projection neurons from ventricular zone to the neocortical plate along the radial array in the developing mouse neocortex (Hirotsune, Takahara et al. 1995; Jossin and Cooper 2011)). And there is no doubt that complex mechanisms and various events are happening

within the migrating cell. However, it is the molecules that are on the surface of that cell that actually provide the physical contact, build the bridge, and conduct the communication with other cells and environment, which eventually guide the cell to reside at a particular position and ensure that it is permitted to stay there. Finding out what these surface molecules are and what they do, therefore, is crucial to address the “why” question.

Identifying these cell surface molecules may also help to explain the different behavior of the early and late precursor populations. As the two donor cell populations are transplanted straight away after isolation from the developing retina and are left in similar recipients for the same length of time, the environment would be largely the same. Therefore it is the different properties of these transplanted cells which make the differences. As integration is a process in which donor cells interact with the host environment, differences on the cell surface should contribute greatly to the interaction process. As soon as the cells are entering the environment, say at the time of injection into the subretinal space, there will probably be some initial contacts made through cell surface molecules. As the transplanted cells need to migrate from the subretinal space into the ONL, cells which have appropriate cell surface molecules will probably be able to connect or “talk” with the host environment and can initiate the migration process. Whereas cells which do not have this surface signature will probably not be recognized by the host environment, hence may not be able to bridge or connect with the host. These cells may remain at the site of injection and may cause unwanted degeneration eventually.

The current approach to select photoreceptor cells from cell mixtures is genetically tagging fluorescent proteins using photoreceptor-specific transcription factor transgenes and sorting photoreceptors out via expression of the fluorescent protein. This method, although valid in scientific research, cannot be applied in clinical practice as genetically tagged fluorescent protein is not desirable for patients. In addition, the TFs are expressed in photoreceptors from birth to death, and do not specifically label a particular stage. These problems can be solved if specific cell surface molecules are identified. On one hand, serving as markers themselves, cell surface molecules allow cell isolation by specific antibody affinity to their extracellular domains without the need of transgenic reporters. On the other hand, as shown in leukocyte differentiation, different clusters of cell surface antigens show different patterns of expression along development (Zola, Swart et al. 2005). Therefore, it is possible to label a particular stage of the photoreceptor cell through a combination of different cell surface markers.

1.8 Approaches for screening cell surface molecules

There are several ways to provide the pool for identification of cell type specific surface antigens. Traditional decoy immunization strategy uses the cells to immunize lymph node cells which are then fused with mouse myeloma cells to produce hybridomas. These hybridomas secrete monoclonal antibodies which can be further characterized and validated. This method was used for ES cells for which around 70 surface molecules are identified but few are new molecules (Choi, Kim et al. 2008).

The second is the classical transcriptome profiling strategy in which RNA microarray is performed to identify genes that are transcribed in the given cell population or compared against other cell populations. Total RNA of the cells were extracted, their cDNA synthesized and hybridised with a gene chip which contains all the genes of that species. Transcribed genes will give a signal on the chip and can be detected. Data obtained from the microarray, however, often contains tens of thousands of genes, the majority of which are probably not surface molecules. Screening only the surface molecules therefore can be highly time-consuming, and whether the protein is present on the cell surface or not remains to be established. Despite these considerations, RNA microarray remains the largest pool for identifying interesting candidates. Some surface markers for definitive endoderm cell population were identified using this strategy (Yasunaga, Tada et al. 2005).

The third method is the proteomic approach which directly identifies and quantifies proteins in the sample using Mass Spectrometry (MS). Proteins were directly extracted from the cells and digested into small peptides. The peptides were then ionized and their mass evaluated. By putting together the fragmented peptides of each protein, the mass and sequence of the protein can be determined. This usually produces a much smaller but more accurately targeted candidate protein data set than microarray. The problem with this assay is that proteins with smaller molecular weight or lower abundance are often masked by proteins with higher abundance during MS analysis. However, this might be improved by cell fractionation through which the abundance of desired proteins could be increased. The ideal cell fraction that cell surface proteins lie in seems to be the membrane fraction which can be obtained via ultracentrifugation or chemical enrichment using combinations of detergents and other reagents.

In this thesis, I used both the microarray and MS methods for the following reasons: 1) the full transcriptome data and proteome data for photoreceptor precursor cells can be obtained; 2)

both the RNA and the protein level are covered; 3) the microarray and MS data probably provides the fullest pool for cell surface molecules to be screened for.

1.9 Hypothesis and aim

During photoreceptor maturation, two processes project in opposing directions along developing photoreceptor precursors: one is the vitread process which will synapse with interneurons in the OPL, and the other is the ventricular process which will develop into IS, CC and OS within the interphotoreceptor matrix in the subretinal space, part of the OS embedding into the RPE. As the processes extend, the cell also seeks the final position for its cell body in the ONL and moves towards there. Cones, and not rods, are known to undergo a late migration so that their cell bodies become located at the outer edge of the ONL (Rich, Zhan et al. 1997). Once the processes are fully established, the position and orientation of the whole cell becomes fixed within the ONL. As the surface of the processes and the cell body interact with the surrounding environment directly, I hypothesize that cell surface molecules enriched there play fundamental roles for the correct localization of the photoreceptors. Furthermore, the same cell surface molecules which are important for the localization of precursors in the developing retina might also be important for the migration and integration of transplanted precursors in the recipient retina. And of wide clinical significance the cell surface molecules can be used as tools to isolate the photoreceptor precursor cells. I therefore, aim to discover these photoreceptor-specific cell surface molecules and examine their function during photoreceptor precursor maturation and integration.

As mentioned earlier, the postnatal photoreceptor precursor cells possess high integration efficiency (MacLaren, Pearson et al. 2006; Lakowski, Baron et al. 2010) and the embryonic photoreceptor precursor cells can give rise to cones after transplantation (Lakowski, Baron et al. 2010). It will be useful to find out what unique molecular properties these cell populations possess. This will not only help us to understand these cells better, but will also facilitate the clinical application of cell therapy. To reveal the most unique properties of photoreceptor precursor cells, I plan to compare them with other retinal cells of the same stage. This is because photoreceptor cells and other retinal cells are all derived from RPCs and they probably share more common properties than that of other cell types. Furthermore, I will compare the properties of the early and late photoreceptor precursor cells to see if I can identify reasons for the different behavior of these cells after transplantation.

I plan to identify the properties of these cells by analyzing transcriptome data from microarray experiments as this will also provide a large enough pool to screen for cell surface molecules. I

will also search for cell surface proteins directly through proteome data obtained from mass spectrometry.

This thesis, therefore, has the following objectives:

1) To understand the properties of embryonic and postnatal photoreceptor precursor cells by comparing their transcriptome expression profiles with other retinal cells of the same stage and comparing CrxGFP or NrlGFP labeled photoreceptor cells of different stages.

2) To identify cell surface molecules on photoreceptor precursors through bioinformatics analysis of proteomic and transcriptomic data.

3) To confirm expression profiles of identified molecules in photoreceptor cells by detecting their mRNA and protein in the developing mouse retina.

4) To test if/where these molecules are expressed on transplanted photoreceptor precursor cells as they interact with the host environment by immunohistochemistry (IHC).

5) To explore the potential interaction partners in the retina of identified molecules, and via over-expression or knock out/down experiments aim to demonstrate the function for selected molecules in photoreceptor integration and correct orientation after transplantation or during photoreceptor development.

6) To validate the performance of selected cell surface molecules as tools to isolate photoreceptor precursor cells for transplantation experiments.

2 Materials and methods

2.1 Mice

The homozygous NrlEGFP transgenic mouse line (referred to as NrlGFP) (mouse strain SV129) (Akimoto, Cheng et al. 2006) was a gift from Anand Swaroop (University of Michigan, USA). The Crx-GfpAP transgenic mouse line (referred to as CrxGFP) (mouse strain C57BL/6) (Samson, Emerson et al. 2009) was provided by C. Cepko's laboratory as a heterozygous line and now has been maintained as a homozygous line. The wildtype CD1 mice were used as a GFP negative control in flow cytometry (FCM) analysis. All animals were maintained in University College London (UCL) animal facilities and experiments performed in accordance with the Animals (Scientific Procedures) Act 1986 and the ARVO Statement for the Use of Animals in Ophthalmic and Vision Research. For timed matings, light-cycle synchronised animals were set up for over-night mating and female checked for vaginal plugs on the following morning. The day of plug discovery was counted as embryonic day (E) 0.5. On the given day of development, embryos were removed from the uterus of sacrificed pregnant mice. Postnatal mice are collected from either timed-mating pairs or non-timed-mating pairs. For non-timed-mating pairs, once pregnancy was confirmed, the cage of a pregnant female was gently checked around the date of birth.

2.2 Dissection of the eye and the retina

2.2.1 Dissection and dissociation of retinal cells

The whole embryos and the postnatal and adult eyes were collected from sacrificed animals into Earle's Balanced Salt Solution (EBSS) on ice in a procedure room. Eyes from the postnatal and adult mice were enucleated with forceps (Dumostar 11cm straight tweezer, Dumont #55). The eyes from the embryos and the postnatal and adult mice were dissected in EBSS under a Zeiss Stemi SV-6 dissection microscope. After removal of the optic nerve, the eye was pulled apart from the hole of the optic nerve revealing the RPE, retina and lens. The RPE and lens were carefully removed and only neural retina tissues were collected for dissociation. Single retina cell suspension was prepared using the Papain Dissociation System (Worthington Biochemical, Lorne Laboratories, UK).

2.2.2 Dissection of eyes for embedding

While the lens from embryonic and postnatal eyes were maintained during embedding for IHC, lens from adult eyes were generally removed as they might damage the retina tissue during cryosectioning. To do this, a hole was punctured on the corneal using a 25G needle, then the

cornea was removed with dissection scissors cutting around it starting from the hole, and the lens removed with forceps.

2.3 Cell sorting and Flow cytometry analysis

2.3.1 Fluorescence-activated cell sorting (FACS)

For microarray, Mass Spectrometry (MS) and quantitative PCR (qPCR) analysis which compared the GFP-positive and GFP-negative cells, two-way sorting which collected both GFP-positive and negative cells were performed with a Beckman Coulter MoFloTM XPD cell sorter. Dissociated retinal cells were prepared at a concentration of 20-40 million/ml in DMEM or DMEM/F-12 medium containing 3% fetal bovine serum (FBS) before sorting and were collected in a FACS tube (or 15 ml falcon tube) containing 0.5 ml (or 1 – 3 ml for 15 ml falcon tube) DMEM or DMEM/F-12 medium with 20 – 50 % serum (or no serum for MS samples) as the serum will be diluted during sorting. FACS-gates were determined according to cell size, cell complexity, and non-GFP retinal cells using stage-matched wild-type retina cells (Figure 2.1). Purity of the sorted GFP-positive cells was checked by re-running a few sorted cells at the end of the sort and was typically >90%.

For microarray and qPCR analysis, around 20 – 30% CrxGFP-positive cells and around 20% CrxGFP-negative cells were collected for E15.5 retinal cells (Figure 2.1 A2 and A3). Around 75% CrxGFP-positive cells and around 13% CrxGFP-negative cells were collected for P4 retinal cells (Figure 2.1 B2 and B3). Previous experience showed that a minimum of 2 million cells per sample was required for microarray analysis. As the cell numbers were low for the E15.5 retinal preparations, several rounds of sorting and collection were performed. Each E15.5 sample was collected from several litters, each P4 GFP-positive sample was from two pups (four retinas) and each P4 GFP-negative sample was from four pups (eight retinas). Cells from different rounds or litters were merged as indicated (Appendix Table 2.1). The sorted GFP positive and negative cell pellets were temporarily frozen at -80°C after centrifugation at 328 g for 15 min at 4°C and removal of the medium. A similar procedure was performed for the NrlGFP-sorted retinal cells for Mass Spectrometry analysis.

2.3.2 Flow cytometry analysis

For cell surface marker expression analysis without collection of cells, Papain dissociated live retinal cells were adjusted to 1×10^6 cells per 100 µl 1% bovine serum albumin (BSA) in Phosphate Buffered Saline (PBS, isotonic, pH 7.3, Oxoid, UK) and blocked on ice for one hour, followed by a 30 min antibody incubation on ice. Cells were then washed in PBS, stained with DAPI/Topro3 and subjected to analysis in the LSRII analyser machine (BD Biosciences). The

following antibodies were used: PerCPCy5.5-conjugated anti-CD80 (0.1 µg, BioLegend), APC-conjugated anti-CD83 (0.25 µg, BioLegend), PE-conjugated anti-CD276 (0.5 µg, BioLegend), eFluor450-conjugated anti-CD73/NT5E (1.2 µg, eBioscience), PECy7-conjugated anti-CD24 (0.2 µg, BD Biosciences), APC-conjugated anti-Prominin-1 (0.06 µg, eBioscience). Background signals of the fluorochrome were visualized using a corresponding isotype control for each antibody (PerCPCy5.5 Armenian Hamster IgG, APC Rat IgG1 κ, PE Rat IgG2a κ were from BioLegend; APC Rat IgG1 κ and eFluor450 Rat IgG1 κ were from eBioscience, PECy7 Rat IgG2b κ was from BD). Live cells are selected for analysis based on cell size, cell complexity, and negative staining of DAPI or Topro3. At least 10, 000 healthy cells were analysed during sorting using the software FACSDiva (BD Biosciences). The data were then analyzed and plotted in FlowJo 8.6.3. Gates for the antibodies in plots were set according to background signals from isotype controls and no-antibody controls. Gates for GFP were set according to retina cells from wild type animals of corresponding stages.

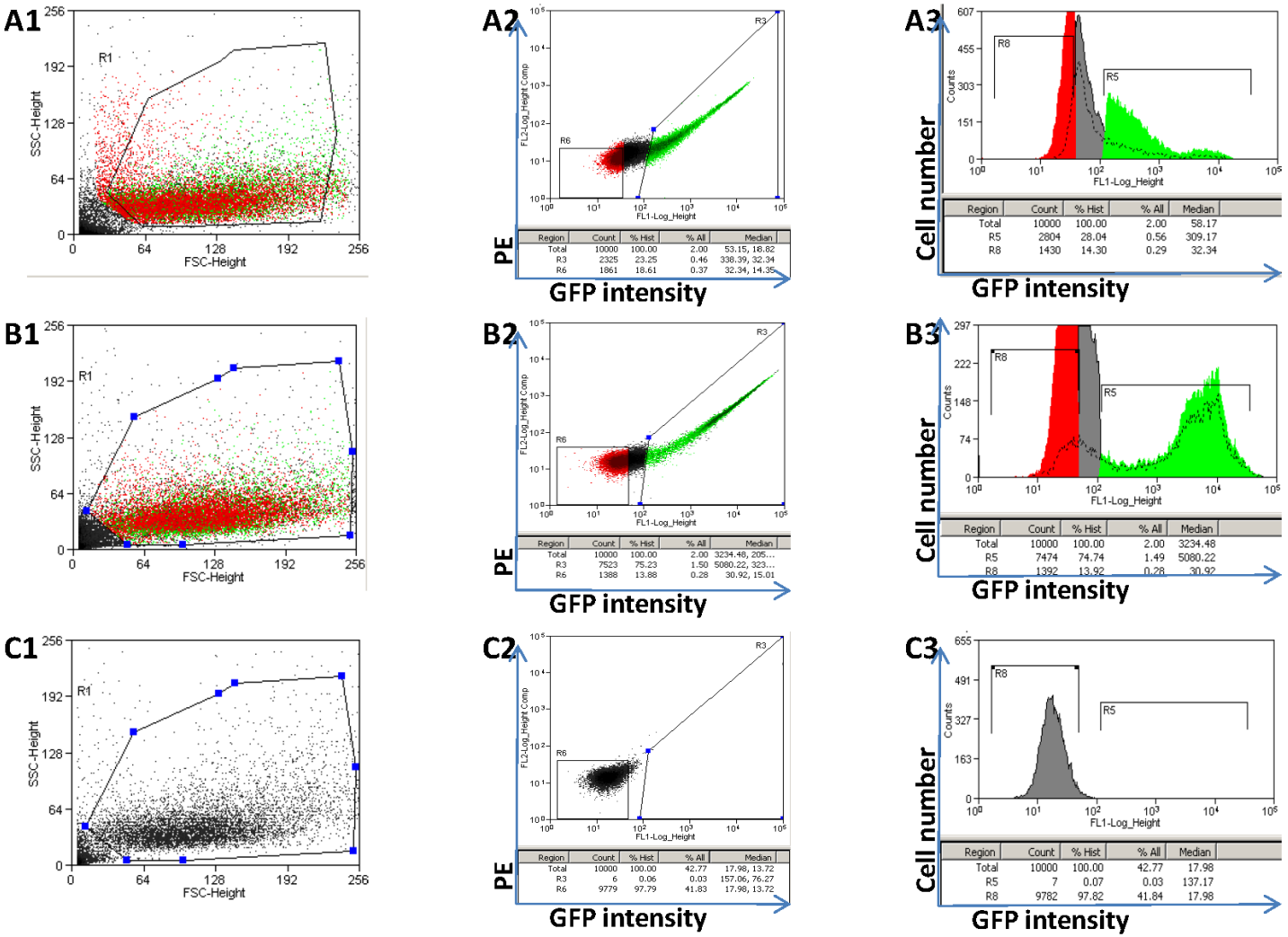

Figure 2.1 FAC-sorting of GFP positive and negative retinal cells. Panel A: E15.5 CrxGFP retinal cells; Panel B: P4 CrxGFP retinal cells; Panel C: P4 wildtype retinal cells; Column 1: Retinal cell population selected and debris excluded by gating with forward scatter (FSC, cell size) and side scatter (SSC, cell complexity). Column 2: Two-way sorting scatter plot of GFP-positive cells (right) and GFP-negative cells (left). Column 3: Histogram plot of GFP-positive cells (right) and GFP-negative cells (left).

2.4 Microarray and bioinformatics analysis

Cells were immediately frozen into -80°C after FACS and triplicates of three million cells per sample were prepared for RNA extraction (Appendix Table 2.1). RNA of the sorted cells was extracted using the RNAeasy mini kit (Qiagene). The concentration and quality of the RNA was examined using NanoDrop and Bioanalyser and all samples showed equivalent high quality, including the E15.5 sample which later emerged as an outlier in the microarray analysis (described in section 2.4.1). cDNA was synthesized for each GFP positive and negative mRNA sample and hybridized with Affymetrix Mouse Gene 1.0ST chip (a whole transcript array that cover 26,166 total RefSeq transcripts) (performed by UCL genomics). Quality control of the array was analyzed to identify possible outliers (see section 2.4.1, performed by UCL genomics). The data was compared between groups and gene lists were generated for significant differentially expressed genes using analysis of variance (ANOVA) statistical model (Table 2.1 and Table 2.2, performed by UCL genomics). Functional bioinformatics analysis of the array gene lists were performed in Database for Annotation, Visualization and Integrated Discovery (DAVID) v6.7 (Dennis, Sherman et al. 2003; Huang da, Sherman et al. 2009) to extract the biological theme of the gene lists or to search for genes of particular functions (section 2.4.2).

Table 2.1 Crx array significant differentially expressed gene numbers (*excluding* outlier)

Comparison	Criteria	Total
E15.5 GFP+ vs. P4 GFP+	FDR<=0.05	3236
E15.5 GFP- vs. P4 GFP-	FDR<=0.05	1215
E15.5 GFP+ vs E15.5 GFP-	**FDR<=0.05**	**103**
P4 GFP+ vs. P4 GFP-	**FDR<=0.05**	**4487**
E15.5 GFP+ vs. P4 GFP+	FDR <= 0.05, FC +/-2.0	1303
E15.5 GFP- vs. P4 GFP-	FDR <= 0.05, FC +/-2.0	538
E15.5 GFP+ vs E15.5 GFP-	FDR <= 0.05, FC +/-2.0	71
P4 GFP+ vs. P4 GFP-	FDR <= 0.05, FC +/-2.0	1628

Table 2.2 Crx array significant differentially expressed gene numbers (*including* outlier)

Comparison	Criteria	Total
E15.5 GFP+ vs. P4 GFP+	FDR<=0.05	2665
E15.5 GFP- vs. P4 GFP-	FDR<=0.05	618
E15.5 GFP+ vs E15.5 GFP-	FDR<=0.05	37
P4 GFP+ vs. P4 GFP-	FDR<=0.05	2622
E15.5 GFP+ vs. P4 GFP+	FDR <= 0.05, FC +/-2.0	1286
E15.5 GFP- vs. P4 GFP-	FDR <= 0.05, FC +/-2.0	396
E15.5 GFP+ vs E15.5 GFP-	FDR <= 0.05, FC +/-2.0	31
P4 GFP+ vs. P4 GFP-	FDR <= 0.05, FC +/-2.0	1384

FDR, false discovery rate; FC, fold change.

2.4.1 Microarray quality control analysis

The quality of the CrxGFP array was analysed by UCL genomics using Partek Genomics Suite in 2010 September and Array Quality Metrics 3.8.0 under R (R is an open source free software environment for statistical computing and graphics) version 2.13.0 (2011-4-13) in 2011 October. Analysis in Partek was performed with the 12 samples all together and one possible outlier was identified (sample number 3, Crx E15.5 GFP+ve 3 as shown in Appendix Table 2.1). Analysis in R was performed as pairwise comparison between E15.5 CrxGFP+ve vs CrxGFP-ve, P4 CrxGFP+ve vs CrxGFP-ve, CrxGFP+ve E15.5 vs P4, and CrxGFP-ve E15.5 vs P4. Sample 3 was detected as an outlier by distance between arrays in E15.5 CrxGFP+ve vs CrxGFP-ve comparison, distance between arrays and box plots in CrxGFP+ve E15.5 vs P4 comparison, but not as an outlier by box plots and MA plots in E15.5 CrxGFP+ve vs CrxGFP-ve comparison and MA plots in CrxGFP+ve E15.5 vs P4 comparison. Results of the quality control analysis here presented the analysis from Partek for all 12 samples and the analysis from R for distance between arrays, box plots, density plots, and MA plots for the E15.5 CrxGFP+ve vs CrxGFP-ve comparison and box plots for CrxGFP+ve E15.5 vs P4.

The raw array data were first processed in Expression Console from Affymetrix. All quality control (QC) parameters from Affymetrix fell within the thresholds, thus passing initial QC. After data export, the raw data were uploaded into Partek Genomics Suite and normalized using Robust Multichip Average (RMA). Overall grouping/separation of the arrays was checked using Principal Component Analysis (PCA). PCA is a dimension reduction and visualisation technique that is here used to project the multivariate data vector of each array into a two-dimensional plot, such that the spatial arrangement of the points in the plot reflects the overall data (dis)similarity between the arrays. PCA plots of the 12 samples showed that sample 3 was away from all other samples (Figure 2.2 Left). After removal of sample 3, the remaining samples clustered as expected (Figure 2.2 Right). Then the signal intensity distribution of the normalized arrays was analysed in box plots (Figure 2.3). Normally one expects the boxes to have similar positions and lengths (or widths if transposed). Here sample 3 showed an overall lower intensity. Further examination of histogram of array signal intensity showed that sample 3 is slightly different from the others (Figure 2.4). The bulge at the upper end of the intensity range for sample 3 indicated signal saturation and the diminishing right tail indicated lack of signal. From these analyses in Partek, it seems that sample 3 showed lower signal intensity and the signals that can be detected were saturated.

Further analysis was performed in R to determine if sample 3 was an outlier or not. Pairwise comparison was performed as the samples were originally paired for such purposes. Distances

between arrays were firstly compared and outliers were detected as arrays whose sum distance to all other arrays was exceptionally large. Both E15.5 CrxGFP+ve vs CrxGFP-ve comparison and CrxGFP+ve E15.5 vs P4 comparison showed that sample 3 was an outlier. Here, as an example, the heatmap of E15.5 CrxGFP+ve vs CrxGFP-ve comparison showed clearly that while the other five samples were near and clustered together, sample 3 was far from the others (Figure 2.5). Array intensity distributions were also examined using box plots (Figure 2.6) and outlier detection performed by computing the Kolmogorov-Smirnov statistic K_a between each array's distribution and the distribution of the pooled data. While sample 3 was not detected as an outlier in E15.5 CrxGFP+ve vs CrxGFP-ve comparison, it was an outlier in CrxGFP+ve E15.5 vs P4 comparison. MA plot examination of individual array quality showed that although sample 3 seem to have different background (trend in the lower range of A) and saturation of the measurements (trend in the upper range of A) in the plot (Figure 2.7), it had the same Hoeffding's statistic D_a as sample 6 (D=0.06) and did not pass the outlier detection threshold D_a >0.15. Finally the density plot of standard deviation versus rank of the mean showed a hump on the right hand of the x-axis for the red dots indicating a saturation of the intensities rather than the trend being approximately horizontal (Figure 2.8). This agreed with the MA plots (Figure 2.7) and histograms (Figure 2.4) of the array signal intensity analysis indicating saturation of the array signals.

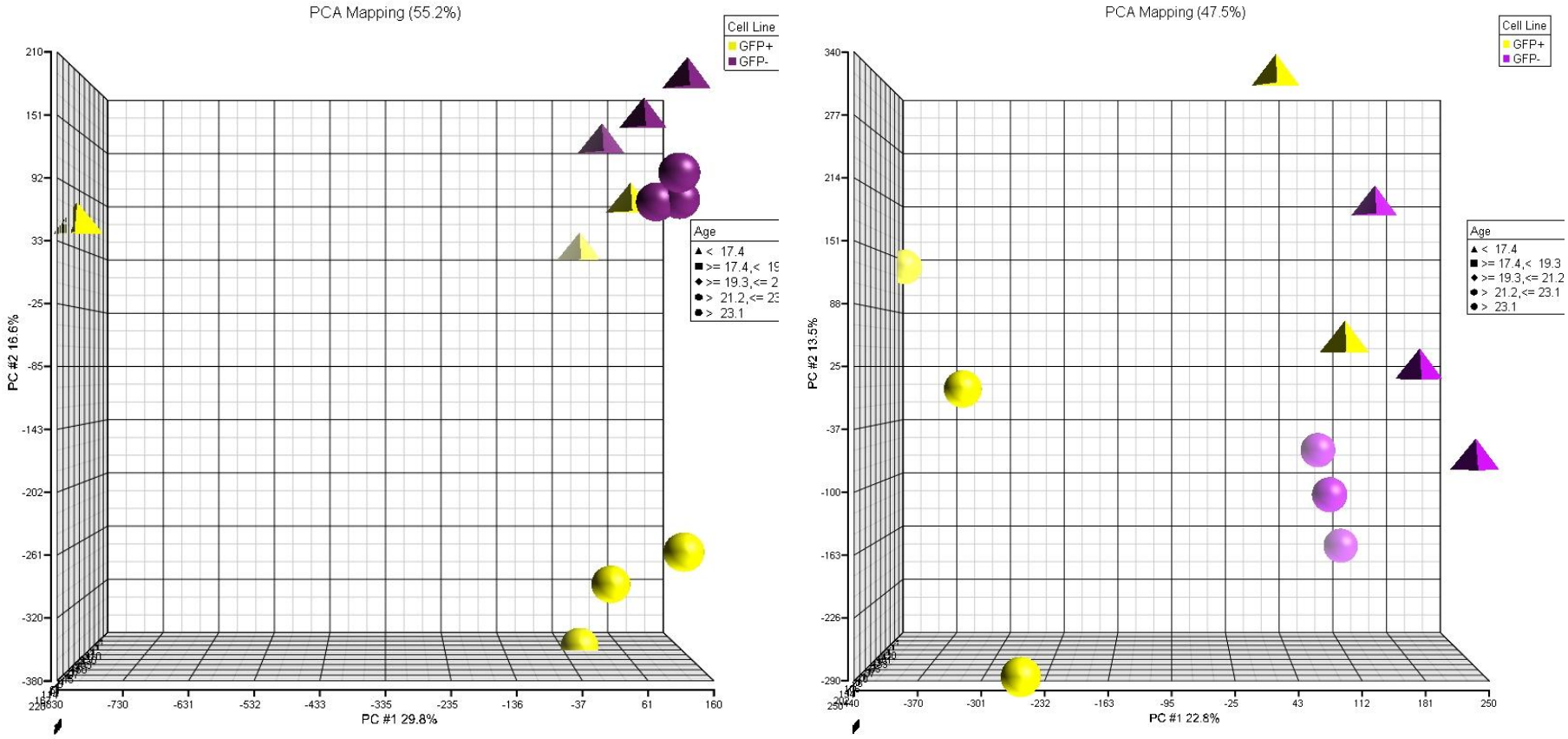

Figure 2.2 PCA plots of the array samples. (Left) Sample 3 (one of E15.5 CrxGFP+ve) falls far from the other 11 samples. (Right) Sample 3 removed from the analysis Yellow indicate CrxGFP+ve, purple indicate CrxGFP-ve, pyramids indicate E15.5, balls indicate P4.

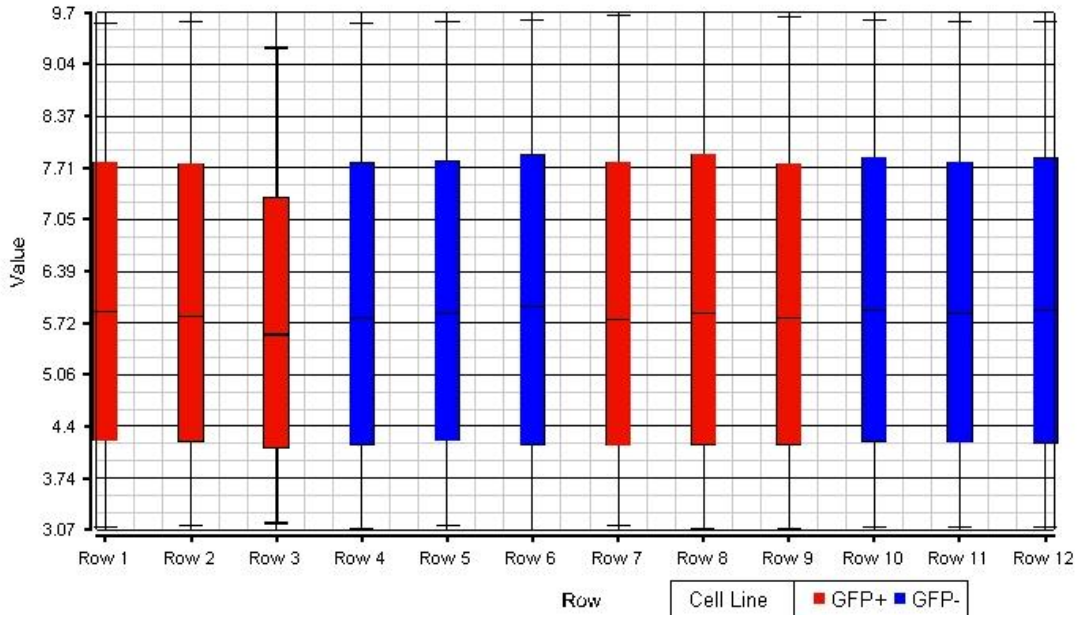

Figure 2.3 Box plots of normalized array signal intensity distributions. Sample 3 shows an overall lower intensity. Red indicates CrxGFP+ve, blue indicates CrxGFP-ve. Each box corresponds to one array.

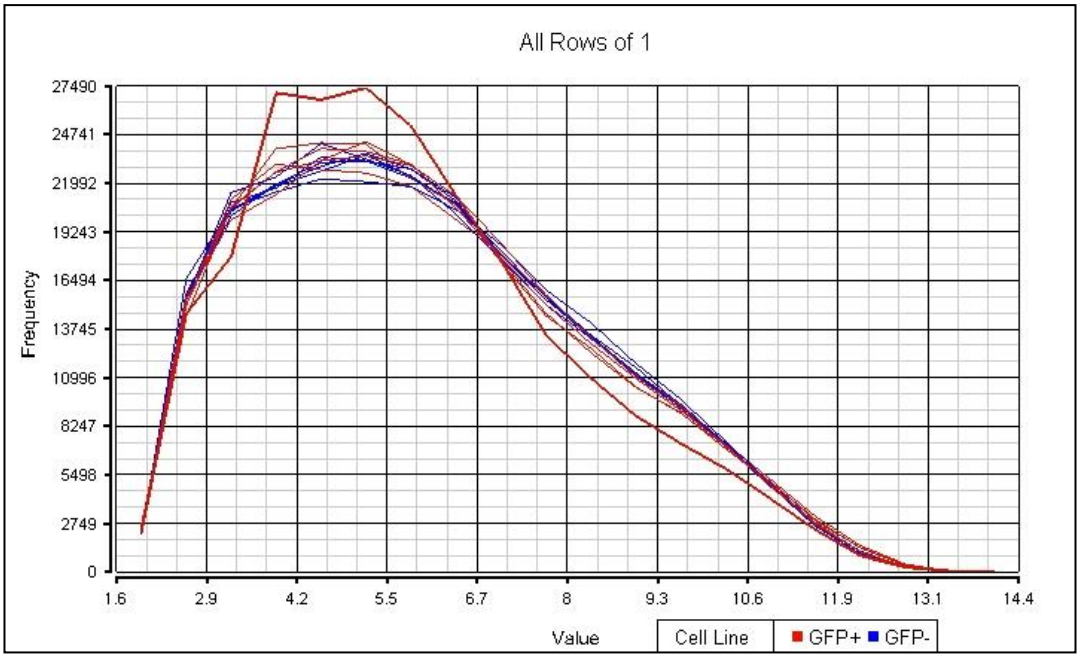

Figure 2.4 Smoothed histograms of array signal density estimates. Sample 3 appears to be out-of-line with the others. Red indicates CrxGFP+ve, blue indicates CrxGFP-ve. Each line corresponds to one array.

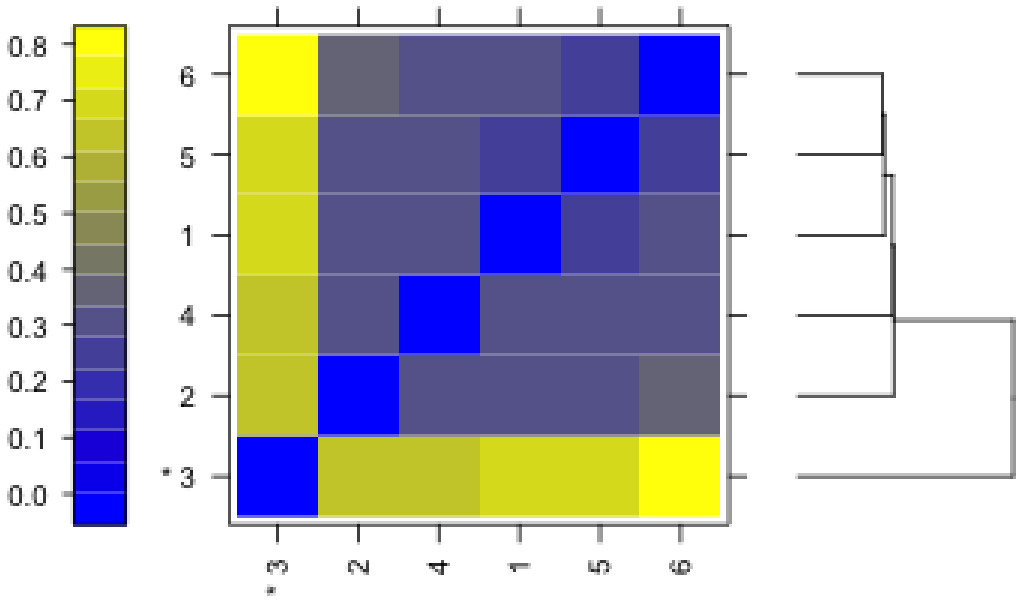

Figure 2.5 Heatmap of the distances between the six embryonic arrays. The color scale is chosen to cover the range of distances encountered in the dataset. Patterns in this plot can indicate clustering of the arrays either because of intended biological or unintended experimental factors (batch effects). The distance d_{ab} between two arrays *a* and *b* is computed as the mean absolute difference (L_1-distance) between the data of the arrays (using the data from all probes without filtering). In formula, d_{ab} = mean $|\ M_{ai} - M_{bi}\ |$, where M_{ai} is the value of the i-th probe on the a-th array. Outlier detection was performed by looking for arrays for which the sum of the distances to all other arrays, $S_a = \Sigma_b\ d_{ab}$ was exceptionally large. One such array was detected, and it is marked by an asterisk, *.

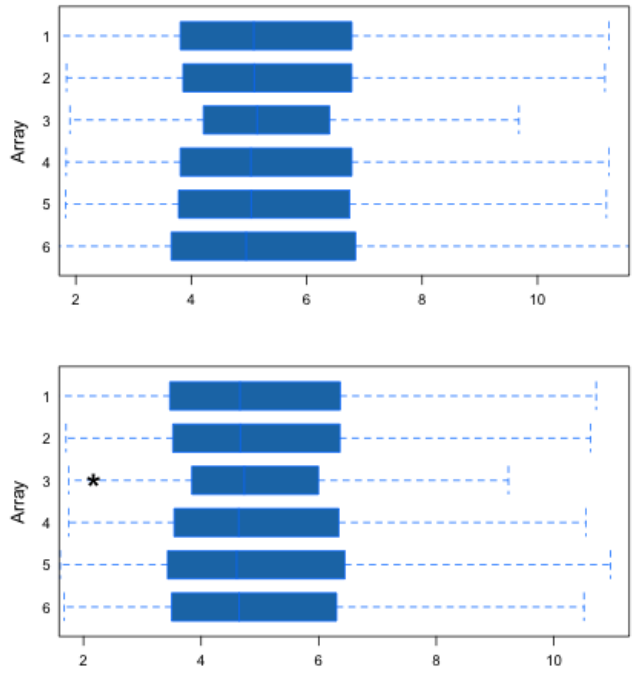

Figure 2.6 Box plots of array signal intensity distribution (pairwise comparisons in R). (Top) E15.5 CrxGFP+ve vs CrxGFP-ve, (bottom) CrxGFP+ve E15.5 vs P4. Each box corresponds to one array.

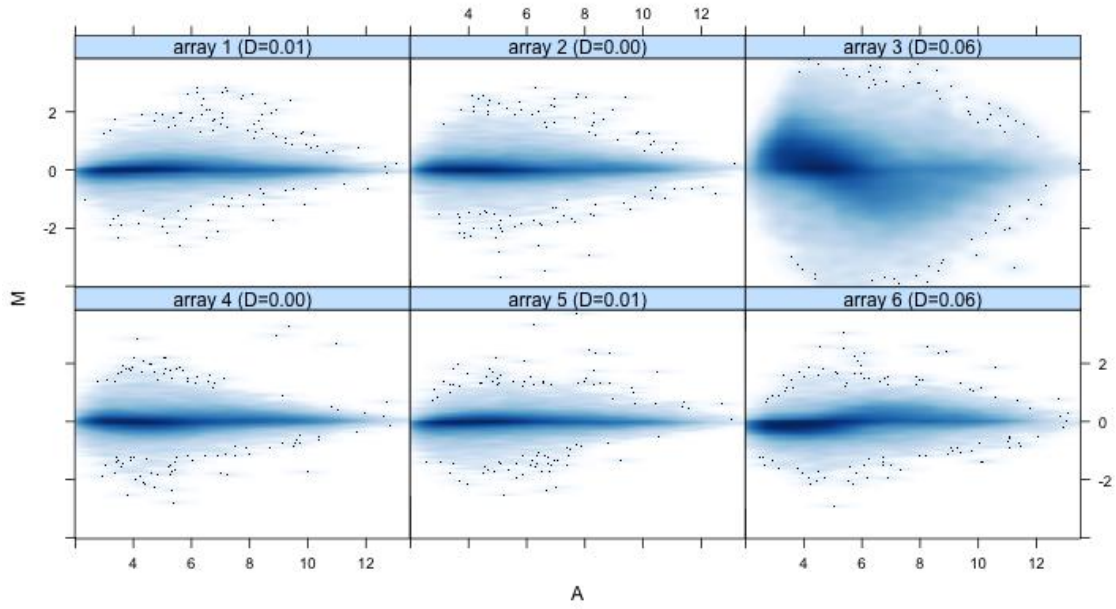

Figure 2.7 MA plots of array samples. M and A are defined as: M = log2(I1) - log2(I2); A = 1/2 (log2(I1)+log2(I2)), where I1 is the intensity of the array studied, and I2 is the intensity of a "pseudo"-array that consists of the median across arrays. Outlier detection was performed by computing Hoeffding's statistic D_a on the joint distribution of A and M for each array.

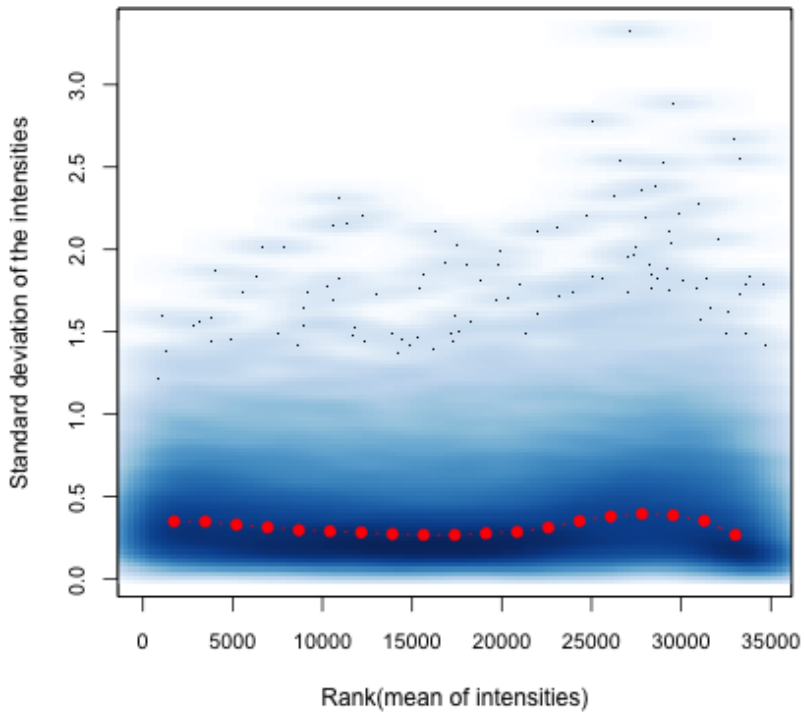

Figure 2.8 Variance mean dependence density plot. Density plot of the standard deviation of the intensities across arrays on the y-axis versus the rank of their mean on the x-axis. The red dots, connected by lines, show the running median of the standard deviation. After normalisation and transformation to a logarithm(-like) scale, one typically expects the red line to be approximately horizontal, that is, show no substantial trend.

2.4.2 Functional bioinformatics analysis of microarray genes by DAVID

Gene lists which compared the GFP+ve and GFP-ve cells of the same stage excluding the outlier were analysed further. Significant genes which expressed more than 2-fold higher in the GFP+ve vs GFP-ve comparison (i.e. genes specific to Crx/NrlGFP+ve) and GFP-ve vs GFP+ve comparison (i.e. genes specific to Crx/NrlGFP-ve) from the Crx array and a previous NrlP4 array were subjected to functional analysis in DAVID. Affymetrix probe IDs of the genes were uploaded onto DAVID and converted into IDs that DAVID uses internally (DAVID ID). Depending on the input gene sets, the percentage of DAVID ID varies from 75 % (E15.5 Crx-ve) to 97 % (E15.5 Crx+ve) for the six gene sets (Table 3.1). These percentages could roughly be considered as the percentage of genes that are annotated from different databases (NCBI's Entrez, Uniprot, Affymetrix, Mouse Genome Informatics (MGI), etc.) as the algorithm to extract annotations are based on these IDs despite not all of them might be annotated. The DAVID IDs were subjected to DAVID Functional Annotation Chart analysis. The Chart provides a table of annotations with genes of similar function enriched under the same annotation. Here Gene Ontology (GO) annotations were analysed further. GO terms are a controlled vocabulary of terms describing gene and gene product characteristics and are widely used in online

databases to annotate genes. Default settings of the GO categories[1] in DAVID were used, total GO chart records were retrieved for each gene set (Table 3.1), and these records were analysed for each gene sets. Depending on the gene sets, further statistical significance thresholds were set for the total GO chart records to allow only the most significant GO annotations to be extracted for biological themes (see table within Figure 3.3 for numbers of these GO terms).

To represent the biological theme of the gene lists, the GO annotations were pulled out and the corresponding percentage of genes annotated with these terms were plotted as bar charts as shown in Chapter 3 Figure 3.3, 3.4 and 3.6. Note, this analysis represent annotations rather than the absolute numbers of genes; a single gene often has multiple annotations.

To search for genes encoding cell surface proteins from the microarray gene list via the annotation approach, I went through the GO terms for each gene list and picked up all the terms which are cell surface related (see also Chapter 3, section 3.2.5.2, and Appendix table 3.4 for GO terms selected). The genes which are annotated with these terms were pulled out from the DAVID analysis results. These genes were then referred back to the original microarray gene lists to extract their corresponding information such as gene name/symbol and expression fold changes and were compared between different arrays to obtain common and different genes. This gave the results of the cell surface related gene lists as shown in Chapter 3 Table 3.3. These analyses were performed in Matlab.

2.5 RNA extraction and PCR

RNA isolation: Retinal tissues or FACS sorted cells were lysed in TRIZol reagent (Invitrogen) and total RNA extracted according to the manufacturer's instructions. Air dried RNA was dissolved in 30 – 50 µl RNase-free water, treated with Turbo DNase (Ambion), analysed on a spectrophotometer for concentration (NanoDrop ND-1000), and stored at -80°C.

cDNA generation: 1 µg RNA and 1 µl random hexamer primers (0.5 µg/µl, Promega) were mixed, heated to 70°C for 10 min and immediately cooled on ice. 4 µl MMLV-RT buffer (5X, Promega), 2 µl dNTP mix (10 mM, Promega), 1 µl RNase Inhibitor (Promega), 1 µl MMLV reverse transcriptase (Promega), and corresponding volume of Nuclease-free water were added to the denatured RNA mixture (final volume 20 µl). The reaction mixture was incubated

[1] Default settings of the gene ontology categories refer to the "FAT" format of Biological Process, Cellular Component and Molecular Function in DAVID, and statistic significance value p<=0.1.

at 42°C for 1 hour followed by 10 min at 95°C to denature the cDNA and deactivate the reverse transcriptase.

PCR: Primers were designed with Primer3 aiming for a melting temperature (Tm) around 60°C and spanning an exon-exon junction where applicable (Table 2.3). The PCR reaction mixture (Table 2.4 top) and thermo-cycler programme (Table 2.5 top) were set up according to manufacturer's recommendation (Bioline, BIO-21040).

Table 2.3 Reverse-transcription PCR primers

Primers	Sequence	Tm	Amplicon size (bp)
Prominin-1	GAAAAGTTGCTCTGCGAACC CTTGTTGCTTGTTTGCTGGA	60	594
Cd276	ACAGGAAGATGCTTCGAGGA TAACAGCAGCGCTGTCAAAG	60	411
Cd80	TGAGCCTAGGAGGTGCCTAA TTCCCAGCAATGACAGACAG	60	330
Cd83	TCCAGCTCCTGTTTCTAGGC TCCTGTCACCTTCAGAACCA	59	344
GAPDH	TTCCAGTATGACTCCACTCACG GGATGCAGGGATGATGTTCT	60	491
Cd73	CAA ATC CCA CAC AAC CAC TG TGC TCA CTT GGT CAC AGG AC	60	158

Real-time quantitative PCR: TaqMan® Gene Expression Assays which contain the PCR primers and a TaqMan® probe with a FAM™ dye label (FAM = 6-carboxy-fluorescein) and minor groove binder (MGB) moiety on the 5' end, and non-fluorescent quencher (NFQ) dye on the 3' end, were purchased from Applied Biosystems for each gene investigated (*Prom1*, *Sema7a*, *Cdhr1*, *Sv2b*). Gapdh FAM™ was used as the internal control. The PCR reaction mixture (Table 2.4 bottom) (TaqMan® Fast Univ PCR Master Mix, 4352046) and thermo-cycler programme (Table 2.5 bottom) were set up according to manufacturer's recommendation. Each sample was triplicated in a 96-well plate and ran on 7500 Fast Real-time PCR System. The data was analysed with Applied Bioscience's 7500 System software.

Table 2.4 Polymerase chain reaction mixture

Reagent	**Volume**
Template DNA	1 µl
dNTPs (2mM, Promega)	2.5 µl
10x NH4 buffer (Bioline)	2.5 µl
$MgCl_2$ (50mM, Bioline)	0.75 µl
Forward primer (25 µM)	1.5 µl
Reverse primer (25 µM)	1.5 µl
Taq DNA polymerase (5U/µl)	0.1 µl (0.5U)
Nuclease-free H_2O	to 25 µl total volume
TaqMan® q-PCR	**1x well**
mQ water	4.7 µl
2x Master Mix buffer	6 µl
assay (probe+FAM, quencher)	0.6 µl
cDNA	0.7 µl
Final volume	total 12 µl per well

Table 2.5 PCR thermocycler programme

95°C	2 min	Denature
95°C	30 sec	
58°C	30 sec	30 cycles
72°C	45 sec	
72°C	5 min	Final elongation
TaqMan® q-PCR		
95°C	20 sec	
95°C	3 sec	60 cycles
60°C	30 sec	

2.6 Immunohistochemistry

2.6.1 Immunohistochemistry of eye cryosections

Eyes or embryos were fixed in 4% paraformaldehyde/PBS (PFA), rinsed in PBS, equilibrated in 30% sucrose, embedded in optimal cutting temperature (OCT) compound (RA Lamb), and

frozen at -80°C. Sections were cut vertically (with the optic nerve in parallel with the section plane) in 12 or 18 µm thickness with a cryostat (Leica CM1900 UV), collected onto Superfrost™ plus glass slides (VWR, Cat No. 631-0108) and stored at -80°C. Upon immunohistochemistry, the sections were air dried on bench for 45 min, washed in 37°C PBS 10 min, incubated with blocking solutions (PBS containing 10 % (v/v) fetal bovine serum and 1 % (w/v) bovine serum albumin (BSA),and 0.1 % (v/v) Triton X-100 when needed) for 1hr at room temperature before antibody incubation. Each slide was incubated with 100 – 200 µl antibody-containing blocking solutions and was covered with a Parafilm to prevent flow or dry out of the solutions. For antibody conditions see Table 2.6 and Table 2.7. The sections were washed in PBS for at least 3 X 10 min following antibody incubations. Nuclear dye Hoechst 33342 (Sigma, 1:2000 to 1:5000) was either added into the secondary antibody blocking solution or added into PBS and incubated with slides for 10 min at room temperature after secondary antibody incubation followed by PBS wash. The slides were then mounted with Citifluor AF-1 (Electron Microscopy Science) and sealed with glass coverslips (Scientific Laboratories Supplies Ltd, 22X50 mm, thickness No. 1.5) using nail-polish.

2.6.2 Immunocytochemistry of dissociated cells

Round coverslips (Scientific Laboratories Supplies Ltd, thickness No. 1.5) were washed with Industrial methylated spirit (IMS) and water and then sterilized by baking in the oven for 4 hr at 180°C. The sterilized coverslips were put into a sterile 24-well plate and coated with 400 µl poly-L-lysine per well (Sigma, P4707). After 2 hrs incubation at 37°C, the poly-L-lysine was removed and the coverslips were washed with PBS three times. The dissociated retinal cells were then seeded onto the coverslips (20,000 cells per well of 24-well plate) and incubated with medium at 37°C for around 2 hrs. After removal of the medium, the coverslips were fixed with 4 % PFA for 10 min and rinsed with PBS three times. The coverslips were then removed from the wells and sequentially incubated with 50 µl blocking solutions, antibody solutions, and Hoechst 33342 solutions with the cell side facing down toward the solution droplets placed on parafilm. The coverslips were then mounted on to Superfrost™ plus glass slides with Citifluor AF-1 and sealed with nail-polish.

2.6.3 Antibodies and peptides

The antibodies and peptides used for immunohistochemistry were listed in Table 2.6 (primary antibodies) and Table 2.7 (secondary antibodies).

2.6.4 Microscopy and image processing

For quantification of the number of integrated cells after transplantation and epifluorescent images, retinal sections were viewed on a Zeiss Axioplan 2 and images captured via a Jenoptik C14 digital camera using OpenLab (Improvision) and dissociated retinal cells were viewed on an Olympus IX71. Confocal images or image stacks were acquired with a Zeiss LSM 710 using ZEN 2009 (Zeiss). Hoechst33342 or AlexaFluor405 was excited by a 405 nm diode laser, GFP or AlexaFluor488 by a 488 nm Argon laser, AlexaFluor594/568 by either a 561 nm diode laser or a 594 nm HeNE laser, and AlexaFluor647 or DyLight™ 649 by a 633 nm laser. The objectives used were 20x Plan Apochromat Dry, 25x LD LCI Plan Apochromat Multi-immersion, 40x C-Apochromat Water immersion, and 63x Plan-Apochromat Oil immersion and transmitted light illumination with differential interference contrast (DIC) prism was often used. Images were processed in Photoshop CS4 (Adobe) or ImageJ (open source) and presented in Illustrator CS4 (Adobe). Quantification of multi-color labeled cells or signal intensity of the images was performed in ImageJ.

Table 2.6 Primary antibodies

Primary antibody	Clonality	Host (Isotype)	Company	Catalogue No.	Dilution	Incubation condition
Prominin-1 (clone 13A4)	monoclonal	Rat (IgG1, κ)	eBioscience	17-1331-81	1:300	4°C, O/N
GFP, Alexa Fluor® 488 Conjugate	polyclonal	Rabbit IgG fraction	Invitrogen	A-21311	1:500	4°C, O/N
Chx10	polyclonal	Sheep	Chemicon	ab9016	1:1000	4°C, O/N
recoverin	polyclonal	Rabbit	Millipore	AB5585	1:1000	4°C, O/N
Rxrγ	polyclonal	Rabbit	Abcam	ab15518	1:300	4°C, O/N
Sema7a	polyclonal	Rabbit	Abcam	ab23578	1:1000	4°C, O/N
Sema7a peptide	N/A	synthetic	Abcam	ab30844	4 µg/ml	4°C, O/N
Itgb1 (CD29)	monoclonal	Hamster	eBioscience	14-0291	1:300	4°C, O/N
Plexin C1 (CD232)	polyclonal	Sheep	R&D systems	AF5375	1:200	4°C, O/N
Pcdh15	polyclonal	Rabbit	The Scripps Research Institute, USA	N/A	1:200	4°C, O/N
Bassoon (SAP7F407)	monoclonal	Mouse (IgG1)	Enzo Life Sciences	ADI-VAM-PS003	1:2000	4°C, O/N
Dystrophin (C-terminus)	monoclonal	Mouse	Novocastra	NCL-DYS2	1:20	4°C, O/N
acetylated tubulin	monoclonal	mouse (IgG2b)	Sigma	T7451	1:1000	4°C, O/N
γ-tubulin	monoclonal	mouse (IgG1)	Sigma	T5326	1:200	4°C, O/N
polyglutamylated tubulin (GT335)	monoclonal	mouse (IgG1κ)	Enzo Life Sciences	ALX-804-885	1:500	4°C, O/N
CENPF	monclonal	mouse (IgG2aκ)	Abcam	ab90	1:200	4°C, O/N

The isotype is IgG if not stated otherwise. Anti-Pcdh15 antibody is a kind gift from U. Mueller, The Scripps Research Institute, USA. Anti-acetylated tubulin, anti-γ-tubulin , anti-polyglutamylated tubulin (GT335), anti-CENPF (Abcam, ab90, 1:200) antibodies are kind gifts aliguots from Prof Philip Beale (UCL Institute of Child Health)

Table 2.7 Secondary antibodies

Secondary antibody	Fluorochrome	Host	Company	Catalogue No.	Dilution	Incubation condition
Anti-rabbit	Alexa Fluor® 647	Goat	Invitrogen	A-21245	1:500	30 min - 1 hr, RT
	Alexa Fluor® 594	Goat	Invitrogen	A-11037		
	Alexa Fluor® 488	Goat	Invitrogen	A-11008		
	Alexa Fluor® 405	Goat	Invitrogen	A-31556		
Anti-sheep	Alexa Fluor® 568	Donkey	Invitrogen	A-21099		
	Alexa Fluor® 488	Donkey	Invitrogen	A-11015		
Anti-goat	Alexa Fluor® 594	Rabbit	Invitrogen	A-11080		
Anti-mouse	Alexa Fluor® 594	Goat	Invitrogen	A-11032		
Anti-mouse IgG, IgM	Alexa Fluor® 488	Goat	Invitrogen	A-10680		
Anti-mouse IgM (μ chain)	Alexa Fluor® 594	Goat	Invitrogen	A-21044		
Anti-hamster (Armenian)	DyLight™ 649	Goat	BioLegend	405505		
Anti-rat	Alexa Fluor® 594	Goat	Invitrogen	A-11007		

The target isotype is IgG if not stated otherwise.

2.7 Hematoxylin and eosin staining for frozen sections

Frozen slides were thawed at room temperature for 20 min and baked at 37°C for 30 min followed by standard hematoxylin and eosin (HE) staining procedure. Briefly, the slides were immersed in distilled water (dH_2O) 1 min to remove OCT followed by immersion in Hematoxylin solution (Mayer's, Sigma) for 2 min and dH_2O for 2 min. The slides were then put under running tap water for 5 min followed by immersion in aqueous 1% Eosin (Acros Organics) for 1 min and under running tap water again for 5 min. The slides were then dehydrated by immersion in 70% ethanol 2 min, 95% ethanol 2 min, 100% ethanol 2 min two times and histoclear (National Diagnostics, Hessle) 5 min sequentially. The slides were mounted with DPX (a mixture of distyrene, a plasticizer, and xylene, BDH) and left in hood overnight until dry. Images were taken with a Zeiss Axiophot 2.

2.8 Western blot

Mouse retina was extracted with RIPA buffer for Western blot. 0.2 ml RIPA buffer were used for every 8 adult retina. The retina tissues were triturated with a pestle and incubated on ice 15 min to lyse and spun down at 14000 rpm 4°C 15 min. The supernatant were collected into a fresh tube and stored at -80°C. Protein concentration was quantified using Pierce BCA protein assay kit (Thermo Scientific Catalogue# 23227). 96-well plates were used and absorbance at 595 nm was read with a Bio-rad Model 680 microplate reader. 40 µg protein samples were mixed with 5 µl 5X loading buffer, boiled at 100°C for 5 min just before loading and resolved in SDS-PAGE (10% resolving gel, 5% stacking gel) at 100 v for around 2 hrs.

The gels were then transferred to nitrocellulose membranes (GE Healthcare, Life Sciences, Whatman™ Protran BA83, Cat#10402495) using Trans-Blot® SD Semi-Dry Transfer Cell (BIO-RAD) at 18v for 1hr. The membranes were blocked in blocking solutions (PBS containing 0.5% Tween and 2% milk) at room temperature for 1 hr, followed by primary antibody incubation at 4°C overnight, PBS wash 3X 10 min, HRP secondary antibody incubation 1hr room temperature, PBS wash 3X 10 min, and ECL (GE Healthcare) developing using Amersham Hyperfilm™. Primary antibodies used here were the same as the ones in Immunohistochemistry but using lower concentrations (Sema7a 1:4000, PlxnC1 1:1000, Itgb1 1:4000, β-actin 1:10000 (mouse)). HRP secondary antibodies were used at 1:4000 dilution (donkey anti sheep HRP (Abcam, ab6900) for PlxnC1, goat anti rabbit HRP (Dako, REF P0448) for Sema7a, rabbit anti hamster (Abcam, ab5745) for Itgb1, and rabbit anti mouse HRP (Dako, REF P0260) for β-actin).

2.8.1 Western blot solutions

10% SDS solution: 100 g SDS dissolved in 1L Milli-Q water keep stirring until the solution becomes clear.

10% Ammonium persulfate (APS): 2 g APS dissolved in 20 ml Milli-Q water.

RIPA Lysis buffer: 50 mM Tris-HCl pH7.4, 150 mM NaCl, 1 mM PMSF (omitted in my current solution as n/a), 1 mM EDTA, 1% Triton X-100, 0.1% SDS, 1% Sodium Deoxycholate, 1 tablet of protease inhibitor mixture (Roche, Complete Mini, REF11836153001) per 10 ml buffer.

5X protein loading buffer: For a total volume of 10 ml, 2.5 ml 20% SDS, 500 µl 1M DTT, 2.5 ml 1M Tris-HCl pH 6.8 and 2.5 ml Glycerol was mixed with 0.1 g (w/v) bromophenol blue. Store at -80°C until use.

10X Western Running buffer: 30 g Tris base, 144 g glycine and 10 g SDS were dissolved in 1L Milli-Q water.

Transfer buffer: For 500 ml transfer buffer: 50 ml 10X Western Running Buffer, 100 ml 100% methanol and 350 ml dH_2O.

0.5% (v/v) PBS-Tween: 5 ml Tween-20 dissolved in 1L PBS.

2.9 Transplantation of photoreceptor cells

Collection of CrxGFP-positive cells was performed via FACS similar to as described in section 2.3. Cells were collected directly into 15 ml falcon tubes with DMEM medium contain 50% serum which will be diluted to around 10% after cell sorting. The cells were then centrifugated at 157 g (900 rpm) for 10 min at 4°C and the medium removed. Cells were resuspended in 1 ml of 10% serum containing DMEM medium and transferred into 1.5 ml eppendorf tubes and transported on ice to the Institute of Ophthalmology for injection. Cells were centrifuged again (157 g (940 rpm), 10 min) and medium removed. Appropriate amounts of injection medium (5.26% DNase in EBSS) was added to the cell pellet to concentrate the cells into 200, 000 cells/µl. The cell suspension was transferred on ice into a round bottomed microtube. 1 µl cell suspension was injected into the subretinal space between the RPE and ONL of each eye of the anesthetised host mice (performed by Dr. Rachael Pearson) and as described (MacLaren, Pearson et al. 2006). Recipient mice were sacrificed 3 days to 1 month after injection and their eyes collected for immunohistochemistry or imaging and quantification as described in section 2.2.2 and 2.6.1.

2.10 Mass Spectrometry

After collection of the GFP positive and negative cells from the FACS cell sorter, the cells (5 million minimum) were lysed and membrane proteins extracted using membrane protein extraction lysis buffer (Mem-PER® Pierce). Briefly, the membrane proteins were solubilized using a detergent and the hydrophobic proteins were separated from hydrophilic proteins through phase partitioning after centrifugation and 37°C incubation. The membrane protein concentration was determined according to a standard curve produced using BSA and bicinchoninic acid assay (BCA assay) through a spectrophotometer UV mini 1240 (Shimadzu). Between 200 to 400 µg proteins per sample were submitted for liquid chromatography/mass spectrometry (LC/MSe) analysis using the ElectroSpray Ionisation-Quadrupole – Time-of-Flight (ESI-QTOF) mass spectrometer (performed by Dr Wendy Heywood and Dr Kevin Mills from Biological Mass Spectrometry Center, ICH, UCL). *S. cerevisiae* enolase 1 (Eno1_Yeast) has always been included in the samples as a positive quality control. The data were run against the mouse database and an all species database for any proteins not described yet in mouse.

2.11 shRNA construction and molecular cloning

For genes of particular interest such as Sema7a, I attempted to evaluate its effect via knocking down with shRNAs (see Chapter 4, section 4.2.5 and Appendix 4.1). Four shRNAs sequences were synthesized (Appendix 2.1, Appendix figure 4.1.2 A) with two of the target sequences based on Origene products and two target sequences designed using Dharmacon siDESIGN Center. The sequences were annealed and ligated with the backbone of mU6 pro vector which was digested with BbsI/XbaI (NEB). The ligations were transformed into competent DH5α (Invitrogen, 18265-017), five colonies for each ligation were randomly picked and minipreped. Correct ligations were confirmed with AscI/SnaB1 (NEB) digestion for 400 bp products. The 2nd colonies of each shRNA ligation were midi-preped and sent to UCL for sequencing (primer M13R2).

Annealing: the shRNA sequences were resuspended into 1ug/ul and equal amounts of both strands were mixed together. The mixture were heated at 95 °C for 3min and cooled down on the bench.

Ligation: 50 -100 ng vector and 5 ng inserts (for molar ration 3:1 between inserts and vector) were incubated with ligase (Promega, T4 DNA ligase, M180A, 28521916) and ligation buffer over night at room temperature.

Transformation: add 10 µl ligation reaction into 50 µl DH5α, incubate on ice for 10 – 15 min followed by 30 sec heat shock at 42°C and immediately on ice for 2 min, spread the

transformed cells onto pre-warmed lysogeny broth (LB) Agar plates (with 50 μg/ml ampicillin) and incubate at 37°C overnight with plates facing down.

Mini or Midi preparation: single colonies from Agar plates (or around 3 ml mini culture for midi culture) were seeded into 5 ml LB broth containing 50 μg/ml ampicillin (or 50 ml LB broth for midi culture) near flame and cultured in a shaker at 187 rpm 37°C overnight. The plasmid DNA was then purified using Qiagen kits (QIA prep Spin Miniprep kit, Cat 27104; Qiagen Plasmid Midi Kit, Cat 12143).

2.12 shRNA transfection of cell lines

Human Embryonic Kidney (HEK) 293 cell line and mouse osteoblastic precursor (MC3T3) cell line were tested for the knocking down efficiency of Sema7a expression using a Sema7a expression vector (Sema7a mouse cDNA clone ORF with C-terminal GFP tag, OriGene, Catalog No. MG209876) co-transfected with the shRNA sequences (see Appendix 4.1). Expression of exogenous Sema7a was evident as shown by the GFP expression in cells transfected only with the expression vector and not the shRNA sequences. The cells were seeded at 1.2 – 1.5 x 10^5 cells per well in 6-well plates the day prior to transfection and were transfected when they reach ~ 70% confluence. For each well to be transfected, 500 ng DNA (mixed into 50 μl PBS) were well mixed (by pipetting) with 6 μl lipofectamine 2000 (Invitrogen, 11668-027) (which is also mixed into 50 μl PBS) and incubated for 20 min at room temperature prior addition to the cell. The cells were incubated with the above transfection mixture for 4 – 6 hr or overnight before changing back to growth medium (DMEM (for HEK293 cells) or MEM alpha (for MC3T3 cells) media + 10 % FBS). Cells were examined for morphology and GFP expression under microscope and RNA was harvested 24 – 48 hr after transfection and subject to PCR and qPCR analysis.

2.13 Statistical analysis

Statistical analysis for standard deviation, Student's t-test (a parametric significance test), generation of bar chart, histogram and dot plot, were performed in Excel 2010 (Microsoft). Generation of box plot and Mann-Whitney test (a non-parametric significance test) were performed in SPSS 16.0 (IBM). The p value in DAVID analysis refers to Benjamini value unless stated otherwise.

3 Transcriptome analysis of photoreceptor precursors

3.1 Introduction

Despite much effort in the field of retina transplantation, demonstration of efficient integration and visual function of transplanted cells was minimal (reviewed in (West, Pearson et al. 2009)). In 2006, it was shown that donor cells, if isolated from an ontogenetic stage when they have just committed to the photoreceptor fate, rather than from the early proliferating stage of stem/progenitor cells, are able to efficiently integrate into the adult recipient retina, form functional synapses with other retinal neurons and improve vision after transplantation (MacLaren, Pearson et al. 2006). This was demonstrated using donor cells isolated from an NrlGFP transgenic line which only labels postmitotic rod photoreceptor cells (Akimoto, Cheng et al. 2006; MacLaren, Pearson et al. 2006). Nrl is a transcription factor which specifies rod fate (see Chapter 1, section 1.4.2.2) and its transcript is detected at E12 from the onset of rod differentiation (Akimoto, Cheng et al. 2006). The NrlGFP line showed GFP expression in a few cells (with long exposure) at E12 and stronger progressive expression from E16 onwards (Akimoto, Cheng et al. 2006). Further work with sorted postnatal NrlGFP labeled rod precursor cells showed around 4-fold higher integration rates than unsorted retinal cells (Pearson, Barber et al. 2012). These data showed that the postnatal photoreceptor precursor cells are potent for efficient transplantation. Yet, it is not understood fully why these cells are of high transplantation potential.

Because cone photoreceptors, although far less than rods in numbers, are responsible for day light vision and visual acuity, it is important to understand their properties as well in order to better utilize these cells for transplantation. Different from rods which are generated from E12 to P10, cones are born over a much shorter window prenatally and peak at E14 (see Chapter 1, Figure 1.2). As Nrl does not label cones, a CrxGFP transgenic line was developed to label both cones and rods (Samson, Emerson et al. 2009). Crx is regarded as the earliest transcription factor to lineate and maintain rod and cone fate (Chapter 1, section 1.4.2.2). It is transcribed from around E12 and progressively increases till photoreceptor maturation (Furukawa, Morrow et al. 1997). CrxGFP expression in the transgenic line was clearly detectable from E13.5 and became prominent in postnatal and adult retina (Lakowski, Baron et al. 2010). At E15.5 shortly after the birth peak of cones, Baron observed over 95% CrxGFP+ve cells stain positively for a cone photoreceptor specific nuclear receptor, Rxrγ (retinoid X receptor-γ) (Figure 3.1 A, (Lakowski, Baron et al. 2010; Baron 2012)) indicating that the CrxGFP+ve cells at E15.5 are mainly cones. Transplantation studies using these cells as donor cells found that the E15.5 CrxGFP+ve cells gave rise to both cones and rods after transplantation ((Lakowski, Baron

et al. 2010), illustrated in Figure 3.1 B). In comparison, the P4 CrxGFP+ve cells only gave rise to rods after transplantation (Lakowski, Baron et al. 2010). However, the integration efficiency of the postnatal cells was 10-fold higher than the embryonic cells (median 5610 range 754 – 15402 integrated cells per eye for P3 vs median 334 range 42 – 1466 integrated cells per eye for E14.5 (Lakowski, Baron et al. 2010)). As the recipient environments are the same, the different behavior of the embryonic and postnatal photoreceptor precursor cells after transplantation must due to their intrinsic properties which remains unknown on this respect. I, therefore, intend to understand the property changes of the photoreceptor precursors from less transplantation-favorable status (E15.5) to more transplantation-favorable status (P4), and to understand why early precursors (E15.5) can give rise to both cones and rods but late precursors (P4) only give rise to rods.

One way to understand the properties of photoreceptor precursors is to analyze their transcriptomes. Then by comparing their transcriptome with other cell types, molecular features that are photoreceptor specific may be identifed. Other retinal cells of the same stage as the photoreceptor precursor cells are the best subject for such comparison. Also differentiated from multipotential RPCs, other retinal cells may share more common features with photoreceptor cells as opposed to other cell types hence their comparison with photoreceptor cells may reveal the most unique feature of photoreceptor cells. Further, by comparing the photoreceptor-specific transcriptomes of the early and late precursors I expect to elucidate some molecular properties that determine their different transplantation behavior.

Most previous microarrays were performed on full retina of postnatal stages without distinguishing between photoreceptor cells and other retinal cells (Dorrell, Aguilar et al. 2004; Hackam, Qian et al. 2004; Zhang, Xu et al. 2005; Liu, Wang et al. 2006; Punzo, Kornacker et al. 2009). Blackshaw et al microdissected ONL from retina cryostat sections and performed serial analysis of gene expression (SAGE) study of E12.5 to P6.5 and adult mice ONL and identified rod-specific genes (Blackshaw, Fraioli et al. 2001) and genes expressed in RPCs and developing PR/interneurons (Blackshaw, Harpavat et al. 2004). Although postnatal ONL mainly contains rods and cones, microdissection cannot exclude the remaining progenitor cells and processes from Müller glia cells in ONL and possibly processes from other inter neurons at OPL. Further in embryonic stages ONL/ONBL is not easily identifiable and contains more progenitor cells, which cannot be separated from photoreceptor cells by microdissection. To compare the transcriptomes of photoreceptor precursor cells of different stages and vs other retinal cells, I aimed to conduct a microarray using E15.5 and P4 retinal cells taking advantage of the newly developed CrxGFP line (Figure 3.1 C) (Samson, Emerson et al. 2009). As CrxGFP labels bipolar

cells and all photoreceptor cells including both cones and rods, FACS allows direct comparison of photoreceptor cells versus other retinal cells.

Previously in our lab a microarray was conducted using the NrlGFP-sorted P4 retinal cells by my colleague Jorn Lakowski although functional bioinformatics analysis wasn't performed. This allows comparison of rod precursors vs non-rod retinal cells. With this data, I also planned to compare the NrlGFP cells with CrxGFP cells. As CrxGFP positive cells should be constituted of rods, cones, and bipolar cells while NrlGFP positive cells should only contain rods, comparison of NrlGFP and CrxGFP positive cells might reveal genes which are specific to cones. In both array experiments, the photoreceptor precursor population was compared with its corresponding non-photoreceptor-precursor retinal cell population to produce a pair of photoreceptor-specific gene set and non-photoreceptor retinal gene set (see workflow in Figure 3.1 B and C) which will be analysed and compared further.

Usage of the Nrl/CrxGFP transgenic line has greatly facilitated our research on retinal cell transplantation by enriching photoreceptor cells, but cannot be used in the clinic as it is not suitable to use such similar system for humans. Furthermore Nrl and Crx are expressed throughout the lifespan of photoreceptor cells; hence they do not allow stage-selection for the precursor cells only. It is therefore necessary to identify new markers that can be used to isolate photoreceptor cells without genetic modification and that only isolate stage specific precursor cells. Therefore, I aimed to screen out photoreceptor-specific cell surface molecules from these microarray data. Not only can these surface molecules be used to identify signatures and isolate the photoreceptor cells, but also they may help to understand the integration process of the migrating cells in the developmental context and transplantation environments.

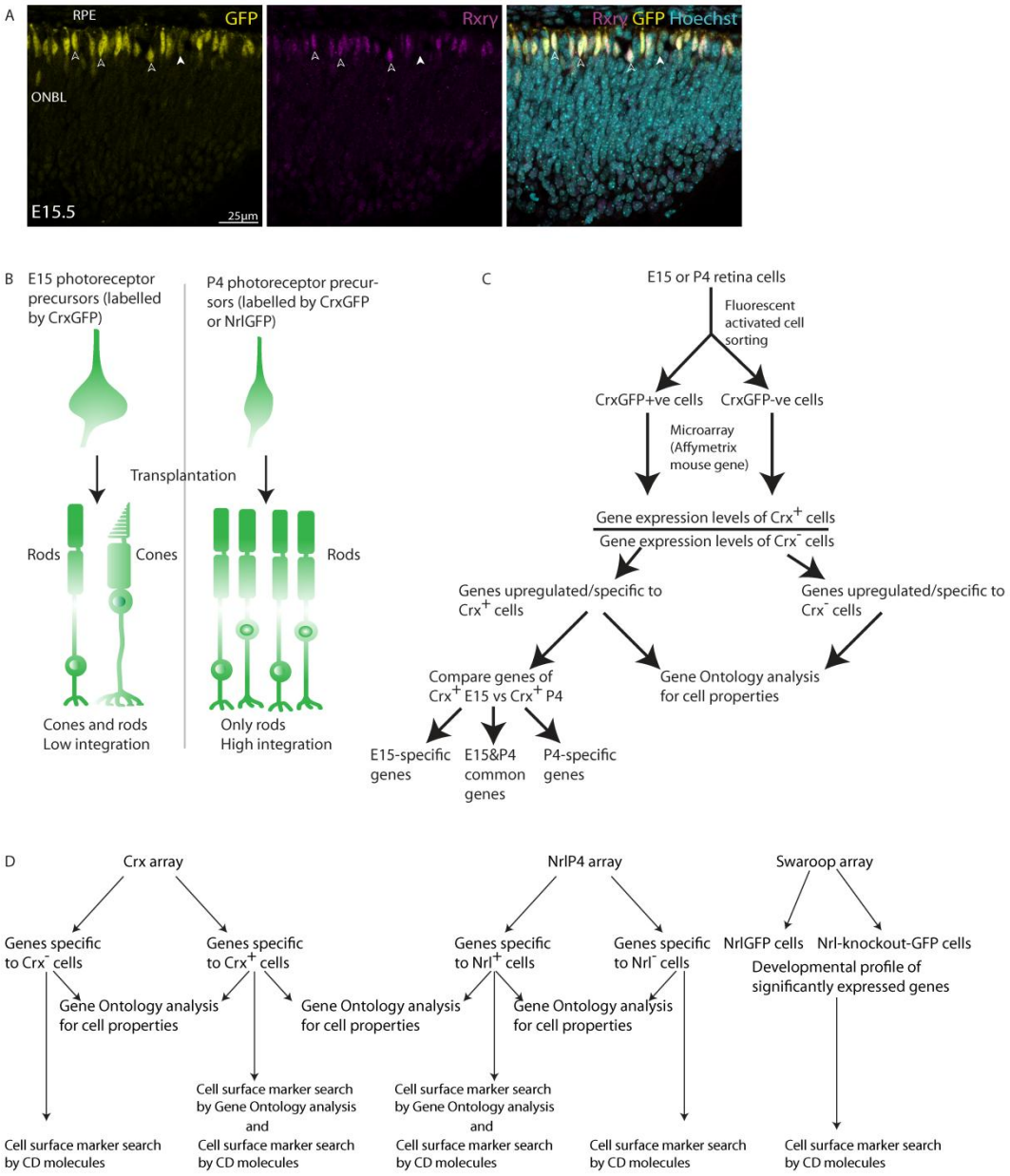

Figure 3.1 Early vs late photoreceptor precursors and work flow (A) The majority of CrxGFP+ve cells is Rxrγ+ve. Adapted from (Baron 2012). (B) Early and late photoreceptor precursors behave differently. Early photoreceptor precursors (embryonic day 15, E15) labelled by CrxGFP give rise to both cones and rods after transplantation, but show low integration (~ median 640 cells) (Lakowski, Baron et al. 2010). Late photoreceptor precursors (postnatal day 4, P4) labelled by CrxGFP or NrlGFP show high integration (~ median 5600 cells) (Lakowski, Baron et al. 2010), but only give rise to rods. (C) Workflow of microarray analysis for early and late CrxGFP positive and negative retinal cells. (D) Workflow of analysis for the three available microarray datasets.

3.2 Results

3.2.1 Expression profiles of transgenic lines and generation of gene lists

Before my preparation of the microarray based on CrxGFP-sorted retinal cells, two other RNA microarray databases were also available for analysis: 1) comparison of P4 NrlGFP positive and negative cells prepared by Jorn Lakowski from our lab (referred to as the NrlP4 array). Generation of the gene list from the NrlP4 array data was prepared by UCL genomics with Bioconductor and R. 11,850 genes were significant differentially expressed between P4 NrlGFP positive and negative cells ($p < 0.05$). I intend to analyse this data using the same method as that of the CrxGFP-based array (see work flow of the analysis in Figure 3.1 D). 2) Comparison of NrlGFP wild-type cells with Nrl-knockout-GFP cells along development (E16, P2, P6, P10 and P28) deposited in Gene Expression Omnibus (GEO) from Anand Swaroop's group (Akimoto, Cheng et al. 2006) (referred to as Swaroop array). This data is used to identify genes showing dynamic temporal expression profiles. Requested by my supervisor Jane Sowden, UCL genomics identified 2,067 genes showing more than 2-fold expression changes during development from this array and generated box plots to show the developmental expression profiles (Lakowski, Han et al. 2011). I used this dataset to search for cell surface molecules and to check for developmental expression profiles of interested genes. Work flow of the analysis was shown in Figure 3.1 D.

3.2.1.1 GFP expression profiles of transgenic reporter lines

I first examined the retinal expression profiles of the transgenic GFP mouse lines by IHC to assess their cell expression specificity. These were CrxGFP, NrlGFP, and Fgf15GFP which is a line labelling RPCs in the early embryonic retina ((Decembrini, Cananzi et al. 2011) Supplementary figure S1). As a member of fibroblast growth factor (FGF) family, Fgf15 is expressed in brain from early stages of neurulation (E8.5) to postnatal period (Gimeno, Brulet et al. 2003). From E9.5 Fgf15 transcript was detected in the neural epithelium of the optic vesicles (Gimeno, Brulet et al. 2003) and was highly expressed at E14 and E16 in outer nuclear blast layer (ONBL) of the retina and stayed until P0 (Blackshaw, Harpavat et al. 2004). Cell specificity of the Fgf15GFP line in later retinal development was uncharacterized. If it specifically labels RPCs, it could be used for microarray comparison with the photoreceptor cell lines to understand why photoreceptor precursor cells can integrate after transplantation but progenitor cells cannot.

Agreeing with previous studies (Samson, Emerson et al. 2009; Lakowski, Baron et al. 2010), CrxGFP labeled a portion of ONBL cells located at the outermost two or three rows of ONBL

cells at E15.5 (Figure 3.2 A1 – A3). Retaining the high expression at the outer edge of ONBL, CrxGFP expression expanded to seven or eight rows in the P4 ONBL (Figure 3.2 B1 – B3). Expression of NrlGFP was also evident at P4 agreeing with the previous study (Akimoto, Cheng et al. 2006). While CrxGFP expression at E15.5 and P4 and NrlGFP expression at P4 seemed comparable for the number of photoreceptors at these stages, expression of Fgf15GFP was in both RPCs and other retinal cells at E15.5 (Figure 3.2, D2 and E2). I then examined Fgf15GFP expression relative to an RPC marker Chx10 (ceh-10 homeo domain containing homolog (*C. elegans*)) and a cone photoreceptor marker Rxrγ. IHC against Chx10 showed that Fgf15GFP not only recognized Chx10+ve cells (filled arrowheads, Figure 3.2 D1 – D3), but also Chx10-ve cells (empty arrowheads, Figure 3.2 D1 – D3). Fgf15GFP was also expressed in Rxrγ+ve cells (filled arrowheads, Figure 3.2 E1 – E3). (Note although labeling the same cell, Fgf15GFP was expressed in the cytoplasm thus it did not colocalize with Chx10 and Rxrγ which were in the nucleus.) This showed clearly that Fgf15GFP not only labeled RPCs, but also non-progenitor cells including photoreceptor cells. Flow cytometry analysis showed that while only ~ 34% GFP+ve cells were detected in the E15.5 CrxGFP retinal cells (Figure 3.2 G), ~ 98% GFP+ve cells were detected in the E15.5 Fgf15GFP retinal cells (Figure 3.2 H) showing that the Fgf15GFP labeled nearly all the retinal cells an not only the progenitor cells. Taken together, the Fgf15GFP population was not considered useful for microarray analysis as a line to provide RPCs as it also coexpressed with the CrxGFP photoreceptor population; the CrxGFP strain, however, remains a good line to label photoreceptor cells.

3.2.1.2 Generation of gene lists from microarray

CrxGFP-sorted cells from E15.5 and P4 retina were collected by FACS (see Chapter 2 section 2.3 for cell sorting and Figure 2.1 for sorting gate) and subjected to microarray analysis (referred to as the CrxE15 array and CrxP4 array respectively or Crx array together) (see Chapter 2 section 2.4 for microarray analysis). In brief, a total of 19 litters E15.5 embryos (~133 embryos) and 24 P4 retinas were used for sorting to collect the GFP+ve and GFP-ve cells. A minimum of 3 million cells per RNA sample and three RNA samples per cell type (E15.5 Crx+ve, E15.5 Crx-ve, P4 Crx+ve, and P4 Crx-ve) were prepared and hybridized to arrays (see Chapter 2 section 2.3 section 2.4 for methods and Appendix Table 2.1 for sample preparation summary). Analysis of the raw microarray data and generation of the gene lists showing significantly altered expression levels were performed by UCL genomics. The array was considered successful but one possible outlier sample was identified (see Chapter 2 section 2.4). Significant differentially expressed genes between pair-wise comparisons were identified using Partek (Table 2.1 and 2.2). Gene lists which exclude the outlier and compared between GFP+ve and GFP-ve cells

were used for further analysis. 4,487 genes were differentially expressed between P4 CrxGFP positive and negative cells while 103 genes were differentially expressed between E15.5 CrxGFP positive and negative cells, and 3,236 genes were differentially expressed between E15.5 CrxGFP positive and P4 CrxGFP positive cells (False Discovery Rate (FDR) <=0.05) (Table 2.1).

For the NrlP4 array data, I divided the total differentially expressed genes into NrlGFP+ve gene set and NrlGFP-ve gene set and performed gene ontology analysis and cell surface marker search on both sets (Work flow of the analysis was shown in Figure 3.1 D). The NrlP4 and Crx array gave direct comparisons between photoreceptor precursors and other retinal cells, so I mainly analysed these two arrays in order to understand the photoreceptor precursor cells and find out markers specific to them. The Swaroop array was constantly referred back to check for developmental expression patterns of a particular gene under examination. Table 3.1 shows a summary of differentially expressed genes and comparison with the previously conducted P4 NrlGFP array experiment (Lakowski, Han et al. 2011).

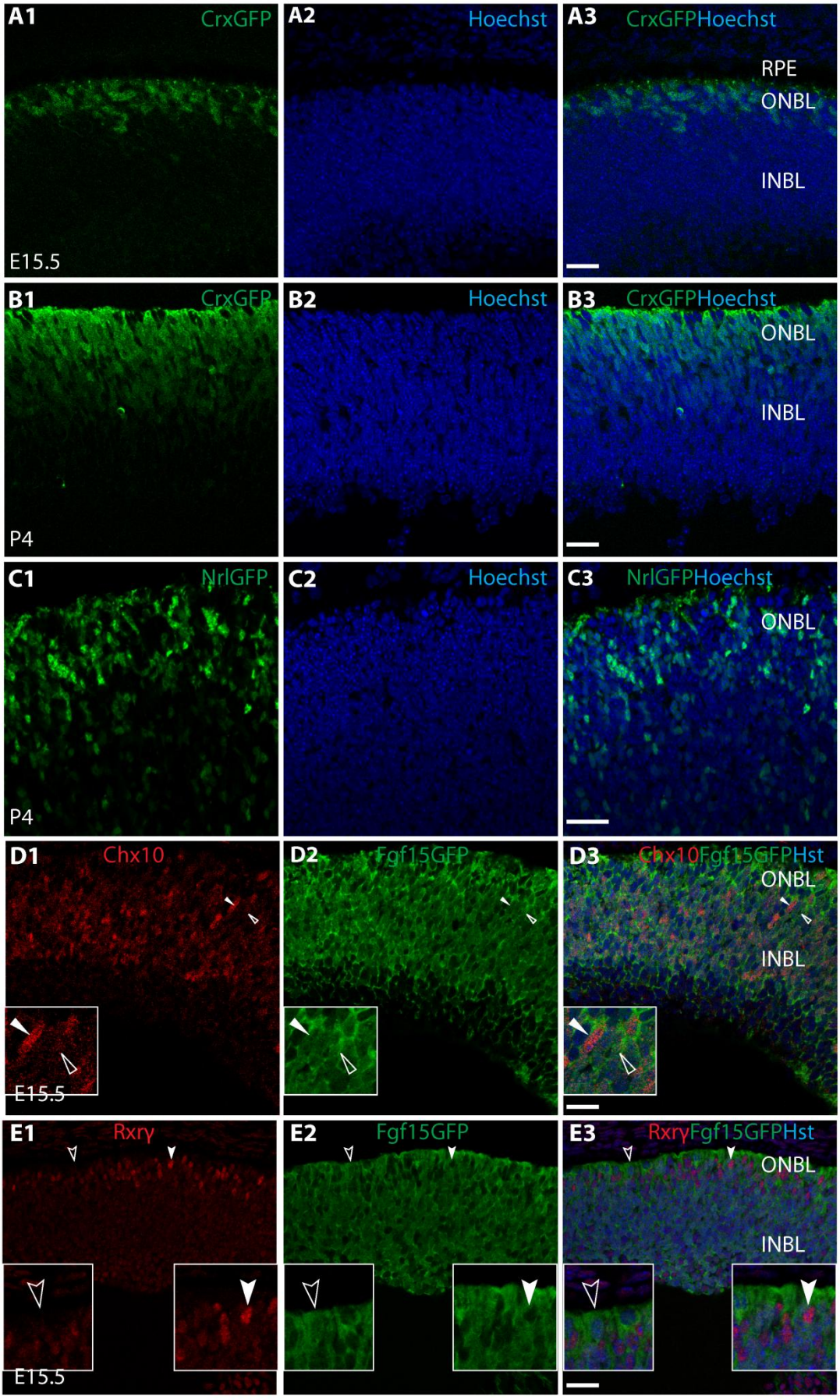

Figure 3.2 Expression profiles of CrxGFP, NrlGFP, and Fgf15GFP transgenic lines in the retina (continues).

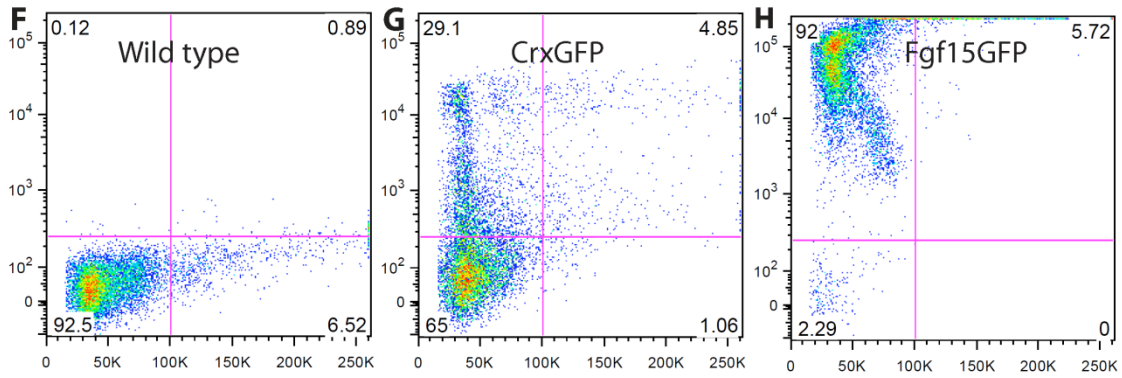

Figure 3.2 Expression profiles of CrxGFP, NrlGFP, and Fgf15GFP transgenic line in the retina – continued. (A1 – E3) Confocal images of CrxGFP retina at E15.5 (A1 – A3) and P4 (B1 – B3), NrlGFP retina at P4 (C1 – C3), and Fgf15GFP retina at E15.5 (D1 – E3) stained with Chx10 (D1) and Rxrγ (E1). Fgf15GFP labels nearly all the embryonic retinal cells and does not differentiate between progenitor cells and other cells. Solid arrowheads denote Chx10 or Rxrγ positive, empty arrowheads denote Chx10 or Rxrγ negative. Red: Chx10 or Rxrγ; Green: GFP; Blue: Hoechst 33342. Scale bar 25 µm. RPE: retina pigment epithelium; INBL: inner neuroblastic layer; ONBL: outer neuroblastic layer. (F – H) Flow cytometry represents the percentage of GFP+ve cells (top two quadrants) in the E15.5 retina of wild type (F), CrxGFP (G), and Fgf15GFP (H) mouse. X-axis: Forward scatter represent cell size; Y-axis: GFP intensity.

Table 3.1 Microarray gene numbers and DAVID analysis of the GFP+ve and GFP-ve gene sets

Array group	Affy ID (p<0.05)	Affy ID (p<0.05, FC>2)	DAVID ID	ID %	GO chart records	Cell surface related genes
E15.5 Crx+ve	85	63	61	97%	94	9
E15.5 Crx-ve	18	8	6	75%	16	
P4 Crx+ve	2147	627	556	89%	210	127
P4 Crx-ve	2340	1001	825	82%	430	
P4 Nrl+ve	5626	978	901	92%	328	197
P4 Nrl-ve	6224	1786	1450	81%	651	

FC: fold change; Affy ID: Affymetrix probe ID, only genes with statistically significant (p<0.05) expression differences and more than 2-fold expression changes were selected for further DAVID analysis; DAVID ID: an internal ID that DAVID use to identify unique gene/protein records; ID %: percentage of DAVID ID out of input Affymetrix ID; GO chart records: total number of gene ontology terms significantly enriched in the gene lists than random gene lists generated from the genome; Cell surface related genes: total number of genes annotated with cell-surface-related GO terms; P4: postnatal day 4; E15.5: embryonic day 15.5; +ve: GFP positive; -ve: GFP negative.

3.2.2 Analysis of photoreceptor precursors vs other retinal cells

I expect that photoreceptor precursor transcriptomes will show different properties from other retinal cells of the same stage. To examine what the differences are, I extracted the biological themes of each gene set based on annotation databases of all genes currently annotated (NCBI's Entrez, Uniprot, Affymetrix, MGI). The biological theme is summarized from the most significant functional annotations obtained from each gene set (significant annotations refer to annotation terms that are significantly enriched in the input gene list compared to random gene lists generated from the whole genome).

Firstly, significantly differently expressed genes with more than 2-fold expression changes were pulled out from the new array and previous array datasets and separated into GFP positive and negative cell gene sets (Table 3.1). Secondly, these gene sets were subjected to *in silico* functional analysis according to their annotations via online software DAVID v6.7 (Dennis, Sherman et al. 2003; Huang da, Sherman et al. 2009) (see Chapter 2, section 2.4.2). Thirdly, DAVID Functional Annotation Chart analysis was performed using GO annotation terms (Table 3.1). Fourthly, the most significantly enriched GO annotations (FDR<0.01) were directly compared between the GFP+ve genes and GFP-ve genes in the category of Biological Process (BP), Cellular Component, and Molecular Function (MF) (Figure 3.3).

It is clear that the photoreceptor precursor cells already showed different transcriptome properties from other retinal cells by E15.5 (Figure 3.3 A, Appendix figure 3.1). In the CrxE15.5 array, the photoreceptor precursor cell gene set mainly functioned in transcription, visual perception, and photoreceptor or eye development whereas the other retinal cells of the same stage mainly functioned in oxygen binding and transport (Figure 3.3 A, Appendix figure 3.1). In detail, the BP GO terms of E15.5 CrxGFP+ve cells is abundant in neurological system process, transcription regulation, and eye related terms such as visual perception, eye development, detection of stimulus, and photoreceptor differentiation (Figure 3.3 A). In contrast, the negative cells only enriched oxygen transport process (Figure 3.3 A). Whereas no Cellular Component GO term was significantly enriched for E15.5 CrxGFP positive cells, the negative cells enriched hemoglobin complex in the retina (Figure 3.3 A). Agreeing with the BP theme, the MF GO terms of the E15.5 CrxGFP+ve cells enriched DNA binding and transcription factor activity whereas the negative cells enriched oxygen binding and oxygen transporter activity (Figure 3.3 A).

The difference between photoreceptor cells and other retinal cells was further enhanced in the CrxP4 array (Figure 3.3 B). While the P4 photoreceptor gene set focused on visual

perception (in BP), photoreceptor or eye development (in BP), and plasma membrane and cell projection (in Cellular Component), the gene set for other retinal cells function in cell cycle or general morphogenesis (in BP), organelle (in Cellular Component), cytoskeleton (in Cellular Component) and chromosome (in Cellular Component) (Figure 3.3 B). To show the most essential information, GO terms from these categories were further compressed and merged to form a more compact chart (Appendix figure 3.1).

In summary based on the analysis of GO annotations of the expressed genes, photoreceptor precursor cells (ie. the GFP+ve cells) demonstrate very different properties from other retina cells of the same stage and from the entire genome transcriptome. These cells not only established their visual perception and photoreceptor commitment features by embryonic stages and maintained such properties, but also gradually evolved their properties and developed more specific functions for themselves (note loss of the initial transcription properties and appearance of the plasma membrane projection properties reflecting the gradual building up of more cell-type specific functions). Whereas other retinal cells only showed some non-cell-type specific functions such as cell cycle, DNA and chromosome. These data are consistent with the onset of photoreceptor differentiation and the emergence of unique properties of these light-sensing cells. The maintenance and changes of photoreceptor properties will be discussed further in section 3.2.3. It is interesting to note the emergence of plasma membrane projection GO terms such as cilium and synapse in photoreceptor cells and not other retinal cells, which will be discussed further in Chapter 5 (section 5.2.1).

A

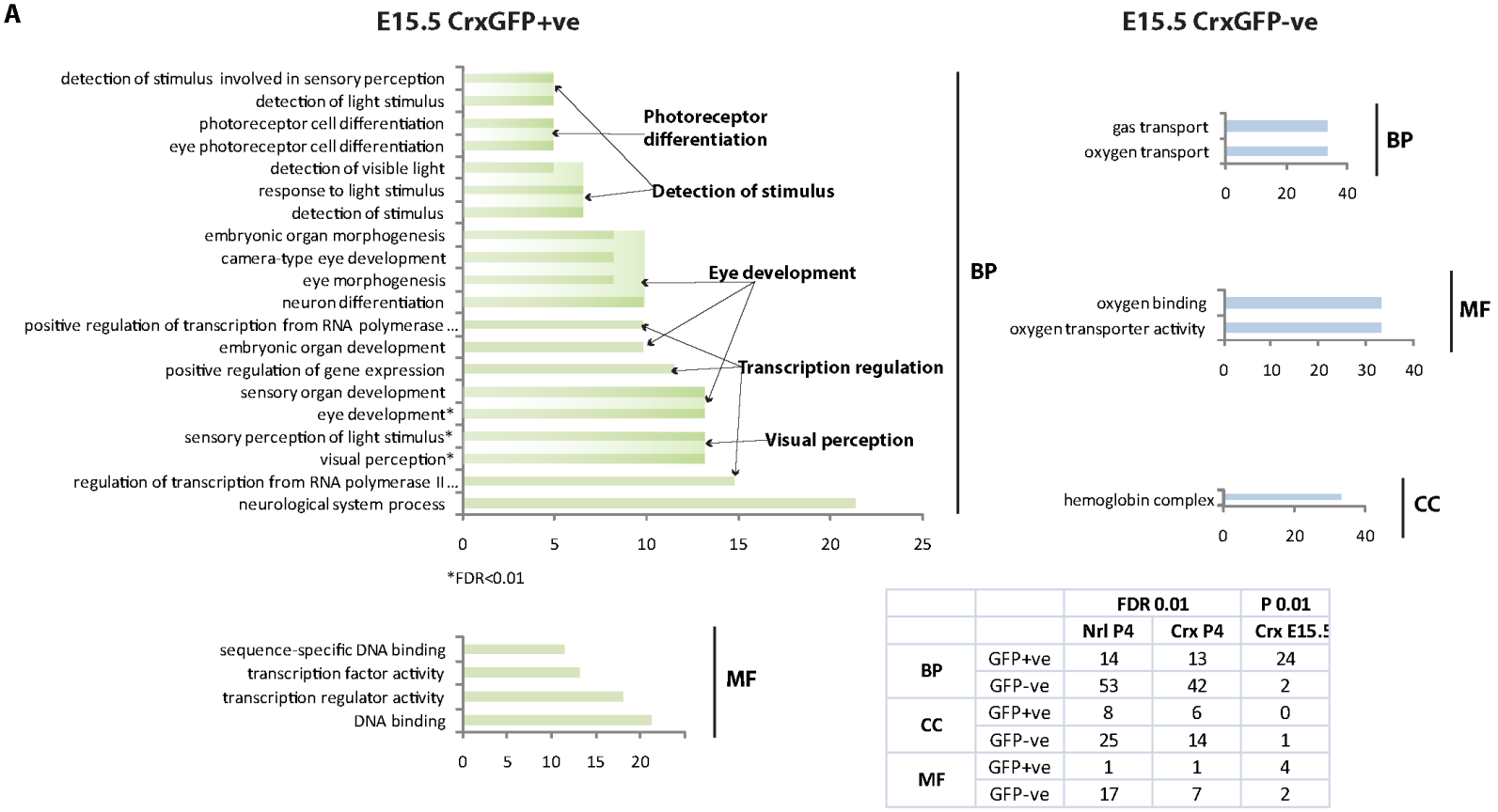

		FDR 0.01		P 0.01
		Nrl P4	Crx P4	Crx E15.5
BP	GFP+ve	14	13	24
	GFP-ve	53	42	2
CC	GFP+ve	8	6	0
	GFP-ve	25	14	1
MF	GFP+ve	1	1	4
	GFP-ve	17	7	2

Figure 3.3 Photoreceptor cell transcriptomes show very different properties from other retinal cells of the same stage (continues). (A) Properties of genes which show >2 fold expression differences significantly for E15.5 CrxGFP+ve cells (green, photoreceptor precursors) and E15.5 CrxGFP-ve cells (blue, other retinal cells) were compared in the category of biological process (BP), molecular function (MF), and cellular component (CC). X-axis: percentage of the genes annotated under each GO term out of the whole input gene lists. Y-axis: GO terms which were most significantly enriched in the gene lists compared with random gene lists generated from the genome. According to the size of the gene sets, the statistic thresholds for the GO terms were set as E15.5Crx+ve p0.01, E15.5Crx-ve p0.01, P4Crx+ve and P4Crx-ve FDR0.01. The table at the bottom represents numbers of the most significant GO terms enriched for gene sets analysed here and in Figure 3.6. For gene lists which produced more than 20 GO terms in each category, only the top 20 significant terms were presented here and in Figure 3.6. BP: Biological process; CC: cellular component; MF: molecular function; FDR: false discovery rate. *indicate GO terms with FDR<0.01.

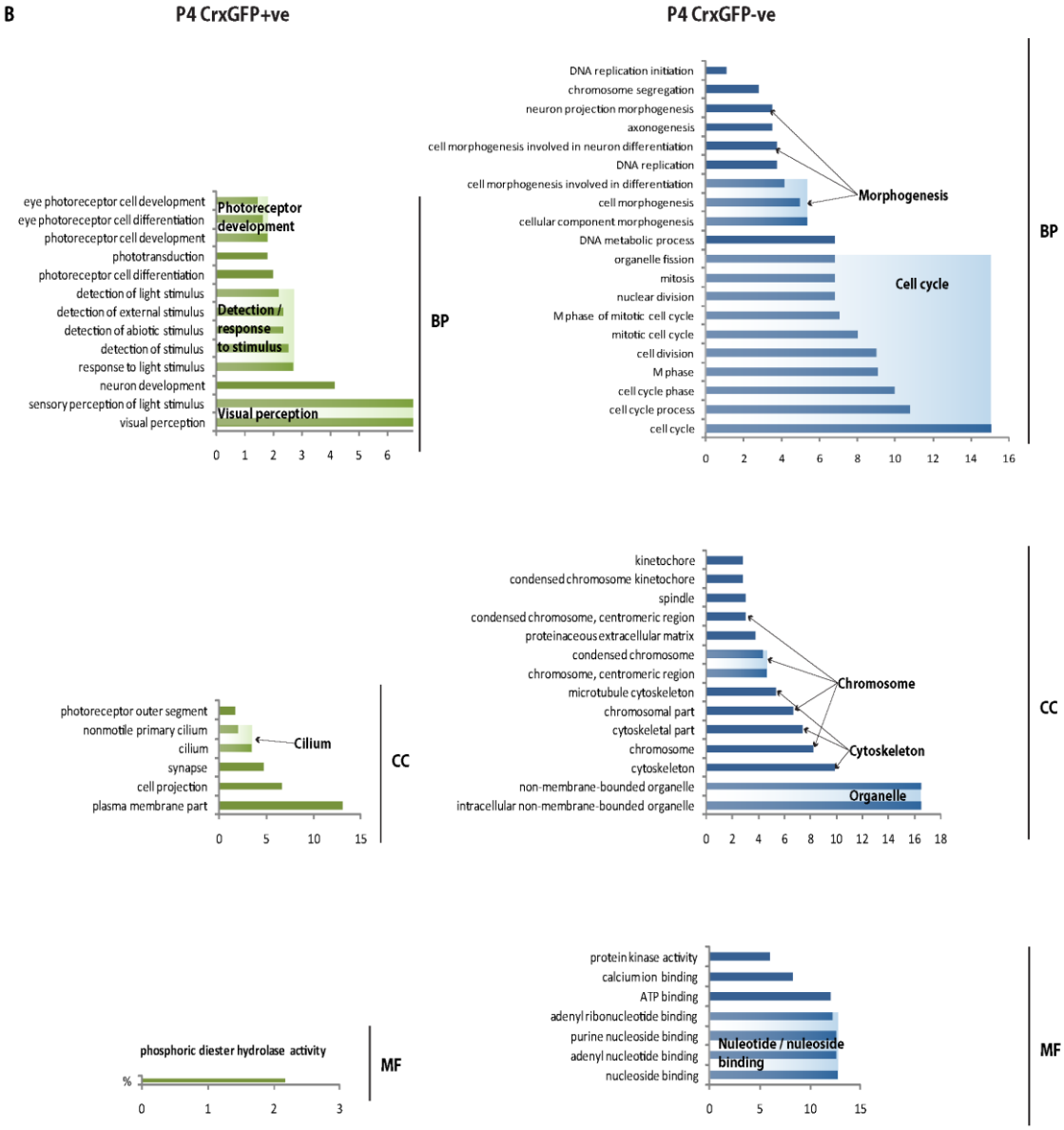

Figure 3.3 Photoreceptor cell transcriptomes show very different properties from other retinal cells of the same stage- continued. (B**) Properties of genes which show >2-fold expression differences significantly for P4 CrxGFP+ve cells (green, photoreceptor precursors) and P4 CrxGFP-ve cells (blue, other retinal cells). Note that each protein can be annotated by more than one functional term.**

3.2.3 Comparative analysis of early and late photoreceptor precursors

As the E15.5 photoreceptor cells labelled by CrxGFP produce more cones than the P4 photoreceptor cells whereas the P4 cells showed much higher integration rates (Lakowski, Baron et al. 2010), I next sought to compare these two cell populations to find properties that are shared and different between these cells. Understanding this could give us the clue as to what the properties of a good transplantable cell population should be like, and what typical genes are expressed in such a population. This will guide what kind of cell population should be screened for when cells are selected from other sources such as ES cells or iPS cells.

I directly compared the E15.5 CrxGFP+ve gene set (significant genes which were expressed more than 2-fold in the E15.5 CrxGFP+ve vs E15.5 CrxGFP-ve comparison, 63 Affymetrix ID, 60 known unique genes) with the P4 CrxGFP+ve gene set (significant genes which were expressed more than 2-fold in the P4 CrxGFP+ve vs P4 CrxGFP-ve comparison, 627 Affymetrix ID, 538 known unique genes) and found that 16 genes (17 Affymetrix ID) were specific to E15.5 CrxGFP+ve cells (Figure 3.4 A, Appendix table 3.1), 494 genes (581 Affymetrix ID) were specific to P4 CrxGFP+ve cells (Figure 3.4 A, Appendix table 3.3), and 44 genes (46 Affymetrix ID) were shared by both early and late photoreceptor precursors (Figure 3.4 A, Appendix table 3.2). I then analyzed the functional annotation of the three gene sets using DAVID and found that the common precursor gene set mainly functioned in transcription regulation, visual perception and cell projection (Figure 3.4 B). On the other hand, while the E15.5-specific genes mainly focused on only a few functions, the P4-specific genes showed a variety of specific functions (Figure 3.4 B & C).

The E15.5 precursor specific genes mainly functioned in transcription regulation, embryonic development, and metabolic process (Figure 3.4 B & C). This gene set included five transcription factors *Meis2*, *Tcfap2b*, *Tcfap2a*, *Nr2f2*, *Onecut1*, four ion transporters and three retinol metabolisers (Appendix table 3.1, Figure 3.5 A). The P4 precursor specific genes were more diverse and included the transcription factors *Nrl*, *Nr2e3,* and *Zranb1*, as well as a large proportion of genes with ion binding activity and enzyme regulator activity (Appendix table 3.3, Figure 3.4 B & C, Figure 3.5 B). The P4-specific genes were also enriched for additional visual perception genes and genes involved in cell projection, cell junction, and synapses (Figure 3.4 B & C).

The 44 common genes between E15.5 and P4 probably contain genes that should be present in a transplantable cell population. Indeed, not only did this set contain many essential transcription factors for photoreceptors such as *Crx*, *Otx2*, but also this set contained genes

encoding cell projection proteins such as *Cdhr1*, *Sv2b*, *Cngb3* etc (Figure 3.5 C, Appendix table 3.2). Interestingly, while I didn't find any genes encoding cell projection proteins in the E15.5-specific gene set, a lot of such genes appeared in the P4-specific gene set. This probably correlates with the low integration efficiency of E15.5 precursor cells and the high integration efficiency of P4 precursor cells and suggest that the onset of cell projection gene expression and the formation of specialized cell projections may be a feature associated with increased cell integration.

In summary, I have found the stage-specific and common genes for the early and late photoreceptor precursor cells. The common genes for transcription, visual perception and cell projection are probably desired for a transplantation competent photoreceptor population. Additional P4 stage-specific genes involved in cell projection, ion binding, and enzyme regulation may be associated with increased integration efficiency for the transplanted late precursor cells.

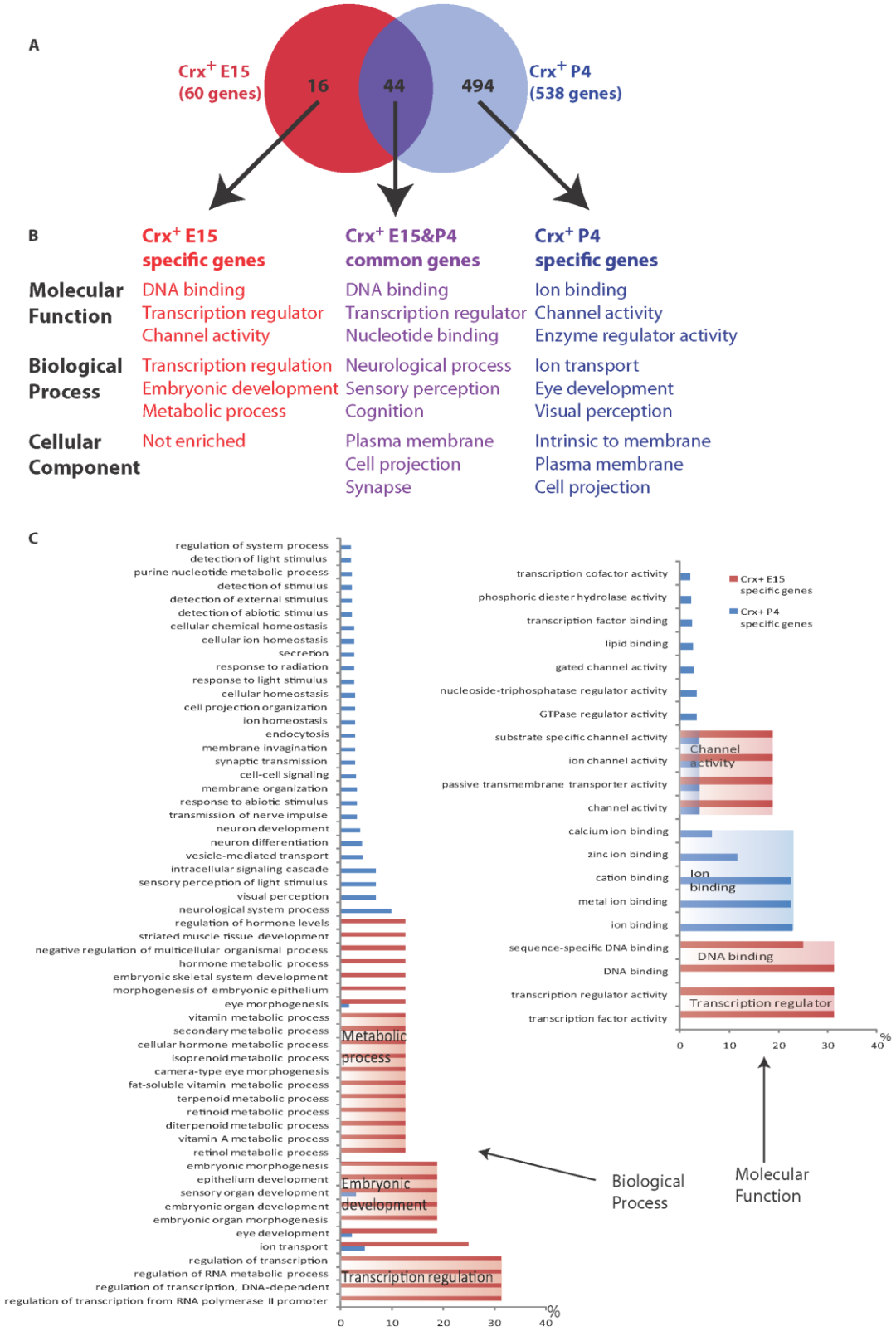

Figure 3.4 Functional comparisons of early and late photoreceptor precursor transcriptomes. (A) Venn diagram showing the number of common and stage-specific genes in E15.5 and P4 photoreceptor precursors. 16 and 494 genes were specific to E15 and P4 Crx+ cells respectively; 44 genes were common in both stages. (B) Comparison of the main function of the common and stage-specific genes for photoreceptor precursor cells. (C) Gene ontology terms (Y-axis) for (Left) Biological Process and (Right) Molecular Function enriched in E15-specific and P4-specific photoreceptor genes. X-axis representing percentage of the genes annotated for each term. GO terms which are significantly enriched are presented ($p<0.1$). Note each protein can be annotated by more than one term.

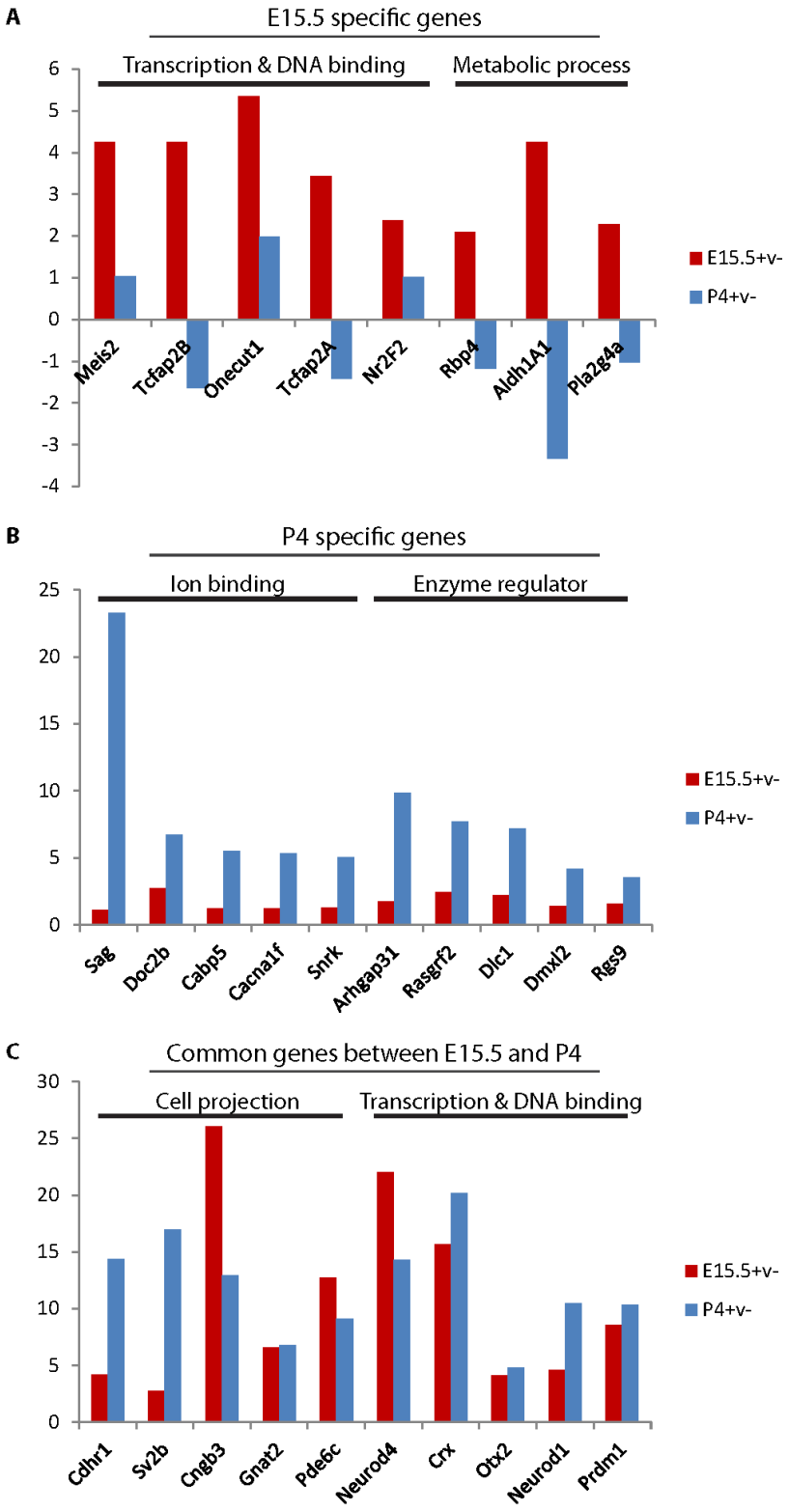

Figure 3.5 Examples of stage-specific and common genes from the comparison of E15.5 and P4 Crx-labelled photoreceptor gene sets. (A) E15.5-specific genes include transcription regulation and DNA binding genes, and genes involved in metabolic processes. (B) P4-specific genes include enzyme regulator and ion binders. (C) Common genes between E15.5 and P4 photoreceptor genes include transcription regulation and DNA binding genes, and genes involved in cell projection. Normalized expression fold changes between GFP-positive and GFP-negative cells from the microarray are shown. Red indicates the fold changes at E15.5, blue indicates the fold changes at P4.

3.2.4 Comparative analysis of NrlGFP and CrxGFP retinal cells

As NrlGFP labels rods and CrxGFP labels rods, cones, and bipolar cells, I next investigated if cone-specific properties could be found by comparing the NrlGFP+ve cells with the CrxGFP+ve cells at P4. Initial functional comparison of the two gene sets showed that the two cell populations were largely the same (Figure 3.6 A). In the category of BP, the NrlGFP+ve cells (Figure 3.6 A, left column, green) were rich in annotations related with visual perception, detection or response to stimulus, and photoreceptor development. This is almost identical to that of P4 CrxGFP positive cells (Figure 3.6 A, right column, green). The largest cellular component genes for both NrlGFP+ve cells and CrxGFP+ve cells were both encoding plasma membrane part and cell projection proteins. Of particular interest, both cells frequently showed GO terms related with cilium. This feature, however, was not found in the GFP-ve cells. The most significant MF GO terms enriched in the GFP+ve cells were also the same being phosphoric diester hydrolase activity including *Pde* genes such as *Pde6a*, *Pde6b*, *Pde6c*, *Pde6g* which hydrolyzes cGMP to 5'-GMP playing an essential role in phototransduction. Sharing of the same properties between the NrlGFP+ve cells and the CrxGFP+ve cells indicates that the two cell populations were very similar. In contrast although some common properties were detected for CrxGFP-ve and NrlGFP-ve cells, the pattern of MF terms and the largest proportion of cellular component terms were different for CrxGFP-ve cells and NrlGFP-ve cells (Figure 3.6 A, blue).

To directly compare between the P4 CrxGFP+ve gene set and the P4 NrlGFP+ve gene set, I pulled out the top 40 genes which showed the highest expression fold changes from both gene sets (Figure 3.6 B). Comparison of the two sets of top genes showed that half of the top genes in one set (20 out of 40) were also the top genes for the other gene set. Even for the remaining top genes which were specifically expressed within the Crx/NrlGFP+ve populations (20 out of 40 for each gene set), nearly all of them can be found in the other gene set albeit with smaller expression fold changes. There were two genes that were only found in the Crx array gene lists: *Gabrr3* and *Gje1*. However, neither has been shown in the literature to be related with cone photoreceptor cells: Gabrr3 is a GABA receptor that mediates inhibitory neurotransmission and in retina it is located in axon terminals of bipolar cells (Feigenspan and Bormann 1998; Schubert, Hoon et al. 2013), whereas Gje1 is a connexin protein found in rods (Eberle, Schubert et al. 2011) and lens (Bassnett, Wilmarth et al. 2009; Sonntag, Sohl et al. 2009).

Further comparison of the full >2-fold gene sets of P4 NrlGFP+ve, P4 CrxGFP+ve and E15.5 CrxGFP+ve identified 205 genes that were only present in CrxGFP+ve cells (including 16 genes in CrxE15.5 alone, 172 genes in CrxP4 alone, and 17 genes in both CrxE15.5 and CrxP4) (Figure

3.6 C, Appendix table 3.5). However, no known genes encoding cone specific proteins were identified in this set whereas general transcription factors (eg. *Meis2*, *Onecut1*, *Neurod1*, *Neurod4*, *Otx2*) or genes in bipolar cells such as GABA receptors (eg. *Gabrr3*, *Gabrr1*, *Gabra1*) (Feigenspan and Bormann 1998) were present. On the other hand, many known genes encoding cone specific proteins such as *Cngb3* (Cyclic nucleotide-gated cation channel beta-3), *Thrb* (Thyroid hormone receptor beta), *Opn1sw* (S opsin), *Chrnb4* (Neuronal acetylcholine receptor subunit beta-4), *Arr3* (cone arrestin), and *Pde6c* (Cone cGMP-specific 3',5'-cyclic phosphodiesterase subunit alpha) were present in the common genes of NrlGFP and CrxGFP gene sets rather than in the Crx-specific gene sets (Appendix table 3.5, known/possible cone genes are highlighted in bold).

Taken together, I showed that by comparing the transcriptomes of CrxGFP+ve and NrlGFP+ve gene sets 1) the transcriptome functional properties of CrxGFP+ve and NrlGFP+ve were very similar; 2) other than some bipolar cell genes and transcription factors specific to CrxGFP+ve I did not identify cone-specific properties or genes in the CrxGFP+ve gene set whereas 3) known cone-specific genes were present in both CrxGFP+ve and NrlGFP+ve gene sets. The most likely explanation is that the abundance of rods in the P4 CrxGFP population masked the properties of cones. Alternatively, it could be that the intrinsic molecular properties of rods and cones may indeed be very similar in early postnatal stages and these cells could not be distinguished. In support of this, Young reported that rods and cones were morphologically indistinguishable until P5 in 0.5 μm sections (Young 1985a).

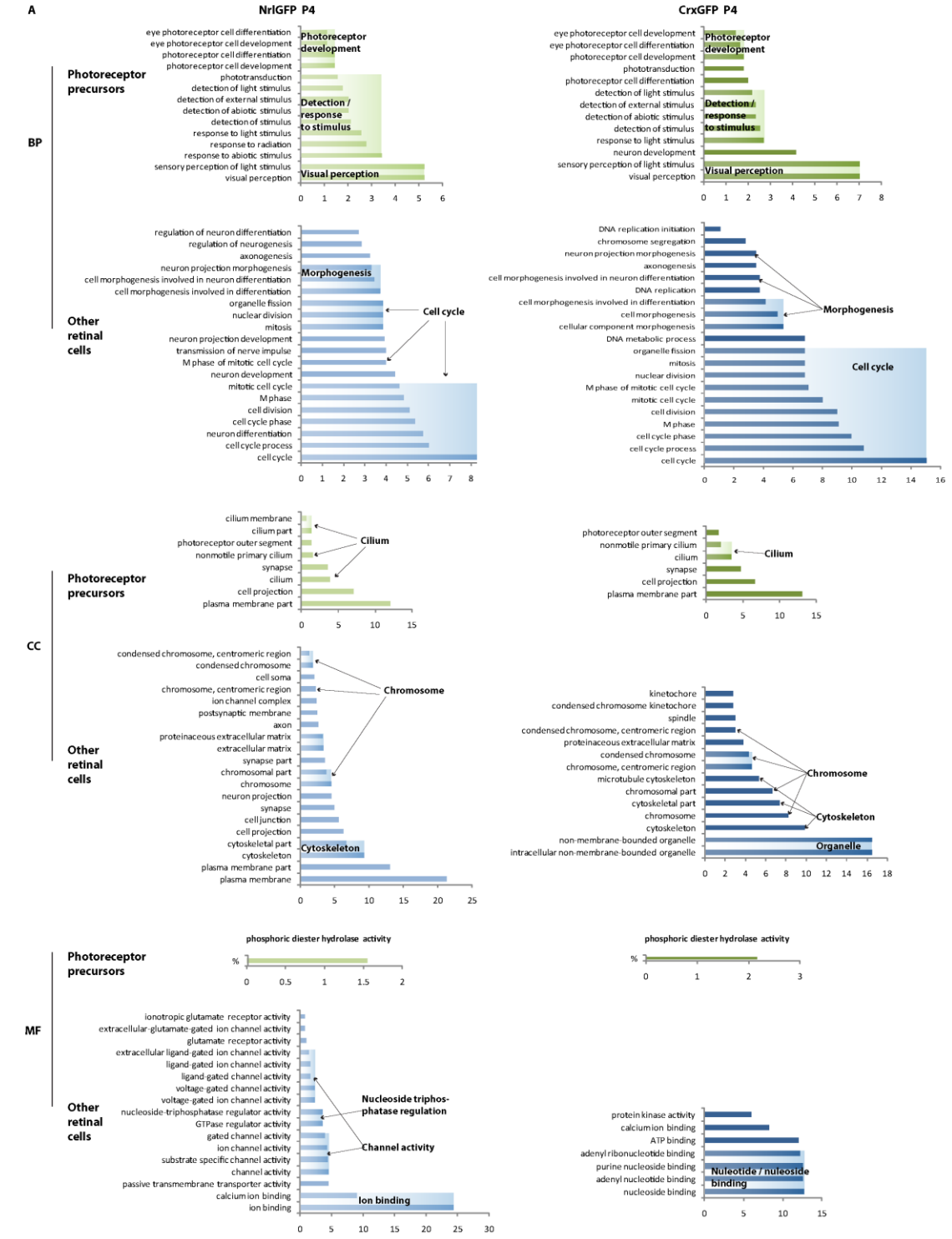

Figure 3.6 Comparison of the P4 CrxGFP-sorted cells and NrlGFP-sorted cells (continues). (A) Gene ontology properties of the CrxGFP-sorted and NrlGFP-sorted P4 retinal cells were similar in the category of biological process (BP), cellular component (CC), and molecular function (MF). Green is GFP+ve and blue is GFP-ve. CrxGFP P4 data were the same as Figure 3.3 B. Note each protein can be annotated by more than one term.

B

Crx only (20)			CrxNrl common (20)			Nrl only (20)		
Gene	FC (Crx)	FC (Nrl)	Gene	FC (Crx)	FC (Nrl)	Gene	FC (Nrl)	FC (Crx)
Gabrr3	47.1376	na	Impg2	51.4033	60.5	Opn1sw	42.2	7.35149
Rbp3	35.0821	12.9	Samd7	45.9339	52.7	Prph2	41.4	9.1317
Cplx4	27.3017	15.7	Rp1h	44.6873	122	Slc17a7	32.4	3.17132
Fabp7	26.1714	1.37	Pdc	43.7619	84.4	Rp1l1	30.3	3.51153
Crx	20.1751	3.81	Pde6b	41.5261	90.5	Pitpnm3	27.1	2.60227
Sv2b	16.9575	8.17	Cnga1	36.0885	34.1	Tulp1	27.1	5.36424
Cerkl	16.1369	11.2	Rho	34.1121	127	Impg1	26.4	9.94632
Slitrk6	15.8267	1.69	Nt5e	31.1249	22.9	Rdh12	25.6	6.16494
Neurod4	14.279	-1.35	Sag	23.2779	62.2	Rcvrn	25.5	3.94552
Adamts3	14.1692	10.9	Mak	22.0808	16.9	Ush2a	24.8	7.01788
Htra1	13.6217	11.5	Rpgrip1	21.604	33.4	Rs1	23.1	9.3161
Cngb3	12.9657	12.6	Ppef2	19.2097	18.9	Cngb1	22.8	5.68943
Samsn1	12.5896	5.43	Nrl	18.4976	24.3	Grk1	21.1	4.58825
Dmd	11.581	12.3	Nr2e3	16.6894	49.5	Kcnv2	20.7	4.32865
Cacna2d4	11.1951	5.35	Gngt1	15.3593	42.2	Rom1	20.1	7.59636
Zfp385b	11.0052	5.21	Cdhr1	14.3479	27.1	Gnat1	18.8	4.24634
Gje1	10.667	na	Slc27a2	12.5943	23.8	Reep6	17.9	4.55004
Neurod1	10.5051	2.75	Lrit2	12.331	29	Llgl2	17.3	1.89211
Prdm1	10.344	2.55	Ano2	12.2319	28.8	Rd3	17.1	3.78289
Pla2g7	10.0114	9.45	Pde6g	10.5799	36	Mpp4	16.1	5.66522

C

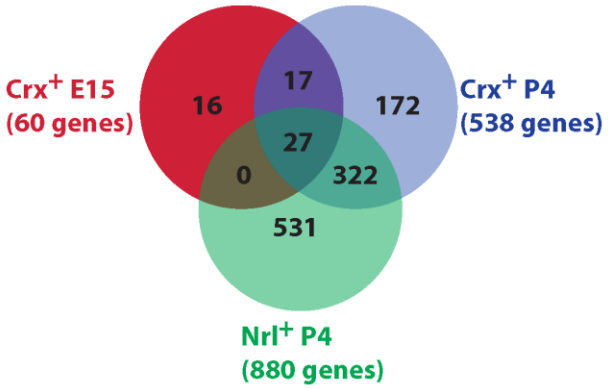

Figure 3.6 Comparison of the P4 CrxGFP-sorted cells and NrlGFP-sorted cells – continued. (B) The top 40 genes from CrxGFP+ve genes and NrlGFP+ve genes share 20 common genes and nearly all the remaining genes can also be found in both gene sets although with smaller fold changes. FC: expression fold changes between the CrxGFP (Crx) or NrlGFP (Nrl) sorted P4 positive and negative cells. (C) Venn diagram comparing the P4 NrlGFP+ve, P4 CrxGFP+ve and E15.5 CrxGFP+ve gene sets with 2-fold cut off.

3.2.5 Possible candidates as cell surface molecules for photoreceptor precursors

Next two approaches were used to find cell surface markers for photoreceptor cells from the array datasets: one is to manually search for the "cluster of differentiation" (CD) genes in the microarray database according to their names, and the other is to pull out the genes which are related with cell surface molecules according to their functional annotations.

It should be noted that with 5,480 transmembrane proteins and 3,129 glycosylated transmembrane proteins currently annotated for humans in the UniProt database (http://www.uniprot.org/), only around 350 proteins are CD antigens (http://hcdm.org/). Therefore, although the CD marker approach gives confirmed cell surface antigens, lots of cell surface proteins will be omitted by this approach. The functional annotation approach, on the other hand, provides a much bigger candidate pool, but interesting candidates will need to be validated individually to determine if they are cell surface antigens or not. This is because there are no defined "cell surface molecule" annotation terms which describe proteins with extracellular domains or extracellular proteins with domains anchored to the cell plasma membrane. GO terms which are related to "cell surface molecule" such as cell projection and plasma membrane not only annotate real cell surface proteins, but also proteins which do not have extracellular domains but are involved in making the cell projection structure. In addition, some annotations may come from electronic protein structure prediction rather than direct experimental assay.

3.2.5.1 CD gene lists

The CD nomenclature was established to classify monoclonal antibodies generated by different laboratories against leukocyte cell surface antigens and antibodies with similar binding patterns at various differentiation stages were clustered together (Zola, Swart et al. 2005). Molecules assigned with a "CD" number are usually cell-surface glycoproteins, and have antibodies available. So far over 350 human CD molecules have been assigned (http://hcdm.org/) and are used to define different cell types in the immune system.

To search for all the CD molecules in the microarray data, the gene symbol of the full 335 mouse CD molecules were compared with the gene symbol lists from the array data, and the common candidates between the CD list and the array lists constitute the CD molecules. A further specific search for "CD" in all the array gene lists including the Swaroop array added in additional CD molecules which were missed by the gene symbol comparison. This was performed for all the GFP positive and negative genes of the three array databases without setting the two-fold change threshold (Table 3.2). 40 CD molecules were found in the P4

NrlGFP+ve cells, with 10 molecules showing more than two-fold expression changes compared with negative cells (above the black line in Table 3.2). 63 CD molecules were found for P4 NrlGFP-ve cells and 26 genes expressed more than two-fold than the positive cells. 13 CD molecules were found in the P4 CrxGFP+ve cells and five expressed two-fold higher than the negative cells. 35 CD molecules were in the P4 CrxGFP-ve cells and 19 genes were more than two-fold. Only one CD molecule *Jam2* was identified in E15.5 CrxGFP+ve cells and one CD molecule for the negative cells. A total of ten CD molecules showed more than two-fold expression changes from the Nrl and Crx arrays for photoreceptor cells. These are *Nt5e* (CD73), *Prom1* (CD133), *Lifr* (CD118), *Sema7a* (CD108), *Itga3* (CD49c), *Sirpa* (CD172a), *Jag1* (CD339), *Cd8a* (CD8a), *Jam2* (CD322), and *Prnp* (CD230). In addition, seven CD molecules were identified in the Swaroop array (CD24a, CD2, CD302, CD53, CD59a, CD80, and CD83). Some of these CD markers will be further discussed in the following chapters.

Table 3.2 CD markers from Crx, NrlP4, and Swaroop array

P4 Nrl+ (40)	FC Nrl-v+	P4Nrl- (63)	FC Nrl-v+	P4 Crx+ (13)	FC P4Crx+v-	P4 Crx- (35)	FC P4Crx+v-
Nt5e	-22.9	Pdgfra	6.5	Nt5e	31.1249	Kit	-7.5178
Prom1	-9.19	Kit	6.15	Prom1	9.40123	Hmmr	-5.66575
Lifr	-6.02	Cxcr4	5.66	Jam2	5.52587	Itga2	-5.40528
Sema7a	-5.03	Cd9	5.21	Sema7a	3.64527	Mcam	-4.74093
Itga3	-3.89	Abcg2	4.89	Lifr	3.45633	Pdgfra	-4.33077
Sirpa	-3.71	Cd1d1	4.89	Darc	1.94085	Abcg2	-3.79395
Jag1	-2.81	Plxnc1	4.32	Itga3	1.87802	Plxnc1	-3.62236
Cd8a	-2.22	Mcam	4.08	Sirpa	1.77622	Bmpr1b	-3.6054
Jam2	-2.2	Hmmr	3.92	Cd164	1.71845	Cd9	-3.36756
Prnp	-2.03	Atp1b3	3.18	Jag1	1.49326	Ptprj	-3.19075
Cd164	-1.72	Ngfr	3.16	Ly75	1.46569	Cxcr4	-3.15292
Fgfr3	-1.63	Fgfr1	2.95	Ccr6	1.39352	Tlr3	-2.42421
Tspan7	-1.6	Cd200	2.93	Cd4	1.37309	Alcam	-2.37286
Cd276	-1.51	Itgav	2.87			Itga6	-2.28179
Igf1r	-1.48	Cd24a	2.87			Il1r1	-2.21358
Tfrc	-1.39	Itga2	2.87			Cd109	-2.18779
Cd37	-1.37	Lrp1	2.85			Atp1b3	-2.14666
Csf2rb	-1.34	Bmpr1b	2.75			Trf	-2.08977
Cd320	-1.33	Sema4d	2.62			Thy1	-2.04565
Ly75	-1.31	Itgb1	2.6			Itgav	-1.94834
Cd209b	-1.26	Ddr1	2.41			Sema4d	-1.93483
Cd4	-1.25	Gstm7	2.38			Cd44	-1.89469
Siglece	-1.24	Ptprj	2.36			Ptprj	-1.88747
Fasl	-1.23	Il4ra	2.13			Fgfr1	-1.87736
Insr	-1.23	Trf	2.11			Cdh2	-1.78236
Cd247	-1.22	L1cam	2.03			Itgb1	-1.74768
Fut4	-1.22	Cdh2	1.99			Ddr1	-1.64655
Entpd1	-1.21	Itga4	1.91			Pvrl3	-1.60783
Icam2	-1.21	Alcam	1.9			Atp1b3	-1.5615
Cd3d	-1.21	B3gat1	1.9			Vcam1	-1.54913
Tnfsf13b	-1.2	Cd151	1.86			Adam17	-1.54468
Itgal	-1.2	Cd99l2	1.85			F3	-1.49366
Tnfrsf17	-1.2	Cd59a	1.75			Pvr	-1.39178
Insr	-1.19	Gypc	1.62			Ngfr	-1.32807
Cd209a	-1.19	Tnfrsf12a	1.57			Cd97	-1.18495
Cd22	-1.18	F11r	1.52				
Itgax	-1.18	Thy1	1.48				
Cd3g	-1.17	Alk	1.47	E15.5 Crx+ (1)	FC E15Crx+v-	E15.5 Crx- (1)	FC E15Crx+v-
Bsg	-1.16	Cd47	1.43	Jam2	1.54415	Bmpr1b	-2.2096
Cd8b1	-1.15	Pdgfrb	1.43				
		Cd44	1.41				
		Cd72	1.41		Swaroop Array (7)		
		Vcam1	1.35		CD24a antigen		
		Cd109	1.35		CD2-associated protein		
		Ace	1.34		CD302 antigen		
		Tlr3	1.34		CD53 antigen		
		Fgfr4	1.34		CD59a antigen		
		F3	1.33		CD80 antigen		
		Sdc1	1.33		CD83 antigen		
		Itga6	1.32				
		Cd68	1.3				
		Il1r1	1.28				
		Pvrl3	1.27				
		Fgfr2	1.27				
		Nrp1	1.27				
		Itga5	1.27				
		Ncam1	1.25				
		Adam17	1.25				
		Cd38	1.22				
		Csf1r	1.21				
		Pvrl2	1.2				
		Cd2bp2	1.2				
		Itgam	1.19				

3.2.5.2 Cell surface-related gene lists

To increase the size of the cell surface marker candidate pool, I also used the functional annotation approach in DAVID. This approach will yield a much higher number of candidates and only genes of the GFP+ve cells with more than two-fold higher expression compared to GFP-ve cells were analysed. All the annotation terms which are related with cell surface molecules were selected and screened (including cell projection terms such as cilium and synapse, see Appendix table 3.4 for all GO terms used), and all the genes annotated with these terms were pulled out and merged to form one gene list named as cell surface-related genes.

197 cell surface-related genes were identified for P4 NrlGFP+ve cells, 127 genes for P4 CrxGFP+ve cells and nine genes for E15.5 CrxGFP+ve cells. These three cell surface-related gene sets were then compared to identify common and cell population-specific genes (Table 3.3). Eight genes were common to all three populations and one gene was common to CrxP4 and CrxE15.5 positive cells. These nine genes may include cell surface molecules that could be used to select both early and late photoreceptor precursors. 89 genes were common to CrxP4 and NrlP4 positive cells, and no genes were found common to CrxE15.5 and NrlP4 positive cells. The CrxP4 and NrlP4 common genes should be able to serve as the pool of cell surface markers for late photoreceptor precursors. Unfortunately no CrxE15.5 specific genes were found to specifically select for embryonic photoreceptor precursors. 29 genes were specific to CrxP4 positive cells and cone specific cell surface markers could come from these genes. 100 genes were specific to NrlP4 positive cells which was unexpected. Considering that the NrlP4 array generated more genes than the CrxP4 array initially, the NrlP4 specific genes identified might actually come from differences between arrays rather than having real biological meanings.

Table 3.3 Cell surface-related gene lists

Common CrxE15+CrxP4+NrlP4+ cell surface related genes (8)

GeneID	GeneSymbol	GeneName	FC NrlP4-v+	FC1 CrxE15+v-	FC2 CrxP4+v-	FC3 Crx+E15vP4	FC4 Crx-E15vP4
10503464	Cngb3	cyclic nucleotide gated channel beta 3	-12.6	26.0673	12.9657	-1.32521	-2.66432
10350530	Pdc	phosducin	-84.4	16.5561	43.7619	-12.2548	-4.63625
10414663	Rpgrip1	retinitis pigmentosa GTPase regulator interacting protein 1	-33.4	5.75074	21.604	-6.26463	-1.66757
10407337	Hcn1	hyperpolarization-activated, cyclic nucleotide-gated K+ 1	-8.17	5.18522	7.23023	-5.12108	-3.67262
10474141	Slc1a2	solute carrier family 1 (glial high affinity glutamate transporter), member 2	-2.48	4.15551	8.43913	-2.41959	-1.19143
10427496	Egflam	EGF-like, fibronectin type III and laminin G domains	-14.7	4.13253	9.67583	-2.75206	-1.1754
10600604	Dmd	dystrophin, muscular dystrophy	-12.3	3.13276	11.581	-3.04372	1.21455
10564646	Sv2b	synaptic vesicle glycoprotein 2 b	-8.17	2.75689	16.9575	-3.62394	1.69731

Common CrxE15+CrxP4+ cell surface related genes (1)

GeneID	GeneSymbol	GeneName	FC NrlP4-v+	FC1 CrxE15+v-	FC2 CrxP4+v-	FC3 Crx+E15vP4	FC4 Crx-E15vP4
10363224	Fabp7			17.3043	26.1714	-3.16354	-2.0917

Common CrxP4+NrlP4+ cell surface related genes (89)

GeneID	GeneSymbol	GeneName	FC NrlP4-v+	FC1 CrxE15+v-	FC2 CrxP4+v-	FC3 Crx+E15vP4	FC4 Crx-E15vP4
10352928	Rp1h	retinitis pigmentosa 1 homolog (human)	-122	1.35926	44.6873	-49.0212	-1.49109
10530503	Cnga1	cyclic nucleotide gated channel alpha 1	-34.1	1.11251	36.0885	-40.8715	-1.25996
10540984	Rho	rhodopsin	-127	-1.04559	34.1121	-44.2423	-1.24041
10540991	---	---	-29.4	1.06174	31.3976	-33.492	-1.13256
10587639	Nt5e	5' nucleotidase, ecto	-22.9	2.25786	31.1249	-17.8497	-1.29485
10459475	Cplx4	complexin 4	-15.7	-1.04124	27.3017	-34.7447	-1.22222
10484261	Cerkl	ceramide kinase-like	-11.2	3.12629	16.1369	-4.13472	1.24837
10536209	Gngt1	guanine nucleotide binding protein (G protein), gamma transducing activity polypeptide 1	-42.2	1.81586	15.3593	-12.1606	-1.43769
10419015	Pcdh21	protocadherin 21	-27.1	4.21158	14.3479	-4.55181	-1.3361
10368021	D230044M03Rik	RIKEN cDNA D230044M03 gene	-14.1	1.05596	10.667	-8.89136	1.13613
10439483	Cdgap	CDC42 GTPase-activating protein	-5.5	1.73977	9.85156	-7.52304	-1.32856
10529824	Prom1	prominin 1	-9.19	1.24535	9.40123	-4.24424	1.77866
10547858	Gnb3	guanine nucleotide binding protein (G protein), beta 3	-6.36	2.78104	9.28214	-3.76594	-1.12832
10462887	Pde6c	phosphodiesterase 6C, cGMP specific, cone, alpha prime	-13	12.758	9.09732	1.07249	-1.3076
10495712	Abca4	ATP-binding cassette, sub-family A (ABC1), member 4	-9.58	1.39594	8.07413	-6.2773	-1.08528
10410995	Rasgrf2	RAS protein-specific guanine nucleotide-releasing factor 2	-10.6	2.42242	7.69304	-5.85925	-1.84499
10543591	Opn1sw	opsin 1 (cone pigments), short-wave-sensitive (color blindness, tritan)	-42.2	1.46211	7.35149	-6.23974	-1.241
10352586	Ush2a	Usher syndrome 2A (autosomal recessive, mild) homolog (human)	-24.8	2.28418	7.01788	-3.4602	-1.12623
10466248	Stx3	syntaxin 3	-8.69	1.61114	6.96566	-6.73011	-1.55666
10495259	Gnat2	guanine nucleotide binding protein, alpha transducing 2	-10.9	6.57846	6.78718	-1.04271	-1.01065
10388465	Doc2b	double C2, beta	-11.7	2.71129	6.75295	-3.03904	-1.22017
10354897	Trak2	trafficking protein, kinesin binding 2	-2.91	1.85247	6.61963	-5.01534	-1.40352
10593947	Cplx3	complexin 3	-4.08	1.91689	6.21274	-4.11427	-1.26943
10482968	Pla2r1	phospholipase A2 receptor 1	-7.57	1.15555	5.93668	-5.09318	1.00871
10366073	Cep290	centrosomal protein 290	-7.01	1.35788	5.92009	-3.28442	1.32742
10436666	Jam2	junction adhesion molecule 2	-2.2	1.54415	5.52587	-2.86082	1.25089
10472549	Bbs5	Bardet-Biedl syndrome 5 (human)	-7.46	1.35512	5.47092	-4.40103	-1.09012
10598309	Cacna1f	calcium channel, voltage-dependent, alpha 1F subunit	-14.6	1.21519	5.36359	-4.31375	1.02319
10497713	Pex5l	peroxisomal biogenesis factor 5-like	-8	1.32106	4.92491	-3.46657	1.07541
10543791	Podxl	podocalyxin-like	-11.2	1.90941	4.76013	-1.97798	1.26037
10473880	Lrp4	low density lipoprotein receptor-related protein 4	-12.8	-1.18694	4.65252	-6.71325	-1.21567
10593767	Chrnb4	cholinergic receptor, nicotinic, beta polypeptide 4	-7.57	1.75116	4.6459	1.17311	3.11231
10482030	Stom	stomatin	-2.46	-1.08347	4.35805	-4.66603	1.01195
10462303	Kcnv2	potassium channel, subfamily V, member 2	-20.7	2.01156	4.32865	-2.71686	-1.26255
10596737	Gnat1	guanine nucleotide binding protein, alpha transducing 1	-18.8	1.15297	4.24634	-4.09312	-1.11137
10593668	Dmxl2	Dmx-like 2	-4.06	1.39853	4.16733	-3.16686	-1.06278
10598359	Syp	synaptophysin	-4.66	1.51843	3.87938	-2.88935	-1.13093
10344935	Kcnb2	potassium voltage gated channel, Shab-related subfamily, member 2	-2.1	1.06275	3.76165	-1.49339	2.37015
10380571	Gngt2	guanine nucleotide binding protein (G protein), gamma transducing activity polypeptide 2	-7.36	2.04152	3.75887	-2.42316	-1.31607
10560919	Atp1a3	ATPase, Na+/K+ transporting, alpha 3 polypeptide	-3.18	-1.23102	3.75012	-6.15319	-1.33288
10593671	Dmxl2	Dmx-like 2	-3.78	1.31459	3.70081	-2.84735	-1.01143
10585778	Sema7a	sema domain, immunoglobulin domain (Ig), and GPI membrane anchor, (semaphorin) 7A	-5.03	-1.05654	3.64527	-3.12341	1.23306
10382376	Ttyh2	tweety homolog 2 (Drosophila)	-2.95	1.81247	3.58817	-3.51552	-1.77577
10594144	Bbs4	Bardet-Biedl syndrome 4 (human)	-4.14	1.26758	3.54791	-2.16995	1.28987
10392415	Rgs9	regulator of G-protein signaling 9	-6.11	1.55203	3.52891	-3.53079	-1.55286
10585484	Chrna5	cholinergic receptor, nicotinic, alpha polypeptide 5	-7.78	1.01644	3.47781	-1.87292	1.82686
10422822	Lifr	leukemia inhibitory factor receptor	-6.02	1.28228	3.45633	-4.20741	-1.56092
10508052	Grik3	glutamate receptor, ionotropic, kainate 3	-2.66	1.3637	3.44141	-2.531	-1.00294
10583847	Bbs9	Bardet-Biedl syndrome 9 (human)	-5.31	-1.20228	3.37727	-4.54105	-1.11837
10600994	Arr3	arrestin 3, retinal	-8.75	1.03877	3.33913	-3.24265	-1.00875
10507500	Slc6a9	solute carrier family 6 (neurotransmitter transporter, glycine), member 9	-3.86	1.1708	3.23292	-3.23045	-1.16991
10421934	Klhl1	kelch-like 1 (Drosophila)	-5.17	1.16602	3.22274	-1.05694	2.61498
10603051	Ap1s2	adaptor-related protein complex 1, sigma 2 subunit	-2.25	1.22257	3.1968	-2.15248	1.21479
10552857	Slc17a7	solute carrier family 17 (sodium-dependent inorganic phosphate cotransporter), member 7	-32.4	1.32034	3.17132	-2.62905	-1.09457
10386951	Hs3st3b1	heparan sulfate (glucosamine) 3-O-sulfotransferase 3B1	-5.86	1.30514	3.15196	-2.13828	1.12943
10348321	Dgkd	diacylglycerol kinase, delta	-2.53	1.44176	3.04502	-2.07896	1.0159
10357164	Epb4.1l5	erythrocyte protein band 4.1-like 5	-2.91	1.15452	2.98192	-1.94708	1.32652
10509441	Ece1	endothelin converting enzyme 1	-3.14	1.30382	2.97518	-2.22003	1.02787

10363921	Pcdh15	protocadherin 15	-5.46	3.09258	2.87036	-6.92572	-7.46191
10512129	B4galt1	UDP-Gal:betaGlcNAc beta 1,4- galactosyltransferase, polypeptide 1	-4.41	-1.39769	2.82217	-3.83449	1.02869
10424607	Ptp4a3	protein tyrosine phosphatase 4a3	-9.78	-1.00227	2.81157	-2.68694	1.04876
10474619	Fmn1	formin 1	-2.1	-1.15986	2.79725	-1.42099	2.2832
10504234	Unc13b	unc-13 homolog B (C. elegans)	-2.87	-1.23641	2.78021	-2.13542	1.60974
10456096	Pde6a	phosphodiesterase 6A, cGMP-specific, rod, alpha	-13.5	1.28197	2.74065	-2.43282	-1.13798
10457357	Mpp7	membrane protein, palmitoylated 7 (MAGUK p55 subfamily member 7)	-2.35	1.48422	2.73373	-2.01633	-1.09472
10497842	Bbs7	Bardet-Biedl syndrome 7 (human)	-3.89	-1.02996	2.64062	-2.5832	1.05286
10444890	Ier3	immediate early response 3	-5.78	1.16517	2.6323	-1.80359	1.25259
10397683	Ttc8	tetratricopeptide repeat domain 8	-3.32	1.19381	2.63163	-2.31089	-1.04831
10476512	Snap25	synaptosomal-associated protein 25	-3.16	1.25319	2.55632	-2.3121	-1.13347
10405253	Cplx2	complexin 2	-3.94	1.39799	2.55392	-1.87899	-1.02854
10584901	Dscaml1	Down syndrome cell adhesion molecule-like 1	-4.11	-1.1683	2.50649	-2.68727	1.08971
10481349	Ntng2	netrin G2	-5.03	1.88705	2.45379	-1.47233	-1.13228
10457359	Mpp7	membrane protein, palmitoylated 7 (MAGUK p55 subfamily member 7)	-2.08	1.2649	2.43801	-2.04372	-1.06033
10510482	Clstn1	calsyntenin 1	-2.35	1.00629	2.30346	-2.56083	-1.11873
10467258	Fer1l3	fer-1-like 3, myoferlin (C. elegans)	-4.69	1.11361	2.29186	-2.58363	-1.25538
10436947	Kcne2	potassium voltage-gated channel, Isk-related subfamily, gene 2	-2.14	1.44492	2.27596	-1.8501	-1.17455
10565910	Plekhb1	pleckstrin homology domain containing, family B (evectins) member 1	-5.03	1.2541	2.27326	-4.14376	-2.28601
10595805	Rasa2	RAS p21 protein activator 2	-2.19	1.2491	2.22509	-1.53475	1.16069
10567964	Cln3	ceroid lipofuscinosis, neuronal 3, juvenile (Batten, Spielmeyer-Vogt disease)	-6.02	1.0286	2.22478	-2.16838	-1.00253
10603598	Rpgr	retinitis pigmentosa GTPase regulator	-2.01	-1.098	2.20675	-2.0735	1.16856
10517521	Epha8	Eph receptor A8	-2.45	1.38766	2.19087	-1.71495	-1.08622
10367775	Stxbp5	syntaxin binding protein 5 (tomosyn)	-2.41	1.69705	2.17653	-2.03053	-1.58321
10577792	Plekha2	pleckstrin homology domain-containing, family A (phosphoinositide binding specific) member 2	-14.7	1.28646	2.17432	-1.902	-1.12534
10587194	Gnb5	guanine nucleotide binding protein (G protein), beta 5	-3.53	1.03198	2.11965	-2.63795	-1.28433
10479379	Slco4a1	solute carrier organic anion transporter family, member 4a1	-8.88	1.01852	2.10709	-1.77365	1.16639
10592001	St14	suppression of tumorigenicity 14 (colon carcinoma)	-2.13	1.05532	2.06456	-1.85796	1.05295
10469335	Stam	signal transducing adaptor molecule (SH3 domain and ITAM motif) 1	-2.19	1.25798	2.06329	-1.46586	1.11891
10519069	Plch2	phospholipase C, eta 2	-6.77	1.28334	2.0309	-1.96427	-1.24124
10483822	Ttc30a2	tetratricopeptide repeat domain 30A2	-2.73	-1.07089	2.02147	-2.19464	-1.0138

CrxP4+ alone cell surface related genes (29)

GeneID	GeneSymbol	GeneName	FC NrlP4-v+	FC1 CrxE15+v-	FC2 CrxP4+v-	FC3 Crx+E15vP4	FC4 Crx-E15vP4
10436416	Gabrr3			1.56298	47.1376	-30.1713	-1.00042
10590623	Cxcr6			2.07137	6.18301	-3.5795	-1.19917
10399046	Vipr2			-1.01688	4.90671	-4.45678	1.11953
10440621	Grik1			1.02031	4.28654	-6.07252	-1.44542
10503866	Gabrr1			-1.04233	3.44093	-2.86596	1.25144
10519815	Cacna2d1			1.42311	3.2895	-1.23462	1.87222
10408268	Scgn			1.21635	3.13135	-2.81532	-1.09359
10415228	Cpne6			1.19314	3.02101	-3.21398	-1.26935
10496192	Tacr3			1.94921	2.98331	-3.31982	-2.16907
10503334	Gem			1.04369	2.92072	-2.59492	1.07843
10410408	Adcy2			1.70573	2.87769	-3.3475	-1.98421
10459671	Dcc			1.7565	2.86387	2.30614	3.76003
10385297	Gabra1			1.54053	2.85675	-10.3722	-5.59335
10485979	Gjd2			-1.1969	2.69682	-4.48856	-1.39059
10418053	Kcnma1			-1.09801	2.67229	-4.41711	-1.50538
10601595	3110007F17Rik			1.34439	2.64575	-1.63947	1.20038
10372503	Lgr5			-1.11738	2.55332	-1.77645	1.60603
10503659	Epha7			-1.04798	2.37221	-2.15222	1.1551
10403796	Amph			-1.1379	2.28951	-3.52346	-1.35245
10360349	Cadm3			1.68219	2.27022	-1.57632	-1.16802
10548118	Prmt8			2.65199	2.24071	-1.50301	-1.77889
10601588	3110007F17Rik			1.29496	2.21928	-1.43976	1.19032
10512949	Abca1			1.20781	2.17968	-8.58166	-4.7553
10548905	Eps8			1.43357	2.17568	-1.90381	-1.25443
10593628	Rab39			1.32043	2.16936	-1.23456	1.33077
10426292	Alg10b			-1.08455	2.16388	-1.59711	1.46943
10553301	Ldha			-1.11543	2.07221	-2.21213	1.04488
10563820	Svip			1.52172	2.04565	-1.34358	1.00054
10439362	Stxbp5l			-1.31005	2.00723	-2.06766	1.27177

NrlP4+ alone cell surface related genes (100)

GeneID	GeneSymbol	GeneName	FC NrlP4-v+
10388098	Aipl1	aryl hydrocarbon receptor-interacting protein-like 1	-12.7
10489872	Kcnb1	potassium voltage gated channel, Shab-related subfamily, member 1	-6.23
10560491	Klc3	kinesin light chain 3	-5.78
10523260	Shroom3	shroom family member 3	-4.92
10478907	Pard6b	par-6 (partitioning defective 6) homolog beta (C. elegans)	-4.41
10378964	Sez6	seizure related gene 6	-4.38
10523579	Arhgap24	Rho GTPase activating protein 24	-4.35
10517842	Crocc	ciliary rootlet coiled-coil, rootletin	-4.23
10432190	Adcy6	adenylate cyclase 6	-4.11
10453636	Svil	supervillin	-3.97
10390117	Itga3	integrin alpha 3	-3.89
10476021	Sirpa	signal-regulatory protein alpha	-3.71
10397835	Slc24a4	solute carrier family 24 (sodium/potassium/calcium exchanger), member 4	-3.61
10510767	Nphp4	nephronophthisis 4 (juvenile) homolog (human)	-3.53
10483819	Ttc30b	tetratricopeptide repeat domain 30B	-3.46
10378549	Rtn4rl1	reticulon 4 receptor-like 1	-3.43
10425335	Syngr1	synaptogyrin 1	-3.41
10464858	Bbs1	Bardet-Biedl syndrome 1 (human)	-3.32
10591978	Hnt	neurotrimin	-3.32
10594679	Tln2	talin 2	-3.29

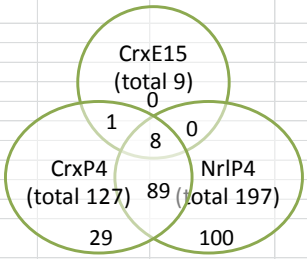

10587023	Rab27a	RAB27A, member RAS oncogene family	-3.23
10573956	Slc6a2	solute carrier family 6 (neurotransmitter transporter, noradrenalin), member 2	-3.14
10427816	Pdzd2	PDZ domain containing 2	-3.12
10555935	Cckbr	cholecystokinin B receptor	-3.12
10547807	Eno2	enolase 2, gamma neuronal	-3.1
10373986	Ap1b1	adaptor protein complex AP-1, beta 1 subunit	-2.97
10488060	Jag1	jagged 1	-2.81
10593384	Dixdc1	DIX domain containing 1	-2.77
10377725	Dlg4	discs, large homolog 4 (Drosophila)	-2.73
10409345	Cltb	clathrin, light polypeptide (Lcb)	-2.71
10548585	Csda	cold shock domain protein A	-2.69
10521626	Cc2d2a	coiled-coil and C2 domain containing 2A	-2.68
10352777	Slc30a1	solute carrier family 30 (zinc transporter), member 1	-2.62
10555460	Stard10	START domain containing 10	-2.62
10566457	Apbb1	amyloid beta (A4) precursor protein-binding, family B, member 1	-2.62
10392152	Scn4a	sodium channel, voltage-gated, type IV, alpha	-2.6
10520173	Accn3	amiloride-sensitive cation channel 3	-2.6
10573954	Capns2	calpain, small subunit 2	-2.6
10464612	Cabp4	calcium binding protein 4	-2.58
10469404	Cacnb2	calcium channel, voltage-dependent, beta 2 subunit	-2.51
10488762	Snta1	syntrophin, acidic 1	-2.51
10487906	Slc23a2	solute carrier family 23 (nucleobase transporters), member 2	-2.5
10383289	Baiap2	brain-specific angiogenesis inhibitor 1-associated protein 2	-2.48
10412773	Slc4a7	solute carrier family 4, sodium bicarbonate cotransporter, member 7	-2.46
10483439	Lrp2	low density lipoprotein receptor-related protein 2	-2.43
10575120	Sntb2	syntrophin, basic 2	-2.43
10595382	Lca5	Leber congenital amaurosis 5 (human)	-2.43
10565634	Myo7a	myosin VIIa	-2.41
10345571	Cnga3	cyclic nucleotide gated channel alpha 3	-2.39
10460498	Slc29a2	solute carrier family 29 (nucleoside transporters), member 2	-2.36
10419854	Slc7a8	solute carrier family 7 (cationic amino acid transporter, y+ system), member 8	-2.33
10529741	Rab28	RAB28, member RAS oncogene family	-2.33
10580733	Bbs2	Bardet-Biedl syndrome 2 (human)	-2.33
10364239	Slc19a1	solute carrier family 19 (sodium/hydrogen exchanger), member 1	-2.3
10387568	Tnfsf12-tnfsf13	tumor necrosis factor (ligand) superfamily, member 12-member 13	-2.3
10448925	Cacna1h	calcium channel, voltage-dependent, T type, alpha 1H subunit	-2.3
10518019	Ddi2	DNA-damage inducible protein 2	-2.3
10546056	Rab43	RAB43, member RAS oncogene family	-2.3
10547888	Gpr162	G protein-coupled receptor 162	-2.3
10489377	Serinc3	serine incorporator 3	-2.28
10514000	Mpdz	multiple PDZ domain protein	-2.28
10588577	Cish	cytokine inducible SH2-containing protein	-2.28
10460356	Gpr152	G protein-coupled receptor 152	-2.27
10540659	Ttll3	tubulin tyrosine ligase-like family, member 3	-2.23
10579776	Arhgap10	Rho GTPase activating protein 10	-2.23
10361887	Perp	PERP, TP53 apoptosis effector	-2.22
10467068	Sgms1	sphingomyelin synthase 1	-2.22
10532784	Svop	SV2 related protein	-2.22
10538993	Cd8a	CD8 antigen, alpha chain	-2.22
10571560	Mtnr1a	melatonin receptor 1A	-2.22
10575844	Cdh13	cadherin 13	-2.22
10443598	Dnahc8	dynein, axonemal, heavy chain 8	-2.2
10455259	Arhgap26	Rho GTPase activating protein 26	-2.2
10517587	Alpl	alkaline phosphatase, liver/bone/kidney	-2.17
10591643	Rab3d	RAB3D, member RAS oncogene family	-2.17
10382393	Dnaic2	dynein, axonemal, intermediate chain 2	-2.14
10408227	Hfe	hemochromatosis	-2.14
10411156	Scamp1	secretory carrier membrane protein 1	-2.13
10418506	Stab1	stabilin 1	-2.11
10540952	Ift122	intraflagellar transport 122 homolog (Chlamydomonas)	-2.11
10368806	Smpd2	sphingomyelin phosphodiesterase 2, neutral	-2.1
10464167	Adrb1	adrenergic receptor, beta 1	-2.1
10474545	Slc12a6	solute carrier family 12, member 6	-2.1
10607806	Ofd1	oral-facial-digital syndrome 1 gene homolog (human)	-2.1
10386652	Aldh3a2	aldehyde dehydrogenase family 3, subfamily A2	-2.08
10533929	Scarb1	scavenger receptor class B, member 1	-2.07
10564960	Furin	furin (paired basic amino acid cleaving enzyme)	-2.07
10404792	Phactr1	phosphatase and actin regulator 1	-2.04
10443730	Abcg1	ATP-binding cassette, sub-family G (WHITE), member 1	-2.04
10577757	Adam9	a disintegrin and metallopeptidase domain 9 (meltrin gamma)	-2.04
10354979	Als2	amyotrophic lateral sclerosis 2 (juvenile) homolog (human)	-2.03
10355456	Mreg	melanoregulin	-2.03
10476314	Prnp	prion protein	-2.03
10483824	Ttc30a1	tetratricopeptide repeat domain 30A1	-2.03
10607366	Shroom2	shroom family member 2	-2.03
10531274	Btc	betacellulin, epidermal growth factor family member	-2.01
10424965	Ppp1r16a	protein phosphatase 1, regulatory (inhibitor) subunit 16A	-2
10451213	1700027N10Rik	RIKEN cDNA 1700027N10 gene	-2
10468344	Col17a1	collagen, type XVII, alpha 1	-2
10535043	Pdgfa	platelet derived growth factor, alpha	-2

3.2.5.3 Genes of top interests

The above analysis produced 227 genes of potential interest as encoding cell surface (or cell surface-related) molecules. Ideally, all these genes should be examined individually. To efficiently select only the most interesting cell surface candidates, I prioritized genes in two non-exclusive groups. Group one: genes common to all three populations (8 genes) and genes common to E15.5 and P4 CrxGFP positive cells (1 gene) (Figure 3.7, Table 3.3). These genes may include cell surface molecules which are shared by both early and late photoreceptor precursors. Group two: genes with more than five-fold expression changes in the photoreceptor cells (Figure 3.7). This allows selection of the most photoreceptor-specific genes. Notably, the above nine genes common to early and late photoreceptor cells also satisfied this standard. For the rest, 54 of the 89 common genes in CrxP4+ve and NrlP4+ve cells, two genes in CrxP4+ve alone and three genes in NrlP4+ve alone satisfied the five-fold standard. These genes may include cell surface markers for late rod or cone precursors. These two groups of genes gave a total of 68 candidates which were then sifted and examined individually in Uniprot to determine the presence of extracellular domains or GPI-anchors as well as their functions and cellular localization (Table 3.4). 32 of them have confirmed extracellular domains or are GPI-anchored. Based on their function and cellular location, I further selected 13 genes which locate in cilium or synapse regions or function in cell migration or adhesion as these features may be important for effective transplantation (Table 3.5).

Of the 13 selected surface markers, *Pcdh21*/*Cdhr1*, *Ush2a*, *Prom1* and *Pcdh15* were annotated to be related with cilium (Table 3.5). *Pcdh15*, *Ush2a*, *Sv2b*, *Slc17a7*, *Chrna5*, *Chrnb4*, and *Gabrr3* were annotated to be related with synapses. *Podxl*, *Sema7a*, *Ntng2* and *Jam2* were annotated to be related with cell migration, adhesion, axon guidance or outgrowth. The pathways in which the 13 candidates are involved and their interacting molecules were also identified (Table 3.5). Prom1 interacts with Cdhr1 in cilium. Sv2b interacts with laminin in extracellular matrix-receptor interaction pathways. Sema7a interacts with Itgb1 and PlexinC1 in axon guidance pathways. And Jam2 interacts with Jam3, Jam2, Magl1, Itga4, and Itgb1 in tight junction and leukocyte transendothelial migration. The interacting molecules of our selected cell surface markers were also detected in our microarrays (Table 3.5).

All the 13 genes selected showed much higher expression in photoreceptor cells than other retinal cells at P4 according to the microarrays (Figure 3.8). Other than *Slc17a7* and *Gabrr3* the expression fold changes of the 13 genes were not widely different between the NrlGFP-sorted and CrxGFP-sorted P4 retinal cells. Except *Sema7a*, most of the 13 genes also showed slightly higher expression in the E15.5 photoreceptor cells than other retinal cells. These indicate the

specificity of these cell surface markers to photoreceptor cells. Other than *Chrnb4*, all remaining genes showed higher expression in late photoreceptor cells than early photoreceptor cells indicating the higher demands of the cell surface molecules for late photoreceptor precursors (Figure 3.8). The absolute expression levels of these genes were also high in the microarrays. Other than *Gabrr3* which was absent in the NrlP4 array, the log2 intensity of the remaining genes were all above 8.7 for NrlP4+ve cells (data not shown). In the Crx array, the minimum log2 intensity of the 13 genes was 4.8 in E15.5 CrxGFP+ve cells and 6.3 in P4 CrxGFP+ve cells demonstrating high expression (Figure 3.9).

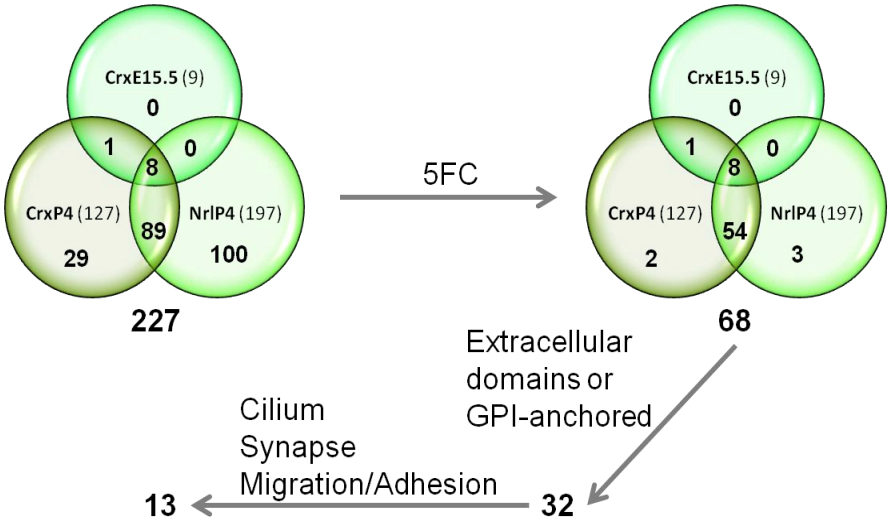

Figure 3.7 Flowchart for sifting through the cell-surface related candidate genes. The 227 cell surface related candidate genes were furthered filtered through a five-fold expression changes which gave 68 candidate genes. The 68 candidates were individually examined for presence of extracellular domains or GPI-anchor which gave 32 candidates. The 32 candidates were further examined for functions involved in cilium, synapses, migration and adhesion and yields 13 candidates of high interests.

Table 3.4 Extracellular domains, function and location of 68 prioritized cell surface candidates

Common CrxE15+CrxP4+NrlP4+ cell surface related genes (8 -> 8)			
GeneSymbo	Extracellular Domain	Function	Location
Cngb3	231-242, 316-351, 431-568	cGMP actived opening of cation channel	multipass mem, OS
Pdc	na	visual phototransduction	cilium
Rpgrip1	na	disk morphogenesis	cilium
Hcn1	157 – 162, 230 – 237, 311 – 333, 356 – 360	cAMP actived hyperpolarization ion channel	multipass mem, apical dendrites
Slc1a2	143 – 238	terminate postsynaptic action of glutmate by removing them from synaptic cleft	multipass mem,axolemma
Egflam	na	ribbon synapse formation	ECM, synapse
Dmd	na	synaptic transmission, signaling, anchors ECM to cytoskeleton	synapse, peripheral mem pr, cytoskeleton, sarcolemma
Sv2b	132 – 148, 204 – 205, 259 – 277, 412 – 535, 587 – 592, 650 – 653	synaptogenesis, control secretion	synapse, ribbon synapses, cell junction, synaptic vesicle mem
Common CrxE15+CrxP4+ cell surface related genes (1-> 1)			
GeneSymbo	Extracellular domain	Function	Location
Fabp7	na	transport of hydrophobic gland	cytoplasm
Common CrxP4+NrlP4+ cell surface related genes (89-> 54)			
GeneSymbo	Extracellular domain	Function	Location
Rho	1 – 36, 99 – 113, 177 – 202, 277 – 284	image-forming vision, postnatal PR viability	multipass mem, IS, OS
Rp1h	soluble fraction?	PR differentiation	cilium, IS, cell bodies of PR
Gngt1	na	GTPase activity, replacement of GDP by GTP, G protein-effector interaction	lipid-anchor, cytoplasmic side, rod OS
Opn1sw	1 – 31, 95 – 108, 172 – 197, 272 – 279	visual pigments, increase spectral sensitivity	multi-pass mem, cones
Cnga1	178 – 190, 254 – 291, 387 – 470	cGMP actived opening cation channel	multipass mem, OS
Slc17a7	85 – 116, 162 – 169, 230 – 236, 324 – 341, 400 – 401, 457 – 469	Mediates the uptake of glutamate into synaptic vesicles at presynaptic nerve terminals of excitatory neural cells	synapse, synaptic vesicle mem, synaptosome
Pcdh21/Cdhr1	22 – 701	may be required for structural integrity of OS	single-pass mem, cilium, OS base, opposite CC
Ush2a	35 – 5033	involved in hearing and vision, required for integration into the basement mem. interact with collagen IV and fibronectin	single-pass type I mem protein, stereocilium mem, apical and basement mem, high in basement mem, synaptic terminals of PR
Nt5e	Signal peptide 1 – 28, GPI-anchored	hydrolyzes extracellular nucleoties into mem permeable nucleosides	GPI-anchor
Kcnv2	185 – 269, 366 – 391, 449 – 461, 483 – 488	Modulates channel activity by shifting the threshold and the half-maximal activation to more negative values	multi-pass mem
Gnat1	na	amplifies and transduces visual impulse, GTP-binding, nucleotide-binding	OS, CC
Cplx4	na	regulate synaptic vesicle exocytosis	lipid-anchor, synapse, synaptic terminal
Plekha2	na	Binds specifically to phosphatidylinositol-3,4-diphosphate (PtdIns3,4P2), but not to other phosphoinositides. May recruit other proteins to the plasma membrane.	peripheral mem, nucleus, cytoplasm
Cacna1f	12 ex domains	give rise to long-lasting calcium currents	multi-pass mem, INL, ONL
D230044M03Ri	na	na	na
Pde6a	na	catalyse guanosine cyclic phosphate into guanosine phosphate, transmits and amplifies visual signal	lipid-anchor, cytoplasmic side
Pde6c	na	catalyse guanosine cyclic phosphate into guanosine phosphate	lipid-anchor, cytoplasmic side
Lrp4	21 – 1725	Potential cell surface endocytic receptor, which binds and internalizes extracellular ligands for degradation by lysosomes.	single-pass mem,
Doc2b	na	stimulate mem fusion by modifying mem curvature, binds calcium/phospholipids	peripheral mem, synapse, synaptic vesicle, cytoplasm
Cerkl	na	Hu:no detectable ceramide-kinase activity	Hu:necleolus, may shuttle, moderate expression in retina
Podxl	22 – 404	migration, regulation of both adhesion and cell morphology and cancer progression	single-pass type I mem protein, microvillus, lamellipodium
Gnat2	na	amplifies and transduces visual impulse, GTP-binding, nucleotide-binding	rod OS,mem
Rasgrf2	na	synaptic plasticity by contributing to the induction of long term potentiation, calcium-regulated nucleotide exchange factor actvating Ras and RAC1	peripheral mem,ER mem
Ptp4a3	na	stimulate progression from G1 to S phase, enhances cell proliferation, motility and invasive activity	early endosome
Abca4	43 – 546, 1397 – 1558	photoresponse, transport retinal	multi-pass mem, rims of rods

Prom1	20 – 107, 180 – 434, 509 – 794	binds cholesterol, regulate disk morphogenesis and MAPK and Akt pathways	multi-pass mem, cilium
Slco4a1	124 – 142, 195 – 224, 296 – 309, 403 – 422, 474 – 582, 641 – 673	Mediates the Na+-independent transport of organic anions such as the thyroid hormone T3 (triiodo-L-thyronine) and of taurocholate	multi-pass mem
Arr3	na	May play a role in an as yet undefined retina-specific signal transduction. Could binds to photoactivated-phosphorylated	IS, OS
Stx3	284 – 289	potentially docking synaptic vesicles	single-pass type IV mem, apical plasma mem
Pex5l	na	Interacts with RAB8B	peripheral mem, cytoplasm
Chrna5	451 - 467, 30 - 254? 305 - 316?	binds acetylcholine and opens an ion-conducting channel	multi-pass mem, synapse, postsynaptic cell mem
Pla2r1	27 - 1396	phospholipase receptor, may affect MAPK	single-pass type I mem,
Chrnb4	21 – 235, 286 – 297, 485 – 495	binds acetylcholine and opens an ion-conducting channel	multi-pass mem, synapse, postsynaptic cell mem,
Bbs5	na	BBSome complex, ciliogenesis	cilium, basal bodies
Gngt2	na	GTPase activity, replacement of GDP by GTP, G protein-effector interaction	lipid-anchor, cytoplasmic side
Cep290	na	localization of ciliary and phototransducin proteins	cilium, nucleus, centrosome
Plch2	na	produce DAG and IP3	plasma mem
Gnb3	na	GTPase activity, replacement of GDP by GTP, G protein-effector interaction	G-protein complex
Rgs9	na	inhibits signal transduction by increasing GTPase activity of G protein alpha subunits	G-protein complex
Lifr	44 - 828	Signal-transducing molecule. May have a common pathway with IL6ST. The soluble form inhibits the biological activity of LIF by blocking its binding to receptors on target cells.	Isoform 1: Cell membrane; Single-pass type I membrane protein. Isoform 2: Secreted.
Cln3	59 - 98, 299 - 357	Battenin	Lysosome membrane; Multi-pass membrane
Hs3st3b1	54 - 390	sulfotransferase 1 family, enzyme	single-pass type II mem protein, Golgi
Ier3	105 - 153	May play a role in the ERK signaling pathway by inhibiting the dephosphorylation of ERK by phosphatase PP2A-PPP2R5C holoenzyme	single-pass type II mem, Golgi
Cdgap/Arhgap31	na	GTPase-activating protein for RAC1 and CDC42, required for cell spreading, polarized lamellipodia formation and cell migration	migration, lamellipodium, focal adhesion
Pcdh15	27 - 1381	Calcium-dependent cell-adhesion protein. Required for inner ear neuroepithelial cell elaboration and cochlear function. Probably involved in the maintenance of normal retinal function	single-pass type I mem (heavy glycosalation), stereocilium, OS,
Bbs9	na	BBSome complex, ciliogenesis	cilium mem, cytoplasm
Klhl1	na	May play a role in organizing the actin cytoskeleton of the brain cells	cytoskeleton
Sema7a	Sema domain and Ig-like C2-type domain, GPI-anchored	Axon guidance, may play an imortant role in the nervous system and in modulating immune function	GPI-anchor
Ntng2	Laminin EGF-like domains, GPI-anchored	Migration, promotes neurite outgrowth of both axons and dendrites. Interacts with LRRC4	GPI-anchor
Plekhb1	na	binds transducins.Interacts with MYO1C	mem-associated. Highly in OS
Cplx3	na	regulate synaptic vesicle exocytosis	lipid-anchor, synapse, synaptic terminal
Atp1a3	99 – 121, 299 – 310, 783 – 792, 857 – 908, 961 – 975	catalytic component of Sodium/potassium-transporting ATPase	multi-pass mem, across plasma mem
Trak2	na	Hu:regulate endosome-to-lysosome trafficking of mem cargo, including EGFR	Cytoplasm, early endosome
Jam2	29 - 236	processes of lymphocyte homing to secondary lymphoid organs	tight junction, single-pass type I mem
CrxP4+ alone cell surface related genes (29->2)			
GeneSymb	**Extracellular domain**	**Function**	**Location**
Gabrr3	24 - 266, 321 -311	Hu: mediates neuronal inhibition by binding to GABA	Hu: synapse, postsynaptic cell mem, multi-pass mem
Cxcr6	1 – 41, 99 – 112, 174 – 196, 269 – 284	Receptor for the C-X-C chemokine CXCL16	multi-pass mem
NrlP4+ alone cell surface related genes (100-> 3)			
GeneSymb	**Extracellular domain**	**Function**	**Location**
Aipl1	na	protein trafficking and/or protein folding and stabilization	cytoplasm, nucleus
Kcnb1	na	mediate voltage-dependent potassium ion permeability of excitable mem	multi-pass mem
Klc3	na	microtubule-associated force-producing protein that may play a role in organelle transport	Elongating spermatid tail midpiece. Localized in outer dense fibers (ODFs) and associates with mitochondria

ECM: extracellular matrix; OS: outer segment; IS: inner segment; PR: photoreceptor; mem: membrane; Hu: Human; CC: connecting cilium; ER: endoplasmic reticulum; INL: inner nuclear layer; ONL: outer nuclear layer. Extracellular domain positions are either directly provided by Uniprot or estimated by positions of transmembrane domains and N-linked glycosylation sites which are known or predicted to be extracellular.

Table 3.5 Pathways and interacting molecules of 13 selected surface markers

	Photoreceptor surface markers				Interacting molecues	
	Gene Symbol	Gene Name	Note	Pathway	Genes in pathway	Expression in microarray (FC)
cilium	Prom1	prominin 1	cilium	Cilium (Yang et al. 2008), Transcriptional misregulation in cancers (Kegg pathway)	Pcdh21 (Yang et al. 2008)	NrlP4+ve Pcdh21 -27.1
cilium	Pcdh21/ Cdhr1	protocadherin 21 / cadherin-related family member 1	cilium	Cadherin signaling pathway (Panther pathway), Wnt signaling pathway (Panther pathway)	Prom1 (Yang et al. 2008)	NrlP4+ve Prom1 -9.19
cilium	Pcdh15	protocadherin 15	adhesion, stereocilium, heavy glycosalation	Cadherin signaling pathway (Panther pathway), Wnt signaling pathway (Panther pathway)		
cilium	Ush2a	Usher syndrome 2A (autosomal recessive, mild) homolog (human)	apical and basement mem	Cilium (Yang et al. 2010; Liu et al, 2007)		
synapse	Sv2b	synaptic vesicle glycoprotein 2 b	synapse	ECM-receptor interaction (Kegg pathway)	laminin	NrlP4-ve Lamb1-1 1.82, Lama1 3.1, Lama2 1.23, Lama5 1.18, Lamb2 3.01, Lamc1 1.37, Sv2c 2.45
synapse	Slc17a7	solute carrier family 17 (sodium-dependent inorganic phosphate cotransporter), member 7	synapse	Ionotropic glutamate receptor pathway (Panther pathway), Metabotropic glutamate receptor group III pathway (Panther pathway)		
synapse	Chrna5	cholinergic receptor, nicotinic, alpha polypeptide 5	synapse	Nicotinic acetylcholine receptor signaling pathway (Panther pathway)		
synapse	Chrnb4	cholinergic receptor, nicotinic, beta polypeptide 4	synapse	Nicotinic acetylcholine receptor signaling pathway (Panther pathway)		
synapse	Gabrr3	Hu:Gamma-aminobutyric acid receptor subunit rho-3	Hu: synapse	na		
migration/adhesion	Sema7a	sema domain, immunoglobulin domain (Ig), and GPI membrane anchor, (semaphorin) 7A	axon guidance	Axon guidance (Kegg pathway)	Itgb1	NrlP4-ve Itgb1 2.6
					plexin C1	NrlP4-ve Plxnc1 4.32
migration/adhesion	Jam2	junction adhesion molecule 2	tight junction	Tight junction (Kegg pathway), Cell adhesion molecules (Kegg pathway)	Jam3 Jam2 Magi1	NrlP4-ve Jam3 3.23 NrlP4+ve Jam2 -2.2 NrlP4-ve Magi1 2.69
				Leukocyte transendothelial migration (Kegg pathway), Cell adhesion molecules (Kegg pathway)	Itga4 Itgb1	NrlP4-ve Itga4 1.91 NrlP4-ve Itgb1 2.6
migration/adhesion	Podxl	podocalyxin-like	migration	na		
migration/adhesion	Ntng2	netrin G2	nuerite outgrowth	Axon guidance mediated by Slit/Robo (Panther pathway), Axon guidance mediated by netrin (Panther pathway)		

OS, outer segment; CC, connecting cilium; mem, membrane; PR, photoreceptor cells

Gene Symbol	NrlP4 +v-	CrxE15 +v-	CrxP4 +v-	Crx+ E15vP4	Crx- E15vP4
Prom1	9.19	1.24535	9.40123	-4.24424	1.77866
Cdhr1	27.1	4.21158	14.3479	-4.55181	-1.3361
Pcdh15	5.46	3.09258	2.87036	-6.92572	-7.46191
Ush2a	24.8	2.28418	7.01788	-3.4602	-1.12623
Sv2b	8.17	2.75689	16.9575	-3.62394	1.69731
Slc17a7	32.4	1.32034	3.17132	-2.62905	-1.09457
Chrna5	7.78	1.01644	3.47781	-1.87292	1.82686
Chrnb4	7.57	1.75116	4.6459	1.17311	3.11231
Gabrr3		1.56298	47.1376	-30.1713	-1.00042
Sema7a	5.03	-1.05654	3.64527	-3.12341	1.23306
Jam2	2.2	1.54415	5.52587	-2.86082	1.25089
Podxl	11.2	1.90941	4.76013	-1.97798	1.26037
Ntng2	5.03	1.88705	2.45379	-1.47233	-1.13228

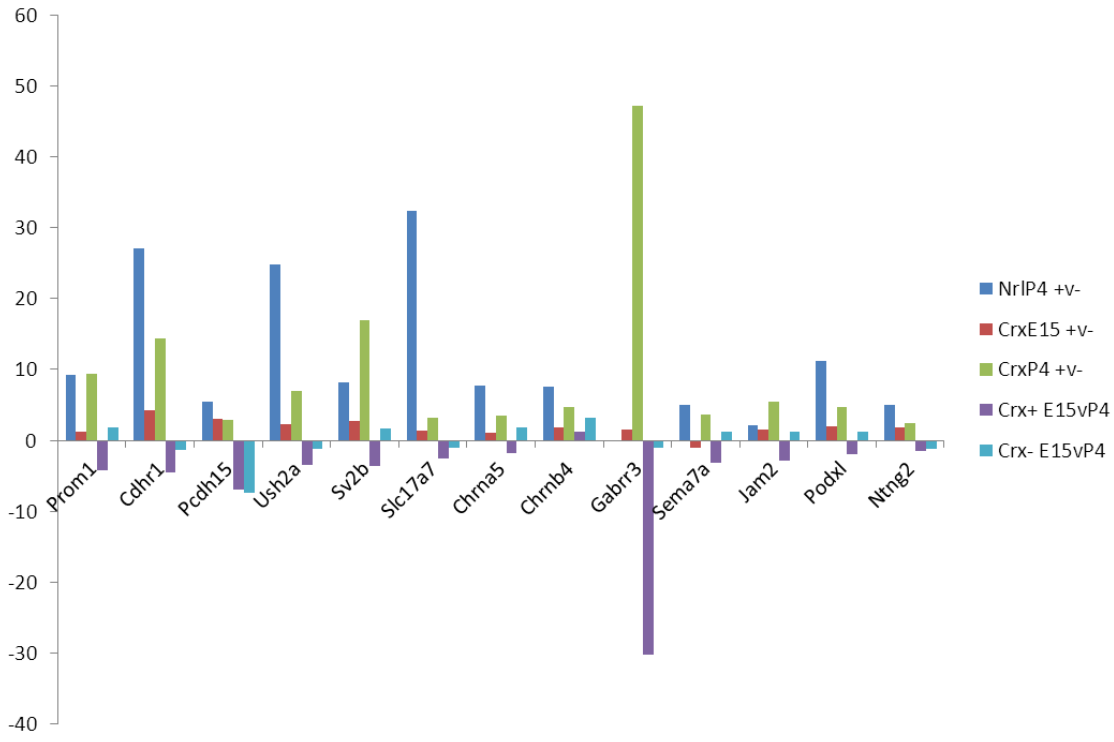

Figure 3.8 Expression fold changes of selected cell surface markers from microarray. (Top**) Table of the normalized expression fold changes of selected markers between different comparisons from the microarrays. (**Bottom**) Chart of the normalized expression fold changes. NrlP4 +v- : P4 NrlGFP+ve vs NrlGFP-ve; CrxE15 +v-: E15.5 CrxGFP+ve vs CrxGFP-ve; CrxP4 +v-: P4 CrxGFP+ve vs CrxGFP-ve; Crx+ E15vP4: CrxGFP+ve E15.5 vs P4; Crx- E15vP4: CrxGFP-ve E15.5 vs P4.**

Gene Symbol	E15+ve		E15-ve		P4+ve		P4-ve	
	Average	Stdev	Average	Stdev	Average	Stdev	Average	Stdev
Prom1	8.35821	0.028157	8.041653	0.095672	10.4437	0.14913	7.210867	0.219296
Cdhr1	6.47519	0.33671	4.400827	0.172311	8.66163	0.417646	4.818857	0.107789
Pcdh15	7.288985	0.363191	5.66017	0.399457	10.08096	0.38391	8.559717	0.231177
Ush2a	5.5172	0.567001	4.325523	0.188166	7.308053	0.328018	4.49702	0.109593
Sv2b	8.271455	0.035645	6.808413	0.340741	10.12903	0.08853	6.045163	0.134221
Slc17a7	4.870175	0.033524	4.46927	0.332747	6.26472	0.290027	4.599633	0.094689
Chrna5	6.55776	0.352464	6.53424	0.169071	7.463047	0.155706	5.66487	0.147782
Chrnb4	9.149725	0.454054	8.341417	0.239726	8.919387	0.632958	6.703427	0.044324
Gabrr3	4.7679	0.194723	4.123593	0.309595	9.683003	0.279764	4.124197	0.035193
Sema7a	5.576905	0.010981	5.65625	0.229596	7.220027	0.292322	5.354	0.069338
Jam2	9.545925	0.073475	8.91911	0.090159	11.06237	0.087387	8.596153	0.093131
Podxl	6.53793	0.482912	5.604807	0.162006	7.52196	0.608996	5.27096	0.259737
Ntng2	5.81083	0.100862	4.89469	0.115697	6.368927	0.350208	5.07392	0.015219

Figure 3.9 Absolute expression levels of selected cell surface markers from Crx microarray. (Top**) Table of the normalized absolute microarray expression levels of selected markers. (**Bottom**) Chart of the normalized expression levels. Error bar represent standard deviation (Stdev) from three independent samples except CrxE15.5+ve which includes two independent samples. E15+ve: E15.5 CrxGFP+ve; E15-ve: E15.5 CrxGFP-ve; P4 +ve: P4 CrxGFP+ve; P4-ve: P4 CrxGFP-ve;**

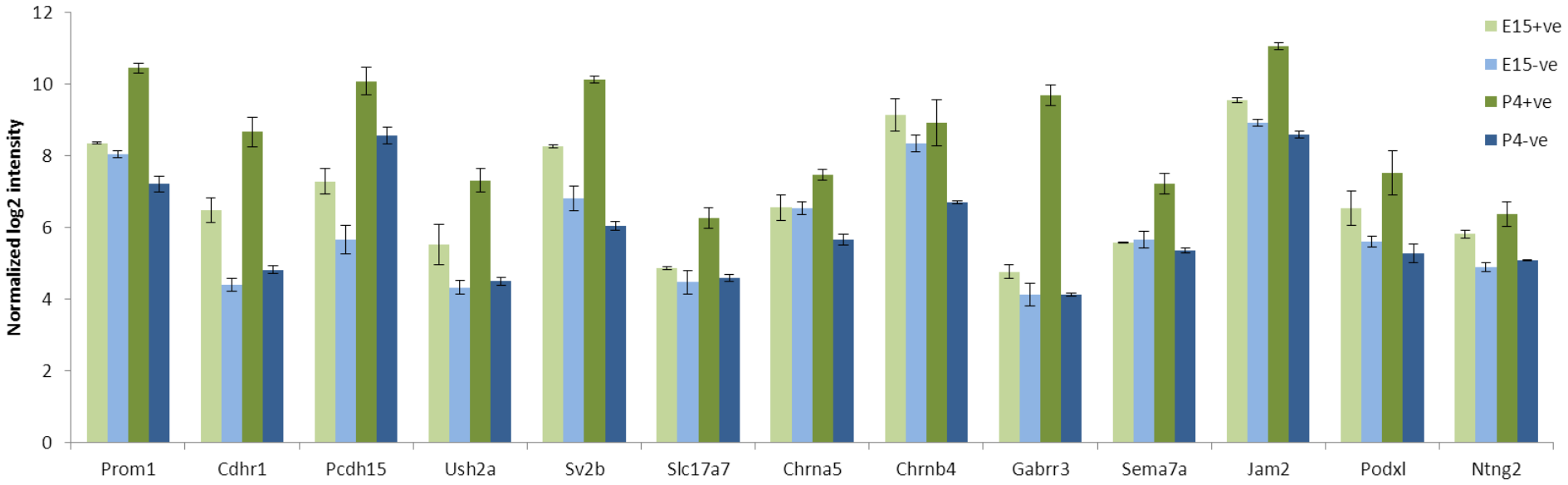

3.2.6 Quantitative RT-PCR validation of selected genes

To validate the microarray expression of the candidate genes, I performed qPCR for four genes of particular interest namely *Prom1*, *Sema7a*, *Cdhr1* and *Sv2b*. Prom1 was reported to interact with Cdhr1 in the cilium at the basement of outer segment involving outer segment formation (Yang, Chen et al. 2008). Sema7a is involved in axon guidance and cell migration interacting with Itgb1 and PlxnC1 (Pasterkamp, Peschon et al. 2003; Pasterkamp, Kolk et al. 2007; Scott, McClelland et al. 2009; Messina, Ferraris et al. 2011). Sv2b was detected in ribbon synapses of the mouse retina, in particular both rod and cone terminals (Rich, Zhan et al. 1997), interacting with laminins (Wang, Janz et al. 2003; Morgans, Kensel-Hammes et al. 2009). Knock out of *Sv2b* in mice reduced neurotransmission between photoreceptor cells and bipolar cells as well as the expression levels of synaptic vesicle proteins synaptotagmin, synaptophysin, and the vesicular glutamate transporter V-GLUT1 (Morgans, Kensel-Hammes et al. 2009). The qPCR expression trends of the four genes agree with the microarray and showed even greater expression fold changes between photoreceptor cells and other retinal cells (Figure 3.10). Expression of *Sema7a* was also higher in the E15.5 photoreceptor cells than other retinal cells according to qPCR despite the microarray indicating slightly higher expression in other retinal cells. Expression of *Prom1* was also examined in NrlGFP-sorted retinal cells, which showed similar expression fold changes as CrxGFP-sorted cells (around 20-fold, Figure 3.10 A, B, F). The expression levels of the four genes in photoreceptor cells as well as the expression fold changes between photoreceptor cells and other retinal cells were all higher in postnatal stages than embryonic stages, agreeing with the microarray data (Figure 3.10 F).

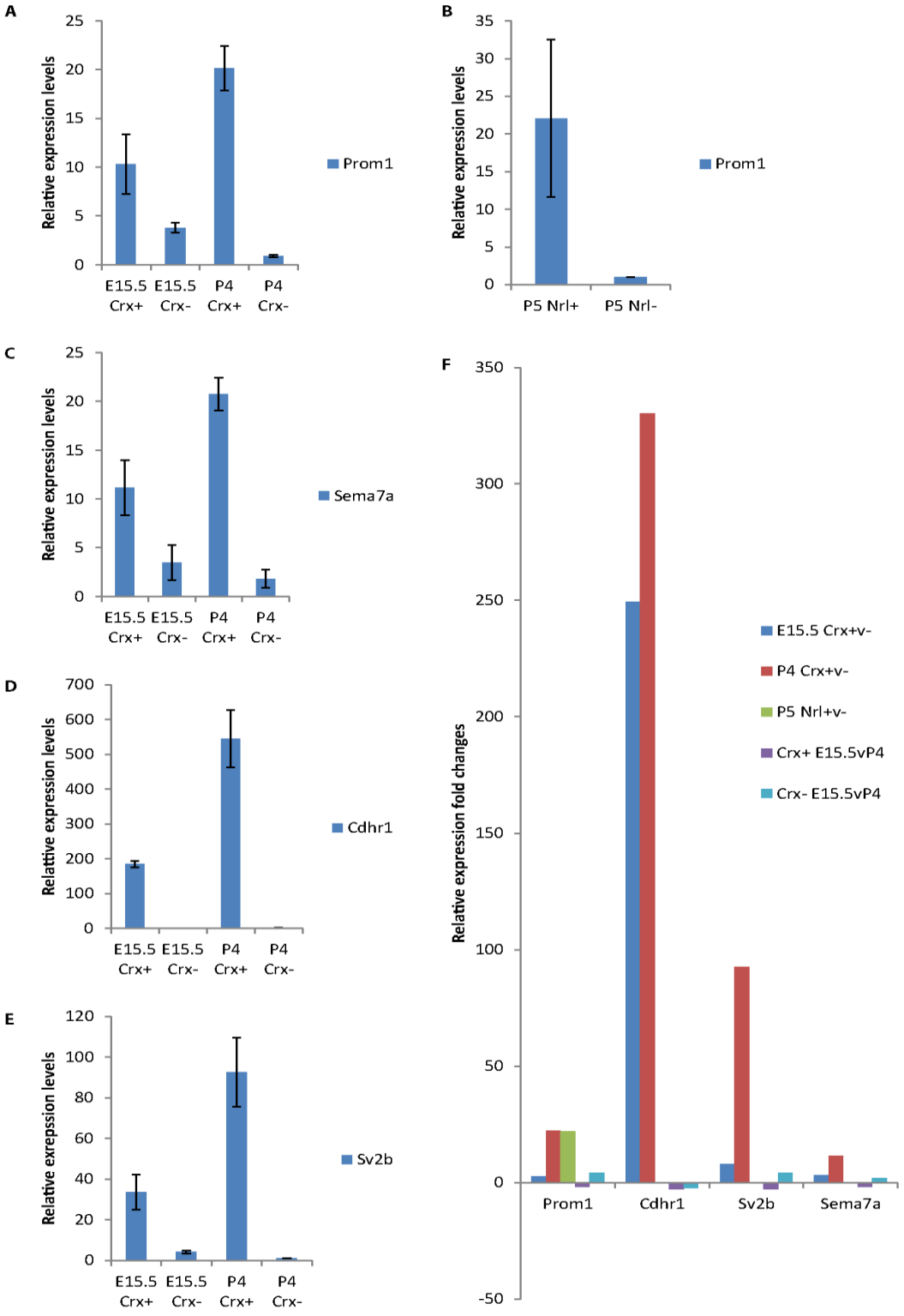

Figure 3.10 qPCR relative expression levels and fold changes of representative markers. Relative expression levels of Prom1 (A, B), Sema7a (C), Cdhr1 (D), and Sv2b (E) from CrxGFP or NrlGFP sorted E15.5 and P4-5 retinal cells. Error bar represent standard deviation of three independent samples. (F) Expression fold changes between comparisons for Prom1, Cdhr1, Sv2b and Sema7a. E15.5 Crx+v-: E15.5 CrxGFP+ve vs CrxGFP-ve; P4 Crx+v-: P4 CrxGFP+ve vs CrxGFP-ve; P5 Nrl+v- : P5 NrlGFP+ve vs NrlGFP-ve (only performed for Prom1); Crx+ E15.5vP4: CrxGFP+ve E15.5 vs P4; Crx- E15.5vP4: CrxGFP-ve E15.5 vs P4.

3.3 Discussion

Despite intensive microarray study in the retina (Dorrell, Aguilar et al. 2004; Hackam, Qian et al. 2004; Zhang, Xu et al. 2005; Liu, Wang et al. 2006; Punzo, Kornacker et al. 2009), rarely has this specifically focused on photoreceptor cells. Microdissection of ONL had been performed (Blackshaw, Fraioli et al. 2001), but contamination from progenitor cells and processes of other retinal neurons was not controlled. With the development of GFP-tagged photoreceptor transcription factor transgenic lines, specific isolation of photoreceptor cells from the retina is possible. Using these transgenic lines Akimoto et al has profiled the gene expression pattern of NrlGFP labelled rod photoreceptor cells and Nrl-knockout-GFP labelled "cone-like-rod" cells during development (Akimoto, Cheng et al. 2006). They also compared the GFP-sorted cells with the whole retina but not with none-photoreceptor retina cells, and hence were less likely to identify photoreceptor-specific properties and genes. During the course of my study, two photoreceptor microarrays after FACS selection of photoreceptor vs other retinal cells were reported: one is on P4 rod cells using a rhoEGFP transgenic line (Eberle, Schubert et al. 2011) and the other is on E17.5 photoreceptor cells using a bacterial artificial chromosome (BAC)-Crx-EGFP line (Muranishi, Sato et al. 2010). The latter studies identified 744 and 168 genes that were upregulated more than 2 fold in the EGFP+ve cells respectively though only limited transcriptome analysis was performed and the array data from only one of these was deposited in public databases. The embryonic photoreceptors I studied are from E15.5 retina which is the earliest time point so far used for photoreceptor microarray. Thirdly, comparison of the E15.5 and P4 photoreceptor microarray revealed specific genes and properties that may be associated with efficient integration and formation of cones after transplantation.

The rod-specific genes reported in the rhoEGFP study (*rhodopsin*, *Pde6b*, *Gngt1*, *recoverin*) and the cell surface markers it reported (*Cd73*, *Cnga1*, *Gje1*, and *Pcdh15*) (Eberle, Schubert et al. 2011) were also present in my study. The BAC-Crx-EGFP study identified 168 genes at E17.5 showing more than 2-fold higher expression in CrxGFP+ve cells than CrxEGFP-ve cells (Muranishi, Sato et al. 2010) whereas I only identified 63 genes at E15.5. This is probably because more transcripts are expressed at later developmental stages than earlier stages as I found 627 genes showing more than 2-fold higher expression in CrxGFP+ve cells at P4. However, I do not exclude the possibility of different sensitivity between my array and Muranishi's array. Similar to the E17.5 photoreceptor array, most of the E15.5 transcripts are transcription factors such as *Otx2*, *NeuroD1*, *Neurod4*, *Meis2*. The genes encoding cone specific proteins reported in the E17.5 array were also present in the E15.5 array (such as *Thrb* and *Opn1sw* but not *Rxrγ*). In addition, I also found *Cngb3* and *Pde6c*, which are more recently

known as cone-specific, present in the E15.5 array (as well as the CrxP4 array) and will be discussed further in section 3.3.1.

3.3.1 The properties of photoreceptor precursor cells

By comparing the CrxGFP or NrlGFP positive versus negative cells, I was able to find the unique transcriptional properties of the photoreceptor precursor cells. Genes within these cells are particularly the ones encoding proteins involved with visual perception, detection to stimulus, and photoreceptor development. These are expected transcriptional properties specifically belonging to photoreceptor cells, and hence demonstrate the accuracy of the microarray analysis. Interestingly, I also found significant enrichment of genes encoding cell projection proteins, in particular genes encoding proteins associated with cilia, which were significantly enriched in the P4 photoreceptor cells, but not other retinal cells of the same stage. The cilium is a very specialized structure on many polarized cells. Much cilia work to date focuses on intracellular molecules which are involved in the genesis of cilium, yet functions, working mechanisms, and detailed subcellular locations of many cilium cell surface molecules are still poorly defined. Some of these molecules will be further studied in Chapter 5 (section 5.2).

Photoreceptor precursors at embryonic stages showed some commitment to photoreceptor differentiation, but remain largely unspecified. One of the major molecular activities of these cells was transcription regulation which agrees well with the early status of these cells and the E17.5 Crx-EGFP array study (Muranishi, Sato et al. 2010). Similarly, the E15.5-specific photoreceptor genes produced by further secondary comparison of the E15.5 versus P4 photoreceptor-specific gene sets were highly focused on transcription regulation, embryonic development, and metabolic process, and not many transcripts showed specific cellular localization. In contrast, the P4-specific genes showed a highly spread-out pattern in many specific functions such as ion binding (eg. *Cadm3, Ppp2r3a, Galnt4, Clstn1*), channel activity (eg. *Grik1, Grik3, Chrna5, Chrnb4*), lipid binding (eg. *Snx14, Cpne6, Fabp12, Nr3c1, Arhgap29*), transcription factor binding ((eg. *Dcc, Ncoa2, Kat2b, Hipk3, Nlk*), phosphoric diester hydrolase activity (eg. *Pde6a, Pde6b, Plcl1, Smpdl3a*), and so on. Importantly, the P4-specific genes enriched lots of cell projection transcripts for cilia and synapses (eg. *Gnat1, Rp1, Bbs4/5/7/9, Rpgr, Ttc30a2, Pcdh15, Ttc8, Cnga1, Plekhb1, Arr3, Cep290*). The limited transcriptional properties of the E15.5 photoreceptor cells and their lack of specific genes encoding cell projection proteins may be associated with their low integration efficiency after transplantation. In contrast, appearance of large amounts of various new transcripts, especially the enrichment of many genes encoding cell projection proteins, along with other diversified detailed functions and properties probably enable the P4 precursor cells more

readily incorporated into the host environment, hence showing higher integration efficiency after transplantation.

In addition to the stage specific genes, the above secondary comparison also revealed common genes and properties for the early and late photoreceptor precursors. This not only included the expected genes encoding photoreceptor-specific transcription regulation factors (*Crx*) and sensory perception proteins (*Pdc*), but also many genes encoding cell projection proteins. Genes in this set seem to be of particular interest as both genes specific to cone photoreceptor cells and genes encoding cell projection proteins can be found here such as *Thrb*, *Pde6c* and *Cngb3*. *Pde6c* encodes the cone-specific alpha subunit of cGMP phosphodiesterase thus playing essential role in cone phototransduction. Mutations of *Pde6c* have been associated with early onset of cone disorders including progressive cone dystrophy (Thiadens, den Hollander et al. 2009), achromatopsia (Chang, Grau et al. 2009; Grau, Artemyev et al. 2011) and cone-rod dystrophy (Huang, Zhang et al. 2013). Containing three extracellular domains, *Cngb3* is specifically involved in the electrical response and cation channel opening of cones (Gerstner, Zong et al. 2000) and its deficiency is associated with retinal disorders characterised by the loss of cones (Kohl, Baumann et al. 2000; Sundin, Yang et al. 2000; Xu, Morris et al. 2011). *Cngb3* mutations were also found in patients with cone-rod dystrophy (Huang, Zhang et al. 2013). In our array, *Cngb3* showed much higher expression fold-changes in the E15.5 CrxGFP+ve and CrxGFP-ve comparison than in the P4 comparison and will be discussed further in Chapter 5 (section 5.2.1).

3.3.2 Cell surface markers for photoreceptor precursor cells

I used two approaches to search for photoreceptor cell surface markers. By searching for CD molecules, I found 10 CD markers expressed more than two-fold in photoreceptor cells compared with other retinal cells from the Crx and Nrl array. By searching with functional annotations in these arrays, I found 227 candidates with two-fold higher expression in photoreceptor cells. Applying more stringent criteria including more than five-fold expression changes, containing confirmed extracellular domains, and function in cilium/synapses/ migration/adhesion prioritized 13 markers of particular interests. These 13 candidates not only showed high expression fold changes between photoreceptor cells and other retinal cells, but also high absolute expression levels in photoreceptor cells. The axon guidance molecule Sema7a was rarely reported in retina and was studied further in Chapter 4 as a candidate molecule possibly involved in photoreceptor migration and ONL organization. The cilia protein Prom1 was studied further in Chapter 5 for the cilia property of photoreceptor cells which may

be involved in photoreceptor orientation, and in Chapter 6 as a biomarker to label photoreceptor cells for transplantation along with CD73 and CD24.

4 The role of cell surface molecule Sema7a on migrating photoreceptor cells in the retina

4.1 Introduction

The mature retina is a laminated neural tissue, organised in three layers of neurons separated by two plexiform layers composed of axons and synapses. This complex structure develops from the pseudostratified neuroepithelium of the embryonic optic cup. Multipotential RPCs from this single layer of optic cup gradually differentiate into different neurons which orient themselves and migrate into their destined positions and finally form all the confined layers. However, the molecular mechanisms governing layer formation are not well understood. Some semaphorins were recently shown to be involved in the correct lamination of the inner retina (Matsuoka, Chivatakarn et al. 2011; Matsuoka, Nguyen-Ba-Charvet et al. 2011). For example, Sema6a is expressed in the IPL and GCL directing lamina-specific neurite arborisation of tyrosine hydroxylase (TH)-expressing dopaminergic amacrine cells, intrinsically photosensitive RGCs (ipRGCs) and calbindin-positive cells via interaction with PlexinA4 (Matsuoka, Nguyen-Ba-Charvet et al. 2011). Sema5a and Sema5b are transiently expressed in the ONBL of the postnatal retina as repulsive molecules to prevent neurite mistargeting of the majority of RGCs, amacrine cells, and bipolar cells via interaction with PlexinA1 and PlexinA3 (Matsuoka, Chivatakarn et al. 2011). However, no molecules have been reported to be involved in the correct lamination of the outer retina, in particular the photoreceptor layer. I, therefore, am interested in finding out cell surface molecules with such functions. This is because although there will be other signals in play such as secreted proteins, chemical and physical stimuli, presence or absence of the proteins at the surface of the migrating cell will almost certainly be a major influence on cell migration and development of the laminated retinal structure. Furthermore, identifying the cell surface molecules that mediate the migration and integration process of the cells following transplantation and correct orientation and organisation within the ONL may aid efforts to repair the retina via photoreceptor transplantation in diseases causing photoreceptor degeneration. My colleagues have previously shown that subretinally transplanted photoreceptor precursor cells can migrate into the ONL and differentiate into correctly integrated photoreceptors (MacLaren, Pearson et al. 2006; Lakowski, Baron et al. 2010; Pearson, Barber et al. 2012). However the processes and mechanisms involved are not understood.

The semaphorins were discovered in 1993 as a family of membrane-associated and secreted proteins (Kolodkin, Matthes et al. 1993). Over 20 members have been identified so far.

Although some of them have been shown to be involved in immune cell regulation (Suzuki, Okuno et al. 2007), organ morphogenesis (Behar, Golden et al. 1996), tumor suppression (Tomizawa, Sekido et al. 2001), and vascularization (Serini, Valdembri et al. 2003; Gu, Yoshida et al. 2005), the semaphorins were largely known for their function in axon guidance and synapses formation. Therefore, the semaphorins seems to be good candidates as cell surface molecules involved in organisation of photoreceptors within the ONL. However, not many semaphorins were known to be expressed in the eye. In addition to Sema6a and Sema5a/5b mentioned above, earlier it was also found that Sema4a is expressed in the GCL, INL and RPE and its deficiency results in disorganized outer segments of photoreceptor cells (Rice, Huang et al. 2004). Yet, semaphorins expressed in the photoreceptor cells remained unknown.

In my microarray screen for cell surface molecules which are highly transcribed in photoreceptor cells, Sema7a was identified as being of potential interest because of its involvement in axon guidance and higher expression in photoreceptor cells than other retinal cells (Chapter 3, Table 3.2 to Table 3.5). Although it has been reported in other systems there is little information about Sema7a in the retina, except one *in situ* hybridization study showed Sema7a expression in RGC at E15 and further in IPL, lens, and lens epithelium at E19 (Pasterkamp, Kolk et al. 2007). A total of 17 semaphorins were identified in our arrays (Table 4.1). Three semaphorins were found to be expressed higher in photoreceptor cells: Sema3f, Sema4b and Sema7a, with Sema7a showing more than 5-fold higher expression in rod photoreceptor cells (5.03 FC) and Sema3f and Sema4b showing less than 2-fold higher expressions (1.79FC and 1.31FC respectively). I also found 14 semaphorins more highly expressed in other retinal cells which include Sema6a (6.87FC), Sema5a (5.28FC), Sema5b (3.25FC), Sema3a (3.1FC), Sema4g (2.95FC), Sema4d (2.62FC), Sema4a (2.43FC), Sema6d (2.14FC), and Sema4f (2.1FC).

All semaphorin family members contain a relatively conserved N terminus extracellular semaphorin (sema) domain and a class-specific C terminus which differs in membrane anchorage and additional sequence motifs. Based on these overall structures as well as phylogenetic tree analyses, the semaphorins were grouped into eight classes (Figure 4.1 A) (Semaphorin-Nomenclature-Committee 1999). Class 1 and 2 are invertebrate semaphorins which include Sema-1a, Sema-1b, and Sema-2a. Class 3 to 7 are expressed in vertebrates which include Sema3 A-F, Sema4 A-G, Sema5 A-B, Sema6 A-C, and Sema7A. The 8th class are the viral semaphorins which are named as Class V. Other than the viral and the class 2 and 3 semaphorins which are secreted, all other semaphorins are associated with membranes. Of these, while class 1, 4, 5 and 6 semaphorins contain a transmembrane domain in their C

terminus, Sema7a is attached to the membrane via a glycosylphosphatidylinositol (GPI)-anchor. Structure of Sema7a without the GPI-anchor mimics the viral semaphorin A39R secreted by smallpox virus (Liu, Juo et al. 2010).

Table 4.1 Semaphorins expressed in the Crx and Nrl array

Name	P4 Nrl- vs. +	E15.5 Crx+ vs. -	P4 Crx+ vs. -	Crx+ E15.5 vs. P4	Crx- E15.5 vs. P4
Sema7a	**-5.03**	-1.05654	3.64527	-3.12341	1.23306
Sema3f	-1.79	1.30482	1.55983	-1.12193	1.06552
Sema4b	-1.31				
Sema6a	**6.87**	-1.4142	-3.70638	2.05435	-1.27575
Sema5a	**5.28**	-1.35661	-4.70013	-1.11271	-3.85511
Sema5b	3.25				
Sema3a	3.1	-1.38269	-2.58841	4.59939	2.45692
Sema4g	2.95				
Sema4d	2.62	-1.7785	-1.93483	1.09753	1.00885
Sema4a	2.43	-1.26067	-1.49504	1.12616	-1.05305
Sema6d	2.14				
Sema4f	2.1				
Sema3e	1.89	-2.33023	-2.2827	1.10998	1.13309
Sema6b	1.62				
Sema3b	1.24				
Sema4c	1.24				
Sema3d	1.2				

Semaphorins in green indicates expression higher in photoreceptor cells, in blue indicate higher in other retinal cells. Expression fold changes were presented for P4 Nrl- vs. +, P4 NrlGFP-ve vs P4 NrlGFP+ve; E15.5 Crx+ vs. -, E15.5 CrxGFP+ve vs E15.5 CrxGFP-ve; P4 Crx+ vs. -, P4 CrxGFP+ve vs P4 CrxGFP-ve; Crx+ E15.5 vs. P4, CrxGFP+ve E15.5 vs P4; Crx- E15.5 vs. P4, CrxGFP-ve E15.5 vs P4.

Initially identified as a ligand-receptor pair through an *in vitro* binding assay, Sema7a was shown to bind to PlexinC1 (PlxnC1) (Tamagnone, Artigiani et al. 1999). However, two later experiments in olfactory neurons and activated T cells respectively suggested that Sema7a may actually bind to integrin β1 (Itgb1) or integrin α1β1 rather than PlxnC1 to promote axon outgrowth (Pasterkamp, Peschon et al. 2003) or induce inflammation (Suzuki, Okuno et al. 2007). Interestingly, a later crystallographic analysis of the Sema7a mimic A39R alone showed that the proposed integrin binding site – a three amino acid RGD motif (arginine-glycine-aspartic acid)– was actually buried and unlikely to be recognized by integrins (Liu, Juo et al. 2010), which indicates either Sema7a does not bind to integrins directly or it has a different conformation when binding to integrins. Crystallography of Sema7a/PlexinC1 complex showed, however, clearly that Sema7a inserts its 4c-4d loop into the groove of PlexinC1 and forms

several salt bridges (Figure 4.1 B and C) (Liu, Juo et al. 2010). The interaction interface extends between residues 202-376 of the Sema domain. It also showed that Sema7a has a homodimer interface within residues 250-405 in human (248-403 in mouse) and proposed that Sema7a may form homodimers which then interact with PlxnC1 and induce PlxnC1 dimerization (Figure 4.1 B) (Liu, Juo et al. 2010). Therefore, it remains perplexing as to which receptors Sema7a interact with *in vivo*. It is possible that in different systems Sema7a might interact with different receptors or both receptors but under different mechanisms.

In this chapter I analysed expression of Sema7a protein in the retina and colocalisation with its two putative receptors, PlexinC1 and integrinβ1. I sought to find out which receptor Sema7a is interacting with in the retina and to investigate the hypothesis that Sema7a interactions are important for orienting and organising developing photoreceptor precursors within the ONL.

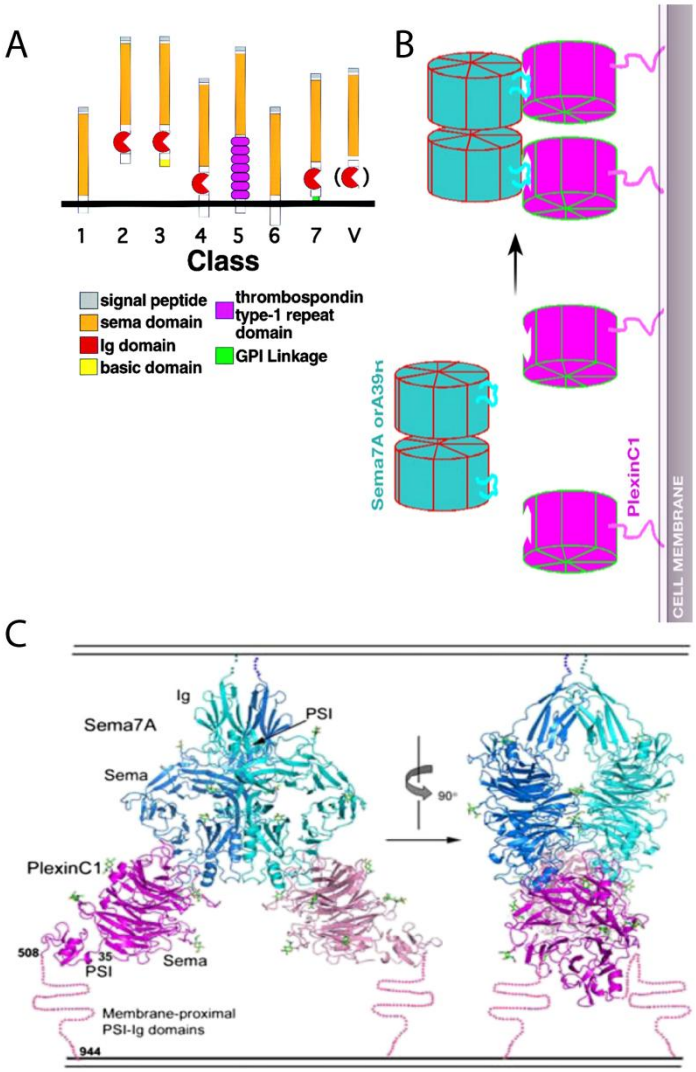

Figure 4.1 Semaphorin classes and Sema7a structure. (A) Semaphorin classes. Adapted from (Semaphorin-Nomenclature-Committee 1999) (B) Illustration of Sema7a dimers interacting with PlexinC1. Adapted from (Liu, Juo et al. 2010). (C) Crystallography structure of Sema7a dimers with PlexinC1. PSI, domains found in Plexins, Semaphorins and Integrins. Adapted from (Liu, Juo et al. 2010).

4.2 Results

4.2.1 Conservation of Sema7a

Based on current genome annotations, the amino acid sequence of human SEMA7A was compared with chimpanzee, dog, cattle, rat, mouse, chicken, and zebrafish to assess conservation. Other than the homologues from chicken and zebrafish which showed less than 50% sequence identity, all other mammalian homologues showed over 80% sequence identity (and mouse showed 89.6% identity) (Table 4.2). Like other semaphorins, Sema7a has a signal peptide (44 amino acid, aa) and a sema domain (~ 436 aa) on the N terminus (Figure 4.2). On its C terminus, Sema7a has a 39 aa Plexin repeat, an 86 aa Ig-like C2-type immunoglobin domain, and an Alanine lipidation site for GPI-anchor. There are five glycosylation sites on the extracellular domains, four of them on the sema domain and one on the Ig domain. There is also the RGD motif within the sema domain predicted for cell attachment or integrin binding. All these structural features are conserved from human to mouse (Figure 4.2). For the lower vertebrate animals, although they maintain the sema domain albeit in a smaller form, several structure elements or features that have emerged in mammals do not seem to be conserved in these species such as the signal peptide, the RGD motif, the lipidation site, and the glycosylation sites (Figure 4.2).

Table 4.2 Sema7a pairwise alignment score

Gene			Identity (%)	
Species		Symbol	Protein	DNA
H.sapiens	Human	SEMA7A		
vs. P.troglodytes	Common chimpanzee	SEMA7A	98.8	99.2
vs. C.lupus	Dog (Gray wolf)	SEMA7A	90.3	89.1
vs. B.taurus	Cattle	SEMA7A	84.2	86.7
vs. M.musculus	House mouse	Sema7a	89.6	87.9
vs. R.norvegicus	Brown rat	Sema7a	89.4	87.5
vs. G.gallus	Chicken (Red Junglefowl)	SEMA7A	49.7	59
vs. D.rerio	Zebrafish	sema7a	38	46.4

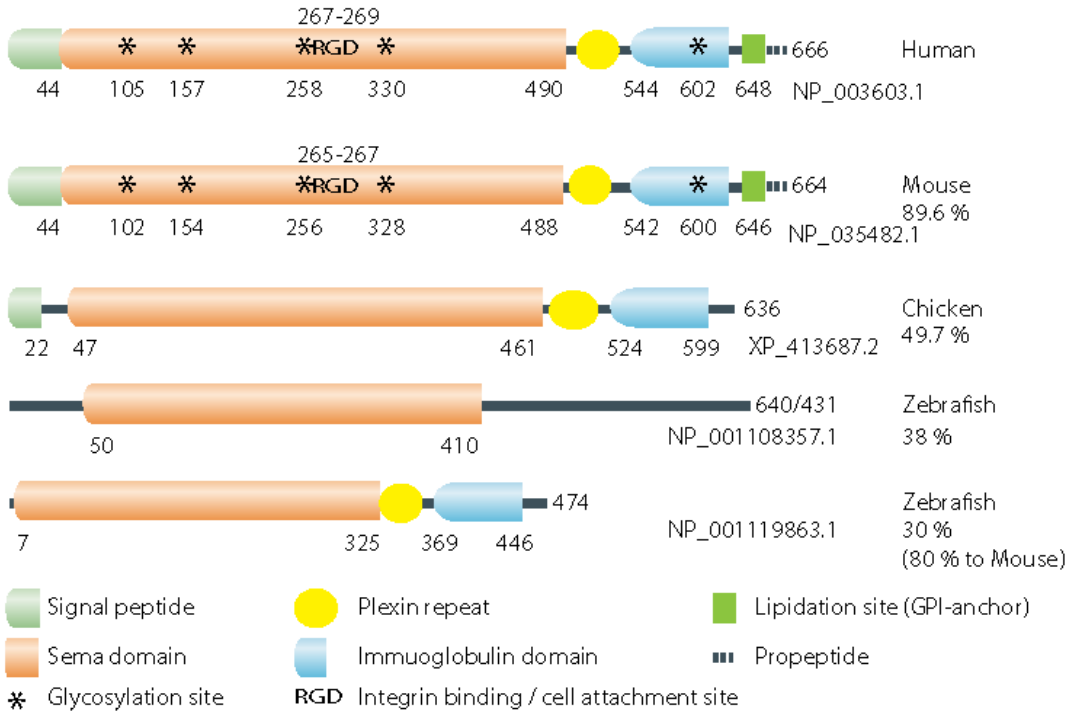

Figure 4.2 Domain organization of Sema7a from Human to Zebrafish. The total number of amino acid residues is shown on the right (uniprot/NCBI) near protein accession number. The percentage of sequence identity with human is shown under species names (performed in NCBI blast).

4.2.2 Sema7a expression in the mouse retina

According to the qPCR analysis (Chapter 3, Figure 3.10), the Sema7a transcript is more than 10-fold and 20-fold higher in CrxGFP FACS sorted photoreceptor cells than other retinal cells at E15.5 and P4 respectively in the mouse retina. I next examined Sema7a protein localisation in the adult and developing retina.

IHC in adult mouse retina showed Sema7a was highly localised in the IS of photoreceptor cells and in the OPL. It was also found as clustered dots on the surface of photoreceptor cell bodies although the levels were lower than the process regions. Sema7a expression was also found in INL and IPL of the inner retina, but the levels were lower than that of the outer retina. In the GCL, however, high levels of Sema7a expression was found on some ganglion cells at the cell bodies and/or the axons (Figure 4.3 A top row).

Specificity of the Sema7a antibody was demonstrated by pre-incubation of the antibody with the peptide that it was raised against in blocking solution before it was incubated with the eye sections. The peptides successfully bind all the antibodies in the solution and no signals can be detected from the sections (Figure 4.3 A middle row), similar with the control where primary antibody was omitted (Figure 4.3 A bottom row). Further, Sema7a antibody only recognized

the expected 75 KD band and the glycosylated form of the adult retina lysates in western blots (Figure 4.3 D and Appendix figure 4.2).

I then went on to examine the developmental expression profile of Sema7a in retina using the CrxGFP transgenic mice which labels the photoreceptor cells (Figure 4.3 B). With higher expression at the apical regions of the developing photoreceptor cells, Sema7a protein can be detected in the whole E15.5 retina. Slightly higher expression remained in the apical region of the ONBL in the early postnatal days (Figure 4.3 B, P1 and P4), and the expression level in the whole retina seems to increase along development. Interestingly, I noticed some individual cells showed particular high levels of Sema7a expression at P4, and some of them were also CrxGFP+ve and appeared as if they were migrating in the retina (Figure 4.3 B, P4, arrow heads).

As the retina began to form different layers from P8 onwards, Sema7a expression seems to be particularly higher at the regions where the borders of the layers are going to form (Figure 4.3 B', P8 and P21). It is highly expressed at the segment regions of the photoreceptor layer, the synapse regions between the photoreceptor layer and bipolar/amacrine cell layer (ie. the OPL), as well as the synapse regions between the INL and GCL (ie. the IPL). Sema7a co-staining with Prom1 which localises at the basement of the OS (see Chapter 5 for study of Prom1) showed that Sema7a expression was below Prom1 demonstrating that Sema7a localises in the inner segments (Figure 4.3 C).

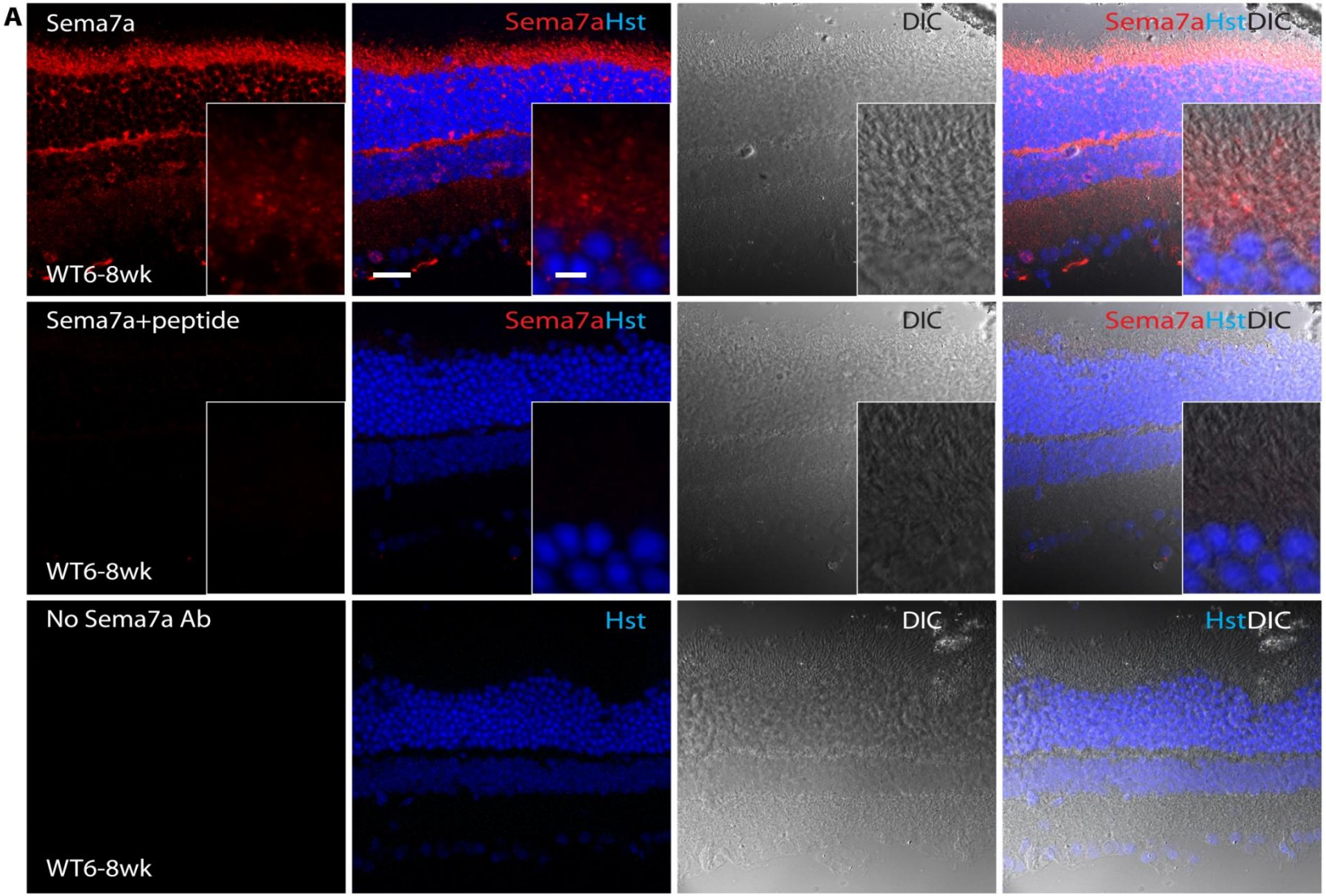

Figure 4.3 Sema7a expression in the retina (continues). (A) Sema7a IHC with blocking peptide on adult eye sections. The wild-type (WT) 6 – 8 weeks adult eye sections were incubated alone with Sema7a antibody (top row), or pre-incubated with the Sema7a peptide followed by co-incubation with Sema7a antibody (middle row), or without the Sema7a antibody (bottom row). Scale bars represent 25 µm except in inserts which represent 5 µm.

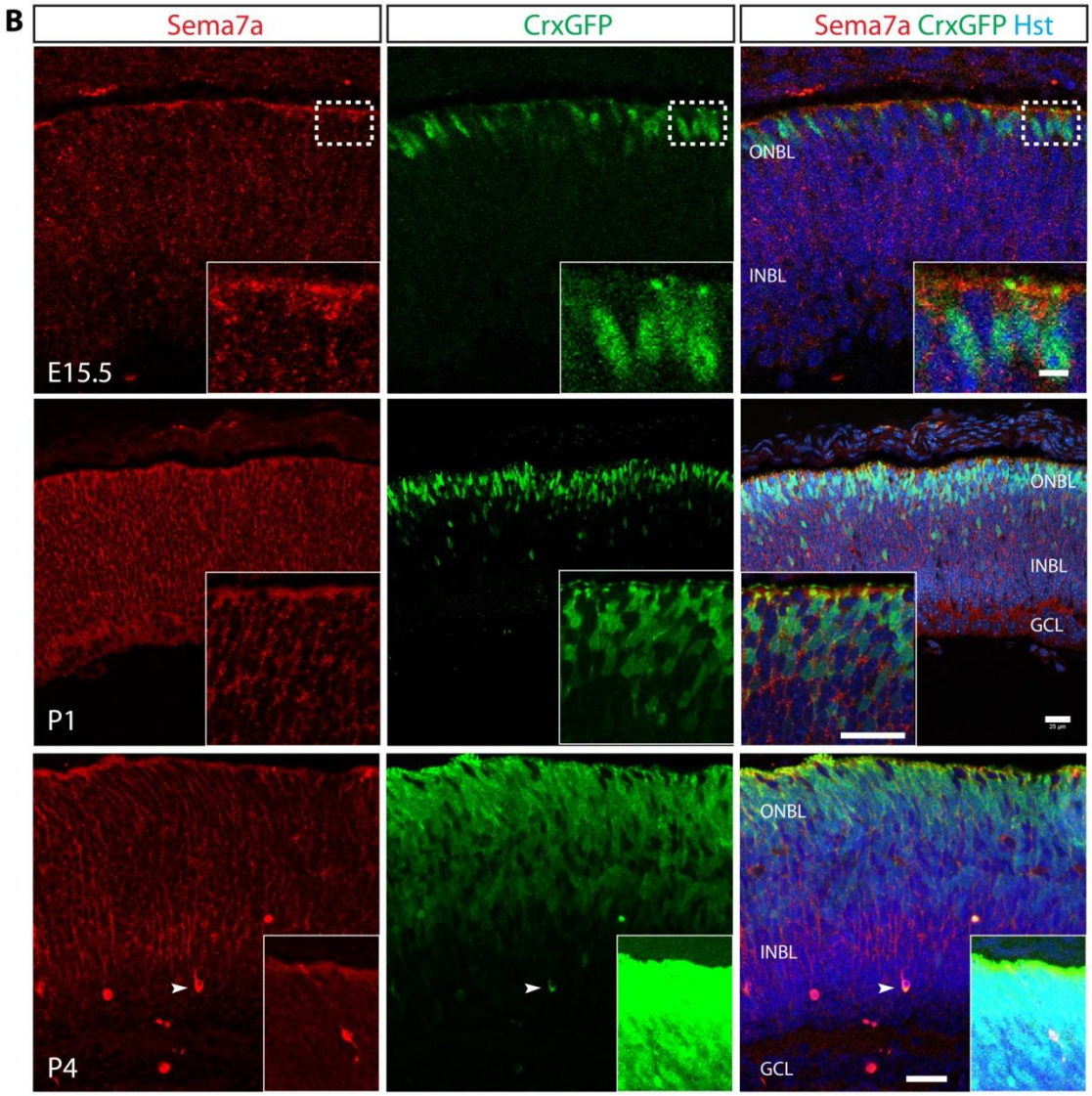

Figure 4.3 Sema7a expression in the retina- continued. (B) Sema7a expression profile in CrxGFP retinal sections along development (E15.5 – P4). Inserts in the P4 retina represent Z-projections. Arrow heads indicate Sema7a+ve CrxGFP expressing cells. Scale bars represent 25 µm except in inserts of top row (E15.5) which represent 5 µm.

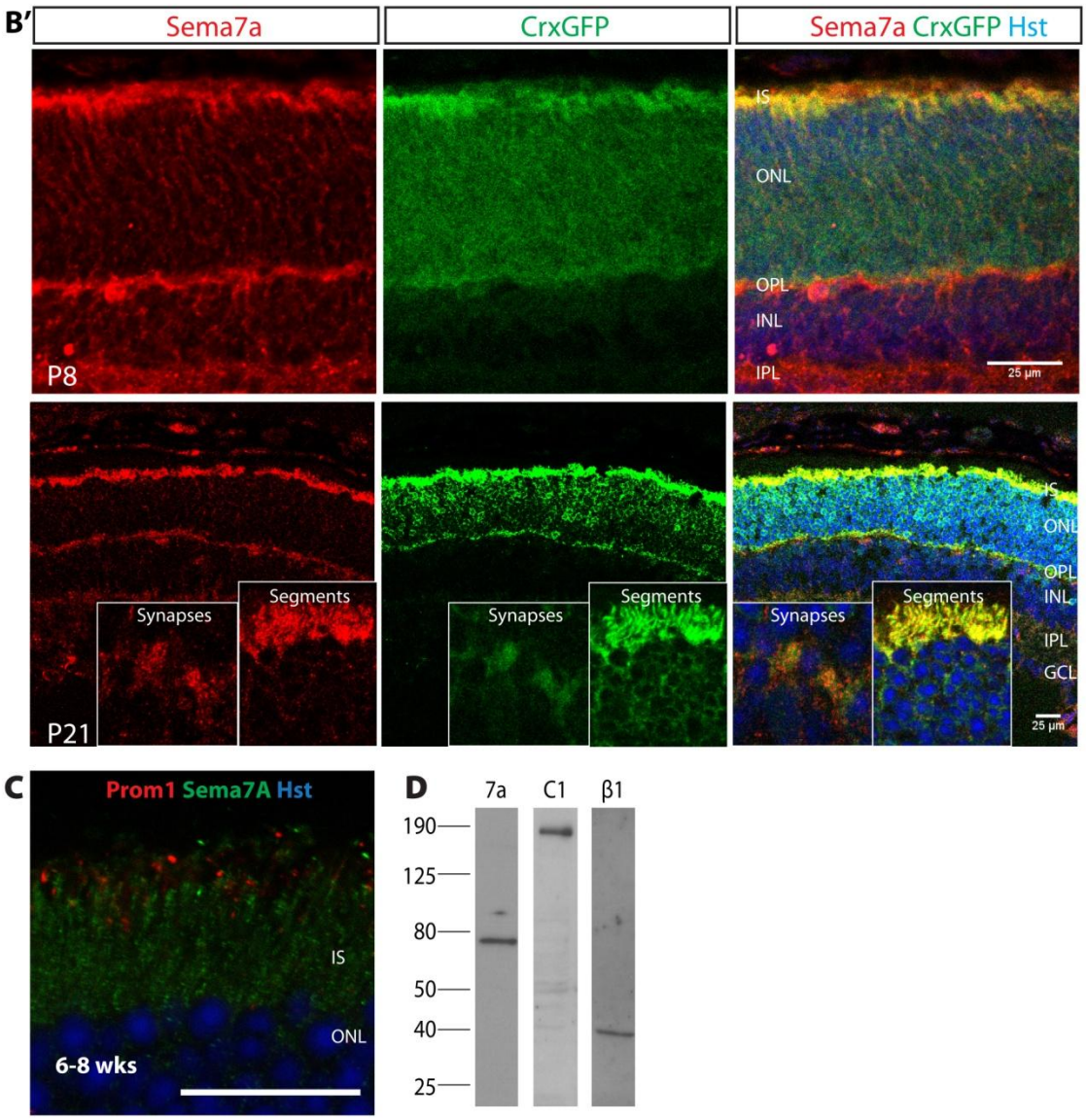

Figure 4.3 Sema7a expression in the retina- continued. (B') Sema7a expression profile in CrxGFP retinal sections along development (P8 – P21). (C) Sema7a costain with Prom1 in adult mouse retina. Scale bars represent 25 µm. (D) Western of Sema7a, PlexinC1, and Integrinβ1 from adult mouse retina lysates. Expected sizes of Sema7a, PlexinC1, and Integrinβ1 are 75 KD (100 KD if glycosylated), ~200 KD and 40KD respectively. Full image of Western blot in Appendix figure 4.2.

4.2.3 Sema7a receptors' expression profiles in the mouse retina

IHC of Itgb1, one of the Sema7a receptors, during eye development shows that the protein was expressed highly in peripheral tissues of retina, but not within the retina (Figure 4.4). It was also expressed in some vascular cells in the retina, but did not seem to be expressed on any neurons.

PlxnC1, the other receptor of Sema7a, was clearly expressed in the retina throughout development (Figure 4.5). It was expressed in both the photoreceptor cells and other retinal neurons. At later stages, its expression became higher in the inner retina, particularly the IPL, and seemed to form an increasing gradient from outer retina to inner retina, in contrast to the distribution of Sema7a which appeared higher in the outer and lower in the inner retina (see Figure 4.3). In adults, expression of PlxnC1 clearly showed the sublayers of the IPL.

To assess the relative localization of Sema7a and its receptors directly, I co-labelled Sema7a and its receptors using different fluorochromes on the same sections (Figure 4.6). Agreeing with the single labelling experiments, no co-localization between Sema7a and Itgb1 was observed. However, PlxnC1 largely colabelled with Sema7a in early postnatal stages. Punctate dots which showed colocalization of both markers on the boarder of cell bodies were clearly observed. The majority of the cells in the P4 retina were positive for both PlexnC1 and Sema7a, including the Sema7a-high expression cells. Despite the overall colocalization, there were a few punctate dots on some cells in the ONBL that showed single immunostaining of either Sema7a or PlexnC1 alone (solid or empty arrow heads) showing presence of domains on the cell surface where the two molecules did not colocalize. The colocalizations in the adults seem to be less than that of the postnatal stages (Appendix figure 4.1). At the segment region of photoreceptor cells where Sema7a strongly immunostained, PlxnC1 signals were weak. And in the IPL I observed strong signals from PlxnC1 but not Sema7a. Where there were colocalizations between Sema7a and PlxnC1, they are shown as punctate dots on the cell bodies of photoreceptor cells or horizontal cells. Hence, I conclude that Sema7a did not colabel with Itgb1, but largely colabels with PlxnC1 as punctate dots on the surface of cell bodies of many retinal cells including photoreceptor cells.

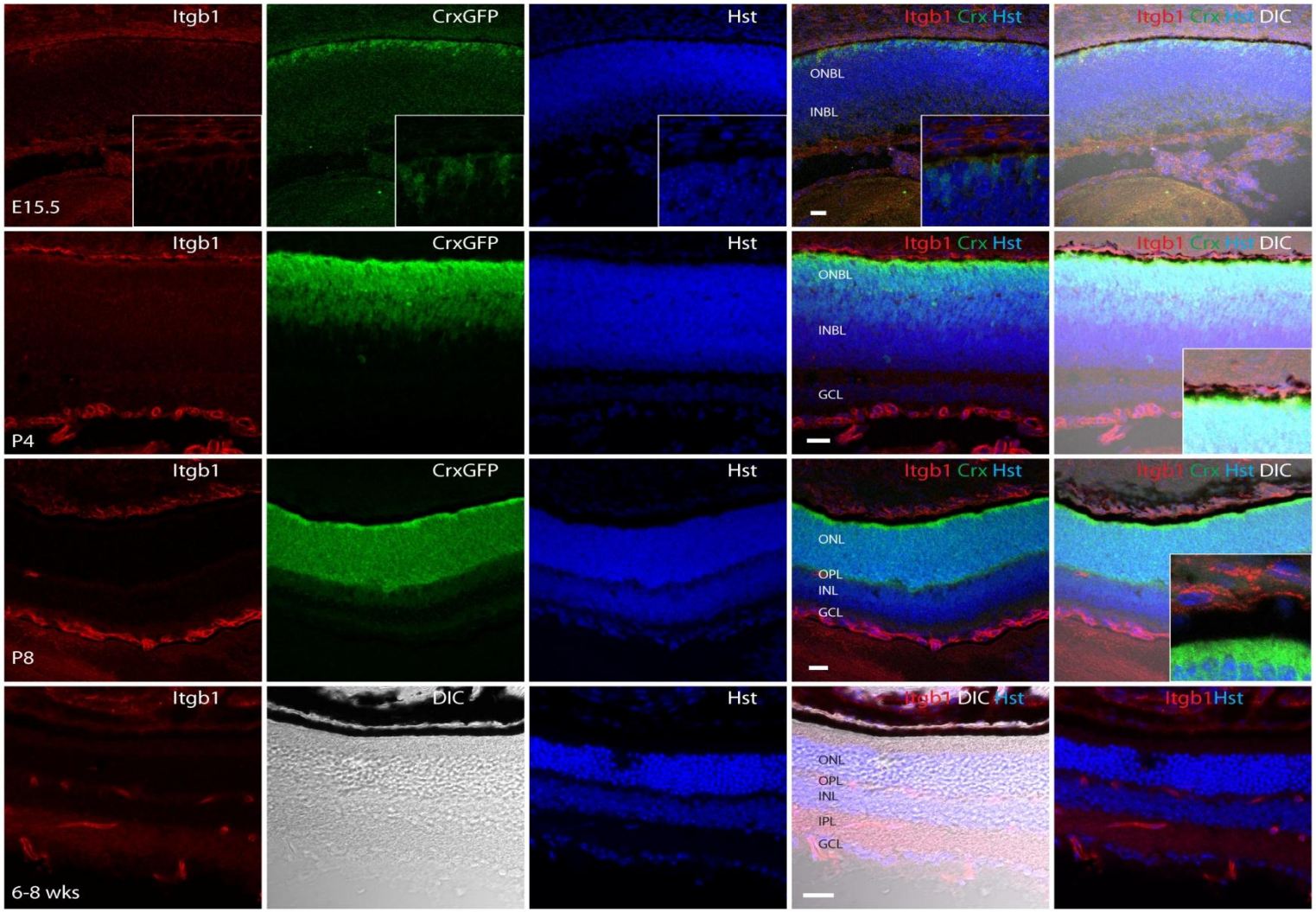

Figure 4.4 Itgb1 expression profile along retina development. Itgb1 Immunohistochemistry on E15.5, P4, P8 CrxGFP eyes and adult WT eyes. Scale bars represent 25 µm.

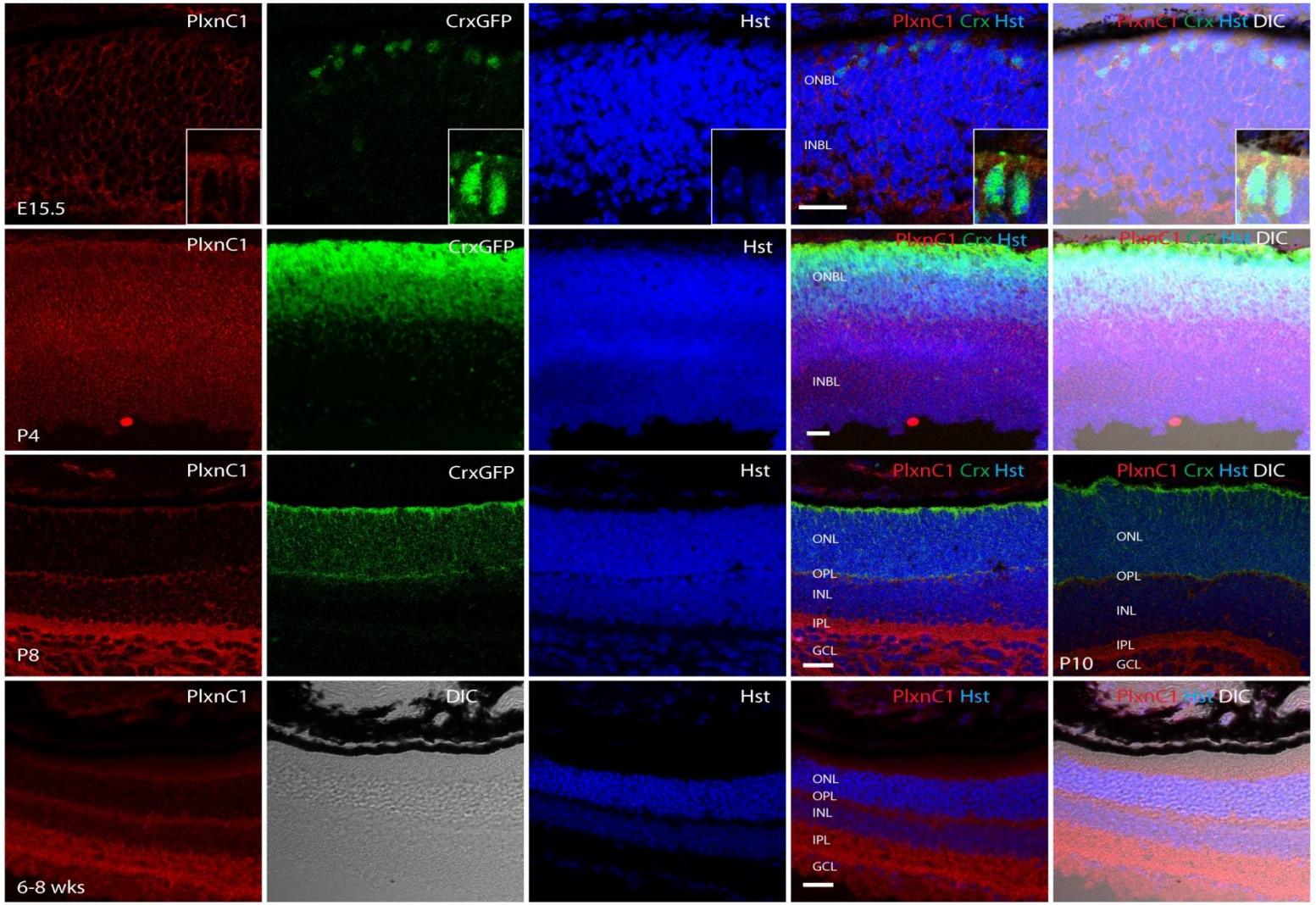

Figure 4.5 PlxnC1 expression profile along retina development. PlxnC1 Immunohistochemistry on E15.5, P4, P8, P10 CrxGFP and adult WT eyes. Scale bars represent 25 µm.

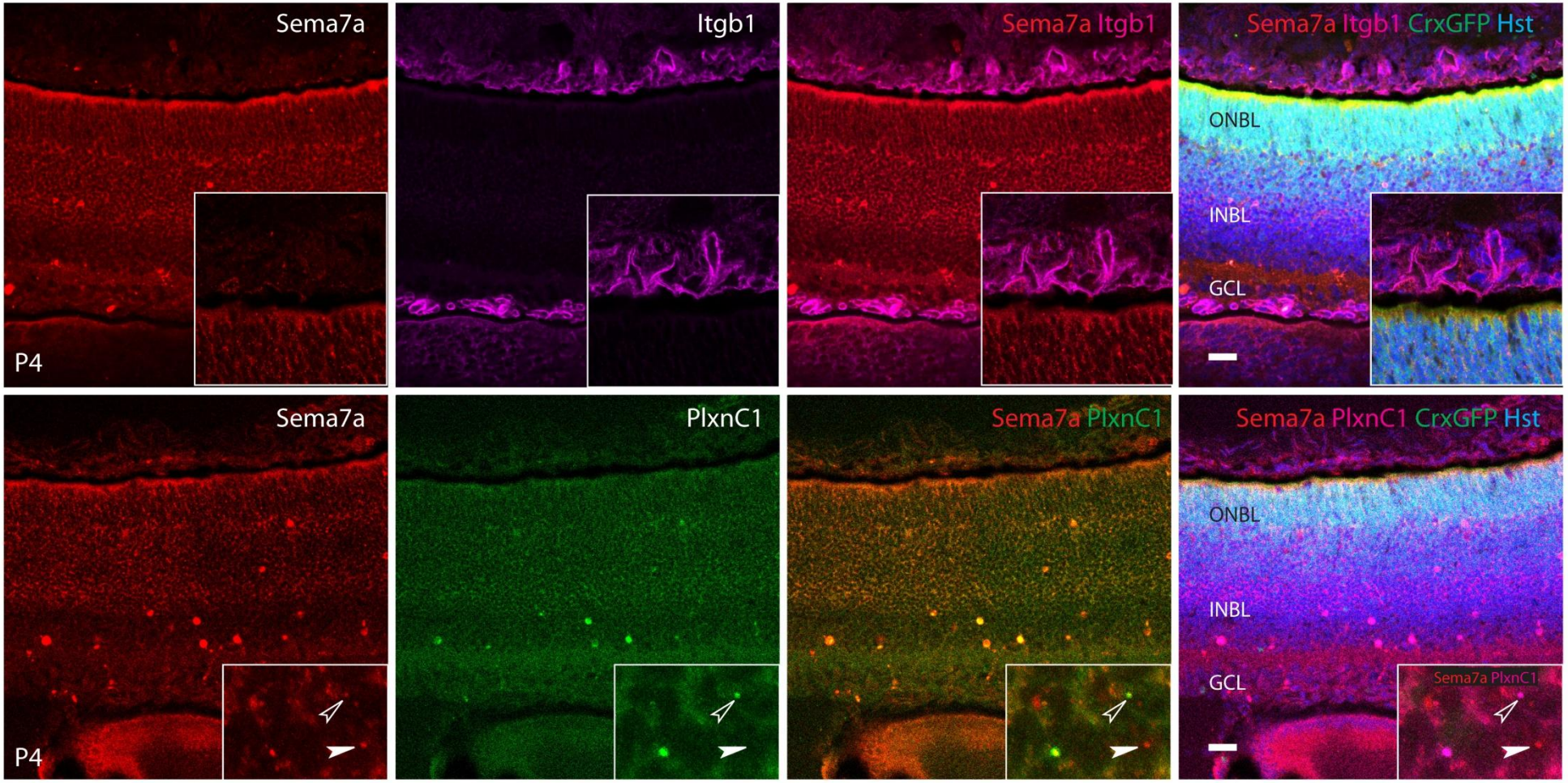

Figure 4.6 Sema7a co-staining with its receptors in P4 retina. Top row: Sema7a does not colable with Itgb1. Bottom row: Sema7a largely colabels with PlxnC1. Despite the overall co-localization of Sema7a with PlxnC1, single domains of Sema7a (solid arrow heads) or PlxnC1 (empty arrow heads) staining also exist on the retinal cells as the inserts show in the bottom row. Scale bars represent 25 µm.

4.2.4 Sema7a is expressed on migrating and integrated transplanted cells

4.2.4.1 Sema7a is expressed on the surface of dissociated retinal cells before transplantation

As Sema7a can be cleaved by caspase-9 (Ohsawa, Hamada et al. 2009) or possibly by phosphatidylinositol-specific phospholipases which cleave GPI anchors (Sharom and Lehto 2002; Sharom and Radeva 2004), I examined if Sema7a is still expressed on the surface of retina cells after dissociation. Retinal cells of both E15.5 and P4 from CrxGFP mice were examined after microdissection and papain dissociation (see method in Chapter 2, section 2.2.1). At E15.5, Sema7a was expressed on the cell surface of both CrxGFP+ve cells and CrxGFP-ve cells (Figure 4.7) (n = 311 retinal cells examined, 12.2% was Sema7a+veCrxGFP+ve and 85.2% was Sema7a+veCrxGFP-ve). At P4, Sema7a expression remained on both CrxGFP+ve and CrxGFP-ve cells (n = 77 retinal cells examined, 59.7% was Sema7a+veCrxGFP+ve and 35.1% was Sema7a+veCrxGFP-ve). Some cells showed particular high localized expression of Sema7a at specific regions of the cell which looks like developing processes (Figure 4.7, 3rd and 4th row).

I also examined the Sema7a receptors on dissociated P4 retinal cells (Figure 4.8). Itgb1 was only found to be expressed in a few CrxGFP-ve cells and not in any CrxGFP+ve cells (n = 106 retinal cells examined, 16% was Itgb1+veCrxGFP-ve and 0% was Itgb1+veCrxGFP+ve). PlxnC1, however, were expressed in both the CrxGFP-ve and CrxGFP+ve cells (n= 183 cells examined, 36.1% was PlxnC1+veCrxGFP+ve and 36.6% was PlxnC1+veCrxGFP-ve) and the expression levels seem to be slightly higher in the CrxGFP-ve cells. The expression of Sema7a and its receptors on dissociated retinal cells agree with their expression on retinal sections. As unlike retinal sections in which the cells might be cut open the dissociated cells remain intact, this confirmed that Sema7a and its receptors are expressed on the cell surface and can still be maintained after dissociation. Immuno-staining of the dissociated cells also showed that the expression of Sema7a could be enriched at particular regions of the cell surface, possibly the lipid rafts of the plasma membrane where GPI-anchored proteins were enriched (Sharom and Lehto 2002).

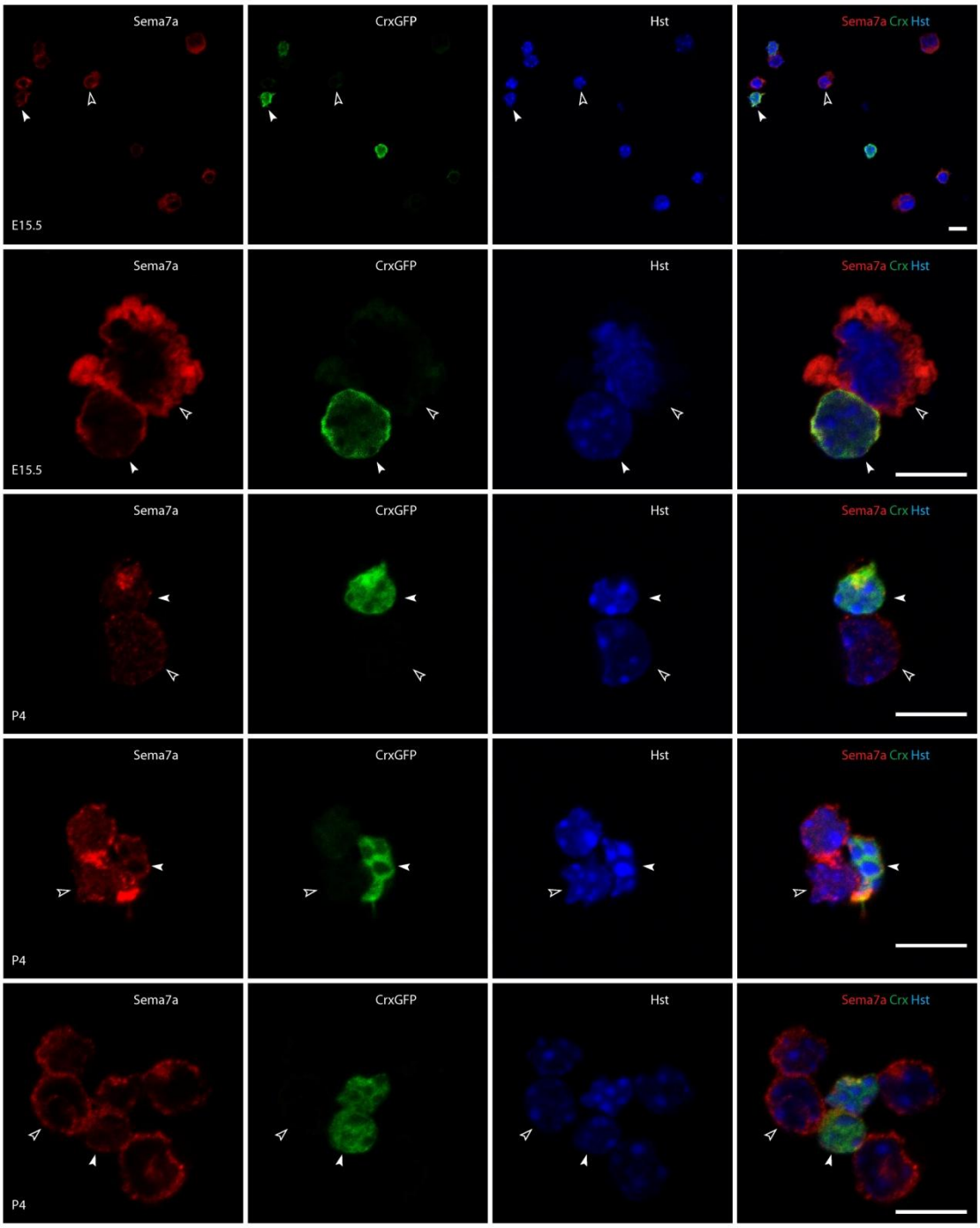

Figure 4.7 Sema7a expression on dissociated retinal cells. E15.5 (top two rows) and P4 (bottom three rows) retinal cells from the CrxGFP (green) mouse strain were dissociated and stained with Sema7a (red) and Hoechst (blue). Solid arrow heads indicate CrxGFP+ve cells; empty arrow heads indicate CrxGFP-ve cells. Scale bar represent 10 µm.

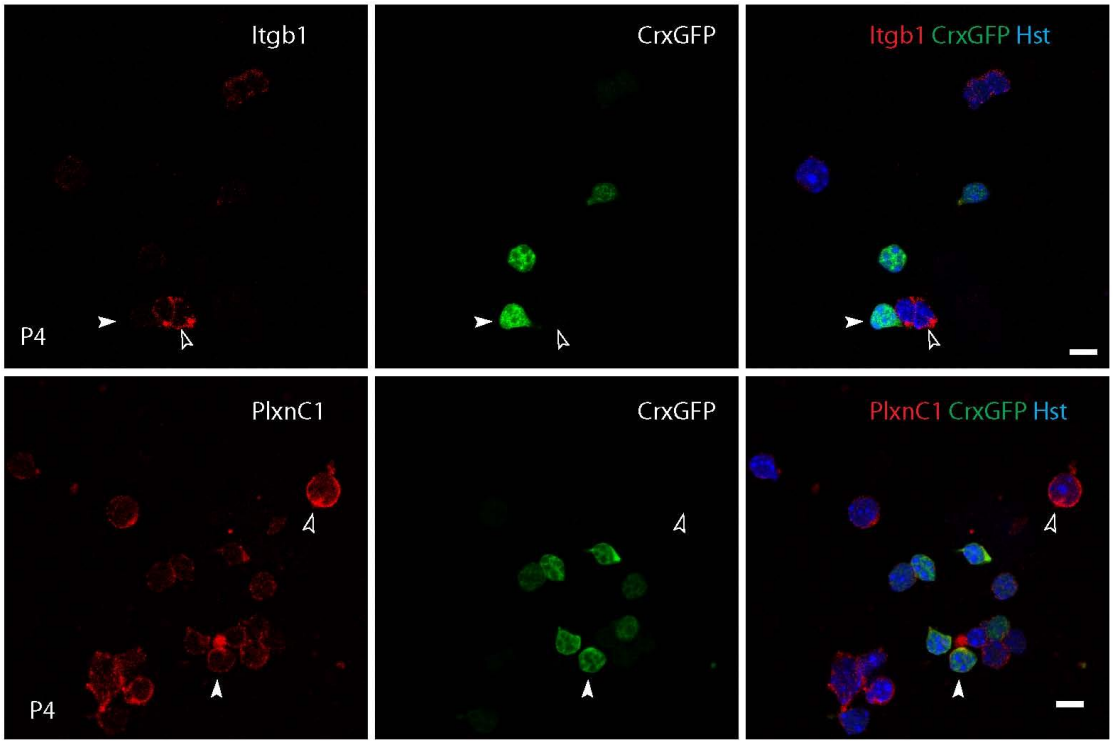

Figure 4.8 Itgb1 and PlxnC1 expression on dissociated retinal cells. P4 retinal cells from the CrxGFP (green) mouse strain were dissociated and stained with Itgb1 or PlxnC1 (red) and Hoechst (blue). Solid arrow heads indicate CrxGFP+ve cells; empty arrow heads indicate CrxGFP-ve cells. Scale bar represent 10 µm.

4.2.4.2 Sema7a is expressed on migrating and integrated cells after transplantation

Earlier my colleagues have established that the transplanted postnatal photoreceptor precursor cells labelled with NrlGFP or CrxGFP can migrate and correctly integrate into the host ONL after subretinal injection (MacLaren, Pearson et al. 2006; Lakowski, Baron et al. 2010; Pearson, Barber et al. 2012). Here I took advantage of this system to assess if Sema7a is expressed during the migration of transplanted photoreceptor cells into the ONL. After subretinal injection of the NrlGFP or CrxGFP labelled postnatal photoreceptor cells (performed by Dr Rachael Pearson), the majority of the cells stay in the SRS between the ONL and the RPE (Figure 4.9 A). A small proportion of the injected cells migrate away from the SRS and go through the outer and inner segment regions of the host retina, and finally integrate and correctly localise into the host ONL. I here define the cells at the SRS as cells that cannot or that have not yet migrated; cells at the inner or outer segment (IS/OS) as migrating cells; and cells at the ONL as migrating or migrated cells (Figure 4.9 A). By comparing Sema7a expression on these cells of different migration ability, it might be possible to infer if Sema7a is involved in migration.

Eyes of the host animals were analyzed for Sema7a expression at 3 – 12 days after transplantation of P4 CrxGFP sorted photoreceptor precursors (n = 8 eyes, N = 6 animals). I clearly observed high Sema7a expression around the cell surface of the transplanted cells (Figure 4.9 E). Strikingly nearly all the migrating/migrated GFP+ve cells expressed Sema7a: 100% GFP cells at ONL (mean ± SD = 100% ± 2%, median = 100%, range = 85 – 100%) and 93% GFP cells at IS/OS (mean ± SD = 93% ± 13%, median = 100%, range = 60 – 100%) (Figure 4.9 B, C and E). However, only about half of the GFP cells at the SRS express Sema7a (mean ± SD = 53% ± 22%, median = 50%, range = 10 – 100%). This highly associates Sema7a expression with migration and correct localisation. Furthermore, while there was no big difference of Sema7a expression on migrating cells (ie GFP cells at IS/OS and ONL) on different days after transplantation, there was a clear decrease of Sema7a expression on GFP cells at the SRS as time proceeds (Figure 4.9 D). This implies that cells that cannot migrate might lose Sema7a expression eventually.

Interestingly, I found that migrating GFP cells in the segment region or ONL which have not yet shown the morphology of mature photoreceptor cells expressed very high level of Sema7a (Figure 4.10 top row). Whereas when the cells developed mature photoreceptor cell morphology such as segments or processes, their Sema7a expression was reduced back to host or endogenous levels (Figure 4.10 bottom row).

I then examined the expression of Sema7a receptors on these transplanted eyes (Figure 4.11). Similar to the colocalization I observed in development, PlxnC1 again colocalized with Sema7a on the surface of the transplanted migrating cells. Because of the close interaction between Sema7a and PlxnC1 (Liu, Juo et al. 2010) and our resolution limit, it is hard to determine if the PlxnC1 signal came from neighbouring cells or the migrating cell itself. On the other hand, Itgb1 only labelled a few scattered vascular cells of the host retina which were far away from the transplanted cells. Together these data suggest a role for Sema7a in photoreceptor migration and that PlxnC1/Sema7a interactions may be involved.

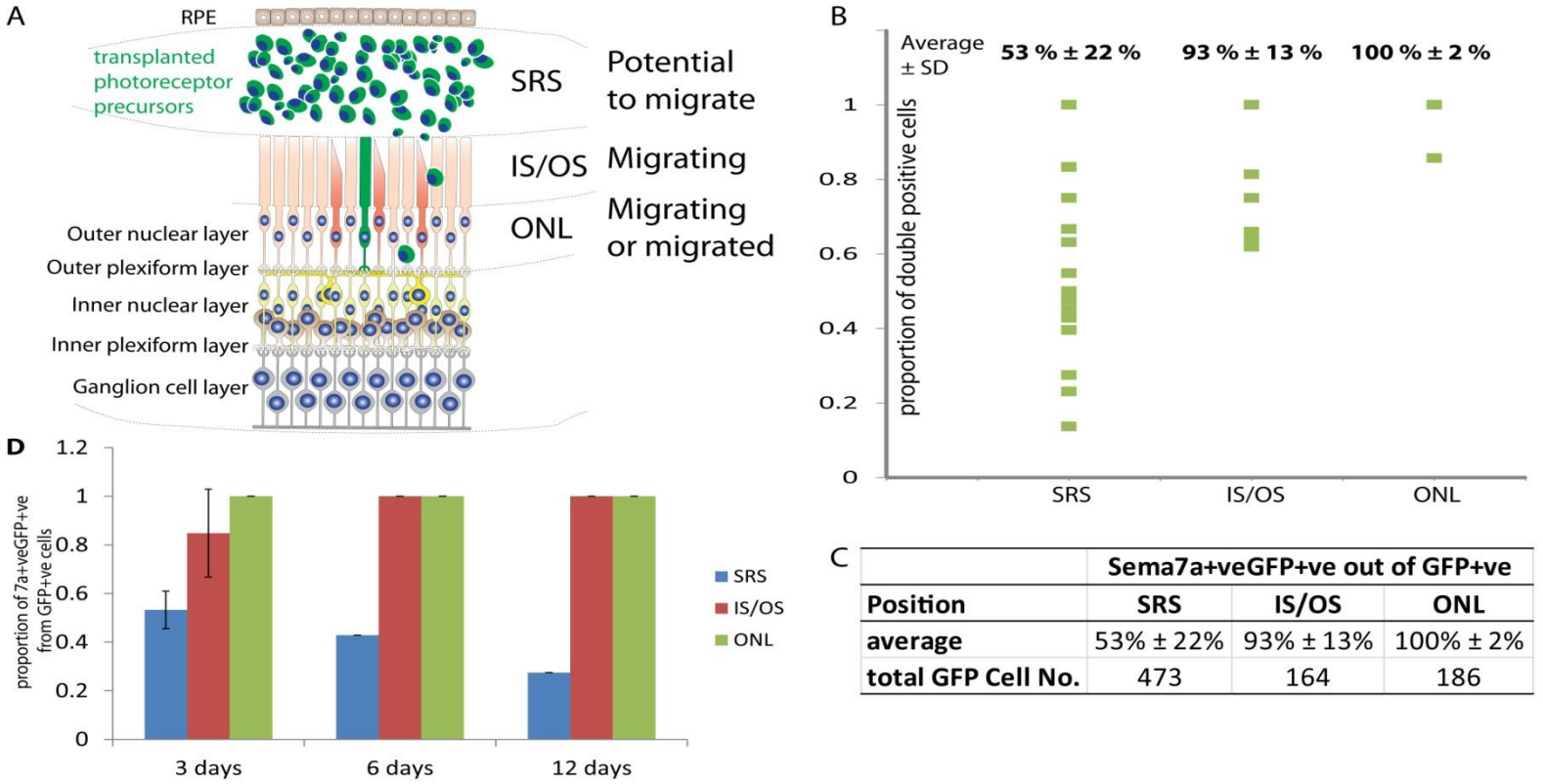

Figure 4.9 Sema7a expression on transplanted eyes (continues). FACS sorted P4 CrxGFP precursor cells were injected into the subretinal space (SRS) between the ONL and the RPE, and Sema7a expression was analysed 3 to 12 days post injection. (A) Illustration of position of transplanted photoreceptor cells after injection. The majority of the cells are located at the SRS; a small proportion of the cells migrate through the outer and inner segment (IS/OS) region and move into the outer nuclear layer (ONL). Cells at the SRS are defined as potential cells to migrate; cells at the IS/OS are defined as migrating cells; and cells at the ONL are defined as migrating or migrated cells. Dot plot (B) and table (C) representing proportion of Sema7a+ve transplanted photoreceptor cells at these positions at 3 to 12 days post injection (n= 8 eyes, 56 confocal stacks). (D) Time-course of Sema7a-expressing transplanted cells. The proportion of Sema7a+veGFP+ve out of the total transplanted GFP+ve cells in the SRS, IS/OS and ONL region were counted at 3 days, 6 days and 12 days after transplantation. Error bars represent standard deviation.

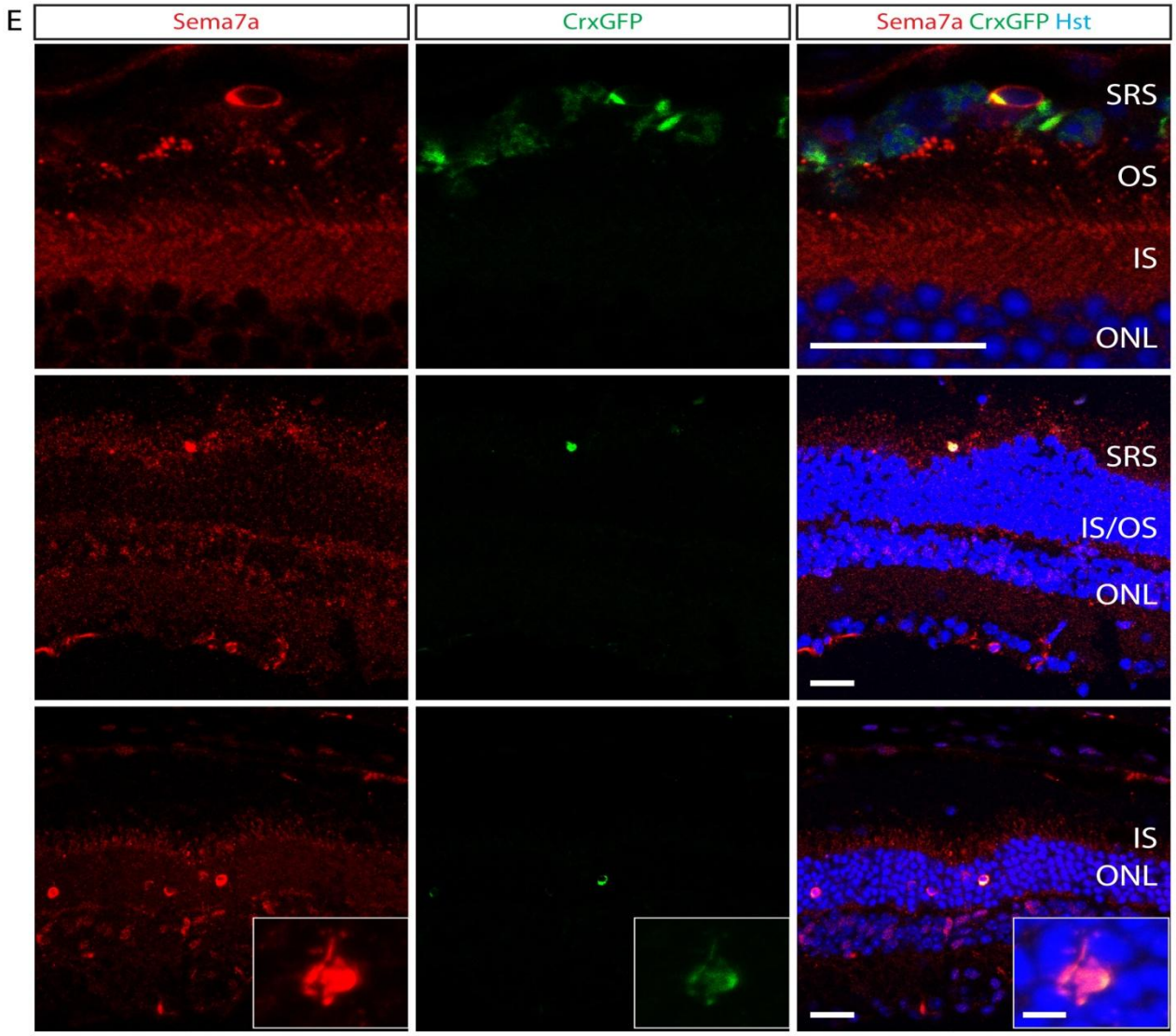

Figure 4.9 Sema7a expression on transplanted eyes- continued. (E) Images of the transplanted photoreceptor cells which are at the SRS (top row), at the IS/OS (middle row), and at the ONL (bottom row). Scale bars represent 25 µm except in inserts which represent 5 µm.

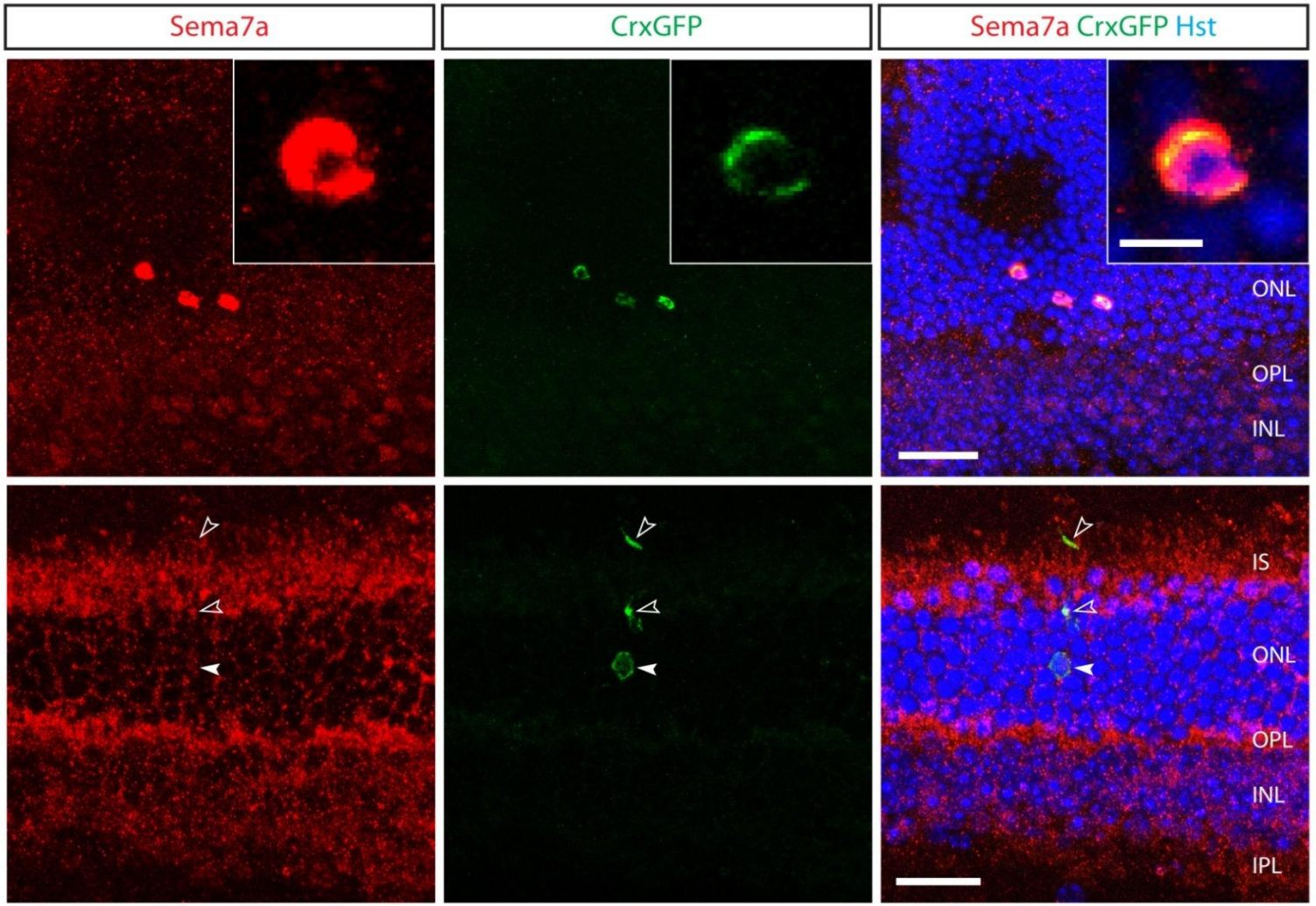

Figure 4.10 Sema7a high and low expression cells after transplantation. (Top row) High Sema7a expression on transplanted cells before they show mature photoreceptor morphology. (Bottom row) sema7a expression return to endogenous levels on transplanted cells which show mature photoreceptor morphology such as segments. Solid arrow heads indicate cell body of the photoreceptor cell; empty arrow heads indicate the process and segments of the photoreceptor cell. Scale bars represent 25 µm except in inserts which represent 5 µm.

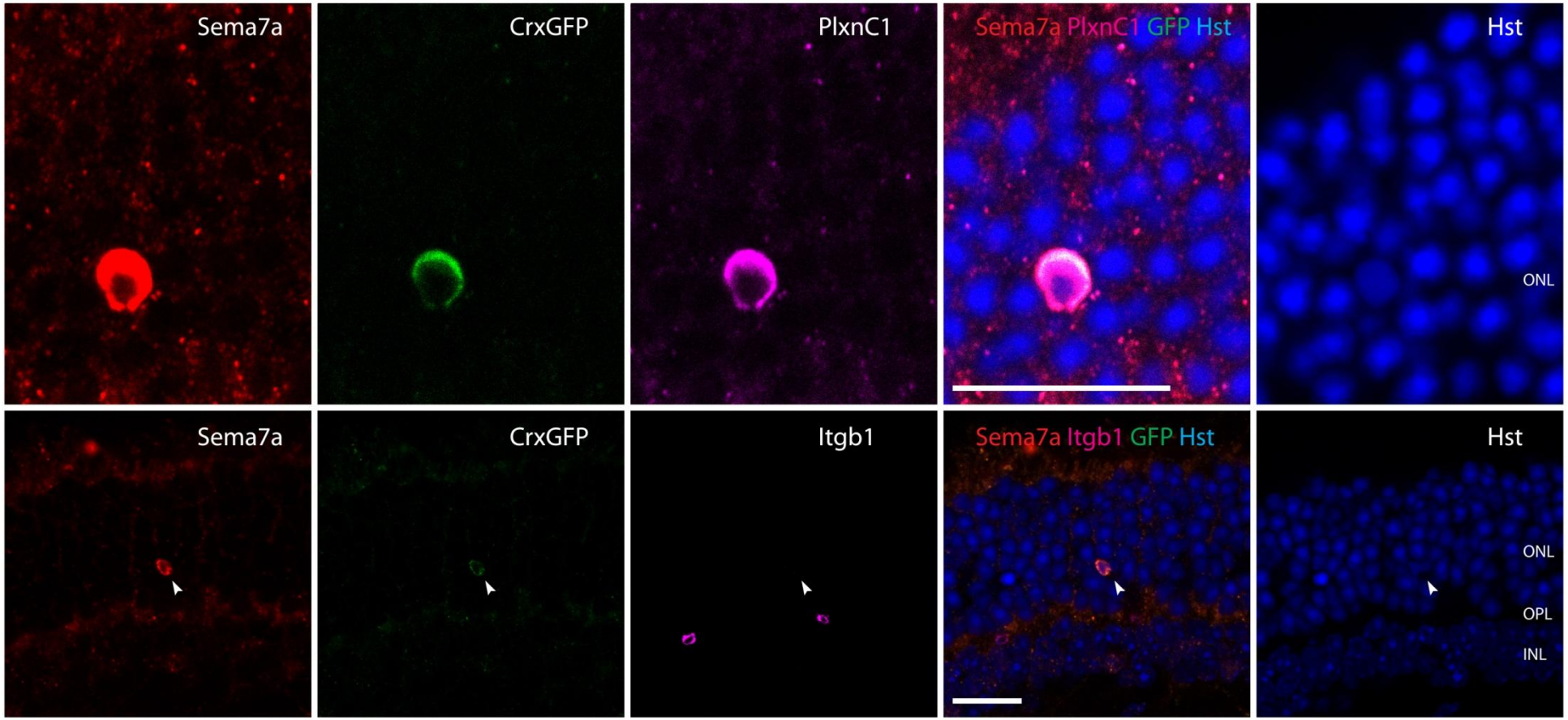

Figure 4.11 PlxnC1 and Itgb1 expression on transplanted eyes. (Top row) PlxnC1 was highly expressed on/adjacent to transplanted migrating cells (n = 57 GFP+ve cells counted). (Bottom row) Itgb1 was not expressed on any cells near the transplanted cell (n = 58 GFP+ve cells counted). Arrow heads indicate the transplanted CrxGFP+ve cells. Scale bars represent 25 µm.

4.2.5 Requirement for Sema7a during outer nuclear layer development

Finally two approaches were taken to more directly assess if Sema7a is required for ONL development: 1) using shRNA to knock down Sema7a expression in cells following transplantation and in the postnatal developing retina; 2) examination of eyes from Sema7a knockout mice.

Preliminary trials for the shRNA experiment with four shRNA sequences on cell lines, however, did not achieve satisfactory knockdown of expression from a Sema7a-IRES-GFP vector (see Appendix 4.1 for details) and future experiments will test more oligos. I also examined eyes from Sema7a knockout mice kindly provided by Alex Kolodokin's group, which generated the *Sema7A* null mice and first showed the axon outgrowth effect of Sema7a in olfactory bulb (Pasterkamp, Peschon et al. 2003). The *Sema7a* null mouse line appeared grossly normal and was generated through homologous recombination and Cre recombinase excision of the first exon and its upstream 1.1kb DNA which leads to loss of the first 59 amino acids of Sema7A including the signal peptide (Pasterkamp, Peschon et al. 2003). Eyes at P8/9 were selected for analysis as at this time point retinal lamination and ONL organisation is ongoing. The Sema7A knockout P8/9 eyes (n = 3) showed loss of Sema7a expression and reduced level of PlxnC1 expression by 50% (Figure 4.12, A and B). Itgb1 expression, however, remained similar between the knockout and the wild type animals. In the eyes where there was no Sema7a expression, holes (regions where cells were missing) were frequently observed in the ONL (Figure 4.12 A and C, arrowheads) (mean ± SD = 51.7 ± 7.1 holes per slide with six 18µm sections on each slide, n = 3 eyes.) although the thickness of ONL looks normal. While the photoreceptor ribbon synapse proteins bassoon and dystrophin showed precise punctate location within the OPL of the wild-type retina, they projected abnormal processes into the INL and ONL in the retina of Sema7a knockout out mice. On the other hand, the bipolar cell dendritic tip marker metabotropic glutamate receptor 6 (mGluR6) and rod bipolar cell marker PKCα showed normal distribution in the knockout retina (Figure 4.12 D). These data indicate that Sema7a is important for the normal synapse formation for photoreceptor cells during retina development.

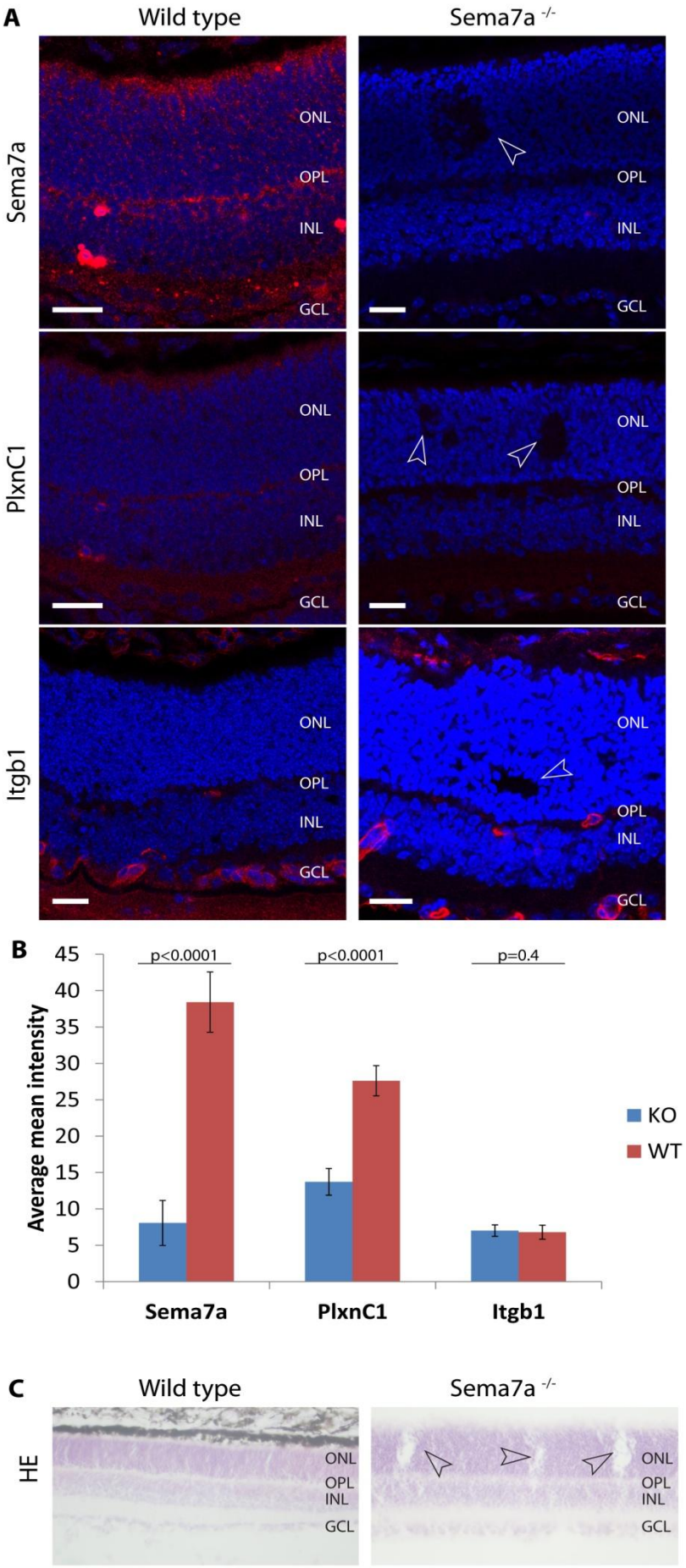

Figure 4.12 Sema7a knockout mouse retina (continues). (A) Expression of Sema7a (top row), PlxnC1 (middle row), and Itgb1 (bottom row) in the retina of wild type (left) and sema7a knockout (right) mice. Scale bars represent 25 µm. (B) Quantification of the expression of Sema7a, PlxnC1, and Itgb1 based on the mean intensity of the signals from confocal images. Each column represents the average of the mean intensity of 20 – 30 confocal slices and the error bar represent standard deviation. The expression in the retina are significantly different between the knockout and wild type animals for Sema7a ($p = 1.52 \times 10^{-32}$) and PlxnC1 ($p = 1.07 \times 10^{-24}$), but not significantly different for Itgb1 ($p = 0.404$) based on students' t-test. (C) Hematoxylin and eosin stain of the retina of wild type (left) and sema7a knockout (right) mice.

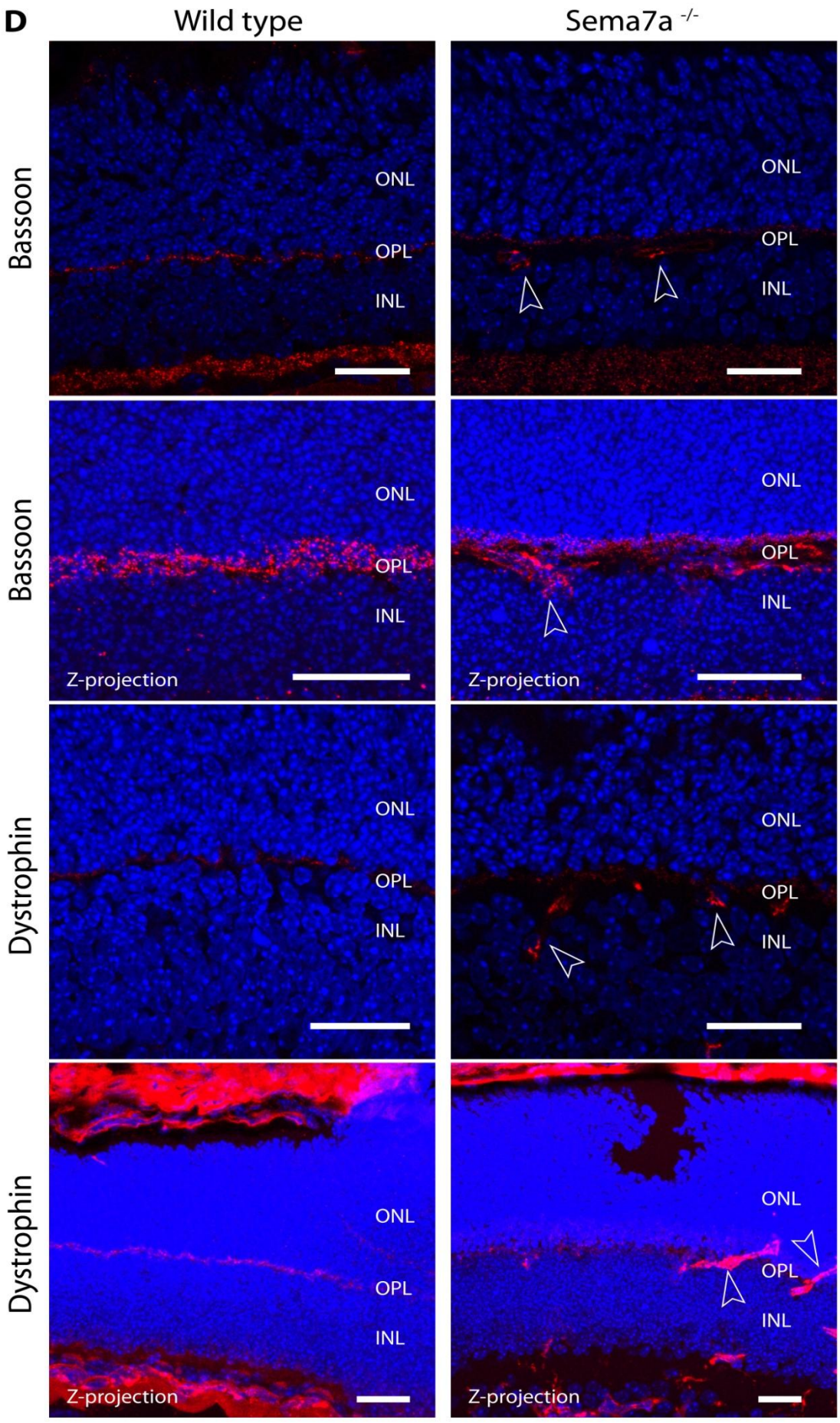
D
Wild type
Sema7a -/-
Bassoon
Bassoon
Dystrophin
Dystrophin
ONL
OPL
INL
Z-projection

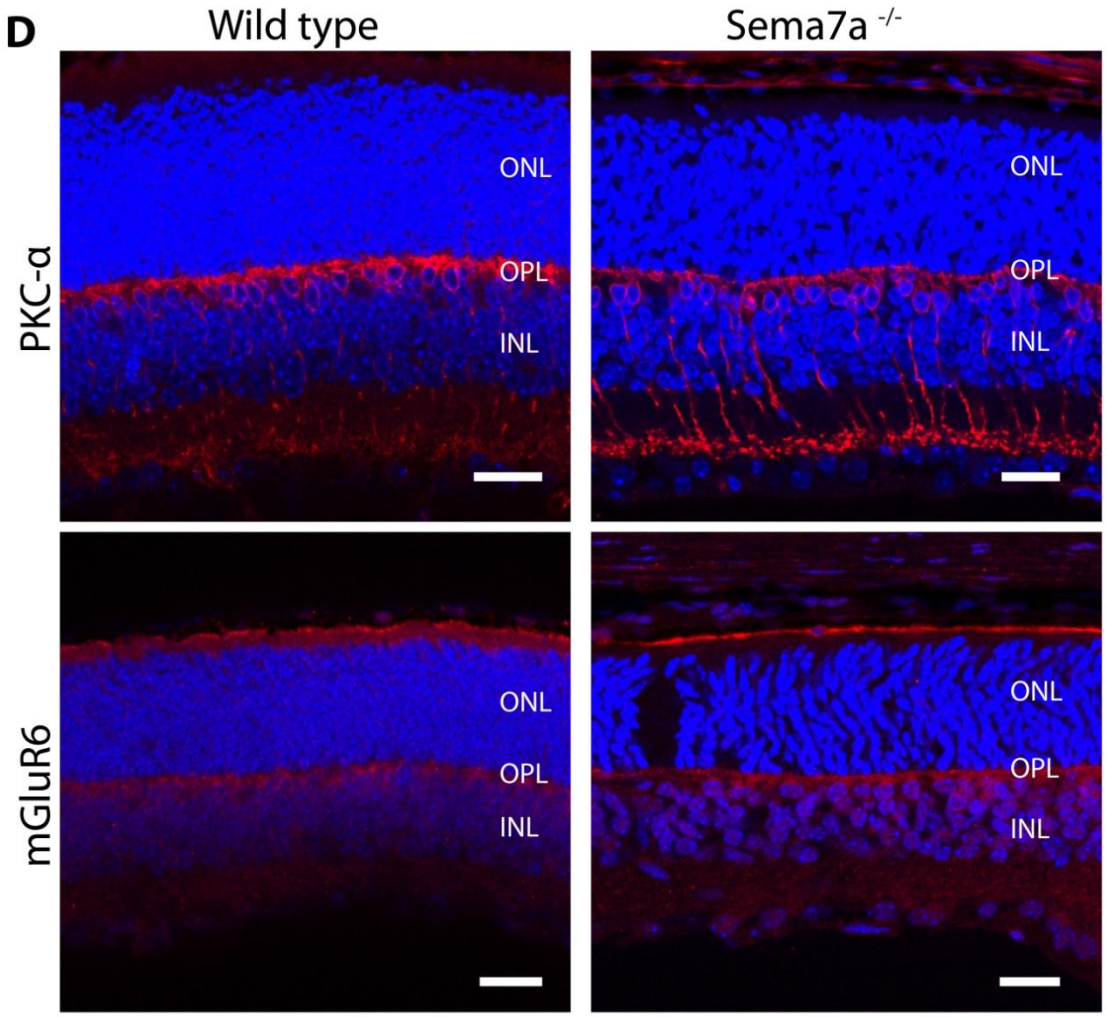

Figure 4.12 Sema7a knockout mouse retina- continued. (D) Expression of Bassoon, Dystrophin, PKCα, and mGluR6 in the retina of wild type and sema7a knockout mice. Scale bars represent 25 µm.

4.3 Discussion

Previously Sema7a has been reported to function in axon/dendrite branching, cell migration and immune responses (Holmes, Downs et al. 2002; Pasterkamp, Peschon et al. 2003; Suzuki, Okuno et al. 2007; Fukunishi, Maruyama et al. 2011; Messina, Ferraris et al. 2011). Its transcripts are highest in the brain, and lower in heart, thymus, spleen, testis and ovary. In the immune system, Sema7a concentrates at the lipid rafts of the immunological synapse of T cells upon their activation and interacts with Itgb1 to stimulate macrophages to produce proinflammatory cytokines (Suzuki, Okuno et al. 2007; Suzuki, Kumanogoh et al. 2008). It is also expressed in the skin keratinocytes to promote attachment, spreading and dendrite outgrowth of melanocytes (Scott, McClelland et al. 2008). Here I report for the first time that Sema7a was highly expressed in photoreceptor cells. I showed that while also expressed in other retinal cells, Sema7a expression level was particularly high in the synapses and segment region of mature photoreceptors where the border of ONL lies. During development Sema7a expression remains high in these apical and basal regions of photoreceptor cells where the processes are about to protrude and layers about to be defined. Upon loss of Sema7a expression, I showed that the photoreceptor synapses but not the processes of bipolar cells, showed abnormal extended processes. Considering the involvement of Sema5a/b and Sema6a in the stratification of the inner retina (Matsuoka, Chivatakarn et al. 2011; Matsuoka, Nguyen-Ba-Charvet et al. 2011), this semaphorin might be the one that is involved in the photoreceptor layer formation of the outer retina.

Sema7a function in the nervous system was initially reported to promote axon growth and branching of the olfactory bulb neurons (Pasterkamp, Peschon et al. 2003). Accumulating evidence also showed that Sema7a is involved in the migration of neurons such as the thalamic neurons (Fukunishi, Maruyama et al. 2011) and GnRH-1 neurons (Messina, Ferraris et al. 2011).Interestingly, I also observed particularly high expression of Sema7a on the migrating photoreceptor cells after cell transplantation as well as on some photoreceptor cells within the developing P4 to P8 retina during normal retina development. This could indicate a role for Sema7a in the migration of the photoreceptor cells. To directly assess how Sema7a might affect the migration of the photoreceptor cells, further shRNA experiments testing more oligos to reduce Sema7a expression in transplanted cells will be needed.

Sema7a was reported in other systems mainly interacting with Itgb1 (Pasterkamp, Peschon et al. 2003; Suzuki, Okuno et al. 2007; Scott, McClelland et al. 2008; Messina, Ferraris et al. 2011). In the olfactory bulb and the skin systems, Sema7a was expressed on the olfactory fibers and the keratinocytes while Itgb1 was expressed on the interacting receptor cell GnRH-1 neurons

and melanocytes to promote their migration and axon/dendrite spreading (Scott, McClelland et al. 2008; Messina, Ferraris et al. 2011). Although PlxnC1 was also expressed on these receptor cells, it seems it inhibited the spreading and migration role of Sema7a (Scott, McClelland et al. 2008; Messina, Ferraris et al. 2011). I, however, found that Itgb1 was not expressed in the retina, in particular not in any adjacent retinal cells that interact with the Sema7a-expressing photoreceptor cells. Therefore it seems unlikely for Itgb1 to interact with Sema7a in the retina. On the other hand, I observed abundant expression of PlxnC1 in the retina, which initially was widespread and overlapped with Sema7a. More interestingly, there were high levels of colocalisation of Sema7a and PlxnC1 on retinal cells during early postnatal development, although such colocalisation was reduced in later stages as Sema7a became more highly expressed in the outer retina and PlxnC1 became more highly expressed in the inner retina. In the photoreceptor transplantation experiments, I also observed such colocalisation of Sema7a and PlxnC1. Therefore my data suggests that it is more likely that Sema7a might actually interact with PlxnC1, rather than Itgb1, to be possibly involved in cell migration and ONL formation in the retina. Further, PlxnC1 expression level was reduced in the Sema7a$^{-/-}$ mouse retina while Itgb1 level was unaffected. Crystallography showed interaction between Sema7a and PlxnC1 (Liu, Juo et al. 2010) but not yet for Sema7a/Itgb1.

Considerable progress has been made in defining the molecular basis of axon guidance patterning in neural circuits formation. One common form of regulation is the graded expression of pairs of axon guidance cues and their receptors in projection neurons or their targets. For example, in the olfactory system, Semaphorin 3A (SEMA3A) and neuropilin 1 (NRP1) are expressed in an opposite anterior-posterior gradient giving each class of olfactory sensory neurons (OSN) unique amounts of SEMA3A and NRP1 (Imai, Yamazaki et al. 2009). This allows axons of the OSN to be sorted based on the expression levels of SEMA3A and NRP1 as the axons progress to the olfactory bulb (Imai, Yamazaki et al. 2009). Further SEMA3F and its receptors NRP2 and plexin A3 (PLXNA3) are expressed complimentarily as a dorsal-ventral gradient in the olfactory epithelium (Takeuchi, Inokuchi et al. 2010). In this way, the early arriving axons release SEMA3F to repel late arriving NRP2–PLXNA3-positive axons to more ventral regions allowing establishment of the dorsal-ventral patterning of olfactory axons (Takeuchi, Inokuchi et al. 2010; Pasterkamp 2012). In the visual system, Sema6a and Sema5a/5b and their plexin receptors are expressed complimentarily on adjacent layers of different retinal cell types with the semaphorins constraining neurites from mistargeting via repulsive interaction with the plexins to regulate the lamination of the inner retina (Matsuoka, Chivatakarn et al. 2011; Matsuoka, Nguyen-Ba-Charvet et al. 2011). The retina data of Sema7a

presented here does not support a repulsive mechanism as the expression of Sema7a and PlxnC1 overlaps and even colocalises. Sema7a and PlxnC1 do show some degree of complimentary expression patern on different cell types in more mature stages. However during early development when the retinal cells are still mobile, Sema7a and PlxnC1 expression largely overlaps in the whole retina. Therefore, Sema7a and PlxnC1 seem to be less confined in their expression in the retina than other semaphorins and plexins. It is possible that at the time when migration of a particular retinal cell is required, Sema7a will be highly expressed on its surface and this will induce the expression of PlxnC1 on its surrounding neighbouring cells no matter if they are the same type of cells or not. I, however, could not exclude the possibility that the colocalized PlxnC1 signal detected is from that Sema7a-expressing cell rather than the surrounding cells. Possible functions of such interactions between Sema7a and PlxnC1 could be (non-exclusively) 1) guiding/limiting migration of the photoreceptor precursor cell to the correct location within developing retina; 2) keeping photoreceptor cells together in ONL; and 3) preventing progenitors/precursors from overshooting the OPL.

During development of olfactory sensory neurons, Sema7a can be cleaved by the Apaf-1/caspase-9 pathway whose deficiency disrupted axonal projections, synaptic formation and maturation of these neurons (Ohsawa, Hamada et al. 2010). It may therefore be possible that the colocalisation of Sema7a and PlxnC1 I detected comes from a secreted (or fragmented) form of Sema7a which binds to PlxnC1. However, I showed clear cell surface expression of Sema7a on dissociated retina cells indicating membrane localisation and Sema7a alone labelled domains were detected in the Sema7a/PlxnC1 costaining experiments. Furthermore I did not detect any of the cleaved fragments of Sema7a in retina western blot like those shown in the Sema7a cleavage by caspase-9 in the aged olfactory bulb (Ohsawa, Hamada et al. 2010). These data instead indicate that in the retina Sema7a acts as a GPI-anchored cell surface molecule rather than any other form to interact with neighbouring cells.

4.4 Conclusions

- I report the first semaphorin, Sema7a, identified in photoreceptor cells. Sema7a is expressed in developing photoreceptors and then in the inner segments and synapses of mature photoreceptors, whereas expression of the putative receptor plexinC1 is initially widespread and then becomes most highly expressed in the inner retina.

- Unlike other systems describing Sema7a/Itgb1 interactions (Pasterkamp, Peschon et al. 2003; Suzuki, Okuno et al. 2007; Scott, McClelland et al. 2008; Messina, Ferraris et al.

2011), Sema7a colabels with PlexinC1, but not Itgb1, as punctate dots on the surface of retinal cell bodies during development.

- Sema7a is highly expressed on transplanted migrating photoreceptors cells, and colabels with PlexinC1 (but not Itgb1).
- In Sema7a$^{-/-}$ mice retina where Sema7a expression was lost, PlxnC1 level was also reduced (but not Itgb1). Loss of Sema7a leads to ONL lesions/holes and over-extended processes of photoreceptor synapses revealed by expression of photoreceptor ribbon synapse proteins bassoon and dystrophin.
- I propose that Sema7a/PlxnC1 interactions may be important for photoreceptor integration and ONL formation.

5 The cilia and cilia surface proteins of photoreceptor precursor cells

5.1 Introduction

From the transcriptome analysis in Chapter 3, I noticed that the postnatal photoreceptor precursor cell transcriptome showed a very unique transcriptome property compared to other retinal cells – expression of genes associated with the cilium – a feature highlighted in both the Crx array and Nrl array (Figure 3.3, Figure 3.6). The cilium is a special filiform extrusion of the plasma membrane and varies in its morphology and microtubule composition according to cell types. Nearly all the polarized cells (including neurons) are ciliated (http://www.bowserlab.org/primarycilia/cilialist.html; (Alberts, Johnson et al. 2008; Louvi and Grove 2011)). However, as other retinal neurons did not enrich this feature or at least not at this stage from the transcriptome analysis, the cilium transcripts seem to be a unique feature for the photoreceptor precursor cells among all the cells in the retina. Little is known about the photoreceptor cilia in early developmental stages, although there are many studies on mature photoreceptor OS which is part of the specialized photoreceptor cilia as re-appreciated in recent years (Liu, Zhang et al. 2010). The first rudimentary OS "disk"(saccule) appears around P7-8 under EM (De Robertis 1960; Olney 1968; Morrow, Furukawa et al. 2005) and the OS become recognizable under light microscope by P10 (Olney 1968). The cilium feature I noticed from photoreceptor precursor transcriptome is at P4, which is before OS formation. On the other hand, embryonic photoreceptor precursor transcriptome did not enrich this feature (Figure 3.3 A, Appendix figure 3.1). The common properties of the E15.5 and P4 photoreceptor cells do include some plasma membrane and cell projection annotations (Figure 3.4 B), but many more cilium-related annotations were enriched in the P4 precursor cells than the E15.5 photoreceptor cells (Figure 3.3, Figure 3.6, and Appendix figure 3.1). I, therefore, want to know if there is a difference in cilium properties between the embryonic and postnatal photoreceptor precursor cells and to better understand the postnatal photoreceptor cilia prior to OS formation.

Despite being a tiny organelle, deficiency of cilium is to be blamed for numerous human pleiotropic disorders. Here I mention several that also show neural defects in the eye. Bardet–Biedl syndrome (BBS), for example, showing symptoms of retinitis pigmentosa, rod-cone dystrophy, anosmia, cognitive disabilities, polydactyly, cystic kidneys, obesity, male hypogonadism and congenital heart defects (Forsythe and Beales 2013), are characterised by autosomal recessive inheritance of BBS genes whose proteins localize within the cilium and are

involved in subcellular targeting of other ciliary proteins (Beales, Warner et al. 1997; Fliegauf, Benzing et al. 2007; Forsythe and Beales 2013). Usher syndrome (USH), another heterogeneous disease displaying hearing loss, vestibular system dysfunction and progressive retinitis pigmentosa, are characterized by absence or abnormality of the USH proteins which are involved in intraflagellar transport (IFT) and rhodopsin transport in photoreceptor cilia (Wolfrum and Schmitt 2000; Reiners, Nagel-Wolfrum et al. 2006) as well as playing a developmental role in sterocilia for the cochlear hair cells (Fliegauf, Benzing et al. 2007; Liu, Bulgakov et al. 2007). Similar to Jeune asphyxiating thoracic dystrophy, Joubert syndrome, Alstrom syndrome and Senior–Løken syndrome, ciliopathies showed vision impairment among other symptoms (Fliegauf, Benzing et al. 2007; Louvi and Grove 2011; Rachel, Li et al. 2012). Joubert syndrome is associated with retinal dystrophy since childhood (Sturm, Leiba et al. 2010). Alstrom syndrome patients lost vision in young adulthood demonstrating retinitis pigmentosa with cone-rod degeneration (Malm, Ponjavic et al. 2008). Senior–Løken syndrome showed severe visual loss from early childhood (Stone, Cideciyan et al. 2011). Genes involved in these retina-related ciliopathies were listed in Chapter 1 Table 1.1.

Although the cilia structure and morphology varies according to cell types, nearly all cilia types share the basic structural units composed of a basal body, transition zone, axoneme, and ciliary membrane (Figure 5.1). Located at the bottom of the cilium, the basal body is made up of the centriole and pericentriolar proteins and is where the transition zone and axoneme are anchored. The transition zone is where the triplet microtubules of the centriole are converted into the doublet microtubule structure of the axoneme. The axoneme contains nine pairs of peripheral microtubule doublets. Depending on cell types, it may contain additional central microtubules and dynein motors. The photoreceptor cilium lacks these additional structures and is thus defined as a primary immotile cilium. It is extended from the inner segment and includes the connecting cilium and the outer segment (Figure 5.1). Axoneme from the connecting cilium extends into the outer segment. In rods the extended axoneme stops at the base of the outer segment where the few open disks are located. In cones where all the disks are open as continuous delineated foldings of the connecting cilium plasma membrane, the axoneme extends the whole length of the outer segment (Figure 1.1, Figure 5.7 A, (Mustafi, Engel et al. 2009)). The connecting cilium is important for OS biogenesis and opsin transport as turnover products from OS and newly synthesized opsins and other proteins from IS are shuttled through it. Around 10^9 molecules of rhodopsin are estimated to be transported in the connecting cilia in the human retina every day (Hildebrandt and Otto 2005). Proteins which need to be transported to the OS are first recruited near the basal bodies where they further

pass the transition fiber and are then loaded onto the IFT complex at the transition zone (Emmer, Maric et al. 2010). The loaded IFT particles interact with the dyneins and kinesins which shuttle along the axoneme to send cargos to the OS or bring recycled products back to the base of the connecting cilium. Disruption of the IFT machinery leads to photoreceptor degeneration (Tsujikawa and Malicki 2004; Boldt, Mans et al. 2011).

Protruding from the cell surface and mainly non-motile, functions of the primary cilia are thought to be to sense and amplify environmental signals. Indeed, several signalling pathways including the sonic hedgehog (SHH) pathway (Huangfu, Liu et al. 2003), platelet-derived growth factor receptor (PDGFR) pathway (Schneider, Clement et al. 2005), and planar cell polarity (PCP) pathways (Ross, May-Simera et al. 2005) are shown to be mediated through cilia. But this may not be the only function of the immotile primary cilia. Some studies suggest that they might also be involved in cell migration. It was found that the primary cilia of the migrating fibroblasts orient in the direction of cell migration (Albrecht-Buehler 1977) and that primary cilia align toward the scratch made in a wound healing assay (Schneider, Cammer et al. 2010). However it remains unexplored if such orientation or guidance also holds for the primary cilia of neural cells (Louvi and Grove 2011), in particular the photoreceptor precursor cells that I am interested in. Despite much being known about the structure of the mature specialised outer segment bearing photoreceptor cilia, little is known about when the photoreceptor cilia begin to form and how their development progresses.

To date, knowledge about the cilium is mainly based on molecules inside the organelle, such as the BBS proteins and IFTs. Little is known about the surface molecules at the cilium membrane. Directly interacting with the environment, the cilium surface proteins are likely to reveal more information about the function and mechanisms of this organelle and the cell. For example, studies of the cyclic nucleotide-gated (CNG) channel proteins revealed that primary cilia also use cAMP (Barzi, Berenguer et al. 2010) and cGMP signalling pathways (Meyer, Angele et al. 2000) in both vertebrate and invertebrate and the cilia may provide a unique compartment to localize these signalling for specific cellular functions (Johnson and Leroux 2010). In addition, study of the cilium-related cell surface proteins may also provide more therapy targets for disease related with ciliopathies.

In this chapter, I aim to investigate the hypothesis that the nascent primitive photoreceptor cilium is important for integration/orientation of developing photoreceptor cells in the ONL. I aim to find out:

1) Which cilium related genes are enriched in photoreceptor precursor cells?

2) Is there a difference in cilium gene expression between the E15.5 and P4 photoreceptor precursor cells? The latter show ~10-fold higher integration efficiency compared with the former after cell transplantation (Lakowski, Baron et al. 2010).

3) Are cilium-related cell surface proteins expressed in the photoreceptor precursor cells and what are their subcellular locations?

4) Are the cilium-related cell surface proteins expressed in the migrating transplanted photoreceptor precursor cells?

Taking together, answers to these questions might reveal how important cilium and cilium-related cell surface proteins are in photoreceptor cell development as well as in establishment of cell transplantation based therapy.

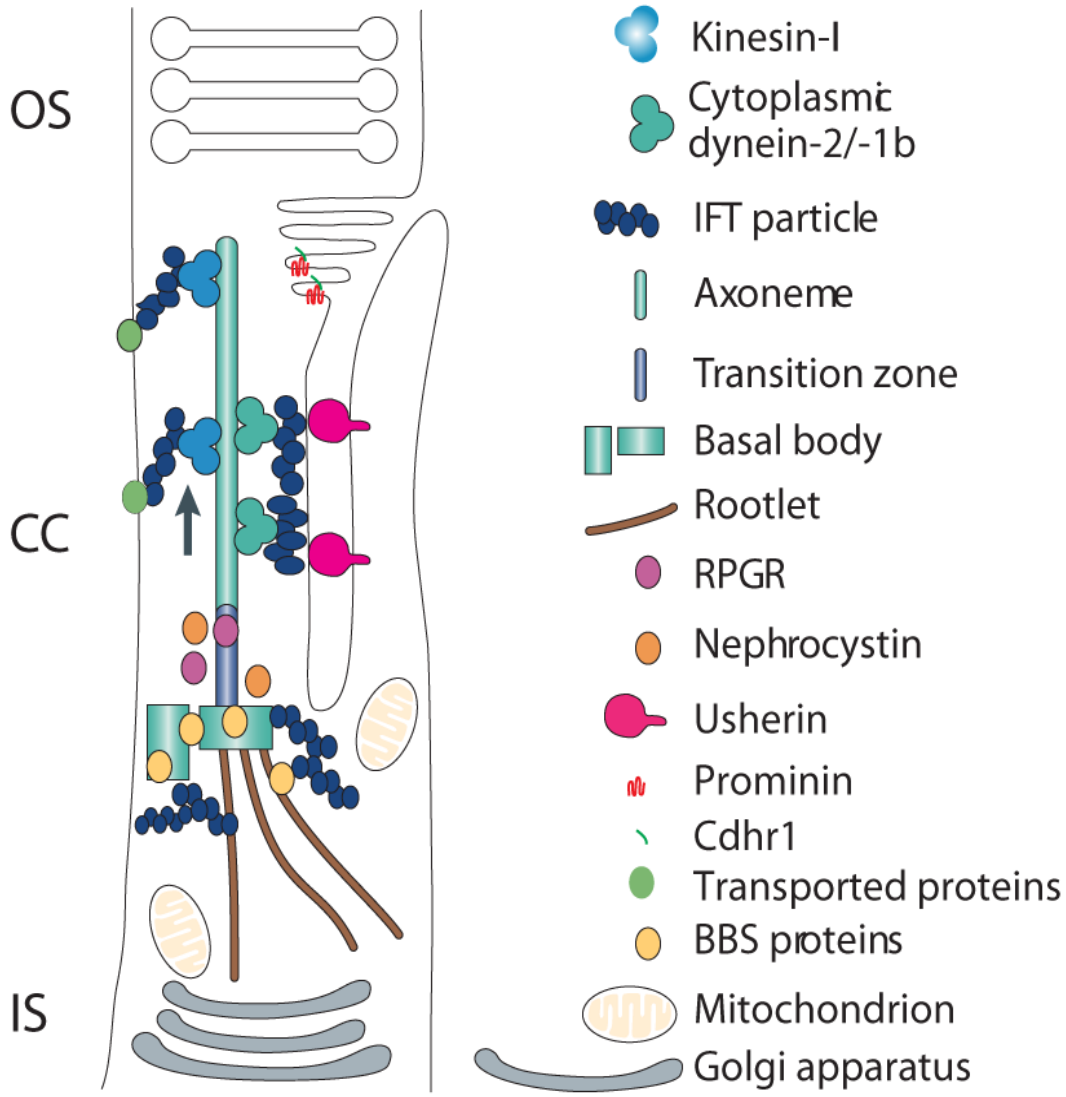

Figure 5.1 Mature rod connecting cilium and cilium protein location. Most cilium proteins are intracellular. The cell surface cilium proteins Prom1 (red) locates at the basement of OS interacting with Cdhr1 (green) (Yang, Chen et al. 2008) while Usherin (pink) locates at the apical inner segment recess that wraps around the connecting cilia (periciliary membrane complex) (Liu, Bulgakov et al. 2007). Other cilia surface molecules which are present in photoreceptor cilia include somatostatin receptor 2a and 3 in newt (Grigoryan, Vasilaki et al. 2003), and possibly polycystin 2 the mutation of which leads to photoreceptor degeneration in rat(Feng, Wang et al. 2009).

5.2 Results

5.2.1 Photoreceptor precursors are enriched with cilium-related genes

To find out what cilium genes are enriched in photoreceptor precursor cells, I uploaded all the genes with more than 2-fold higher expression in the photoreceptor gene sets from the E15.5 CrxGFP, P4 CrxGFP, and P4 NrlGFP array to DAVID. Genes which were annotated to be related with cilium (see Appendix table 3.4 for cilium-related GO terms used) were pulled out and compared between the Nrl and Crx array (Table 5.1, Figure 5.2 A). Expression of three genes *Cngb3* (synonyms *Cng6*), *Pdc*, and *Rpgrip1* were enriched in all three cell populations. CNG ion channels depolarize cilium potential to amplify cAMP signals and lack of this amplification leads to severely blunted odorant responsiveness in mice (Hengl, Kaneko et al. 2010). *Cngb3* (protein name Cyclic nucleotide-gated cation channel beta-3) encodes the beta subunit of a CNG cation channel protein which upon activation leads to opening of the cone cation channel and causes an electrical response (Gerstner, Zong et al. 2000). Loss or mutation of *Cngb3* is associated with achromatopsia (Kohl, Baumann et al. 2000; Sundin, Yang et al. 2000; Xu, Morris et al. 2011), a retina disorder characterised by inability to distinguish colours and low visual acuity. *Cngb3* expression was 26-fold higher in the E15.5 CrxGFP+ve cells than the E15.5 CrxGFP-ve cells. Such a difference agrees with the concept that embryonic photoreceptor cells are mainly cones. As development proceeds and rods outnumber cones, the difference is decreased. Nevertheless, its absolute expression in photoreceptor cells is still increased from E15.5 to P4 by 1.3-fold indicating the continued requirement of Cngb3 by cones.

Also showing higher expression in E15.5 photoreceptor cells than other retinal cells are *Pdc* and *Rpgrip1*, although their expression fold changes were even higher in the P4+ve vs P4–ve comparison and the P4+ve vs E15.5+ve comparison indicating more demand of these genes in the rods. *Pdc* (protein name Phosducin) is involved in regulating phototransduction by interaction with transducin subunits in the OS (Lee, Ting et al. 1992). Rpgrip1 (protein name X-linked retinitis pigmentosa GTPase regulator-interacting protein 1, RPGR-interacting protein 1) forms stable polymers to tether RPGR in the photoreceptor connecting cilium. It is required for normal outer segment disk morphogenesis and its deficiency is a known cause of LCA (Zhao, Hong et al. 2003). Rpgrip1 protein is located between the axonemal microtubules and the plasma membrane in the connecting cilium of photoreceptor cells (Zhao, Hong et al. 2003).

18 cilium annotated genes were shared between the P4 CrxGFP+ve and NrlGFP+ve cells and 17 genes were present only in the NrlP4 array probably because of its higher sensitivity (Table 5.1). Therefore a total of 35 cilium annotated genes were enriched in the postnatal photoreceptor

precursor cells. Many of these proteins are known to be located in different regions of the mature photoreceptor cilia such as the OS disks (eg. *Rho*, *Opn1sw*, *Arr3*), the axoneme (eg. *Ttll3*, *Dnaic2*), the transition zone (eg. *Cep290*) and the basal body (eg. *BBS5*) (Table 5.2). Most of these proteins are intracellular, particularly the ones at basal bodies, transition zones, and rod OS disks. But some are located on the plasma membrane and contain extracellular domains (highlighted as bold in Table 5.1).

In summary, expression of 38 cilium-related genes was found to be enriched in the photoreceptor precursor cells, among which 23 are associated with retinal diseases (Table 5.2). As well as the higher expression fold changes in the P4 photoreceptor cells than other retinal cells, three cilium genes also showed much higher expression in the E15.5 photoreceptor cells than other retinal cells (Figure 5.2 B, Table 5.1) suggesting cilium development as early as embryonic stages. It should be noted, however, that all 38 cilium related genes identified showed higher expression in P4 photoreceptor cells than E15.5 photoreceptor cells (Figure 5.2 B, Table 5.1). In addition, many more genes were enriched in the P4 photoreceptor cells than the E15.5 photoreceptor cells (35 genes vs 3 genes). This shows that the postnatal photoreceptor precursor cells are indeed more enriched with expression of cilium-related genes than the embryonic photoreceptor precursor cells.

Table 5.1 Cilium-related gene lists from array

Array	Gene Symbol	Gene Name	Expression Fold Change			
			CrxE15 + vs. -	CrxP4 + vs. -	NrlP4 + vs. -	Crx+ E15 vs. P4
CrxE15+ve CrxP4+ve NrlP4+ve common (3)	**Cngb3**	cyclic nucleotide gated channel beta 3	26.0673	12.9657	12.6	1.32521
	Pdc	phosducin	16.5561	43.7619	84.4	12.2548
	Rpgrip1	retinitis pigmentosa GTPase regulator interacting protein 1	5.75074	21.604	33.4	6.26463
CrxP4+ve NrlP4+ve common (18)	Rp1h	retinitis pigmentosa 1 homolog (human)	1.35926	44.6873	122	49.0212
	Cnga1	cyclic nucleotide gated channel alpha 1	1.11251	36.0885	34.1	40.8715
	Rho	rhodopsin	-1.04559	34.1121	127	44.2423
	Prom1	prominin 1	1.24535	9.40123	9.19	4.24424
	Opn1sw	opsin 1 (cone pigments), short-wave-sensitive (color blindness, tritan)	1.46211	7.35149	42.2	6.23974
	Ush2a	Usher syndrome 2A (autosomal recessive, mild) homolog (human)	2.28418	7.01788	24.8	3.4602
	Cep290	centrosomal protein 290	1.35788	5.92009	7.01	3.28442
	Bbs5	Bardet-Biedl syndrome 5 (human)	1.35512	5.47092	7.46	4.40103
	Gnat1	guanine nucleotide binding protein, alpha transducing 1	1.15297	4.24634	18.8	4.09312
	Bbs4	Bardet-Biedl syndrome 4 (human)	1.26758	3.54791	4.14	2.16995
	Bbs9	Bardet-Biedl syndrome 9 (human)	-1.20228	3.37727	5.31	4.54105
	Arr3	arrestin 3, retinal	1.03877	3.33913	8.75	3.24265
	Pcdh15	protocadherin 15	3.09258	2.87036	5.46	6.92572
	Bbs7	Bardet-Biedl syndrome 7 (human)	-1.02996	2.64062	3.89	2.5832
	Ttc8	tetratricopeptide repeat domain 8	1.19381	2.63163	3.32	2.31089
	Plekhb1	pleckstrin homology domain containing, family B (evectins) member 1	1.2541	2.27326	5.03	4.14376
	Rpgr	retinitis pigmentosa GTPase regulator	-1.098	2.20675	2.01	2.0735
	Ttc30a2	tetratricopeptide repeat domain 30A2	-1.07089	2.02147	2.73	2.19464
NrlP4+ve alone (17)	Klc3	kinesin light chain 3			5.78	
	Crocc	ciliary rootlet coiled-coil, rootletin			4.23	
	Nphp4	nephronophthisis 4 (juvenile) homolog (human)			3.53	
	Ttc30b	tetratricopeptide repeat domain 30B			3.46	
	Bbs1	Bardet-Biedl syndrome 1 (human)			3.32	
	Rab27a	RAB27A, member RAS oncogene family			3.23	
	Cc2d2a	coiled-coil and C2 domain containing 2A			2.68	
	Stard10	START domain containing 10			2.62	
	Slc4a7	solute carrier family 4, sodium bicarbonate cotransporter, member 7			2.46	
	Lca5	Leber congenital amaurosis 5 (human)			2.43	
	Myo7a	myosin VIIa			2.41	
	Cnga3	cyclic nucleotide gated channel alpha 3			2.39	
	Bbs2	Bardet-Biedl syndrome 2 (human)			2.33	
	Ttll3	tubulin tyrosine ligase-like family, member 3			2.23	
	Dnaic2	dynein, axonemal, intermediate chain 2			2.14	
	Ttc30a1	tetratricopeptide repeat domain 30A1			2.03	
	1700027N10Rik	RIKEN cDNA 1700027N10 gene			2	
CrxP4+ve alone (0)						

Bolded genes encode cell surface proteins

Table 5.2 Cilium-related gene function, location and associated retinal diseases

Gene Symbol	Function	Location	Retinal disease
Cngb3	cGMP actived opening of cation channel	multipass mem, OS	recessive achromatopsia Pingelapese; recessive, progressive cone dystrophy
Pdc	visual phototransduction	cilium	na
Rpgrip1	disk morphogenesis	cilium	recessive Leber congenital amaurosis; recessive cone-rod dystrophy
Rp1h	PR differentiation	CC, IS, cell bodies of PR	na
Cnga1	cGMP actived opening cation channel	multipass mem, OS	recessive retinitis pigmentosa
Rho	image-forming vision, postnatal PR viability	multipass mem, IS, OS	dominant retinitis pigmentosa; dominant congenital stationary night blindness; recessive retinitis pigmentosa
Prom1	binds cholesterol, regulate disk morphogenesis and MAPK and Akt pathways	multi-pass mem, cilium, base of rod OS	recessive retinitis pigmentosa with macular degeneration; dominant Stargardt-like macular dystrophy; dominant macular dystrophy, bull's-eye; dominant cone-rod dystrophy
Opn1sw	visual pigments, increase spectral sensitivity	multi-pass mem, cone OS	dominant tritanopia
Ush2a	involved in hearing and vision, required for integration into the basement mem. interact with collagen IV and fibronectin	single-pass type I mem protein, stereocilium mem, apical and basement mem, high in basement mem, synaptic terminals of PR	recessive Usher syndrome, type 2a; recessive retinitis pigmentosa
Cep290	localization of ciliary and phototransducin proteins	cilium transition zone, nucleus, centrosome	recessive Senior-Loken syndrome; recessive Joubert syndrome; recessive Leber congenital amaurosis; recessive Meckel syndrome
Bbs5	BBSome complex, ciliogenesis	cilium basal bodies	recessive Bardet-Biedl syndrome
Gnat1	amplifies and transduces visual impulse, GTP-binding, nucleotide-binding	OS, CC	dominant congenital stationary night blindness, Nougaret type; recessive congenital stationary night blindness
Bbs4	BBSome complex, ciliogenesis	cilium mem, cytoplasm	recessive Bardet-Biedl syndrome
Bbs9	BBSome complex, ciliogenesis	cilium mem, cytoplasm	recessive Bardet Biedl syndrome
Arr3	May play a role in an as yet undefined retina-specific signal transduction. Could binds to photoactivated-phosphorylated red/green opsins.	IS, OS	na
Pcdh15	Calcium-dependent cell-adhesion protein. Required for inner ear neuroepithelial cell elaboration and cochlear function. Probably involved in the maintenance of normal retinal function	single-pass type I mem (heavy glycosalation), stereocilium, OS,	recessive Usher syndrome, type 1f; recessive deafness without retinitis pigmentosa; digenic Usher syndrome with CDH23
Bbs7	BBSome complex, ciliogenesis	cilium mem, cytoplasm	recessiveBardet Biedl syndrome
Ttc8/Bbs8	BBSome complex, ciliogenesis	cilium mem, cytoplasm	recessive Bardet-Biedl syndrome; recessive retinitis pigmentosa
Plekhb1	binds transducins.Interacts with MYO1C	mem-associated. Highly in OS	na
Rpgr	PR integrity, ciliogenesis	centrosome, cilium basal body and axoneme	X-linked retinitis pigmentosa, recessive; X-linked retinitis pigmentosa, dominant; X-linked cone dystrophy 1; X-linked atrophic macular dystrophy, recessive
Ttc30a2	polyglutamylation of axonemal tubulin; anterograde intraflagellar transport	cilium	na
Klc3	microtubule-associated force-producing protein that may play a role in organelle transport	Elongating spermatid tail midpiece. Localized in outer dense fibers (ODFs) and associates with mitochondria	na
Crocc	Rootletin,structural component of the ciliary rootlet; contributes to centrosome cohesion before mitosis	In ciliated cells, associated with ciliary rootlets. In non-ciliated cells, localized between, around and at the proximal ends of the centrioles.	na
Nphp4	organization of apical junctions in kidney cells; may not strictly required for ciliogenesis	cilium basal body; centrosome; tight junction	recessive Senior-Loken syndrome; recessive nephronophthisis, juvenile
Ttc30b	polyglutamylation of axonemal tubulin; anterograde intraflagellar transport	cilium	na
Bbs1	BBSome complex, ciliogenesis	cilium, basal bodies	recessive Bardet-Biedl syndrome
Rab27a	cytotoxic granule exocytosis in lymphocytes	Lipid-anchor. Melanosome; Late endosome; Lysosome	na
Cc2d2a	in tectonic-like complex acting as a barrier that prevents diffusion of transmembrane proteins between the cilia and plasma membranes. Required for ciliogenesis and sonic hedgehog/SHH signaling	cilium transition zone between basal body and axoneme	recessive retinitis pigmentosa and mental retardation; recessive Joubert syndrome
Stard10	Phospholipid transfer protein	cilium flagellum; cytoplasm; membrane	na
Slc4a7	Electroneutral sodium- and bicarbonate-dependent cotransporter	multi-pass membrane protein; apical cell membrane; stereocilium	na
Lca5	minus end-directed microtubule transport	cilium axoneme and basal body	recessive Leber congenital amaurosis
Myo7a	outer PR disks renewal; regulation of opsin transport; ditribution and migration of RPE melanosomes and phagosomes; RPE65 transport	inner and base of OS and synaptic ending region; cytoskeleton	recessive Usher syndrome, type 1b; recessive congenital deafness without retinitis pigmentosa; recessive atypical Usher syndrome (USH3-like)
Cnga3	Cyclic nucleotide-gated cation channel alpha-3; essential for the generation of light-evoked electrical responses in the red-, green- and blue sensitive cones	multi-pass membrane protein; OS	recessive achromatopsia
Bbs2	BBSome complex, ciliogenesis	cilium, basal bodies	recessive Bardet-Biedl syndrome
Ttll3	Tubulin monoglycylase generating side chains of glycine on the gamma-carboxyl groups of glutamate residues within the C-terminal tail of alpha- and beta-tubulin	cilium axoneme; cytoskeleton	na
Dnaic2	Dynein intermediate chain 2, axonemal	cilium axoneme	na
Ttc30a1	polyglutamylation of axonemal tubulin; anterograde intraflagellar transport	cilium	na
1700027N10Rik/Rsph9	Radial spoke head protein 9 homolog, component of the axonemal radial spoke head appears to interact with the projections from the central pair of microtubules	cilium axoneme, radial spoke	na

Retnet last updated July 25, 2013 (last access 31 July 2013) for retinal diseases. Uniprot last updated July 24, 2013 (last acess 31 July 2013) for protein fucntion and location. CC, connecting cilium; OS, outer segment; IS, inner segment; mem, membrane; na, not available

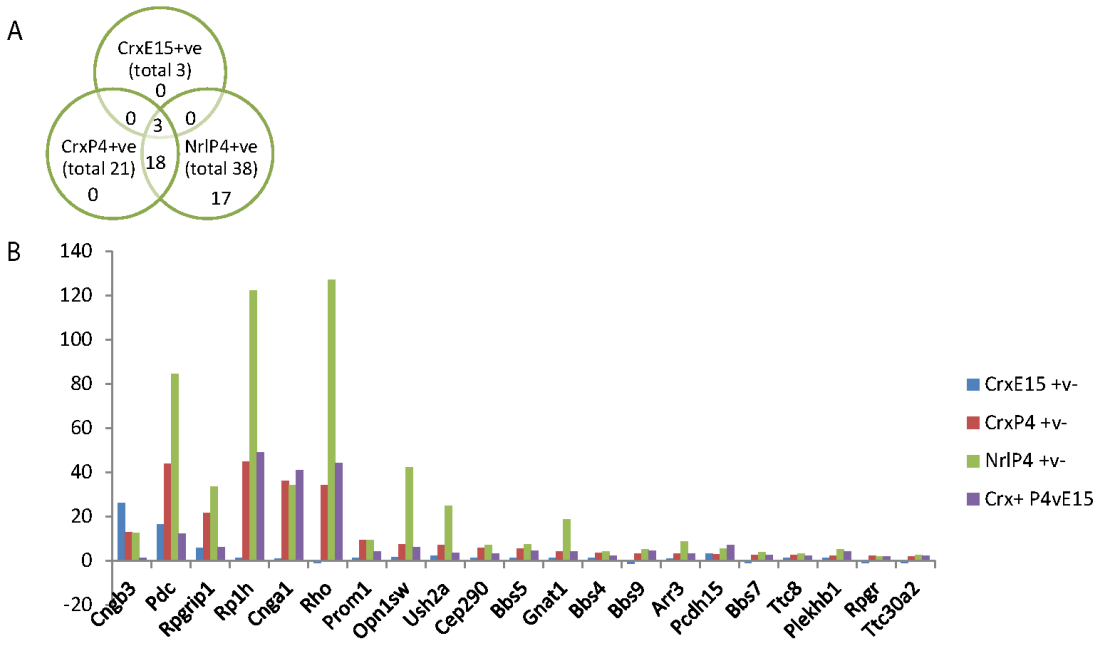

Figure 5.2 Cilium-related genes comparison and expression fold changes (A) Venn diagram showing the number of common and different cilium-related genes in E15.5 Crx+ve, P4 Crx+ve cells and P4 Nrl+ve cells (B) Histogram of expression fold changes of the common cilium-related genes.

5.2.2 Cilium development in photoreceptor cells

To test if there is any cilium-related difference between the E15.5 and P4 photoreceptor cells at the protein level, I examined the IHC of three proteins which are established cilium markers in other systems. Acetylated α-tubulin (AcTub) marks the axoneme (Fliegauf, Benzing et al. 2007) and has been used as a cilia marker in mouse embryonic fibroblasts, embryonic nodes and perineural mesenchyme tissues etc (Garcia-Gonzalo, Corbit et al. 2011). CenpF is a centromere protein that is transiently associated with the outer kinetochore plate of chromosomes for their segregation in M phase (Liao, Winkfein et al. 1995; Zhu, Mancini et al. 1995; Yang, Guo et al. 2003) and relocalizes at different phases of cell cycle (Zhu, Mancini et al. 1995; Yang, Guo et al. 2003; Pooley, Moynihan et al. 2008). In differentiated cells CenpF is found to localize at the centrosome (Moynihan, Pooley et al. 2009; Bolhy, Bouhlel et al. 2011) which is composed of centrioles which form basal bodies in interphase to assemble primary cilia (Kobayashi and Dynlacht 2011). Upon ablation of the CenpF protein, the centrosomal proteins which CenpF colocalize with redistribute and the nucleation, anchoring and repolymerization of centrosome specific microtubules are disrupted (Moynihan, Pooley et al. 2009). GT335 is a monoclonal antibody raised against glutamylated tubulins and specifically recognizes polyglutamylation which is a unique posttranslational modification that is highly

abundant in cilia. It stains the basal bodies and the axonemes of nearly all ciliated cells such as human nasal epithelia cells (Million, Larcher et al. 1999), mouse tracheal cilia (Ikegami, Sato et al. 2010), mouse and sea urchin sperm flagellar microtubules and basal bodies (Kann, Soues et al. 2003), lung ciliated cells axonemes and basal bodies (Kann, Soues et al. 2003).

At E15.5, AcTub expression was detected mainly at the apical region of the ONBL and the bottom of the INBL (Figure 5.3 A). By P4, AcTub was expressed all over the retina, but was particularly high in the apical region of the photoreceptor layer (Figure 5.3 B). CenpF was weakly expressed also at the apical region of the ONBL in E15.5 retina (Figure 5.3 C). At P4, CenpF expression at the apical region of the ONBL was much higher and was more specifically localized at the interphase between the apical protrusion and the remaining of the cell body (Figure 5.3 D) although expression in the inner INBL was also observable. Similar to CenpF and AcTub, GT335 was also weakly expressed at the apical region of the ONBL at E15.5 and more highly expressed there at P4 (Figure 5.3 E, F). So clearly these cilium markers were expressed in E15.5 retina, but were more highly expressed in P4.

It is also noticeble that while location of these cilium markers were not so different at E15.5 (all at the tip of the protrusion), their location in the cilium at P4 differs slightly. While GT335 expression spread into the axoneme and the basal bodies of the cilia, CenpF expression was only confined at the bottom of the cilia where the centrosome locates and AcTub stained the thin axoneme structures of cilia. Such differences probably reflect the more developed structure of the cilia.

Therefore, I conclude that the cilium marker proteins began to localise in photoreceptor cells as early as E15.5, but much more abundant expression as well as more defined localization was seen in P4 when the cilium structure is more developed. This indicates cilium began to form as early as E15.5 and was more established by P4. This agrees well with the early electron micrographs showing protrusions (and even centrioles in the protrusions) in some photoreceptor cells (Chapter 1, Figure 1.3) (Hinds and Hinds 1979) and the microarray analysis that a few cilium related genes can already be detected at E15.5 but much more were enriched at P4 and that cilium was a feature for the P4 photoreceptor cells.

However these cilium markers are located within the cell. Because I am interested in cell surface proteins as these have the potential to interact with other extracellular molecules to organise cell location or affect migration, I went on to examine if the cilium-related cell surface proteins show the same expression pattern.

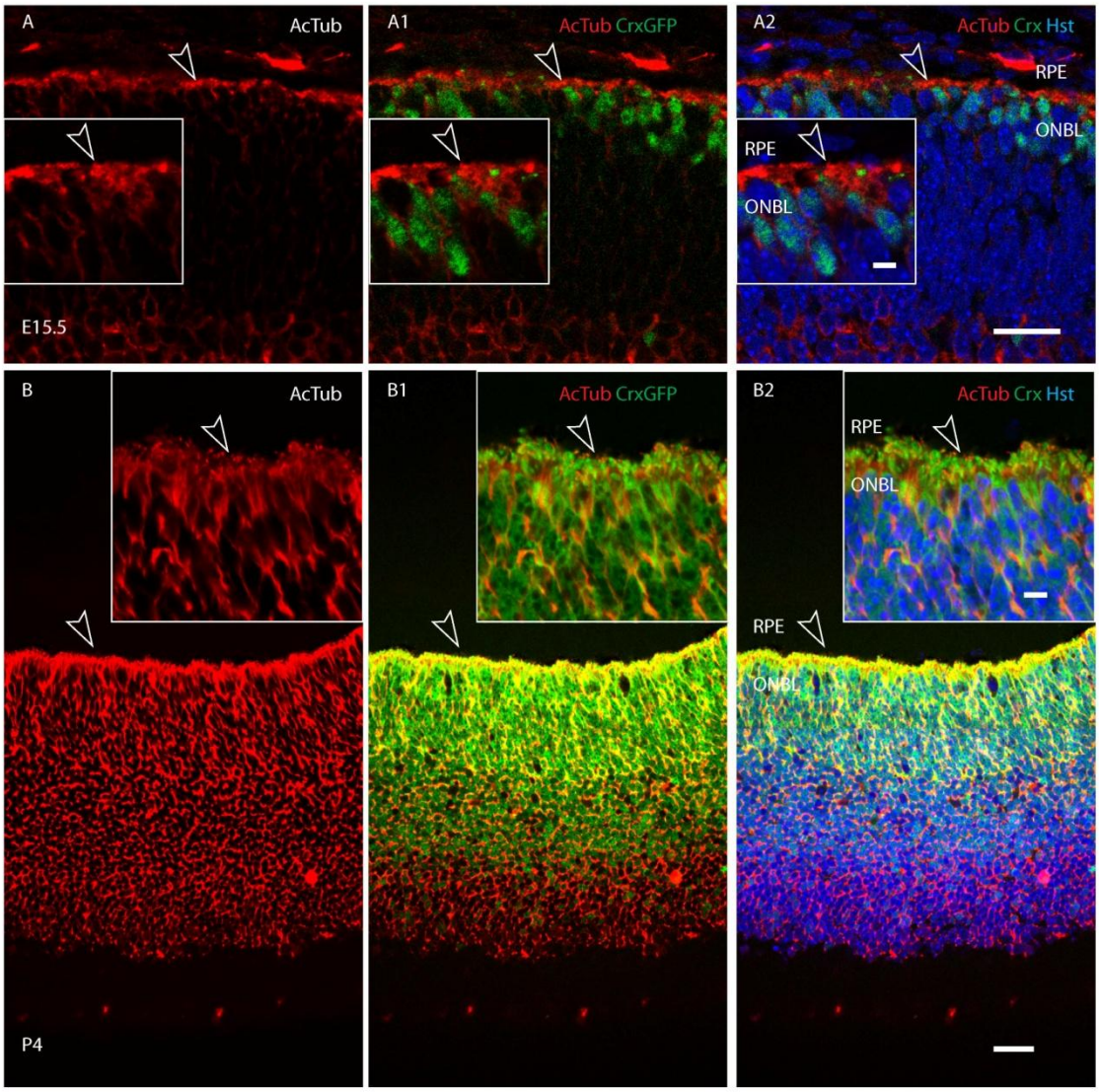

Figure 5.3 Cilium markers expression in mouse retina (continues). Confocal images of AcTub (panel A and B), CenpF (panel C and D), and GT335 (panel E and F) on E15.5 and P4 CrxGFP retina. Cilium markers (red), CrxGFP (green), Hoechst 33342 (Hst, blue). Scale bars represent 25 µm except in inserts which are 5 µm.

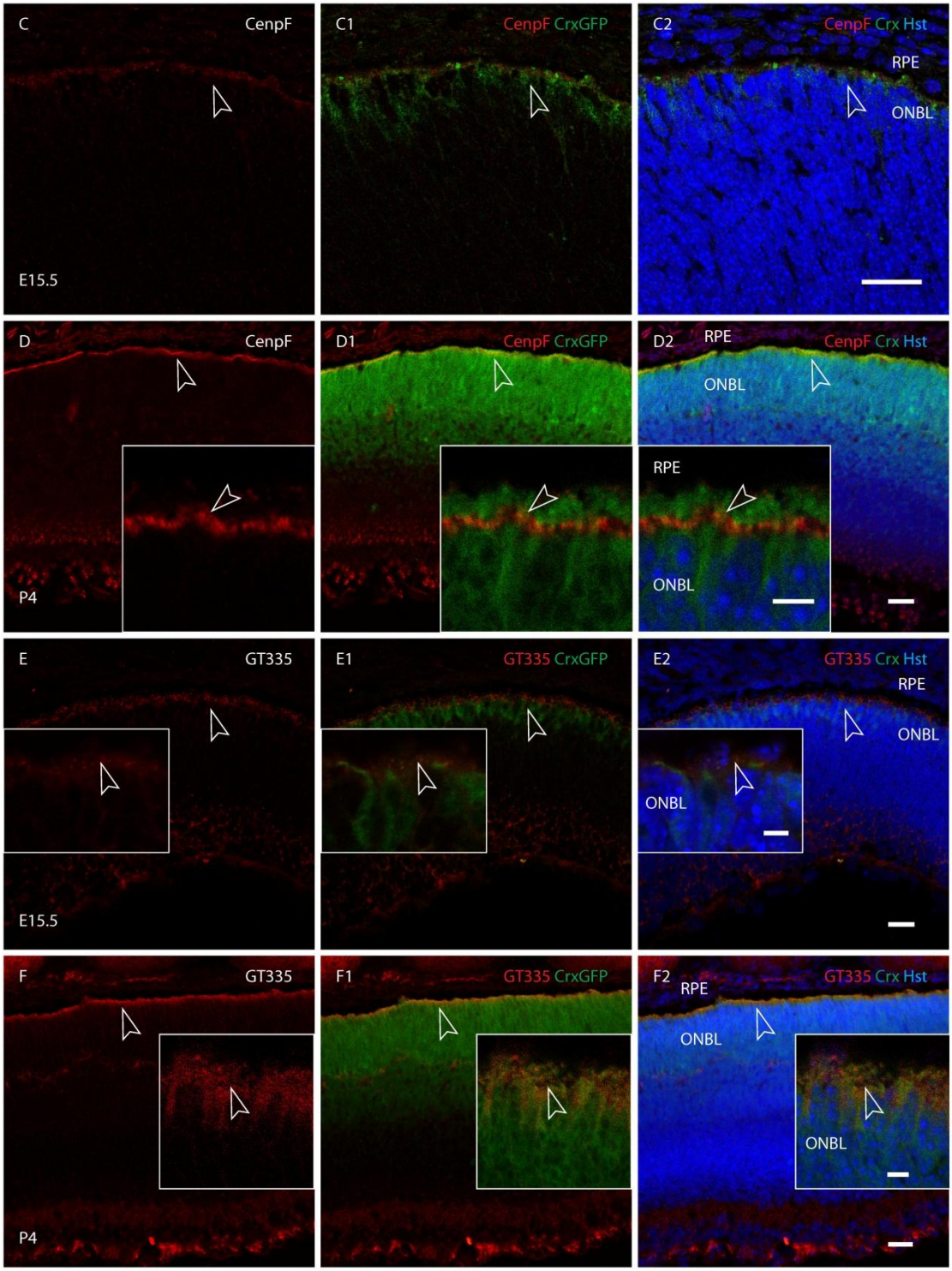

Figure 5.3 Cilium markers expression in mouse retina- continued. Confocal images of AcTub (panel A and B), CenpF (panel C and D), and GT335 (panel E and F) on E15.5 and P4 CrxGFP retina. Cilium markers (red), CrxGFP (green), Hoechst 33342 (Hst, blue). Scale bars represent 25 µm except in inserts which are 5 µm.

5.2.3 Prom1 is expressed in the cilium regions of photoreceptor cells throughout retinal development

Despite involvement with the protruding cilium structure, not all the cilium proteins I pulled out above from the transcriptome analysis (Table 5.1) are located on the cell surface or have extracelluar domains. The BBS proteins, for example, are located within the cell at the bottom of the cilium region around the basal bodies. And pericentriolar marker Cep290 only shows a centrosome localization (Valente, Silhavy et al. 2006; Otto, Hurd et al. 2010). In fact, only 9 out of the 38 proteins above are annotated to contain extracellular domains. These are *Cngb3*, *Cnga1*, *Rho*, *Opn1sw*, *Prom1*, *Ush2a*, *Pcdh15, Slc4a7* and *Cnga3* (Table 5.1 and Table 5.2, highlight in bold). The CNG proteins, Rhodopsin and opsins have been well studied and are involved in phototransduction. In the case of Rhodopsin, although it is annotated to contain four extracellular domains, these domains are probably only extracellular when the protein is at the base of the OS where new disks remain open. The most common presence of Rhodopsin, however, is on membranes of mature rod OS disks which are inside the cell. The CNG proteins and S-opsin, located on the open disks of cone OS, are true cell surface molecules. In Chapter 3, I prioritized some cell surface protein candidates (Table 3.5) which included *Prom1*, *Cdhr1/Pcdh21*, *Pcdh15* and *Ush2a* implicated in cell projection and showed high level up regulation (> 5-fold). Prom1 was reported to locate at the basement of outer segments interacting with Cdhr1 for OS formation (Yang, Chen et al. 2008) (see Figure 5.1 for locations of Prom1, Cdhr1 and Ush2a/Usherin in rod cilia). Pcdh15 and Ush2a mutations are associated with Usher syndromes which initially affected photoreceptor cells followed by RPE pathology in the eye (Jacobson, Cideciyan et al. 2008). As Prom1 and Pcdh15 showed higher expression levels from the microarray (Figure 3.9) and their antibodies were available, I first examined the retina development expression profile of these two proteins.

From E15.5 to P4, Prom1 showed intense polarised staining at the apical regions of the developing photoreceptor layer where the cilia will develop (Figure 5.4, A, B, C, A2, B2, C2). The discrete punctate distribution of Prom1 along development at the cilium region colocalizes with the CrxGFP signals there (Figure 5.4, inserts in row A and row C). A lower level of Prom1 staining within the developing neuroblastic layer at these stages was also detected, but the expression was more diffuse and seemed to be outlining the cell borders (Figure 5.4, A2, B2, and inserts in row A and C). At later stages when the photoreceptor cells are matured, Prom1 expression was confined to the basement of the outer segments and no expression was observed in other retinal cell types (Figure 5.4, row D and E). Quantitative PCR showed that Prom1 transcripts showed more than 5 – 8 folds higher expression after birth relative to its expression in embryonic stages (Figure 5.4, F).

Therefore, Prom1 seemed to label the nascent cilia in photoreceptor precursor cells, and in the mature rod photoreceptor cells at the bottom of rod OS disks near the top of the connecting cilium.

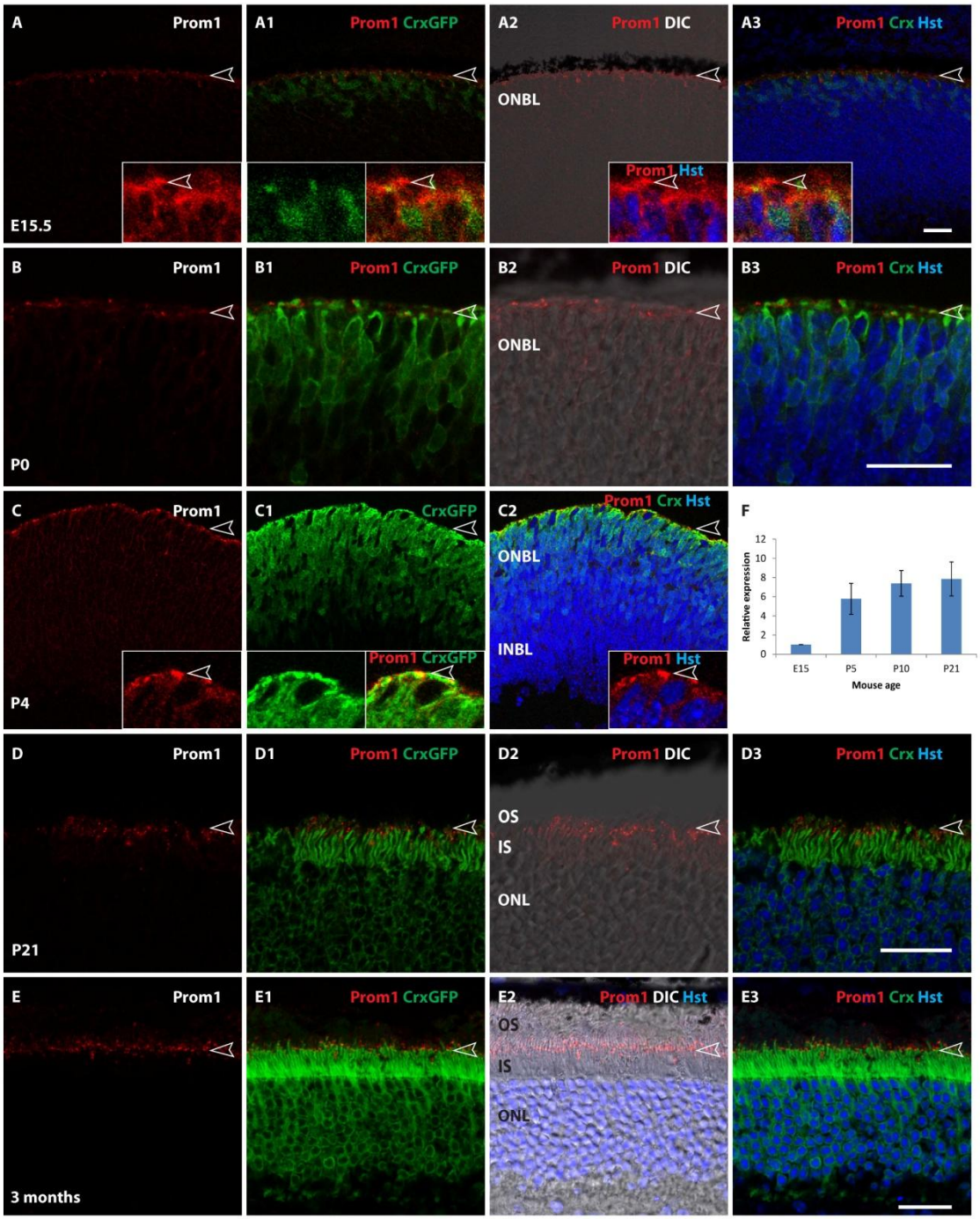

Figure 5.4 Prom1 expression profile during retinal development. (A – E) Confocal images of Prom1 IHC in CrxGFP mouse eye sections along development, scale bar represent 25 µm; (F) Prom1 qPCR in retinal development, error bar represents standard deviation of three independent samples.

5.2.4 Pcdh15 is expressed in cilium and synapses of photoreceptor cells as well as other retinal cells throughout retinal development

In embryonic stages, Pcdh15 showed intense punctate staining at the apical regions of the developing ONBL (Figure 5.5, row A), similar to Prom1. But unlike Prom1, strong punctate staining near the bottom of the INBL was also observed for Pcdh15. After birth while it maintained the high expression at the outer edge of the photoreceptor cells, Pcdh15 was also expressed at the emerging OPL where photoreceptor synapses locate (Figure 5.5, row B, C and D). In addition, it was also expressed in the inner retina including the INBL/INL and GCL (Figure 5.5, row B to E) whereas expression in these regions was not observed for Prom1. When the retina was fully developed by P21, Pcdh15 expression in the photoreceptor apical regions was mainly in the outer segments and filled the whole structure (Figure 5.5, row E and inserts) in contrast to Prom1 which was only confined at the bottom of the OS.

Therefore, the cell surface molecule Pcdh15 is expressed in the photoreceptor cilia during development and in particular the outer segments. This, in addition to Prom1, provides a further cell surface marker to study the photoreceptor cilium. However, it should be noted that Pcdh15 is also expressed in the photoreceptor synapses regions and other retinal cell types.

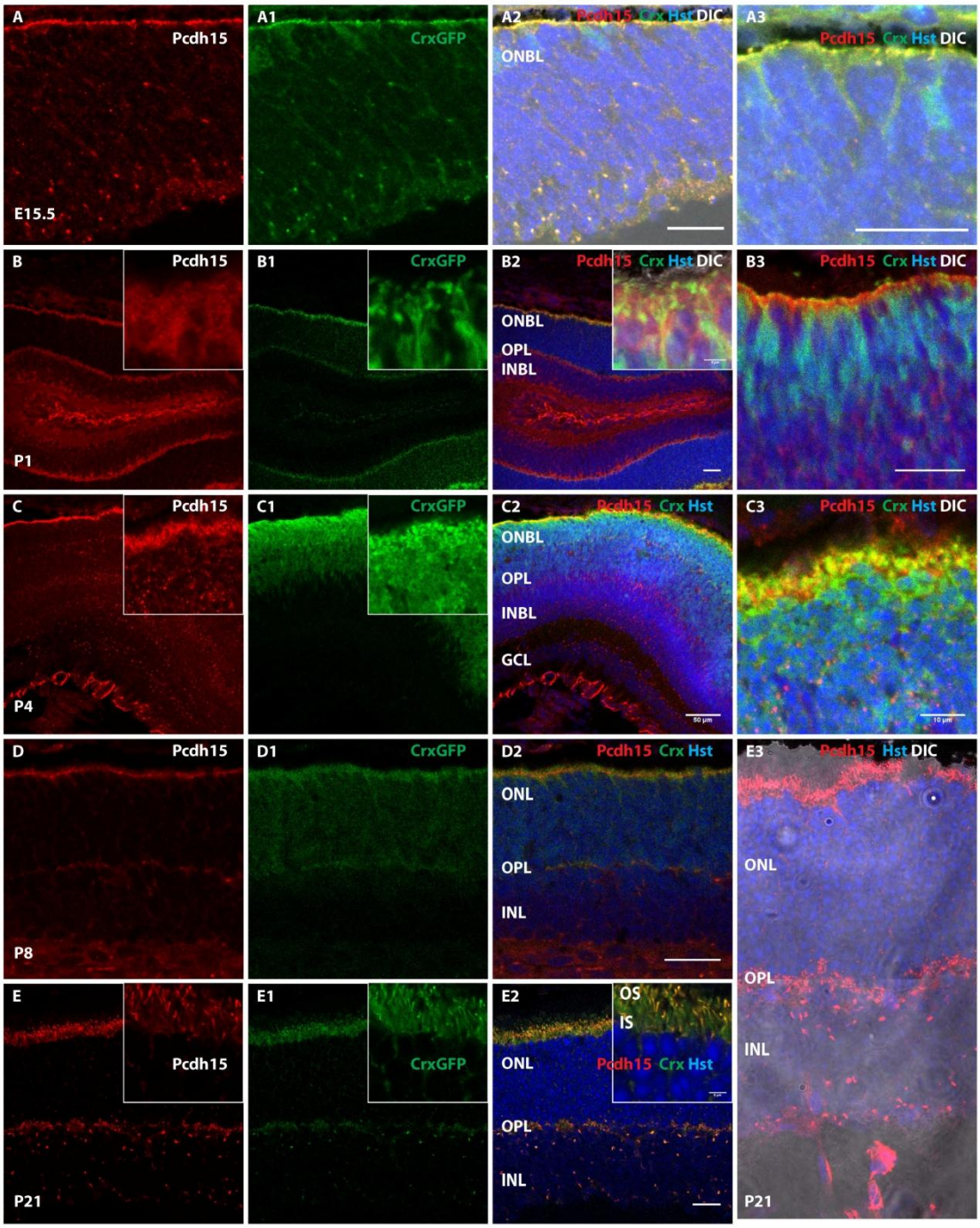

Figure 5.5 Pcdh15 expression profile in CrxGFP retinal sections along development. (A - E) Confocal images of Pcdh15 IHC in CrxGFP mouse eye sections along development. (C3) shows the enlarged image of the inserts for (C – C2). Scale bar represent 25 µm for all except (C2) for 50 µm, (C3) for 10 µm, and the inserts for (B – B2) and (E – E2) for 5 µm.

5.2.5 Prom1 is expressed on migrating transplanted photoreceptor cells

Because Prom1 more specifically labeled the photoreceptor cilia than Pcdh15, I examined if this cilium-related cell surface marker is involved in the migration of transplanted photoreceptor cells. P4 CrxGFP+ve cells were FACS sorted and injected into the SRS of adult wildtype mouse eyes. 3 to 12 days after injection, eyes of the host animals were collected and analysed for Prom1 expression. The transplanted photoreceptor cells which can migrate away from the SRS to the segment region or ONL clearly expressed Prom1 (Figure 5.6). Interestingly, while the transplanted cells at the segment region mostly show Prom1 expression all over the cell body (Figure 5.6 A2, B2, n = 76 GFP+ve cells counted), transplanted cells in the ONL seemed have higher enrichment of Prom1 in particular directions/regions (Figure 5.6 C2, n = 38 GFP+ve cells counted), although the directions/regions varied in different cells.

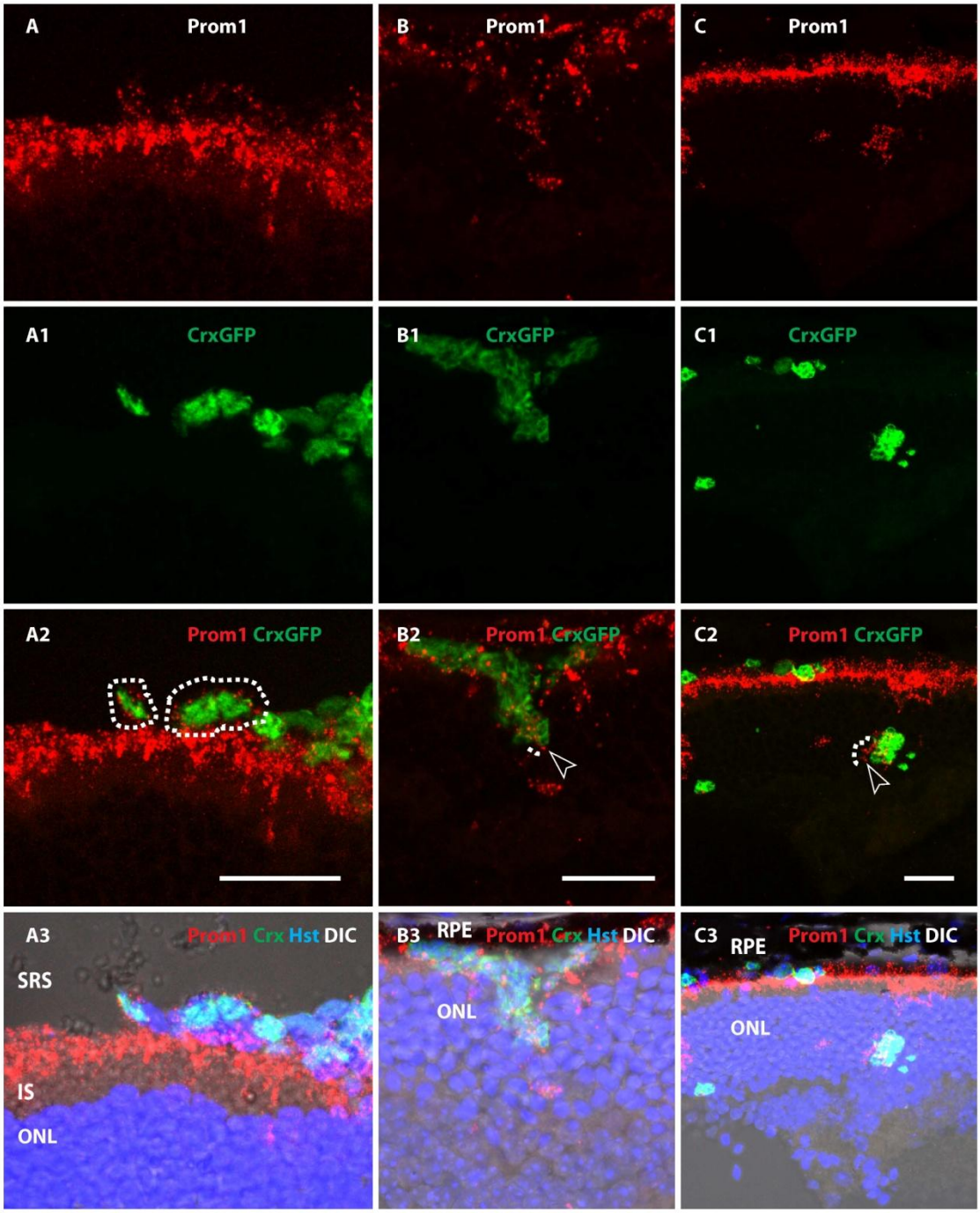

Figure 5.6 Prom1 expression on transplanted photoreceptor cells. All confocal Z-projections. (A – A3) 3 days after transplantation; (B – B3, and C – C3) 6 days after transplantation. Prom1 (red), CrxGFP (green), Hoechst 33342 (Hst, blue). Dashed line or arrow heads indicate Prom1 expression on transplanted cells. Scale bar represent 25 µm. N = 76 GFP+ve cells counted in segment region and n = 38 GFP+ve cells counted in ONL.

5.3 Discussion

I noticed that the postnatal photoreceptor cells featured the cilium property according to the gene ontology analysis of the transcriptome study in Chapter 3 (Figure 3.3, Figure 3.6). Here in this chapter, I confirmed that these cells indeed enriched expression of many cilium related genes (Table 5.1). These genes are mainly retinitis pigmentosa genes, nucleotide channel or binding proteins, opsins or arrestins, and BBS proteins. In addition, all these genes showed higher expression in postnatal photoreceptor cells than embryonic photoreceptor cells (Figure 5.2 B, Table 5.1). And all their expressions were higher in photoreceptor cells than other retinal cells at the postnatal stage (Figure 5.2 B, Table 5.1). Three of these genes also showed much higher expression in photoreceptor cells than other retinal cells at the embryonic stage indicating cilium development as early as E15.5. I, therefore, propose that cilium genesis starts at E15.5 if not earlier and is quite developed as a feature structure for the photoreceptor cells by P4 – well before establishment of the outer segment. Further examination of the E15.5 and P4 retina using established cilium markers has confirmed this observation. Not only were the cilium markers detected at E15.5, but also more abundant protein expression as well as more defined localization was observed at P4 (Figure 5.3).

To explore the cilium property further, I examined two cilium surface molecules Prom1 and Pcdh15. Prom1 belong to the prominin family. Prominin family includes prominin-1, prominin-2 and prominin-like proteins and contains a conserved region of around 800 amino acid residues. They are pentaspan membrane proteins with two large extracellular glycosylated loops (over 250 residues, Prom1: 180 – 434 and 509 – 794,) and two small cytoplasmic loops, with the N-terminal domain (Prom1: 20 – 107) extruding out of the cell and C-terminal inside (Fargeas, Florek et al. 2003) (see Figure 5.7 B for Prom1 protein structure). The 115-KDa glycoprotein prominin-1 is expressed in a $CD34^{bright}$ subset of human hematopoietic stem and progenitor cells (Miraglia, Godfrey et al. 1997) and many epithelial cells and has been regarded as a surface marker for stem cells (Boivin, Labbe et al. 2009). In the context of retina, Prom1 protein has previously been reported to be expressed in photoreceptor cells (Maw, Corbeil et al. 2000; Yang, Chen et al. 2008; Zacchigna, Oh et al. 2009), and our data agrees with this (Figure 5.4, and (Lakowski, Han et al. 2011)). Transcripts of *Prom1* were nine fold higher in the photoreceptor cells than other retinal cells from our arrays (Figure 3.8) and in the ONBL or ONL throughout development except a few cells in INL also showed Prom1 expression in postnatal stages (Jaszai, Fargeas et al. 2011). The protein of Prominin-1 preferentially localizes to the apical surface of polarized cells and specifically associates with plasma membrane protrusions such as microvilli and microvilli-related structures of neuroepithelium and other epithelial cells

(Weigmann, Corbeil et al. 1997; Corbeil, Roper et al. 2000), filopodia, lamellipodia, and microspikes of CHO cells (Weigmann, Corbeil et al. 1997), and plasma membrane protrusions of fibroblasts and hematopoietic stem cells (Corbeil, Roper et al. 2000). In mature photoreceptor cells, prominin-1 was previously described to be concentrated in the plasma membrane evaginations at the base of the OS of rods (Maw, Corbeil et al. 2000; Yang, Chen et al. 2008; Zacchigna, Oh et al. 2009), and possibly spreads into the entire OS of cones (Jaszai, Fargeas et al. 2007). Our Immunohistochemistry of Prom1 in retina showed the same specificity toward the cilia region of the developed photoreceptor cells, ie at the basement of rod OS (Figure 5.4, and (Lakowski, Han et al. 2011)) and the entire cone OS (Figure 6.6 A' in chapter 6).

Furthermore, I showed that similar to our Immunohistochemistry of the established cilium markers, this cilium surface protein was also expressed in the apical protrusions of photoreceptor cells as early as E15.5. This is before birth when rod ciliogenesis was proposed to start in a recent study (Sedmak and Wolfrum 2011). The embryonic expression of the cilium markers and cilium surface proteins therefore highly indicate the cone cilia genesis at this stage. Early identification of centriole in the apical protrusion of E15 photoreceptor cells by electron microscopy images also agrees with this hypothesis (Hinds and Hinds 1979). Studies about initiation of cone ciliogenesis have been lacking except one study in tree shrew suggesting cone ciliogenesis starts around E20 (Knabe and Kuhn 1997). Our observation therefore provides mammalian evidence suggesting mouse cone ciliogenesis starts at least at E15.5. As rod ciliogenesis coincides with the birth peak of rods at P0 in mice, it is plausible that cone ciliogenesis may also coincide with the birth peak of cones at E14.5.

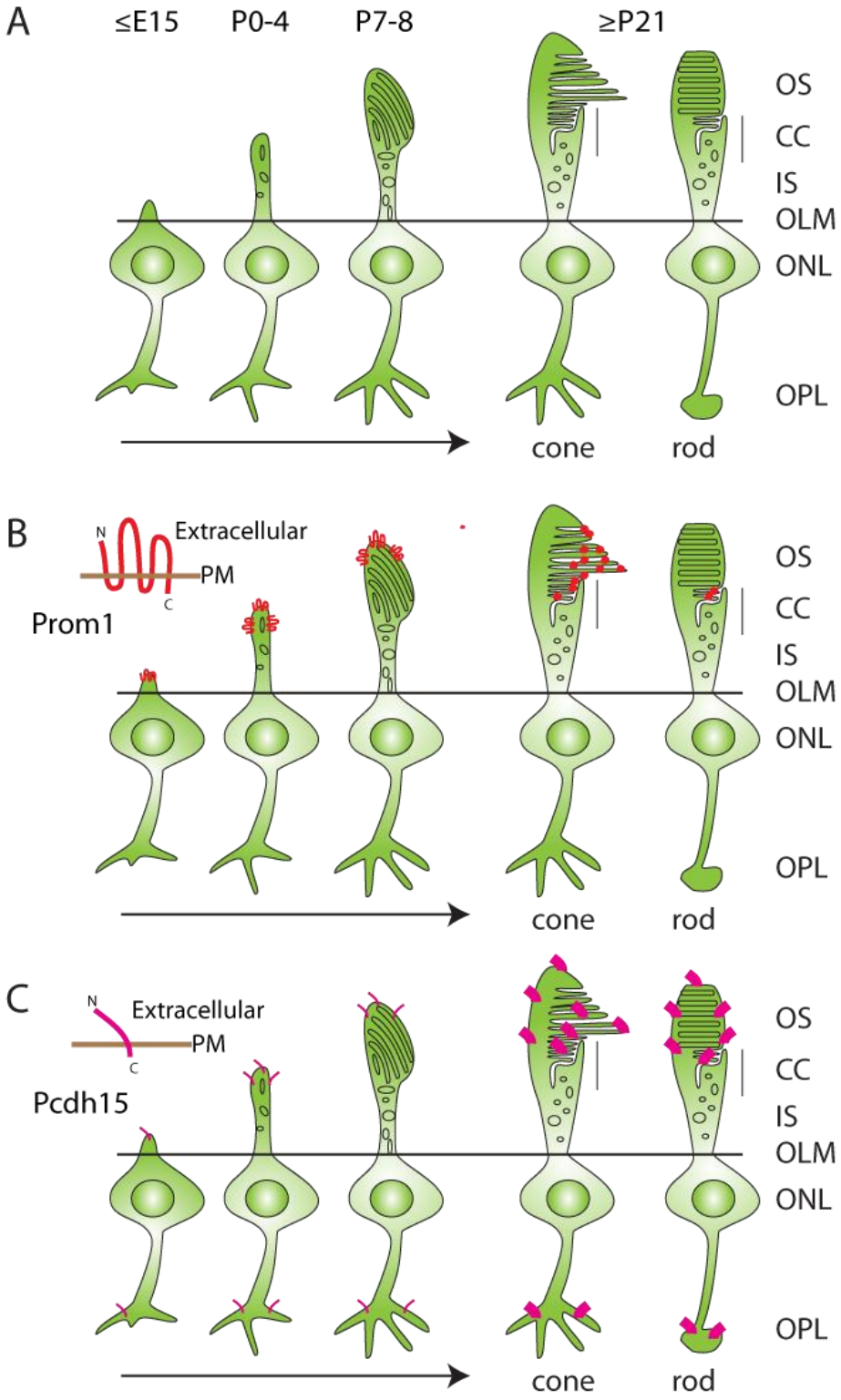

Figure 5.7 Model of photoreceptor cell cilia development and cilium surface proteins Prom1 and Pcdh15 location (A) Development of cilia and photoreceptor cells. (B) Structure and localisation of Prom1 on developing photoreceptor cells. (C) Structure and localisation of Pcdh15 on developing photoreceptor cells. E, embryonic day; P, postnatal day; OS, outer segment; CC, connecting cilium; IS, inner segment; OLM, outer limiting membrane; ONL, outer nuclear layer; OPL, outer plexing layer; Extracellular, extracellular side of the cell; PM, plasma membrane; N, N-terminus; C, C-terminus.

My colleagues showed that the E14.5 photoreceptor cells gave the maximum integration of cones and postnatal photoreceptor cells gave around 10 fold higher integration of rods after transplantation (Lakowski, Baron et al. 2010). The presence of cilia structures on E15.5 cones and the abundant and more defined cilia structures on P4 rods interestingly match the integration properties of the transplanted photoreceptor cells. It is therefore tempting to propose that the presence of cilia structures on photoreceptor cells might play a role in the integration of transplanted photoreceptor cells in the host environment. The primary cilia of fibroblasts were reported to align toward the direction of migration possibly helping fibroblasts to migrate (Albrecht-Buehler 1977; Schneider, Cammer et al. 2010). Our finding that the cilium surface protein Prom1 was directionally/regionally enriched on transplanted migrating photoreceptor cells (Figure 5.6) further supports this possibility. Interestingly while cells migrating in the ONL showed directional/local enrichment, cells in the segment region did not show such enrichment (Figure 5.6). It might be possible that the orientation roles of photoreceptor cilia only function after cells migrated in the ONL which might provide some directional cues that the cilia can sense and use to orient the cells. While before cells migrated in the ONL, the cilium surface molecules could be all over the cell body to search for such directional cues.

In addition to the intensive punctate staining at the apical protrusion, I also observed relatively weak expression of Prom1 around the cell body of photoreceptor cells in early development. Expression around the whole cell body was also observed on photoreceptor precursor cells after dissociation (Lakowski, Han et al. 2011) and after transplantation (Figure 5.6). The all around expression on developing photoreceptor cell bodies gradually diminished as more expression was concentrated to the apical regions as development proceeds. This observation has not been reported before. This may imply the translocation of this surface molecule from around the cell body to the cilium region. How this translocation works and whether it is coupled with the genesis of cilium will be worth further investigation. It is less likely to be based on direct interaction with the cytoskeleton, because neither studies which disturbed the actin-bundling protein villin and profoundly altered cytoskeletal architecture of epithelial microvilli abolished the preferential microvilli localization of prominin (supplementary data in (Roper, Corbeil et al. 2000)) nor did deletion of the C-terminal domain of Prom1 – the potential cytoskeleton interaction domain – impaired Prom1's microvilli specification in epithelial cells (Corbeil, Roper et al. 1999). Interestingly, when mild cholesterol depletion was applied to Prom1-transfected MDCK cells (using methyl-β-cyclodextrin), Prom1 was redistributed from microvilli to the entire apical plasma membrane (Roper, Corbeil et al. 2000). Indeed, Prom1

directly interacts with cholesterol (Roper, Corbeil et al. 2000) and is enriched in the cholesterol-based Lubrol lipid rafts (Roper, Corbeil et al. 2000; Corbeil, Roper et al. 2001). Although this may only explain the specification of Prom1 from microvilli to apical surface, it is possible that transportation of Prom1 from the Golgi complex and around the cell body to the apical surface may also involve cholesterol.

I also examined another cilium cell surface molecule Pcdh15. Pcdh15 is a single-pass type I membrane protein (see Figure 5.7 C for cartoon of Pcdh15 protein structure), usually heavily glycosylated. It is a calcium-dependent cell-adhesion protein, required for inner ear neuroepithelial cell elaboration (Lefevre, Michel et al. 2008) and cochlear function (Alagramam, Murcia et al. 2001). It can be found in the stereocilium of hair cells (Alagramam, Murcia et al. 2001; Kazmierczak, Sakaguchi et al. 2007; Lefevre, Michel et al. 2008) as well as photoreceptor cilia (Reiners, Marker et al. 2005). Interestingly there are two orthologues of Pcdh15 in zebrafish with Pcdh15a necessary for integrity of the stereociliary bundle while Pcdh15b knock down results in clumped photoreceptor outer segments positioned perpendicular to RPE (Seiler, Finger-Baier et al. 2005). PCDH15 (USH1F) mutation in human is associated with Usher syndromes (Jacobson, Cideciyan et al. 2008). Mouse Pcdh15 localizes in rod and cone outer segments and synapses and costains with peanut agglutinin (PNA), as well as in connecting cilium (Reiners, Marker et al. 2005). It also colocalizes with harmonin (USH1C) at the base of the photoreceptor outer segment where newly synthesized disk membranes are present (Reiners, Marker et al. 2005). Our Immunohistochemistry of Pcdh15 showed expression in the cilia (in particular OS) and synapses region of photoreceptor cells (Figure 5.5) which agrees with previous findings, but also expression in other types of retinal cells. As previous Immunohistochemistry in retina for Pcdh15 did not show the inner retina (Reiners, Marker et al. 2005), I do not know if that antibody also labels inner retina cells. It is possible that either murine Pcdh15 indeed labels other retinal cells or our antibody has non-specific effects. Although also expressed in the synapses of photoreceptor cells, Pcdh15 remains an interesting cilium surface molecule because its expression in the cilia is within the whole outer segment and is different from Prom1 (Figure 5.5). Interestingly, a PCDH15 mutation is associated with increased total cholesterol levels as well as high plasma triglycerides concentration and apolipoprotein B levels in Finnish dyslipidemic patients with hyperlipidemia (Huertas-Vazquez, Plaisier et al. 2010). This again links cholesterol with cilium surface molecule, but whether Pcdh15 affects the cholesterol levels in photoreceptor cells and cilia requires further investigation.

To sum, based on some early electron microscopy images of developing photoreceptors (Robertis 1960; Hinds and Hinds 1979) as well as my own immunohistochemical staining of retina with cilium markers and cilium cell surface protiens, a simple cartoon was drawn to illustrate the process of cilia development and the cell surface protein location along this process (Figure 5.7). Initially the apical region of the cell gradually buds out. The bud continues to grow into the primitive cilium which is filled with vesicular materials at the apical end. The apical region of the primitive cilium expands as the vesicles accumulate and grow. These vesicles gradually remodel and reorient themselves into stacked disks vertical to the growing axis of the buds and finally form the outer segment. More recent investigation in ciliogenesis further revealed that IFT proteins were associated with ciliary apparatus as early as appearance of the primary ciliary vesicle and electron dense centriolar satellites around P0 (Sedmak and Wolfrum 2011). However studies so far are mainly in rods, and little is known about the cones which are born early and which might use a different mechanism because their disks are the continuous invagination of the plasma membrane rather than closed disks. Expression of Prom1 is mainly at the apical protrusions of the cilia in embryonic and early postnatal stages, but is specifically at the base of rod OS and the whole of cone OS disks (Figure 5.7 B). Expression of Pcdh15 is in both the apical protrusion (the whole OS surface in the case of mature photoreceptor cells) as well as the synapse region of the photoreceptor cells throughout development (Figure 5.7 C).

5.4 Conclusions

- I identified 38 cilium annotated genes enriched in photoreceptor precursor cells from the transcriptome analysis, among which 23 are known to be associated with retinal diseases.
- Nine cilium cell surface molecules were identified. Two of them Prom1 and Pcdh15 were examined in detail and both showed high expression in the cilia, although Pcdh15 was also expressed in the photoreceptor synapses and other retinal cells. Prom1 specifically labeled the cilia (cone OS and base of rod OS) in photoreceptor cells in retina and was also expressed on the migrating photoreceptor cells after transplantation.
- I found three cilia annotated genes showed higher transcript levels in photoreceptor precursor cells compared with other retinal cells at E15.5 from the transcriptome analysis and observed protein expression of cilium markers (AcTub, CenpF and GT335) and cilium cell surface proteins (Prom1 and Pcdh15) at E15.5, which indicates possible cone ciliogenesis at this stage.

- I found 38 cilia genes showed higher transcript levels in photoreceptor precursor cells compared with other retinal cells at P4 and all 38 genes showed higher transcript expression in P4 than E15.5 photoreceptor precursors. More abundant expression and more defined localization of cilium proteins (ie. the above cilium markers and cilium cell surface proteins) were also seen in P4 than E15.5. I speculate such differences in the cilium property may correlate with the higher integration rate of the postnatal photoreceptor precursor cells compared with the embryonic photoreceptor precursor cells after transplantation. In support of this, the migrating photoreceptor cells express the photoreceptor cilium specific cell surface protein Prom1 after transplantation.

6 Cell surface molecules can be used to select photoreceptor precursors for cell transplantation

6.1 Introduction

As demonstrated in mice, transplantation of rod photoreceptor cells is a feasible approach to restore vision if the donor cells are from the early postnatal stages (MacLaren, Pearson et al. 2006; Pearson, Barber et al. 2012). As a means of therapy for human, the corresponding stage of donor cells would have to come from fetal tissue of 13 to 28 wks in pregnancy, which is not ideal. With much more availability and easy access, ES cells or induced pluripotent stem cells (iPS cells) offer this therapy more promising sources. Several groups have demonstrated that given certain conditions, these cells are able to differentiate into retinal cells including photoreceptor cells (Lamba, Karl et al. 2006; Osakada, Ikeda et al. 2008; Meyer, Shearer et al. 2009; Eiraku, Takata et al. 2011). However, these cultures are mostly heterogeneous containing cells of different types and developmental stages. To obtain homogeneous correctly staged photoreceptor precursor cells, cell selection strategy has to be applied to these cultures. Although photoreceptor cells have been selected using GFP-tagged transgenic genes in research, this is not desirable for human therapy.

It is known that in the immune system, during development as differentiation proceeds different types of cells begin to present different cell surface antigens to interact with neighboring cells or the environment, and monoclonal antibodies raised against these surface antigens are termed as the “CD” markers (Zola, Swart et al. 2005) (although the antigen itself or the gene that encodes the antigen are often referred to the CD name as well). The end result is that each type of cell in the immune system has a unique pattern of expressed CD markers along development. Using combinations of antibodies against these antigens, cells of a particular type and stage are successfully enriched. As the photoreceptor cells are able to correctly position themselves in the ONL during development, these cells must also express cell surface markers helping them to interact with the surroundings. In addition, the transplanted photoreceptor precursor cells can correctly migrate from SRS to ONL which is a process that probably involves lots of interactions between the cell and its environment and thus will require the presence of cell surface molecules. Therefore, if I can identify the photoreceptor specific cell surface marker profile, these markers could be used to enrich and isolate these cells by cell sorting using antibodies recognising cell surface molecules without any genetic manipulation. Previously in Chapter 3, I have developed ways to identify cell surface markers based on microarray analysis (section 3.2.5) and also listed all the CD markers

identified from the different arrays (Table 3.2). In this chapter, I will evaluate the potential of using some of these markers to isolate live photoreceptor precursor cells in flow cytometry and test the feasibility of using cell surface molecules to prepare donor cells for transplantation experiments.

With my supervisor Jane Sowden, I selected several CD markers (CD73/Nt5e, CD24, CD80, CD83, CD276, and Prom1/CD133) for analysis from the combined data sets: NrlGFP P4 array (generated by Jorn Lakowski), the previously reported Swaroop array (Akimoto, Cheng et al. 2006) and the CrxGFP P4 array (produced as part of this thesis). CD73, CD24, CD80, CD83 and CD276 were initially focussed on based on the array data existing before the start of my study. My identification protocol also confirmed the presence of these molecules (Table 3.2 and Table 3.3). In addition I found Prom1/CD133 quite interesting as it was found to be highly enriched in human retina (Carter, Dick et al. 2009). These markers were chosen because they showed dynamic developmental expression profiles in the Swaroop array (Figure 6.1 A – F) and (i) potentially can label photoreceptor precursors at specific developmental stages; and (ii) may label cones specifically or cones as well as rods.

To assess if the antigens were present on the cell surface in order to be useful for live cell selection, I plan to examine their protein expression using fluorochrome-conjugated antibodies in flow cytometry using live retinal cells. For each marker under examination, the retina was collected after microdissection of the mouse eye and subjected to Papain treatment to obtain dissociated single retinal cells (see Chapter 2, section 2.2.1). These live cells were directly incubated with the antibody after blocking (without fixation) and analysed in flow cytometry machine. My colleague Jorn Lakowski had successfully tested CD73 and CD24 with this approach and my aim was to examine the remaining markers in combination with CD73/CD24 with the same approach. Most of the markers were examined for several timepoints throughout development so that their expression profiles along retina development can be obtained.

6.2 Results

6.2.1 Trials on CD80, CD83 and CD276

CD80

In the Swaroop array (Akimoto, Cheng et al. 2006), the mRNA level of Cd80 was very low from E16 to P10 but increased at P28 (log2 intensity from around 2 to around 5, Figure 6.1 C). If its protein is also expressed in the adult photoreceptor cells but not the younger cells, CD80 could

be used as an adult marker to deplete the more matured cells from the mixed cell population. Flow cytometry results showed that after subtraction of the background from isotype control, however, very few retina cells could be recognized by CD80 except 1 – 2% cells positive for CD80 staining at P10 and P20 (Figure 6.2 A). These 1 – 2% cells were further analysed against NrlGFP which labels developing and mature rod photoreceptors. Although there was a slight increase in the NrlGFP positive population at P10 and P20 (0.1% and 0.6% respectively), the CD80 positive cells were mainly in the non-rod retina cells (2% at P20 and 1.3% at P10, Figure 6.2 B). Because non-rod retina cells also contain cone photoreceptors, to rule out if the CD80 positive cells might be cone photoreceptors, retina cells from the CrxGFP line were analysed. GFP expression in this transgenic line labels both rod and cone photoreceptors. Similar to the NrlGFP line, around 2% cells were CD80 positive but were mainly in the CrxGFP negative population (Figure 6.2 C) indicating that the CD80 positive cells are not photoreceptor cells.

CD83

Transcript of Cd83 was also low in wild type rod precursor cells in the array data (log2 intensity around 3, Figure 6.1 D), but sharply increased (log2 intensity 6.8) at P10 in the cone-like rod cells where Nrl was knocked out (Akimoto, Cheng et al. 2006). This suggests that Cd83 might label cone cells. Therefore, P10 retina cells of the CrxGFP line were analysed in flow cytometry. 2.4% of the whole retina cells were found being both CD83 positive and CrxGFP positive (Figure 6.3 A). This number nearly corresponds to the percentage of cones in the whole retina cells. However, intensity of the CD83 signals here was only slightly higher than the background and no distinct cell population was identified. In addition, 1.4% retina cells which were CD83+ve were CrxGFP-ve showing that CD83 also labels non-photoreceptor retina cells.

CD276

Transcript of Cd276 was relatively high in the P4 NrlGFP microarray and was higher in the NrlGFP positive population than the negative population (log2 intensity 8.5 vs 7.9, Figure 6.1 E). I wanted to know if it could be used to enrich rod precursor cells. After subtraction of the background from isotype non-specific binding, there seemed to be a small percentage of CD276 binding cells in all time points tested (0.24% at P4, 0.28% at P6, 0.43% at P10, and 0.49% at P20, Figure 6.3 B). However, such a percentage is too low to be considered as a marker to enrich photoreceptor precursor cells.

Validation of CD80, CD83, and CD276

To examine the mRNA levels of these genes as well as to validate their microarray expression, conventional reverse-transcription PCR was performed for retina tissues. Results showed that while Cd73 and Prom1 were highly expressed, Cd83 was only detectable at lower level. Cd276 could be detected at relatively higher levels, but Cd80 was not detected in the retina at all although it was detected in activated dendritic cells which were used as a positive control (Figure 6.2 D).

None of the antibodies for CD80, CD83, and CD276 tested identified any distinct cell populations nor sufficiently increased the percentage of the expected cell population. To rule out the possibility that the antibodies are not working, I examined these antibodies on dendritic cells which are known to be able to present the antigens of CD80, CD83, and CD276 on the cell surface after maturation or lipopolysaccharide (LPS) activation. Results showed that over 70% dendritic cells were positive for CD80 and over 30% were positive for CD83 and CD276 (Figure 6.3 C) which agrees with their expression levels after LPS activation. This shows that all three antibodies were properly functioning. To rule out possible protocol problems in flow cytometry analysis with retina cells, two molecules, CD24 and CD73, recently shown in the lab to be highly expressed in retinal cells (by Jorn Lakowski), were tested along with the three antibodies following the same procedure. Around 45% and 30% retina cells were positive for CD24 and CD73 at E18.5 and 3 months respectively (Figure 6.3 C). Therefore, it is highly likely that the majority of the antigens of CD80, CD83, and CD276 are not yet present on the surface of the retina cells. Further analysis with western blot may reveal if the proteins are translated at all.

In summary, Cd80 with maximum log2 intensity at 5 in microarray analysis labeled around 1% non-photoreceptor cells in FCM analysis, but did not label any photoreceptor cells and was not detectable by PCR. For Cd83 and Cd276, their log2 intensity in microarray was around 7 and their transcripts were detectable in PCR. But in FCM analysis, CD83 labeled non-photoreceptor cells as well as photoreceptor cells (both around 2%), while CD276 barely labeled more than 0.5% cells. Therefore I conclude that none of the three candidates could be used as surface markers for positive selection of photoreceptor precursors. However, CD80 and CD276 might be used as negative cell surface markers for photoreceptor cells. Indeed CD80 showed high expression in ES cells and low expression in neural progenitors during the controlled differentiation of ES cells (Wollscheid, Bausch-Fluck et al. 2009). Therefore, when isolating

photoreceptor precursor cells from ES cells, CD80 could be a useful negative marker for photoreceptors.

From these preliminary studies, I also found that genes with log2 intensity below 6 in the arrays were difficult to be detected by conventional PCR. I therefore prioritized genes with log2 intensity higher than 6 in future studies. These include CD73, CD24, and Prom1 which will be focused on the following sections.

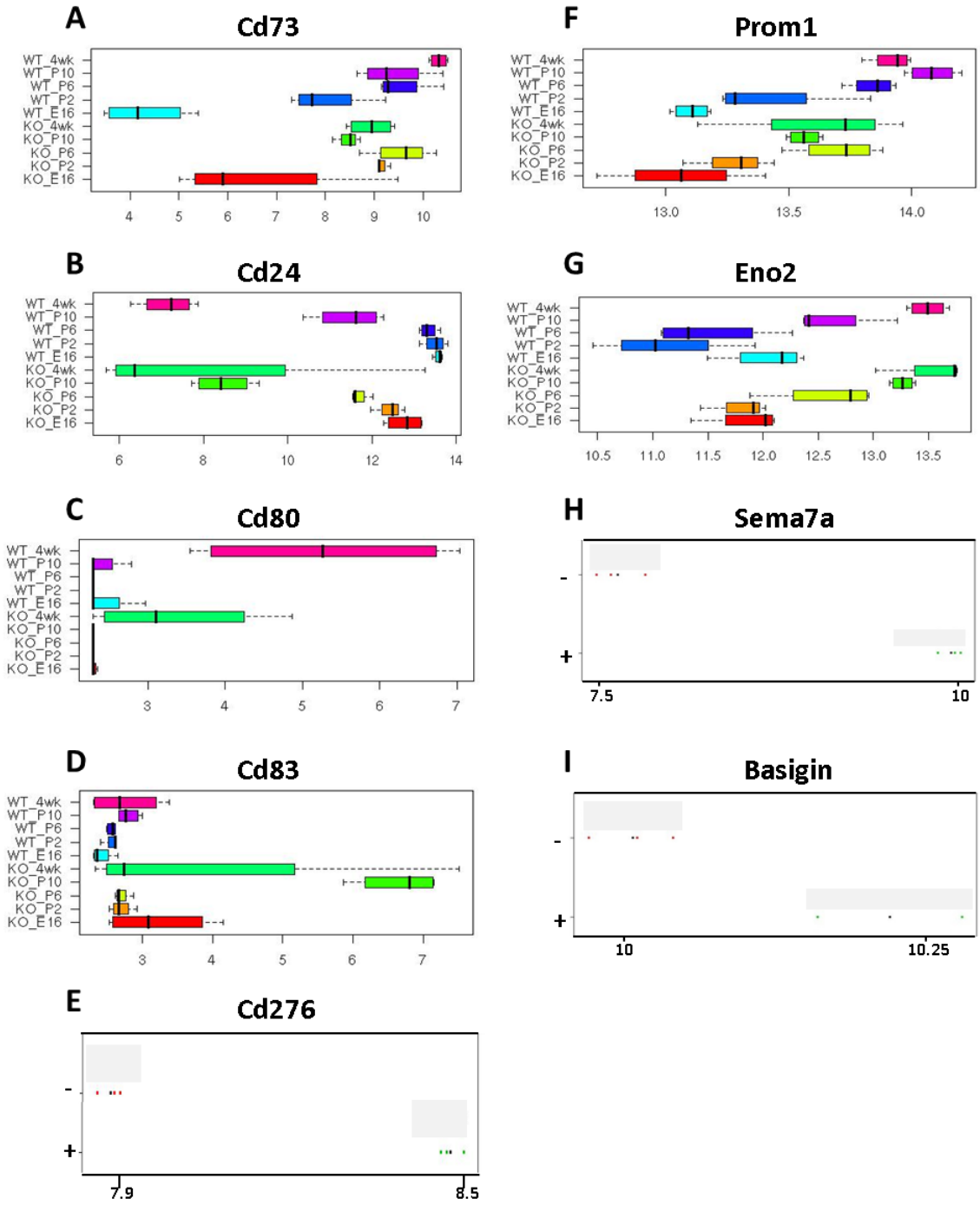

Figure 6.1 Expression levels of candidate genes in Swaroop array and NrlP4 array. The Swaroop array compares NrlGFP+ve cells in wildtype (WT) and Nrl-knockout (KO) background at the time point of E16, P2, P6, P10 and 4 wks. The box plots of the Swaroop array represent the absolute gene expression levels (ie. the log2 array signal intensity on X-axis) of Cd73, Cd24, Cd80, Cd83, Prom1 and Eno2 (A, B, C, D, F and G). The NrlP4 array compares NrlGFP+ve cells (+) and NrlGFP-ve cells (-) at P4. The dot plots of the NrlP4 array represent the absolute gene expression levels (ie. the log2 array signal intensity on X-axis) of Cd276, Sema7a and Basigin (E, H and I). Each dot represents the expression level of the gene under examination from each array chip. WT, wildtype; KO, Nrl knockout; +, NrlGFP+ve; -, NrlGFP-ve.

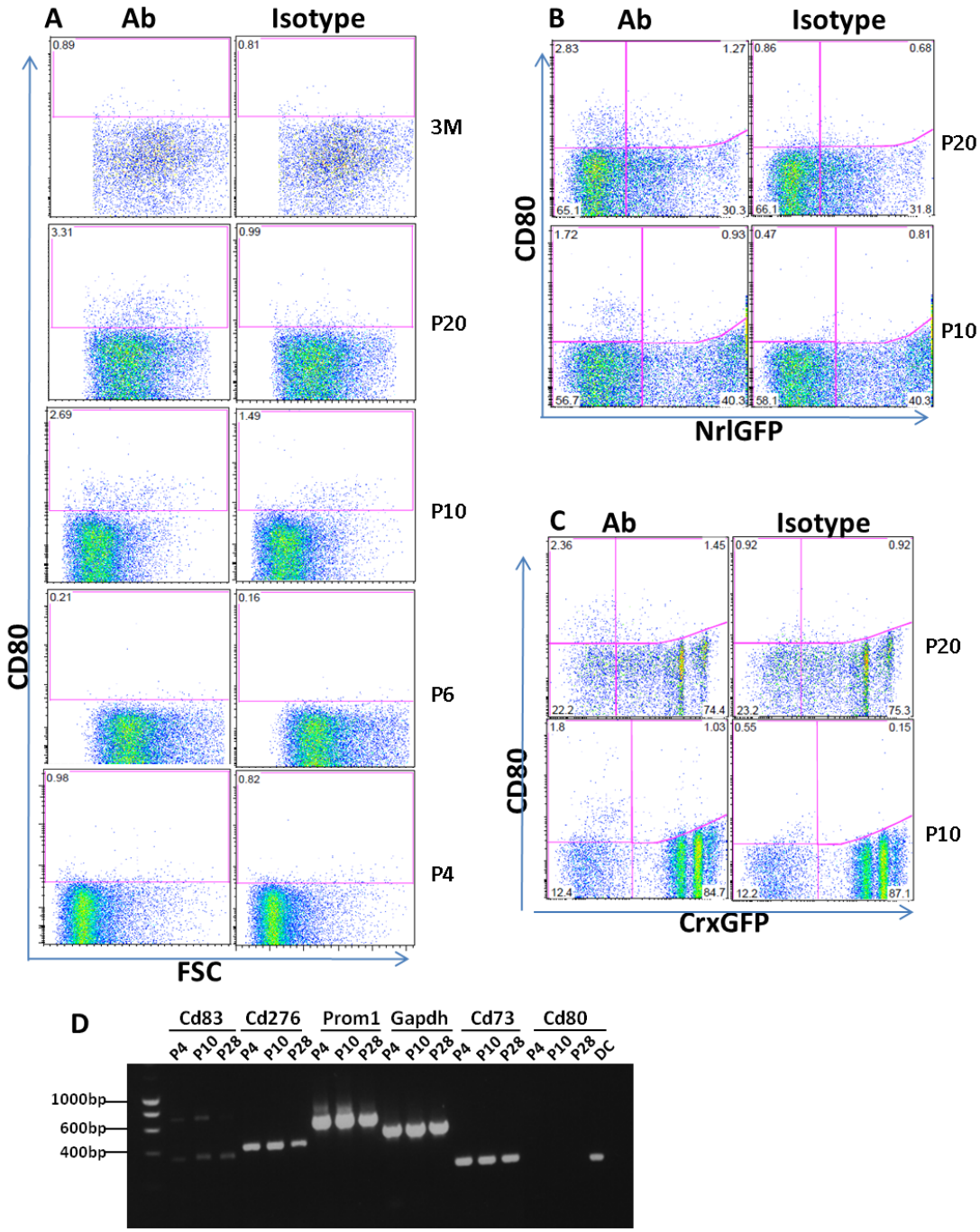

Figure 6.2 FCM analysis of CD80 and PCR analysis of *Cd80*, *Cd83*, *Cd276*, *Prom1*, *Gapdh* and *Cd73*. Representative dot plot patterns of CD80 labelled cells compared with forward scatter (FSC, roughly equals cell size) (A), or compared with NrlGFP (B) or CrxGFP (C) at each developmental time point. Pink boxes indicate positive signals determined using matched isotype control stained cells. When X-axis is NrlGFP or CrxGFP, the top right hand quadrants in each plot indicate cells that are double positive for GFP and CD80. (D) PCR analysis of *Cd80*, *Cd83*, *Cd276*, *Prom1*, *Gapdh* and *Cd73* on P4, P10, P28 retinae and activated dendritic cells (DC).

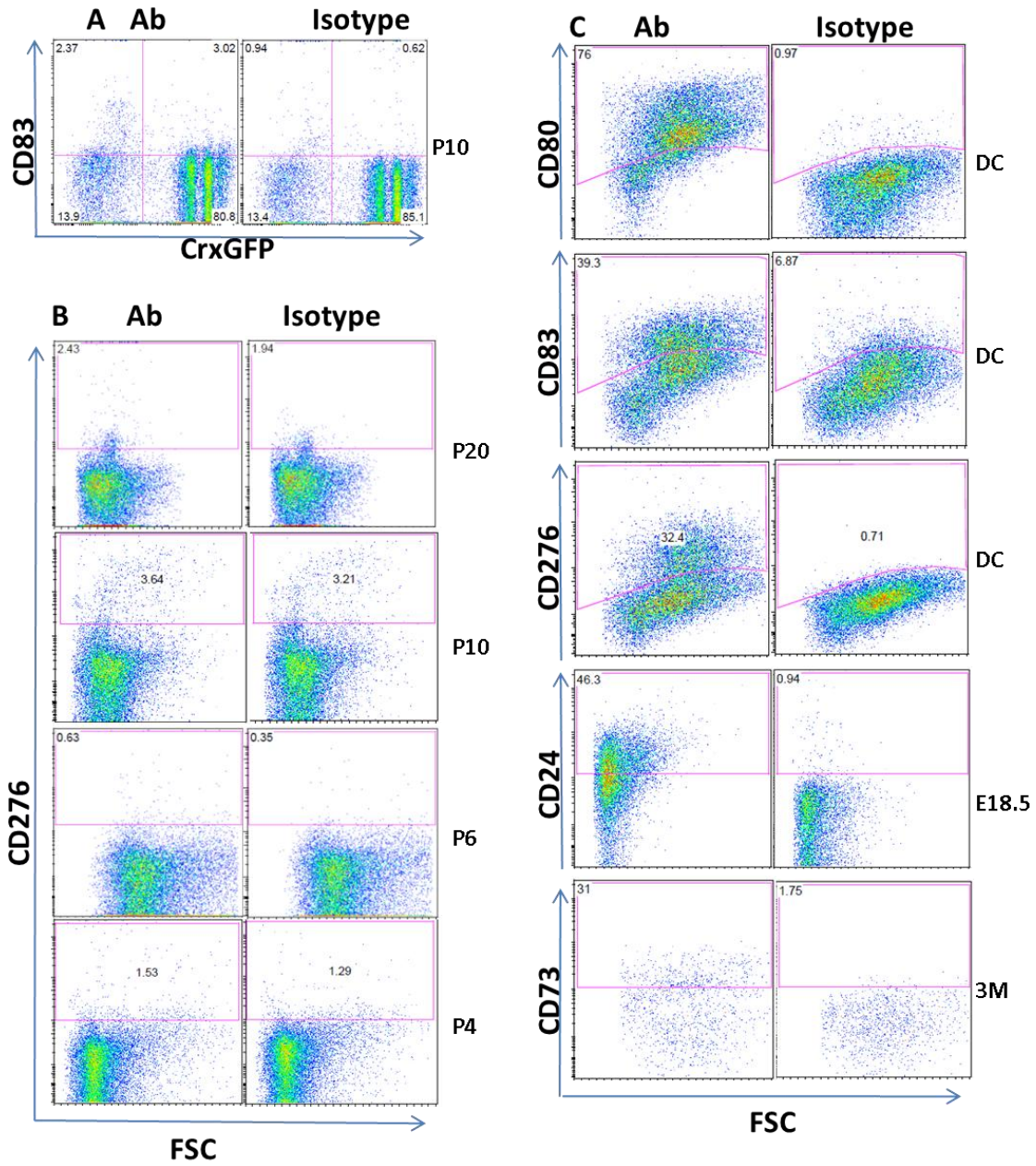

Figure 6.3 (A) FCM analysis of CD83 against CrxGFP. (B) FCM analysis of CD276 against FSC. (C) FCM analysis of CD80, CD83, CD276 on dendritic cells and CD24 and CD73 on retinal cells at E18.5 and 3 months respectively.

6.2.2 Flow cytometry analysis of Prom1, CD73, and CD24 in NrlGFP line

To evaluate the possibility of using Prom1, CD73, and CD24 to isolate live photoreceptor cells, my colleague Jorn Lakowski and I tested the corresponding antibodies in dissociated NrlGFP retinal cells using flow cytometry (CD73 and CD24 by Dr Lakowski, Prom1 by Y. Han). Firstly, the percentage of retinal cells labelled by each candidate cell surface antigen at different developmental time points was established. At E17, only a very small number (2%) of retinal cells is stained with CD73 and this increased markedly in the postnatal period to more than 60% of all cells persisting into adulthood (Figure 6.4 B, F). By contrast, CD24 showed an inverse pattern (Figure 6.4 C, F): more than 80% of cells were labelled at E17 and this decreased in the postnatal period to very low levels in the mature retina of less than 8% consistent with its reported down regulation in maturing neurons in the central nervous system (Shirasawa, Akashi et al. 1993; Nieoullon, Belvindrah et al. 2007). Prom1 (CD133) stained a significant number of retinal cells during embryonic and postnatal development (>70%) but levels decreased in adulthood (Figure 6.4 D, F).

By gating for each fluorochrome and GFP, the proportion of each cell surface marker population that colabels with NrlGFP was assessed. At E17, very few of the NrlGFP cells colabeled with CD73 (Figure 6.4 G) indicating that CD73 is not a marker of the very early stages of rod photoreceptor differentiation. By P5, and at later stages, the majority of retinal cells (>60%) were colabeled for CD73 and NrlGFP (Figure 6.4 G; top right hand quadrants). Conversely, at E17 the vast majority of the CD24+ve cells were NrlGFP-ve (Figure 6.4 H, left hand panel; top left hand quadrant, 70%). The proportion of retinal cells that colabeled with CD24 and NrlGFP initially increased postnatally so that by P5 more than 40% of all retinal cell colabeled and then subsequently declined such that less than 10% of cells colabel after P10 (Figure 6.4 H; top right hand quadrants). At E17, Prom1 labeled approximately 70% of all cells, but the majority of these were NrlGFP-ve (Figure 6.4 I; left hand panel; top left hand quadrant). In the postnatal period, Prom1 labeled both GFP+ve cells and GFP-ve cells with approximately 50% of all cells colabeling for GFP and Prom1 at P5 and more than 60% at P10 decline thereafter (Figure 6.4 I).

CD73 and CD24 were evaluated as a candidate surface marker combination that could define postnatal stage photoreceptor precursors as previous qPCR and immunohistochemistry analysis indicated that these markers were coexpressed in developing photoreceptors at P4–P7 but not at earlier or later stages (Lakowski, Han et al. 2011). Here flow cytometry analysis confirmed that more than 30% of retinal cells colabeled with CD73 and CD24 at P5, whereas negligible levels colabel at embryonic and adult stages (Figure 6.4 J). For easy comparison of

the performance of the markers in flow cytometry analysis, I defined two terms to evaluate these markers, namely “specificity” and “efficiency”. **Specificity** refers to the percentage of marker labelled cells that are NrlGFP+ve. This parameter evaluates how specifically the markers label photoreceptor cells and is particularly useful for cell resources of mixed population. **Efficiency** refers to the percentage of NrlGFP+ve cells that are labelled by the new marker(s). This parameter evaluates how many photoreceptor cells can be labelled by the markers and is useful when the cell resources are limited. Although when applying to *in vitro* differentiation of stem cells, if cell resources are abundant, efficiency may not represent a restricting factor. The majority of CD73 and CD24 double-labelled and CD73 single labelled cells expressed the NrlGFP transgene at P5 (98.4 ± 0.3% and 98.8 ± 0.1% respectively; Figure 6.4 K) showing high specificity. Only 43.3 ± 5.1% of NrlGFP precursors label with both CD73 and CD24 at P5 showing lower efficiency compared to single labelling (Figure 6.4 K). The specificity and efficiency of the double labelling is illustrated in Figure 6.4 L.

Therefore, m colleague and I identified three cell surface molecules, CD73, CD24 and Prom1, highly expressed in retinal cells in flow cytometry experiments. Each of them shows a unique expression pattern against NrlGFP along retinal development. Both single labelling of CD73 and double labelling of CD73CD24 can isolate rod photoreceptor cells with high specificity, but the CD73CD24 combination add further specificity to a developmental stage around P5 in expense of efficiency.

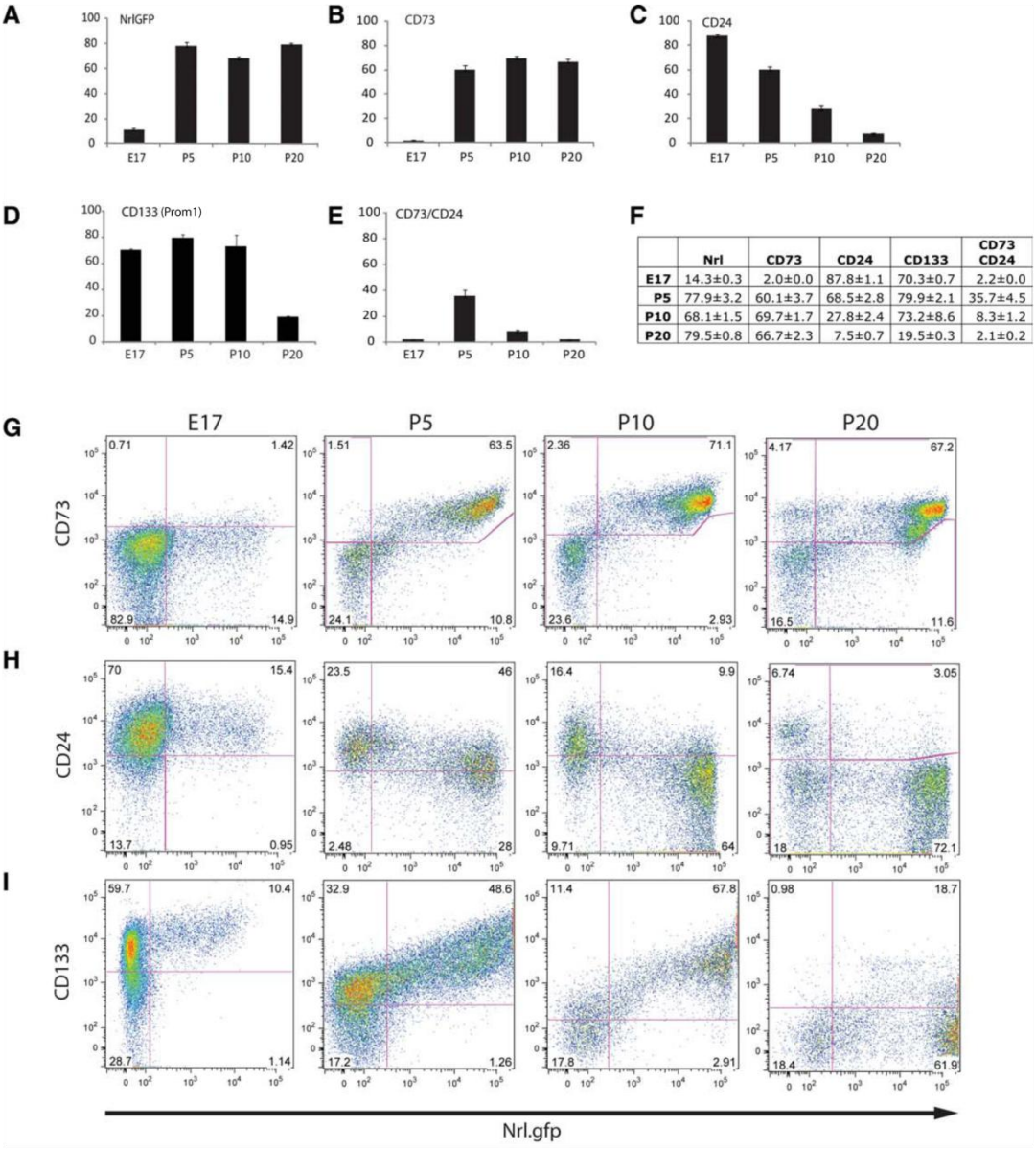

	Nrl	CD73	CD24	CD133	CD73 CD24
E17	14.3±0.3	2.0±0.0	87.8±1.1	70.3±0.7	2.2±0.0
P5	77.9±3.2	60.1±3.7	68.5±2.8	79.9±2.1	35.7±4.5
P10	68.1±1.5	69.7±1.7	27.8±2.4	73.2±8.6	8.3±1.2
P20	79.5±0.8	66.7±2.3	7.5±0.7	19.5±0.3	2.1±0.2

Figure 6.4 FCM analysis of Prom1 (ie CD133), CD24, and CD73 in NrlGFP (continues). (A–E) Graph of surface marker expression profiles from three independent retinal cell samples derived from NrlGFP mice at E17, P5, P10, and P20. (F) Table of the average percentage of viable cells expressing each marker or combination of markers and the respective standard deviation (n = 3). (G–I) Representative dot plot patterns of CD73, CD24, and Prom1 labelled cells compared with NrlGFP expression at each developmental time point. Pink lines demarcate detection thresholds for positive signal determined using matched isotype control stained cells. Top right hand quadrants in each plot indicate percentage of total cells that are double labelled (from (Lakowski, Han et al. 2011)).

J

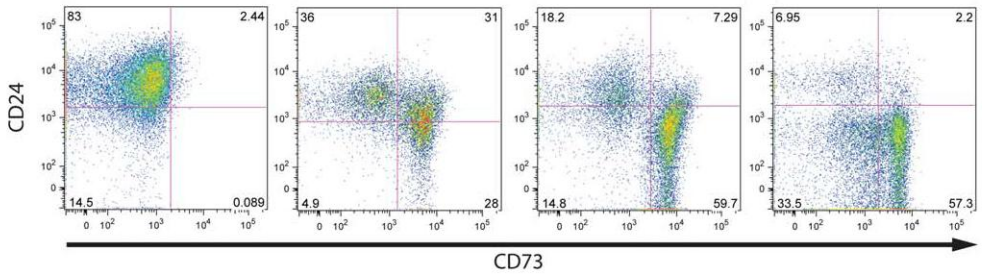

K

		CD73	CD73 & CD24	CD24	Prom1
Specificity	% of NrlGFP from surface marker labelled cells (mean ± SD)	98.8±0.1	98.4±0.3	79.2±3.9	51.3±5.9
Efficiency	% of surface markers from NrlGFP labelled cells (mean ± SD)	82.1±1.7	43.3±5.1	63.6±9	95.7±0.4

L

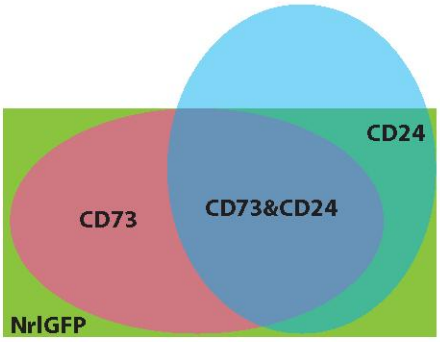

Figure 6.4 FCM analysis of Prom1, CD24, and CD73 in NrlGFP-continued. (J) Representative dot plot patterns of double labeled CD73 and CD24 cells from E17 to P20 as labelled in (G). (K) Table of the average percentage of NrlGFP cells expressing the markers (Specificity) or percentage of the marker expressing cells that are NrlGFP+ve (Efficiency) (n = 3) at P5. (L) Venn diagram showing expression overlap between CD73, CD24, and NrlGFP at P5.

6.2.3 Flow cytometry analysis of Prom1, CD73 and CD24 in CrxGFP line

As NrlGFP does not label cones, I next examined if these markers also label cones by using the CrxGFP line which labels cones, rods, and bipolar cells (Furukawa, Morrow et al. 1997; Lakowski, Baron et al. 2010). As the three types of cells are different in terms of cell numbers in the retina, expression levels of CrxGFP, and probably cell size and cell complexity, they might show up as different populations when passing the lasers of the flow cytometry machine and being presented in the flow cytometry scatter plot which provides 2-dimentional visual separation to these cells. Therefore, using the CrxGFP population might reveal more information as to what retinal cells these surface markers label. Further, the specificity and efficiency of the surface marker labelling were examined.

CrxGFP vs NrlGFP

First I compared the flow cytometry plots of the CrxGFP and NrlGFP line. Similar to the NrlGFP line, more CrxGFP-ve cells appear to transfer into the CrxGFP+ve population as development proceeds (Figure 6.6 A). However, different from the NrlGFP line which contains only one cell population with a slight continuous gradient of GFP intensity (Figure 6.5 A right), the CrxGFP+ve cells showed about three distinct differently sized cell populations with increased CrxGFP intensity at late postnatal periods (Figure 6.5 A left and Figure 6.6 A). The biggest cell population (around 54.6% live retinal cells at P8) is likely to be the rods which roughly cluster their CrxGFP levels around 10^5. On its right is a very small CrxGFP+ve population (around 4.27%) with CrxGFP levels higher than 10^5 and on its left is a median sized CrxGFP+ve population (around 18.5%) with maximum CrxGFP levels around $10^{4.4}$. Considering the size of the population and levels of the CrxGFP signals, the weak CrxGFP+ve cells (ie. the left population) is likely to be bipolar cells and the strong CrxGFP+ve cells (ie. the right population) to be cones. Immunohistochemistry showed that the weak CrxGFP+ve cells locate in INL and are mostly positive for PKCα staining indicating they are bipolar cells (Figure 6.5 B). The percentage of the possible bipolar cells here in flow cytometry agrees with Young's autoradiography study that around 20% ventricular cells produced postnatally are bipolar cells and this decreased to 10.3% in adults (Young 1985a). Percentage of adult mouse rods represent 97% of photoreceptor cells while cones represent 3% (Carter-Dawson and LaVail 1979b). The three cell populations also expressed different levels of the cell surface markers (Figure 6.6 A).

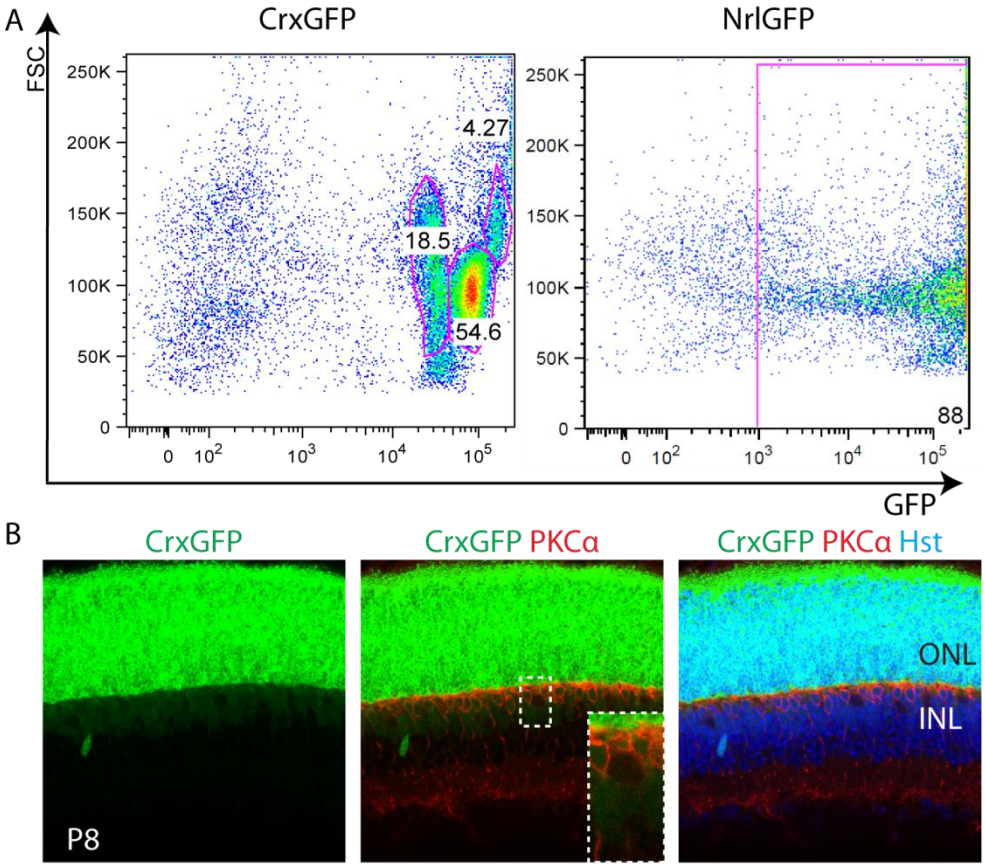

Figure 6.5 CrxGFP+ve cell populations. (A) Flow cytometry analysis comparing the CrxGFP (left, at P8) and NrlGFP (right, at P10) retina cells. X-axis GFP intensity, Y-axis forward scatter. (B) Immunohistochemistry of P8 CrxGFP retina with rod bipolar cell marker PKCα.

Prom1

The developmental pattern of the biggest cell population of the CrxGFP+ve cells (ie. the CrxGFP+ve cells with middle intensity, the rods) resembled the NrlGFP profile in terms of Prom1 expression (Figure 6.6 A vs Figure 6.4 I). Before maturation, all these rods are labelled by Prom1, although in the adult only a portion was Prom1+ve. Prom1 did not label the putative bipolar cells (ie. the weak CrxGFP+ve cells) but labelled all the putative cones (ie. the strong CrxGFP+ve cells) (Figure 6.6 A). Immunohistochemistry of Prom1 and cone arrestin confirmed that Prom1 indeed labelled the cones, specifically at the cone OS (Figure 6.6 A'), agreeing with previous finding that Prom1 colabels with another cone marker PNA (Supplemental figures in (Zacchigna, Oh et al. 2009)). This shows that Prom1 labelled all the NrlGFP or CrxGFP labelled rods and cones in postnatal stages.

Prom1 also labelled many CrxGFP-ve cells early in development, but this percentage decreased as development proceeds and was negligible by adult stage (Figure 6.6 A), similar to the

pattern in NrlGFP (Figure 6.4 I). The percentage decrease of the Prom1+veGFP-ve cells corresponded to the increase of Prom1+veGFP+ve cells as if the Prom1+ve cells were shifting from GFP-ve to GFP+ve throughout development till all the Prom1+ve cells became GFP+ve in adult (Figure 6.6 A, Figure 6.4 I). Intriguingly, throughout postnatal development the percentage of Prom1 expressing cells in the retina was maintained between 70 – 80 % which roughly equals the total percentage of photoreceptor cells in adult retina (Figure 6.4 D, F; Figure 6.6 C, D). This suggests Prom1 may label a progenitor/precursor cell population which is destined to become photoreceptor cells even before they begin to express NrlGFP or CrxGFP.

It is notable that at P20 when the photoreceptor cells were fully matured, Prom1 no longer labelled the bulk of rod photoreceptor cells in flow cytometry, although it still can label cones (Figure 6.6 A). Immunohistochemistry showed that Prom1 was expressed in the adults, but was specifically located at the bottom of rod OS and was just above the connecting cilium (Figure 6.6 A', Chapter 5, Figure 5.4 and (Lakowski, Han et al. 2011)). As the connecting cilium is prone to damage, it is likely that these delicate structures were broken during the dissociation procedure resulting loss of rod OS and proteins around this region.

Therefore, Prom1 seem to be a photoreceptor specific marker in retina. It not only labels the rods and cones from early embryonic development, but also the postnatal rods and cones. Its ability to label mature rods was decreased in flow cytometry analysis because of the dissociation procedure, but it is still able to label adult cones.

CD24

In contrast to Prom1, CD24 labelled all the putative bipolar cells (the median sized relatively low CrxGFP-expression population) as well as the CrxGFP-ve cells as shown on P8 (Figure 6.6 A). But it also labelled all the cones (the small tight high CrxGFP-expression population) and a small portion of rods at this stage. This agrees with the NrlGFP line in which by P10 CD24 recognized a portion of the NrlGFP+ve cells and a portion of the NrlGFP-ve cells. Later CD24 is lost from photoreceptor cells.

CD73

CD73, on the other hand, did not label the CrxGFP-ve cells and only labelled the CrxGFP+ve cells throughout retinal development. For the CrxGFP+ve cells, CD73 did not label many of them at around birth ie only around 3% comparing to over 30% by Prom1 or CD24. But this percentage greatly increased to over 30% at P4 and to over 60% between P8 to P12, which then decreased to around 47% in matured retina. The majority of these cells were rods which

constantly showed high levels of CD73 throughout development. But the small sized high CrxGFP signal cells (ie. the possible cones) showed decreased CD73 levels at P20 although their CD73 levels were high between P4 to P12. Similar to Prom1, CD73 did not label the medium sized CrxGFP+ve cell population with weaker GFP signals (ie the possible bipolar cells). Therefore, CD73 seem to label relatively late stages of immature photoreceptor cells (including rods and cones) and mature rods, but not early stages of immature photoreceptor precursors and mature cones.

Prom1 CD24 combination

To find if a combination of these markers are more specific to isolate photoreceptor cells at particular developmental stages than single labelling, I combined staining of the CrxGFP retinal cells with these markers. Combined analysis of Prom1 and CD24 in the CrxGFP line showed that similar to the NrlGFP line there seem to be two cell populations (Figure 6.6 B). Most of the cells were positive for Prom1 throughout P0 to P12. About half of the Prom1+ve cells were also positive for CD24 between P0 to P8 and the other half was CD24-ve. The majority of the CD24+ve cells were Prom1+ve. The CD24+veProm1-ve cells contained about 70% CrxGFP+ve cells (likely to be bipolar cells) whereas the CD24-veProm1+ve cells contained 98% CrxGFP+ve cells around P8 (data not shown) indicating that CD24 has not labelled many photoreceptor cells and labelled more non-photoreceptor cells. The double positive cells (32 – 49% of total retinal cells between P0 and P8) although not forming a homogenous population, were mainly from the stage before P8. As both markers seemed also to enrich cones, this combination could be useful to select cones and rods which are born early.

Prom1 CD73 combination

Combined analysis of Prom1 and CD73 showed that these two markers seemed to show a rough linear relationship (Figure 6.6 B). Neonatal stages (P0 – P4) saw many Prom1+veCD73-ve cells but they seem to migrate into the double positive cells as more CD73 was expressed along development. The cells seemed to be relatively homogeneous double negative or double positive for both markers in particular between P8 and P12. Combining with the single labelling plot, the double negative cells were expected to be mainly GFP-ve cells and bipolar cells whereas the double positive cells (17 – 62% of total retinal cells between P4 and P20) should be rods and cones. Indeed, consistently 94 – 99% of the double positive cells were CrxGFP+ve throughout postnatal development (Figure 6.6 C). Therefore, the combination of these two markers seems to purely enrich photoreceptor precursor cells taking into account

that Prom1 eliminated the very mature photoreceptor cells and CD73 eliminated the very young photoreceptor cells.

CD73 CD24 combination

Double labelling with CD73 and CD24 showed that these two markers showed a much smaller percentage of overlap in comparison with the other two combinations (12 – 37% of total retinal cells between P4 and P8) (Figure 6.6 B). Around 90% of these double positive cells were also CrxGFP+ve between P0 and P8 (Figure 6.6 C). This combination, however, seems to particularly enrich retinal cells between P4 and P8.

Prom1 CD24 CD73 combination

Triple labelling of all three markers at P8 showed that over 98% triple positive cells express CrxGFP (Table 6.1). This is slightly lower than CD73 alone or in combination with Prom1 (probably because of the unspecificity that CD24 brought in), but higher than any other single or double labelling. However, only one third of the CrxGFP cells can be triple labelled at P8 (Table 6.1).

Table 6.1 Percentage of Triple stain for P8 CrxGFP cells

		CD24	CD73	Prom1	CD24Prom1	CD73Prom1	CD24CD73	CD24CD73Prom1
Specificity	% of CrxGFP from surface marker labelled cells (mean ± SD)	84.3±1.69	99±0.058	94.5±1.14	92.8±0.84	99.3±0.1	98.1±0.4	98.6±0.2
Efficiency	% of surface markers from CrxGFP labelled cells (mean ± SD)	56±13.9	73.5±2.17	81±0.31	39.1±11	70.9±1.15	31.5±9.85	33.0±8.18

Expression stages

I then directly compared the developmental profile of these markers with that of CrxGFP (Figure 6.6 D and C left). First of all, from all the live retinal cells, CrxGFP expression gradually increased from around 40% at P0 to around 90% at P20. CD73 largely resembled the trend of CrxGFP along development albeit was constantly 20 – 45% lower with a further 15% decrease from P12 to P20. However, at P0 when over 40% retinal cells already expressed CrxGFP, CD73 barely labelled anything. CD24 showed an opposite trend of CrxGFP despite some fluctuations, with relatively high expression (40 – 70%) until P8 followed by a sharp decrease when it barely labelled any cells. Prom1 was also high at early stages, but the expression was maintained at around 70% from birth to P12 and dropped in mature retinal cells. Therefore when in combinations, CD24 and Prom1 enriched P0 – P8 cells, Prom1 and CD73 enriched P4 – P20

cells, whereas CD73 and CD24 (or triple staining of Prom1, CD73 and CD24) enriched P4 – P8 cells (Figure 6.6 C, Table 6.1, and Figure 6.7).

Specificity and efficiency

I then assessed the specificity of these labelling in the CrxGFP line (Figure 6.6 C). Around 40 – 50% CD24+ve cells expressed CrxGFP at P0 and P20, and around 70 – 80% between P4 to P12. Over 90% CD73+ve cells expressed CrxGFP throughout postnatal development. Although only around 40% Prom1+ve cells were CrxGFP+ve at P0, from P4 onwards over 80 – 90% Prom1+ve cells were CrxGFP+ve. Double labelling mostly showed higher specificity than single markers. Around 90% CD24+veProm1+ve cells were CrxGFP+ve between P4 and P8, although only around 60% were CrxGFP+ve at birth and after P12. Nearly all of the CD73+veProm1+ve cells were CrxGFP+ve throughout development. The CD73+veCD24+ve cells showed around 80 – 90% CrxGFP+ve cells from P0 to P8, but the percentage decreased thereafter.

Therefore, single labelling with CD73 was highly specific and combination with Prom1 further enhanced the specificity. CD73 CD24 combination was also specific at early stages but the specificity decreased after P8 probably because of the low expression and low specificity that CD24 brought in. Single labelling with Prom1 was also specific except at early stages when CrxGFP expression was still low. Prom1 CD73 combination showed higher specificity than Prom1 alone but was in expense of loss of early born photoreceptor cells. Prom1 CD24 combination showed slightly higher specificity than Prom1 alone at early stages but was lower than Prom1 alone at stages after P8. Single labelling of CD24 was much less specific than single labelling of Prom1 or CD73, but in combination with either of them showed higher specificity than CD24 alone. Triple labelling of CD73 CD24 and Prom1 was not more specific than CD73 alone or double labelling of CD73 and Prom1, but was more specific than other single or double labelling (Table 6.1).

The efficiency analysis shows that Prom1 is the most efficient surface markers among the three to isolate photoreceptor cells (Figure 6.6 C). CD73 was only relatively more efficient than Prom1 after maturation. CD24 was not a very efficient marker except when neonatal photoreceptor cells were desired. Combination of these markers greatly reduced efficiency comparing to single labelling, but Prom1+veCD73+ve was still highly efficient for isolation of P8 photoreceptor cells.

The expression of Prom1, CD73, and CD24 in relative to CrxGFP and their specificity and efficiency was illustrated as venn diagrams in Figure 6.6 E.

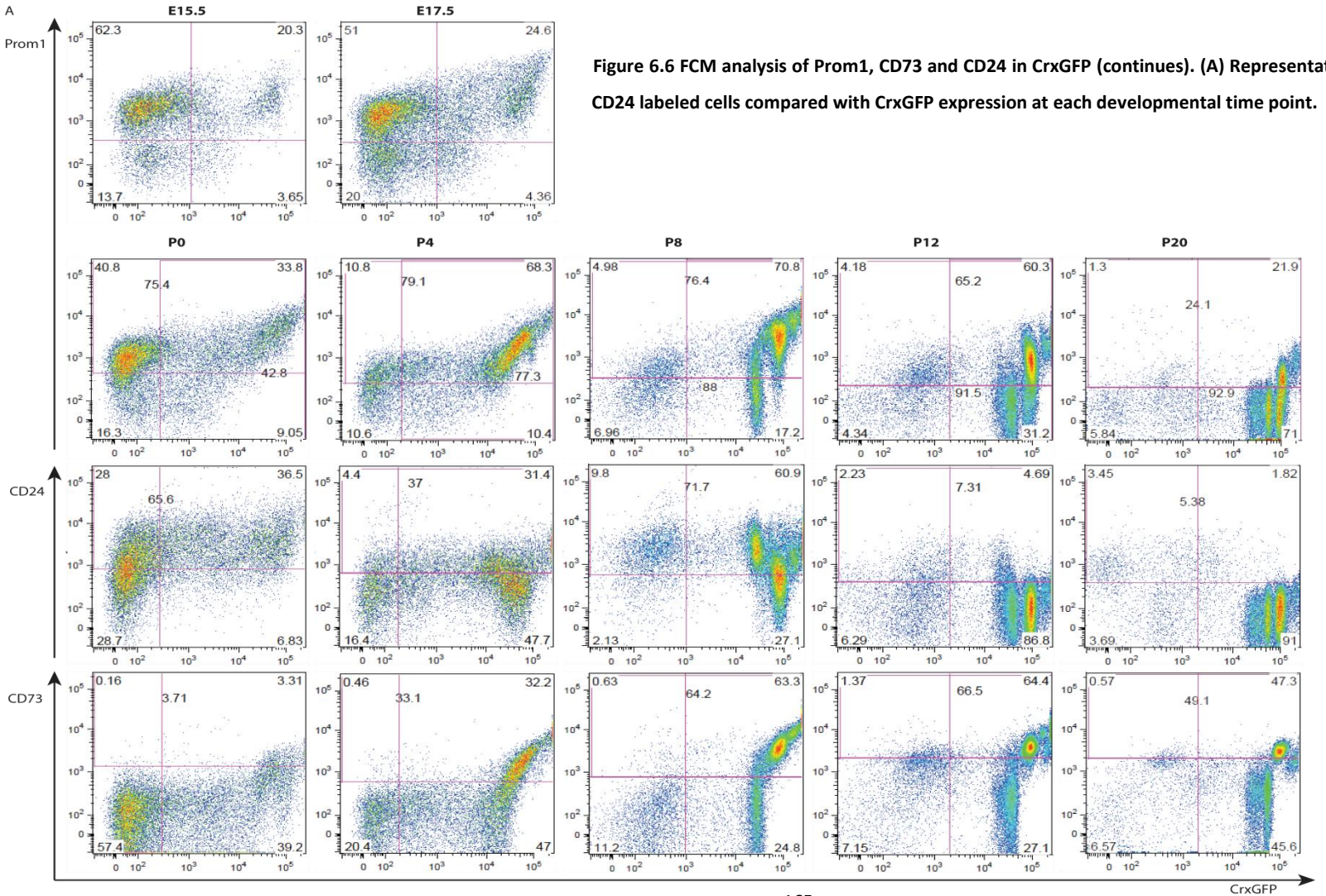

Figure 6.6 FCM analysis of Prom1, CD73 and CD24 in CrxGFP (continues). (A) Representative dot plot of Prom1, CD73, and CD24 labeled cells compared with CrxGFP expression at each developmental time point.

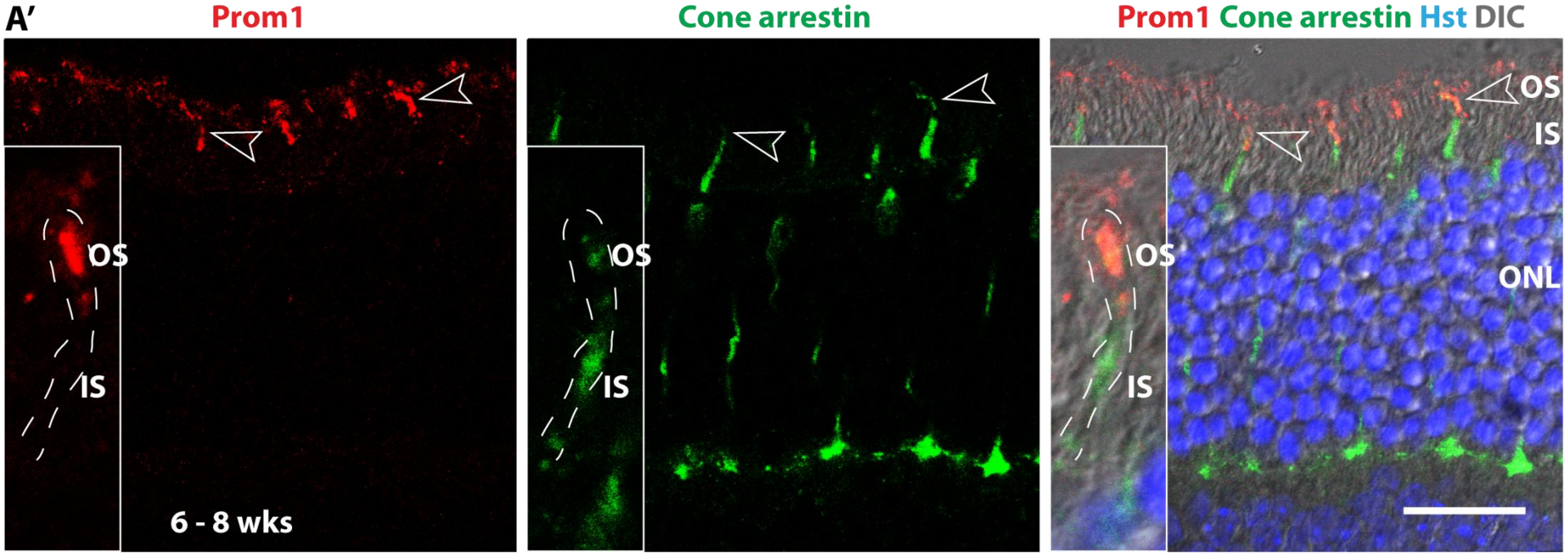

Figure 6.6 FCM analysis of Prom1, CD73 and CD24 in CrxGFP- continued. (A') Immunohistochemistry of Prom1 (red) with Cone arrestin (green) in 6 – 8 wks wild type mouse retina. Hst, Hoechst 33342; OS, outer segment; IS, inner segment; ONL, outer nuclear layer. Inserts: layout the OS and IS of a cone photoreceptor cell. Scale bars represent 25 µm.

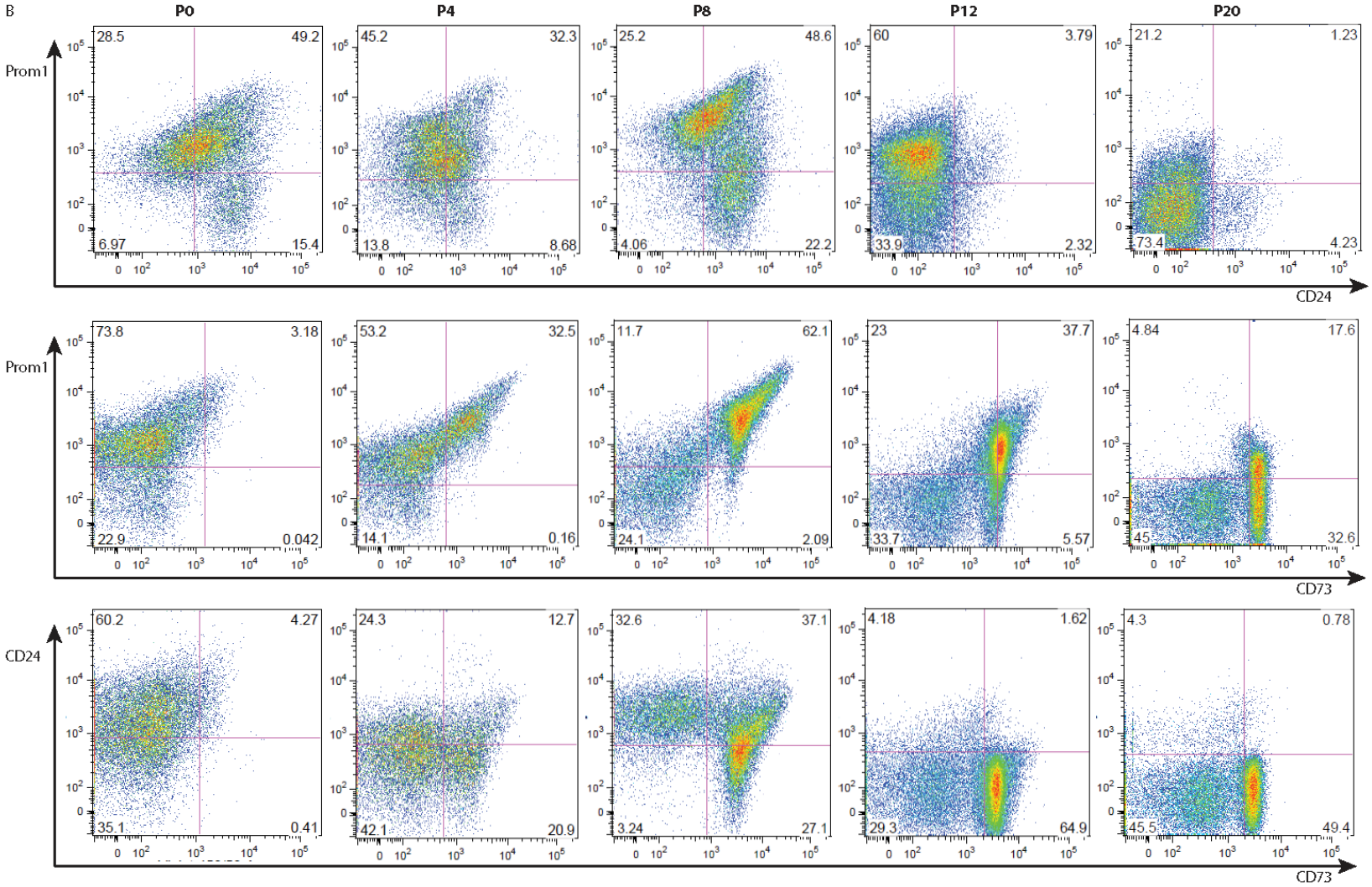

Figure 6.6 FCM analysis of Prom1, CD73 and CD24 in CrxGFP- continued. (B) Representative dot plot of combined analysis of Prom1, CD73, and CD24 in CrxGFP cells at the indicated time point.

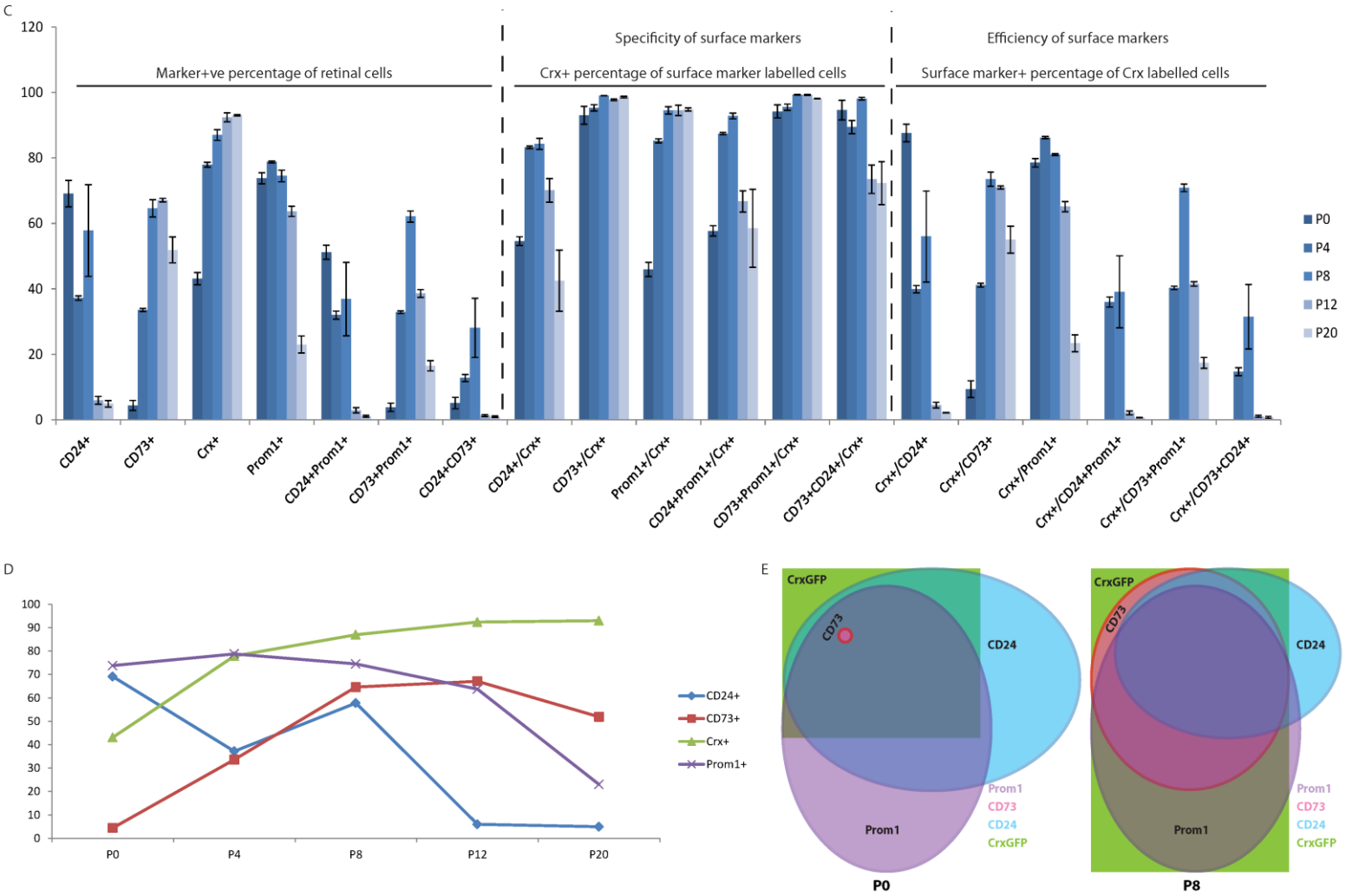

Figure 6.6 FCM analysis of Prom1, CD73 and CD24 in CrxGFP-continued. (C) Graph showing marker+ve percentage of retinal cells (left), marker specificity (middle), and marker efficiency (right) at the indicated time point; Error bar represent standard deviation of three independent sample preparation; (D) Expression trend line of the surface markers at the indicated time point in comparison with CrxGFP expression. (E) Venn diagram showing expression of the three markers relative to CrxGFP based on expression percentage at P0 (left) and P8 (right).

6.2.4 Cell surface marker flow cytometry analysis summary

In summary (Figure 6.7):

- CD80 and CD276 showed very low or no expression in photoreceptor cells in flow cytometry analysis and may be used as negative markers.
- CD83 showed unspecific low expression and may not be useful for selection.
- CD73 specifically isolate photoreceptor cells from P4 onwards but not early rods and cones and mature cones.
- CD24 labels early photoreceptor cells before P8 but is not specific as also labels the possible bipolar cells.
- Prom1 specifically labels all photoreceptor cells (both rods and cones) in the retina and some Nrl/CrxGFP-ve cells during early embryonic development.
- Prom1 CD73 combination or CD73 alone showed the highest specificity and was also relatively efficient in isolating photoreceptor cells among all single and combined labelling experiments (Figure 6.7, Table 6.1). This combination can isolate pure photoreceptor cells from retina from P4 onwards (Figure 6.7).
- Prom1 CD24 combination is good to isolate rods and cones which are born early ie before P8 and is more specific than Prom1 or CD24 alone for this stage.
- CD24 CD73 combination labels the fewest photoreceptor cells among all single and double labelling, but specifically isolates these cells between P4 to P8, an optimal developmental stage for transplantation competent rod precursors.
- Triple staining of CD73, CD24 and Prom1 resembles that of CD24 CD73 combination albeit with less cells.

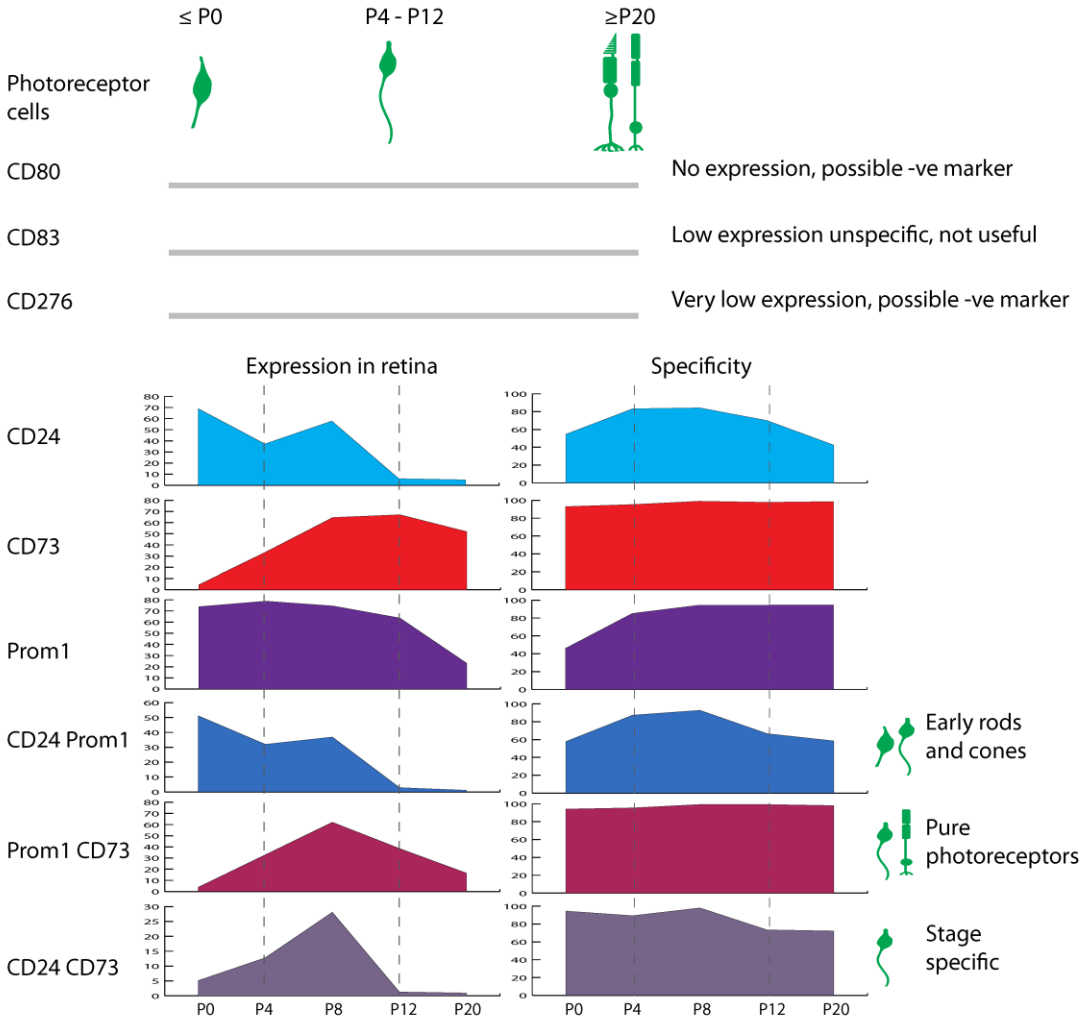

Figure 6.7 Surface marker flow cytometry summary. CD80 and CD276 showed no or very low expression in retinal cells in flow cytometry and may be used for negative selection. CD83 showed low unspecific expression for both photoreceptor cells and other retinal cells and is not useful. CD73, CD24, and Prom1 showed high expression in retina/photoreceptor cells and different developmental profiles. CD24 was high in early photoreceptor cells, CD73 was high in late photoreceptor cells, and Prom1 was high throughout photoreceptor development. The coloured shapes indicate percentage of total live retinal cells that express the markers (left, Expression in retina) or percentage of marker labelled cells that express CrxGFP (right, Specificity) at P0, P4, P8, P12, and P20.

6.2.5 Transplantation of photoreceptor precursor cells selected via CD73 and CD24

Finally to examine if cell surface markers can isolate viable retinal cells for transplantation experiments, transplantation with cells sorted using CD73 and CD24 were tested. Postnatal day four retina cells which were double positive for CD73 and CD24 in FACS were injected into the subretinal space of adult wild-type recipients (performed by Rachael Pearson). The transplanted cells were tracked based on GFP expression of the NrlGFP or CbaGFP (which labels all retinal cells injected based on GFP expression under the control of a chicken β–actin promoter) mice. The CbaGFP line allows comparison of the transplantation efficiency between unsorted retinal cells vs cells sorted by NrlGFP or cell surface markers. Three weeks post transplantation the recipient eyes were collected and assessed (performed by Jorn Lakowski). Large numbers of the transplanted cells had migrated and correctly located into the recipient ONL. These cells showed the morphology of mature photoreceptor cells and also expressed mature photoreceptor cell markers such as recoverin, retinal guanylate cyclase (RetGC), and phosducin (Figure 6.8, experiments performed by J. Lakowski (Lakowski, Han et al. 2011)). In addition, the number of integrated cells sorted by CD73 and CD24 (median = 10,899, range 544 – 32,826, n = 10) was two fold higher than the number of integrated cells sorted by NrlGFP (median = 4,649, range 1,953 – 8,206, n = 12) and around 18-fold higher than unsorted cells (median = 606, range 131 – 4,032, n = 15) (Figure 6.8, experiments performed by J. Lakowski (Lakowski, Han et al. 2011)).

The same approach was then applied to mouse models of retinal degeneration to assess if integration can also be achieved. Transplanting into a degenerating environment is more challenging because of the worsened physiological and structural changes in the eye. The *Prph2*$^{rd2/rd2}$ (*Rds*) mutant mice and the *Crb1*$^{rd8/rd8}$ (*Crb1*) mutant mice were used. The *Rds* mouse is homozygous for a null mutation in the *Prph2* gene and represents a slow rod degeneration model LCA. In this model, photoreceptor cells lack the disk structures of outer segments and contain reduced amounts of rhodopsin. The *Crb1* mutant mice contain a single base pair deletion in the *Crb1* gene. In this model, the OLM is compromised and retinitis pigmentosa and LCA may eventually occur. Similar to transplantation to wild-type recipients above, I analysed the degenerating mouse eyes which were collected three weeks after transplantation. Rod precursors isolated by CD73CD24 expression clearly integrated into the ONL of both *Rds* (median = 4,406, range 0 – 25,742, n = 8) and *Crb1* (median = 1,008, range 876 – 3,284, n = 4) retina. The *Rds* mice seem to be quite varied in the number of integrated cells (Figure 6.9). Both mutant mice did not show higher integration than the wild type (Figure 6.9 E).

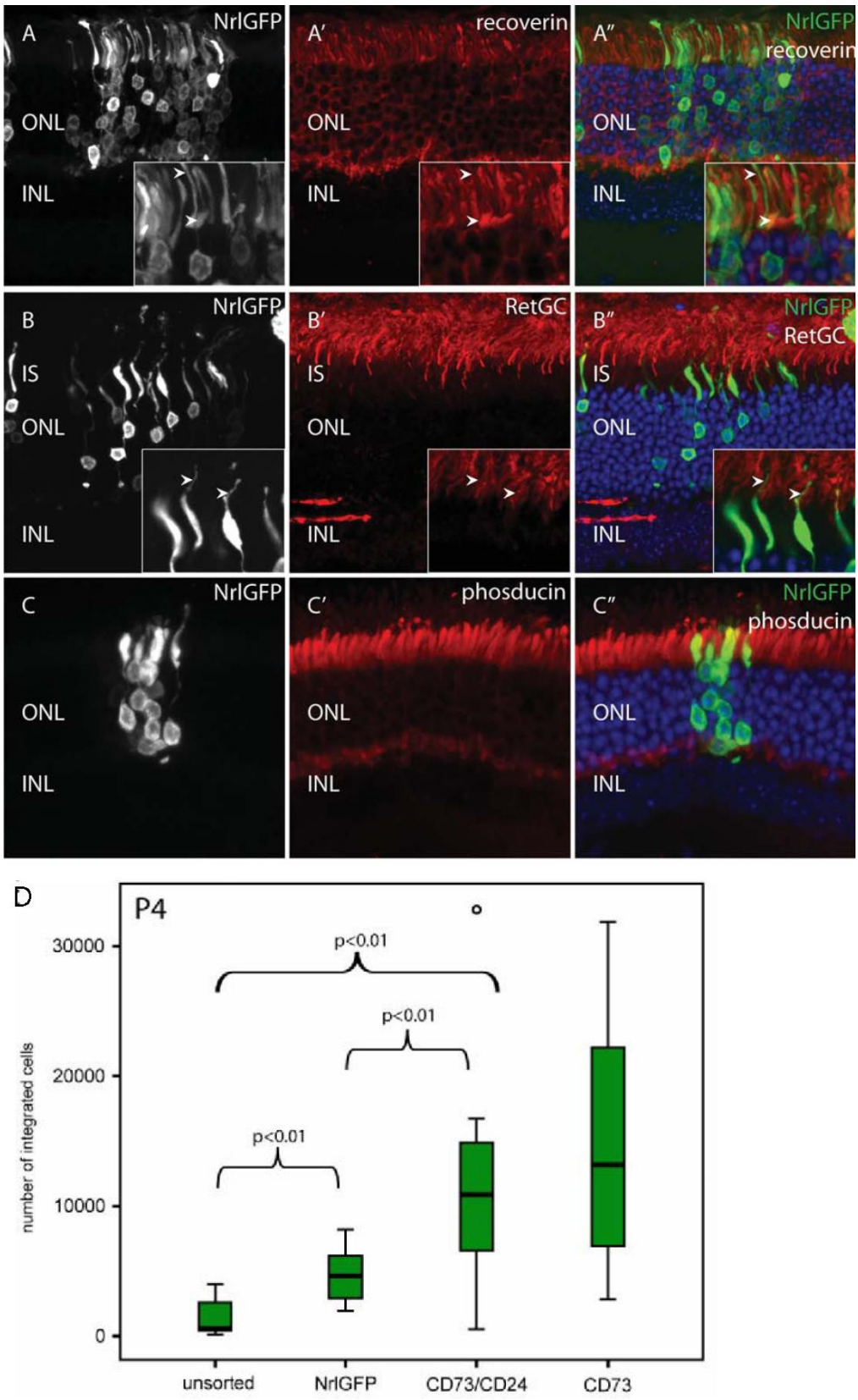

Figure 6.8 Transplantation of CD73 and CD24 sorted cells into wildtype mice. (A – C'') Confocal Z-projections of integrated NrlGFP+ve cells 3 wks after transplantation showing expression of photoreceptor markers recoverin (A'), RetGC (B'), and phosducin (C'). (D) CD73 and CD24 sorted cells integrate more efficiently than NrlGFP sorted or unsorted cells. Mann-Whitney, p < .05 ((Lakowski, Han et al. 2011) Experiments performed by Lakowski).

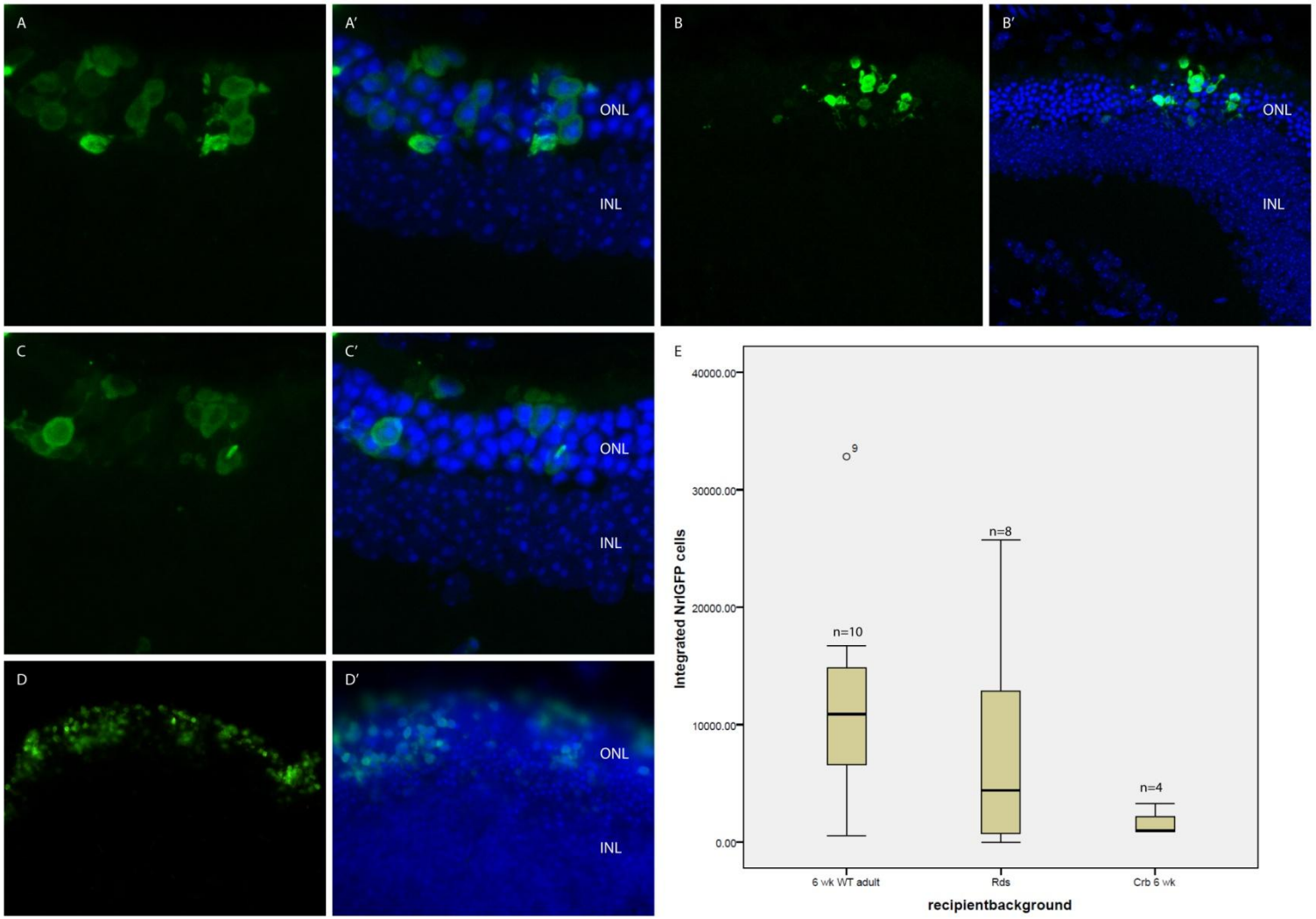

Figure 6.9 Transplantation of CD73 and CD24 sorted cells into mutant mice. (A – D) Images of CD73CD24 double-sorted P4 NrlGFP cells transplanted into 6-8wks Prph2$^{rd2/rd2}$ (*Rds*) mutant mice; (A – C) are confocal Z-projections, (D) is normal microscope image; (E) comparison of the total number of integrated P4 NrlGFP cells in mutant (*Rds* and *Crb1*) and wild-type recipient retina.

6.3 Discussion

Here six cell surface molecules were tested for their ability to isolate photoreceptor cells. Three of them CD80, CD83, CD276 could not enrich photoreceptor cells. CD73 efficiently enriched rod photoreceptor cells from retina of late postnatal stages onwards. CD24, although not as specific as CD73, only enriched immature photoreceptor cells of early stages and is turned off after P10. CD73 CD24 combination, therefore, delineated a narrow window of the precursor stage (P4 – P8) from which transplanted cells showed high integration efficiency (MacLaren, Pearson et al. 2006). Our transplantation experiments further confirmed that cells isolated by this combination are viable and can integrate into the host ONL (either wild type or degenerated retina) and mature normally. These experiments prove the concept of using cell surface markers to isolate donor cells for retinal transplantations and future experiments will test the integration efficiency of cell populations isolated using different marker combinations.

Prom1 is the 3rd surface marker which I found can efficiently enrich both cones and rods with high specificity in flow cytometry. Constantly around 70% of total mouse retinal cells can be labelled by Prom1 before P10, agreeing with a magnetic automated cell sorting (MACS) analysis where at least 67% of total human retinal cells can be isolated by Prom1 (Carter, Dick et al. 2009). Initially suggested as a marker for hematopoietic stem/progenitor cells (Yin, Miraglia et al. 1997), Prom1 is found to be expressed mainly in neuroepithelium and some embryonic and adult epithelia (Weigmann, Corbeil et al. 1997). It was also reported to label around 3% cells of neural or oligodendrocyte progenitor potential in fetal human brain dissociates (Uchida, Buck et al. 2000; Wang, O'Bara et al. 2013) as well as some cancer cells (Li, Liu et al. 2010; Wang, Chadalavada et al. 2010; Nishida, Hirohashi et al. 2012; Ji, Greening et al. 2013; Walker, Wierick et al. 2013). IHC analysis in adult mouse retina showed that Prom1 specifically labels photoreceptor cells (Chapter 5, Figure 5.4) agreeing with previous confocal and electron images (Yang, Chen et al. 2008; Zacchigna, Oh et al. 2009). Therefore if cells were only isolated from retina, using Prom1 alone may be enough and both rods and cones could be enriched. However, when in the context of *in vitro* differentiated stem cells, combination with CD73 and/or CD24 will be necessary. The combination of Prom1 with CD73 further enhanced the specificity to all rods, combination of Prom1 with CD24 might be useful to isolate rods and in particular cones of prenatal and early postnatal stages, and combination of all three may reduce contamination from other types of progenitor or differentiated cells from stem cell cultures.

It is interesting to note that when isolating the gradually maturing photoreceptor cells, CD73 showed a clear homogeneous level of expression as seen by the round tight cell cluster on the

scatter plot whereas Prom1 showed a continuous gradient level of expression. This is possibly due to the different localization of Prom1 and CD73 in matured photoreceptor cells. While Prom1 was mainly located at the cilium region which could be sheared during dissociation, CD73 was expressed mainly on the cell bodies and could be more robust to dissociation.

7 Proteomic study of rod precursors and other retinal cells at P4

7.1 Introduction

To complement the transcriptome analysis described in Chapter 3, I am interested in directly finding out proteins which are highly expressed on the surface of photoreceptor precursor cells. This was considered potentially useful as transcripts identified from microarray do not always lead to coincident high levels of protein. One method is the proteomic approach which identifies individual proteins from protein mixtures by mass mapping and peptide sequencing. Because most cell surface proteins are hydrophobic and not suitable for gel-based analysis, a technique that couples a mass spectrometer with a liquid chromatography (LC) interface, ElectroSpray Ionisation – Quadrupole-Time-of-Flight Mass Spectrometry (ESI-QTOF MS) were used. Combination of the electrospray ionisation source with LC also gives greater separation of the peptides before they enter the mass spectrometer and reduced effects of ion suppression by salts and other co-eluting molecules, thereby providing more accurate molecule identification and sequence coverage.

7.2 Results

7.2.1 Mass spectrometry of NrlGFP positive population: whole cell vs. membrane extraction

Ideally MS will provide a high-throughput mapping of all the protein candidates from the cell lysates. In reality, proteins with lower abundance could be masked by highly abundant proteins and cannot be detected. Therefore, I tested if fractionation of the cells by enriching the membrane-associated proteins using a membrane protein extraction kit (see section 2.7) will improve the number of membrane and cell surface proteins identified.

Similar to the microarray, I FACS sorted GFP positive versus negative P4 cells from NrlGFP mouse retina. Whole cell lysates (prepared by Dr Lakowski) and membrane-enriched proteins were separately prepared and submitted for MS analysis. A total of 366 proteins comparing with all species were reported for the whole cell lysates of photoreceptor cells, of which 27 are known mouse proteins (Appendix Table 7.1, mouse proteins are above the black line on 1st page of the table). In contrast, 60 mouse proteins were identified for the membrane fractions of photoreceptor cells (Appendix Table 7.2 A). 12 mouse proteins overlap between whole cell lysates and the membrane fractions (yellow highlighted in Appendix Table 7.1). All the proteins identified by both methods for photoreceptor cells were then submitted to DAVID functional chart and their Cellular Component GO terms were analysed. All GO terms with a Benjaminin value (a type of modified p value) smaller than 0.05 were compared between the whole cell

lysates (red) and the membrane fraction of photoreceptor cells (green) (Figure 7.1). Many GO terms appeared in both protein lists, and for these GO terms there were always more proteins in the membrane fractionation than the whole cell lysates either by comparing absolute protein numbers (dark colours) or the percentage of these proteins of the whole input lists (light colours). There were also GO terms that only appeared in the whole cell lysates, but these were mainly chromatin or nucleosome proteins. As expected, there were more proteins for the membrane-related GO terms in the membrane fraction than the whole cell extraction (comparing both absolute protein numbers and percentage). In addition, several GO terms which are related to cell surface molecules or membranes including cell projection, membrane-bounded vesicle and vesicle only appeared in the membrane fractionated proteins and not the whole cell extracted proteins. This shows that enriching the membrane fraction from the cells indeed enabled us to identify relatively more cell surface molecules or membrane proteins than from the whole cell extraction.

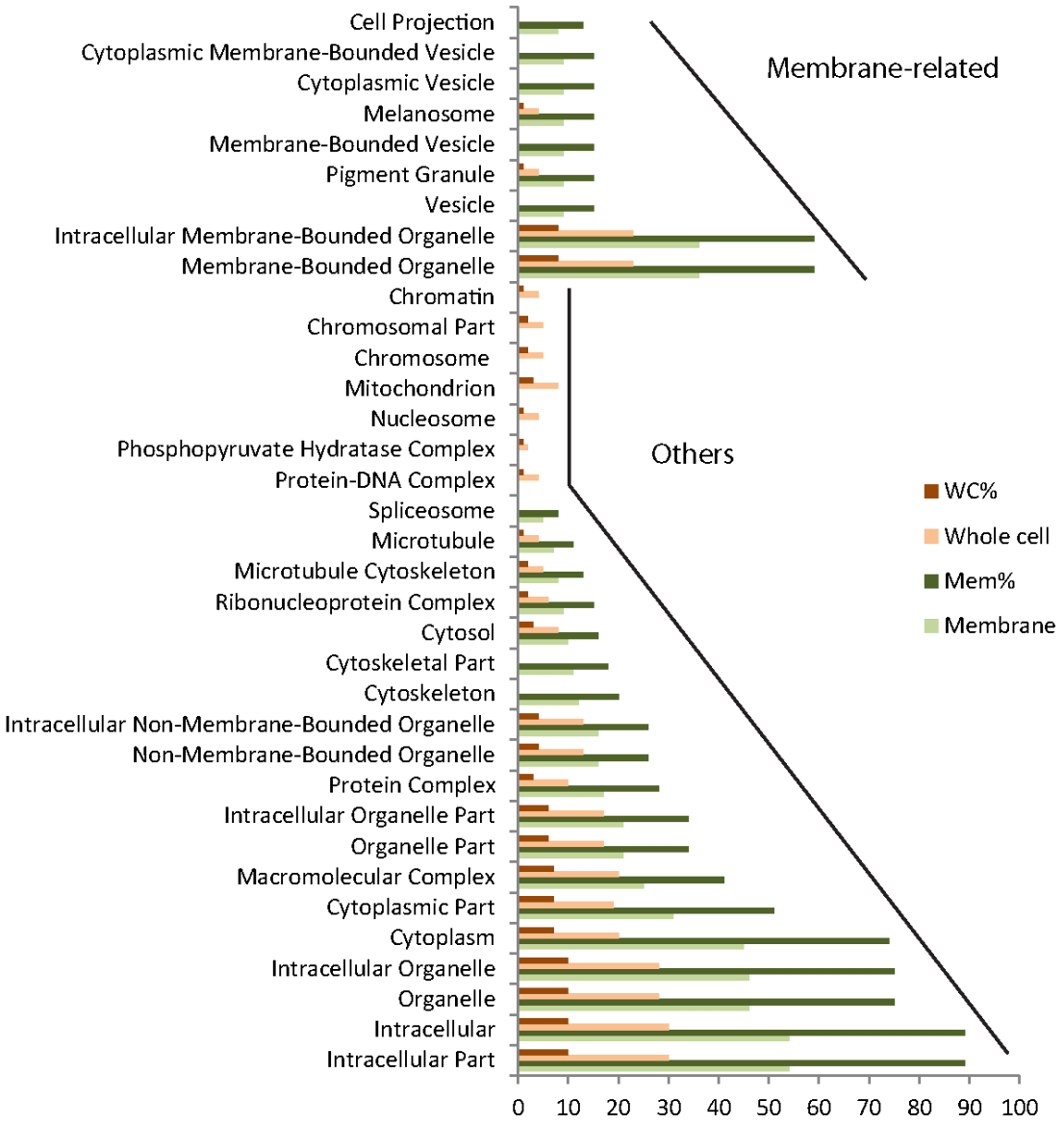

Figure 7.1 Cellular component analysis of P4 NrlGFP+ve cell proteomics: whole cell lysates versus membrane fraction. Red, whole cell lysates; Green, membrane fraction. X-axis: dark colour, percentage of proteins annotated under each GO term; light colour, absolute numbers of proteins annotated under each GO term. Note each protein can be annotated by more than one functional annotation term. Y-axis, GO terms.

7.2.2 Mass spectrometry of membrane fraction of NrlGFP positive vs. negative

I then went on to examine for the enriched membrane proteins if there are any differences between the photoreceptor precursor cells and other retinal cells. To do this, I compared the Cellular Component GO terms of the MS results of the membrane fractions of the P4 NrlGFP positive and negative cells (Figure 7.2 A and B, Appendix Table 7.2). 16 GO terms which are related with intracellular proteins were present in both NrlGFP positive and negative populations, and similar numbers of proteins for these terms were being enriched for both cell populations (Figure 7.2 A and B right of the dashed line; Figure 7.2 C). 12 GO terms were found only in the photoreceptor precursor population (Figure 7.2 C, GO terms in green). 9 out of the 12 GO terms are membrane-related, such as cell projection, cytoplasmic membrane-bounded vesicle, membrane-bounded organelles, membrane-bounded vesicle etc (Figure 7.2 A, left of the dashed line). The term “cell projection” enriched the fewest proteins of the 9 GO terms (8 proteins vs 36 proteins in “membrane-bounded organelles”) (Figure 7.2 C). In contrast, 7 GO terms were found only in the negative population which are mainly chromatin, nucleosome, protein-DNA complex, and only one membrane related GO term was enriched which is organelle inner membrane (Figure 7.2 B, left of the dashed line; Figure 7.2 C, GO terms in blue). This shows that there are more membrane proteins in the photoreceptor precursor cells than other retinal cells after membrane fractionation of both cell types.

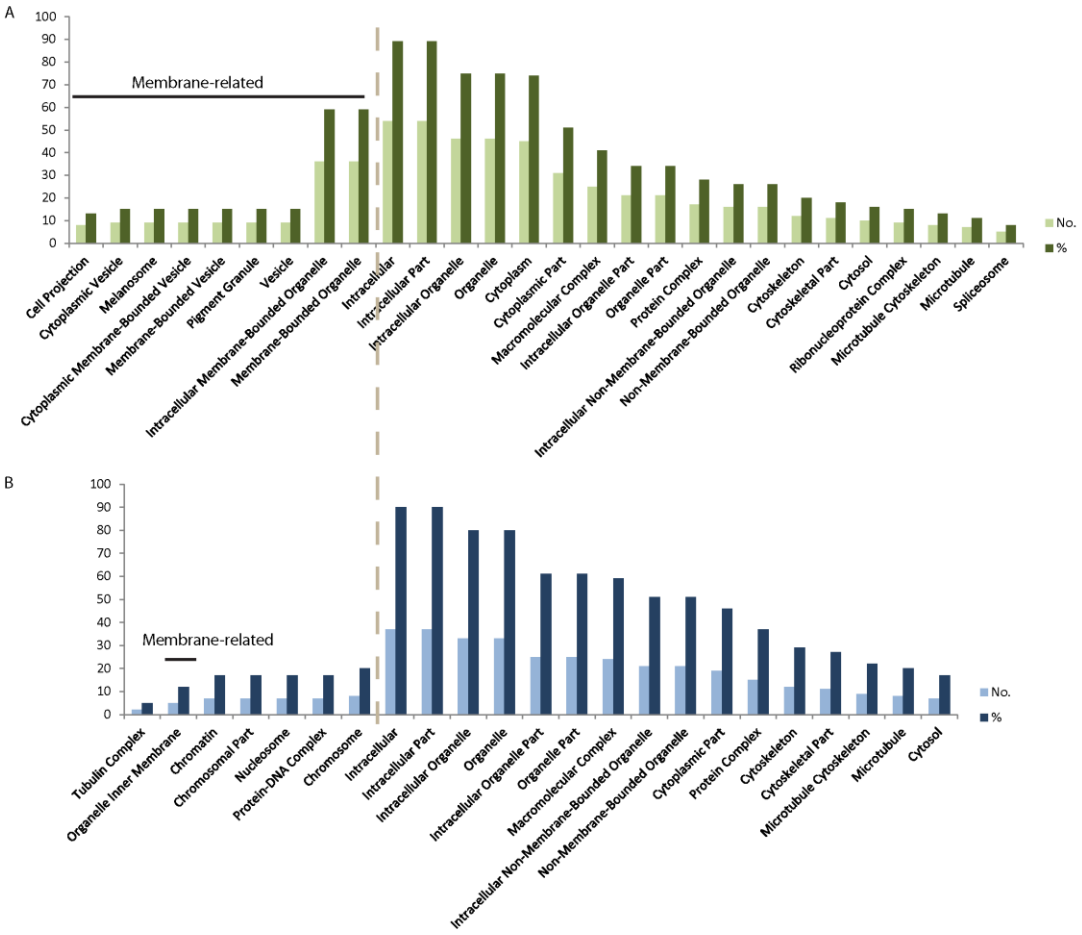

C

GO term (cellular component)	Nrl+ve (No.)	Pos%	Nrl-ve (No.)	Neg%
Cytoplasm	45	74		
Intracellular Membrane-Bounded Organelle	36	59		
Membrane-Bounded Organelle	36	59		
Cytoplasmic Membrane-Bounded Vesicle	9	15		
Cytoplasmic Vesicle	9	15		
Melanosome	9	15		
Membrane-Bounded Vesicle	9	15		
Pigment Granule	9	15		
Ribonucleoprotein Complex	9	15		
Vesicle	9	15		
Cell Projection	8	13		
Spliceosome	5	8		
Intracellular	54	89	37	90
Intracellular Part	54	89	37	90
Intracellular Organelle	46	75	33	80
Organelle	46	75	33	80
Cytoplasmic Part	31	51	19	46
Macromolecular Complex	25	41	24	59
Intracellular Organelle Part	21	34	25	61
Organelle Part	21	34	25	61
Protein Complex	17	28	15	37
Intracellular Non-Membrane-Bounded Organelle	16	26	21	51
Non-Membrane-Bounded Organelle	16	26	21	51
Cytoskeleton	12	20	12	29
Cytoskeletal Part	11	18	11	27
Cytosol	10	16	7	17
Microtubule Cytoskeleton	8	13	9	22
Microtubule	7	11	8	20
Chromosome			8	20
Chromatin			7	17
Chromosomal Part			7	17
Nucleosome			7	17
Protein-DNA Complex			7	17
Organelle Inner Membrane			5	12
Tubulin Complex			2	5

Figure 7.2 Cellular component analysis of membrane proteomics of P4 NrlGFP sorted cells (A) P4 NrlGFP+ve cells (B) P4 NrlGFP-ve cells. Dark colour, percentage of proteins annotated under each GO term; light colour, absolute numbers of proteins annotated under each GO term. X-axis, GO terms. The dashed line separate the cell-specific GO terms (left) from the common GO terms (right); (C) Direct comparison of the cellular component GO terms for P4 NrlGFP+ve cells and NrlGFP-ve cells. Green indicates terms only appeared in the photoreceptor precursors and blue indicates terms only appeared in other retinal cells.

7.2.3 Repeats of membrane fractionation for MS of NrlGFP positive vs. negative

Our initial trial of ESI-QTOF MS with membrane preparations of sorted retinal cells seems indeed to enrich some membrane proteins, although the total number of proteins identified was low (60 for rod photoreceptor cells and 39 for non-rod retinal cells) (Run 1, Appendix Table 7.2). To confirm the repeatability of the method as well as to see if more cell surface proteins could be identified, I performed another run of MS with new FACS sorted retinal cells. Membrane proteins of the new sorted cells were again extracted using the same Pierce Mem-Per kit as before. This time two different precipitation reagents were used, acetone as before and also chloroform as the latter is better to remove fat tissues. Using chloroform 31 proteins were detected for rods and 34 for non-rod retinal cells (Run 2, Appendix Table 7.3). Using acetone 47 proteins were detected for rods and 32 for non-rod retinal cells (Run 3, Appendix Table 7.4).

Comparison of the three runs for the rods shows that while six proteins were common in the 1st and 3rd run, only two and three proteins were common between the 2nd and 1st, 3rd run (Figure 7.3). This suggests that the precipitation method indeed affects the number of proteins enriched and that acetone is better to precipitate photoreceptor membrane proteins than chloroform. Numbers of proteins identified in non-rod retinal cells were comparable between all three runs (Figure 7.3).

As common proteins between different runs are probably the most robust proteins present in the cells, I examined what these proteins are. There were 13 proteins found to be common in at least two runs for the photoreceptor cells, of which lamin B1 (Lmnb1) and heterogeneous nuclear ribonucleoproteins A2/B1 (Hnrnpa2b1) could be detected in all three runs (Table 7.1). These two proteins were also common proteins found in the non-rod retinal cells. Of the remaining 11 common proteins, six proteins were also present in the non-rod retinal cells. These include HnrnpK, Voltage dependent anion selective channel protein 1 (Vdac1), Tubulin beta 5 chain (Tubb5), Tubb2c, Myristoylated alanine rich C kinase substrate (Marcks), and ATP synthase subunit beta mitochondrial (Atp5b). These proteins, although not specific to photoreceptor cells, might be important for the development of the whole retina. Five proteins were specific to photoreceptor cells from the common proteins, of which Sodium potassium transporting ATPase subunit alpha 3 (Atp1a3), Sodium potassium transporting ATPase subunit beta 2 (Atp1b2), and Alpha enolase (Eno1) were interesting candidates which will be discussed further in the next section.

A total of 15 common proteins were found in at least two runs for the non-rod retinal cells (Table 7.1). Other than the above mentioned eight proteins which were present in both rod and non-rod retinal cells, the remaining proteins were three tubulin chains, one phosphate dehydrogenase, one histone protein, one heterogeneous nuclear ribonucleoprotein, and Brain acid soluble protein 1 (Basp1) which will also be further discussed below.

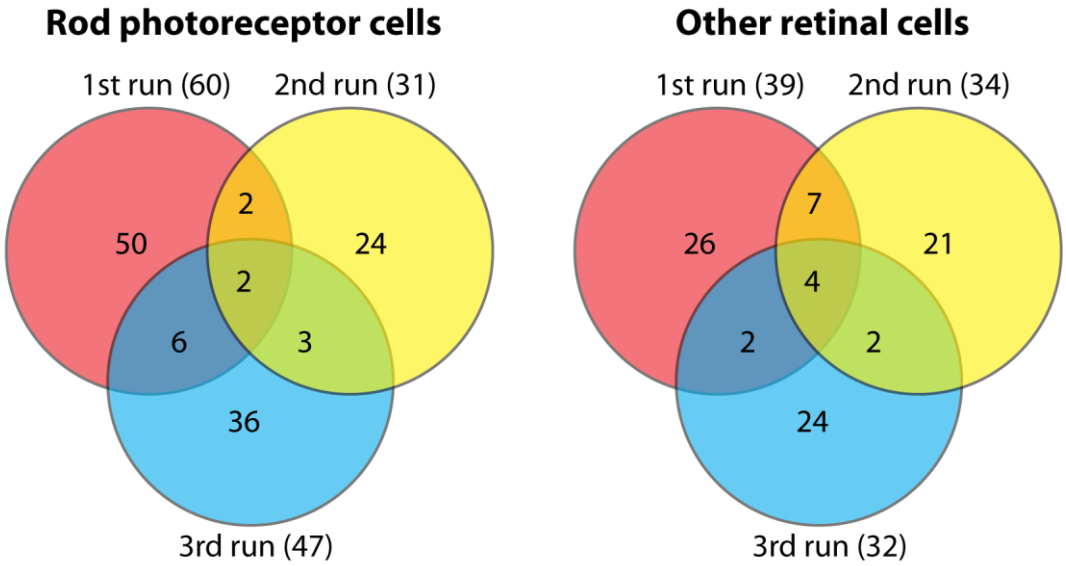

Figure 7.3 Comparison of three Mass Spectrometry runs of membrane fraction from FAC-sorted retinal cells.

Table 7.1 Common proteins from three runs of Mass Spectrometry

Proteins in photoreceptor cells	Amount (fmoles)			Proteins in other retinal cells	Amount (fmoles)		
	Run 1	Run 2	Run 3		Run 1	Run 2	Run 3
Common in all 3 runs (2)				**Common in all 3 runs (4)**			
Lamin B1	31.5536	1.7757	21.4516	Histone H4	113.2583	1.201	10.2123
Heterogeneous nuclear ribonucleoproteins A2/B1	25.3172	0	0	Voltage dependent anion selective channel protein 1	11.4354	9.4427	53.8539
				Lamin B1	20.2837	19.1796	79.612
				ATP synthase subunit beta mitochondrial	12.2702	4.7696	37.1476
Common in 2 of the 3 runs (11)				**Common in 2 of the 3 runs (11)**			
Heterogeneous nuclear ribonucleoprotein K	33.4423	1.1821		Glyceraldehyde 3 phosphate dehydrogenase	235.7324	2.0879	
Voltage dependent anion selective channel protein 1	20.6201	2.11		Tubulin beta 5 chain	166.0173	1.0231	
Sodium potassium transporting ATPase subunit alpha 3		1.022	11.2294	Tubulin beta 2B chain	2.2063	2.7463	
Beta actin like protein 2		0	0	Tubulin alpha 1C chain	186.3768	4.4704	
Sodium potassium transporting ATPase subunit beta 2		0	10.6499	Brain acid soluble protein 1	4.2734	0.8403	
Tubulin beta 5 chain	130.4988		0	Myristoylated alanine rich C kinase substrate	10.3172	4.1355	
Tubulin beta 2C chain	24.1877		6.808	Heterogeneous nuclear ribonucleoprotein K	25.4271	4.8244	
Creatine kinase B type	72.1535		5.5526	Heterogeneous nuclear ribonucleoproteins A2/B1		3.2446	23.2192
Alpha enolase	54.6878		1.1967	Heterogeneous nuclear ribonucleoprotein H		2.9709	43.4083
Myristoylated alanine rich C kinase substrate	18.29		1.3756	Tubulin beta 2C chain	15.8904		0
ATP synthase subunit beta mitochondrial	11.4701		7.2057	Tubulin alpha 1A chain	28.1914		29.374

Of these proteins, Voltage dependent anion selective channel protein 1 (Vdac1), Sodium potassium transporting ATPase subunit alpha 3 (Atp1a3), Sodium potassium transporting ATPase subunit beta 2 (Atp1b2) and Myristoylated alanine rich C kinase substrate (Marcks) are regarded as plasma membrane proteins.
Red indicates common proteins found in both photoreceptor cells and other retinal cells.

7.2.4 Marker candidates from MS of NrlGFP positive vs. negative membrane fractions

To assess whether any of these proteins are cell surface molecules, I merged the three runs of MS of the membrane fractions from the P4 NrlGFP positive and negative cells to give a total of 123 proteins in P4 NrlGFP positive population and 86 proteins in negative population (Table 7.2 A). To find out which of these proteins could be possible cell surface molecules, all the candidates were examined individually in Mouse Genome Informatics (MGI) (http://www.informatics.jax.org/) and UniProt Knowledgebase (http://www.uniprot.org/). As for searches of the microarray data as there are no specific annotation terms for cell surface proteins, I screened for plasma membrane proteins using the following criteria: proteins which are membrane-bound but annotated as located in the intracellular membrane system, such as cytoskeleton, nuclear envelope, and subcellular organelles (eg. endoplasmic reticulum, microtube, mitochondria, Golgi body, lysosome/vacuole etc) were not considered as surface proteins. Proteins which are annotated as located on plasma membranes, or annotated with extracellular or cell surface GO terms such as “plasma membrane”, “cell projection”, “secreted”, “cell membrane” etc were considered as plasma membrane proteins. Plasma membrane proteins identified in this way from each run of the MS were labelled red in Appendix Tables 7.2, 7.3, and 7.4. A total of 15 and 9 plasma membrane proteins were identified for the rods and non-rod retinal cells respectively (Table 7.2 A and B). Among them, four proteins could be detected in both rods and non-rod retinal cells (Table 7.2 B). All the plasma membrane proteins were further examined in the database to assess if they contain extracellular domains. Plasma membrane proteins whose domain structures were not annotated in the databases were also examined using transmembrane domain prediction software Tmhmm and MEMSAT, and signal peptide prediction software Signal P. Transcript levels of these genes from the Swaroop array and NrlGFP P4 array as well as the molecular function and biological process GO terms that these proteins are annotated were also examined. Interesting candidates from these examinations are presented in Table 7.3.

Table 7.2 Plasma membrane proteins from Mass Spectrometry

A	Total proteins		Plasma membrane proteins			
	rods	other cells	rods		other cells	
	protein No.	protein No.	protein No.	% of total	protein No.	% of total
1st run	60	39	8	13.33333	6	15.384615
2nd run	31	34	7	22.58065	3	8.8235294
3rd run	47	32	5	10.6383	4	12.5
Total	123	86	15	12.19512	9	10.465116

B	Plasma membrane proteins		
	rods alone (11)	common (4)	others alone (5)
	Fabp7	Eno1	Serpina3k
	Eno2	Marcks	Ntsr1
	Rab10	Basp1	Syn1
	Rab8a	Vdac1	Stxbp1
	Atp1a1		Slc2a1
	Atp1a3		
	Atp1a2		
	Atp1b2		
	V2Rp5		
	V2Rp2		

Table 7.3 Surface marker candidates from Mass Spectrometry.

Family	Protein	Gene	Gene ontology	NrlGFP microarray (Fold change and log2 intensity)		NrlGFP MassSpec (P4, fmoles)		Protein domains/location	Extracellular domain
				E16-P28 NrlGFP	P4 NrlGFP +vs-	positive	negative		
BASP1 family	Brain acid soluble protein 1	Basp1	negative regulation of gene-specific transcription, cytoplasm, growth cone, nuclear speck, plasma membrane, promoter binding, specific transcriptional repressor activity, transcription corepressor activity	high from E16 to P10 (log2 around 13), decrease at P28 (log2 around 11).	2-fold higher in negative cells (log2 at 9.2 and 10.2)	5.3663	4.2734	Tmhmm: no TMHs; MEMSAT:(in) 110-127; Signal P: no signal peptide, non-secretory protein	
enolase family	Alpha-enolase	Eno1	glycolysis, phosphopyruvate hydratase complex, plasma membrane, magnesium ion binding, phosphopyruvate hydratase activity, protein binding	low from E16 to P10 (log2 around 6), increase at P28 (log2 at 10)	2-fold higher in negative cells (log2 at 11.6 and 12.6)	54.6878	56.9848	Tmhmm: no TMHs, mainly outside; MEMSAT:(in) 106-124; Signal P: no signal peptide, non-secretory protein	
	Gamma-enolase	Eno2	glycolysis, perikaryon, phosphopyruvate hydratase complex, photoreceptor inner segment, plasma membrane, magnesium ion binding, phosphopyruvate hydratase activity	high at E16 (log2 at 12.2), decreased at P2 (log2 at 11), but increased from P6 to P28 (log2 range 11.3 – 13.5)	3-fold higher in positive cells (log2 at 9.8 and 8.2)	10.4937	N/A	Tmhmm: no TMHs, mainly outside; MEMSAT: (in) 106-124; Signal P: no signal peptide, non-secretory protein	
MARCKS family	Myristoylated alanine-rich C-kinase substrate	Marcks	cell cortex, centrosome, germinal vesicle, membrane, actin binding, calmodulin binding, protein kinase C binding	high in E16 to P6 and decreased in P10 and P28 (from 13.2 – 11.7)	1.7-fold higher in negative cells (log2 at 11.3 and 12.1)	18.29	10.3172	Tmhmm: no TMHs, mainly outside; MEMSAT:(out) 275-291; Signal P: no signal peptide, non-secretory protein	
eukaryotic mitochondrial porin family	Voltage-dependent anion-selective channel protein 1	Vdac1	anion transport, apoptosis, behavioral fear response, learning, nerve-nerve synaptic transmission, transmembrane transport, plasma membrane, pore complex, nucleotide binding, voltage-gated anion channel activity	N/A	N/A	20.6201	53.8539	Multi-pass membrane protein locates on plasma membrane, mainly transmembrane beta stranded; Tmhmm: no TMHs: MEMSAT: (out) 255-276; Signal P: signal peptide cleavage site 21-22	yes
calycin superfamily, Fatty-acid binding protein family	Fatty acid-binding protein, brain	Fabp7	cell proliferation in forebrain, neurogenesis, prepulse inhibition, transport, cell projection, cytoplasm, neuronal cell body, lipid binding, transporter activity	high from E16 to P6 (log2 around 12), decreased at P10 (log2 at 9), very low at P28 (log2 at 2)	1.37-fold higher in positive cells (log2 at 10.9 and 10.5)	17.6197	N/A	Tmhmm: no TMHs; MEMSAT: (out) 23-43; Signal P: no signal peptide, non-secretory protein	
small GTPase superfamily, Rab family	Ras-related protein Rab-8A	Rab8a	protein transport, small GTPase mediated signal transduction, plasma membrane, GTP binding, protein binding	N/A	N/A	1.3939	N/A	Tmhmm: no TMHs; MEMSAT: (out) 7-26; Signal P: no signal peptide, non-secretory protein	
	Ras-related protein Rab-10	Rab10	intracellular protein transport, small GTPase mediated signal transduction, Golgi apparatus, plasma membrane, GTP binding, protein binding	N/A	1.42-fold higher in negative cells (log2 at 9.85 and 10.35)	3.2215	N/A	Tmhmm: no TMHs; MEMSAT: (out) 8-27; Signal P: conatin signal peptide cleavage site between residual 23 and 24, non-secretory protein	
Sodium potassium transporting ATPase subunit	Sodium potassium transporting ATPase subunit alpha 3	Atp1a3	basolateral plasma membrane, regulation of glucocorticoid biosynthetic process, blood pressure and the force of heart contraction, sodium:potassium-exchanging ATPase activity	N/A	3.18-fold higher in positive cells (log2 at 12.4 and 10.6)	11.2294	N/A	4 to 5 extracellular domains; Tmhmm: 8 TMHs; MEMSAT: 8 TMHs; Signal P: no signal peptide	yes
	Sodium potassium transporting ATPase subunit beta 2	Atp1b2	cytoplasm, cell adhesion, sodium:potassium-exchanging ATPase activity	N/A	4.35-fold higher in positive cells (log2 at 12.5 and 10.3)	10.6499	N/A	1 extracellular domain (aa. 68 -290); Tmhmm: 1TMHs; MEMSAT: 1TMHs; Signal P: no signal peptide	yes
G-protein coupled receptor 1 family	Neurotensin receptor type 1	Ntsr1	G-protein coupled receptor protein signaling pathway, adult locomotory behavior, signal transduction, integral to membrane, plasma membrane, neurotensin receptor activity, G-protein coupled	N/A	N/A	N/A	44.2043	Cell membrane, four extracellular domains (aa. 1-64, 122-143, 211-235, 331-348), Tmhmm: 7 TMHs, Signal P: no signal peptide, non-secretory protein	yes
serpin family	Serine protease inhibitor A3K / Contrapsin / SPI-2	Serpina3k / Mcm2 / Spi2	response to cytokine stimulus and peptide hormone stimulus, extracellular region, serine-type endopeptidase inhibitor activity	N/A	N/A	N/A	16.5039	Tmhmm: no TMHs; MEMSAT: 1: (in) 7-23, 2: 72-90; Signal P: contain signal peptide cleavage site 21-22; The serpin-protease complex is covalently bound and highly stable	
synapsin family	Synapsin 1	Syn1	presynaptic active zone, synaptic vesicle membrane, neurotransmitter secretion	N/A	1.64-fold higher in negative cells (log2 at 7.5 and 8.2)	N/A	68.2297	Tmhmm: no TMHs; MEMSAT: no TMHs; Signal P: no signal peptide	
Sugar transporter family, Glucose transporter subfamily	Solute carrier family 2 facilitated glucose transporter member 1	Slc2a1	basolateral plasma membrane, cytoplasm, cellular response to glucose starvation, dehydroascorbic acid transporter activity, D-glucose transmembrane transporter activity	N/A	1.48-fold higher in negative cells (log2 at 5.7 and 6.2)	N/A	12.0599	6 extracellular domains; Tmhmm: 12 TMHs; MEMSAT: 12 TMHs; Signal P: no signal peptide	yes

Tmhmm and MEMSAT are protein transmembrane helix prediction program, Signal P is signal peptide prediction program. TMH: transmembrane helix

E16-P28 NrlGFP data from Swaroop array. P4 NrlGFP +vs- (ie GFP+ve versus GFP-ve) data from Lakowski.

7.2.4.1 Plasma membrane proteins identified in both populations

The four plasma membrane proteins identified from the *in silico* analysis in rod and non-rod populations are Vdac1, Marcks, Basp1, and Eno1. The protein expression levels of Basp1 and Eno1 are largely similar between the positive and negative population (Table 7.3). Transcript levels of Basp1 and Eno1 were higher in the non-rod retinal cells than rods (Table 7.3). Despite this, both genes showed high transcript levels and interesting expression profiles in the rods during retinal development. While Basp1 was high in early rod development from E16 to P10 and decreased in the adult at P28, Eno1 was low between E16 to P10 but increased at P28 (Appendix Figure 7.1). This indicates that although both proteins may not be specific for rods, they may still be involved for rod development at different stages. However, my *in silico* analysis suggests that they do not contain any extracellular domains.

Marcks showed 1.8-fold higher protein levels in rod photoreceptor cells than the non-rod retina cells according to MS (Table 7.3). However, transcript level of Marcks was slightly higher in the non-rod retinal cells although its level was also high in the rods from the microarrays (Table 7.3). As rod development proceeds, Marcks expression gradually decreased (Appendix Figure 7.1) indicating down regulation as the retina matures. Although this protein is described as being located on the membrane and may contain a lipid-anchor, being the substrate for protein kinase C (Herget, Oehrlein et al. 1995) this protein is more likely to be intracellular than extracellular and I didn't find any evidence suggesting extracellular domains.

Vdac1 showed high proteins levels from the MS, but its transcript was not detected in the microarrays. There are two isoforms for the multi-pass membrane channel protein Vdac1. Mitochondrial VDAC-1 (Mt-Vdac1) locates on mitochondrion outer membrane while plasmalemmal VDAC-1 (Pl-Vdac1) locates on plasma membrane (Buettner, Papoutsoglou et al. 2000). Pl-Vdac1 has confirmed extracellular domains. Pl-Vdac1-transfected cells exhibited higher rates of ATP release than control groups in response to medium change (Okada, O'Neal et al. 2004). On the other hand, cells from the Vdac1 knock out mice released less ATP and showed slower regulatory volume decrease after luminal hypotonic challenged cell volume increase than wild type cells (Okada, O'Neal et al. 2004). This shows that Vdac1 is associated with ATP release which is highly relevant for the high-energy-demanding photoreceptor cells. Although there is no information about it in retina yet, Vdac1 could be an interesting protein to study.

These proteins were detected in both rods and non-rod retinal cells, hence are less likely to be specific for rods. However because of their higher abundance, they might be important for rod

development. Among them only Vdac1 was confirmed to have extracellular domains and could possibly be used as a cell surface marker.

7.2.4.2 Plasma membrane proteins identified only in NrlGFP positive population

11 plasma membrane proteins were identified to exist only in rod precursor cells and not in other retinal cells. These include Gamma-enolase (Eno2), brain Fatty acid-binding protein (Fabp7), two Ras-related proteins Rab8a and Rab10, four subunits of sodium potassium transporting ATPase alpha 1 (Atp1a1), alpha 2 (Atp1a2), alpha 3 (Atp1a3) and beta 2 (Atp1b2), and two Vomeronasal 2 receptors V2Rp5 and V2Rp2. The vomeronasal receptor V2Rp5 and V2Rp2 were expressed at very low levels from the MS (less than 2 fmoles, Appendix Table 7.3). Although being inferred to locate on plasma membrane and predicted to have extracellular domains and signal peptides according to Tmhmm, MEMSAT and Signal P (data not shown), little is known about these two proteins other than a role in female mouse sexual receptive behaviour (Haga, Hattori et al. 2010).

10 fmoles Eno2 protein was detected in NrlGFP-positive cells by MS and the transcript levels were three fold higher than non-rod retinal cells (Table 7.3). During development Eno2 transcript level was high at E16 (log2 intensity 12), but decreased at P2 (log2 intensity 11) from which transcription gradually increased again (log2 intensity 11 – 13.5) (Appendix Figure 7.1). Nrl KO mice showed a similar trend of increase but with higher transcripts levels than wild type mice from P2 onwards (log2 intensity 11.8 – 13.8) and lower levels at E16 (Appendix Figure 7.1). In Zebrafish, endogenous Eno2 mRNA was detected in the developing retina from 2dpf and by 12dpf it localized to the retinal ganglion cell, inner and outer nuclear layers including rods (Bai, Garver et al. 2007; Bai, Wei et al. 2009). This indicates that Eno2 is probably involved in rod development. Then I examined if Eno2 contains any cell surface domains. Although Tmhmm and Signal P predicted it did not contain transmembrane helixes (TMHs), extracellular domains, or signal peptides, MEMSAT predicted a TMH at residual 106 –124 and an extracellular domain. It is also predicted to translocate to the plasma membrane when forming dimmers by computational similarity, but there is no experimental data in mammalians yet. It is found that the enolase of *S. cerevisiae* (Lopez-Villar, Monteoliva et al. 2006) and some prokaryotic microorganism locates on the cell surface (Bernal, de la Rubia et al. 2004; Schaumburg, Diekmann et al. 2004). This protein, therefore, remains an interesting surface molecule candidate for photoreceptor cells. Of particular note, antibodies to a neuron-specific enolase were found to preferentially label cones (Rich, Zhan et al. 1997).

18 fmole Fabp7 protein was detected in the NrlGFP positive cells by MS and the transcript levels were slightly higher in rod precursor cells than non-rod retinal cells in microarray (Table 7.3). With gradually a slight decrease, Fabp7 transcripts levels remain high from E16 to P6 (log2 intensity around 12), but decreased clearly at P10 (log2 intensity 9) and dramatically at P28 (log2 intensity 2) (Appendix Figure 7.1). When Nrl was knocked out, Fabp7 transcript levels increased at all time points tested especially at P28 where log2 intensity increased from 2 to 12 (Appendix Figure 7.1). During chick retina genesis, protein levels of Fabp7 also showed three fold decrease from E12 to P33 by ESI-MS (Finnegan, Robson et al. 2008). These clearly show that Fabp7 could be highly involved in photoreceptor development. However, there was no evidence of extracellular domains for Fabp7 except a transmembrane helix (residual 23-43) predicted by MEMSAT.

Two members of the Rab family, Rab10 and Rab8a, were also found to be present exclusively in the NrlGFP positive cells, although the expression levels were low (3 fmole and 1 fmole respectively) (Table 7.3). Rab10 was predicted to have a transmembrane helix (residual 8-27) and a signal peptide with a possible cleavage site between residual 23 and 24 by MEMSAT and Signal P. It is a member of RAS oncogene family, involved in transport, small GTPase mediated signal transduction, membrane nucleotide binding, protein binding, and GTP binding. Rab8a was predicted to have a transmembrane helix (residual 7-26) and no signal peptides. It interacts with Myo5c tubules (Jacobs, Weigert et al. 2009) and EHD1 which regulates endocytosis and associates with tubular membranes to facilitate recycling (Sharma, Giridharan et al. 2009). Rab8a and Rab8b are essential for ciliary trafficking and their knockouts in addition with Rab10 knockdown greatly affected ciliogenesis (Sato, Iwano et al. 2013). Without confirmed extracellular domains, these two proteins could not serve as cell surface molecules.

Four subunits of the sodium potassium transporting ATPase Atp1a1, Atp1a2, Atp1a3 and Atp1b2 were exclusively found in the rod photoreceptor cells. This type of ATPase couples the catalysis of ATP hydrolysis and the exchange of Na^+ and K^+ ions to create the electrochemical gradient of these ions and provide energy for active transport of nutrients. Although the expression levels of Atp1a1 and Atp1a2 were below 1 fmole, Atp1a3 and Atp1b2 showed relatively higher expression (around 11 fmoles). Transcript levels of Atp1a3 and Atp1b2 were also 3 – 4 folds higher in the rods than other retinal cells. All of these four proteins have confirmed extracellular domains. Atp1a3 is a multipass membrane protein and is the catalytic component of the ATPase. Atp1b2 is a single-pass type II membrane protein and is a non-catalytic component of the ATPase.

Considering all these 11 proteins, Eno2, Atp1a3 and Atp1b2 seem to be the most promising candidates as cell surface markers for rod photoreceptor cells.

7.2.4.3 Plasma membrane proteins identified only in NrlGFP negative population

Five plasma membrane proteins were identified in MS to exist only in the non-rod retinal cells: Neurotensin receptor type 1 (Ntsr1), Serine protease inhibitor A3K (Serpina3k), Synapsin 1 (Syn1), Syntaxin binding protein 1 (Stxbp1), and Solute carrier family 2 facilitated glucose transporter member 1 (Slc2a1). Although both Syn1 and Stxbp1 are involved in synaptic transmission, no evidence of TMHs or extracellular domains were found or predicted.

Serpina3k is a secreted protein that belongs to the serpin family. Its decrease in retina may contribute to retinal inflammation in diabetic retinopathy and is thus suggested to have an anti-inflammatory and antioxidant effect (Zhang, Hu et al. 2009). Although it is secreted out of the cell, serpin binds covalently to proteases and forms a stable complex. Further investigation of its specificity and the protease it binds to may tell if serpina3k could serve as a surface marker or not.

Slc2a1 belongs to the glucose transporter subfamily and facilitates glucose uptake. It has six confirmed extracellular domains and 12 TMHs. Ntsr1 belongs to the rhodopsin-like G protein-coupled receptor (GPCR) family that binds to neurotensin which plays important roles in neurotransmission and neuromodulation. It can activate phospholipase C, stimulate inositol phosphate (IP) production, and is also linked to the Gs-mediated pathway which increases intracellular cAMP levels (reviewed in (Hwang, Kim et al. 2009)). It contains four extracellular domains including the N-terminal domain and four cytoplasmic domains. There is no report about Slc2a1 and Ntsr1 function in retina development yet. If they are specific to non-rod retina cells, they could possibly be used as markers to deplete these cells from cell mixtures that contain the desired rod precursor cells.

7.3 Discussion

By comparing the proteome of rod photoreceptor cells from whole cell lysates versus membrane preparations, I have found that membrane fractionation indeed allowed us to identify more membrane proteins (Figure 7.1). By comparing the proteome of rod photoreceptor cells versus other retinal cells from membrane preparations, I have found that rod photoreceptor cells enriched more membrane proteins than other retinal cells (Figure 7.2), which was as expected and also agrees with the microarray analysis (Chapter 3, section 3.2.2 and 3.2.4).

I have repeated the membrane preparation MS of sorted retinal cells. The results, however, showed high variability. For the photoreceptor cells which are membrane rich, the number of proteins detected varied from 60 to 31 between the three runs. Only two proteins can be detected in all three runs and 11 proteins common in two runs. It is noticeable that when the precipitation reagent was changed from chloroform to acetone for the 3rd run, 6 common proteins were detected between the 1st and 3rd run despite they were different biological samples. In contrast, only two proteins were common between the 2nd and 3rd run which used the same biological sample but different precipitation reagents. In addition, more proteins were detected in the 1st and 3rd run which used acetone than the 2nd run which used chloroform. This shows that different precipitation reagents will affect the protein yield for MS of membrane preparations, at least for photoreceptor cells.

On the other hand, I also noticed that for other retinal cells which are less membrane rich, the numbers of proteins detected were less different between the runs (39 to 32). There were also slightly more common proteins detected among the runs for these cells (four common proteins in three runs) despite fewer total proteins. The repeatability for these cells was 17.4% (ie. 15 common proteins out of 86 total proteins), nearly 2-fold higher than the membrane rich photoreceptor cells which was 10.6% (ie. 13 common proteins out of 123 total proteins). Because the photoreceptor cells have more membrane proteins, this suggests that the variability might be related with the amount of membrane proteins and possibly contaminating detergents from the Pierce Mem-Per kit used for solubilisation. In future experiments, we could try to dialyse the membrane preparations to see if these detergents can be removed from the samples prior to precipitation for MS and to see if the repeatability increased. Future experiments could also seek to evaluate the quality of the protein preparation prior to MS analysis. Normal procedure which was followed, is to perform a protein assay (BCA assay) to determine the concentration of the samples, and to ensure the samples are the same concentration and volume before they are loaded for MS. Unlike labelling based or in-gel based MS, no other quality control is normally required for direct MS with protein mixtures. However, as the protein concentration assay will not determine whether the proteins are degraded or not, as peptides will give colour reactions, a useful additional quality control step would be to visualise the protein preps on a Coomassie or Silver stained gel prior to MS analysis.

For all the proteins identified from the three runs of the membrane proteomics of the rods and non-rod retinal cells, I individually examined them in the protein database to search for cell surface protein candidates. 20 proteins were found to be plasma membrane related. Of these

plasma membrane proteins, Vdac1, Ntsr1, Slc2a1, Atp1a3, and Atp1b2 were the ones that have confirmed extracellular domains and were relatively abundant. Atp1a3 and Atp1b2 were only found in the rod membrane proteomics and possibly could be developed as cell surface markers for rods. Ntsr1 and Slc2a1 were only found in the non-rod retinal cells and thus might be used as a negative marker to deplete these cells from cell mixtures. Vdac1 was abundant in both rods and non-rod retinal cells. So although it is not specific to rods, it possibly could serve as a general retinal marker for cell cultures which may contain non-retinal cells. Further analysis will be required to confirm the different abundance of these proteins in rod and non-rod cells, for example by Western blot analysis. Notably the identified proteins differed from the list of 13 cell surface markers identified from the RNA microarray analysis; and only 10 of them showed significantly altered expression pattern at the mRNA level in the microarray.

8 Summary and final discussion

8.1 Properties of photoreceptor precursor cells

I identified gene expression properties of the photoreceptor precursor cells by comparing their transcriptome with other retinal cells of the same stage and comparing different stages of the photoreceptor cells. Comparison with other retinal cells of the same stage showed the unique properties of photoreceptor precursor cells. This includes the expected properties such as visual perception and photoreceptor development as well as notable properties such as the enrichment of genes encoding cell projection proteins, and in particular many cilium-related genes.

I found the cilium property to be quite a unique feature for photoreceptor precursor cells in comparison with other retinal cells from the functional bioinformatics analysis. By studying the expression of some cilium markers and cilium cell surface molecules, I found the cilium property of photoreceptor cells is present as early as E15.5. As this is earlier than the recent evidence in rods suggesting photoreceptor cilia genesis starts around P0 (which coincides with the birth peak of rods) (Sedmak and Wolfrum 2011), it may represent early cone ciliogenesis coinciding with the period for the birth peak of cones. If it is indeed early cone ciliogenesis, it may represent a property of embryonic photoreceptor precursors (which give rise to cones after transplantation) that is important for integration. As there is little literature about cone ciliogenesis in mammals and considering the importance of cones, it will be important for future work to confirm if these embryonic ciliogenesis are cone specific.

Consistent with cilium marker expression, the cilium property was more established in P4 matching the higher integration rate of postnatal photoreceptor precursor cells after transplantation. Also many more cilium genes and other genes encoding cell projection proteins were expressed in P4 photoreceptor cells than E15.5 photoreceptor cells. Most of the cilium-related cell surface molecules, such as Prom1, Pcdh15 were also more highly expressed at P4 than E15.5. The cilium study here provided the starting point for further investigation of cone ciliogenesis as well as the role of cilium and cilium cell surface molecules in the migration and integration processes of photoreceptor cells.

Using the NrlGFP (rod marker) and CrxGFP (rod and cone marker) mouse strains I attempted to identify properties for cone photoreceptor cells. Comparison of the two strains showed that GO annotations of the two lines were largely the same at postnatal stages. As the cones are at low abundance, transcripts with lower expression level may have been undetected due to the limits of the array methodology. Alternatively, these two populations may in fact be largely

similar at the early postnatal stages prior to photoreceptor maturation. Surprisingly, I detected cone transcripts (*Opn1sw*) within the NrlGFP population. The embryonic CrxGFP cells showed some unique properties. However, none of the genes responsible for these properties seem to be particularly related with cones. On the other hand, I found some genes in the common gene set between the embryonic and postnatal CrxGFP+ve cells that have cone specific functions, such as *Cngb3*, *Pde6c*. Furthermore, I did find a total of 205 genes (among which 29 are genes encoding cell projection proteins) which are exclusive to the postnatal CrxGFP line despite the similarity between the postnatal CrxGFP and NrlGFP cells. Further individual examination of these genes may identify more cone-specific genes and may give more clues about cone properties.

8.2 Approaches for screening cell surface molecules

I performed bioinformatics analysis of the microarray and mass spectrometry data on the photoreceptor cells to search for cell surface molecules using several different approaches. Initially I searched for all members from several families of proteins which are known to have extracellular domains and for which a single member was initially identified as showing a significant expression pattern in microarray data. For example, tetraspanin (Tspan) is a family of highly conserved transmembrane proteins. It contains four transmembrane domains with two extracellular domains (the N and C-termini are within the cell). There are 34 mammalian tetraspanin in total and I have found five (Tspan 5, 6, 7, 9 and 33) in the Swaroop array and 13 (Tspan 1, 2, 5, 6, 7, 9, 10, 12, 14, 15, 17, 18, and 33) in the Nrl array. Of the five Tspan identified in both the Swaroop array and NrlGFP array, Tspan 6 is high in P4 NrlGFP negative population while Tspan 5, 7, 9, 33 are high in NrlGFP-positive population. Semaphorin is another family of proteins which contains extracellular domains and I found 17 of them present in the Nrl and Crx array. Similarly members of the solute carrier family, basic immunoglobulin superfamily were all present in our arrays (data not shown). This method, although exhaustive to search for all members of one particular family, relies on prior knowledge of all the families which have members with extracellular domains.

I then collected the names (both the CD name and the gene name) of all the mouse CD molecules and searched for these within the microarray data. Over 100 CD molecules were found in our arrays and 10 of them were expressed over two-fold higher in photoreceptor cells than other retinal cells. Although these candidates are confirmed cell surface molecules and have antibodies available, the number of highly differentially expressed molecules was low. To further enlarge the pool of candidates, I used the gene ontology search approach. It has to be noted that there are no specific gene ontology terms that define cell surface molecules (or

surface molecular domains). There are terms that are often used to annotate cell surface molecules such as transmembrane proteins, plasma membrane. However, transmembrane proteins can be either trans subcellular organelle membrane or trans plasma membrane. Even for trans plasma membrane, the proteins can be either intracellular or extracellular. In addition, the cell surface molecules I am seeking for are not uniform – both transmembrane proteins which have extracellular domains and proteins for which the whole structure is extracellular but are attached to the plasma membrane via some linkers all count. Therefore, it is important to go through the whole gene annotations of each gene list and check all the terms that may be used to annotate any type of cell surface molecules. This has given 227 cell surface molecule candidates which are expressed more than two fold higher in photoreceptor cells. This method probably provides the fullest list for photoreceptor cell surface molecules. Reassuringly, all the top ten CD molecules and the above mentioned members of known protein families with extracellular domains highly expressed in photoreceptor cells were in this list.

I also performed a complementary mass spectrometry analysis with the photoreceptor precursor cells. To reduce the extent of cell surface proteins being masked by other high abundant proteins, I tried to enrich for the membrane fraction of the cells in which cell surface molecules are located. Indeed more membrane-related proteins were identified in the fractionation than in the whole cell lysates. Also more membrane-related proteins were in the photoreceptor cells than in other retinal cells. This shows that the membrane fractionation was successful. However, I did not identify many cell surface molecules and there was not a good correlation with the microarray data, likely reflecting the different sensitivities of the two techniques – detection of thousands of mRNAs versus detection of tens of proteins. There are several possible reasons. Firstly, despite cell fractionation, the abundance of surface proteins in the sample may still be too low to be detected by this method initially. Secondly, cell surface proteins which are anchored to plasma membrane through lipid linkers might be sheared off during the procedure. Thirdly, if the final dissociation of proteins from the membrane is not efficient after membrane fractionation, some proteins may not even be released for detection. These reasons probably accounts for why cell surface markers such as CD73, Prom1, CD24 etc. which I know are present in photoreceptors were not detected by MS in the experiments presented here.

In the future, to search cell surface markers through the mass spectrometry approach, we could try to chemically tag cell surface glycoproteins with a linker molecule, such as biocytin hydrazide (BH), and enrich the labelled peptides by affinity purification (Wollscheid, Bausch-

Fluck et al. 2009). Compared with other MS strategies, this method seems to be more comprehensive and specific for surface membrane proteomics. The key issue with this method is the oxidation of cell surface carbohydrate-containing proteins on living cells followed by BH labeling, which needs to be carefully optimized to not only increase candidate capturing, but also prevent cell death and side reactions. Considering the high sensitivity/limited viability of photoreceptor cells, a substantial amount of effort will be required to optimize the conditions.

There is another type of analysis called membrane-polysome translation state array analysis (TSAA) which we could try in the future. This method separates membrane-bound and secreted RNA from cytosolic and nuclear RNA (Kolle, Ho et al. 2009). Basically cells were lysed, nuclei removed, and supernatant applied to sucrose gradient. The membrane-bound and secreted RNA were separated by ultracentrifugation and then hybridized with Illumina microarray chips. This selects only the membranes-associated or secreted RNA from total mRNA, therefore produce a data set that is better targeted than normal microarray. It detects more genes than MS and also avoids the problems for hydrophobic proteins. The problem remains, however, that it cannot differentiate plasma membrane proteins with intracellular/subcellular membrane proteins. Therefore bioinformatics analysis is still required to select only the cell surface candidates. Although this method analyses the polyribosome-bound RNA, it is still at RNA level and protein existence still needs to be confirmed.

8.3 The cell surface molecules

I have identified 227 cell surface molecule candidates that are expressed more than two fold higher in photoreceptor precursor cells than other retinal cells from the Nrl and Crx array. 68 of them are more than five-fold higher, among which 32 are confirmed cell surface molecules. In this thesis, I have intensively studied Prom1, CD73, CD24, and Sema7a.

8.3.1 Prom1 and isolation of photoreceptor cells for transplantation

In our microarray databases, Prom1 is highly expressed with log2 intensity over 13 in the Swaroop array and between 7 – 11 in the NrlP4 and Crx array (Figure 3.9, Figure 6.1 F). Its expression is nine fold higher in P4 photoreceptor precursor cells than other retinal cells according to both the NrlP4 array and CrxP4 array and is four-fold higher in P4 than E15.5 photoreceptor precursors in the Crx array (Table 3.3). Preliminary conventional PCR confirmed the presence of *Prom1* transcript between P4 to P28 retina tissues (Figure 6.2 D). Quantative PCR showed that *Prom1* expression is 6 – 8 fold higher from P5 to P21 than E15.5 in retina (Figure 5.4 F) and is 20 times higher in photoreceptor cells than other retina cells at P4-5 (Figure 3.10 A & B). Confocal images of developmental retina also confirmed the expression of

Prom1 protein at the cilia region from embryonic stages onwards (Figure 5.4). It is found in human that two different frameshift mutations of *PROM1* which result in truncated proteins that could not be delivered to cell surface, are responsible for the severe autosomal-recessive retinitis pigmentosa found in a Pakistan family (Zhang, Zulfiqar et al. 2007) and an India consanguineous pedigree respectively (Maw, Corbeil et al. 2000). Further an R373C missense mutation of *PROM1* was reported to cause autosomal-dominant macular degeneration in three pedigrees of Stargardt disease 4, bull's-eye macular dystrophy, and cone-rod dystrophy (Yang, Chen et al. 2008). Knockout or mutant Prom1 transgenic mice exhibited underdeveloped and disorganized disk membranes in both rods and cones (Yang, Chen et al. 2008; Zacchigna, Oh et al. 2009) as well as mislocalized rod and cone opsins and shortened cone OS and increased photoreceptor apoptosis (Zacchigna, Oh et al. 2009). All these suggest that Prom1 plays important roles in OS morphogenesis and sorting of opsin proteins.

I found that Prom1 is also expressed on transplanted photoreceptor cells (Figure 5.6). Interestingly while Prom1 expression was all over the cell body surface before the cells entered the host ONL, it is localised into specific regions of the cell surface once the cells are in the ONL. During normal retina development, I also observed Prom1 expression all over the cell body in embryonic stages, and a gradual reduction of overall expression but increased apical expression as development proceeds. Based on these expression patterns, I propose that the overall expression and the foci expression may represent two stages for photoreceptor migration with the former function more of a spreading out and searching for cues and the latter orienting and migration in the retina. The exact mechanism of how Prom1 translocates from the cell body to the cilium is still unknown, but cholesterol is likely to be involved. Further study of loss of function of Prom1 in migrating transplanted cells may indicate if Prom1 plays roles in the migration of photoreceptor cells.

Flow cytometry analysis with conjugated anti-Prom1 antibody using dissociated retina cells from Nrl/CrxGFP mouse showed that, firstly Prom1 labelled all the NrlGFP labelled cells and the "strong" CrxGFP+ve cells, secondly Prom1 did not stain the "weak" CrxGFP+ve population, thirdly Prom1 stained some Nrl/CrxGFP-ve cells in early development but much less in late development (Figure 6.4 and 6.6). As immunostaining of Prom1 showed clearly that Prom1 stains specifically to the outer layer of the retina where photoreceptor cells lie and does not stain the inner retina (Figure 5.4 in this thesis, Figure 3 in (Lakowski, Han et al. 2011)), I propose that the weak CrxGFP+ve cells which Prom1 did not stain in flow cytometry (Figure 6.6 A) are likely to be bipolar cells (as discussed in Chapter 6, section 6.2.4); the GFP-veProm1+ve cells in early development (Figure 6.6 A) are likely to be cells destined to become

photoreceptor cells/ progenitor cells as these GFP-veProm1+ve cells gradually decreased while the GFP+veProm1+ve cells correspondingly increased (as discussed in Chapter 6, section 6.2.4).

Prom1 did not label many adult photoreceptor cells in flow cytometry and showed a decreased gradient there. Conversely, confocal images of adult mouse eye cryosections showed clearly that Prom1 stains specifically between the inner and outer segments of adult rod photoreceptor cells (Figure 5.4). This agrees with previous confocal and electron microscopy images which showed Prom1 localization at the membrane evaginations of the base of rod photoreceptor outer segments (Yang, Chen et al. 2008; Zacchigna, Oh et al. 2009) and coexpression of Prom1 with Recoverin, Rhodopsin, and PNA both in sections and dissociated cells (Supplemental figures in (Zacchigna, Oh et al. 2009; Lakowski, Han et al. 2011)). It was shown in neocortex neuroepithelial (NE) cells that the Prom1-enriched-apical midbodies can be released into the neural tube fluid as NE cells divide (Dubreuil, Marzesco et al. 2007). However, these processes are observed mainly around E10.5 and E11.5 and no later than E14.5 (Dubreuil, Marzesco et al. 2007) whereas the mouse retina I studied were from E15.5 onwards and I did not notice this phenomenon. The decrease of Prom1 expression in adult photoreceptor cells in flow cytometry however, considering its gradient pattern, is most likely to be caused by damage of the cilia region of adult photoreceptor cells during the dissociation procedure as normally the more mature the photoreceptors are, the more delicate and thinner the cilia regions will be. Our flow cytometry also showed that the total Prom1+ve cells were consistently between 70 – 80% of the whole retinal before P10. This agrees with a reported MACS analysis where at least 67% of the total human retinal cells are labelled by Prom1 from post-mortem tissues (Carter, Dick et al. 2009). Further, the transplanted cells which migrate and integrate into the host retina indeed express Prom1 (Figure 5.6 in this thesis, and Figure 6 in (Lakowski, Han et al. 2011)). Taken together, these data indicate that Prom1 labels all the cone and rod photoreceptor cells in the retina from the early stages of development. Because it labels the rod and cone precursor cells, and not photoreceptor cells which lost their cilia during dissociation, it serves very well to select desired photoreceptor cells for transplantation.

Prom1, together with two other cell surface molecules CD73 and CD24 that my colleague and I showed labelled photoreceptor cells from the retina (Figure 6.4, Figure 6.6 – 6.9 in this thesis, (Lakowski, Han et al. 2011)), may be used in combination to isolate photoreceptor populations for transplantation. Firstly, all three markers labelled a relatively large proportion of photoreceptor cells on their own. Secondly, all three markers showed different expression profiles. CD73 did not label early photoreceptor precursors (before P4) and adult cones, but

labelled late photoreceptor precursors (P4 onwards) and adult rods. CD24 did not label photoreceptor cells older than P12, but labelled early rod and cone precursor cells (embryonic to P8) as well as bipolar cells. Prom1 specifically labelled all the photoreceptor cells since their birth, although its expression was reduced in adult photoreceptor cells. As each marker has a different expression profile, different combinations give rise to different photoreceptor populations. For example, a combination of Prom1 and CD24 may enrich embryonic to P8 photoreceptor cells (in particular cones), a combination of CD24 and CD73 enriched P4 to P8 photoreceptor cells, and a combination of CD73 and Prom1 enriched P4 to P12 pure photoreceptor cells. Future comparisons of the transplantation behaviour of these photoreceptor cells from different combinations will determine which population gives the highest number of integrated cells and cone photoreceptor cells.

Further to confirm if the combinations of all three markers labels photoreceptor cells specifically in different cell mixtures, it will be necessary to examine marker combinations on other types of cells which express these markers as well as stem cell sources of donor cells for transplantation. For example, high expression of both CD73 and CD24 was detected by flow cytometry on immortalized human amniotic epithelial cells (Zhou, Koike et al. 2013) and Prom1 also labels hematopoietic progenitor cells and epithelial cells (reviewed in (Corbeil, Roper et al. 2001)). Currently the three markers define photoreceptor cells if donor cells are isolated only from the developing retina. If the donor cells are derived from differentiated stem cell cultures, they may not be sufficient and further markers will be required to define the retinal context and increase stringency. It will be important to examine the expression profiles of the remaining cell surface molecules from our candidate list so that more retinal or photoreceptor-specific cell surface markers can be found.

8.3.2 Sema7a and retinal stratification

8.3.2.1 Sema7a

In this thesis I intensively studied Sema7a, a GPI-anchored semaphorin much studied in the olfactory bulb and other systems, but not in the retina. This is a migration related cell surface molecule. The transcript was highly expressed in photoreceptor cells according to the microarrays and qPCR (Figure 3.8 – 3.10). The protein was initially expressed in the whole retina but became more highly expressed in the outer retina, especially in the segments and synapses of photoreceptor cells (Figure 4.3). On the other hand, while the receptor Itgb1 did not show much expression in the retina, the other receptor PlxnC1 showed initial widespread expression in the retina followed by higher expression in the inner retina (Figure 4.4 – 4.6).

PlxnC1 also colabeled with Sema7a on the surface of photoreceptor cells in normal development as well as on migrating photoreceptor cells after transplantation (Figure 4.6, 4.11). In Sema7a$^{-/-}$ mice retina where Sema7a expression was lost, expression of PlxnC1 was also reduced (Figure 4.12). This indicates that Sema7a is interacting with PlxnC1 in the retina which is different from the Sema7a/Itgb1 interactions in many other systems (Pasterkamp, Peschon et al. 2003; Suzuki, Okuno et al. 2007; Scott, McClelland et al. 2008; Messina, Ferraris et al. 2011).

Study of Sema5a/5b and Sema6a shed the first light on the regulation of the layer formation of the inner retina (Matsuoka, Chivatakarn et al. 2011; Matsuoka, Nguyen-Ba-Charvet et al. 2011) while stratification of the outer retina is still virtually unknown. I here report the first semaphorin, Sema7a, expressed in the outer retina and in particular photoreceptor cells, and whose loss leads to Bassoon and Dystrophin in photoreceptor synapses over shooting into the ONL/INL. This indicates Sema7a may prevent over extension of photoreceptor synapses. This is likely to be achieved via interaction with PlxnC1, but the exact mechanism of this process need to be examined further.

Sema7a and PlxnC1 are also expressed on migrating transplanted photoreceptor cells as well as on some migrating-like cells in the developing retina and loss of Sema7a leads to holes in the ONL. These indicate additional roles of Sema7a and PlxnC1 in photoreceptor migration and possibly ONL formation. Further examination of the Sema7a knockout or knockdown photoreceptor cells in the developmental context as well as the transplantation context might help to answer these questions.

Because Sema7a is also expressed at lower levels in other retinal cells, it does not seem to be a specific marker to isolate photoreceptor cells from the retina for transplantation. However, it might be used in combination with other markers as a retinal cell marker.

8.3.2.2 Retina lamination

Although well known for its layered structure, little is known about the molecular mechanism that control the stratification of the retina. To form the synaptic layers, neurites must first be guided to the correct plexiform layer, then to the correct sublamination layer (where it applies) and thirdly to establish synaptic contacts with the correct partner. For example, following Sema5a/5b's repulsive guidance to constrain neurites in IPL, Sema6a and PlxnA4 guide a small subset of neurites to the correct sublamination of IPL. Yet, molecules that mediate direct synapse formation remain unidentified in the retina. These are likely to be short-range adhesive cues like the sidekicks and DSCAMs found in *Drosophila* (Yamagata, Weiner et al.

2002; Yamagata and Sanes 2008) but are largely unidentified in mammals. Further, Sema6a is only expressed in a small number of inner retinal cells and Sema5a/5b only functions in the early postnatal stages of retina to establish IPL lamination indicating additional stratification cues must exist.

Not only establishment of the synaptic layers need to be further investigated, but also formation of the nuclear layers remains enigmatic. For example, how do cell bodies of photoreceptor cells stack into such a regular layer of ONL? What makes cone photoreceptor cells stay only in the apical region of the ONL? What controls photoreceptor cells to not migrate into other cell layers? Similar questions also apply to other inner retinal cells. This thesis provided some preliminary evidence suggesting Sema7a's involvement in some of these processes. But it cannot be the only one involved and other molecules need to be identified.

In the microarray analysis, I also found Sema3f and Sema4b more highly expressed in photoreceptor cells and 14 other semaphorins (mostly Sema3s, Sema4s and Sema6s) more highly expressed in inner retinal cells. Sema3s have been recently implicated in the control of synaptic specificity in mammalian cortical–thalamic–striatal circuits (Ding, Oh et al. 2011) and spinal reflex circuitry (Sema3e with PlxnD1) (Pecho-Vrieseling, Sigrist et al. 2009) and cortex and hippocampus (Sema3f with Nrp2 or PlxnA3) (Tran, Rubio et al. 2009). Our future work will focus on these molecules. Understanding the molecular mechanisms regulating retinal neuron migration and retinal layer formation will not only facilitate the cell transplantation approach, but may also shed light on the design of more strategies in general neural injuries and diseases.

8.4 The photoreceptor cilium and its implications in retinal repair

The tiny organelle cilium has been under intensive study over the last decades, but understanding of the development of photoreceptor cilia remains limited. The work in this thesis suggests that the nascent cilium, prior to OS formation, may be important during photoreceptor development for ONL organisation. Current knowledge about photoreceptor cilium mainly focuses on ciliopathy genes that cause retinal degeneration and that the organelle itself is critical for protein transport between the OS and IS. As a primary sensory organelle, the photoreceptor cilia may function more than just as a sorting machine. Primiary cilia in other cell types such as fibroblasts (Schneider, Cammer et al. 2010) and endothelial cells (Jones, Adapala et al. 2012) have been indicated to function in orientation and migration; it is possible that the photoreceptor cilia may also have such functions. Study in this thesis found that the postnatal photoreceptor precursor cells which have high integration potential are featured with cilia properties and the transplanted migrating photoreceptor cells express the

cilium protein Prom1. These indicate that the cilia may be involved in the migration of transplanted photoreceptor cells. Future work will examine this hypothesis in detail.

Firstly, whether there is an association between intact photoreceptor cilia and integration efficiency need to be evaluated. Since Prom1 locates at the base of rod OS which are just above the connecting cilium, Prom1 could be used as an indicator for cilia intactness. As all early postnatal NrlGFP cells are labelled by Prom1, if use of a harsher digestion protocol yields NrlGFP+veProm1-ve cells, these cells are most likely to have lost the Prom1-labelled cilia region leaving the cilia impaired. Comparison of the integration efficiency of these cells with the NrlGFP+veProm1+ve cells may tell us if there is an association between cilia and integration efficiency. Since over time cells may replenish the lost cilia, it will be important to analyse a time course of cells following transplantation.

Secondly, if there is association between cilia and integration efficiency, what exact role cilia may play in the migration of photoreceptor cells will need to be further examined. It has to be noted that the role of cilia in transplanted migrating photoreceptor cells may not be exactly the same as the new born photoreceptor cells in a developmental context. Unlike the new photoreceptor cells which are born in the ONL, the transplanted cells need to migrate all the way from SRS through the interphotoreceptor matrix into ONL. It is quite possible that these cells may be orientated and guided during this migration process. Whether cilium is playing such a role can be assessed by comparing the migration path of the transplanted cells which have cilia and which do not have cilia. Again the Prom1 and NrlGFP combination may help to answer this question.

On a separate note, this thesis also observed expression of cilia markers at embryonic stages. Since rod ciliogenesis was proposed to start not until around P0 (Sedmak and Wolfrum 2011), I speculate that such early expression of cilia markers indicates ciliogenesis of cones. Different from rods, the axoneme of cones extends the whole length of OS thus probably making cilia even more critical for cones than for rods. Not much is known about cone ciliogenesis so far. Our future work is to further examine the apical protrusions of photoreceptor cells in embryonic stages at more time points using cone markers combining with cilia markers in immunohistochemistry. Electron microscopy will provide more solid evidence as to if cilia are really forming. Immunogold labelling with cone markers will probably give a firm conclusion on my speculation. As embryonic photoreceptor cells give rise to cones after transplantation but the integration efficiency is low, detailed investigation of the embryonic photoreceptor

precursor cells and their subcellular structure may also shed light on how to increase the integration efficiency of embryonic photoreceptor cells and the number of cones to be formed.

8.5 Cell transplantation and retinal repair

8.5.1 Transplantation efficiency

Since the start of cell transplantation being tested for retinal repair, the integration efficiency have been low with a typical number of 1,000 – 5,000 new cells per eye (MacLaren, Pearson et al. 2006; West, Pearson et al. 2008; Lakowski, Baron et al. 2010; Pearson, Barber et al. 2010; West, Pearson et al. 2010; West, Pearson et al. 2012). On-going optimizations have been performed to increase the integration efficiency including disruption of the host OLM (West, Pearson et al. 2008; Pearson, Barber et al. 2010), providing neurotrophic growth factors to the host environment (West, Pearson et al. 2012), preselection of donor cells (Lakowski, Baron et al. 2010; Pearson, Barber et al. 2012), increasing the number of injected cells (Pearson, Barber et al. 2012), introducing scleral punctures (Pearson, Barber et al. 2012), pre-detaching the injection site (Pearson, Barber et al. 2012), dual injections (Pearson, Barber et al. 2012) and so on. All these have contributed to increase the integration efficiency to such an extent that at present up to 26,000 cells can be integrated into a wildtype host retina (Pearson, Barber et al. 2012). With an optimized number of 200,000 donor cells in 1 µl injection buffer to inject, this gives a maximum integration efficiency of 16% (Pearson, Barber et al. 2012). This number, although substantial enough to guide optokinetic head tracking and visually guided behaviour in a rod-deficient mouse model Gnat1$^{-/-}$ (Pearson, Barber et al. 2012), remains low considering that in an experiment with viral vector delivery of *Gnat1* transgene in this model, 60,000 rod α-transducin^{+ve} cells cannot evoke an ERG response but 150,000 cells can after dual injection of AAV2/8.Rho.GNAT1 (Pearson, Barber et al. 2012). Therefore, substantial improvement of the integration efficiency remains to be achieved for cell transplantation therapy. Further refinement and characterisation of the donor population selected for transplantation as explored in this thesis is one strategy to improve integration levels.

8.5.2 Cone transplantation

Of crucial importance to human vision are the cone photoreceptor cells. However, there are far fewer studies in cone transplantation than in rod transplantation. Occasionally cone-like cells were observed after transplantation with neonatal retinal cells (MacLaren, Pearson et al. 2006) or RPCs (Klassen, Ng et al. 2004) or ES cell derived retinal cells (Lamba, Gust et al. 2009). However numbers of such cells are finger countable. Some may express cone opsins (Klassen, Ng et al. 2004; Lamba, Gust et al. 2009), but the featured cone morphology of stubby

inner/outer segment, multiple heterochromatin loci, and large cone pedicle were not shown (Lamba, Gust et al. 2009). Lakowski and Baron *et al* found that cells isolated from the embryonic stage close to the birth peak of cones (E14.5) gave the highest percentage of cones after transplantation (Lakowski, Baron et al. 2010). The new cones unambiguously demonstrated the morphology of cone features and expressed cone markers. Up to 54 integrated cones per eye was observed (Lakowski, Baron et al. 2010), yet taking into account both rods and cones formed by the transplanted cells, the integration efficiency of the embryonic photoreceptor precursor cells was 10-fold lower than postnatal photoreceptor cells which only give rise to rods. Although the ratio of the newly formed rods and cones are close to host retina, the degenerated cone-rich macular region of the human retina will require a much higher number of cones to be integrated. Therefore increasing the number of integrated cones remains a priority.

The optimization of the transplantation procedure mentioned above can be adopted here for cone transplantation. Of particular importance is probably the preselection of cone-forming cells for transplantation. This thesis found that the embryonic photoreceptor precursor cells which form cones after transplantation contain some stage-specific genes and cone-specific genes which are shared with postnatal photoreceptor precursor cells. Therefore selecting cells which express these genes, in particular the cone-specific genes and testing them for transplantation could be the next step for cone transplantation. Of particular convenience, many cone-specific genes identified here encode cell surface molecules such as *Cngb3, Opn1sw, Chrnb4,* and *Arr3*, making live cell selection potentially feasible and easy, although the stage at which these proteins are present on the cell surface and the availability of antibodies to extracellular domains first needs to be established. The recipient environment can also be manipulated to increase cone integration. It was shown that cone yield was increased in the *Gucy2e*$^{-/-}$ mutant in which endogenous cones were degenerated (Lakowski, Baron et al. 2010).

There is no purpose for transplantation if the injected cones don't function. To determine if the newly formed cones function or not, ERG responses and behavioural tests can be assessed. To separate cone function from rod function in ERGs, light-adaption can be applied to saturate the rod system so that the ERG mainly reflects activities in the cone system which shows waves of small amplitude but very fast kinetics (Hood and Finkelstein 1986; Alexander, Umino et al. 2007). If in a dark-adapted state, bright red light stimulus induces a cone-mediated ERG response of fast kinetics (known as X-waves) followed by a rod-mediated slow-time-to-peak response (Bornschein, Goodman et al. 1957; Berson and Howard 1971). This property can be

used to assess the function of both rods and cones after transplantation. Visual acuity can be assessed by measuring optomotor head-tracking responses and its ERG responses to a rotating grating using the OptoMotry© system (Alexander, Umino et al. 2007). Other behaviour tests such as the Prusky water maze system in which rodents learn to associate visual grating display with escape can also be used to assess visual acuity (Prusky, West et al. 2000).

Using mice, a nocturnal species, for cone transplantation to restore photopic vision is in general less ideal, although the many transgenic lines greatly facilited our research. Domestic animals such as pig, sheep, and cattle as well as the rodent ground squirrel and nile rat are all diurnal species. It may be worthwhile to explore the possibility of using these species as the recipients for cone transplantation. Although there aren't any cone-degenerating models in these species, it may still be possible to generate a cone-deficient retina to test new cone function after transplantation. It is found that excessive thyroid hormone or triiodothyronine (T3) leads to cone apoptosis in mice (Ng, Lyubarsky et al. 2010), therefore it may be worth injecting T3 or thyroid hormone to these diurnal species to see if their cones are eliminated or not.

8.5.3 ES cells and iPS cells

Being considered renewable and immortal cell resources, ES cells and iPS cells have been the focus of regenerative medicine over decades. Retinal cell transplantation studies with these sources have also evolved greatly. A recent breakthrough in ES cell technology showed spontaneous formation of optic cups and even properly layered ONL using a 3-dimentional (3D) culture system (Eiraku, Takata et al. 2011). Rod precursors labelled with RhoGFP transgenes derived from mouse ES cells using this 3D protocol successfully integrated into ONL of degenerating mice retina and matured into healthy OS-bearing photoreceptor cells (Gonzalez-Cordero, West et al. 2013). These new data suggest that ES cell sources are likely to be useful to provide photoreceptor precursor cells for human transplantation and treatment of retinal diseases. The immediate next step will be to evaluate if these cells can rescue vision in these models with behaviour tests, ERG recordings and so on. Protocols of human ES cell and iPS cells differentiation into photoreceptor precursors will need to be improved to increase photoreceptor-precursor-forming-efficiency and similar functional assessments are needed. Cell surface molecules identified in the postnatal retina will need to be assessed in the human ES cell and iPS cell cultures to select for cells of the right type and time for transplantation, and so that cells can be selected without the use of transgenic markers. Last but not least, Good Manufacturing Practice will need to be established to ensure safe transplantation for retinal repair.

9 Appendix

9.1 Appendix Table 2.1

Appendix Table 2.1 RNA extraction and FACS of CrxGFP+ve vs CrxGFP-ve cells for microarray

All extracted RNA are in 30 µl RNase-free water at -80°C.

First set of 6 samples from CrxGFP E15.5

Sample Number	Sample Name	Cell No. (10^6)	A260/280	[RNA] ng/µl	RNA Extractn date	Cell sort date (million cells)
#1	**Crx E15.5 GFP+tive 1**	3.02	2.09	81.1	26.5.10	31.3.10 (1.86) 31.3.10 (0.51) 7.4.10 (0.65)
#2	**Crx E15.5 GFP+tive 2**	3.03	1.98	107.1	27.5.10	25.2.10 (0.78) 25.2.10 (0.96) 25.2.10 (1.29)
#3	**Crx E15.5 GFP+tive 3**	3.97	1.96	99.4	27.5.10	29.1.10 (1.06) 19.2.10 (1.47) 26.2.10 (1.44)
#4	**Crx E15.5 GFP-tive 1**	3.02	1.98	100.7	27.5.10	31.3.10 (1.54) 31.3.10 (0.9) 7.4.10 (0.4) 9.4.10 (0.17)
#5	**Crx E15.5 GFP-tive 2**	5	2.08	76.5	1.7.10	17.6.10 (5 from 3 litters)
#6	**Crx E15.5 GFP-tive 3**	2.47	2.09	65.9	1.7.10	25.6.10 (2.47)

Second set of 6 samples from CrxGFP P4

Sample Number	Sample Name	Cell No. (10^6)	A260/280	[RNA] ng/µl	RNA Extractn date	Cell sort date (million)
#7	**Crx P4 GFP+tive 1**	5.96	2.06	81.3	2.8.10	29.7.10 (5.96)
#8	**Crx P4 GFP+tive 2**	8.09	2.06	106.9	2.8.10	29.7.10 (8.09)
#9	**Crx P4 GFP+tive 3**	9.5	2.08	115.3	2.8.10	29.7.10 (9.5)
#10	**Crx P4 GFP-tive 1**	4.92	2.08	72	3.8.10	29.7.10 (2.02) 2.8.10 (2.9)
#11	**Crx P4 GFP-tive 2**	5.4	2.07	86.4	3.8.10	29.7.10 (1.9) 2.8.10 (3.5)
#12	**Crx P4 GFP-tive 3**	5.54	2.08	65.1	3.8.10	29.7.10 (2) 2.8.10 (3.54)

9.2 Appendix 2.1

Appendix 2.1 shRNA sequences for Sema7a

shRNAsema7a1 (Target seq: TGGACGTGGCAAGGTCTACCACTTCAACT)

5’ - TTTG TGAGCGA **TGGACGTGGCAAGGTCTACCACTTCAATT** CTGTAAAGCCACAGATGGG **AGTTGAAGTGGTAGACCTTGCCACGTCCA**

CCGCCTA TTTT-3’

5’ – CTAGAAAA TAGGCGG **TGGACGTGGCAAGGTCTACCACTTCAATT** CCCATCTGTGGCTTTACAG **AATTGAAGTGGTAGACCTTGCCACGTCCA** TCGCTCA -3’

shRNAsema7a2 (Target seq: TCTGTCTCCAAGTGGAACACCTTCCTGAA)

5’ - TTTG TGAGCGA **TCTGTCTCCAAGTGGAACACCTTCCTTAA** CTGTAAAGCCACAGATGGG **TTCAGGAAGGTGTTCCACTTGGAGACAGA**

CCGCCTA TTTT-3’

5’ – CTAGAAAA TAGGCGG **TCTGTCTCCAAGTGGAACACCTTCCTGAA** CCCATCTGTGGCTTTACAG **TTAAGGAAGGTGTTCCACTTGGAGACAGA** TCGCTCA -3’

shRNAsema7a3 (Target seq: GAACTGTACACAAGTGATA)

5’ - TTTG TGAGCGA **GAACTGTACACAAGTGATA** CTGTAAAGCCACAGATGGG **TATCACTTGTGTACAGTTC** CCGCCTA TTTT-3’

5’ – CTAGAAAA TAGGCGG **GAACTGTACACAAGTGATA** CCCATCTGTGGCTTTACAG **TATCACTTGTGTACAGTTC** TCGCTCA -3’

shRNAsema7a4 (Target seq: GCTTGGTGACATTGACAGA)

5’ - TTTG TGAGCGA **GCTTGGTGACATTGACAGA** CTGTAAAGCCACAGATGGG **TCTGTCAATGTCACCAAGC** CCGCCTA TTTT-3’

5’ – CTAGAAAA TAGGCGG **GCTTGGTGACATTGACAGA** CCCATCTGTGGCTTTACAG **TCTGTCAATGTCACCAAGC** TCGCTCA -3’

9.3 Appendix figure 3.1

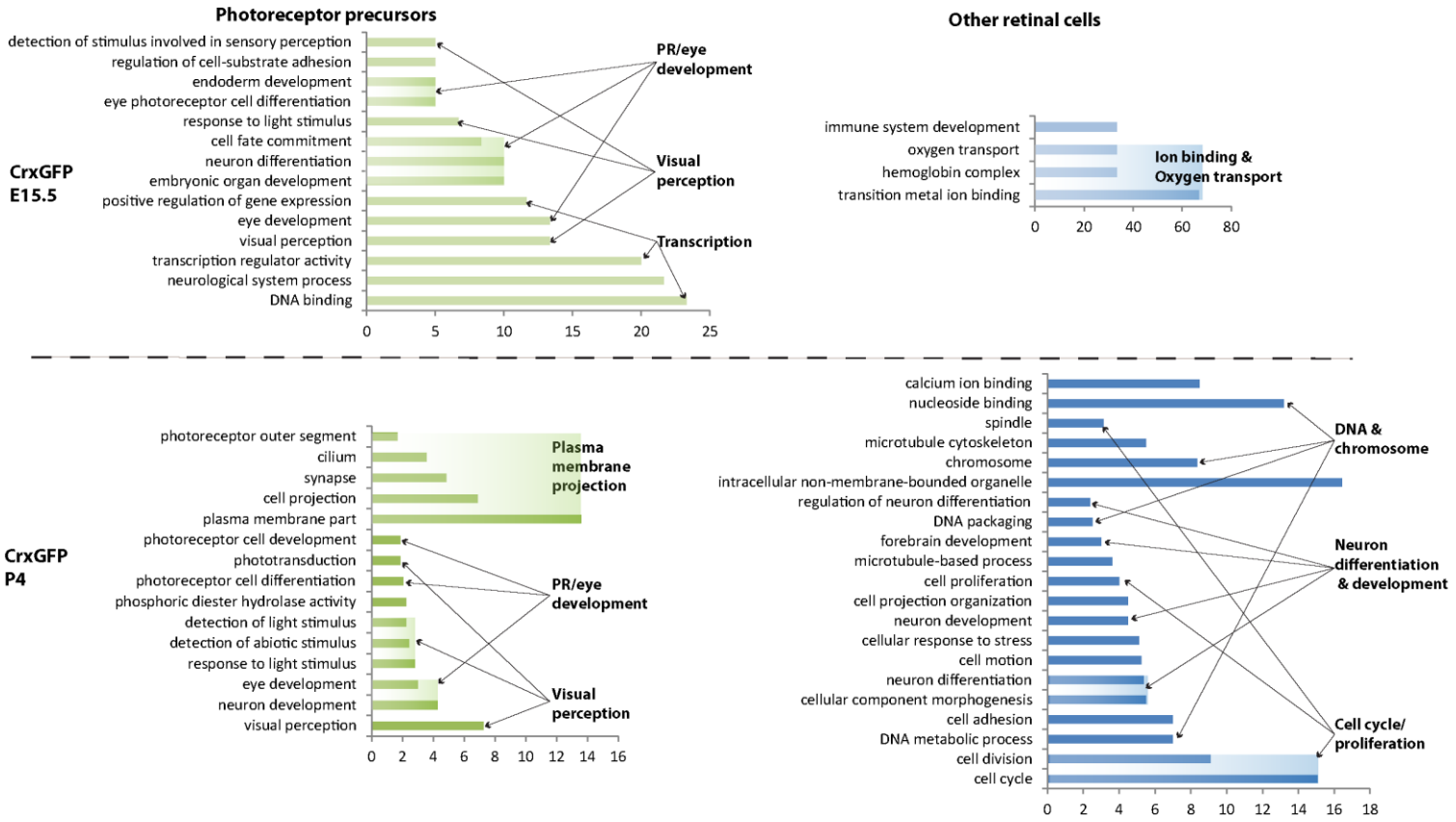

Appendix figure 3.1 Photoreceptor cell transcriptomes show very different properties from other retinal cells of the same stage. (A**) Properties of gene sets for E15.5 CrxGFP positive cells (green, photoreceptor precursors) vs CrxGFP negative cells (blue, other retinal cells). (**Bottom row**) Main properties of gene sets for P4 CrxGFP positive cells (green, photoreceptor precursors) vs CrxGFP negative cells (blue, other retinal cells). X-axis: percentage of the genes annotated under each GO term out of the whole input gene lists. Y-axis: Gene ontology terms which were significantly enriched in the gene lists compared with random generated gene lists from the genome. Here only the most general GO terms merged and compressed from the original full GO lists were compared (Figure3.6 and Appendix figure 3.1 showed the full lists of GO term comparison). According to the size of the gene sets, the statistic thresholds were set as E15.5Crx+ve p0.01, E15.5Crx-ve p0.01, P4Crx+ve and P4Crx-ve FDR0.01. PR: photoreceptor cell.**

9.4 Appendix table 3.1

Appendix table 3.1 Crx+ve E15.5 specific gene list and expression fold changes

GeneID	GeneSymbol	Fold Change between copmarison			
		E15.5+v-	P4+v-	Pos E15.5vP4	Neg E15.5vP4
10575227	Pmfbp1	7.40171	1.11228	11.3425	1.70448
10426385	Muc19	6.7345	1.70728	3.79409	-1.03967
10587077	Onecut1	5.34908	1.98551	6.61816	2.45658
10426383	Muc19	5.32521	1.23673	4.18323	-1.02932
10553477	Ano5	5.29653	1.11665	5.18558	1.09326
10486041	Meis2	4.25981	1.03087	-1.61024	-6.65395
10461979	Aldh1a1	4.24871	-3.32572	7.53073	-1.87632
10345016	Tcfap2b	4.24378	-1.63453	1.06917	-6.48781
10432831	Krt73	4.10624	1.16921	3.4788	-1.00954
10408798	Tcfap2a	3.4392	-1.40821	1.27202	-3.80743
10492402	Kcnab1	3.20919	-1.02407	2.05693	-1.59773
10514240	Slc24a2	2.74261	-1.99407	1.86717	-2.92901
10357339	Lypd1	2.45636	1.15356	1.65555	-1.2862
10564527	Nr2f2	2.37387	1.01021	1.7306	-1.35784
10358434	Pla2g4a	2.2837	-1.03389	3.95443	1.67483
10364402	Slc1a6	2.26781	1.23661	1.82212	-1.00646
10467319	Rbp4	2.08783	-1.16647	2.33731	-1.04196

9.5 Appendix table 3.2

Appendix table 3.2 Crx+ve E15.5 & P4 common gene list and expression fold changes

GeneID	GeneSymbol	Fold Change between copmarison			
		E15.5+v-	P4+v-	Pos E15.5vP4	Neg E15.5vP4
10412882	Thrb	10.993	3.16205	3.78172	1.08778
10428376	Angpt1	11.0135	4.6791	1.75939	-1.33783
10502881	St6galnac5	5.00706	3.00236	1.64386	-1.01451
10344679	St18	3.71804	4.31443	1.52956	1.77491
10372023	Gm4792	3.49235	2.79062	1.23951	-1.00964
10462887	Pde6c	12.758	9.09732	1.07249	-1.3076
10495259	Gnat2	6.57846	6.78718	-1.04271	-1.01065
10528864	Cnpy1	2.33203	2.23657	-1.05128	-1.09615
10406817	Enc1	2.20788	2.2026	-1.09166	-1.09428
10382492	Otop3	3.04043	3.41933	-1.16554	-1.03639
10503464	Cngb3	26.0673	12.9657	-1.32521	-2.66432
10503259	Trp53inp1	2.06685	2.00654	-1.34396	-1.38435
10548118	Prmt8	2.65199	2.24071	-1.50301	-1.77889
10402020	Eml5	2.57303	2.94343	-1.51782	-1.32681
10440393	Samsn1	8.39357	12.5896	-1.53622	-1.02421
10411782	Pik3r1	2.72947	3.13696	-1.67729	-1.45941
10368970	Prdm1	8.55711	10.344	-1.70707	-1.41218
10422244	Slitrk6	28.2526	15.8267	-1.81468	-3.23941
10446334	Glcci1	2.97587	6.0902	-1.90631	1.07356
10402061	Eml5	2.91839	3.66592	-1.9167	-1.52586
10462195	Kank1	2.09994	4.2985	-1.94368	1.05314
10428004	Ankrd33b	2.11933	3.06033	-1.9743	-1.36724
10543118	Glcci1	2.65454	5.13945	-2.02176	-1.04424
10529923	Lcorl	2.44664	4.65032	-2.14844	-1.13034
10484276	Neurod1	4.60123	10.5051	-2.38507	-1.04466
10474141	Slc1a2	4.15551	8.43913	-2.41959	-1.19143
10419356	Otx2	4.11957	4.80459	-2.56417	-2.19858
10454369	Fhod3	2.97124	7.20721	-2.73701	-1.12836
10427496	Egflam	4.13253	9.67583	-2.75206	-1.1754
10480139	C1ql3	6.62908	6.34843	-2.79417	-2.91769
10560168	Crx	15.6546	20.1751	-2.83702	-2.20134
10373680	Neurod4	22.0025	14.279	-2.98079	-4.59311
10600604	Dmd	3.13276	11.581	-3.04372	1.21455
10363224	Fabp7	17.3043	26.1714	-3.16354	-2.0917
10413981	Gm626	6.58336	20.5644	-3.41173	-1.09221
10564646	Sv2b	2.75689	16.9575	-3.62394	1.69731
10408812	Mak	6.25322	22.0808	-3.82327	-1.08274
10419015	Cdhr1	4.21158	14.3479	-4.55181	-1.3361
10484237	Zfp385b	2.64113	11.0052	-4.92003	-1.18076
10531348	Ppef2	5.50396	19.2097	-5.10044	-1.46138
10407337	Hcn1	5.18522	7.23023	-5.12108	-3.67262
10414663	Rpgrip1	5.75074	21.604	-6.26463	-1.66757
10436282	Impg2	13.7527	51.4033	-6.59326	-1.764
10400904	4930403N07Rik	2.07776	17.7718	-9.09124	-1.06289
10414034	Rbp3	10.0091	35.0821	-9.55153	-2.72511
10350530	Pdc	16.5561	43.7619	-12.2548	-4.63625

9.6 Appendix table 3.3

Appendix table 3.3 Crx+ve P4 specific gene list and expression fold changes

GeneID	GeneSymbol	Fold Change between copmarison			
		E15.5+v-	P4+v-	Pos E15.5vP4	Neg E15.5vP4
10436416	Gabrr3	1.56298	47.1376	-30.1713	-1.00042
10491252	Samd7	1.23482	45.9339	-78.2068	-2.10239
10352928	Rp1	1.35926	44.6873	-49.0212	-1.49109
10522366		-1.1787	42.613	-52.0424	-1.03613
10523979	Pde6b	1.06469	41.5261	-67.4317	-1.72889
10530503	Cnga1	1.11251	36.0885	-40.8715	-1.25996
10540984	Rho	-1.04559	34.1121	-44.2423	-1.24041
10540991	Rho	1.06174	31.3976	-33.492	-1.13256
10587639	Nt5e	2.25786	31.1249	-17.8497	-1.29485
10459475	Cplx4	-1.04124	27.3017	-34.7447	-1.22222
10348301	Sag	1.13769	23.2779	-29.9094	-1.46181
10420013	Nrl	1.89248	18.4976	-13.1307	-1.3434
10594188	Nr2e3	-1.09344	16.6894	-23.1088	-1.26632
10484261	Cerkl	3.12629	16.1369	-4.13472	1.24837
10536209	Gngt1	1.81586	15.3593	-12.1606	-1.43769
10413993	Gm626	4.29368	15.3371	-4.15283	-1.1626
10485357		1.54624	14.1963	-5.03205	1.82454
10531177	Adamts3	1.08234	14.1692	-6.7008	1.95368
10558150	Htra1	1.33505	13.6217	-14.2355	-1.3952
10475653	Slc27a2	-1.13881	12.5943	-9.69793	1.47892
10414168	Lrit2	2.02075	12.331	-6.86066	-1.1243
10541968	Ano2	1.51876	12.2319	-9.85965	-1.22422
10413979	Gm626	3.80615	11.1979	-3.80604	-1.29366
10541144	Cacna2d4	1.97631	11.1951	-7.68082	-1.35592
10413991	Gm626	3.24716	10.676	-3.94013	-1.19841
10368021	Gje1	1.05596	10.667	-8.89136	1.13613
10393793	Pde6g	1.29125	10.5799	-12.7712	-1.55869
10445293	Pla2g7	-1.27454	10.0114	-5.60963	2.27464
10595306	Impg1	1.15089	9.94632	-10.0882	-1.16732
10439483	Arhgap31	1.73977	9.85156	-7.52304	-1.32856
10529824	Prom1	1.24535	9.40123	-4.24424	1.77866
10602966	Rs1	1.07405	9.3161	-10.2494	-1.18164
10547858	Gnb3	2.78104	9.28214	-3.76594	-1.12832
10497276	Fabp12	1.12878	9.20939	-8.51571	-1.04375
10445633	Prph2	1.23823	9.1317	-8.48423	-1.15044
10408838	Elovl2	1.35792	8.63188	-4.36834	1.45518
10531179	Adamts3	-1.16794	8.61017	-7.63127	1.31776
10495712	Abca4	1.39594	8.07413	-6.2773	-1.08528
10413985	Gm626	2.14426	8.02536	-3.99514	-1.06744
10410995	Rasgrf2	2.42242	7.69304	-5.85925	-1.84499
10465833	Rom1	1.10279	7.59636	-7.09602	-1.03016
10543591	Opn1sw	1.46211	7.35149	-6.23974	-1.241
10531195	Adamts3	1.05045	7.21243	-4.63592	1.48104
10578222	Dlc1	2.22912	7.21027	-3.4664	-1.07167
10379176	Unc119	1.71948	7.19371	-3.81745	1.09593
10428124	Rgs22	2.21332	7.12397	-2.75136	1.16985
10352586	Ush2a	2.28418	7.01788	-3.4602	-1.12623
10466248	Stx3	1.61114	6.96566	-6.73011	-1.55666
10476795	4930529M08Rik	1.10935	6.95721	-4.34872	1.44213
10488804	Gm14214	1.20456	6.94072	-5.01794	1.14829
10388465	Doc2b	2.71129	6.75295	-3.03904	-1.22017
10413977	Gm626	2.04713	6.69868	-3.35515	-1.02534
10504672	Tdrd7	1.00695	6.64456	-6.68964	-1.01378
10354897	Trak2	1.85247	6.61963	-5.01534	-1.40352
10413999	Gm626	1.48267	6.55424	-4.74664	-1.07376
10578709	Wdr17	-1.25406	6.48935	-5.92946	1.37248
10593947	Cplx3	1.91689	6.21274	-4.11427	-1.26943
10590623	Cxcr6	2.07137	6.18301	-3.5795	-1.19917
10396840	Rdh12	1.013	6.16494	-6.00956	1.01269
10542738	Rassf8	1.93907	6.11243	-3.00378	1.04943
10452729	BC027072	1.08423	6.05408	-6.10163	-1.09275
10531193	Adamts3	1.09541	6.04745	-3.49286	1.58058
10402268	Lgmn	1.05821	6.0078	-6.92171	-1.21919
10597978	Fyco1	2.1969	5.97841	-3.48501	-1.28065
10482968	Pla2r1	1.15555	5.93668	-5.09318	1.00871
10366073	Cep290	1.35788	5.92009	-3.28442	1.32742
10414001	Gm626	1.62035	5.84266	-3.32439	1.08465
10461268	1810009A15Rik	1.0168	5.82991	-5.19098	1.10453
10514892	2210012G02Rik	1.93319	5.79579	-3.03297	-1.01165
10457475	Abhd3	1.64751	5.74139	-4.29229	-1.23169
10413995	Gm626	1.93989	5.7	-2.82912	1.0386

10580829	Cngb1	1.1839	5.68943	-5.41098	-1.12596
10354955	Mpp4	1.41652	5.66522	-5.1472	-1.287
10351665	Ccdc72	1.49154	5.64424	-3.48898	1.08461
10440314	Cadm2	1.65796	5.5947	-3.47506	-1.02982
10436666	Jam2	1.54415	5.52587	-2.86082	1.25089
10398459	Ppp2r5c	-1.00481	5.51938	-4.45568	1.24469
10436623	Chodl	2.52038	5.51542	1.22612	2.68314
10550146	Cabp5	1.21357	5.48416	-4.7383	-1.04852
10453049	Cdc42ep3	1.49641	5.48076	-3.53911	1.0349
10472549	Bbs5	1.35512	5.47092	-4.40103	-1.09012
10420631	Ebpl	1.21116	5.36451	-5.12711	-1.15756
10449435	Tulp1	1.77893	5.36424	-3.5291	-1.17034
10598309	Cacna1f	1.21519	5.36359	-4.31375	1.02319
10531191	Adamts3	1.11941	5.31394	-4.20883	1.12789
10607064	Gucy2f	1.16859	5.25875	-5.33025	-1.18448
10523977	Gm10419	-1.00634	5.16872	-6.16471	-1.18518
10531203	Adamts3	-1.01664	5.16042	-2.85969	1.83457
10471675	Glo1	1.19349	5.1155	-5.25575	-1.22621
10531197	Adamts3	-1.04658	5.11408	-3.53137	1.51565
10514128	Ttc39b	1.59538	5.11125	-3.69123	-1.15215
10550217	Crxos1	2.61861	5.08755	-2.66619	-1.37231
10503234	Clvs1	-1.10758	5.0791	-1.98019	2.8409
10458645	Ppp2r2b	-1.28521	5.07785	-4.03172	1.61869
10374578	Fam161a	-1.16891	5.06097	-3.74481	1.57973
10538206	Ccdc126	1.46046	5.03828	-4.05328	-1.17493
10590445	Snrk	1.26359	5.02082	-4.01741	-1.01106
10476791	4930529M08Rik	1.43901	4.95348	-2.10477	1.63547
10419366	Gm534	1.17769	4.95253	-4.22477	-1.00464
10449644	Glo1	1.09345	4.93538	-4.9488	-1.09642
10497713	Pex5l	1.32106	4.92491	-3.46657	1.07541
10399046	Vipr2	-1.01688	4.90671	-4.45678	1.11953
10412335	Isl1	-1.59131	4.89052	1.3737	10.6906
10517731	Igsf21	2.17235	4.84819	-2.64916	-1.18702
10571657	Acsl1	1.35559	4.81671	-4.58377	-1.29003
10543791	Podxl	1.90941	4.76013	-1.97798	1.26037
10356154	Sphkap	2.37251	4.73331	-3.36976	-1.68905
10420503	Setdb2	1.2769	4.69231	-3.99343	-1.08672
10366595	Dyrk2	1.2676	4.66271	-3.4899	1.054
10473880	Lrp4	-1.18694	4.65252	-6.71325	-1.21567
10593767	Chrnb4	1.75116	4.6459	1.17311	3.11231
10373622	Olfr773	1.07792	4.5998	-4.40506	-1.03229
10570379	Grk1	1.13827	4.58825	-4.73281	-1.17414
10414003	Gm626	1.63183	4.56862	-2.55118	1.09741
10364784	Reep6	1.66124	4.55004	-3.23403	-1.18076
10531183	Adamts3	-1.09222	4.53914	-3.65957	1.35473
10531173	Adamts3	1.27644	4.53009	-3.21892	1.10255
10494509	Pias3	1.06588	4.52989	-4.01447	1.05864
10413983	Gm626	1.96447	4.42784	-2.36186	-1.04787
10493189	Mef2d	1.40113	4.39043	-3.74915	-1.19648
10387505	Atp1b2	1.84192	4.38038	-5.26182	-2.21256
10531187	Adamts3	1.15843	4.3781	-3.30351	1.14404
10363231	Smpdl3a	1.86284	4.36274	-2.27175	1.03091
10482030	Stom	-1.08347	4.35805	-4.66603	1.01195
10536827	Ccdc136	1.51521	4.3569	-2.441	1.17797
10462303	Kcnv2	2.01156	4.32865	-2.71686	-1.26255
10519855	Cacna2d1	1.71996	4.32617	-1.29466	1.9428
10440621	Grik1	1.02031	4.28654	-6.07252	-1.44542
10596737	Gnat1	1.15297	4.24634	-4.09312	-1.11137
10411171	Pde8b	1.05532	4.24144	-3.85799	1.04176
10414163	Lrit1	1.63678	4.21884	-2.90364	-1.12653
10458046	D0H4S114	1.26789	4.17311	-2.26477	1.4533
10593668	Dmxl2	1.39853	4.16733	-3.16686	-1.06278
10580850		1.30427	4.15638	-3.12241	1.02061
10427159	Gm9918	1.88072	4.14065	-2.29928	-1.04435
10596982	Ccdc72	1.33164	4.093	-2.74202	1.12095
10384572	1110067D22Rik	1.32883	4.08823	-2.9098	1.05731
10350247	Kif21b	-1.03458	4.07574	-1.94014	2.17339
10393166	St6galnac2	1.20908	4.07183	-3.32342	1.01333
10420532	Atp8a2	-1.66213	4.04273	-3.1637	2.12395
10528031	Zfp804b	1.21134	4.03227	-4.2329	-1.27161
10352792	Gm10124	1.01887	4.01934	-3.22902	1.22171
10429140	Ndrg1	1.38675	3.97818	-4.7455	-1.65423
10505623	D4Bwg0951e	2.16305	3.95598	-2.14892	-1.17498
10377235	Rcvrn	1.15175	3.94552	-3.04709	1.12425
10598359	Syp	1.51843	3.87938	-2.88935	-1.13093
10460157	Cpt1a	-1.42002	3.8496	-2.90429	1.88222
10352781	Rd3	1.19109	3.78289	-3.55745	-1.12011

10565360		1.01877	3.78087	-3.21852	1.15308
10454580	Bin1	1.63083	3.77643	-2.03404	1.13845
10404848	Jarid2	1.21986	3.76638	-3.58258	-1.16033
10479726	Pcmtd2	1.79527	3.76561	-2.73496	-1.30391
10344935	Kcnb2	1.06275	3.76165	-1.49339	2.37015
10380571	Gngt2	2.04152	3.75887	-2.42316	-1.31607
10560919	Atp1a3	-1.23102	3.75012	-6.15319	-1.33288
10366554	Mdm1	1.05751	3.74959	-2.79738	1.26749
10465764	C730048C13Rik	1.58344	3.72027	-2.84627	-1.21145
10593671	Dmxl2	1.31459	3.70081	-2.84735	-1.01143
10440292	Gm5488	1.19193	3.64536	-3.27652	-1.07133
10585778	Sema7a	-1.05654	3.64527	-3.12341	1.23306
10344743	3110035E14Rik	2.45765	3.62666	-2.53073	-1.71498
10382376	Ttyh2	1.81247	3.58817	-3.51552	-1.77577
10558285	Zranb1	1.35197	3.58516	-3.13773	-1.18325
10386359	Guk1	1.02499	3.57025	-3.18173	1.09475
10423293	Myo10	1.15711	3.5634	-3.23297	-1.04981
10476628	Otor	1.01212	3.56107	-3.60789	-1.02543
10594144	Bbs4	1.26758	3.54791	-2.16995	1.28987
10440329	9330155M09Rik	1.36482	3.53727	-1.89354	1.36874
10413987	Gm626	1.8556	3.53418	-2.03247	-1.06714
10392415	Rgs9	1.55203	3.52891	-3.53079	-1.55286
10502696	Spata1	1.25963	3.51568	-2.7608	1.01095
10415890	Rp1l1	1.85238	3.51153	-2.27284	-1.19895
10389738	Dgke	1.14266	3.50347	-3.31513	-1.08123
10548899	Rerg	1.10718	3.49827	-3.49271	-1.10542
10531370	Naaa	1.8812	3.49207	-2.66921	-1.43792
10594747	C2cd4b	1.65077	3.48033	-2.04134	1.0328
10585484	Chrna5	1.01644	3.47781	-1.87292	1.82686
10422822	Lifr	1.28228	3.45633	-4.20741	-1.56092
10404612	Rreb1	1.7541	3.44475	-2.32251	-1.18264
10508052	Grik3	1.3637	3.44141	-2.531	-1.00294
10503866	Gabrr1	-1.04233	3.44093	-2.86596	1.25144
10588495	Dusp7	1.19357	3.4291	-2.1887	1.31264
10347073	Unc80	2.28709	3.42583	-2.24305	-1.49747
10479698	Myt1	1.10897	3.42219	-1.64882	1.8716
10503992	Tmem215	1.3805	3.4179	-2.79354	-1.12832
10476814	Insm1	1.15923	3.4161	-1.67268	1.76177
10429218	Fam135b	1.03943	3.41505	-3.53511	-1.07597
10429203	Fam135b	1.13181	3.41276	-3.85884	-1.27975
10405753	Me1	-1.59932	3.40088	-4.27204	1.27318
10554392	D330012F22Rik	-1.19786	3.38468	-4.15748	-1.02543
10583847	Bbs9	-1.20228	3.37727	-4.54105	-1.11837
10398455	Ppp2r5c	1.00942	3.35747	-2.97174	1.11925
10600994	Arr3	1.03877	3.33913	-3.24265	-1.00875
10531544	Paqr3	1.1238	3.32818	-2.28076	1.29849
10589685	Lrrc2	1.1572	3.31093	-2.98485	-1.04323
10595392	Elovl4	1.10098	3.2966	-3.0154	-1.00707
10519815	Cacna2d1	1.42311	3.2895	-1.23462	1.87222
10505568	Frmd3	-1.46895	3.27672	-1.28644	3.74158
10572050	Mar	1.00628	3.27366	-3.14373	1.03483
10543572	Impdh1	1.20914	3.27104	-2.65554	1.01873
10565210	Fam154b	-1.03032	3.25567	-2.66788	1.25732
10507500	Slc6a9	1.1708	3.23292	-3.23045	-1.16991
10421934	Klhl1	1.16602	3.22274	-1.05694	2.61498
10389581	Ypel2	2.17532	3.22264	-1.98577	-1.34042
10346330	Plcl1	1.55175	3.20984	-1.41739	1.4594
10400006	Ahr	-1.18259	3.19761	-2.12326	1.78097
10603051	Ap1s2	1.22257	3.1968	-2.15248	1.21479
10499988	2310007A19Rik	2.26686	3.19467	-1.27402	1.10618
10481711	Stxbp1	1.29356	3.19363	-1.60619	1.5371
10552857	Slc17a7	1.32034	3.17132	-2.62905	-1.09457
10545014	Vopp1	-1.13459	3.1695	-2.84351	1.26466
10386951	Hs3st3b1	1.30514	3.15196	-2.13828	1.12943
10578477	Fam149a	1.20713	3.14455	-2.23838	1.16379
10511258	Fam132a	1.31156	3.14312	-2.22264	1.07821
10408268	Scgn	1.21635	3.13135	-2.81532	-1.09359
10531189	Adamts3	1.19495	3.12801	-2.51826	1.03948
10427428	AW549877	1.27932	3.11818	-2.5872	-1.06147
10428388	Rspo2	1.44061	3.11568	-2.29199	-1.05976
10347060	Unc80	1.59891	3.06919	-2.16611	-1.12844
10443027	A930001N09Rik	1.64011	3.06786	-2.13955	-1.14383
10494069	Celf3	1.56155	3.05124	-1.03229	1.89287
10348321	Dgkd	1.44176	3.04502	-2.07896	1.0159
10431697	Abcd2	1.6015	3.04069	-1.78767	1.06208
10415228	Cpne6	1.19314	3.02101	-3.21398	-1.26935
10346000	Gulp1	1.03064	3.01726	-2.72265	1.07526

10471533		1.76433	3.00824	-1.45441	1.17232
10476793	4930529M08Rik	1.36797	3.00181	-1.87722	1.16893
10372745	Dyrk2	1.30078	2.99886	-1.76422	1.30678
10366196	Ppfia2	1.44206	2.99559	-2.31388	-1.11389
10370471	Agpat3	1.15365	2.9879	-3.63302	-1.40273
10496192	Tacr3	1.94921	2.98331	-3.31982	-2.16907
10557498	Fam57b	1.26172	2.98234	-2.6136	-1.10572
10357164	Epb4.1l5	1.15452	2.98192	-1.94708	1.32652
10497214	Tpd52	2.07922	2.97897	-2.69683	-1.8823
10531181	Adamts3	-1.038	2.97697	-2.86936	1.07693
10509441	Ece1	1.30382	2.97518	-2.22003	1.02787
10420637	Kpna3	-1.06575	2.96294	-2.5819	1.22304
10399337	Klhl29	1.55869	2.95826	-1.59453	1.19026
10405174	Nxnl2	1.27952	2.94979	-2.92087	-1.26698
10362186	Moxd1	-1.1496	2.94717	-5.06671	-1.49545
10503334	Gem	1.04369	2.92072	-2.59492	1.07843
10440288	Zfp654	1.33596	2.91946	-2.50776	-1.14757
10354168	Tbc1d8	1.19189	2.90283	-3.38802	-1.39111
10533026	Prkab1	1.02719	2.89211	-2.74227	1.02672
10484941	Madd	1.13194	2.88858	-2.45471	1.03958
10440206	Arl6	1.03534	2.88748	-2.53435	1.10045
10531201	Adamts3	-1.12074	2.88198	-2.81566	1.14713
10410408	Adcy2	1.70573	2.87769	-3.3475	-1.98421
10438442	A930003A15Rik	1.10558	2.87673	-2.70085	-1.03798
10506754	Slc1a7	1.19328	2.87647	-2.3181	1.03989
10363921	Pcdh15	3.09258	2.87036	-6.92572	-7.46191
10476355	Chgb	2.16377	2.86612	-1.51893	-1.14671
10376579	Lrrc48	1.08212	2.86585	-2.97611	-1.12376
10459671	Dcc	1.7565	2.86387	2.30614	3.76003
10510708	Icmt	1.13795	2.86375	-2.41985	1.03998
10385297	Gabra1	1.54053	2.85675	-10.3722	-5.59335
10538658	Herc3	-1.22121	2.84603	-3.19077	1.08927
10578504	1700029J07Rik	1.1973	2.83941	-2.52064	-1.06289
10451665	Apobec2	1.22229	2.82865	-2.01891	1.14627
10505779	Acer2	1.13593	2.82837	-2.50931	-1.00779
10458569	Nr3c1	1.19687	2.82501	-2.22422	1.0612
10512129	B4galt1	-1.39769	2.82217	-3.83449	1.02869
10504564	Dcaf10	1.12929	2.81388	-2.64939	-1.06328
10424607	Ptp4a3	-1.00227	2.81157	-2.68694	1.04876
10514133	Ttc39b	1.05217	2.80373	-2.61427	1.0193
10596051	Tmem22	1.00746	2.79934	-2.41405	1.15101
10474619	Fmn1	-1.15986	2.79725	-1.42099	2.2832
10523974	Gm10419	1.18895	2.7921	-4.54438	-1.93512
10406941	Sgtb	1.16552	2.78381	-1.82113	1.31153
10504234	Unc13b	-1.23641	2.78021	-2.13542	1.60974
10558295	Zranb1	1.5612	2.77866	-2.28927	-1.28623
10382409	Kif19a	1.66908	2.76537	-1.90095	-1.14735
10607619	Cdkl5	-1.01453	2.76243	-2.35022	1.19247
10357155	Inhbb	1.96871	2.75733	-1.73812	-1.241
10592802	C2cd2l	1.00512	2.75266	-2.34036	1.17018
10456096	Pde6a	1.28197	2.74065	-2.43282	-1.13798
10415700	Mtmr6	1.00137	2.7378	-2.03351	1.3445
10568586	Fam53b	1.60333	2.73505	-1.79093	-1.04987
10457357	Mpp7	1.48422	2.73373	-2.01633	-1.09472
10427997	Ankrd33b	1.63131	2.71887	-2.01761	-1.21056
10452516	Ankrd12	-1.0798	2.71568	-2.4652	1.18951
10598586	Xk	-1.42407	2.70977	-3.43488	1.12344
10474201	Lmo2	-1.05567	2.70938	1.1399	3.26034
10493177	Mef2d	1.4956	2.70611	-2.12104	-1.17225
10383819	Sec14l2	1.29941	2.69709	-2.38621	-1.14963
10485979	Gjd2	-1.1969	2.69682	-4.48856	-1.39059
10405576	Fbxl21	-1.08335	2.69453	-2.08493	1.40011
10535017	Gal3st4	1.03226	2.69193	-2.22368	1.17274
10400896	2810055F11Rik	1.08203	2.68509	-2.15911	1.14933
10579976	Elmod2	1.22104	2.67817	-1.45985	1.50246
10418053	Kcnma1	-1.09801	2.67229	-4.41711	-1.50538
10440513	Cyyr1	1.10767	2.6722	-1.5343	1.57235
10475324	Ckmt1	-1.09544	2.66946	-2.92836	-1.00141
10466903	4430402I18Rik	-1.00989	2.66415	-3.86708	-1.43731
10601598	3110007F17Rik	1.35392	2.65714	-1.64652	1.19194
10582464		2.0879	2.65675	-1.47599	-1.15996
10476782	4930529M08Rik	-1.05079	2.65533	-1.87978	1.48432
10601595	3110007F17Rik	1.34439	2.64575	-1.63947	1.20038
10597162	Klhl18	-1.10229	2.64435	-2.84441	1.02477
10414417	Peli2	1.08565	2.64333	-1.55296	1.56785
10549849	Zfp78	1.29619	2.64314	-1.92444	1.05961
10497842	Bbs7	-1.02996	2.64062	-2.5832	1.05286

10449971	Zfp763	1.34705	2.63689	-1.77355	1.10374
10444890	Ier3	1.16517	2.6323	-1.80359	1.25259
10397683	Ttc8	1.19381	2.63163	-2.31089	-1.04831
10595480	Me1	-1.53876	2.62763	-3.37354	1.19853
10495685	Arhgap29	1.4234	2.6274	1.06996	1.97499
10575693	Vat1l	-1.32856	2.60801	-5.11672	-1.47673
10388109	Pitpnm3	1.03938	2.60227	-2.73164	-1.09104
10404059	Hist1h1c	-1.08298	2.59884	-2.89983	-1.03032
10462313	Slc1a1	-1.15036	2.59651	-5.52904	-1.85107
10390080	Tmem92	-1.15972	2.59546	-2.71718	1.10776
10488497	Vsx1	1.22303	2.58552	-2.31751	-1.09625
10421293	Ppp3cc	1.15836	2.58299	-4.99214	-2.23875
10585976	Myo9a	-1.07853	2.57451	-1.40664	1.97398
10407792	Gpr137b-ps	1.2761	2.56242	-1.64637	1.21966
10388884	Nlk	1.97632	2.56031	-1.45093	-1.11998
10476512	Snap25	1.25319	2.55632	-2.3121	-1.13347
10405253	Cplx2	1.39799	2.55392	-1.87899	-1.02854
10372503	Lgr5	-1.11738	2.55332	-1.77645	1.60603
10459469		1.00703	2.54678	-2.70641	-1.07015
10401997	Ptpn21	1.24906	2.54603	-3.261	-1.59981
10597575	Plcd1	1.46896	2.53973	-1.80767	-1.04555
10510422	Casz1	1.03073	2.53881	-1.98703	1.2396
10386427	Flcn	1.16211	2.53421	-2.55719	-1.17264
10437073	Ripply3	1.32277	2.53308	-1.53558	1.24707
10453178	Map4k3	1.18416	2.53214	-1.92912	1.10845
10541260	Cecr2	1.31431	2.52845	-1.68569	1.14124
10382830	Gm11744	1.35351	2.52115	-1.91253	-1.02677
10566723	Lmo1	-1.03536	2.52057	-1.6287	1.60233
10494335	Otud7b	1.06421	2.51915	-2.45023	-1.0351
10536390	Glcci1	1.6809	2.5188	-1.4647	1.02306
10470564	Ralgds	-1.01054	2.51151	-2.16531	1.17211
10531185	Adamts3	-1.01479	2.51105	-2.6502	-1.04003
10584901	Dscaml1	-1.1683	2.50649	-2.68727	1.08971
10413997	Gm626	1.65771	2.50559	-1.58726	-1.05014
10448064	Prdm9	1.019	2.50297	-2.52273	-1.02704
10468517	Mxi1	1.31963	2.50087	-2.34576	-1.23778
10404380	Dusp22	1.0172	2.4953	-2.41507	1.01575
10589913	Dync1li1	1.00299	2.4947	-1.62335	1.53217
10542731	Rassf8	1.30299	2.4925	-1.62952	1.17391
10415714	Fam123a	1.64993	2.48717	-1.40519	1.07277
10516393	Eif2c4	1.44993	2.48711	-2.02748	-1.18197
10505587	Kdm4c	1.29667	2.48068	-2.32971	-1.21775
10581088	Ccdc79	1.02861	2.47912	-2.28003	1.05707
10355227	1110028C15Rik	1.4499	2.47181	-1.91011	-1.12042
10565525		1.04168	2.46806	-2.36697	1.00098
10555205	Gdpd5	-1.09979	2.46511	-2.22872	1.21644
10395805	1700047I17Rik1	-1.25084	2.45843	-2.98213	1.03117
10352867	Plxna2	2.09998	2.45662	-2.46729	-2.1091
10481349	Ntng2	1.88705	2.45379	-1.47233	-1.13228
10479765	Suv39h2	1.07371	2.44852	-1.49869	1.52162
10366038	Galnt4	1.10656	2.44791	-2.59401	-1.1726
10585980	Myo9a	1.3176	2.44732	-1.15365	1.61002
10364249		1.14195	2.44384	-2.16608	-1.01216
10423503	Gm6624	1.14011	2.44203	-1.60707	1.33282
10457359	Mpp7	1.2649	2.43801	-2.04372	-1.06033
10585974	Myo9a	1.1752	2.43166	-1.26475	1.63601
10465336	Mrpl49	1.26941	2.42919	-1.98741	-1.03855
10440186	Crybg3	-1.32496	2.42703	-1.4546	2.21071
10506274	Dnajc6	-1.05403	2.42057	-1.86679	1.36671
10582890		1.14925	2.42013	-2.07298	1.01585
10408935	Gm10786	1.09708	2.41891	-9.32868	-4.23098
10549276	Bhlhe41	1.17499	2.41634	-2.78479	-1.35416
10409265	Auh	1.03038	2.41491	-2.19766	1.06646
10456577		1.26201	2.41189	1.02853	1.96567
10573803	Cyld	1.11107	2.40853	-2.4033	-1.10866
10587655	4930422I07Rik	1.15882	2.40743	-1.92842	1.07729
10363762	Tmem26	1.47596	2.40008	-1.36817	1.18853
10514713	Wdr78	1.02061	2.39664	-1.72246	1.3633
10349208	Cntnap5a	1.11821	2.39655	-2.46587	-1.15055
10359027	Lhx4	1.34343	2.39105	-1.84029	-1.03398
10546272	Iqsec1	-1.0654	2.39032	-2.06505	1.23321
10363161	Tmem229b	-1.26663	2.3814	-2.06134	1.4633
10555303	Pgm2l1	1.00793	2.38018	-1.28074	1.84382
10384566		1.09431	2.3783	-2.23159	-1.0268
10500378	Nudt17	1.19826	2.37306	-1.68756	1.17354
10503659	Epha7	-1.04798	2.37221	-2.15222	1.1551
10511984	1700003M02Rik	-1.09058	2.37137	-1.47089	1.75824

10399148	Rapgef5	-1.00601	2.36846	-1.63243	1.4596
10586971	Prtg	1.85034	2.36644	1.54169	1.97169
10417841	Ttc18	1.088	2.36636	-2.05137	1.06024
10376425	Gm12258	1.17875	2.36303	-1.94358	1.03144
10467766	Loxl4	1.36379	2.3588	-1.99434	-1.15307
10589541	Kif9	1.15006	2.35126	-2.24149	-1.09637
10366026	Poc1b	1.00025	2.34234	-1.80012	1.30088
10384179		1.14282	2.34132	-2.19547	-1.07163
10463254	D19Ertd386e	1.3349	2.33547	-1.78598	-1.02083
10533055	Srrm4	1.71307	2.33335	-1.25933	1.0816
10423593	Laptm4b	-1.09566	2.33175	-2.60445	-1.01943
10554076	Lysmd4	1.15492	2.33123	-2.15199	-1.06613
10403081	Wdr60	1.04056	2.32707	-2.27688	-1.01812
10549222	Bcat1	1.28512	2.32183	-1.65279	1.09312
10513544	Zfp37	1.1335	2.31879	-1.73716	1.1776
10523297	Ccng2	1.18806	2.31875	-1.78402	1.094
10505747	Rraga	-1.00205	2.31479	-2.06033	1.12581
10519607	4930420K17Rik	1.38246	2.31233	-2.16099	-1.29198
10500899	Fam19a3	1.15151	2.30366	-2.44354	-1.22143
10453900	Riok3	1.1333	2.30349	-2.02635	1.00306
10510482	Clstn1	1.00629	2.30346	-2.56083	-1.11873
10513592	Wdr31	-1.01541	2.29736	-1.98659	1.17425
10467258	Myof	1.11361	2.29186	-2.58363	-1.25538
10403796	Amph	-1.1379	2.28951	-3.52346	-1.35245
10545065	Gprin3	1.29	2.28272	-2.23518	-1.26314
10436947	Kcne2	1.44492	2.27596	-1.8501	-1.17455
10411059	Zfyve16	1.40197	2.2755	-1.89514	-1.16763
10504373	Gm12472	-1.02543	2.27396	-2.50775	-1.07547
10565910	Plekhb1	1.2541	2.27326	-4.14376	-2.28601
10415784	Trim13	-1.08624	2.27324	-1.34249	1.83933
10557397	D430042O09Rik	1.02247	2.27274	-2.24411	-1.00959
10390841	Krt12	2.68669	2.27203	1.24205	1.05036
10360349	Cadm3	1.68219	2.27022	-1.57632	-1.16802
10585956	Myo9a	-1.07383	2.27005	-1.47266	1.65528
10380289	Mmd	-1.15768	2.26916	-1.65084	1.59128
10379410	Rhot1	-1.05858	2.26584	-2.2992	1.04322
10531437	Scarb2	1.01393	2.26162	-2.18803	1.01943
10533304	Trafd1	1.18001	2.26052	-1.62718	1.17729
10439114	Iqcg	1.0811	2.25812	-1.50637	1.3866
10521757		1.02461	2.24788	-2.00027	1.09679
10573472	Rtbdn	1.20968	2.24604	-1.85841	-1.00091
10604922	BC023829	-1.00888	2.23622	-2.26447	-1.00371
10420899	Gulo	1.56687	2.23377	-1.48563	-1.04209
10585978	Myo9a	1.13842	2.22944	-1.24585	1.57192
10383564	Fn3k	1.30148	2.22889	-1.92774	-1.12564
10595805	Rasa2	1.2491	2.22509	-1.53475	1.16069
10536949	Fam40b	1.20194	2.22505	-2.29755	-1.24111
10567964	Cln3	1.0286	2.22478	-2.16838	-1.00253
10570573	Agpat5	1.08463	2.22385	-2.17805	-1.06229
10601588	3110007F17Rik	1.29496	2.21928	-1.43976	1.19032
10476482	6330527O06Rik	1.04855	2.21879	-4.22842	-1.99825
10402997	LOC630837	-1.02872	2.21805	-1.85338	1.23114
10535532	Tecpr1	1.37514	2.21479	-1.58918	1.01347
10546152	Podxl2	-1.08348	2.2104	-2.29707	1.04261
10465770		-1.041	2.20845	-2.17928	1.05493
10561337	1700049G17Rik	-1.10437	2.2077	-2.07049	1.17756
10603598	Rpgr	-1.098	2.20675	-2.0735	1.16856
10388098	Aipl1	1.07247	2.20669	-2.13161	-1.03598
10461311	Eml3	-1.00388	2.20492	-2.22045	-1.00315
10460468	Ctsf	1.61068	2.19978	-1.7328	-1.26875
10485562	Hipk3	-1.01041	2.19735	-2.28409	-1.02877
10344624	Lypla1	1.33908	2.19673	-1.59739	1.02697
10422962	1110020G09Rik	1.07829	2.19593	-1.85069	1.1004
10375343	Rnf145	-1.09035	2.19571	-2.43642	-1.01768
10565532	Ankrd42	1.00715	2.19203	-1.1651	1.86805
10503835	Rragd	1.18228	2.19164	1.03103	1.91126
10517521	Epha8	1.38766	2.19087	-1.71495	-1.08622
10474371	Gm16488	1.36197	2.19081	-1.54407	1.04176
10400948	Six6os1	1.28714	2.18967	-1.88958	-1.11073
10571647	4933411K20Rik	1.05066	2.18522	-1.70932	1.21677
10515242	Nsun4	1.24089	2.18252	-1.74716	1.00668
10512949	Abca1	1.20781	2.17968	-8.58166	-4.7553
10544148	Jhdm1d	1.43131	2.17772	-1.1825	1.28667
10367775	Stxbp5	1.69705	2.17653	-2.03053	-1.58321
10548905	Eps8	1.43357	2.17568	-1.90381	-1.25443
10577792	Plekha2	1.28646	2.17432	-1.902	-1.12534
10566714	Ric3	1.08115	2.17347	-1.86949	1.07533

10577922	Hook3	1.01113	2.17237	-1.68917	1.2719
10350341	Mir181b-1	-1.07804	2.17122	-3.19297	-1.36413
10465742	Gm5631	1.04453	2.17028	-2.17622	-1.04738
10573939	Lpcat2	1.27082	2.17007	-3.69117	-2.16159
10593628	Rab39	1.32043	2.16936	-1.23456	1.33077
10427494		1.79659	2.16521	-1.25686	-1.04288
10578207	Lonrf1	-1.02076	2.16451	-1.87362	1.17924
10426292	Alg10b	-1.08455	2.16388	-1.59711	1.46943
10458122	Nme5	1.61234	2.16355	-3.32809	-2.48019
10395770	Ppp2r3c	-1.19096	2.16173	-2.50351	1.02838
10395780	Ppp2r3c	-1.19096	2.16173	-2.50351	1.02838
10544150	Jhdm1d	1.39405	2.16103	-1.21453	1.27637
10535739	Usp12	1.03475	2.15935	-1.61905	1.28892
10529858	Tapt1	1.12817	2.15877	-2.40475	-1.25672
10518726	Slc25a33	1.17505	2.15779	-2.06038	-1.122
10579872	Tpd52	1.58348	2.15388	-2.1913	-1.61099
10504169	4933409K07Rik	-1.4825	2.1537	-1.84143	1.7339
10520043	Lhfpl3	-1.28171	2.15023	-3.16497	-1.1484
10346678	Carf	1.1419	2.14812	-2.51364	-1.3362
10402630	Stk30	-1.15501	2.14303	-2.38694	1.03698
10549813	Zfp444	1.11829	2.13958	-1.88343	1.01583
10481827	Zbtb34	-1.01796	2.1378	-1.96002	1.11029
10516823	Epb4.1	1.07544	2.13485	-1.75052	1.13401
10555946	Smpd1	-1.07388	2.13465	-2.45271	-1.06995
10585972	Myo9a	1.12797	2.12991	-1.20818	1.56291
10571634	Lrp2bp	1.20479	2.12887	-1.77923	-1.00692
10407040	Esco1	1.40538	2.12829	-1.90666	-1.25904
10593589		1.05284	2.12803	-1.93685	1.04357
10365344	Tcp11l2	1.6286	2.12286	-3.7141	-2.84936
10587194	Gnb5	1.03198	2.11965	-2.63795	-1.28433
10504137	4933409K07Rik	-1.35551	2.1182	-1.74545	1.64499
10504201	4933409K07Rik	-1.35551	2.1182	-1.74545	1.64499
10512350	4933409K07Rik	-1.35551	2.1182	-1.74545	1.64499
10512352	4933409K07Rik	-1.35551	2.1182	-1.74545	1.64499
10401829	Gm8300	1.12387	2.11714	-1.5146	1.24376
10595126	Fbxo9	1.13091	2.11614	-2.36893	-1.266
10523670	Aff1	1.49592	2.11355	-1.2643	1.11752
10472562	Kbtbd10	1.37807	2.11335	-1.36929	1.11997
10527982	A330021E22Rik	-1.05632	2.11288	-2.43777	-1.09225
10585990	Myo9a	1.25857	2.11235	-1.2234	1.37189
10406598	Serinc5	2.7583	2.11145	-1.47936	-1.93256
10366337	Nap1l1	-1.04725	2.10939	-1.66763	1.32467
10580852		1.17064	2.10871	-1.83421	-1.01825
10403193	Sp4	1.04901	2.10842	-1.56748	1.28227
10457959	Sft2d3	1.22832	2.10826	-1.44233	1.18999
10525741	Snrnp35	1.00125	2.10802	-1.95643	1.07613
10479379	Slco4a1	1.01852	2.10709	-1.77365	1.16639
10531342	U90926	1.23034	2.10705	-1.90332	-1.11138
10482434	Gtdc1	1.1703	2.10282	-2.15118	-1.19721
10487945	Gpcpd1	1.20501	2.10052	-2.05652	-1.17978
10378271	1200014J11Rik	1.19733	2.10007	-1.37081	1.27951
10426991	Ankrd33	1.2135	2.09874	-1.80867	-1.04578
10413967	Gm626	1.42072	2.0948	-1.73369	-1.17581
10350046	Kdm5b	1.34336	2.09329	-1.51746	1.02688
10449401	Tcp11	1.36504	2.09174	-1.58381	-1.03358
10584067	Zbtb44	1.2467	2.09105	-2.02224	-1.20568
10451851	Armcx3	-1.04473	2.0904	-2.06491	1.05763
10585970	Myo9a	1.18676	2.09	-1.26566	1.39144
10452613	Arhgap28	1.50142	2.08688	-1.36591	1.01759
10424370	Trib1	1.25436	2.08665	-2.35639	-1.4165
10374553	Tmem17	-1.05783	2.08652	-1.82436	1.20984
10363894	Ipmk	1.00121	2.08431	-2.1167	-1.01677
10556812	Lyrm1	-1.11394	2.0824	-2.04802	1.13264
10467110	AI747699	1.32044	2.07825	-1.08335	1.45282
10353036	Gm10567	1.04938	2.07801	-2.10224	-1.06162
10372139	Nts	1.07829	2.07593	-2.05189	-1.06581
10596072	Ppp2r3a	1.05744	2.07572	-1.76189	1.11412
10515924	Rimkla	1.00017	2.07436	-1.59674	1.29889
10553301	Ldha	-1.11543	2.07221	-2.21213	1.04488
10588509	Pcbp4	1.11088	2.07071	-1.49086	1.25031
10429222	Fam135b	-1.00237	2.0661	-2.13955	-1.0331
10566488	Trim3	1.04975	2.06475	-2.01297	-1.02343
10592001	St14	1.05532	2.06456	-1.85796	1.05295
10469335	Stam	1.25798	2.06329	-1.46586	1.11891
10397541	Gm8300	1.09855	2.06098	-1.46251	1.28279
10431140	1810041L15Rik	-1.02246	2.05893	-1.69905	1.23902
10590487	Zfp660	1.38539	2.05885	-1.40033	1.06126

10454632	Camk4	1.26742	2.05865	-2.04904	-1.2615
10506134	Atg4c	-1.02451	2.0582	-2.59715	-1.23166
10422259	Tgds	1.22912	2.05705	-1.95866	-1.17033
10531175	Adamts3	1.018	2.05251	-1.67641	1.20269
10397543	Gm8300	1.09322	2.05233	-1.55773	1.20517
10554650	1700010L04Rik	1.14587	2.05169	-1.96922	-1.09982
10595573	Snx14	-1.0674	2.04777	-2.22153	-1.01635
10563820	Svip	1.52172	2.04565	-1.34358	1.00054
10451613	Foxp4	1.35316	2.04212	-1.13202	1.33314
10459193	Ppargc1b	-1.05391	2.04047	-2.16289	-1.00578
10511139	Ssu72	1.02821	2.03801	-1.89689	1.04492
10487021	Slc30a4	1.09468	2.03749	-2.06522	-1.10957
10429216	Fam135b	1.05881	2.03702	-2.10378	-1.09351
10446763	Lbh	1.3168	2.0365	-1.73979	-1.12495
10585992	Myo9a	-1.14623	2.03649	-1.40658	1.65953
10467102	Rnls	1.35423	2.03633	-1.49501	1.00581
10496387	Dnajb14	1.13824	2.03496	-1.65085	1.08296
10553324	Tmem86a	1.13331	2.03479	-2.04523	-1.13913
10376778	Mfap4	1.39867	2.03456	-1.05358	1.38066
10525487	4932422M17Rik	1.35421	2.03417	-1.45005	1.03591
10603627	Bcor	1.14635	2.03376	-1.48152	1.1975
10369738	Sirt1	1.19377	2.03305	-1.64817	1.03329
10437023	Morc3	1.09707	2.03101	-1.78815	1.03532
10519069	Plch2	1.28334	2.0309	-1.96427	-1.24124
10430770	Tob2	1.06923	2.02825	-2.10573	-1.11008
10529801	Fbxl5	1.15052	2.02786	-2.10563	-1.19464
10365199	Gm10778	1.24651	2.02748	-1.42394	1.14226
10445909	Kat2b	1.16198	2.0266	-2.38149	-1.36546
10491695	Bbs12	1.07234	2.02639	-1.54232	1.22523
10512301	Arid3c	1.21719	2.02191	-1.77027	-1.0657
10483822	Ttc30a2	-1.07089	2.02147	-2.19464	-1.0138
10562486	Rgs9bp	-1.13057	2.02123	-2.02237	1.12994
10383353	Tspan10	1.04183	2.02104	-2.06699	-1.06552
10599335	Mcts1	1.16614	2.01959	-1.67971	1.03104
10446756	Ypel5	1.44447	2.01913	-1.8708	-1.33836
10369783	Zfp365	1.10912	2.01435	-1.70094	1.06775
10580870	Zfp319	1.01706	2.0115	-1.54536	1.27981
10435345	Mylk	1.1583	2.00958	1.09541	1.90047
10353135	Ncoa2	-1.08333	2.00934	-1.80923	1.20316
10474477	Gm13961	1.24295	2.00862	-1.39656	1.15714
10379795	Synrg	1.13049	2.00754	-1.74904	1.0153
10439362	Stxbp5l	-1.31005	2.00723	-2.06766	1.27177
10531126	Igj	1.15894	2.00508	-1.92729	-1.11398
10376096	Acsl6	1.01149	2.00453	-2.08545	-1.05233
10419216	Gnpnat1	1.26108	2.00387	-1.29288	1.22904
10557481	Ypel3	1.36552	2.00212	-1.93489	-1.31967
10358991	BC034090	1.38022	2.00117	-1.31056	1.10632
10456296	Malt1	1.0351	2.00077	-1.87827	1.0291

9.7 Appendix table 3.4

Appendix table 3.4 Gene ontology terms enriched in the annotations of photoreceptor gene sets and classified here as encoding cell surface and cilium proteins

NrlGFP+ve P4		CrxGFP+ve E15.5		CrxGFP+ve P4	
Cell surface protein	**Cilium protein**	**Cell surface protein**	**Cilium protein**	**Cell surface protein**	**Cilium protein**
'cell projection'	'cilium'	'cell projection'	'cilium'	'cell projection'	'cilium'
'plasma membrane'	'cilium part'	'synapse'	'nonmotile primary cilium'	'cell projection membrane'	'cilium membrane'
'plasma membrane part'	'nonmotile primary cilium'	'photoreceptor outer segment'		'plasma membrane'	'cilium part'
'apical plasma membrane'	'stereocilium bundle'	'cilium'		'plasma membrane part'	'nonmotile primary cilium'
'basolateral plasma membrane'	'stereocilium'	'nonmotile primary cilium'		'extrinsic to plasma membrane'	'stereocilium bundle'
'extrinsic to plasma membrane'	'cilium axoneme'			'intrinsic to plasma membrane'	'photoreceptor connecting cilium'
'cilium'	'motile secondary cilium'			'integral to plasma membrane'	
'cilium part'	'photoreceptor connecting cilium'			'cilium'	
'intrinsic to plasma membrane'	'cilium membrane'			'cilium membrane'	
'nonmotile primary cilium'				'cilium part'	
'photoreceptor outer segment'				'nonmotile primary cilium'	
'apical plasma membrane'				'stereocilium bundle'	
'cell projection membrane'				'photoreceptor connecting cilium'	
'stereocilium bundle'				'photoreceptor outer segment'	
'stereocilium'				'synapse'	
'cilium axoneme'				'synapse part'	
'motile secondary cilium'				'neuron projection'	
'photoreceptor connecting cilium'					
'photoreceptor inner segment'					
'cilium membrane'					
'synapse'					
'synapse part'					
'cell projection part'					

9.8 Appendix table 3.5

Appendix table 3.5 Gene lists comparsion between Crx and Nrl array

CrxE15.5 only (16)	CrxP4 only (172)	CrxE15.5&P4 common (17	common to all three (27)	CrxE15.5 and NrlP4 common (0)	CrxP4 and NrlP4 common (322)	NrlP4 only (531)
Pmfbp1	Gabrr3	Slitrk6	**Cngb3**		Samd7	Rp1h
Muc19	Rp1	Neurod4	Pdc		Pde6b	---
Onecut1	Gje1	Fabp7	**Crx**		Cnga1	Pcdh21
Ano5	Arhgap31	Angpt1	Impg2		Rho	1700008G05Rik
Meis2	Fabp12	St6galnac5	**Pde6c**		Nt5e	Llgl2
Aldh1a1	Gm14214	Cdhr1	**Thrb**		Cplx4	434166
Tcfap2b	Cxcr6	Otx2	Rbp3		Sag	4930430E16Rik
Krt73	Chodl	St18	Prdm1		Nrl	D230044M03Rik
Tcfap2a	Gm10419	Gm4792	Samsn1		Nr2e3	EG432988
Kcnab1	Clvs1	Glcci1	C1ql3		Cerkl	Gucy2e
Slc24a2	Fam161a	Pik3r1	Gm626		Gngt1	Abhd14b
Lypd1	Gm534	Prmt8	Gnat2		Adamts3	Gm1614
Nr2f2	Vipr2	Lcorl	Mak		Htra1	Vtn
Pla2g4a	Isl1	Cnpy1	Rpgrip1		Slc27a2	BC016201
Slc1a6	Sphkap	Enc1	Ppef2		Lrit2	OTTMUSG00000003947
Rbp4	Smpdl3a	Ankrd33b	Hcn1		Ano2	Nxnl1
	Cacna2d1	Trp53inp1	Neurod1		Cacna2d4	**Rxrg**
	Grik1		Slc1a2		Pde6g	Peli3
	D0H4S114		Egflam		Pla2g7	1500016O10Rik
	Gm9918		Dmd		Impg1	Ubxn11
	Zfp804b		Otop3		Prom1	Guca1a
	Gm10124		Fhod3		Rs1	Camkk1
	Gm5488		Eml5		Gnb3	BC042720
	3110035E14Rik		Sv2b		Prph2	Hspb6
	Otor		Zfp385b		Elovl2	RP23-433P19.11
	C2cd4b		Kank1		Abca4	Kcnb1
	Gabrr1		4930403N07Rik		Rasgrf2	2010001M09Rik
	Unc80				Rom1	BC035537
	Myt1				**Opn1sw**	Gata3
	Tmem215				Dlc1	Klc3
	Fam135b				Unc119	Padi2
	Paqr3				Rgs22	ENSMUSG00000054339
	Frmd3				Ush2a	Tshz2
	Fam154b				Stx3	Abcg4
	Plcl1				4930529M08Rik	C030018G13Rik
	Stxbp1				Doc2b	Ephx2
	Vopp1				Tdrd7	Cdgap
	Fam149a				Trak2	Shroom3
	Fam132a				Wdr17	1700020C11Rik
	Scgn				Cplx3	Tub
	Celf3				Rdh12	C1qdc2
	Abcd2				Rassf8	Bhlhb3
	Cpne6				BC027072	Crb2
	Tacr3				Lgmn	Lrguk
	Fam57b				Fyco1	Fer1l3
	Tpd52				Pla2r1	Dhrs3
	Gem				Cep290	F630110N24Rik
	Adcy2				1810009A15Rik	1700007K13Rik
	A930003A15Rik				2210012G02Rik	Zdhhc2
	Dcc				Abhd3	AW146242

Known/possible cone genes were **bold**

	Gabra1				Cngb1	Elfn1
	Acer2				Mpp4	Osbp2
	Dcaf10				Ccdc72	Pard6b
	Mtmr6				Cadm2	Sez6
	Fam53b				Jam2	Arhgap24
	Lmo2				Ppp2r5c	AI118078
	Gjd2				Cabp5	Phyhd1
	Kcnma1				Cdc42ep3	Chchd10
	Cyyr1				Bbs5	Zdhhc23
	4430402I18Rik				Ebpl	1190005I06Rik
	3110007F17Rik				Tulp1	Vps13b
	Zfp763				Cacna1f	Paqr4
	Arhgap29				Gucy2f	Crocc
	Vat1l				Glo1	Rage
	Vsx1				Ttc39b	Pip4k2c
	Gpr137b-ps				Crxos1	Mthfr
	Nlk				Ppp2r2b	Adcy6
	Lgr5				Ccdc126	Rhbdf2
	Gm11744				Snrk	Pde6h
	Ralgds				Pex5l	BC022687
	Mxi1				Igsf21	Pacrg
	Fam123a				Acsl1	EG628705
	Kdm4c				Podxl	Svil
	Ccdc79				Setdb2	Rhpn1
	Gm6624				Dyrk2	Lass4
	Crybg3				Lrp4	Itga3
	Gm10786				**Chrnb4**	Nefh
	Bhlhe41				Olfr773	Ogdhl
	Cntnap5a				Grk1	Rdh8
	Lhx4				Reep6	Sirpa
	Tmem229b				Pias3	Wdtc1
	Pgm2l1				Mef2d	Tbc1d24
	Nudt17				Atp1b2	Scube3
	Epha7				Stom	Ppap2c
	Gm12258				Ccdc136	4932418E24Rik
	Loxl4				Kcnv2	Slc24a4
	Poc1b				Gnat1	Rabepk
	Srrm4				Pde8b	Plekhb2
	Lysmd4				Lrit1	Pitpnm1
	Bcat1				Dmxl2	Fance
	Zfp37				1110067D22Rik	Krt18
	Ccng2				Kif21b	Nphp4
	Fam19a3				St6galnac2	A930008G19Rik
	Riok3				Atp8a2	C030014K22Rik
	Myof				Ndrg1	Obox6
	Amph				D4Bwg0951e	Ndrg3
	Zfyve16				Rcvrn	Synpo2
	Gm12472				Syp	Tmem176a
	Trim13				Cpt1a	Ttc30b
	Krt12				Rd3	Bcar3
	Cadm3				Bin1	Slc11a1
	Scarb2				Jarid2	Rtn4rl1
	Fam40b				Pcmtd2	Syngr1
	6330527O06Rik				Kcnb2	AI427515
	LOC630837				Gngt2	Pdk2
	Tecpr1				Atp1a3	Slc31a2
	1700049G17Rik				Mdm1	Grina
	Lypla1				C730048C13Rik	Akna
	Rnf145				Sema7a	Bbs1
	Rragd				Ttyh2	Hnt
	Gm16488				Zranb1	C79127
	Six6os1				Guk1	Tln2
	Abca1				Myo10	Tnfsf9
	Jhdm1d				Bbs4	Cst3
	Eps8				9330155M09Rik	Tmem135
	Ric3				Rgs9	Jmjd2c
	Mir181b-1				Spata1	Olfr772
	Gm5631				Rp1l1	433036
	Rab39				Dgke	Rab27a
	Alg10b				Rerg	D930005D10Rik
	Ppp2r3c				Naaa	Farp2
	Stk30				Chrna5	1110038D17Rik
	Epb4.1				Lifr	5430407P10Rik
	Lrp2bp				Rreb1	Ramp3
	Esco1				Grik3	Cetn4
	Tcp11l2				Dusp7	2310031A18Rik
	Gm8300				Insm1	6330442E10Rik

	Aff1				Me1	Uckl1
	Kbtbd10				D330012F22Rik	Lrit3
	Serinc5				Bbs9	Tle2
	Sft2d3				**Arr3**	Pde8a
	Snrnp35				Lrrc2	Sys1
	U90926				Elovl4	Slc6a2
	Gtdc1				Mar-01	Sox30
	Gpcpd1				Impdh1	Pdzd2
	1200014J11Rik				Slc6a9	6530418L21Rik
	Kdm5b				Klhl1	Akap1
	Zbtb44				Ypel2	2210010N04Rik
	Armcx3				Ahr	Cckbr
	Arhgap28				Ap1s2	Pnpla3
	AI747699				2310007A19Rik	Rorc
	Gm10567				Slc17a7	Mamld1
	Nts				Hs3st3b1	Eno2
	Ppp2r3a				AW549877	Ccdc113
	Rimkla				Rspo2	Pomt2
	Ldha				A930001N09Rik	Tead3
	Pcbp4				Dgkd	St3gal5
	1810041L15Rik				Gulp1	Pter
	Zfp660				Ppfia2	3110001A13Rik
	Camk4				Agpat3	Vasn
	1700010L04Rik				Epb4.1l5	4631416L12Rik
	Svip				Ece1	Susd2
	Foxp4				Kpna3	Dynlrb2
	Slc30a4				Klhl29	Zbtb4
	Lbh				Nxnl2	Ap1b1
	Rnls				Moxd1	ENSMUSG00000072890
	Mfap4				Zfp654	5430411C19Rik
	4932422M17Rik				Tbc1d8	4930578G10Rik
	Bcor				Prkab1	4930546H06Rik
	Sirt1				Madd	Prickle1
	Morc3				Arl6	Lrrc4
	Fbxl5				Slc1a7	ENSMUSG00000053531
	Gm10778				Pcdh15	Phlppl
	Tspan10				Chgb	Tect1
	Mcts1				Lrrc48	Cdk2ap2
	Ypel5				Icmt	Ctbp2
	Zfp319				Herc3	Mlf1
	Gm13961				1700029J07Rik	Clip4
	Synrg				Apobec2	1700030J22Rik
	Stxbp5l				Nr3c1	Mif4gd
	Gnpnat1				B4galt1	Adck4
	Malt1				Ptp4a3	Angel1
					Tmem22	Dusp26
					Fmn1	Tube1
					Sgtb	Mmd2
					Unc13b	Tmem9
					Kif19a	Shisa2
					Cdkl5	ENSMUSG00000074917
					Inhbb	1700129I04Rik
					C2cd2l	Hmgn2
					Pde6a	Syne2
					Mpp7	1110012J17Rik
					Ankrd12	Jag1
					Xk	Dixdc1
					Sec14l2	Lmln
					Fbxl21	Dhdh
					Gal3st4	Lactb
					2810055F11Rik	1110007C09Rik
					Elmod2	Dlg4
					Ckmt1	Mtfr1
					Klhl18	Spint1
					Peli2	Dnaja4
					Zfp78	Slc44a1
					Bbs7	Cltb
					Ier3	Ccdc64
					Ttc8	BC062109
					Pitpnm3	Csda
					Hist1h1c	Cbx7
					Slc1a1	3110056O03Rik
					Tmem92	Txndc5

Ppp3cc	Taok3
Myo9a	6430571L13Rik
Snap25	Cc2d2a
Cplx2	Ppargc1a
Ptpn21	Morn1
Plcd1	B130055M24Rik
Casz1	A930018M24Rik
Flcn	Wdr34
Ripply3	Calml4
Map4k3	Pwwp2b
Cecr2	Slc30a1
Lmo1	Gpr180
Otud7b	Stard10
Dscaml1	Lrrc46
Prdm9	Apbb1
Dusp22	Sh3bgrl2
Dync1li1	Frmd4b
Eif2c4	Rxra
1110028C15Rik	Arid3b
Gdpd5	Scn4a
1700047I17Rik1	Pygm
Plxna2	Accn3
Ntng2	Capns2
Suv39h2	Slc24a1
Galnt4	Cabp4
Mrpl49	Dnajc12
Dnajc6	Zfp787
Auh	D10Bwg1364e
Cyld	Crtc3
4930422I07Rik	ENSMUSG00000055181
Tmem26	Zbtb7b
Wdr78	Tyrp1
Iqsec1	100039909
1700003M02Rik	Pacsin2
Rapgef5	8030462N17Rik
Prtg	Nr6a1
Ttc18	Zfp516
Kif9	Armc9
D19Ertd386e	Pih1d2
Laptm4b	Snta1
Wdr60	Cacnb2
Rraga	Atp6v0b
4930420K17Rik	Slc23a2
Clstn1	Got1
Wdr31	1110007L15Rik
Gprin3	4930466F19Rik
Kcne2	Clu
Plekhb1	Zdbf2
D430042O09Rik	Baiap2
Mmd	Ccdc65
Rhot1	Slc4a7
Trafd1	Scp2
Iqcg	Epb4.1l2
Rtbdn	1110051M20Rik
BC023829	1810043G02Rik
Gulo	Wfs1
Fn3k	Cyp46a1
Rasa2	Rnf150
Cln3	Ap1gbp1
Agpat5	Lca5
Podxl2	Lrp2
Rpgr	Sntb2
Aipl1	Rhbdd2
Eml3	Myo7a
Ctsf	Lycat
Hipk3	Arl13b
1110020G09Rik	D230014K01Rik
Ankrd42	Insm2
Epha8	Dyx1c1
4933411K20Rik	ENSMUSG00000074230
Nsun4	5730557B15Rik
Stxbp5	Cnga3
Plekha2	Pgf

					Hook3	Cited1
					Lpcat2	AI427122
					Lonrf1	Itpk1
					Nme5	Agl
					Usp12	Galt
					Tapt1	BC029684
					Slc25a33	Hagh
					4933409K07Rik	2810051F02Rik
					Lhfpl3	Rdh9
					Carf	Slc29a2
					Zfp444	Tex264
					Zbtb34	Zbtb7a
					Smpd1	Pla2g5
					Gnb5	Xrcc4
					Fbxo9	Klhdc8b
					A330021E22Rik	Fntb
					Nap1l1	EG624121
					Sp4	Bbs2
					Slco4a1	Zfp715
					Ankrd33	Map3k1
					Tcp11	Ufsp2
					Trib1	Rab28
					Tmem17	Slc7a8
					Ipmk	Mbnl1
					Lyrm1	Nfkbia
					Trim3	Kifc3
					St14	Fryl
					Stam	4930565B19Rik
					Atg4c	4833412L08Rik
					Tgds	6330409N04Rik
					Snx14	Ddi2
					Ppargc1b	Asah3l
					Ssu72	Dcun1d3
					Dnajb14	Nfic
					Tmem86a	Slc25a10
					Plch2	Slc19a1
					Tob2	Cacna1h
					Kat2b	Rab43
					Bbs12	Ccdc96
					Arid3c	Dohh
					Ttc30a2	Gpr162
					Rgs9bp	4930485B16Rik
					Zfp365	OTTMUSG00000005931
					Mylk	Ptges
					Ncoa2	Ppara
					Igj	Tnfsf12-tnfsf13
					Acsl6	Serinc3
					Ypel3	Rffl
					BC034090	Mzf1
						Cish
						Mpdz
						6330512M04Rik
						Ppil6
						Bcl2l1
						Gpr152
						4930573I19Rik
						Mllt6
						Pde6d
						Dctn1
						Zdhhc16
						Irf5
						Nrtn
						Cabc1
						St3gal3
						Sirt4
						Ttll3
						Dbndd2
						Ahdc1
						Nkiras2
						Arhgap10
						Wwc2
						Atxn1
						BC017158
						Wdr51b
						C130023O10Rik
						Fbxw9
						Mgat1
						Klc4
						Commd1
						Man2a2
						Dhdds
						Pink1
						Ccdc52
						1110049F12Rik

						Perp
						Sgms1
						Cd8a
						Cdh13
						Svop
						Mtnr1a
						Rora
						Cul4a
						Btbd9
						Agtpbp1
						Gramd1b
						Dnahc8
						H6pd
						Eno3
						Arhgap26
						Lad1
						Tmem158
						C030048H21Rik
						Sesn1
						Wdr19
						D330017J20Rik
						Rab3d
						Scap
						Lpgat1
						Ppa2
						Alpl
						Pbx3
						Zfpm1
						Susd3
						Chn1
						4932417I16Rik
						Tet3
						Ddhd1
						St6galnac4
						Dennd3
						Chchd5
						2900052L18Rik
						Cxxc5
						BC057022
						Ano10
						0610037D15Rik
						Oxct1
						Stk11ip
						Npepl1
						Hfe
						Dnaic2
						Heatr5b
						Katnal2
						4930578N16Rik
						4930430O22Rik
						Qsox2
						Sfrs2ip
						Gas6
						Arl4a
						Tmem27
						Scamp1
						Synj1
						AI462493
						Kbtbd3
						Fscn2
						Acadvl
						Msh5
						Hist2h3c2
						Ttll1
						Hint3
						Ift122
						Gse1
						Stab1
						Snx25
						4933432B09Rik
						Bmp15
						Slc12a6
						Plagl2
						5530400B01Rik
						Dusp8
						Slc26a2
						BC032203
						Plcxd2
						2310006M14Rik
						Dnajc16
						Higd2a
						Ofd1
						Slc38a9
						Smpd2
						Ccl21a
						EG624367
						Adrb1
						Ift81

						Aldh3a2
						4833439L19Rik
						Smarcd2
						2600011E07Rik
						9130008F23Rik
						Lpin1
						D9Ertd402e
						Pnpla7
						Slc4a5
						Scarb1
						Tmem42
						Furin
						Itfg2
						Rnf32
						Slc25a22
						Akap7
						D3Ertd751e
						Tacc2
						Otub2
						Ezh1
						Ercc2
						Cab39l
						Slc9a7
						Rpl3l
						Abcg1
						Adam9
						6430537H07Rik
						Lingo3
						Lrrc16a
						2600009E05Rik
						Phactr1
						Chst12
						Mknk1
						Zbtb26
						Lpcat1
						Usp6nl
						Prnp
						Mreg
						Akr1e1
						Mpped2
						Als2
						Shroom2
						Gm166
						Dock8
						Nfat5
						2310047B19Rik
						4930562D19Rik
						Urod
						Ttc30a1
						Btc
						Dalrd3
						Pitpnc1
						Ccpg1
						6720456H20Rik
						6620401K05Rik
						Galnt7
						Unc84a
						Max
						1110002L01Rik
						Slc7a4
						4930451G09Rik
						Klhdc1
						Pmm1
						Rdh14
						Als2cr4
						Stk40
						Punc
						Tbc1d9
						Ccndbp1
						9630058J23Rik
						Col17a1
						Foxo3a
						Gfpt1
						7530404M11Rik
						Wdr32
						Zbtb22
						Arfip2
						Slc46a3
						Mlh3
						Tbc1d30
						Pdgfa
						Ppp1r16a
						1700027N10Rik
						Ptges2
						Ppapdc2
						EG639396

9.9 Appendix figure 4.1

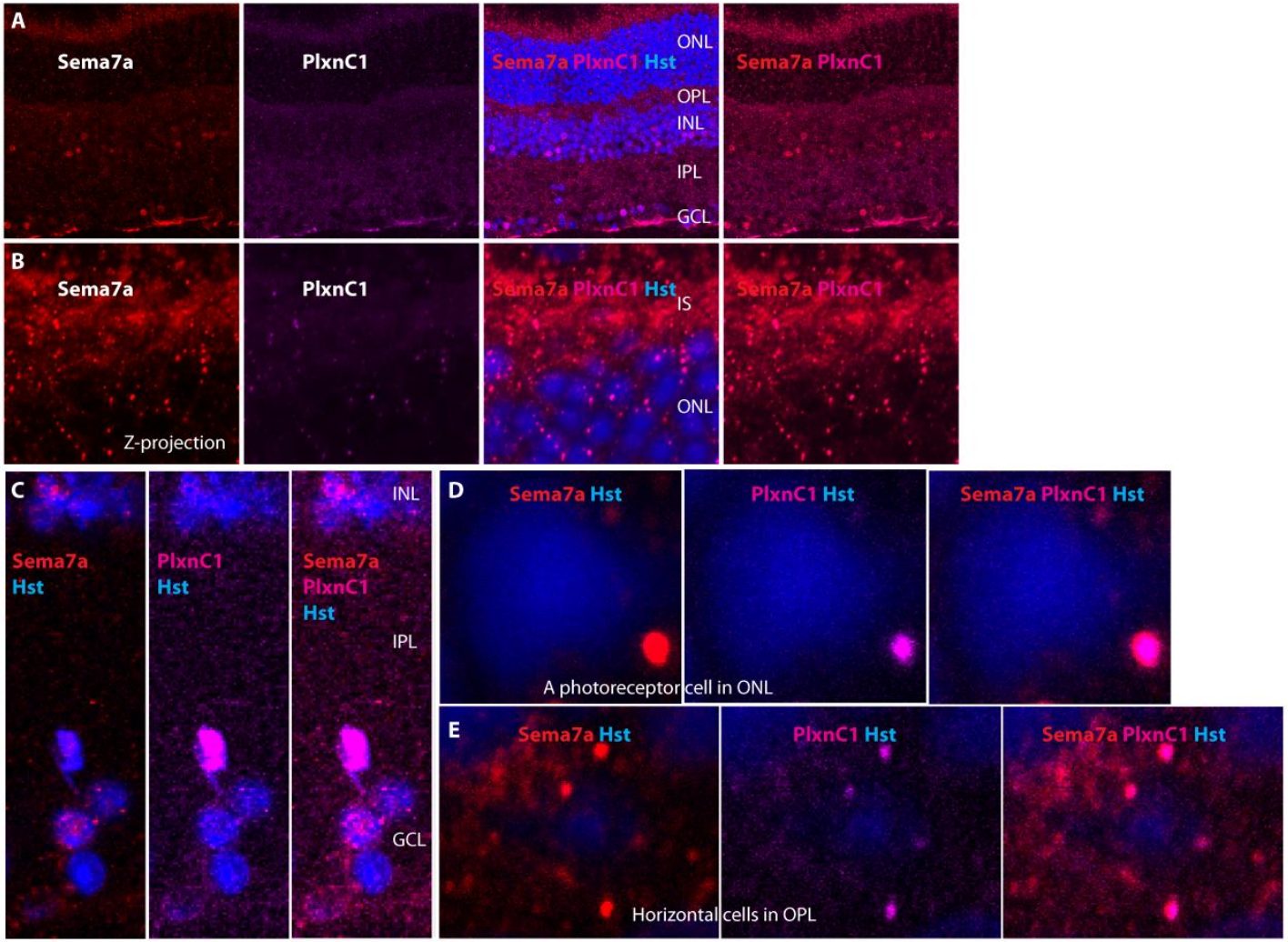

Appendix figure 4.1 Sema7a and PlxnC1 co-staining in adult mouse retina. (A) Sema7a (red) and PlxnC1 (mergenta) co-staining in 2 month adult mouse retina. (B) Z-projection of Sema7a and PlxnC1 immuno-staining in the segment and ONL region. (C) Sema7a and PlxnC1 immuno-staining in INL to GCL region. (D) Sema7a and PlxnC1 co-labeling on a single photoreceptor cell in ONL. (E) Sema7a and PlxnC1 co-labeling on horizontal cells in OPL.

9.10 Appendix figure 4.2

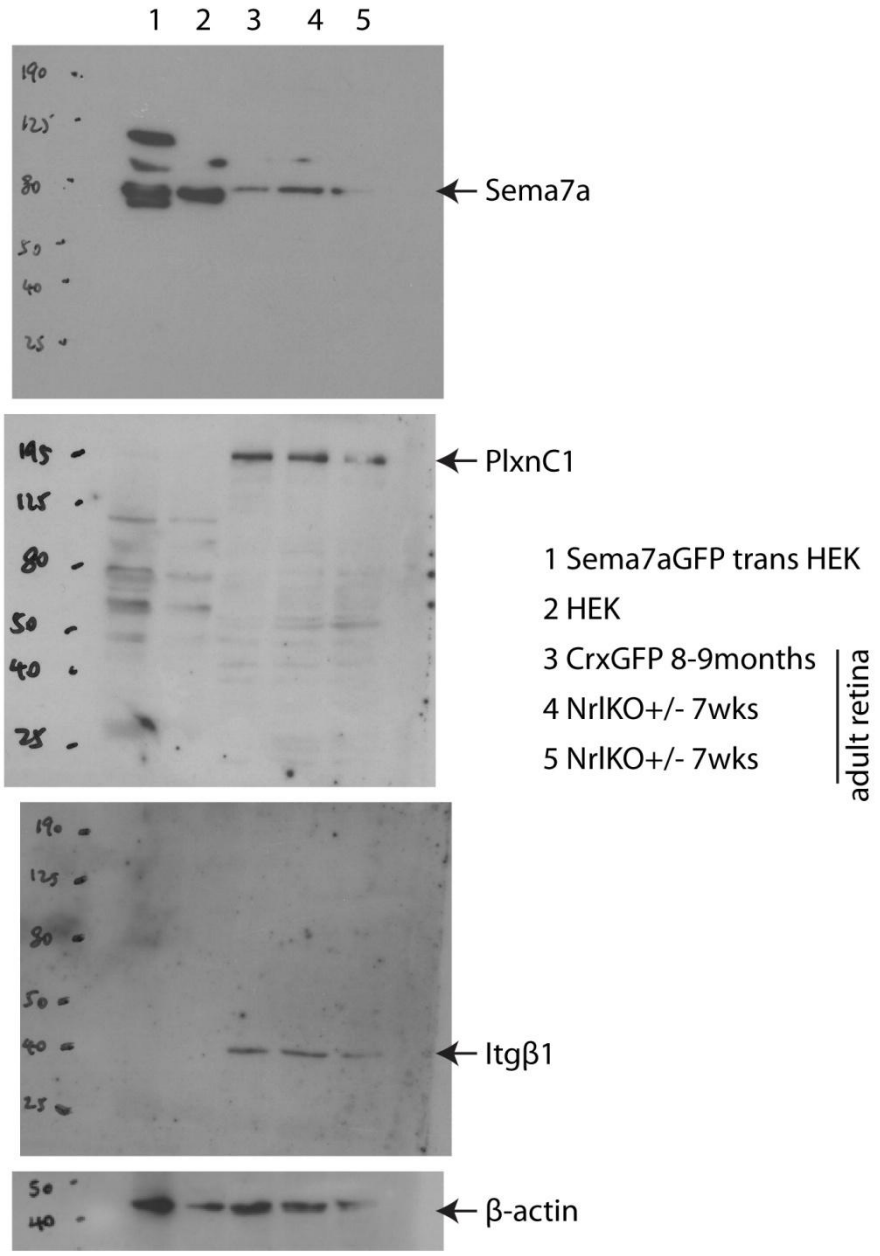

Appendix figure 4.2 Western blot of Sema7a and receptors full image. Lane 1: Sema7aGFP expression vector transfected HEK293 cells (for details about the vector, transfection and cells, see Appendix 4.1). Lane 2: untransfected HEK293 cells. Lane 3: retina lysates of 8 – 9 months CrxGFP mice. Lane 4 and lane 5: retina lysates of 7 weeks NrlKO+/- mice.

9.11 Appendix 4.1

Appendix 4.1 Sema7a shRNA knock down

Purpose: I proposed to use shRNA to knockdown Sema7a expression in neonatal mice and transplant these cells into the host animals in order to examine if the migration and

integration efficiency of the transplanted cells might be affected. It is also possible to assess how the knockdown affects retina development to confirm the knockout effect I observed.

Experimental design: I planned to use adeno-associated virus (AAV) infection which has been shown as the most efficient way to infect retina. This involved two-steps of sub-cloning (Appendix figure 4.1.1). The initial step was to construct several mU6 shRNA vectors and test their knock-down efficiency in cell lines. Then the most efficient mU6 shRNA vector would be subcloned into an AAV production vector PD10 and its effect examined in transplantation experiments.

Results: I designed and synthesized four Sema7a shRNA sequences (Appendix 2.1, Appendix figure 4.1.2 A) and correctly inserted them into the mU6 vectors as confirmed by digestion and sequencing (Appendix figure 4.1.1). Initial validation of the Sema7a mU6 shRNA constructs was performed by visiting Erasmus student Veronika Haunerdinger under my supervision in cell lines by co-transfection with a Sema7a expression vector (Sema7a mouse cDNA clone ORF with C-terminal GFP tag, OriGene, Catalog No. MG209876). In HEK 293 cells, none of the four shRNAs can decrease Sema7a expression except shRNA1 which seemed to have some reduction although the effect was not significant (Appendix figure 4.1.2 B). Reduction in Sema7a expression was detected by qRTPCR and fluorescent microscopy in MC3T3 cells which express mouse Sema7a endogenously at low levels (Sudo, Kodama et al. 1983; Fratzl-Zelman, Fratzl et al. 1998; Delorme, Saltel et al. 2005). shRNA1 decreased endogenous Sema7a expression by around 30 – 40 % whereas the other three shRNA did not show effective reduction (Appendix figure 4.1.2 D left). For exogenous Sema7a expression, shRNA1, shRNA2, and the all four pooled shRNAs decreased the expression levels by around 50 %, 40 %, and 30 % (Appendix figure 4.1.2 D right) and the other two shRNA showed no reduction at all.

9.12 Appendix figure 4.1.1

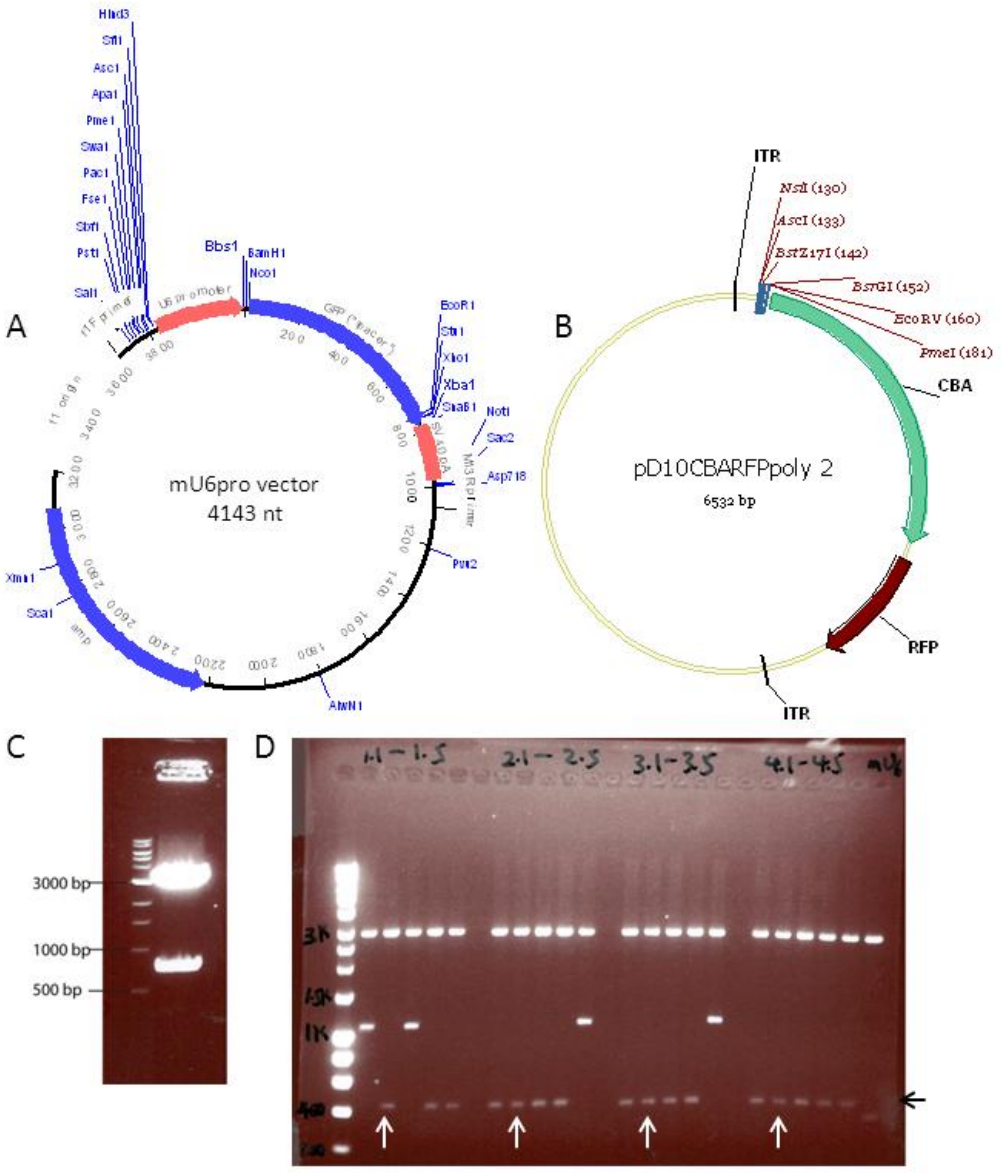

Appendix figure 4.1.1 Sema7a shRNA construction. The mU6pro vector (A) was cut with BbsI/XbaI and the 3 KB backbone (C) was gel purified for ligation with the Sema7a shRNA inserts which were synthesized with the cutting sites of BbsI/XbaI. The ligations were confirmed with AscI/SnaB1 for 400 bp products (D, black arrow). The 2nd colonies from five randomly chosen colonies of each shRNA ligation were mini and midi-preped and sequenced (D, white arrow). After validation of the mU6 shRNA in cell lines for knocking down effect of Sema7a, the most potent mU6 shRNA plasmid will be cut with AscI/SnaBI and the 400 bp product will be ligated with the backbone of PD10 (B) which will be cut with AscI/Bstz17I.

9.13 Appendix figure 4.1.2

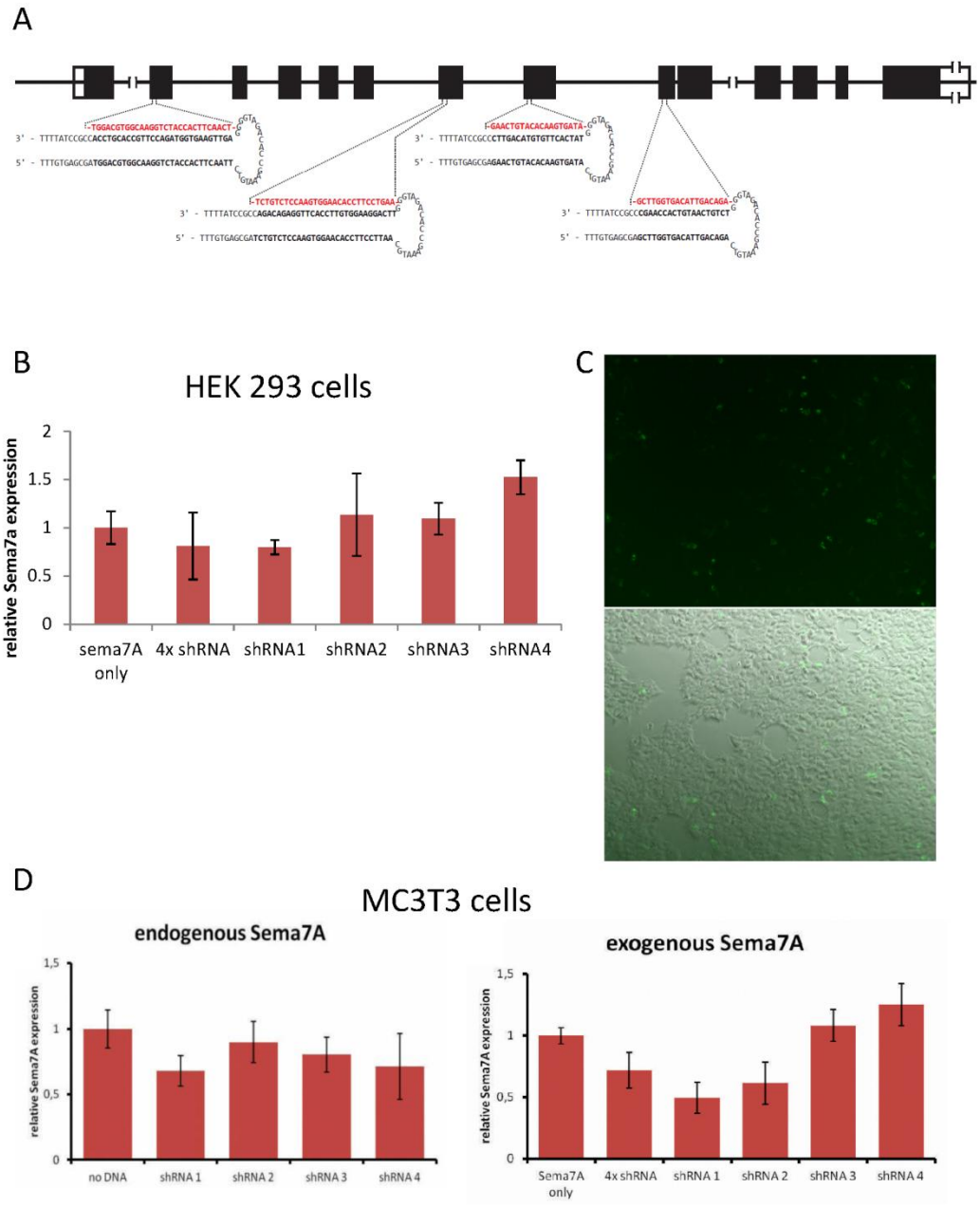

Appendix figure 4.1.2 Sema7a shRNA knockdown validation. The four shRNA sequences (A) were incubated with a Sema7a expression plasmid in HEK293 cells (B&C) and MC3Y3 cells (D). (B&C) 24hrs incubation for target:shRNA=1:20 in HEK 293 cells, images at 10X; (D) Transfection of MC3T3 cells with shRNA plasmid alone (Left) or shRNA plasmid and Sema7a expression plasmid (Right). no DNA: control group without transfection. Sema7A only: transfection with Sema7A overexpression plasmid alone. 4x shRNA: Sema7A overexpression plasmid and all 4 shRNAs pooled. shRNA#: one shRNA plasmid alone (left) or shRNA plasmid and Sema7A overexpression plasmid together (right)

9.14 Appendix figure 7.1

Appendix figure 7.1 Swaroop array plot of marker candidates

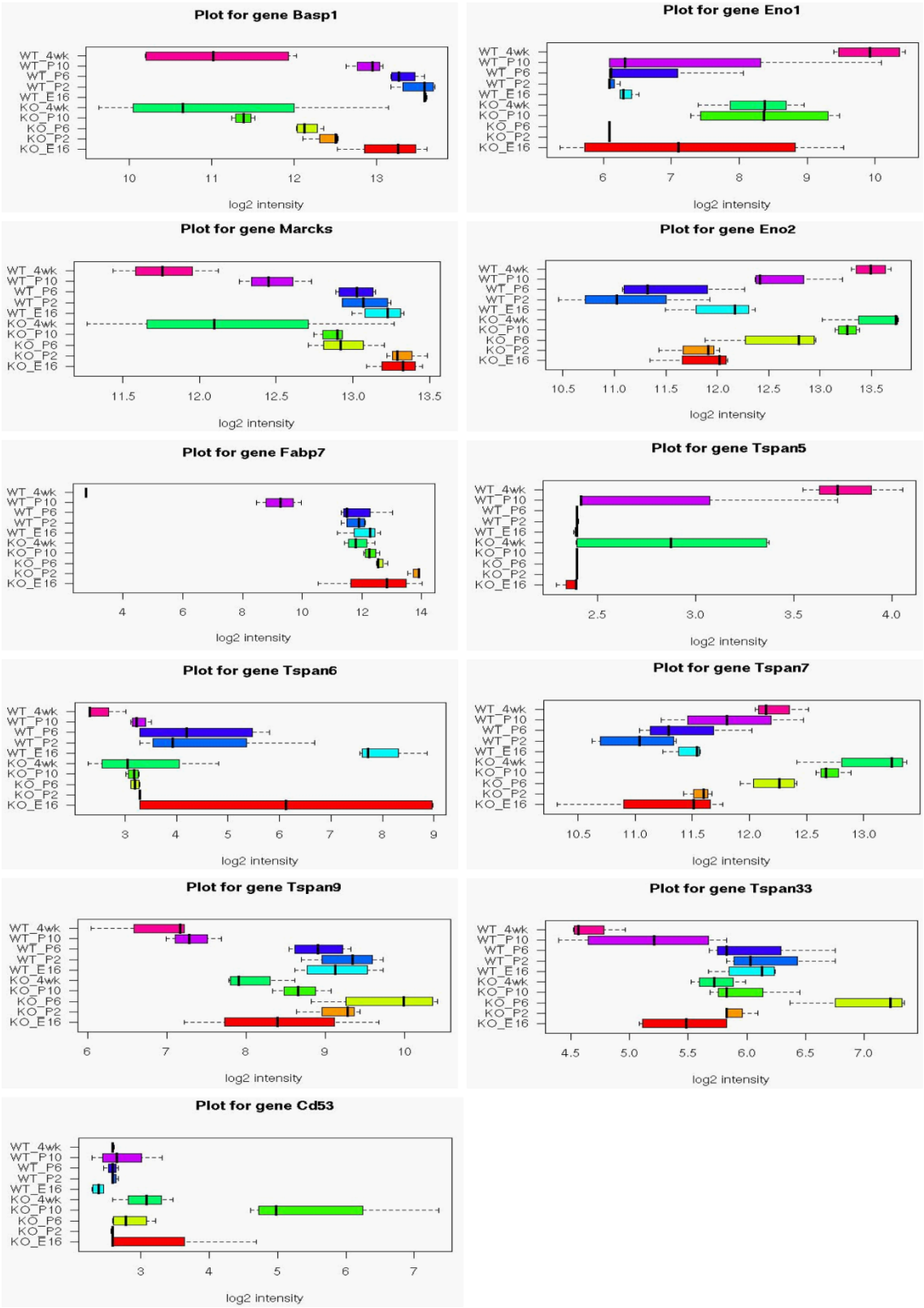

9.15 Appendix table 7.1

Appendix table 7.1 photoreceptor whole cell lysates

Accession	Entry	Description	mW (Da)	pI (pH)	PLGS Score	Peptides	Theoretical Peptides	Coverage (%)	Precursor RMS Mass Error (ppm)	Products	Modified Peptides	Products RMS Mass Error (ppm)	Products RMS RT Error (min)	Amount (fmol)	Amount (ngrams)	Protein ID
P52480	KPY2_MOUSE	Pyruvate kinase M2 isozyme EC 2 7 1 40	57719	7.2131	552.8033	25	44	65.283	6.2573	173	1	17.574	0.014	56.1897	3.2453	41095
P17182	ENOA_MOUSE	Alpha enolase EC 4 2 1 11 2 phospho D glycerate	46980	6.3752	735.7579	24	30	72.2864	4.3705	234	1	16.8074	0.0125	253.3919	11.9119	23162
P40142	TKT_MOUSE	Transketolase EC 2 2 1 1 TK P68	67587	7.2307	271.3765	22	44	44.9438	6.6353	101	0	16.4018	0.0136	15.05	1.0178	79962
P14733	LAM1_MOUSE	Lamin B1	66613	4.9213	523.8222	22	68	47.7002	4.5622	149	1	18.225	0.0137	79.3386	5.2883	41701
Q04447	KCRB_MOUSE	Creatine kinase B chain EC 2 7 3 2 B CK	42686	5.2866	605.1655	19	23	79.5276	4.2425	249	1	16.1442	0.0122	451.1776	19.2713	40228
P17751	TPIS_MOUSE	Triosephosphate isomerase EC 5 3 1 1 TIM	26564	7.0833	238.9937	18	20	79.0323	5.3306	134	1	18.945	0.0132	10.9721	0.2917	80571
P11499	HS9B_MOUSE	Heat shock protein HSP 90 beta HSP 84 Tumor spe	83142	4.775	364.1511	15	66	32.6418	5.4351	67	0	15.8408	0.0137	55.9171	4.652	35631
Q02053	UBA1_MOUSE	Ubiquitin activating enzyme E1 1	117734	5.2956	270.6295	15	68	21.5501	6.2061	82	2	17.3191	0.0144	13.8487	1.6315	82546
P06151	LDHA_MOUSE	L lactate dehydrogenase A chain EC 1 1 1 27 LDH	36344	7.669	395.7395	15	28	59.5166	3.7905	145	1	16.1084	0.0128	118.809	4.3208	41976
P16858	G3P_MOUSE	Glyceraldehyde 3 phosphate dehydrogenase EC 1 2 1	35656	8.3507	1044.0819	13	19	58.4337	3.8951	253	0	15.673	0.0114	307.4733	10.9703	27737
P16627	HS7T_MOUSE	Heat shock related 70 kDa protein	70651	5.722	214.5654	10	51	32.1373	7.0539	50	2	14.702	0.0136	29.414	2.0794	35583
P35700	PDX1_MOUSE	Peroxiredoxin 1 Thioredoxin peroxidase 2 Thiore	22162	8.2344	140.6652	8	18	60.804	6.3721	44	0	19.4475	0.0136	5.217	0.1157	55598
P17183	ENOG_MOUSE	Gamma enolase EC 4 2 1 11 2 phospho D glycerate	47136	4.7996	295.1113	7	30	25.4042	5.7158	45	1	13.736	0.0145	115.0281	5.4254	23174
P14206	RSP4_MOUSE	40S ribosomal protein SA P40 34 67 kDa laminin	32698	4.5458	186.5374	7	25	39.322	5.102	35	0	12.7818	0.0143	22.8984	0.7492	71622
P17918	PCNA_MOUSE	Proliferating cell nuclear antigen PCNA Cyclin	28766	4.4643	132.3064	7	21	36.0153	6.8104	29	0	17.2591	0.0173	11.8413	0.3409	55375
Q61937	NPM_MOUSE	Nucleophosmin NPM Nucleolar phosphoprotein B23	32539	4.4242	131.7983	7	22	33.9041	3.7509	47	1	15.6858	0.0135	11.4286	0.3721	50670
P56480	ATPB_MOUSE	ATP synthase beta chain mitochondrial precursor	56344	4.9709	358.4167	6	37	25.7089	2.8273	45	0	14.6173	0.0105	44.6235	2.5159	6274
P05218	TBB5_MOUSE	Tubulin beta 5 chain	49638	4.5903	1261.9083	6	31	26.8018	4.4825	123	0	13.7544	0.0116	406.6357	20.198	78289
P05213	TBA2_MOUSE	Tubulin alpha 2 chain	50133	4.7622	920.6479	5	35	23.7251	3.1307	100	0	14.6719	0.0114	467.847	23.4699	78136
P20029	GR78_MOUSE	78 kDa glucose regulated protein precursor GRP 78	72377	4.8748	313.7196	4	52	8.2443	6.8555	20	0	13.0869	0.0124	34.4199	2.4928	30757
Q9R1P3	PSB2_MOUSE	Proteasome subunit beta type 2 EC 3 4 25 1 Prot	22891	6.6086	129.2958	4	19	39.801	9.1596	22	1	18.2472	0.0192	4.2576	0.0975	60344
P02551	TBA1_MOUSE	Tubulin alpha 1 chain	50103	4.7622	926.8679	4	35	19.9557	4.0742	95	1	13.604	0.0113	467.847	23.4559	78114
P08109	HS7C_MOUSE	Heat shock cognate 71 kDa protein	70827	5.1998	465.8573	3	50	8.8235	2.0273	39	0	13.6022	0.0119	62.6054	4.4369	35566
P26369	U2AF_MOUSE	Splicing factor U2AF 65 kDa subunit U2 auxiliary	53483	9.3635	146.2892	3	26	8.4211	5.6791	17	0	14.5612	0.011	16.806	0.8994	82501
Q9JJZ2	TBA8_MOUSE	Tubulin alpha 8 chain Alpha tubulin 8	50019	4.7966	496.3186	2	35	10.9131	3.3523	53	1	14.789	0.0119	152.7005	7.6429	78163
P14701	TCTP_MOUSE	Translationally controlled tumor protein TCTP p	19449	4.5679	135.8492	2	16	15.6977	8.9695	15	0	13.158	0.0115	16.4748	0.3206	78658
P47955	RLA1_MOUSE	60S acidic ribosomal protein P1	11467	4.0217	127.8643	2	7	75.4386	4.1428	29	1	14.1487	0.0141	26.0309	0.2987	67834
P53675	CLH2_HUMAN	Clathrin heavy chain 2 CLH 22	186909	5.4738	445.8013	28	133	22.3171	6.3253	100	5	18.4335	0.0151	11.9929	2.243	12981
Q04619	HS9B_CHICK	Heat shock cognate protein HSP 90 beta	83375	4.7514	339.7942	22	68	34.4828	6.6605	112	1	18.3962	0.015	44.2634	3.6928	35629
P00924	ENO1_YEAST	Enolase 1 EC 4 2 1 11 2 phosphoglycerate dehydr	46642	6.1527	314.0052	22	28	64.9083	4.8703	172	2	18.3509	0.0136	50	2.3335	23153
P06576	ATPB_HUMAN	ATP synthase beta chain mitochondrial precursor	56524	5.0955	349.7532	20	38	60.8696	5.6867	131	0	17.6918	0.0131	44.6235	2.5239	6261
P70615	LAM1_RAT	Lamin B1	66434	4.9711	477.9323	20	67	37.7133	6.427	117	3	14.8809	0.0141	61.0764	4.0601	41702
P11142	HS7C_HUMAN	Heat shock cognate 71 kDa protein	70854	5.1998	422.0086	19	50	38.3901	5.325	163	0	18.0179	0.0127	44.1048	3.1269	35564
Q39043	BIP2_ARATH	Luminal binding protein 2 precursor BiP2 AtBP2	73515	4.9235	273.3715	17	63	34.1317	6.1609	68	0	15.719	0.0147	29.414	2.1637	7797
P00829	ATPB_BOVIN	ATP synthase beta chain mitochondrial precursor	56248	4.9759	355.17	17	36	46.5909	5.7204	71	0	13.6274	0.0145	44.6235	2.5116	6228
P49118	BIP_LYCES	Luminal binding protein precursor BiP 78 kDa gl	73189	4.9078	290.8727	16	63	37.5375	4.5357	57	0	14.4983	0.0171	29.414	2.1541	7805
Q9AWL7	GIGA_ORYSA	Gigantea like protein	128526	6.3582	292.1222	15	88	22.3359	7.2972	80	4	19.3741	0.0165	3.745	0.4816	29340
O19049	ROK_RABIT	Heterogeneous nuclear ribonucleoprotein K hnRNP K	50928	5.2203	270.1672	15	39	37.581	4.3507	135	0	18.3713	0.0112	39.4178	2.0087	68581
Q9SQJ2	GIGA_ARATH	GIGANTEA protein	127794	6.5971	224.1116	14	83	15.0043	6.6213	65	2	17.6253	0.0164	1.7297	0.2212	29339
P20030	HS7C_TRYBB	Heat shock cognate HSP70 protein	73649	4.9292	217.5527	14	46	30.4734	5.8369	59	0	17.2546	0.0163	29.414	2.1677	35568
P16019	HS70_THEAN	Heat shock 70 kDa protein HSP 70 1	70929	5.1449	255.481	14	53	40.5573	5.9387	78	3	14.8114	0.0162	29.414	2.0876	35492
P11981	KPY2_RAT	Pyruvate kinase M2 isozyme EC 2 7 1 40	57613	7.1938	529.2921	13	43	37.9245	6.0249	88	0	16.3264	0.015	56.1897	3.2393	41097
P29844	HS7C_DROME	Heat shock 70 kDa protein cognate 3 precursor 78	72190	5.0424	298.4409	13	58	31.7073	7.4544	65	2	17.6798	0.0156	34.3664	2.4825	35563
Q07437	HS70_LEIAM	Heat shock 70 kDa protein	71153	5.2989	264.9041	13	49	26.9939	6.0661	72	1	15.2569	0.0147	29.414	2.0942	35471
Q65729	POLG_BSTVG	Genome polyprotein Contains Nuclear inclusion pr	105480	5.9213	256.6098	13	70	20.4883	7.1721	51	0	16.3606	0.0161	7.2525	0.7655	58108
P08418	HS70_SCHMA	Heat shock 70 kDa homolog protein HSP70 Major s	69831	5.2527	252.8508	13	47	30.2983	5.8999	56	2	17.0747	0.0143	29.414	2.0553	35490
P40918	HS70_CLAHE	Heat shock 70 kDa protein Allergen Cla h 4 Cla	69933	4.8289	248.2131	13	56	37.014	6.2701	62	2	16.5429	0.0141	29.414	2.0583	35466

Yellow colour indicates overlap proteins between whole cell lysates and membrane preparations. Proteins above the thick black line are mouse proteins. Whole cell lysates data from Lakowski.

The protein accession number (accession), name (description), molecular weight (mW), isoelectric point (pI), number of detected peptides (peptides) and theoretical peptides, and the amount of the proteins detected are given in columns.

P18669	PMGB_HUMAN	Phosphoglycerate mutase brain form EC 5 4 2 1	28654	6.7861	297.7026	12	20	67.5889	4.1206	94	0	17.4523	0.0123	81.6361	2.3407	57841
P48720	HS70_BLAEM	Heat shock 70 kDa protein	70790	5.0475	293.5657	12	50	30.3544	5.8081	71	3	17.1228	0.0153	29.414	2.0835	35460
P22202	HS74_YEAST	Heat shock protein SSA4	69477	4.8327	265.3275	12	53	25.117	7.7568	45	0	15.8954	0.0123	29.414	2.0449	35540
P22996	PAA4_ECOLI	Resolvase	24145	10.3881	133.0365	12	23	49.3151	8.3028	45	1	15.7272	0.0174	33.5173	0.8098	54637
P24722	KCRT_ONCMY	Creatine kinase testis isozyme EC 2 7 3 2	42976	6.2034	356.4003	12	24	38.9034	5.7931	69	0	15.2883	0.0143	124.6657	5.3612	40247
P00548	KPYK_CHICK	Pyruvate kinase muscle isozyme EC 2 7 1 40	57846	7.3508	439.3006	11	43	31.38	6.9566	61	2	16.2102	0.015	49.3656	2.8575	41120
P37899	HS70_PYRSA	Heat shock 70 kDa protein	72035	4.879	281.5872	11	59	29.8921	7.873	56	1	15.0008	0.0149	29.414	2.1202	35488
Q42434	BIP_SPIOL	Luminal binding protein precursor BiP 78 kDa gl	73547	4.8398	281.3997	11	64	18.4132	4.656	46	0	15.3573	0.0148	29.414	2.1646	7807
P11147	HS7D_DROME	Heat shock 70 kDa protein cognate 4 Heat shock 70	71087	5.1848	275.0262	11	50	21.9662	4.7256	57	2	14.074	0.0132	29.414	2.0923	35569
P24629	HS71_LYCES	Heat shock cognate 70 kDa protein 1	71242	4.9545	258.6985	11	54	27.5385	5.1695	48	1	14.8074	0.0159	29.414	2.0968	35505
Q14103	ROD_HUMAN	Heterogeneous nuclear ribonucleoprotein D0 hnRNP	38410	7.8979	179.4634	11	24	31.2676	4.6626	55	0	16.119	0.0161	58.7947	2.2597	68567
P42897	ENO_ALLMI	Enolase EC 4 2 1 11 2 phosphoglycerate dehydrat	42857	5.4666	521.7158	11	28	29.1139	3.283	74	0	13.9656	0.0135	213.1057	9.1388	23178
Q06331	TBA_OCTDO	Tubulin alpha chain	50161	4.8904	424.7603	10	36	25.4989	5.9941	90	0	18.6419	0.0117	119.1692	5.9816	78188
Q01859	ATP2_ORYSA	ATP synthase beta chain mitochondrial precursor	59022	6.308	372.9282	10	39	30.6715	7.1172	64	1	17.19	0.0131	31.8105	1.8787	5837
P53459	ACT6_DIPDE	Actin 6 Fragment	41496	5.1608	300.455	10	33	43.1635	4.7414	74	2	16.1758	0.0141	109.6464	4.5529	1905
P53623	HS72_PICAN	Heat shock protein 70 2	69898	4.7461	293.3205	10	53	38.0062	9.2399	50	1	17.0853	0.0159	29.414	2.0573	35523
P34933	HS73_BOVIN	Heat shock 70 kDa protein 3	69156	5.1396	262.1818	10	49	26.149	6.3177	46	0	15.2486	0.0157	29.414	2.0354	35528
P05456	HS70_TRYCR	Heat shock 70 kDa protein	73762	5.2678	225.9714	10	46	13.9706	6.947	41	0	15.1003	0.0144	29.414	2.171	35494
P22954	HS72_ARATH	Heat shock cognate 70 kDa protein 2 Hsc70 2	71342	4.8344	221.3224	10	51	22.3583	7.036	43	0	12.9069	0.0164	29.414	2.0998	35515
P08734	ENO_XENLA	Enolase EC 4 2 1 11 2 phosphoglycerate dehydrat	47343	5.8427	544.176	10	29	28.8684	6.356	68	0	14.3779	0.0147	213.1057	10.0955	23240
P46561	ATPB_CAEEL	Probable ATP synthase beta chain mitochondrial pr	60961	5.6904	319.5997	9	41	25.0877	6.3354	61	1	15.7805	0.015	31.8105	1.9404	6232
Q01233	HS70_NEUCR	Heat shock 70 kDa protein HSP70	70558	4.8261	304.1837	9	53	18.7306	5.3861	41	1	14.9318	0.0159	29.414	2.0767	35478
P38482	ATP2_CHLRE	ATP synthase beta chain mitochondrial precursor	61783	4.8029	290.588	9	38	25.4355	6.6177	55	3	17.695	0.0138	18.7214	1.1574	5832
P09446	HS7A_CAEEL	Heat shock 70 kDa protein A	69780	5.0823	271.66	9	53	26.25	6.8642	41	1	19.2901	0.0145	29.414	2.0538	35553
P16394	HS70_BRELC	Heat shock 70 kDa protein	74041	5.1255	256.1414	9	57	18.6391	8.4455	45	2	14.8541	0.017	29.414	2.1792	35461
P27420	HS7C_CAEEL	Heat shock 70 kDa protein C precursor	73303	4.9133	219.858	9	56	27.2315	6.6996	48	1	14.4625	0.0159	29.414	2.1575	35560
P22623	HS72_PARLI	Heat shock 70 kDa protein II HSP70 II Fragment	41321	8.3611	216.4324	9	33	29.8387	5.8897	44	2	15.9305	0.0144	29.414	1.2162	35522
P87047	HS70_PARBR	Heat shock 70 kDa protein	70461	5.1189	204.632	9	53	35.4391	6.3925	50	3	16.459	0.0167	29.414	2.0738	35482
Q01105	SET_HUMAN	SET protein HLA DR associated protein II PHAPII	32083	3.9111	197.4204	9	16	44.4043	6.221	60	0	18.6397	0.0118	28.2188	0.9059	73379
O80585	MTHR_ARATH	Probable methylenetetrahydrofolate reductase EC 1	68216	5.1101	149.1151	9	50	22.9373	8.31	37	0	20.3854	0.0159	1.5378	0.105	47390
O16808	ACT_MAYDE	Actin	41789	5.0709	478.6162	9	35	32.7128	2.5889	79	0	15.2199	0.0131	240.733	10.0667	2030
P09652	TBB4_CHICK	Tubulin beta 4 chain Beta tubulin class III	50388	4.6778	716.2647	8	32	32.0713	6.1811	85	1	14.5855	0.0138	204.2637	10.2992	78277
Q91060	TBA_NOTVI	Tubulin alpha chain	50061	4.7567	634.3005	8	35	28.2222	6.3971	115	0	16.4019	0.0114	266.282	13.339	78187
O18919	KPY2_RABIT	Pyruvate kinase M2 isozyme EC 2 7 1 40	57737	7.7569	525.4713	8	42	15.8491	6.1914	55	0	15.9018	0.0144	56.1897	3.2463	41096
Q9Y707	ACT2_SUIBO	Actin 2	41636	5.1594	502.4036	8	34	38.4	6.3981	84	1	15.0447	0.0116	240.733	10.0298	1861
P08108	HS70_ONCMY	Heat shock cognate 70 kDa protein HSP70	71239	5.0493	404.8638	8	52	26.7281	6.4875	54	0	16.3634	0.0133	44.1048	3.1439	35479
P49741	TBAA_SCHCO	Tubulin alpha 1A chain	49413	4.9124	395.3371	8	35	27.9018	5.8999	61	1	15.4146	0.014	107.0527	5.2932	78165
P17614	ATP2_NICPL	ATP synthase beta chain mitochondrial precursor	59819	5.9019	337.4333	8	39	21.4286	6.821	50	1	19.7345	0.0119	31.8105	1.9041	5836
P06761	GR78_RAT	78 kDa glucose regulated protein precursor GRP 78	72302	4.8748	313.7196	8	52	18.0428	5.3297	39	0	15.9867	0.0147	34.4199	2.4902	30762
P07323	ENOG_RAT	Gamma enolase EC 4 2 1 11 2 phospho D glycerate	46979	4.8424	313.4042	8	29	29.5612	5.981	44	0	14.1087	0.0133	115.0281	5.4074	23175
P41797	HS71_CANAL	Heat shock protein SSA1	70150	4.862	301.151	8	52	24.4275	7.0895	38	0	14.1924	0.0159	29.414	2.0647	35499
P47773	HS7C_ICTPU	Heat shock cognate 71 kDa protein	71296	5.0079	292.9524	8	53	20.0308	6.1125	49	3	15.5632	0.0136	29.414	2.0984	35565
P09435	HS73_YEAST	Heat shock protein SSA3	70503	4.8563	287.8965	8	51	20.9553	7.0982	36	0	15.2719	0.0155	29.414	2.0751	35532
P15429	ENOB_RAT	Beta enolase EC 4 2 1 11 2 phospho D glycerate	46800	7.6655	287.6051	8	29	26.097	6.3228	43	0	14.7072	0.0154	115.0281	5.3867	23171
Q27727	ENO_PLAFA	Enolase EC 4 2 1 11 2 phosphoglycerate dehydrat	48673	6.1838	272.441	8	33	36.3229	6.2853	52	2	14.5333	0.0147	115.0281	5.6023	23223
P11143	HS70_MAIZE	Heat shock 70 kDa protein	70559	5.0295	269.2604	8	51	18.7597	6.9825	32	0	13.0053	0.0164	29.414	2.0735	35477
P26413	HS70_SOYBN	Heat shock 70 kDa protein	70835	5.1815	249.2893	8	51	18.2946	7.7617	42	1	17.3097	0.0164	29.414	2.0849	35491
Q43725	CYSM_ARATH	Cysteine synthase mitochondrial precursor EC 4 2	45153	8.2429	128.1766	8	35	25.2358	7.4137	42	2	14.1903	0.0136	9.585	0.4331	18138
O87862	ADCC_STRPN	Zinc transport system ATP binding protein adcC	26525	7.0426	98.7626	8	16	46.5812	5.9546	26	0	16.2341	0.0176	2.2861	0.0607	2160
O17449	TBB1_MANSE	Tubulin beta 1 chain Beta 1 tubulin	50198	4.5593	983.6111	8	31	31.3199	3.3181	98	0	13.4775	0.0107	216.9111	10.8956	78224
Q00215	ACTC_STYPL	Actin cytoplasmic	41902	5.1581	600.474	7	35	38.4	5.3355	87	2	15.4865	0.0134	258.4635	10.8374	1945
Q9W7L0	ENOA_PYTRG	Alpha enolase EC 4 2 1 11 2 phospho D glycerate	47409	7.1027	537.61	7	34	33.2564	6.4352	65	2	14.4998	0.0145	213.1057	10.1096	23163
P90689	ACT_BRUMA	Actin	41682	5.1478	515.4861	7	34	25.5319	4.9924	63	0	14.4976	0.0127	253.1386	10.5584	2003
P19120	HS7C_BOVIN	Heat shock cognate 71 kDa protein	71195	5.3269	422.0086	7	50	20.1538	5.8514	55	1	14.6316	0.0135	44.1048	3.142	35557
P04350	TBB5_HUMAN	Tubulin beta 5 chain	49598	4.617	414.342	7	31	29.955	4.334	72	3	14.4043	0.014	206.0144	10.2247	78287
Q05524	ENOL_HUMAN	Alpha enolase lung specific EC 4 2 1 11 2 phos	49446	5.705	372.8593	7	30	26.6376	5.2429	45	1	14.799	0.0147	97.2268	4.8105	23176
P37399	ATP2_DAUCA	ATP synthase beta chain mitochondrial precursor	59098	5.5018	318.3439	7	42	20.6581	6.9267	38	0	14.3226	0.0107	31.8105	1.8811	5833
Q16956	GR78_APLCA	78 kDa glucose regulated protein precursor GRP 78	73652	4.6066	287.3463	7	52	18.5907	5.963	42	0	15.6766	0.0127	34.3664	2.5327	30751

P22953	HS71_ARATH	Heat shock cognate 70 kDa protein 1 Hsc70 1	71313	4.8272	274.2661	7	53	16.4363	4.771	30	0	13.5203	0.0135	29.414	2.0989	35497
O57391	ENOG_CHICK	Gamma enolase EC 4 2 1 11 2 phospho D glycerate	47278	4.6481	272.2957	7	29	29.4931	7.2268	49	2	15.6149	0.0148	117.7532	5.5707	23172
P27541	HS70_BRUMA	Heat shock 70 kDa protein	70176	5.131	264.4902	7	51	29.9689	5.8174	39	3	15.9194	0.0169	29.414	2.0655	35462
P11833	TBB_PARLI	Tubulin beta chain	50019	4.5416	1031.4604	7	31	31.3199	3.6016	102	1	13.1257	0.0118	293.374	14.6838	78336
P09244	TBB7_CHICK	Tubulin beta 7 chain Tubulin beta 4	49638	4.5903	1261.9083	6	31	26.8018	3.6	124	0	13.4644	0.0117	406.6357	20.198	78298
P02554	TBB_PIG	Tubulin beta chain	49828	4.5903	1184.696	6	31	23.3708	2.5977	110	0	13.0881	0.0113	347.0077	17.3022	78341
P32882	TBB2_CHICK	Tubulin beta 2 chain Beta tubulin class II	49920	4.5903	1178.4197	6	31	23.3708	3.2098	106	0	13.1812	0.0118	347.0077	17.3342	78241
P13602	TBB2_XENLA	Tubulin beta 2 chain	49691	4.6168	1175.2455	6	31	20.9932	3.501	105	0	13.4833	0.0114	347.0077	17.2546	78264
P09203	TBB1_CHICK	Tubulin beta 1 chain Beta tubulin class I	49876	4.5903	1169.7322	6	31	23.5955	2.8998	105	0	13.4235	0.0117	347.0077	17.3189	78210
P04691	TBB1_RAT	Tubulin beta chain T beta 15	49930	4.5961	1164.7333	6	31	24.0449	2.6787	111	1	13.6926	0.0113	347.0077	17.3376	78232
P09206	TBB3_CHICK	Tubulin beta 3 chain Beta tubulin class IV	49829	4.5767	982.2007	6	31	29.2135	3.8821	90	0	12.9801	0.0115	293.374	14.628	78267
P07437	TBB1_HUMAN	Tubulin beta 1 chain	49726	4.5593	933.8457	6	31	27.2523	3.5076	84	0	13.6127	0.0118	216.9111	10.7933	78221
Q91240	TBB_PSEAM	Tubulin beta chain	49743	4.602	927.7854	6	31	27.191	4.3739	88	0	12.5351	0.011	293.374	14.603	78347
P04797	G3P_RAT	Glyceraldehyde 3 phosphate dehydrogenase EC 1 2 1	35682	8.3491	820.9352	6	19	44.5783	3.9963	104	2	12.8737	0.0121	303.4024	10.833	27760
P36221	TBB1_NOTCO	Tubulin beta 1 chain	49773	4.5903	638.713	6	31	24.6637	6.7168	79	0	15.5237	0.0129	247.7534	12.3396	78226
P12456	TBB7_CAEEL	Tubulin beta chain	49228	4.6926	612.2667	6	31	19.7279	4.9816	72	0	12.8091	0.0115	250.9069	12.3598	78297
Q25009	TBB1_HOMAM	Tubulin beta 1 chain Beta I tubulin	50710	4.6888	575.4449	6	32	21.5078	6.1517	53	0	15.508	0.0121	107.6477	5.4624	78220
Q9XSJ4	ENOA_BOVIN	Alpha enolase EC 4 2 1 11 2 phospho D glycerate	47116	6.4534	569.0612	6	31	29.3303	4.491	82	2	14.1129	0.0135	387.8564	18.2858	23159
P06733	ENOA_HUMAN	Alpha enolase EC 4 2 1 11 2 phospho D glycerate	47008	7.1713	510.7335	6	31	24.7113	7.3371	64	1	14.7713	0.0143	210.3806	9.8959	23161
Q9W7L2	ENOA_SCEUN	Alpha enolase EC 4 2 1 11 2 phospho D glycerate	47332	6.6982	507.2524	6	32	29.0993	6.9896	55	0	13.0621	0.0137	213.1057	10.0931	23165
P29511	TBA6_ARATH	Tubulin alpha 6 chain	49506	4.743	501.9935	6	35	20.2222	1.5475	62	0	14.0185	0.0121	315.8264	15.6454	78158
P06351	H33_HUMAN	Histone H3 3 H3 A H3 B H3 3Q	15187	11.6797	488.1847	6	12	52.5926	6.2782	93	0	15.7912	0.0132	101.3608	1.5404	32328
P38669	TBA2_NEUCR	Tubulin alpha B chain	50222	4.8345	409.081	6	37	23.0599	5.9008	52	0	15.8961	0.0128	107.0527	5.3799	78137
P10719	ATPB_RAT	ATP synthase beta chain mitochondrial precursor	56318	5.0198	395.6592	6	36	25.7089	4.8278	39	0	14.3422	0.0112	40.0093	2.2547	6303
P08238	HS9B_HUMAN	Heat shock protein HSP 90 beta HSP 84 HSP 90	83081	4.7726	357.0724	6	66	11.065	5.6659	34	0	12.0904	0.0133	55.9171	4.6486	35630
P07823	GR78_MESAU	78 kDa glucose regulated protein precursor GRP 78	72334	4.8748	311.789	6	52	17.737	5.8234	34	1	14.9562	0.0138	34.4199	2.4913	30756
P26300	ENO_LYCES	Enolase EC 4 2 1 11 2 phosphoglycerate dehydrat	47768	5.5746	299.0548	6	35	32.8829	4.621	52	2	16.6988	0.0141	115.0281	5.4982	23210
P93587	ACT1_SOLTU	Actin 42 Fragment	36830	5.3156	297.8023	6	30	33.1325	4.6349	45	1	14.9387	0.0136	109.6464	4.0409	1822
P29357	HS7E_SPIOL	Chloroplast envelope membrane 70 kDa heat shock re	71555	5.1747	284.0978	6	53	17.1779	7.0756	39	2	16.9212	0.0155	29.414	2.106	35572
P46406	G3P_RABIT	Glyceraldehyde 3 phosphate dehydrogenase EC 1 2 1	35666	8.515	278.9782	6	18	28.012	3.6251	43	0	14.7237	0.0111	84.4838	3.0057	27758
P09189	HS7C_PETHY	Heat shock cognate 70 kDa protein	71182	4.9092	275.2816	6	54	12.1352	5.528	32	0	19.0806	0.0164	29.414	2.0951	35567
Q00043	HS70_AJECA	Heat shock 70 kDa protein	77510	5.374	231.6771	6	57	15.461	6.4494	30	0	14.5093	0.0158	29.414	2.2813	35458
P53421	HS71_PICAN	Heat shock protein 70 1 HSP72	69963	4.9131	231.3553	6	51	14.9068	8.2286	31	0	15.4872	0.0138	29.414	2.0592	35507
P29843	HS7A_DROME	Heat shock 70 kDa protein cognate 1 Heat shock 70	70642	5.17	219.5867	6	47	18.2527	6.0572	35	0	13.51	0.0124	32.1355	2.2715	35554
Q09810	YABA_SCHPO	Hypothetical 44 4 kDa protein C2G11 10c in chromos	44386	7.8794	158.3309	6	29	26.1845	8.7346	31	2	17.957	0.0145	8.8534	0.3932	94141
P24518	NADR_SALTY	Transcriptional regulator nadR	47070	5.5527	143.4372	6	37	29.7561	5.539	26	1	12.9372	0.0158	36.0724	1.699	48590
P41387	TBB_ONCGI	Tubulin beta chain	49920	4.7141	741.7727	5	33	23.4234	2.2127	77	1	13.3563	0.0122	320.5922	16.0144	78335
P18700	TBB_STRPU	Tubulin beta chain Fragment	33322	4.496	617.9194	5	20	30.8219	3.724	68	0	12.0254	0.0123	254.311	8.4799	78351
P12277	KCRB_HUMAN	Creatine kinase B chain EC 2 7 3 2 B CK	42617	5.2167	595.6894	5	24	18.8976	4.6797	64	0	14.3038	0.0116	449.1597	19.1541	40227
P05122	KCRB_CHICK	Creatine kinase B chain EC 2 7 3 2 B CK	42843	5.902	535.2069	5	25	13.9108	5.8823	69	0	16.2265	0.01	444.8338	19.0704	40226
Q9PVK2	ENOA_ALLMI	Alpha enolase EC 4 2 1 11 2 phospho D glycerate	47161	6.6953	534.1151	5	31	21.709	5.087	57	1	13.2714	0.0145	213.1057	10.0567	23157
Q00214	ACTM_STYPL	Actin muscle	42327	5.077	492.7652	5	34	21.6359	4.6288	57	0	13.1492	0.0137	253.1386	10.7215	1968
Q03342	ACT3_ECHGR	Actin 3 Fragment	34742	5.0958	489.6795	5	25	30.7443	6.9534	62	0	15.2079	0.0129	253.1386	8.8004	1874
P50138	ACT_PUCGR	Actin	41717	5.1594	450.1362	5	30	29.3333	7.0752	59	1	13.9674	0.0133	240.733	10.0494	2041
P05124	KCRB_CANFA	Creatine kinase B chain EC 2 7 3 2 B CK	42674	5.3763	443.5303	5	23	26.7717	4.4454	56	2	14.2236	0.0133	128.9916	5.5081	40225
P04689	TBA2_SCHPO	Tubulin alpha 2 chain	50547	4.6829	413.0338	5	36	21.1581	9.2095	50	1	15.1596	0.0148	107.0527	5.4147	78140
P49742	TBAB_SCHCO	Tubulin alpha 1B chain	49331	5.0449	404.2228	5	38	18.8341	5.6318	52	1	15.8332	0.0136	107.0527	5.2844	78166
Q9BE24	LDHA_MACFA	L lactate dehydrogenase A chain EC 1 1 1 27 LDH	36511	8.3721	382.9194	5	31	22.3565	2.2703	52	0	14.8247	0.0101	118.809	4.3406	41974
P00338	LDHA_HUMAN	L lactate dehydrogenase A chain EC 1 1 1 27 LDH	36534	8.3652	381.2604	5	31	22.6586	4.4012	54	1	12.8845	0.0106	118.809	4.3434	41972
P19023	ATP2_MAIZE	ATP synthase beta chain mitochondrial precursor	59067	5.9729	363.2227	5	37	15.5515	5.7389	37	0	15.5441	0.0095	33.9353	2.0057	5835
P34058	HS9B_RAT	Heat shock protein HSP 90 beta HSP 84	83133	4.8671	357.7866	5	66	8.4371	4.9509	26	0	12.346	0.0108	55.9171	4.6515	35633
P00340	LDHA_CHICK	L lactate dehydrogenase A chain EC 1 1 1 27 LDH	36360	7.8153	323.0299	5	29	41.6918	5.7615	48	3	14.646	0.0136	103.0729	3.7501	41960
P08439	G3P_ZYGRO	Glyceraldehyde 3 phosphate dehydrogenase EC 1 2 1	35579	6.3382	319.9025	5	34	22.5225	6.3325	49	2	15.6706	0.012	82.2635	2.9287	27779
P11021	GR78_HUMAN	78 kDa glucose regulated protein precursor GRP 78	72288	4.8748	318.4182	5	52	9.7859	7.8302	28	0	17.9372	0.0123	34.4199	2.4897	30754
Q9Y896	ACT2_SCHCO	Actin 2	41766	5.315	302.4552	5	34	15.4667	5.2057	41	1	15.1829	0.0148	109.6464	4.5825	1858
P26197	ACT2_ABSGL	Actin 2	42039	5.2359	292.8569	5	34	29.7082	7.2528	41	1	14.3434	0.015	109.6464	4.6125	1831
P00544	FGR_FSVGR	Tyrosine protein kinase transforming protein FGR	61476	5.7171	289.4366	5	37	11.9266	2.3865	32	0	15.8299	0.0132	109.6464	6.7451	25497
Q9U639	HS7D_MANSE	Heat shock 70 kDa protein cognate 4	71387	5.1482	283.0701	5	49	13.1902	5.9238	30	1	17.2803	0.0148	29.414	2.1011	35570
Q9TM41	ATPB_CYACA	ATP synthase beta chain EC 3 6 3 14	53244	6.5651	273.0966	5	40	19.5918	6.9577	32	1	16.0703	0.0105	18.7214	0.9974	6240
O65314	ACT_SCHDU	Actin	41828	5.0599	271.7023	5	34	35.1852	5.861	45	2	16.3479	0.0148	109.6464	4.5893	2042
Q05944	HS70_HYDMA	Heat shock 70 kDa protein	71423	5.5344	269.3019	5	52	12.9969	6.7853	36	3	15.8691	0.0152	29.414	2.1022	35469

P10592	HS72_YEAST	Heat shock protein SSA2	69296	4.7487	266.986	5	54	12.3824	5.9871	24	0	16.0218	0.0159	29.414	2.0395	35526
P50137	TKT_RAT	Transketolase EC 2 2 1 1 TK	67600	7.2133	265.2631	5	44	15.0883	5.742	31	0	14.0356	0.0157	15.05	1.018	79968
P08106	HS70_CHICK	Heat shock 70 kDa protein HSP70	69707	5.3604	264.2122	5	48	9.1483	9.0065	28	0	15.153	0.0125	29.414	2.0517	35464
P11145	HS74_TRYBB	Heat shock 70 kDa protein 4 HSP70	71391	5.0638	244.7078	5	46	15.4312	7.3351	39	2	13.6904	0.0132	29.414	2.0914	35539
P38982	RSP4_CRIGR	40S ribosomal protein SA P40 34 67 kDa laminin	32860	4.6617	210.6422	5	26	27.7966	7.0346	29	0	14.9986	0.0157	22.8984	0.7529	71617
P07029	ROU2_HUMAN	Heterogeneous nuclear ribonucleoprotein UP2 Fragm	24183	7.8327	160.8986	5	14	55.5556	4.6946	40	3	14.6267	0.0152	58.7947	1.4227	68615
P17132	ROC_RAT	Heterogeneous nuclear ribonucleoprotein C hnRNP C	18008	10.0571	147.6805	5	12	39.2405	4.5801	40	0	14.5678	0.0136	58.7947	1.0595	68556
P26368	U2AF_HUMAN	Splicing factor U2AF 65 kDa subunit U2 auxiliary	53467	9.3635	146.2892	5	26	18.1053	5.8569	29	0	19.2939	0.0134	16.806	0.8991	82500
P13084	NPM_RAT	Nucleophosmin NPM Nucleolar phosphoprotein B23	32539	4.4242	131.7983	5	22	21.2329	4.9501	29	0	17.3049	0.013	11.4286	0.3721	50671
Q63716	PDX1_RAT	Peroxiredoxin 1 Thioredoxin peroxidase 2 Thiore	22095	8.2425	113.4073	5	18	38.6935	4.5117	31	0	15.7277	0.0174	5.217	0.1153	55599
P30050	RL12_HUMAN	60S ribosomal protein L12	17807	9.8965	84.6366	5	15	35.1515	8.1959	19	0	20.9483	0.0148	10.8617	0.1935	66070
P05209	TBA1_CRIGR	Tubulin alpha 1 chain	50119	4.7622	829.1841	4	35	15.2993	3.76	83	0	14.0228	0.0104	467.847	23.4634	78105
P52273	TBA_BOMMO	Tubulin alpha chain	49873	4.7864	723.8331	4	35	18.6667	7.6634	79	2	15.1349	0.012	299.8134	14.9624	78175
P18258	TBA1_PARLI	Tubulin alpha 1 chain	50176	4.7194	718.2768	4	35	19.0265	2.993	75	0	15.3247	0.0113	299.8134	15.0533	78117
P02552	TBA1_CHICK	Tubulin alpha 1 chain Fragment	45871	4.7818	713.7037	4	33	16.9903	7.5928	74	0	13.6879	0.0115	394.6305	18.1139	78103
P04764	ENOA_RAT	Alpha enolase EC 4 2 1 11 2 phospho D glycerate	46955	6.1377	694.4021	4	31	18.9376	1.4724	67	0	14.259	0.0124	253.3919	11.9055	23164
P53478	ACT5_CHICK	Actin cytoplasmic type 5	41808	5.1537	642.4346	4	34	20.7447	2.5515	67	0	13.3118	0.014	258.4635	10.8131	1899
P53506	ACT8_XENLA	Actin cytoplasmic type 8	41820	5.1594	631.5379	4	35	21.2766	7.0435	66	0	12.9169	0.0138	258.4635	10.8162	1916
P10987	ACT1_DROME	Actin 5C	41794	5.1535	629.274	4	34	20.7447	2.5515	67	0	13.3118	0.014	258.4635	10.8095	1798
P53485	ACT2_FUGRU	Actin cytoplasmic 2 Beta actin 2	41739	5.1478	614.7429	4	34	17.6	4.9187	65	0	13.7237	0.0137	258.4635	10.7952	1842
P18603	ACT4_ARTSX	Actin clone 403	41810	5.1478	600.527	4	34	22.0745	4.115	64	0	13.5251	0.014	258.4635	10.8136	1889
Q94571	TBB2_HOMAM	Tubulin beta 2 chain Beta II tubulin	50897	4.6456	593.1722	4	32	28.9823	6.1277	63	3	13.308	0.0121	134.5784	6.8542	78251
P49128	ACT1_AEDAE	Actin 1	41763	5.6785	584.1883	4	36	27.3936	5.8148	69	1	13.4184	0.0141	258.4635	10.8014	1791
P20670	H2AO_HUMAN	Histone H2A o H2A o H2A 2 H2a 615	13955	11.3333	535.3417	4	7	49.6124	5.9353	98	0	13.9693	0.0094	72.2351	1.0087	32192
P19140	ENOA_ANAPL	Alpha enolase EC 4 2 1 11 2 phospho D glycerate	47079	6.3734	533.5181	4	31	17.552	6.7777	55	1	15.484	0.0131	210.3806	9.9108	23158
Q25008	TBA1_HOMAM	Tubulin alpha 1 chain Alpha I tubulin	50041	4.8278	533.3693	4	35	16.408	3.8857	66	1	15.5418	0.0123	152.7005	7.6463	78110
P51913	ENOA_CHICK	Alpha enolase EC 4 2 1 11 2 phospho D glycerate	47144	6.1403	532.0462	4	31	14.7806	4.1129	49	0	12.9011	0.0137	210.3806	9.9245	23160
P09653	TBB5_CHICK	Tubulin beta 5 chain Beta tubulin class V	49939	4.5842	523.5466	4	31	13.2287	3.9344	45	0	14.7192	0.0127	107.6477	5.3793	78285
P30436	TBA_ONCKE	Tubulin alpha chain	49283	4.7406	508.3869	4	34	11.9369	3.6427	59	0	15.7824	0.0113	149.3157	7.3635	78190
P53466	ACT2_LYTPI	Actin cytoskeletal 2 LPC2	41846	5.142	500.5599	4	34	18.883	2.5066	55	1	14.8182	0.0121	240.733	10.0805	1846
P53465	ACT1_LYTPI	Actin cytoskeletal 1 LPC1	41814	5.2414	491.3668	4	34	17.0213	4.4696	56	1	15.013	0.0125	240.733	10.0728	1805
P02576	ACTA_PHYPO	Actin plasmodial isoform	41641	5.0771	484.4079	4	34	22.6667	8.2723	52	0	16.3958	0.0114	240.733	10.031	1922
P53470	ACT1_SCHMA	Actin 1	41704	5.1537	483.5381	4	34	17.8191	5.3435	50	0	14.7766	0.0122	240.733	10.0462	1821
Q92193	ACT_CRAVI	Actin Fragment	29694	5.3216	466.5921	4	23	30.0752	4.0618	58	1	13.6104	0.0131	253.1386	7.5216	2015
P02577	ACT1_DICDI	Actin	41574	5.0711	465.4265	4	34	22.9333	1.7107	51	0	13.0593	0.0126	240.733	10.0149	1797
P10986	ACT4_CAEEL	Actin 4	41750	5.1478	443.0655	4	34	24.4681	3.5038	50	0	13.7365	0.0152	139.7823	5.8398	1891
O94128	TBA_MYCGR	Tubulin alpha chain	49976	4.7168	415.1623	4	36	22.8889	4.2607	50	1	14.3991	0.0127	107.0527	5.3535	78185
P24633	TBA1_EMENI	Tubulin alpha 1 chain	50339	4.7322	408.7271	4	36	16.4811	5.6955	48	1	15.5329	0.0136	107.0527	5.3924	78108
P08841	TBB3_DROME	Tubulin beta 3 chain	50867	4.6243	399.2384	4	31	15.859	4.6202	41	1	13.4072	0.0137	78.5938	4.0005	78268
P41385	TBB_BOMMO	Tubulin beta chain	50302	4.5414	365.9926	4	32	20.2222	7.2632	45	2	12.3553	0.0113	78.5938	3.956	78310
P04642	LDHA_RAT	L lactate dehydrogenase A chain EC 1 1 1 27 LDH	36427	8.3699	361.9266	4	31	18.9759	2.4322	45	0	13.1053	0.0115	118.809	4.3307	41986
Q25117	ATPB_HEMPU	ATP synthase beta chain mitochondrial precursor	56040	4.9167	352.419	4	35	17.9732	5.9095	36	1	14.0211	0.0111	31.8105	1.7838	6258
P35394	TBB_OCTDO	Tubulin beta chain	50415	4.6573	333.4316	4	32	23.7136	4.6779	44	2	14.0583	0.0127	47.0857	2.3754	78334
P27131	ACT1_NAEFO	Actin I	41700	5.0967	328.448	4	36	21.8667	3.5277	33	0	14.6265	0.0144	109.6464	4.5753	1807
P18602	ACT3_ARTSX	Actin clone 302 Fragment	36867	5.2297	328.3654	4	29	16.5138	6.1575	37	0	16.0112	0.0131	109.6464	4.045	1868
P53476	ACT_TOXGO	Actin	41880	4.8704	323.1953	4	39	19.4149	3.3582	34	1	15.6042	0.0137	109.6464	4.5951	2047
P13363	ACT_PHYME	Actin	41960	5.4694	322.0128	4	36	20.2667	5.9022	36	0	14.6816	0.0135	109.6464	4.6039	2034
P00360	G3P1_YEAST	Glyceraldehyde 3 phosphate dehydrogenase 1 EC 1 2	35596	8.5448	319.5415	4	30	33.8369	5.0807	38	1	14.2562	0.0114	82.2635	2.9301	27598
P29685	ATP2_HEVBR	ATP synthase beta chain mitochondrial precursor	60221	5.9171	318.7723	4	39	15.4804	4.8116	32	0	14.4633	0.011	31.8105	1.9169	5834
Q03341	ACT2_ECHGR	Actin 2	41855	5.2408	306.5767	4	34	14.3617	8.6095	36	1	15.1214	0.012	109.6464	4.5923	1841
P30169	ACT7_SOLTU	Actin 75	41900	5.1414	305.2027	4	33	22.5464	2.608	34	0	16.5251	0.0138	109.6464	4.3288	1911
O50290	ATPB_RICPR	ATP synthase beta chain EC 3 6 3 14	51237	4.662	304.1544	4	30	16.4557	5.3381	31	1	13.5892	0.012	22.8239	1.1702	6308
P34690	TBA2_CAEEL	Tubulin alpha 2 chain	49881	4.7516	298.7104	4	34	14.0625	6.7386	37	0	15.6429	0.0137	73.8964	3.6884	78127
P25113	PMGB_RAT	Phosphoglycerate mutase brain form EC 5 4 2 1	28496	6.2014	296.352	4	20	32.8063	6.0711	36	1	13.8033	0.0127	81.6361	2.3278	57842
Q40831	TBA1_PELFA	Tubulin alpha 1 chain	49905	4.7518	293.039	4	34	17.8808	5.1266	31	0	15.256	0.0148	73.8964	3.6902	78119
P22275	TBA3_MAIZE	Tubulin alpha 3 chain Alpha 3 tubulin	49529	4.9188	290.3136	4	35	14.2222	7.8369	31	0	14.9647	0.0134	73.8964	3.6624	78148
Q9Y701	ACT1_SUIBO	Actin 1	41624	5.3423	287.7543	4	35	15.7333	6.5588	37	1	13.7627	0.0131	109.6464	4.5668	1826
P20904	ACT_VOLCA	Actin	41731	5.1537	283.5714	4	34	20.4244	4.6445	41	1	16.3255	0.0137	109.6464	4.5787	2050
Q92G88	ATPB_RICCN	ATP synthase beta chain EC 3 6 3 14	51076	4.6813	277.955	4	28	16.0677	3.1141	28	0	15.9784	0.0114	22.8239	1.1665	6307
P10591	HS71_YEAST	Heat shock protein SSA1 Heat shock protein YG100	69483	4.799	273.838	4	52	12.9485	6.3276	25	1	16.9536	0.0144	29.414	2.045	35513
P04106	TBA_TRYBR	Tubulin alpha chain	49755	4.7512	267.8998	4	35	11.9734	8.5535	39	0	16.0094	0.0116	78.8041	3.9235	78202
Q00715	H2B_RAT	Histone H2B	13850	10.7878	263.1908	4	10	30.6452	3.1105	41	0	15.4406	0.012	548.0758	7.5958	32310
P30161	ACT_COSCS	Actin Fragment	37199	5.3551	263.1786	4	30	10.574	6.8729	27	0	15.3532	0.0126	109.6464	4.0814	2013
P02827	HS70_XENLA	Heat shock 70 kDa protein HSP70	70871	5.1392	252.3545	4	51	14.8377	4.7391	27	1	13.8216	0.0132	29.414	2.0859	35495
P24067	BIP2_MAIZE	Luminal binding protein 2 precursor BiP2 Heat s	73039	4.9103	246.8104	4	62	9.8039	3.8877	26	1	17.1434	0.0119	29.414	2.1497	7798
P42896	ENO_RICCO	Enolase EC 4 2 1 11 2 phosphoglycerate dehydrat	47882	5.4379	246.2456	4	34	18.2022	4.4923	37	1	16.6088	0.0154	115.0281	5.5113	23227
P34931	HS7H_HUMAN	Heat shock 70 kDa protein 1 HOM HSP70 HOM	70355	5.6453	229.189	4	48	13.1045	7.4203	21	0	16.4024	0.0122	29.414	2.0707	35574
P08865	RSP4_HUMAN	40S ribosomal protein SA P40 34 67 kDa laminin	32833	4.5932	206.448	4	26	28.1356	5.352	33	0	16.7333	0.0144	22.8984	0.7523	71621

P38983	RSP4_RAT	40S ribosomal protein SA P40 34 67 kDa laminin	32803	4.6022	196.1643	4	26	16.2712	4.8964	26	0	15.7664	0.0135	22.8984	0.7516	71623
Q24751	ATPB_DROVI	ATP synthase beta chain mitochondrial precursor	23949	5.7958	196.1096	4	16	26.7544	4.7995	26	0	19.5366	0.0121	18.7214	0.4487	6247
P14643	TBB_PLAFK	Tubulin beta chain	49718	4.5359	170.3184	4	31	12.5843	4.747	18	0	14.6598	0.0131	32.9732	1.6405	78343
P14140	TBB_PLAFA	Tubulin beta chain	49781	4.5018	169.892	4	31	12.5843	6.8777	20	0	18.1076	0.0164	32.9732	1.6425	78342
P15259	PMGM_HUMAN	Phosphoglycerate mutase muscle form EC 5 4 2 1	28616	9.2446	154.2681	4	20	26.9841	4.9358	25	0	16.9303	0.0127	48.0933	1.3772	57862
Q9ZSW1	TBB1_CYAPA	Tubulin beta 1 chain Beta 1 tubulin	49791	4.5961	148.0945	4	31	16.3311	8.1549	21	1	16.6308	0.0144	32.9732	1.6429	78214
P12457	TBB_EUGGR	Tubulin beta chain	49385	4.4242	130.49	4	31	14.2534	7.8963	18	0	19.597	0.0132	32.9732	1.6295	78320
P06748	NPM_HUMAN	Nucleophosmin NPM Nucleolar phosphoprotein B23	32554	4.444	109.0942	4	22	16.3265	2.2165	26	0	13.6549	0.0145	11.4286	0.3723	50669
Q9X767	PFLA_LISMO	Pyruvate formate lyase activating enzyme EC 1 97	28097	4.9609	103.9476	4	24	20.9677	6.4594	21	0	13.2573	0.0183	4.9016	0.1378	56248
P23358	RL12_RAT	60S ribosomal protein L12	17834	9.8965	81.0238	4	15	34.5455	5.988	20	1	16.4973	0.0138	10.8617	0.1938	66079
P08578	RUXE_HUMAN	Small nuclear ribonucleoprotein E snRNP E Sm pr	10796	9.7804	78.3456	4	4	72.8261	5.4146	29	2	17.3829	0.0153	11.7064	0.1265	72001
P17244	G3P_CRIGR	Glyceraldehyde 3 phosphate dehydrogenase EC 1 2 1	35594	8.4987	590.2339	3	19	20.4819	5.6523	68	1	13.5796	0.0114	233.6207	8.3208	27706
P07335	KCRB_RAT	Creatine kinase B chain EC 2 7 3 2 B CK	42685	5.2004	589.0782	3	23	12.8609	1.7064	57	0	13.4363	0.011	451.1776	19.2709	40231
P80534	G3P1_JACOR	Glyceraldehyde 3 phosphate dehydrogenase muscle	39388	8.9141	573.4907	3	25	23.1405	4.405	68	1	13.8309	0.0118	233.6207	9.2078	27593
P06605	TBA3_DROME	Tubulin alpha 3 chain	49858	4.8285	536.5869	3	35	12.4444	3.5436	51	0	14.4468	0.0112	152.7005	7.6183	78144
P53471	ACT2_SCHMA	Actin 2	41713	5.1537	512.759	3	34	18.883	3.8913	55	1	13.9976	0.0128	253.1386	10.5662	1859
Q9NY65	TBA8_HUMAN	Tubulin alpha 8 chain Alpha tubulin 8	50061	4.7567	503.489	3	35	10.9131	7.9814	51	0	15.3957	0.0114	152.7005	7.6493	78162
Q93131	ACTC_BRAFL	Actin cytoplasmic BfCA1	41693	5.1478	501.6621	3	34	14.9333	1.585	47	0	13.945	0.0116	240.733	10.0436	1937
P41339	ACTA_LIMPO	Actin acrosomal process isoform Actin 5	41747	5.2304	497.3423	3	34	12.766	8.4276	51	1	15.1575	0.0116	240.733	10.0566	1920
P92176	ACT2_LUMTE	Actin 2	41812	5.2357	496.0553	3	34	18.617	2.7329	47	0	13.9393	0.0124	240.733	10.0723	1844
P07829	ACT3_DICDI	Actin 3 SUB1	41757	5.0861	492.968	3	35	17.6	4.2501	53	1	13.8012	0.0123	240.733	10.059	1871
P41113	ACT3_PODCA	Actin 3	41799	5.142	491.4865	3	34	21.0106	1.8821	53	1	13.8008	0.0122	240.733	10.0691	1882
O22347	TBA1_ELEIN	Tubulin alpha 1 chain Alpha 1 tubulin	49699	4.7108	490.9277	3	35	15.0776	4.0915	50	0	13.6764	0.0125	321.528	15.99	78107
P25704	ENOB_RABIT	Beta enolase EC 4 2 1 11 2 phospho D glycerate	46908	7.6827	489.8306	3	29	10.8545	3.1743	45	0	14.1112	0.0123	158.0394	7.418	23170
Q07903	ACTC_STRPU	Actin cytoskeletal IIA	41773	5.142	480.225	3	34	15.4255	2.9886	48	0	13.873	0.0124	240.733	10.0629	1944
P45886	ACT3_BACDO	Actin 3 muscle specific	41788	5.1478	477.3292	3	34	12.5	3.2856	48	0	14.0441	0.0114	240.733	10.0665	1869
Q9Y702	ACT1_SCHCO	Actin 1 Beta actin	41591	5.1537	475.8036	3	34	22.6667	5.2438	50	1	13.6086	0.0115	240.733	10.0187	1820
P45887	ACT5_BACDO	Actin 5 muscle specific	41743	5.1478	475.4858	3	34	17.2872	5.9594	48	0	13.6414	0.0117	240.733	10.0556	1898
P12431	ACTM_STRPU	Actin muscle	41530	5.809	469.2625	3	36	15.7754	6.1926	47	0	13.7391	0.0112	240.733	9.8971	1966
P91754	ACT_LUMRU	Actin Fragment	41296	5.341	468.522	3	33	15.8602	1.7035	47	0	13.7722	0.0113	240.733	9.9479	2028
P00567	KCRB_RABIT	Creatine kinase B chain EC 2 7 3 2 B CK	42636	5.2097	464.7339	3	24	14.4357	3.1151	45	1	14.3872	0.0121	128.9916	5.5032	40230
P92182	ACT1_LUMTE	Actin 1	41818	5.1478	461.5403	3	34	20.2128	3.7559	55	1	13.6758	0.0134	240.733	10.0737	1803
O65316	ACT_MESVI	Actin	41562	5.1537	444.1467	3	32	15.1194	7.497	47	0	14.6437	0.0118	240.733	9.9852	2031
P10984	ACT2_CAEEL	Actin 2	41778	5.142	443.0655	3	34	23.9362	4.3453	51	1	14.5211	0.0153	139.7823	5.8437	1836
P09644	TBA5_CHICK	Tubulin alpha 5 chain	49916	4.7567	429.9084	3	35	16.2946	4.7679	50	2	14.6072	0.0119	119.1692	5.9523	78156
P50719	TBA_HAECO	Tubulin alpha chain	50078	4.8301	425.1556	3	35	10.2222	5.2341	47	1	15.5751	0.0116	119.1692	5.9717	78182
Q94572	TBA3_HOMAM	Tubulin alpha 3 chain Alpha III tubulin	49974	4.7567	410.7083	3	35	17.2949	5.8076	47	1	15.2311	0.0107	119.1692	5.9593	78146
P24637	TBB_PNECA	Tubulin beta chain	49086	4.7009	403.6846	3	29	13.3484	5.8362	38	1	16.523	0.0126	72.0362	3.5383	78345
P53372	TBA1_PNECA	Tubulin alpha chain	50350	4.9951	392.6057	3	35	13.8085	5.4515	42	1	13.6134	0.0127	107.0527	5.3936	78120
P50259	TBB1_PORPU	Tubulin beta 1 chain	50014	4.4899	391.6796	3	31	17.5055	5.1384	35	1	15.6538	0.0104	72.0362	3.6052	78231
Q92335	TBA_SORMA	Tubulin alpha chain	49786	4.7875	389.0664	3	31	14.4766	1.7994	44	1	13.473	0.0129	107.0527	5.3332	78197
P50258	TBAD_PHYPO	Tubulin alpha 1A chain	49821	4.823	374.4113	3	35	6.2222	7.6483	29	0	17.8458	0.0118	73.8964	3.684	78167
P04688	TBA1_SCHPO	Tubulin alpha 1 chain	51119	4.7897	363.6262	3	37	12.3077	7.039	42	1	14.3549	0.0132	107.0527	5.476	78121
P41937	TBB2_CAEEL	Tubulin beta chain	49767	4.6049	359.7253	3	31	18.2432	7.6623	34	1	11.9094	0.0131	45.6206	2.2719	78240
Q07244	ROK_HUMAN	Heterogeneous nuclear ribonucleoprotein K hnRNP K	50944	5.2203	358.5522	3	39	15.1188	3.0517	43	0	14.0008	0.0109	98.4876	5.0205	68579
P17317	H2AZ_HUMAN	Histone H2A z H2A z	13413	11.0354	346.671	3	7	34.6457	4.8224	57	0	14.2596	0.011	32.8996	0.4416	32206
P33625	TBA_EUGGR	Tubulin alpha chain	49860	4.8014	343.2773	3	35	15.7428	5.288	37	1	15.0966	0.0143	79.7969	3.9813	78179
P33623	TBA1_ANEPH	Tubulin alpha 1 chain	49754	4.8439	334.2202	3	35	10.643	6.4639	32	0	16.5227	0.0135	73.8964	3.6708	78101
P05304	TBB_GIALA	Tubulin beta chain	49924	4.6456	333.8278	3	31	10.9865	2.7695	33	1	15.9625	0.0132	99.2543	4.9584	78324
P13929	ENOB_HUMAN	Beta enolase EC 4 2 1 11 2 phospho D glycerate	46826	7.658	328.5745	3	28	8.545	7.7748	28	0	15.3006	0.013	115.0281	5.3897	23168
Q9W7L1	ENOA_TRASC	Alpha enolase EC 4 2 1 11 2 phospho D glycerate	47172	6.0417	324.7036	3	31	9.0069	6.4725	25	0	11.6682	0.0132	116.8358	5.5149	23166
P16106	H31_HUMAN	Histone H3 1 H3 a H3 c H3 d H3 f H3 h H	15263	11.5404	324.0855	3	12	34.8148	6.6852	48	0	14.1068	0.0121	116.5931	1.7807	32316
P09243	TBA2_STYLE	Tubulin alpha 2 chain	49326	4.8274	322.9846	3	36	11.3586	2.4447	30	0	18.8898	0.0119	73.8964	3.6474	78141
Q91883	GR78_XENLA	78 kDa glucose regulated protein precursor GRP 78	72590	4.7635	320.6134	3	52	8.5106	5.4072	19	0	13.5908	0.0135	32.6253	2.3698	30764
Q9PW07	LDHA_COLLI	L lactate dehydrogenase A chain EC 1 1 1 27 LDH	36373	7.8116	319.4906	3	29	11.1782	6.0058	32	0	14.0871	0.0109	103.0729	3.7515	41961
P17304	ACTM_APLCA	Actin muscle	41738	5.1478	316.838	3	34	13.8298	2.477	29	0	11.9312	0.0126	143.4923	5.9931	1956
P22132	ACT2_PHYIN	Actin 2	41930	5.2533	314.5078	3	36	15.2	9.4847	30	0	16.2785	0.0129	109.6464	4.6006	1855
P30171	ACTB_SOLTU	Actin 97	41615	5.1583	309.4706	3	35	15.1194	6.2073	33	0	13.7594	0.0138	113.8373	4.7405	1932
Q40832	TBA2_PELFA	Tubulin alpha 2 chain	49948	4.7197	296.2566	3	35	11.9205	9.3492	34	1	16.58	0.014	73.8964	3.6934	78139
Q90593	GR78_CHICK	78 kDa glucose regulated protein precursor GRP 78	71974	4.9341	292.5913	3	52	6.2883	2.7456	19	0	13.0756	0.0121	29.414	2.1184	30752
P26182	ACT_ACHBI	Actin	41823	5.1509	292.4547	3	37	21.8085	4.8973	34	1	15.568	0.0133	109.6464	4.5888	1999
P02581	ACT1_SOYBN	Actin 1	41330	5.2258	286.5408	3	27	21.4854	7.2385	35	1	14.7609	0.0114	109.6464	4.498	1824
P00358	G3P2_YEAST	Glyceraldehyde 3 phosphate dehydrogenase 2 EC 1 2	35693	6.5068	282.1055	3	28	16.3142	5.7169	35	1	14.9559	0.0083	82.2635	2.9381	27615
P27132	ACT2_NAEFO	Actin II Fragment	41126	5.0696	276.049	3	34	21.8329	5.7593	33	1	15.5362	0.0136	109.6464	4.5123	1848
O65719	HS73_ARATH	Heat shock cognate 70 kDa protein 3 Hsc70 3	71103	4.7708	271.4206	3	54	8.9368	6.2769	22	1	13.6877	0.0159	29.414	2.0927	35527
Q07972	TBAA_PNECA	Tubulin alpha chain Fragment	23819	7.164	268.722	3	16	15.566	6.1432	28	0	16.0163	0.0129	73.8964	1.7613	78164
P09643	TBA4_CHICK	Tubulin alpha 4 chain Fragment	35912	4.5738	244.638	3	23	24.8447	8.6999	36	1	14.9225	0.0123	78.8041	2.8319	78152
P27322	HS72_LYCES	Heat shock cognate 70 kDa protein 2	70662	4.8807	221.092	3	51	9.9379	7.5663	18	0	12.2623	0.0125	29.414	2.0798	35520
P55063	HS73_RAT	Heat shock 70 kDa protein 3 HSP70 3	70505	5.8319	219.4503	3	52	10.2964	5.5854	20	1	12.6571	0.0144	29.414	2.0751	35531
Q9JJ54	ROD_RAT	Heterogeneous nuclear ribonucleoprotein D0 hnRNP	38168	7.8979	177.8547	3	24	14.1643	1.9366	26	0	14.7249	0.0131	58.7947	2.2455	68568

P04961	PCNA_RAT	Proliferating cell nuclear antigen PCNA Cyclin	28730	4.3755	149.9738	3	23	15.3257	4.0426	14	0	15.9288	0.0204	11.8413	0.3404	55384
Q9RSG0	LYTB_DEIRA	LytB protein homolog	36294	5.1324	127.4708	3	23	11.6418	7.1055	12	0	20.0054	0.0166	1.4142	0.0514	43948
P40307	PSB2_RAT	Proteasome subunit beta type 2 EC 3 4 25 1 Prot	22897	7.2667	125.683	3	19	20.398	8.3605	16	1	13.269	0.0155	4.2576	0.0976	60347
P27278	NADR_ECOLI	Transcriptional regulator nadR	47315	5.2917	125.5729	3	35	16.8293	7.4027	18	1	12.9465	0.0146	36.0724	1.7079	48587
P36255	RL7_MYCGE	50S ribosomal protein L7 L12	13052	4.8206	106.4994	3	10	25.4098	7.6979	19	0	15.8577	0.0129	4.2576	0.0556	67691
P55272	CDN5_RAT	Cyclin dependent kinase 4 inhibitor B P14 INK4B	13739	5.3254	90.3335	3	12	18.4615	3.913	14	0	22.0112	0.0137	1.6149	0.0222	11111
P18288	TBAT_ONCMY	Tubulin alpha chain testis specific	49961	4.7966	717.1216	3	35	15.1111	3.013	74	1	14.292	0.0113	299.8134	14.9888	78171
P29510	TBA2_ARATH	Tubulin alpha 2 alpha 4 chain	49509	4.743	498.7438	2	35	8.4444	5.143	47	1	13.3283	0.0119	315.8264	15.6464	78126
P53473	ACTB_STRPU	Actin cytoskeletal IB	41738	5.1418	496.3771	2	34	15.1596	1.7223	47	1	13.4513	0.0117	240.733	10.0544	1933
Q10453	H33_CAEEL	Histone H3 3	15201	11.6797	486.5024	2	12	42.2222	6.7429	79	0	14.0841	0.0133	101.3608	1.5418	32327
P92179	ACT_BIOGL	Actin	41909	5.1478	484.8539	2	34	14.8936	2.8838	51	1	13.1355	0.0121	240.733	10.0957	2001
P53458	ACT5_DIPDE	Actin 5 Fragment	41156	5.4575	484.7069	2	33	15.0943	2.9737	51	2	13.7975	0.0128	240.733	9.9142	1900
P53501	ACT3_DROME	Actin 57B	41807	5.0709	466.1548	2	35	11.9681	4.9647	49	1	13.6465	0.0121	240.733	10.0711	1873
P10875	TBB_CANAL	Tubulin beta chain	49910	4.4381	391.2248	2	30	14.6993	6.043	35	1	15.046	0.0126	72.0362	3.5976	78312
P35432	ACT1_ECHGR	Actin 1	41800	5.155	369.2443	2	32	16.8	3.9983	31	1	15.9107	0.0124	109.6464	4.5863	1799
P08985	H2AV_DROME	Histone H2A variant	14841	10.6794	364.3352	2	11	27.8571	6.4026	51	0	13.0718	0.0113	32.8996	0.4886	32196
P30163	ACT2_ONCVO	Actin 2	41791	5.1537	353.3517	2	34	16.7553	6.0481	34	1	15.0161	0.0139	122.0519	5.1041	1849
P08991	H2AV_STRPU	Histone H2A variant Fragment	13156	11.0354	346.671	2	7	34.4	3.8319	51	0	13.4492	0.0114	32.8996	0.4331	32198
P11480	TBAE_PHYPO	Tubulin alpha 2B chain Tubulin alpha E chain	49607	4.8223	342.0682	2	35	6.0134	1.4085	26	0	15.2209	0.0127	73.8964	3.6682	78168
P46258	ACT3_PEA	Actin 3	41607	5.1638	332.4516	2	35	12.7321	7.6142	33	1	15.1063	0.0132	111.5741	4.6454	1881
P53494	ACT4_ARATH	Actin 4	41751	5.2397	324.4822	2	35	9.5491	7.1557	27	0	14.5546	0.0119	109.6464	4.5809	1888
P00359	G3P3_YEAST	Glyceraldehyde 3 phosphate dehydrogenase 3 EC 1 2	35593	6.5068	323.6433	2	29	6.3444	5.7318	27	0	13.2821	0.0073	82.2635	2.9299	27622
P81228	ACT5_SOLTU	Actin 66 Fragment	37171	5.4441	322.6461	2	31	10.119	2.4171	29	0	14.5409	0.0116	121.16	4.5066	1902
P30162	ACT1_ONCVO	Actin 1	41744	5.1537	319.665	2	34	16.7553	5.509	35	1	15.0962	0.0133	122.0519	5.0983	1808
P93584	ACT9_SOLTU	Actin 82 Fragment	37208	5.4397	315.5777	2	31	11.9048	5.566	27	0	14.6863	0.0125	109.6464	4.0824	1917
Q05825	ATPB_DROME	ATP synthase beta chain mitochondrial precursor	54105	5.0821	313.5788	2	32	13.2673	5.564	27	1	13.8353	0.0095	31.8105	1.7222	6246
P53497	ACTC_ARATH	Actin 12	41767	5.2397	312.2555	2	35	16.1804	6.0725	30	1	15.4585	0.0121	109.6464	4.5827	1935
P09104	ENOG_HUMAN	Gamma enolase EC 4 2 1 11 2 phospho D glycerate	47124	4.7518	307.0987	2	30	9.4688	4.6971	23	0	12.1291	0.0128	115.0281	5.4241	23173
P30167	ACT3_SOLTU	Actin 58	41759	5.3458	305.6437	2	34	12.2016	3.8524	27	0	15.3462	0.0122	111.1465	4.6444	1883
Q05214	ACT1_TOBAC	Actin	41711	5.3414	302.9246	2	34	9.0186	11.0981	27	0	15.854	0.0117	109.6464	4.5765	1828
O65315	ACT_COLSC	Actin	41678	5.1537	301.5899	2	34	9.0186	4.3497	27	0	15.0067	0.0134	109.6464	4.5729	2011
P22131	ACT1_PHYIN	Actin 1	41854	5.1568	296.0745	2	37	18.3511	4.9723	36	2	15.3512	0.0133	109.6464	4.5922	1815
P53504	ACT1_SORBI	Actin 1	41835	5.3236	295.4765	2	34	10.8753	7.2842	28	0	15.1278	0.0126	109.6464	4.5901	1823
P30668	TBB_SCHCO	Tubulin beta chain	49883	4.5665	291.9617	2	31	8.0899	1.7861	23	0	12.7517	0.0113	99.2543	4.9543	78349
P07304	TBA1_STYLE	Tubulin alpha 1 chain	49104	4.7188	291.6006	2	34	10.1124	6.5532	28	0	14.3942	0.0137	73.8964	3.631	78122
P11139	TBA1_ARATH	Tubulin alpha 1 chain	49768	4.7355	291.1344	2	31	6.2222	4.3126	25	0	14.8386	0.0125	73.8964	3.6801	78102
Q03684	BIP4_TOBAC	Luminal binding protein 4 precursor BiP 4 78 kD	73477	4.8787	290.4351	2	66	10.3448	6.6865	27	3	14.869	0.0143	29.414	2.1626	7802
P30168	ACT6_SOLTU	Actin 71	41755	5.2449	289.9611	2	34	18.0371	5.876	44	3	15.9418	0.014	109.6464	4.5691	1907
Q03685	BIP5_TOBAC	Luminal binding protein 5 precursor BiP 5 78 kD	73699	4.8904	286.1054	2	64	7.0359	0.7109	15	0	11.6747	0.0131	29.414	2.1691	7803
Q27352	TBA_TRYCR	Tubulin alpha chain	49696	4.7142	278.9905	2	34	11.3082	7.5567	34	1	14.5881	0.0119	81.7158	4.0636	78203
P14659	HS72_RAT	Heat shock related 70 kDa protein 2 Heat shock pr	69485	5.2674	278.5038	2	50	6.1611	5.487	15	0	13.5643	0.0164	29.414	2.0451	35524
P93375	ACT7_TOBAC	Actin 104 Fragment	37120	5.4706	274.9634	2	30	7.1429	6.8865	25	0	15.3149	0.0116	109.6464	4.0728	1913
P54652	HS72_HUMAN	Heat shock related 70 kDa protein 2 Heat shock 70	69977	5.4073	271.6127	2	50	5.1643	1.6098	15	0	14.5999	0.0147	29.414	2.0596	35519
Q28259	G3P_CANFA	Glyceraldehyde 3 phosphate dehydrogenase EC 1 2 1	6678	6.0192	266.5935	2	3	53.9683	8.6615	29	0	14.5447	0.0089	82.2635	0.5497	27690
P30164	ACT1_PEA	Actin 1	41699	5.2599	264.3018	2	35	8.5106	2.3985	27	0	14.9186	0.0121	109.6464	4.5751	1814
P02553	TBA_LYTPI	Tubulin alpha chain Fragment	18012	4.5196	263.6154	2	15	11.8012	3.1953	23	0	14.9993	0.012	73.8964	1.3319	78184
P02279	H2B_CHICK	Histone H2B	13782	10.6934	261.483	2	11	20	5.946	33	0	13.8751	0.0123	548.0758	7.5585	32295
Q01877	HS71_PUCGR	Heat shock protein HSS1	70538	4.9391	246.2297	2	53	11.8827	6.1798	20	2	15.3496	0.0149	29.414	2.0761	35509
O24581	BIP3_MAIZE	Luminal binding protein 3 precursor BiP3	73111	4.9411	245.8451	2	62	6.4857	4.4234	17	1	13.1331	0.0155	29.414	2.1518	7800
P24263	ACTD_PHYPO	Actin spherule isoform	40492	5.4232	241.6961	2	29	15.847	4.116	30	1	15.1206	0.0131	109.6464	4.4427	1946
P16865	H2A3_VOLCA	Histone H2A III	13545	10.6395	238.3276	2	7	25.5814	6.473	31	0	11.9397	0.0137	225.23	3.0527	32178
P14834	HS70_LEIMA	Heat shock 70 kDa protein Fragment	56500	6.4658	202.6228	2	38	6.2016	0.7452	14	0	13.553	0.0121	29.414	1.6629	35474
P50890	RSP4_CHICK	40S ribosomal protein SA P40 34 67 kDa laminin	33000	4.6022	196.1643	2	26	19.5946	5.7353	21	1	11.537	0.0137	22.8984	0.7561	71613
P19208	HS7C_CAEBR	Heat shock 70 kDa protein C precursor Fragment	48799	5.432	194.1835	2	33	12.9252	6.1127	19	1	13.6831	0.0155	29.414	1.4363	35559
P26452	RSP4_BOVIN	40S ribosomal protein P40 C10 protein	32876	4.6022	173.3223	2	26	7.1186	2.7124	12	0	10.3363	0.0136	12.353	0.4064	71610
Q9N2N6	TBB_EUPFO	Tubulin beta chain Beta tubulin	49774	4.6626	151.2619	2	31	7.2072	2.0839	12	0	14.384	0.0133	32.9732	1.6423	78322
P34108	TBB_NAEGR	Tubulin beta chain	50478	4.5652	149.126	2	31	13.082	4.2679	17	1	12.8207	0.0178	32.9732	1.6655	78332
P57761	PCNA_CRIGR	Proliferating cell nuclear antigen PCNA	28776	4.3755	148.848	2	23	18.0077	5.4444	15	1	16.0059	0.0199	11.8413	0.341	55366
P20365	TBB_EUPCR	Tubulin beta chain Beta tubulin	49892	4.5593	145.3324	2	31	8.9686	8.0862	11	0	16.0979	0.0093	32.9732	1.6462	78321
Q08115	TBB_EUPOC	Tubulin beta chain Beta tubulin	49586	4.602	143.5899	2	31	11.036	5.2531	15	1	13.3429	0.0129	32.9732	1.6361	78323
Q9V1C7	Y339_PYRAB	Hypothetical protein PAB0339	24459	5.5366	121.3101	2	17	15.5556	11.4975	11	0	17.3911	0.0086	5.1785	0.1267	91474
O02722	TIM1_HORSE	Metalloproteinase inhibitor 1 precursor TIMP 1	23031	7.6326	70.824	2	13	13.5266	9.0085	10	0	18.7899	0.01	1.8269	0.0421	79815
P16105	H32_BOVIN	Histone H3 H3 2	15247	11.6797	542.5127	2	12	28.1481	5.6535	66	0	13.6936	0.0111	364.5874	5.5625	32320

9.16 Appendix table 7.2

Appendix table 7.2 Mass Spectrometry results of membrane preparation of P4 NrlGFP sorted cells (Run 1)

Appendix Table 7.2 A Mass spectrometry results of P4 NrlGFP positive cells

Entry	Description	mW (Da)	pI (pH)	Theoretical Peptides	Coverage (%)	Digest Peptides	Amount (fmol)	Amount (ngrams)
P16858	G3P MOUSE Glyceraldehyde 3 phosphate dehydrogenase OS Mus musculus GN Gapdh PE 1 SV 2	35787	8.3507	19	49.8498	13	292.2957	10.4671
P99024	TBB5 MOUSE Tubulin beta 5 chain OS Mus musculus GN Tubb5 PE 1 SV 1	49638	4.5903	30	68.4685	20	130.4988	6.482
P68372	TBB2C MOUSE Tubulin beta 2C chain OS Mus musculus GN Tubb2c PE 1 SV 1	49799	4.602	30	54.6067	17	24.1877	1.2053
Q7TMM9	TBB2A MOUSE Tubulin beta 2A chain OS Mus musculus GN Tubb2a PE 1 SV 1	49874	4.5903	30	47.4157	13	2.8681	0.1431
P17742	PPIA MOUSE Peptidyl prolyl cis trans isomerase A OS Mus musculus GN Ppia PE 1 SV 2	17959	8.003	12	53.6585	6	74.5241	1.3393
P68369	TBA1A MOUSE Tubulin alpha 1A chain OS Mus musculus GN Tuba1a PE 1 SV 1	50103	4.7622	34	56.0976	19	25.2345	1.2651
P05213	TBA1B MOUSE Tubulin alpha 1B chain OS Mus musculus GN Tuba1b PE 1 SV 2	50119	4.7622	34	53.2151	19	161.4343	8.0962
Q64467	G3PT MOUSE Glyceraldehyde 3 phosphate dehydrogenase testis specific OS Mus musculus GN Gapdhs PE 1	47626	7.8001	30	7.0455	4	1.9385	0.0924
Q9ERD7	TBB3 MOUSE Tubulin beta 3 chain OS Mus musculus GN Tubb3 PE 1 SV 1	50386	4.6326	30	25.5556	11	0	
Q04447	KCRB MOUSE Creatine kinase B type OS Mus musculus GN Ckb PE 1 SV 1	42686	5.2866	23	41.2073	12	72.1535	3.0819
P17182	ENOA MOUSE Alpha enolase OS Mus musculus GN Eno1 PE 1 SV 3	47111	6.3752	30	21.4286	10	54.6878	2.578
P63260	ACTG MOUSE Actin cytoplasmic 2 OS Mus musculus GN Actg1 PE 1 SV 1	41765	5.1594	34	30.4	17	79.84	3.33
P00924	ENO1 YEAST Enolase 1 EC 4 2 1 11 2 phosphoglycerate dehydr	46642	6.1527	28	22.2477	12	50	2.3335
Q922F4	TBB6 MOUSE Tubulin beta 6 chain OS Mus musculus GN Tubb6 PE 1 SV 1	50058	4.5903	31	19.2394	7	36.5173	1.8292
P26645	MARCS MOUSE Myristoylated alanine rich C kinase substrate OS Mus musculus GN Marcks PE 1 SV 2	29643	4.1239	25	26.5372	8	18.29	0.5425
P68033	ACTC MOUSE Actin alpha cardiac muscle 1 OS Mus musculus GN Actc1 PE 1 SV 1	41991	5.0709	34	8.4881	10	22.4112	0.9417
O89086	RBM3 MOUSE Putative RNA binding protein 3 OS Mus musculus GN Rbm3 PE 1 SV 1	16594	7.6776	13	20.915	2	47.5206	0.7891
P10126	EF1A1 MOUSE Elongation factor 1 alpha 1 OS Mus musculus GN Eef1a1 PE 1 SV 3	50082	9.3417	32	12.987	9	34.7412	1.741
P18760	COF1 MOUSE Cofilin 1 OS Mus musculus GN Cfl1 PE 1 SV 3	18547	8.2196	19	16.8675	4	13.5565	0.2516
P47955	RLA1 MOUSE 60S acidic ribosomal protein P1 OS Mus musculus GN Rplp1 PE 1 SV 1	11467	4.0217	7	14.0351	1	44.287	0.5082
Q91XV3	BASP1 MOUSE Brain acid soluble protein 1 OS Mus musculus GN Basp1 PE 1 SV 3	22073	4.2828	22	15.9292	4	5.3663	0.1185
P68254	1433T MOUSE 14 3 3 protein theta OS Mus musculus GN Ywhaq PE 1 SV 1	27760	4.4934	24	4.898	8	14.9078	0.4141
Q61171	PRDX2 MOUSE Peroxiredoxin 2 OS Mus musculus GN Prdx2 PE 1 SV 3	21765	5.0387	17	4.0404	6	22.7988	0.4965
P61979	HNRPK MOUSE Heterogeneous nuclear ribonucleoprotein K OS Mus musculus GN Hnrnpk PE 1 SV 1	50944	5.2203	38	7.5594	10	33.4423	1.7048
P01942	HBA MOUSE Hemoglobin subunit alpha OS Mus musculus GN Hba PE 1 SV 2	15075	8.6376	9	8.4507	1	44.4156	0.67
P14733	LMNB1 MOUSE Lamin B1 OS Mus musculus GN Lmnb1 PE 1 SV 3	66744	4.9213	69	2.7211	13	31.5536	2.1073
P28667	MRP MOUSE MARCKS related protein OS Mus musculus GN Marcksl1 PE 1 SV 2	20153	4.3993	15		2	4.4322	0.0894
Q60932	VDAC1 MOUSE Voltage dependent anion selective channel protein 1 OS Mus musculus GN Vdac1 PE 1 SV 3	32331	8.6711	21		6	20.6201	0.6671
P52480	KPYM MOUSE Pyruvate kinase isozymes M1 M2 OS Mus musculus GN Pkm2 PE 1 SV 4	57808	7.2131	45		12	22.4032	1.2959
P63101	1433Z MOUSE 14 3 3 protein zeta delta OS Mus musculus GN Ywhaz PE 1 SV 1	27753	4.5273	25		7	8.3832	0.2328
P63158	HMGB1 MOUSE High mobility group protein B1 OS Mus musculus GN Hmgb1 PE 1 SV 2	24878	5.4465	17		4	13.321	0.3316
P51880	FABP7 MOUSE Fatty acid binding protein brain OS Mus musculus GN Fabp7 PE 1 SV 2	14883	5.2996	12		2	17.6197	0.2624
P56480	ATPB MOUSE ATP synthase subunit beta mitochondrial OS Mus musculus GN Atp5b PE 1 SV 2	56265	5.0259	37		8	11.4701	0.6458
Q9D0J8	PTMS MOUSE Parathymosin OS Mus musculus GN Ptms PE 2 SV 3	11423	3.9613	9		1	1.9717	0.0225
O88569	ROA2 MOUSE Heterogeneous nuclear ribonucleoproteins A2 B1 OS Mus musculus GN Hnrnpa2b1 PE 1 SV 2	37379	9.1939	29	2.8329	6	25.3172	0.9469
Q37595	COX2 PERFA Cytochrome c oxidase subunit 2 OS Perognathus flavus GN MT CO2 PE 3 SV 1	25630	4.3949	11		2	0	
P06151	LDHA MOUSE L lactate dehydrogenase A chain OS Mus musculus GN Ldha PE 1 SV 3	36475	7.669	28		4	7.9637	0.2907
P62827	RAN MOUSE GTP binding nuclear protein Ran OS Mus musculus GN Ran PE 1 SV 3	24407	7.312	17		3	11.3994	0.2784
P11499	HS90B MOUSE Heat shock protein HSP 90 beta OS Mus musculus GN Hsp90ab1 PE 1 SV 2	83273	4.775	67		9	16.3153	1.3595
P62259	1433E MOUSE 14 3 3 protein epsilon OS Mus musculus GN Ywhae PE 1 SV 1	29155	4.4355	29		4	9.7774	0.2852
P07724	ALBU MOUSE Serum albumin OS Mus musculus GN Alb PE 1 SV 3	68647	5.6752	54		3	27.355	1.8791
P14206	RSSA MOUSE 40S ribosomal protein SA OS Mus musculus GN Rpsa PE 1 SV 4	32817	4.6022	25		4	6.9119	0.227
P07901	HS90A MOUSE Heat shock protein HSP 90 alpha OS Mus musculus GN Hsp90aa1 PE 1 SV 4	84734	4.7357	91		4	3.804	0.3225
O35737	HNRH1 MOUSE Heterogeneous nuclear ribonucleoprotein H OS Mus musculus GN Hnrnph1 PE 1 SV 3	49168	5.8513	27		6	12.3296	0.6066
Q8BG05	ROA3 MOUSE Heterogeneous nuclear ribonucleoprotein A3 OS Mus musculus GN Hnrnpa3 PE 1 SV 1	39627	9.2212	32		6	16.3854	0.6497
P49312	ROA1 MOUSE Heterogeneous nuclear ribonucleoprotein A1 OS Mus musculus GN Hnrnpa1 PE 1 SV 2	34175	9.5198	29		3	5.2826	0.1806
P09411	PGK1 MOUSE Phosphoglycerate kinase 1 OS Mus musculus GN Pgk1 PE 1 SV 4	44521	7.9043	32		4	8.783	0.3913
P17183	ENOG MOUSE Gamma enolase OS Mus musculus GN Eno2 PE 1 SV 2	47267	4.7996	30		4	10.4937	0.4963
Q62433	NDRG1 MOUSE Protein NDRG1 OS Mus musculus GN Ndrg1 PE 1 SV 1	42980	5.6483	20		3	8.0218	0.345
P35564	CALX MOUSE Calnexin OS Mus musculus GN Canx PE 1 SV 1	67235	4.2949	44		3	12.1988	0.8207
P28656	NP1L1 MOUSE Nucleosome assembly protein 1 like 1 OS Mus musculus GN Nap1l1 PE 1 SV 2	45316	4.1589	25		3	10.6917	0.4848
Q9CQV8	1433B MOUSE 14 3 3 protein beta alpha OS Mus musculus GN Ywhab PE 1 SV 3	28068	4.5745	22		3	0.543	0.0153
P70459	ERF MOUSE ETS domain containing transcription factor ERF OS Mus musculus GN Erf PE 2 SV 1	59013	6.9192	31		1	10.9955	0.6493
P61027	RAB10 MOUSE Ras related protein Rab 10 OS Mus musculus GN Rab10 PE 1 SV 1	22526	8.5735	18		4	3.2215	0.0726
P63017	HSP7C MOUSE Heat shock cognate 71 kDa protein OS Mus musculus GN Hspa8 PE 1 SV 1	70827	5.1998	50		9	6.0082	0.4258
Q6P5F9	XPO1 MOUSE Exportin 1 OS Mus musculus GN Xpo1 PE 1 SV 1	123013	5.6552	88		6	12.9072	1.5888
P56695	WFS1 MOUSE Wolframin OS Mus musculus GN Wfs1 PE 1 SV 1	100514	7.8706	52		3	12.8751	1.295
P55258	RAB8A MOUSE Ras related protein Rab 8A OS Mus musculus GN Rab8a PE 1 SV 2	23653	9.4319	17		3	1.3939	0.033
P70168	IMB1 MOUSE Importin subunit beta 1 OS Mus musculus GN Kpnb1 PE 1 SV 1	97090	4.4865	62		5	6.8265	0.6632
P60335	PCBP1 MOUSE Poly rC binding protein 1 OS Mus musculus GN Pcbp1 PE 1 SV 1	37473	6.7136	24		3	4.9154	0.1843
O08553	DPYL2 MOUSE Dihydropyrimidinase related protein 2 OS Mus musculus GN Dpysl2 PE 1 SV 2	62238	5.9229	43		5	2.4237	0.1509

Red indicates plasma membrane proteins. Note P00924 ENO1 Yeast is a positive control that added during Mass Spec mapping.

Appendix Table 7.2 B Mass spectrometry results of P4 NrlGFP negative cells

Entry	Description	mW (Da)	pI (pH)	Theoretical Peptides	Coverage (%)	Digest Peptides	Amount (fmol)	Amount (ngrams)
Q8CGP6	H2A1H MOUSE Histone H2A type 1 H OS Mus musculus GN Hist1h2ah PE 1 SV 3	13941	11.454	7	37.5	2	683.5786	9.5361
Q64523	H2A2C MOUSE Histone H2A type 2 C OS Mus musculus GN Hist2h2ac PE 1 SV 3	13979	11.333	7	14.7287	2	0	
P62806	H4 MOUSE Histone H4 OS Mus musculus GN Hist1h4a PE 1 SV 2	11360	11.767	11	48.5437	6	113.2583	1.2874
P16858	G3P MOUSE Glyceraldehyde 3 phosphate dehydrogenase OS Mus musculus GN Gapdh PE 1 SV 2	35787	8.3507	19	47.4474	11	235.7324	8.4416
P10853	H2B1F MOUSE Histone H2B type 1 F J L OS Mus musculus GN Hist1h2bf PE 1 SV 2	13927	10.739	11	28.5714	3	409.44	5.71
P99024	TBB5 MOUSE Tubulin beta 5 chain OS Mus musculus GN Tubb5 PE 1 SV 1	49638	4.5903	30	43.018	15	166.0173	8.2462
P68372	TBB2C MOUSE Tubulin beta 2C chain OS Mus musculus GN Tubb2c PE 1 SV 1	49799	4.602	30	32.809	12	15.8904	0.7918
Q9CWF2	TBB2B MOUSE Tubulin beta 2B chain OS Mus musculus GN Tubb2b PE 1 SV 1	49920	4.5903	30	30.1124	12	2.2063	0.1102
P68369	TBA1A MOUSE Tubulin alpha 1A chain OS Mus musculus GN Tuba1a PE 1 SV 1	50103	4.7622	34	33.2594	16	28.1914	1.4134
P68373	TBA1C MOUSE Tubulin alpha 1C chain OS Mus musculus GN Tuba1c PE 1 SV 1	49877	4.7856	34	33.4076	16	186.3768	9.302
P05213	TBA1B MOUSE Tubulin alpha 1B chain OS Mus musculus GN Tuba1b PE 1 SV 2	50119	4.7622	34	27.2727	16	0	
P47955	RLA1 MOUSE 60S acidic ribosomal protein P1 OS Mus musculus GN Rplp1 PE 1 SV 1	11467	4.0217	7	14.0351	1	46.4574	0.5331
P63260	ACTG MOUSE Actin cytoplasmic 2 OS Mus musculus GN Actg1 PE 1 SV 1	41765	5.1594	34	9.0667	9	0	
P17742	PPIA MOUSE Peptidyl prolyl cis trans isomerase A OS Mus musculus GN Ppia PE 1 SV 2	17959	8.003	12	27.439	4	53.3011	0.9579
P68433	H31 MOUSE Histone H3 1 OS Mus musculus GN Hist1h3a PE 1 SV 2	15394	11.54	12	23.5294	5	66.3964	1.0228
Q9ERD7	TBB3 MOUSE Tubulin beta 3 chain OS Mus musculus GN Tubb3 PE 1 SV 1	50386	4.6326	30	3.1111	8	0	
P00924	ENO1 YEAST Enolase 1 EC 4 2 1 11 2 phosphoglycerate dehydr	46642	6.1527	28	8.945	11	50	2.3335
Q04447	KCRB MOUSE Creatine kinase B type OS Mus musculus GN Ckb PE 1 SV 1	42686	5.2866	23	7.874	6	118.6838	5.0694
Q922F4	TBB6 MOUSE Tubulin beta 6 chain OS Mus musculus GN Tubb6 PE 1 SV 1	50058	4.5903	31	3.132	8	1.5514	0.0777
P17182	ENOA MOUSE Alpha enolase OS Mus musculus GN Eno1 PE 1 SV 3	47111	6.3752	30	10.8295	8	56.9848	2.6863
P10126	EF1A1 MOUSE Elongation factor 1 alpha 1 OS Mus musculus GN Eef1a1 PE 1 SV 3	50082	9.3417	32		5	46.8196	2.3463
P63268	ACTH MOUSE Actin gamma enteric smooth muscle OS Mus musculus GN Actg2 PE 2 SV 1	41849	5.1594	33		6	21.6764	0.9077
P84228	H32 MOUSE Histone H3 2 OS Mus musculus GN Hist1h3b PE 1 SV 2	15378	11.68	12		5	8.9884	0.1383
P02088	HBB1 MOUSE Hemoglobin subunit beta 1 OS Mus musculus GN Hbb b1 PE 1 SV 2	15830	7.4969	13		4	28.5083	0.4516
P07759	SPA3K MOUSE Serine protease inhibitor A3K OS Mus musculus GN Serpina3k PE 1 SV 2	46850	4.8693	31		2	16.5039	0.7737
Q91XV3	BASP1 MOUSE Brain acid soluble protein 1 OS Mus musculus GN Basp1 PE 1 SV 3	22073	4.2828	22		2	4.2734	0.0944
P11499	HS90B MOUSE Heat shock protein HSP 90 beta OS Mus musculus GN Hsp90ab1 PE 1 SV 2	83273	4.775	67		5	11.2115	0.9342
P63158	HMGB1 MOUSE High mobility group protein B1 OS Mus musculus GN Hmgb1 PE 1 SV 2	24878	5.4465	17		2	8.9752	0.2234
Q3V132	ADT4 MOUSE ADP ATP translocase 4 OS Mus musculus GN Slc25a31 PE 2 SV 1	35235	9.8932	34		2	32.1351	1.133
P01942	HBA MOUSE Hemoglobin subunit alpha OS Mus musculus GN Hba PE 1 SV 2	15075	8.6376	9		3	33.0378	0.4984
P00405	COX2 MOUSE Cytochrome c oxidase subunit 2 OS Mus musculus GN Mtco2 PE 1 SV 1	25959	4.4103	11		4	0	
P07901	HS90A MOUSE Heat shock protein HSP 90 alpha OS Mus musculus GN Hsp90aa1 PE 1 SV 4	84734	4.7357	91		6	6.7891	0.5756
P26645	MARCS MOUSE Myristoylated alanine rich C kinase substrate OS Mus musculus GN Marcks PE 1 SV 2	29643	4.1239	25		4	10.3172	0.306
Q60932	VDAC1 MOUSE Voltage dependent anion selective channel protein 1 OS Mus musculus GN Vdac1 PE 1 SV 3	32331	8.6711	21		3	11.4354	0.37
P14733	LMNB1 MOUSE Lamin B1 OS Mus musculus GN Lmnb1 PE 1 SV 3	66744	4.9213	69		6	20.2837	1.3547
P61979	HNRPK MOUSE Heterogeneous nuclear ribonucleoprotein K OS Mus musculus GN Hnrnpk PE 1 SV 1	50944	5.2203	38		5	25.4271	1.2962
Q9R0M8	S35A2 MOUSE UDP galactose translocator OS Mus musculus GN Slc35a2 PE 2 SV 1	40740	10.133	18		2	8.7346	0.3561
O88319	NTR1 MOUSE Neurotensin receptor type 1 OS Mus musculus GN Ntsr1 PE 2 SV 1	47186	9.4257	21		1	44.2043	2.0872
P56480	ATPB MOUSE ATP synthase subunit beta mitochondrial OS Mus musculus GN Atp5b PE 1 SV 2	56265	5.0259	37		5	12.2702	0.6908
Q64692	SIA8D MOUSE CMP N acetylneuraminate poly alpha 2 8 sialyltransferase OS Mus musculus GN St8sia4 PE 2	41229	10.156	27		1	3.8582	0.1592

Red indicates plasma membrane proteins. Note P00924 ENO1 Yeast is a positive control that added during Mass Spec mapping.

9.17 Appendix table 7.3

Appendix table 7.3 Mass Spectrometry results of membrane preparation of P4 NrlGFP sorted cells (Run 2)

Appendix Table 7.3 A Mass spectrometry results of P4 NrlGFP positive cells 2nd run

Accession	Entry	Description	mW (Da)	pI (pH)	Theoretical Peptides	Coverage (%)	Digest Peptides	Amount (fmol)	Amount (ngrams)
ENO1_YEAST	P00924	Enolase 1 OS Saccharomyces cerevisiae GN ENO1 PE 1 SV 2	46773	6.1527	28	51.9451	29	100	4.6802
Q64426	tr	Q64426 MOUSE Histone H2A Fragment OS Mus musculus domesticus GN Hist2h2aa1 PE 2 SV 1	14737	11.0358	8	34.3066	3	0	
Q8CGP4	tr	Q8CGP4 MOUSE Histone H2A OS Mus musculus GN Hist1h2aa PE 2 SV 1	14047	11.6213	9	50.3876	3	2.2004	0.0309
Q6IWE2	tr	Q6IWE2 MOUSE Beta actin Fragment OS Mus musculus GN Actb PE 2 SV 1	8588	4.2336	9	45.4545	2	1.9972	0.0172
A2A513	tr	A2A513 MOUSE Keratin 10 OS Mus musculus GN Krt10 PE 3 SV 1	57006	4.8127	37	7.4866	4	2.1369	0.1219
Q8CIT7	tr	Q8CIT7 MOUSE Retinoblastoma binding protein 1 Fragment OS Mus musculus GN Arid4a PE 2 SV 1	4025	9.9765	2	45.9459	1	0.348	0.0014
LMNB1_MOUSE	P14733	Lamin B1 OS Mus musculus GN Lmnb1 PE 1 SV 3	66744	4.9213	69	25.1701	11	1.7757	0.1186
K2C1_MOUSE	P04104	Keratin type II cytoskeletal 1 OS Mus musculus GN Krt1 PE 1 SV 4	65565	8.1526	47	5.9655	4	1.7558	0.1152
Q08EK4	tr	Q08EK4 MOUSE Keratin 77 OS Mus musculus GN Krt77 PE 2 SV 1	61264	8.2932	47	14.711	7	3.8485	0.2359
Q99NC5	tr	Q99NC5 MOUSE Beta actin FE 3 Fragment OS Mus musculus GN Actb PE 2 SV 1	14973	5.5602	11	21.6418	2	0	
UCP1_MOUSE	P12242	Mitochondrial brown fat uncoupling protein 1 OS Mus musculus GN Ucp1 PE 2 SV 2	33226	9.3928	25	8.7948	2	17.6048	0.5853
VDAC1_MOUSE	Q60932	Voltage dependent anion selective channel protein 1 OS Mus musculus GN Vdac1 PE 1 SV 3	32331	8.6711	21	40.2027	7	2.11	0.0648
ROA2_MOUSE	O88569	Heterogeneous nuclear ribonucleoproteins A2 B1 OS Mus musculus GN Hnrnpa2b1 PE 1 SV 2	37379	9.1939	29	11.6147	3	0	
AT1A1_MOUSE	Q8VDN2	Sodium potassium transporting ATPase subunit alpha 1 OS Mus musculus GN Atp1a1 PE 1 SV 1	112909	5.1374	72	10.4594	7	0	
AT1A3_MOUSE	Q6PIC6	Sodium potassium transporting ATPase subunit alpha 3 OS Mus musculus GN Atp1a3 PE 1 SV 1	111620	5.0881	66	19.2498	13	1.022	0.1141
HNRPK_MOUSE	P61979	Heterogeneous nuclear ribonucleoprotein K OS Mus musculus GN Hnrnpk PE 1 SV 1	50944	5.2203	38	23.1102	7	1.1821	0.0574
Q8R3A9	tr	Q8R3A9 MOUSE Atp1a2 protein Fragment OS Mus musculus GN Atp1a2 PE 2 SV 1	53815	4.9867	34	26.9547	8	0	
KRT35_MOUSE	Q497I4	Keratin type I cuticular Ha5 OS Mus musculus GN Krt35 PE 2 SV 1	50497	4.7047	40	7.033	2	1.9649	0.0993
D3YZY0	tr	D3YZY0 MOUSE Uncharacterized protein OS Mus musculus GN Actg2 PE 3 SV 1	30045	4.7576	24	20	4	0	
D3YV05	tr	D3YV05 MOUSE Uncharacterized protein OS Mus musculus GN Atp1b2 PE 3 SV 1	25564	8.6801	18	30.3571	5	0.3241	0.0083
Q80ZV2	tr	Q80ZV2 MOUSE Tubb5 protein Fragment OS Mus musculus GN Tubb5 PE 2 SV 1	21440	4.5701	13	15.5914	2	0	
AT1A2_MOUSE	Q6PIE5	Sodium potassium transporting ATPase subunit alpha 2 OS Mus musculus GN Atp1a2 PE 1 SV 1	112145	5.2291	77	16.2745	11	0	
Q61272	tr	Q61272 MOUSE Alpha actin Aa 40 375 Fragment OS Mus musculus GN Acta1 PE 2 SV 1	37787	5.326	30	16.0714	4	0	
CRYM_MOUSE	O54983	Mu crystallin homolog OS Mus musculus GN Crym PE 1 SV 1	33502	5.3161	22	13.738	1	1.1092	0.0372
B1AQ77	tr	B1AQ77 MOUSE Keratin 15 OS Mus musculus GN Krt15 PE 3 SV 1	49463	4.593	42	7.2368	3	1.8835	0.0932
ACTBL_MOUSE	Q8BFZ3	Beta actin like protein 2 OS Mus musculus GN Actbl2 PE 1 SV 1	41977	5.1535	35	11.4362	3	0	
AT1B2_MOUSE	P14231	Sodium potassium transporting ATPase subunit beta 2 OS Mus musculus GN Atp1b2 PE 1 SV 2	33322	8.3441	22	25.1724	5	0	
Q8BK71	tr	Q8BK71 MOUSE Putative uncharacterized protein Fragment OS Mus musculus GN Tpr PE 2 SV 1	47597	5.1226	44	11.1922	3	2.5077	0.1194
Q3U9U3	tr	Q3U9U3 MOUSE Putative uncharacterized protein OS Mus musculus GN Tubb6 PE 2 SV 1	42127	4.5709	25	8.5333	2	0	
D7URW5	tr	D7URW5 MOUSE Vomeronasal 2 receptor p5 OS Mus musculus domesticus GN V2Rp5 PE 2 SV 1	97640	7.0688	52	11.4486	4	1.9876	0.1942
D7URW2	tr	D7URW2 MOUSE Vomeronasal 2 receptor p2 OS Mus musculus domesticus GN V2Rp2 PE 2 SV 1	97583	7.1554	48	9.8016	4	0	
K2C71_MOUSE	Q9R0H5	Keratin type II cytoskeletal 71 OS Mus musculus GN Krt71 PE 1 SV 1	57346	6.626	45	15.458	5	0	

Appendix Table 7.3 B Mass spectrometry results of P4 NrlGFP negative cells 2nd run

Accession	Entry	Description	mW (Da)	pI (pH)	Theoretical Peptides	Coverage (%)	Digest Peptides	Amount (fmol)	Amount (ngrams)
ENO1_YEAST	P00924	Enolase 1 OS Saccharomyces cerevisiae GN ENO1 PE 1 SV 2	46773	6.1527	28	55.6064	21	100	4.6802
MARCS_MOUSE	P26645	Myristoylated alanine rich C kinase substrate OS Mus musculus GN Marcks PE 1 SV 2	29643	4.1239	25	86.0841	13	4.1355	0.1227
LMNB1_MOUSE	P14733	Lamin B1 OS Mus musculus GN Lmnb1 PE 1 SV 3	66744	4.9213	69	46.5986	26	19.1796	1.2809
K2C74_MOUSE	Q6IFZ9	Keratin type II cytoskeletal 74 OS Mus musculus GN Krt74 PE 2 SV 1	54712	5.3787	46	17.3737	5	0	
K2C71_MOUSE	Q9R0H5	Keratin type II cytoskeletal 71 OS Mus musculus GN Krt71 PE 1 SV 1	57346	6.626	45	23.6641	8	0	
K2C1_MOUSE	P04104	Keratin type II cytoskeletal 1 OS Mus musculus GN Krt1 PE 1 SV 4	65565	8.1526	47	16.0126	9	11.6692	0.7656
HNRPL_MOUSE	Q8R081	Heterogeneous nuclear ribonucleoprotein L OS Mus musculus GN Hnrnpl PE 1 SV 2	63923	8.042	34	13.4812	3	2.9811	0.1907
H4_MOUSE	P62806	Histone H4 OS Mus musculus GN Hist1h4a PE 1 SV 2	11360	11.7665	11	30.0971	4	1.201	0.0137
BASP1_MOUSE	Q91XV3	Brain acid soluble protein 1 OS Mus musculus GN Basp1 PE 1 SV 3	22073	4.2828	22	44.6903	8	0.8403	0.0186
ACTB_MOUSE	P60710	Actin cytoplasmic 1 OS Mus musculus GN Actb PE 1 SV 1	41709	5.142	34	21.3333	6	6.4839	0.2706
ROA2_MOUSE	O88569	Heterogeneous nuclear ribonucleoproteins A2 B1 OS Mus musculus GN Hnrnpa2b1 PE 1 SV 2	37379	9.1939	29	31.728	8	3.2446	0.1214
VDAC1_MOUSE	Q60932	Voltage dependent anion selective channel protein 1 OS Mus musculus GN Vdac1 PE 1 SV 3	32331	8.6711	21	16.5541	4	9.4427	0.3055
ACTA_MOUSE	P62737	Actin aortic smooth muscle OS Mus musculus GN Acta2 PE 1 SV 1	41981	5.077	34	17.2414	6	0	
K1C10_MOUSE	P02535	Keratin type I cytoskeletal 10 OS Mus musculus GN Krt10 PE 1 SV 3	57734	4.8534	38	12.807	5	7.6891	0.4442
ACTBL_MOUSE	Q8BFZ3	Beta actin like protein 2 OS Mus musculus GN Actbl2 PE 1 SV 1	41977	5.1535	35	20.2128	4	0	
HNRPK_MOUSE	P61979	Heterogeneous nuclear ribonucleoprotein K OS Mus musculus GN Hnrnpk PE 1 SV 1	50944	5.2203	38	22.4622	7	4.8244	0.2459
ATPB_MOUSE	P56480	ATP synthase subunit beta mitochondrial OS Mus musculus GN Atp5b PE 1 SV 2	56265	5.0259	37	22.8733	7	4.7696	0.2685
PGRC1_MOUSE	O55022	Membrane associated progesterone receptor component 1 OS Mus musculus GN Pgrmc1 PE 1 SV 4	21680	4.3422	19	15.8974	1	7.2572	0.1574
TBB2B_MOUSE	Q9CWF2	Tubulin beta 2B chain OS Mus musculus GN Tubb2b PE 1 SV 1	49920	4.5903	30	38.6517	13	2.7463	0.1372
TBA1C_MOUSE	P68373	Tubulin alpha 1C chain OS Mus musculus GN Tuba1c PE 1 SV 1	49877	4.7856	34	38.5301	9	0	
RANDOM4525	RANDOM4525	Random Sequence 4525	54700	5.4809	34	10.7071	2	5.0781	0.278
TBB5_MOUSE	P99024	Tubulin beta 5 chain OS Mus musculus GN Tubb5 PE 1 SV 1	49638	4.5903	30	35.1351	13	0	
Q8R5E7	tr	Q8R5E7 MOUSE Tmem106b protein Fragment OS Mus musculus GN Tmem106b PE 2 SV 1	12153	5.5521	6	76.6355	4	1.4954	0.0182
Q2NKW2	tr	Q2NKW2 MOUSE Olfr847 protein Fragment OS Mus musculus GN Olfr847 PE 2 SV 1	34585	8.1442	9	31.5113	6	36.2647	1.2551
D3YU91	tr	D3YU91 MOUSE Uncharacterized protein OS Mus musculus GN C87414 PE 4 SV 1	31706	6.6694	19	18.705	4	1.8201	0.0577
Q9R0U5	tr	Q9R0U5 MOUSE Matrin3 OS Mus musculus GN Matr3 PE 2 SV 1	34083	6.4517	29	13.3987	3	2.3795	0.0812
D3YX94	tr	D3YX94 MOUSE Uncharacterized protein OS Mus musculus GN Gm6205 PE 4 SV 1	41713	9.3898	26	13.0919	3	0	
Q3T9Y9	tr	Q3T9Y9 MOUSE Putative uncharacterized protein Fragment OS Mus musculus GN Ptpn1 PE 2 SV 1	28612	5.805	28	42.5703	7	0.4141	0.0119
VAPA_MOUSE	Q9WV55	Vesicle associated membrane protein associated protein A OS Mus musculus GN Vapa PE 1 SV 2	27837	8.5909	21	6.4257	1	1.2341	0.0344
Q3TNH0	tr	Q3TNH0 MOUSE Putative uncharacterized protein OS Mus musculus GN Tmpo PE 1 SV 1	46021	9.6059	36	28.1553	7	1.7539	0.0808

Accession	Entry	Description	mW (Da)	pI (pH)	Theoretical Peptides	Coverage (%)	Digest Peptides	Amount (fmol)	Amount (ngrams)
ENO1_YEAST	P00924	Enolase 1 OS Saccharomyces cerevisiae GN ENO1 PE 1 SV 2	46773	6.1527	28	55.8352	23	100	4.6802
LMNB1_MOUSE	P14733	Lamin B1 OS Mus musculus GN Lmnb1 PE 1 SV 3	66744	4.9213	69	41.3265	18	11.782	0.7869
MARCS_MOUSE	P26645	Myristoylated alanine rich C kinase substrate OS Mus musculus GN Marcks PE 1 SV 2	29643	4.1239	25	64.7249	9	2.1255	0.063
ROA3_MOUSE	Q8BG05	Heterogeneous nuclear ribonucleoprotein A3 OS Mus musculus GN Hnrnpa3 PE 1 SV 1	39627	9.2212	32	29.8153	7	4.3662	0.1731
K1C10_MOUSE	P02535	Keratin type I cytoskeletal 10 OS Mus musculus GN Krt10 PE 1 SV 3	57734	4.8534	38	7.193	4	4.5484	0.2628
G3P_MOUSE	P16858	Glyceraldehyde 3 phosphate dehydrogenase OS Mus musculus GN Gapdh PE 1 SV 2	35787	8.3507	19	20.7207	3	2.0879	0.0748
HNRPK_MOUSE	P61979	Heterogeneous nuclear ribonucleoprotein K OS Mus musculus GN Hnrnpk PE 1 SV 1	50944	5.2203	38	15.1188	4	2.8757	0.1396

Accession	Entry	Description	mW (Da)	pI (pH)	Theoretical Peptides	Coverage (%)	Digest Peptides	Amount (fmol)	Amount (ngrams)
ENO1_YEAST	P00924	Enolase 1 OS Saccharomyces cerevisiae GN ENO1 PE 1 SV 2	46773	6.1527	28	52.4027	22	100	4.6802
LMNB1_MOUSE	P14733	Lamin B1 OS Mus musculus GN Lmnb1 PE 1 SV 3	66744	4.9213	69	37.2449	17	9.6148	0.6421
MARCS_MOUSE	P26645	Myristoylated alanine rich C kinase substrate OS Mus musculus GN Marcks PE 1 SV 2	29643	4.1239	25	79.6117	8	2.3784	0.0705
ACTB_MOUSE	P60710	Actin cytoplasmic 1 OS Mus musculus GN Actb PE 1 SV 1	41709	5.142	34	31.2	8	6.5801	0.2746
ACTBL_MOUSE	Q8BFZ3	Beta actin like protein 2 OS Mus musculus GN Actbl2 PE 1 SV 1	41977	5.1535	35	31.9149	6	0	
TBA1C_MOUSE	P68373	Tubulin alpha 1C chain OS Mus musculus GN Tuba1c PE 1 SV 1	49877	4.7856	34	32.7394	7	4.4704	0.2231
HNRH1_MOUSE	O35737	Heterogeneous nuclear ribonucleoprotein H OS Mus musculus GN Hnrnph1 PE 1 SV 3	49168	5.8513	27	25.6125	7	2.9709	0.1462
CALX_MOUSE	P35564	Calnexin OS Mus musculus GN Canx PE 1 SV 1	67235	4.2949	44	14.5516	4	1.0114	0.068
HNRH2_MOUSE	P70333	Heterogeneous nuclear ribonucleoprotein H2 OS Mus musculus GN Hnrnph2 PE 1 SV 1	49248	5.8511	27	12.6949	4	0	
ROA3_MOUSE	Q8BG05	Heterogeneous nuclear ribonucleoprotein A3 OS Mus musculus GN Hnrnpa3 PE 1 SV 1	39627	9.2212	32	12.4011	3	3.5508	0.1408
BASP1_MOUSE	Q91XV3	Brain acid soluble protein 1 OS Mus musculus GN Basp1 PE 1 SV 3	22073	4.2828	22	58.4071	9	0.4424	0.0098
ROA2_MOUSE	O88569	Heterogeneous nuclear ribonucleoproteins A2 B1 OS Mus musculus GN Hnrnpa2b1 PE 1 SV 2	37379	9.1939	29	20.3966	5	1.1189	0.0418
VDAC1_MOUSE	Q60932	Voltage dependent anion selective channel protein 1 OS Mus musculus GN Vdac1 PE 1 SV 3	32331	8.6711	21	13.1757	2	6.1123	0.1977
PGRC1_MOUSE	O55022	Membrane associated progesterone receptor component 1 OS Mus musculus GN Pgrmc1 PE 1 SV 4	21680	4.3422	19	29.7436	3	4.7642	0.1034
K1C10_MOUSE	P02535	Keratin type I cytoskeletal 10 OS Mus musculus GN Krt10 PE 1 SV 3	57734	4.8534	38	10.3509	3	5.0049	0.2891
ATPB_MOUSE	P56480	ATP synthase subunit beta mitochondrial OS Mus musculus GN Atp5b PE 1 SV 2	56265	5.0259	37	17.7694	4	3.9583	0.2229
HNRPK_MOUSE	P61979	Heterogeneous nuclear ribonucleoprotein K OS Mus musculus GN Hnrnpk PE 1 SV 1	50944	5.2203	38	12.527	4	1.6616	0.0847
TBB5_MOUSE	P99024	Tubulin beta 5 chain OS Mus musculus GN Tubb5 PE 1 SV 1	49638	4.5903	30	17.7928	6	1.0231	0.0508

Red indicates plasma membrane proteins; Proteins from technichal replicates were presented separately.

9.18 Appendix table 7.4

Appendix table 7.4 Mass Spectrometry results of membrane preparation of P4 NrlGFP sorted cells (Run 3)

Appendix Table 7.4 A Mass spectrometry results of P4 NrlGFP positive cells 3rd run

Accession	Entry	Description	mW (Da)	pI (pH)	Theoretical Peptides	Coverage (%)	Digest Peptides	Amount (fmol)	Amount (ngrams)
P00924	ENO1_YEAST	Enolase 1 EC 4 2 1 11 2 phosphoglycerate dehydr	46642	6.1527	28	45.4128	20	100	4.6671
LMNB1_MOUSE	P14733	Lamin B1 OS Mus musculus GN Lmnb1 PE 1 SV 3	66744	4.9213	69	35.2041	16	21.4516	1.4327
AT1B2_MOUSE	P14231	Sodium potassium transporting ATPase subunit beta 2 OS Mus musculus GN Atp1b2 PE 1 SV 2	33322	8.3441	22	24.1379	3	10.6499	0.3551
ROA2_MOUSE	O88569	Heterogeneous nuclear ribonucleoproteins A2 B1 OS Mus musculus GN Hnrnpa2b1 PE 1 SV 2	37379	9.1939	29	25.4958	7	0	
MARCS_MOUSE	P26645	Myristoylated alanine rich C kinase substrate OS Mus musculus GN Marcks PE 1 SV 2	29643	4.1239	25	25.5663	4	1.3756	0.0408
ATPA_MOUSE	Q03265	ATP synthase subunit alpha mitochondrial OS Mus musculus GN Atp5a1 PE 1 SV 1	59715	9.5021	46	31.4647	12	7.0848	0.4233
ADT2_MOUSE	P51881	ADP ATP translocase 2 OS Mus musculus GN Slc25a5 PE 1 SV 3	32910	10.0303	31	31.8792	7	6.2345	0.2053
AT1A3_MOUSE	Q6PIC6	Sodium potassium transporting ATPase subunit alpha 3 OS Mus musculus GN Atp1a3 PE 1 SV 1	111620	5.0881	66	22.2113	15	11.2294	1.2542
A2BDV8	tr	A2BDV8 MOUSE Heterogeneous nuclear ribonucleoprotein H2 OS Mus musculus GN Hnrnph2 PE 4 SV 1	49248	5.8511	27	30.2895	10	7.2114	0.3554
F6ZQM8	tr	F6ZQM8 MOUSE Uncharacterized protein Fragment OS Mus musculus PE 4 SV 1	35556	8.0825	19	42.2492	12	18.2757	0.6502
TBA8_MOUSE	Q9JJZ2	Tubulin alpha 8 chain OS Mus musculus GN Tuba8 PE 1 SV 1	50019	4.7966	34	23.608	6	0	
ACTBL_MOUSE	Q8BFZ3	Beta actin like protein 2 OS Mus musculus GN Actbl2 PE 1 SV 1	41977	5.1535	35	28.4574	7	0	
ATPB_MOUSE	P56480	ATP synthase subunit beta mitochondrial OS Mus musculus GN Atp5b PE 1 SV 2	56265	5.0259	37	17.5803	6	7.2057	0.4057
ENOA_MOUSE	P17182	Alpha enolase OS Mus musculus GN Eno1 PE 1 SV 3	47111	6.3752	30	26.0369	8	1.1967	0.0564
HNRPF_MOUSE	Q9Z2X1	Heterogeneous nuclear ribonucleoprotein F OS Mus musculus GN Hnrnpf PE 1 SV 3	45700	5.1652	26	4.8193	1	0	
ADT1_MOUSE	P48962	ADP ATP translocase 1 OS Mus musculus GN Slc25a4 PE 1 SV 4	32883	10.0181	31	25.1678	6	0.5776	0.019
H4_MOUSE	P62806	Histone H4 OS Mus musculus GN Hist1h4a PE 1 SV 2	11360	11.7665	11	46.6019	6	5.7579	0.0655
TBB2C_MOUSE	P68372	Tubulin beta 2C chain OS Mus musculus GN Tubb2c PE 1 SV 1	49799	4.602	30	29.2135	9	6.808	0.3393
KCRB_MOUSE	Q04447	Creatine kinase B type OS Mus musculus GN Ckb PE 1 SV 1	42686	5.2866	23	19.685	5	5.5526	0.2372
TBB5_MOUSE	P99024	Tubulin beta 5 chain OS Mus musculus GN Tubb5 PE 1 SV 1	49638	4.5903	30	22.5225	7	0	
Q3TFP8	tr	Q3TFP8 MOUSE Uncharacterized protein OS Mus musculus GN Pgrmc1 PE 2 SV 1	19733	4.4806	19	14.8571	2	2.611	0.0516
Q3TQ70	tr	Q3TQ70 MOUSE Beta1 subnuit of GTP binding protein OS Mus musculus GN Gnb1 PE 2 SV 1	37353	5.5351	21	33.2353	7	5.4029	0.2019
E9Q9J0	tr	E9Q9J0 MOUSE Uncharacterized protein OS Mus musculus GN Uba52 PE 4 SV 1	10906	8.2344	7	26.0417	2	0.7498	0.0082
F2Z471	tr	F2Z471 MOUSE Uncharacterized protein OS Mus musculus GN Vdac1 PE 4 SV 1	28139	7.2405	17	31.1024	6	2.1967	0.0619
PHB_MOUSE	P67778	Prohibitin OS Mus musculus GN Phb PE 1 SV 1	29801	5.4293	21	14.3382	2	5.0522	0.1507
E9Q7H5	tr	E9Q7H5 MOUSE Uncharacterized protein OS Mus musculus GN Gm8991 PE 4 SV 1	32554	8.482	28	24	8	4.338	0.1413
COX2_MOUSE	P00405	Cytochrome c oxidase subunit 2 OS Mus musculus GN Mtco2 PE 1 SV 1	25959	4.4103	11	29.5154	4	4.3326	0.1125
VDAC2_MOUSE	Q60930	Voltage dependent anion selective channel protein 2 OS Mus musculus GN Vdac2 PE 1 SV 2	31712	7.372	20	29.8305	8	3.8052	0.1207
Q3TNH0	tr	Q3TNH0 MOUSE Uncharacterized protein OS Mus musculus GN Tmpo PE 2 SV 1	46021	9.6059	36	24.2718	6	2.1125	0.0973
GBB4_MOUSE	P29387	Guanine nucleotide binding protein subunit beta 4 OS Mus musculus GN Gnb4 PE 2 SV 4	37355	5.6975	22	14.7059	3	0	
QCR2_MOUSE	Q9DB77	Cytochrome b c1 complex subunit 2 mitochondrial OS Mus musculus GN Uqcrc2 PE 1 SV 1	48205	9.5676	26	5.9603	2	2.7056	0.1305
F7C5V8	tr	F7C5V8 MOUSE Uncharacterized protein Fragment OS Mus musculus GN Ncam1 PE 4 SV 1	118069	4.5053	68	16.6365	9	1.165	0.1376
K1C10_MOUSE	P02535	Keratin type I cytoskeletal 10 OS Mus musculus GN Krt10 PE 1 SV 3	57734	4.8534	38	17.0175	7	1.8954	0.1095
PGRC2_MOUSE	Q80UU9	Membrane associated progesterone receptor component 2 OS Mus musculus GN Pgrmc2 PE 1 SV 2	23319	4.8098	25	11.5207	3	0	
F6UTR6	tr	F6UTR6 MOUSE Uncharacterized protein Fragment OS Mus musculus GN Shox2 PE 4 SV 1	26010	9.8201	18	4.5833	1	16.1676	0.419
DX39B_MOUSE	Q9Z1N5	Spliceosome RNA helicase Ddx39b OS Mus musculus GN Ddx39b PE 1 SV 1	49004	5.3124	37	12.1495	2	2.7805	0.1363
THOC4_MOUSE	O08583	THO complex subunit 4 OS Mus musculus GN Thoc4 PE 1 SV 3	26923	11.5563	18	13.3333	2	2.0199	0.0544
TMX3_MOUSE	Q8BXZ1	Protein disulfide isomerase TMX3 OS Mus musculus GN Tmx3 PE 1 SV 2	51815	4.8246	46	8.3333	2	2.9089	0.1508
HNRPU_MOUSE	Q8VEK3	Heterogeneous nuclear ribonucleoprotein U OS Mus musculus GN Hnrnpu PE 1 SV 1	87862	5.8418	53	19.125	11	3.8375	0.3374
RANDOM32305	RANDOM32305	Random Sequence 32305	23294	6.6923	13	19.2488	3	4.0383	0.0941
GNAI2_MOUSE	P08752	Guanine nucleotide binding protein G i subunit alpha 2 OS Mus musculus GN Gnai2 PE 1 SV 5	40463	5.1172	29	10.4225	3	3.5965	0.1456
A2RTD1	tr	A2RTD1 MOUSE Interleukin 6 OS Mus musculus GN Il6 PE 2 SV 1	24368	7.2167	18	17.0616	2	0	
D3Z4C7	tr	D3Z4C7 MOUSE MCG20459 isoform CRA a OS Mus musculus GN Dus2l PE 4 SV 1	42641	6.4949	36	10	2	1.5406	0.0657
A2AH75	tr	A2AH75 MOUSE Kinesin family member 1B OS Mus musculus GN Kif1b PE 3 SV 1	129969	8.3945	116	10.6957	11	6.9699	0.9064
E9Q664	tr	E9Q664 MOUSE Uncharacterized protein OS Mus musculus GN Ube4b PE 4 SV 1	133402	5.7237	99	10.7234	7	1.532	0.2045
A2ACG7	tr	A2ACG7 MOUSE Ribophorin II OS Mus musculus GN Rpn2 PE 4 SV 1	67460	5.7918	39	13.4959	7	0	
DIDO1_MOUSE	Q8C9B9	Death inducer obliterator 1 OS Mus musculus GN Dido1 PE 1 SV 4	247022	7.7889	179	1.7287	4	20.1923	4.9911
F6UYF1	tr	F6UYF1 MOUSE Uncharacterized protein Fragment OS Mus musculus GN Ppfia3 PE 4 SV 1	115093	5.5847	94	17.8917	12	1.3224	0.1523

Appendix Table 7.4 B Mass spectrometry results of P4 NrlGFP negative cells 3rd run

Accession	Entry	Description	mW (Da)	pI (pH)	Theoretical Peptides	Coverage (%)	Digest Peptides	Amount (fmol)	Amount (ngrams)
P00924	ENO1_YEAST	Enolase 1 EC 4 2 1 11 2 phosphoglycerate dehydr	46642	6.1527	28	23.6239	9	100	4.6671
B1ATY0	tr	B1ATY0 MOUSE Actin gamma cytoplasmic 1 OS Mus musculus GN Actg1 PE 3 SV 1	32599	4.9788	27	30.5085	4	0	
TBA1A_MOUSE	P68369	Tubulin alpha 1A chain OS Mus musculus GN Tuba1a PE 1 SV 1	50103	4.7622	34	20.8426	5	16.6004	0.8323
LMNB1_MOUSE	P14733	Lamin B1 OS Mus musculus GN Lmnb1 PE 1 SV 3	66744	4.9213	69	6.8027	2	26.2848	1.7554
HNRH1_MOUSE	O35737	Heterogeneous nuclear ribonucleoprotein H OS Mus musculus GN Hnrnph1 PE 1 SV 3	49168	5.8513	27	7.5724	2	17.1212	0.8424

Accession	Entry	Description	mW (Da)	pI (pH)	Theoretical Peptides	Coverage (%)	Digest Peptides	Amount (fmol)	Amount (ngrams)
P00924	ENO1_YEAST	Enolase 1 EC 4 2 1 11 2 phosphoglycerate dehydr	46642	6.1527	28	28.211	11	100	4.6671
LMNB1_MOUSE	P14733	Lamin B1 OS Mus musculus GN Lmnb1 PE 1 SV 3	66744	4.9213	69	39.6259	21	79.612	5.3169
ROA2_MOUSE	O88569	Heterogeneous nuclear ribonucleoproteins A2 B1 OS Mus musculus GN Hnrnpa2b1 PE 1 SV 2	37379	9.1939	29	17.2805	7	23.2192	0.8654
VDAC1_MOUSE	Q60932	Voltage dependent anion selective channel protein 1 OS Mus musculus GN Vdac1 PE 1 SV 3	32331	8.6711	21	49.3243	8	53.8539	1.7423
HNRPF_MOUSE	Q9Z2X1	Heterogeneous nuclear ribonucleoprotein F OS Mus musculus GN Hnrnpf PE 1 SV 3	45700	5.1652	26	17.3494	4	1.2509	0.0572
HNRH1_MOUSE	O35737	Heterogeneous nuclear ribonucleoprotein H OS Mus musculus GN Hnrnph1 PE 1 SV 3	49168	5.8513	27	24.9443	8	43.4083	2.1357
TBA1A_MOUSE	P68369	Tubulin alpha 1A chain OS Mus musculus GN Tuba1a PE 1 SV 1	50103	4.7622	34	35.9202	9	29.374	1.4727
ACTC_MOUSE	P68033	Actin alpha cardiac muscle 1 OS Mus musculus GN Actc1 PE 1 SV 1	41991	5.0709	34	35.0133	11	0	
H4_MOUSE	P62806	Histone H4 OS Mus musculus GN Hist1h4a PE 1 SV 2	11360	11.7665	11	29.1262	3	10.2123	0.1161
SYN1_MOUSE	O88935	Synapsin 1 OS Mus musculus GN Syn1 PE 1 SV 2	74051	10.1462	38	16.4306	5	68.2297	4.7785
TBA8_MOUSE	Q9JJZ2	Tubulin alpha 8 chain OS Mus musculus GN Tuba8 PE 1 SV 1	50019	4.7966	34	14.0312	4	0	
ATPB_MOUSE	P56480	ATP synthase subunit beta mitochondrial OS Mus musculus GN Atp5b PE 1 SV 2	56265	5.0259	37	13.0435	4	37.1476	2.0914
VDAC2_MOUSE	Q60930	Voltage dependent anion selective channel protein 2 OS Mus musculus GN Vdac2 PE 1 SV 2	31712	7.372	20	19.661	4	16.5292	0.5245
D3Z6F5	tr	D3Z6F5 MOUSE ATP synthase subunit alpha OS Mus musculus GN Atp5a1 PE 3 SV 1	54560	8.4943	44	7.7535	3	24.5487	1.3402
E9Q9J0	tr	E9Q9J0 MOUSE Uncharacterized protein OS Mus musculus GN Uba52 PE 4 SV 1	10906	8.2344	7	41.6667	4	20.4005	0.2226
F6ZQM8	tr	F6ZQM8 MOUSE Uncharacterized protein Fragment OS Mus musculus PE 4 SV 1	35556	8.0825	19	26.1398	5	34.4755	1.2266
E9Q8D6	tr	E9Q8D6 MOUSE Uncharacterized protein OS Mus musculus GN Hnrnpk PE 4 SV 1	49847	5.5633	40	31.1111	10	24.7583	1.2349
STXB1_MOUSE	O08599	Syntaxin binding protein 1 OS Mus musculus GN Stxbp1 PE 1 SV 2	67525	6.509	48	3.7037	2	33.1267	2.2383
GTR1_MOUSE	P17809	Solute carrier family 2 facilitated glucose transporter member 1 OS Mus musculus GN Slc2a1 PE 1 SV	53949	9.0406	19	14.6341	5	12.0599	0.651
ADT1_MOUSE	P48962	ADP ATP translocase 1 OS Mus musculus GN Slc25a4 PE 1 SV 4	32883	10.0181	31	11.4094	3	13.6549	0.4493
E0CZ27	tr	E0CZ27 MOUSE Histone H3 OS Mus musculus GN H3f3a PE 3 SV 1	13314	11.4359	10	5.8824	1	13.8015	0.1839
E9Q3T0	tr	E9Q3T0 MOUSE Uncharacterized protein OS Mus musculus GN Gm10073 PE 4 SV 1	11425	4.0849	7	43.8596	3	18.6066	0.2127
F6QXX3	tr	F6QXX3 MOUSE Uncharacterized protein Fragment OS Mus musculus GN Tmpo PE 4 SV 1	30568	10.3727	19	25.8993	4	11.9151	0.3644
E9PVI9	tr	E9PVI9 MOUSE Uncharacterized protein OS Mus musculus GN Gm17695 PE 4 SV 1	63342	10.3176	43	23.3096	9	38.6237	2.4481
PHB_MOUSE	P67778	Prohibitin OS Mus musculus GN Phb PE 1 SV 1	29801	5.4293	21	20.2206	4	13.1861	0.3932
TBB4_MOUSE	Q9D6F9	Tubulin beta 4 chain OS Mus musculus GN Tubb4 PE 1 SV 3	49553	4.5903	30	3.1532	1	0	
TBB2C_MOUSE	P68372	Tubulin beta 2C chain OS Mus musculus GN Tubb2c PE 1 SV 1	49799	4.602	30	13.4831	5	0	
ZBTB3_MOUSE	Q91X45	Zinc finger and BTB domain containing protein 3 OS Mus musculus GN Zbtb3 PE 2 SV 3	55865	4.9343	35	20.8494	4	5.9341	0.3317
E9Q754	tr	E9Q754 MOUSE Uncharacterized protein OS Mus musculus GN Vrk3 PE 4 SV 1	18284	9.1172	18	27.6471	3	9.239	0.169
GBB1_MOUSE	P62874	Guanine nucleotide binding protein G I G S G T subunit beta 1 OS Mus musculus GN Gnb1 PE 1 SV 3	37353	5.5351	21	35	5	9.9462	0.3718
F6YPY4	tr	F6YPY4 MOUSE Uncharacterized protein Fragment OS Mus musculus PE 4 SV 1	32725	11.7314	24	40.3846	8	17.4456	0.5712
Q71S36	tr	Q71S36 MOUSE TAGL M splice variant OS Mus musculus GN Pglyrp2 PE 2 SV 1	40540	5.5474	18	6.8602	1	4.3011	0.1745

Red indicates plasma membrane proteins; Proteins from technichal replicates were presented separately.

10 References

Adams, M. K., J. A. Simpson, K. Z. Aung, G. A. Makeyeva, G. G. Giles, D. R. English, J. Hopper, R. H. Guymer, P. N. Baird and L. D. Robman (2012). "Abdominal obesity and age-related macular degeneration." Am J Epidemiol **173**(11): 1246-55.

Agathocleous, M. and W. A. Harris (2009). "From progenitors to differentiated cells in the vertebrate retina." Annu Rev Cell Dev Biol **25**: 45-69.

Akimoto, M., H. Cheng, D. Zhu, J. A. Brzezinski, R. Khanna, E. Filippova, E. C. Oh, Y. Jing, J. L. Linares, M. Brooks, S. Zareparsi, A. J. Mears, A. Hero, T. Glaser and A. Swaroop (2006). "Targeting of GFP to newborn rods by Nrl promoter and temporal expression profiling of flow-sorted photoreceptors." Proc Natl Acad Sci U S A **103**(10): 3890-5.

Alagramam, K. N., C. L. Murcia, H. Y. Kwon, K. S. Pawlowski, C. G. Wright and R. P. Woychik (2001). "The mouse Ames waltzer hearing-loss mutant is caused by mutation of Pcdh15, a novel protocadherin gene." Nat Genet **27**(1): 99-102.

Alberts, B., A. Johnson, J. Lewis, M. Raff, K. Roberts and P. Walter (2008). Molecular Biology of The Cell. New York, Garland Science, Taylor & Francis Group.

Albrecht-Buehler, G. (1977). "Phagokinetic tracks of 3T3 cells: parallels between the orientation of track segments and of cellular structures which contain actin or tubulin." Cell **12**(2): 333-9.

Alexander, J. J., Y. Umino, D. Everhart, B. Chang, S. H. Min, Q. Li, A. M. Timmers, N. L. Hawes, J. J. Pang, R. B. Barlow and W. W. Hauswirth (2007). "Restoration of cone vision in a mouse model of achromatopsia." Nat Med **13**(6): 685-7.

Allikmets, R., N. F. Shroyer, N. Singh, J. M. Seddon, R. A. Lewis, P. S. Bernstein, A. Peiffer, N. A. Zabriskie, Y. Li, A. Hutchinson, M. Dean, J. R. Lupski and M. Leppert (1997). "Mutation of the Stargardt disease gene (ABCR) in age-related macular degeneration." Science **277**(5333): 1805-7.

Allikmets, R., N. Singh, H. Sun, N. F. Shroyer, A. Hutchinson, A. Chidambaram, B. Gerrard, L. Baird, D. Stauffer, A. Peiffer, A. Rattner, P. Smallwood, Y. Li, K. L. Anderson, R. A. Lewis, J. Nathans, M. Leppert, M. Dean and J. R. Lupski (1997). "A photoreceptor cell-specific ATP-binding transporter gene (ABCR) is mutated in recessive Stargardt macular dystrophy." Nat Genet **15**(3): 236-46.

Altmann, C. R., R. L. Chow, R. A. Lang and A. Hemmati-Brivanlou (1997). "Lens induction by Pax-6 in Xenopus laevis." Dev Biol **185**(1): 119-23.

Aoki, H., A. Hara, M. Niwa, Y. Yamada and T. Kunisada (2009). "In vitro and in vivo differentiation of human embryonic stem cells into retina-like organs and comparison with that from mouse pluripotent epiblast stem cells." Dev Dyn **238**(9): 2266-79.

Atchaneeyasakul, L. O., W. Jinda, N. Sakolsatayadorn, A. Trinavarat, N. Ruangvoravate, N. Thanasombatskul, W. Thongnoppakhun and C. Limwongse (2008). "Mutation analysis of the VMD2 gene in thai families with best macular dystrophy." Ophthalmic Genet **29**(3): 139-44.

Bai, Q., J. A. Garver, N. A. Hukriede and E. A. Burton (2007). "Generation of a transgenic zebrafish model of Tauopathy using a novel promoter element derived from the zebrafish eno2 gene." Nucleic Acids Res **35**(19): 6501-16.

Bai, Q., X. Wei and E. A. Burton (2009). "Expression of a 12-kb promoter element derived from the zebrafish enolase-2 gene in the zebrafish visual system." Neurosci Lett **449**(3): 252-7.

Bainbridge, J. W., A. J. Smith, S. S. Barker, S. Robbie, R. Henderson, K. Balaggan, A. Viswanathan, G. E. Holder, A. Stockman, N. Tyler, S. Petersen-Jones, S. S. Bhattacharya, A. J. Thrasher, F. W. Fitzke, B. J. Carter, G. S. Rubin, A. T. Moore and R. R. Ali (2008). "Effect of gene therapy on visual function in Leber's congenital amaurosis." N Engl J Med **358**(21): 2231-9.

Baron, M. (2012). Towards cone photoreceptor transplantation for retinal repair. Institute of Child Health. London, University College London. **PhD:** 220.

Barzi, M., J. Berenguer, A. Menendez, R. Alvarez-Rodriguez and S. Pons (2010). "Sonic-hedgehog-mediated proliferation requires the localization of PKA to the cilium base." J Cell Sci **123**(Pt 1): 62-9.

Bassnett, S., P. A. Wilmarth and L. L. David (2009). "The membrane proteome of the mouse lens fiber cell." Mol Vis **15**: 2448-63.

Baye, L. M. and B. A. Link (2007). "Interkinetic nuclear migration and the selection of neurogenic cell divisions during vertebrate retinogenesis." J Neurosci **27**(38): 10143-52.

Baye, L. M. and B. A. Link (2008). "Nuclear migration during retinal development." Brain Res **1192**: 29-36.

Beales, P. L., A. M. Warner, G. A. Hitman, R. Thakker and F. A. Flinter (1997). "Bardet-Biedl syndrome: a molecular and phenotypic study of 18 families." J Med Genet **34**(2): 92-8.

Behar, O., J. A. Golden, H. Mashimo, F. J. Schoen and M. C. Fishman (1996). "Semaphorin III is needed for normal patterning and growth of nerves, bones and heart." Nature **383**(6600): 525-8.

Behesti, H., V. E. Papaioannou and J. C. Sowden (2009). "Loss of Tbx2 delays optic vesicle invagination leading to small optic cups." Dev Biol **333**(2): 360-72.

Bernal, D., J. E. de la Rubia, A. M. Carrasco-Abad, R. Toledo, S. Mas-Coma and A. Marcilla (2004). "Identification of enolase as a plasminogen-binding protein in excretory-secretory products of Fasciola hepatica." FEBS Lett **563**(1-3): 203-6.

Berson, E. L. and J. Howard (1971). "Temporal aspects of the electroretinogram in sector retinitis pigmentosa." Arch Ophthalmol **86**(6): 653-65.

Blackshaw, S., R. E. Fraioli, T. Furukawa and C. L. Cepko (2001). "Comprehensive analysis of photoreceptor gene expression and the identification of candidate retinal disease genes." Cell **107**(5): 579-89.

Blackshaw, S., S. Harpavat, J. Trimarchi, L. Cai, H. Huang, W. P. Kuo, G. Weber, K. Lee, R. E. Fraioli, S. H. Cho, R. Yung, E. Asch, L. Ohno-Machado, W. H. Wong and C. L. Cepko (2004). "Genomic analysis of mouse retinal development." PLoS Biol **2**(9): E247.

Boivin, D., D. Labbe, N. Fontaine, S. Lamy, E. Beaulieu, D. Gingras and R. Beliveau (2009). "The stem cell marker CD133 (prominin-1) is phosphorylated on cytoplasmic tyrosine-828 and tyrosine-852 by Src and Fyn tyrosine kinases." Biochemistry **48**(18): 3998-4007.

Boldt, K., D. A. Mans, J. Won, J. van Reeuwijk, A. Vogt, N. Kinkl, S. J. Letteboer, W. L. Hicks, R. E. Hurd, J. K. Naggert, Y. Texier, A. I. den Hollander, R. K. Koenekoop, J. Bennett, F. P. Cremers, C. J. Gloeckner, P. M. Nishina, R. Roepman and M. Ueffing (2011). "Disruption of intraflagellar protein transport in photoreceptor cilia causes Leber congenital amaurosis in humans and mice." J Clin Invest **121**(6): 2169-80.

Bolhy, S., I. Bouhlel, E. Dultz, T. Nayak, M. Zuccolo, X. Gatti, R. Vallee, J. Ellenberg and V. Doye (2011). "A Nup133-dependent NPC-anchored network tethers centrosomes to the nuclear envelope in prophase." J Cell Biol **192**(5): 855-71.

Bornschein, H., G. Goodman and R. D. Gunkel (1957). "Temporal aspects of the human electroretinogram; a study of the implicit time-amplitude relationship of the B-wave." AMA Arch Ophthalmol **57**(3): 386-92.

Buettner, R., G. Papoutsoglou, E. Scemes, D. C. Spray and R. Dermietzel (2000). "Evidence for secretory pathway localization of a voltage-dependent anion channel isoform." Proc Natl Acad Sci U S A **97**(7): 3201-6.

Carter-Dawson, L. D. and M. M. LaVail (1979a). "Rods and cones in the mouse retina. I. Structural analysis using light and electron microscopy." J Comp Neurol **188**(2): 245-62.

Carter-Dawson, L. D. and M. M. LaVail (1979b). "Rods and cones in the mouse retina. II. Autoradiographic analysis of cell generation using tritiated thymidine." J Comp Neurol **188**(2): 263-72.

Carter, D. A., A. D. Dick and E. J. Mayer (2009). "CD133+ adult human retinal cells remain undifferentiated in Leukaemia Inhibitory Factor (LIF)." BMC Ophthalmol **9**: 1.

Cavodeassi, F., F. Carreira-Barbosa, R. M. Young, M. L. Concha, M. L. Allende, C. Houart, M. Tada and S. W. Wilson (2005). "Early stages of zebrafish eye formation require the coordinated activity of Wnt11, Fz5, and the Wnt/beta-catenin pathway." Neuron **47**(1): 43-56.

Chang, B., T. Grau, S. Dangel, R. Hurd, B. Jurklies, E. C. Sener, S. Andreasson, H. Dollfus, B. Baumann, S. Bolz, N. Artemyev, S. Kohl, J. Heckenlively and B. Wissinger (2009). "A homologous genetic basis of the murine cpfl1 mutant and human achromatopsia linked to mutations in the PDE6C gene." Proc Natl Acad Sci U S A **106**(46): 19581-6.

Chen, J., A. Rattner and J. Nathans (2005). "The rod photoreceptor-specific nuclear receptor Nr2e3 represses transcription of multiple cone-specific genes." J Neurosci **25**(1): 118-29.

Chen, J., C. L. Tucker, B. Woodford, A. Szel, J. Lem, A. Gianella-Borradori, M. I. Simon and E. Bogenmann (1994). "The human blue opsin promoter directs transgene expression in short-wave cones and bipolar cells in the mouse retina." Proc Natl Acad Sci U S A **91**(7): 2611-5.

Chen, S., Q. L. Wang, Z. Nie, H. Sun, G. Lennon, N. G. Copeland, D. J. Gilbert, N. A. Jenkins and D. J. Zack (1997). "Crx, a novel Otx-like paired-homeodomain protein, binds to and transactivates photoreceptor cell-specific genes." Neuron **19**(5): 1017-30.

Cheng, H., T. S. Aleman, A. V. Cideciyan, R. Khanna, S. G. Jacobson and A. Swaroop (2006). "In vivo function of the orphan nuclear receptor NR2E3 in establishing photoreceptor identity during mammalian retinal development." Hum Mol Genet **15**(17): 2588-602.

Cheng, H., H. Khanna, E. C. Oh, D. Hicks, K. P. Mitton and A. Swaroop (2004). "Photoreceptor-specific nuclear receptor NR2E3 functions as a transcriptional activator in rod photoreceptors." Hum Mol Genet **13**(15): 1563-75.

Choi, H. S., H. Kim, A. Won, J. J. Kim, C. Y. Son, K. S. Kim, J. H. Ko, M. Y. Lee, C. H. Kim and C. J. Ryu (2008). "Development of a decoy immunization strategy to identify cell-surface molecules expressed on undifferentiated human embryonic stem cells." Cell Tissue Res **333**(2): 197-206.

Chow, R. L., C. R. Altmann, R. A. Lang and A. Hemmati-Brivanlou (1999). "Pax6 induces ectopic eyes in a vertebrate." Development **126**(19): 4213-22.

Coles, B. L., B. Angenieux, T. Inoue, K. Del Rio-Tsonis, J. R. Spence, R. R. McInnes, Y. Arsenijevic and D. van der Kooy (2004). "Facile isolation and the characterization of human retinal stem cells." Proc Natl Acad Sci U S A **101**(44): 15772-7.

Corbeil, D., K. Roper, C. A. Fargeas, A. Joester and W. B. Huttner (2001). "Prominin: a story of cholesterol, plasma membrane protrusions and human pathology." Traffic **2**(2): 82-91.

Corbeil, D., K. Roper, M. J. Hannah, A. Hellwig and W. B. Huttner (1999). "Selective localization of the polytopic membrane protein prominin in microvilli of epithelial cells - a combination of apical sorting and retention in plasma membrane protrusions." J Cell Sci **112 (Pt 7)**: 1023-33.

Corbeil, D., K. Roper, A. Hellwig, M. Tavian, S. Miraglia, S. M. Watt, P. J. Simmons, B. Peault, D. W. Buck and W. B. Huttner (2000). "The human AC133 hematopoietic stem cell antigen is also expressed in epithelial cells and targeted to plasma membrane protrusions." J Biol Chem **275**(8): 5512-20.

De Robertis, E. (1960). "Some observations on the ultrastructure and morphogenesis of photoreceptors." J Gen Physiol **43(6)Suppl**: 1-13.

Decembrini, S., M. Cananzi, S. Gualdoni, A. Battersby, N. Allen, R. A. Pearson, R. R. Ali, P. De Coppi and J. C. Sowden (2011). "Comparative analysis of the retinal potential of embryonic stem cells and amniotic fluid-derived stem cells." Stem Cells Dev **20**(5): 851-63.

Del Bene, F., A. M. Wehman, B. A. Link and H. Baier (2008). "Regulation of neurogenesis by interkinetic nuclear migration through an apical-basal notch gradient." Cell **134**(6): 1055-65.

Delorme, G., F. Saltel, E. Bonnelye, P. Jurdic and I. Machuca-Gayet (2005). "Expression and function of semaphorin 7A in bone cells." Biol Cell **97**(7): 589-97.

Dennis, G., Jr., B. T. Sherman, D. A. Hosack, J. Yang, W. Gao, H. C. Lane and R. A. Lempicki (2003). "DAVID: Database for Annotation, Visualization, and Integrated Discovery." Genome Biol **4**(5): P3.

Dewan, A., M. Liu, S. Hartman, S. S. Zhang, D. T. Liu, C. Zhao, P. O. Tam, W. M. Chan, D. S. Lam, M. Snyder, C. Barnstable, C. P. Pang and J. Hoh (2006). "HTRA1 promoter polymorphism in wet age-related macular degeneration." Science **314**(5801): 989-92.

Ding, J. B., W. J. Oh, B. L. Sabatini and C. Gu (2011). "Semaphorin 3E-Plexin-D1 signaling controls pathway-specific synapse formation in the striatum." Nat Neurosci **15**(2): 215-23.

Dorrell, M. I., E. Aguilar, C. Weber and M. Friedlander (2004). "Global gene expression analysis of the developing postnatal mouse retina." Invest Ophthalmol Vis Sci **45**(3): 1009-19.

Dreher, B. and S. R. Robinson (1988). "Development of the retinofugal pathway in birds and mammals: evidence for a common 'timetable'." Brain Behav Evol **31**(6): 369-90.

Dubreuil, V., A. M. Marzesco, D. Corbeil, W. B. Huttner and M. Wilsch-Brauninger (2007). "Midbody and primary cilium of neural progenitors release extracellular membrane particles enriched in the stem cell marker prominin-1." J Cell Biol **176**(4): 483-95.

Eberle, D., S. Schubert, K. Postel, D. Corbeil and M. Ader (2011). "Increased integration of transplanted CD73-positive photoreceptor precursors into adult mouse retina." Invest Ophthalmol Vis Sci **52**(9): 6462-71.

Eiraku, M., N. Takata, H. Ishibashi, M. Kawada, E. Sakakura, S. Okuda, K. Sekiguchi, T. Adachi and Y. Sasai (2011). "Self-organizing optic-cup morphogenesis in three-dimensional culture." Nature **472**(7341): 51-6.

Emmer, B. T., D. Maric and D. M. Engman (2010). "Molecular mechanisms of protein and lipid targeting to ciliary membranes." J Cell Sci **123**(Pt 4): 529-36.

Fargeas, C. A., M. Florek, W. B. Huttner and D. Corbeil (2003). "Characterization of prominin-2, a new member of the prominin family of pentaspan membrane glycoproteins." J Biol Chem **278**(10): 8586-96.

Feigenspan, A. and J. Bormann (1998). "GABA-gated Cl- channels in the rat retina." Prog Retin Eye Res **17**(1): 99-126.

Feng, Y., Y. Wang, O. Stock, F. Pfister, N. Tanimoto, M. W. Seeliger, J. L. Hillebrands, S. Hoffmann, H. Wolburg, N. Gretz and H. P. Hammes (2009). "Vasoregression linked to neuronal damage in the rat with defect of polycystin-2." PLoS One **4**(10): e7328.

Finnegan, S., J. L. Robson, M. Wylie, A. Healy, A. W. Stitt and W. J. Curry (2008). "Protein expression profiling during chick retinal maturation: a proteomics-based approach." Proteome Sci **6**: 34.

Fliegauf, M., T. Benzing and H. Omran (2007). "When cilia go bad: cilia defects and ciliopathies." Nat Rev Mol Cell Biol **8**(11): 880-93.

Forsythe, E. and P. L. Beales (2013). "Bardet-Biedl syndrome." Eur J Hum Genet **21**(1): 8-13.

Frade, J. M. (2002). "Interkinetic nuclear movement in the vertebrate neuroepithelium: encounters with an old acquaintance." Prog Brain Res **136**: 67-71.

Fratzl-Zelman, N., P. Fratzl, H. Horandner, B. Grabner, F. Varga, A. Ellinger and K. Klaushofer (1998). "Matrix mineralization in MC3T3-E1 cell cultures initiated by beta-glycerophosphate pulse." Bone **23**(6): 511-20.

Fukunishi, A., T. Maruyama, H. Zhao, M. Tiwari, S. Kang, A. Kumanogoh and N. Yamamoto (2011). "The action of Semaphorin7A on thalamocortical axon branching." J Neurochem **118**(6): 1008-15.

Furukawa, T., E. M. Morrow and C. L. Cepko (1997). "Crx, a novel otx-like homeobox gene, shows photoreceptor-specific expression and regulates photoreceptor differentiation." Cell **91**(4): 531-41.

Furukawa, T., E. M. Morrow, T. Li, F. C. Davis and C. L. Cepko (1999). "Retinopathy and attenuated circadian entrainment in Crx-deficient mice." Nat Genet **23**(4): 466-70.

Garcia-Gonzalo, F. R., K. C. Corbit, M. S. Sirerol-Piquer, G. Ramaswami, E. A. Otto, T. R. Noriega, A. D. Seol, J. F. Robinson, C. L. Bennett, D. J. Josifova, J. M. Garcia-Verdugo, N. Katsanis, F. Hildebrandt and J. F. Reiter (2011). "A transition zone complex regulates mammalian ciliogenesis and ciliary membrane composition." Nat Genet **43**(8): 776-84.

Garelli, A., N. P. Rotstein and L. E. Politi (2006). "Docosahexaenoic acid promotes photoreceptor differentiation without altering Crx expression." Invest Ophthalmol Vis Sci **47**(7): 3017-27.

Gerstner, A., X. Zong, F. Hofmann and M. Biel (2000). "Molecular cloning and functional characterization of a new modulatory cyclic nucleotide-gated channel subunit from mouse retina." J Neurosci **20**(4): 1324-32.

Gimeno, L., P. Brulet and S. Martinez (2003). "Study of Fgf15 gene expression in developing mouse brain." Gene Expr Patterns **3**(4): 473-81.

Glaser, T., L. Jepeal, J. G. Edwards, S. R. Young, J. Favor and R. L. Maas (1994). "PAX6 gene dosage effect in a family with congenital cataracts, aniridia, anophthalmia and central nervous system defects." Nat Genet **7**(4): 463-71.

Gonzalez-Cordero, A., E. L. West, R. A. Pearson, Y. Duran, L. S. Carvalho, C. J. Chu, A. Naeem, S. J. Blackford, A. Georgiadis, J. Lakowski, M. Hubank, A. J. Smith, J. W. Bainbridge, J. C. Sowden and R. R. Ali (2013). "Photoreceptor precursors derived from three-dimensional embryonic stem cell cultures integrate and mature within adult degenerate retina." Nat Biotechnol **31**(8): 741-7.

Grau, T., N. O. Artemyev, T. Rosenberg, H. Dollfus, O. H. Haugen, E. Cumhur Sener, B. Jurklies, S. Andreasson, C. Kernstock, M. Larsen, E. Zrenner, B. Wissinger and S. Kohl (2011). "Decreased catalytic activity and altered activation properties of PDE6C mutants associated with autosomal recessive achromatopsia." Hum Mol Genet **20**(4): 719-30.

Grigoryan, E. N., A. Vasilaki, N. Mastrodimou and K. Thermos (2003). "Somatostatin receptor immunoreactivity in the eye of the adult newt (Pleurodeles waltlii Michan)." Neurosci Lett **337**(3): 143-6.

Gu, C., Y. Yoshida, J. Livet, D. V. Reimert, F. Mann, J. Merte, C. E. Henderson, T. M. Jessell, A. L. Kolodkin and D. D. Ginty (2005). "Semaphorin 3E and plexin-D1 control vascular pattern independently of neuropilins." Science **307**(5707): 265-8.

Hackam, A. S., J. Qian, D. Liu, T. Gunatilaka, R. H. Farkas, I. Chowers, M. Kageyama, G. Parmigiani and D. J. Zack (2004). "Comparative gene expression analysis of murine retina and brain." Mol Vis **10**: 637-49.

Haga, S., T. Hattori, T. Sato, K. Sato, S. Matsuda, R. Kobayakawa, H. Sakano, Y. Yoshihara, T. Kikusui and K. Touhara (2010). "The male mouse pheromone ESP1 enhances female sexual receptive behaviour through a specific vomeronasal receptor." Nature **466**(7302): 118-22.

Haider, N. B., P. Demarco, A. M. Nystuen, X. Huang, R. S. Smith, M. A. McCall, J. K. Naggert and P. M. Nishina (2006). "The transcription factor Nr2e3 functions in retinal progenitors to suppress cone cell generation." Vis Neurosci **23**(6): 917-29.

Han, Z., S. M. Conley, R. S. Makkia, M. J. Cooper and M. I. Naash (2012). "DNA nanoparticle-mediated ABCA4 delivery rescues Stargardt dystrophy in mice." J Clin Invest **122**(9): 3221-6.

Harman, A. M. and L. D. Beazley (1989). "Generation of retinal cells in the wallaby, Setonix brachyurus (quokka)." Neuroscience **28**(1): 219-32.

Hartong, D. T., E. L. Berson and T. P. Dryja (2006). "Retinitis pigmentosa." Lancet **368**(9549): 1795-809.

Hengl, T., H. Kaneko, K. Dauner, K. Vocke, S. Frings and F. Mohrlen (2010). "Molecular components of signal amplification in olfactory sensory cilia." Proc Natl Acad Sci U S A **107**(13): 6052-7.

Hennig, A. K., G. H. Peng and S. Chen (2008). "Regulation of photoreceptor gene expression by Crx-associated transcription factor network." Brain Res **1192**: 114-33.

Herget, T., S. A. Oehrlein, D. J. Pappin, E. Rozengurt and P. J. Parker (1995). "The myristoylated alanine-rich C-kinase substrate (MARCKS) is sequentially phosphorylated by conventional, novel and atypical isotypes of protein kinase C." Eur J Biochem **233**(2): 448-57.

Heussen, F. M., N. F. Fawzy, S. Joeres, A. Lux, K. Maaijwee, J. C. Meurs, B. Kirchhof and A. M. Joussen (2008). "Autologous translocation of the choroid and RPE in age-related macular degeneration: 1-year follow-up in 30 patients and recommendations for patient selection." Eye (Lond) **22**(6): 799-807.

Hildebrandt, F. and E. Otto (2005). "Cilia and centrosomes: a unifying pathogenic concept for cystic kidney disease?" Nat Rev Genet **6**(12): 928-40.

Hill, R. E., J. Favor, B. L. Hogan, C. C. Ton, G. F. Saunders, I. M. Hanson, J. Prosser, T. Jordan, N. D. Hastie and V. van Heyningen (1991). "Mouse small eye results from mutations in a paired-like homeobox-containing gene." Nature **354**(6354): 522-5.

Hinds, J. W. and P. L. Hinds (1979). "Differentiation of photoreceptors and horizontal cells in the embryonic mouse retina: an electron microscopic, serial section analysis." J Comp Neurol **187**(3): 495-511.

Hirotsune, S., T. Takahara, N. Sasaki, K. Hirose, A. Yoshiki, T. Ohashi, M. Kusakabe, Y. Murakami, M. Muramatsu, S. Watanabe and et al. (1995). "The reeler gene encodes a protein with an EGF-like motif expressed by pioneer neurons." Nat Genet **10**(1): 77-83.

Hollyfield, J. G. (1971). "Differential growth of the neural retina in Xenopus laevis larvae." Dev Biol **24**(2): 264-86.

Holmes, S., A. M. Downs, A. Fosberry, P. D. Hayes, D. Michalovich, P. Murdoch, K. Moores, J. Fox, K. Deen, G. Pettman, T. Wattam and C. Lewis (2002). "Sema7A is a potent monocyte stimulator." Scand J Immunol **56**(3): 270-5.

Holt, C. E., T. W. Bertsch, H. M. Ellis and W. A. Harris (1988). "Cellular determination in the Xenopus retina is independent of lineage and birth date." Neuron **1**(1): 15-26.

Hood, D. C. and M. A. Finkelstein (1986). Sensitivity to light. New York, John Wiley and Sons.

Huang da, W., B. T. Sherman and R. A. Lempicki (2009). "Systematic and integrative analysis of large gene lists using DAVID bioinformatics resources." Nat Protoc **4**(1): 44-57.

Huang, L., Q. Zhang, S. Li, L. Guan, X. Xiao, J. Zhang, X. Jia, W. Sun, Z. Zhu, Y. Gao, Y. Yin, P. Wang, X. Guo, J. Wang and Q. Zhang (2013). "Exome sequencing of 47 chinese families with cone-rod dystrophy: mutations in 25 known causative genes." PLoS One **8**(6): e65546.

Huangfu, D., A. Liu, A. S. Rakeman, N. S. Murcia, L. Niswander and K. V. Anderson (2003). "Hedgehog signalling in the mouse requires intraflagellar transport proteins." Nature **426**(6962): 83-7.

Huertas-Vazquez, A., C. L. Plaisier, R. Geng, B. E. Haas, J. Lee, M. M. Greevenbroek, C. van der Kallen, T. W. de Bruin, M. R. Taskinen, K. N. Alagramam and P. Pajukanta (2010). "A nonsynonymous SNP within PCDH15 is associated with lipid traits in familial combined hyperlipidemia." Hum Genet **127**(1): 83-9.

Humayun, M. S., J. D. Dorn, L. da Cruz, G. Dagnelie, J. A. Sahel, P. E. Stanga, A. V. Cideciyan, J. L. Duncan, D. Eliott, E. Filley, A. C. Ho, A. Santos, A. B. Safran, A. Arditi, L. V. Del Priore and R. J. Greenberg (2012). "Interim results from the international trial of Second Sight's visual prosthesis." Ophthalmology **119**(4): 779-88.

Hwang, J. I., D. K. Kim, H. B. Kwon, H. Vaudry and J. Y. Seong (2009). "Phylogenetic history, pharmacological features, and signal transduction of neurotensin receptors in vertebrates." Ann N Y Acad Sci **1163**: 169-78.

Ikegami, K., S. Sato, K. Nakamura, L. E. Ostrowski and M. Setou (2010). "Tubulin polyglutamylation is essential for airway ciliary function through the regulation of beating asymmetry." Proc Natl Acad Sci U S A **107**(23): 10490-5.

Imai, T., T. Yamazaki, R. Kobayakawa, K. Kobayakawa, T. Abe, M. Suzuki and H. Sakano (2009). "Pre-target axon sorting establishes the neural map topography." Science **325**(5940): 585-90.

Jacobs, D. T., R. Weigert, K. D. Grode, J. G. Donaldson and R. E. Cheney (2009). "Myosin Vc is a molecular motor that functions in secretory granule trafficking." Mol Biol Cell **20**(21): 4471-88.

Jacobson, S. G., A. V. Cideciyan, T. S. Aleman, A. Sumaroka, A. J. Roman, L. M. Gardner, H. M. Prosser, M. Mishra, N. T. Bech-Hansen, W. Herrera, S. B. Schwartz, X. Z. Liu, W. J. Kimberling, K. P. Steel and D. S. Williams (2008). "Usher syndromes due to MYO7A, PCDH15, USH2A or GPR98 mutations share retinal disease mechanism." Hum Mol Genet **17**(15): 2405-15.

Jacobson, S. G., A. V. Cideciyan, J. Bennett, R. M. Kingsley, V. C. Sheffield and E. M. Stone (2002). "Novel mutation in the TIMP3 gene causes Sorsby fundus dystrophy." Arch Ophthalmol **120**(3): 376-9.

Jaszai, J., C. A. Fargeas, M. Florek, W. B. Huttner and D. Corbeil (2007). "Focus on molecules: prominin-1 (CD133)." Exp Eye Res **85**(5): 585-6.

Jaszai, J., C. A. Fargeas, S. Graupner, E. M. Tanaka, M. Brand, W. B. Huttner and D. Corbeil (2011). "Distinct and conserved prominin-1/CD133-positive retinal cell populations identified across species." PLoS One **6**(3): e17590.

Ji, H., D. W. Greening, T. W. Barnes, J. W. Lim, B. J. Tauro, A. Rai, R. Xu, C. Adda, S. Mathivanan, W. Zhao, Y. Xue, T. Xu, H. J. Zhu and R. J. Simpson (2013). "Proteome profiling of exosomes derived from human primary and metastatic colorectal cancer cells reveal differential expression of key metastatic factors and signal transduction components." Proteomics **13**(10-11): 1672-86.

Jia, L., E. C. Oh, L. Ng, M. Srinivas, M. Brooks, A. Swaroop and D. Forrest (2009). "Retinoid-related orphan nuclear receptor RORbeta is an early-acting factor in rod photoreceptor development." Proc Natl Acad Sci U S A **106**(41): 17534-9.

Johnson, J. L. and M. R. Leroux (2010). "cAMP and cGMP signaling: sensory systems with prokaryotic roots adopted by eukaryotic cilia." Trends Cell Biol **20**(8): 435-44.

Johnson, P. T., R. R. Williams, K. Cusato and B. E. Reese (1999). "Rods and cones project to the inner plexiform layer during development." J Comp Neurol **414**(1): 1-12.

Jones, T. J., R. K. Adapala, W. J. Geldenhuys, C. Bursley, W. A. AbouAlaiwi, S. M. Nauli and C. K. Thodeti (2012). "Primary cilia regulates the directional migration and barrier integrity of endothelial cells through the modulation of hsp27 dependent actin cytoskeletal organization." J Cell Physiol **227**(1): 70-6.

Jonsson, F., M. S. Burstedt, O. Sandgren, A. Norberg and I. Golovleva (2013). "Novel mutations in CRB1 and ABCA4 genes cause Leber congenital amaurosis and Stargardt disease in a Swedish family." Eur J Hum Genet.

Jossin, Y. and J. A. Cooper (2011). "Reelin, Rap1 and N-cadherin orient the migration of multipolar neurons in the developing neocortex." Nat Neurosci **14**(6): 697-703.

Kanda, A., W. Chen, M. Othman, K. E. Branham, M. Brooks, R. Khanna, S. He, R. Lyons, G. R. Abecasis and A. Swaroop (2007). "A variant of mitochondrial protein LOC387715/ARMS2, not HTRA1, is strongly associated with age-related macular degeneration." Proc Natl Acad Sci U S A **104**(41): 16227-32.

Kanda, A., J. S. Friedman, K. M. Nishiguchi and A. Swaroop (2007). "Retinopathy mutations in the bZIP protein NRL alter phosphorylation and transcriptional activity." Hum Mutat **28**(6): 589-98.

Kann, M. L., S. Soues, N. Levilliers and J. P. Fouquet (2003). "Glutamylated tubulin: diversity of expression and distribution of isoforms." Cell Motil Cytoskeleton **55**(1): 14-25.

Kazmierczak, P., H. Sakaguchi, J. Tokita, E. M. Wilson-Kubalek, R. A. Milligan, U. Muller and B. Kachar (2007). "Cadherin 23 and protocadherin 15 interact to form tip-link filaments in sensory hair cells." Nature **449**(7158): 87-91.

Kishan, A. U., B. S. Modjtahedi, L. S. Morse and P. Lee (2013). "Radiation therapy for neovascular age-related macular degeneration." Int J Radiat Oncol Biol Phys **85**(3): 583-97.

Klassen, H. J., T. F. Ng, Y. Kurimoto, I. Kirov, M. Shatos, P. Coffey and M. J. Young (2004). "Multipotent retinal progenitors express developmental markers, differentiate into retinal neurons, and preserve light-mediated behavior." Invest Ophthalmol Vis Sci **45**(11): 4167-73.

Knabe, W. and H. J. Kuhn (1997). "Ciliogenesis in photoreceptor cells of the tree shrew retina." Anat Embryol (Berl) **196**(2): 123-31.

Kobayashi, T. and B. D. Dynlacht (2011). "Regulating the transition from centriole to basal body." J Cell Biol **193**(3): 435-44.

Kohl, S., B. Baumann, M. Broghammer, H. Jagle, P. Sieving, U. Kellner, R. Spegal, M. Anastasi, E. Zrenner, L. T. Sharpe and B. Wissinger (2000). "Mutations in the CNGB3 gene encoding the beta-subunit of the cone photoreceptor cGMP-gated channel are responsible for achromatopsia (ACHM3) linked to chromosome 8q21." Hum Mol Genet **9**(14): 2107-16.

Koike, C., A. Nishida, S. Ueno, H. Saito, R. Sanuki, S. Sato, A. Furukawa, S. Aizawa, I. Matsuo, N. Suzuki, M. Kondo and T. Furukawa (2007). "Functional roles of Otx2 transcription factor in postnatal mouse retinal development." Mol Cell Biol **27**(23): 8318-29.

Kolle, G., M. Ho, Q. Zhou, H. S. Chy, K. Krishnan, N. Cloonan, I. Bertoncello, A. L. Laslett and S. M. Grimmond (2009). "Identification of human embryonic stem cell surface markers by combined membrane-polysome translation state array analysis and immunotranscriptional profiling." Stem Cells **27**(10): 2446-56.

Kolodkin, A. L., D. J. Matthes and C. S. Goodman (1993). "The semaphorin genes encode a family of transmembrane and secreted growth cone guidance molecules." Cell **75**(7): 1389-99.

Kumar, J. P. and K. Moses (2001). "EGF receptor and Notch signaling act upstream of Eyeless/Pax6 to control eye specification." Cell **104**(5): 687-97.

La Vail, M. M., D. H. Rapaport and P. Rakic (1991). "Cytogenesis in the Monkey Retina." The Journal of Comparative Neurology **309**: 86 - 114.

Lakowski, J., M. Baron, J. Bainbridge, A. C. Barber, R. A. Pearson, R. R. Ali and J. C. Sowden (2010). "Cone and rod photoreceptor transplantation in models of the childhood retinopathy Leber congenital amaurosis using flow-sorted Crx-positive donor cells." Hum Mol Genet **19**(23): 4545-59.

Lakowski, J., Y. T. Han, R. A. Pearson, A. Gonzalez-Cordero, E. L. West, S. Gualdoni, A. C. Barber, M. Hubank, R. R. Ali and J. C. Sowden (2011). "Effective transplantation of photoreceptor precursor cells selected via cell surface antigen expression." Stem Cells **29**(9): 1391-404.

Lamb, T. D., S. P. Collin and E. N. Pugh, Jr. (2007). "Evolution of the vertebrate eye: opsins, photoreceptors, retina and eye cup." Nat Rev Neurosci **8**(12): 960-76.

Lamba, D. A., J. Gust and T. A. Reh (2009). "Transplantation of human embryonic stem cell-derived photoreceptors restores some visual function in Crx-deficient mice." Cell Stem Cell **4**(1): 73-9.

Lamba, D. A., M. O. Karl, C. B. Ware and T. A. Reh (2006). "Efficient generation of retinal progenitor cells from human embryonic stem cells." Proc Natl Acad Sci U S A **103**(34): 12769-74.

LaVail, M. M. (1973). "Kinetics of rod outer segment renewal in the developing mouse retina." J Cell Biol **58**(3): 650-61.

Lee, R. H., T. D. Ting, B. S. Lieberman, D. E. Tobias, R. N. Lolley and Y. K. Ho (1992). "Regulation of retinal cGMP cascade by phosducin in bovine rod photoreceptor cells. Interaction of phosducin and transducin." J Biol Chem **267**(35): 25104-12.

Lefevre, G., V. Michel, D. Weil, L. Lepelletier, E. Bizard, U. Wolfrum, J. P. Hardelin and C. Petit (2008). "A core cochlear phenotype in USH1 mouse mutants implicates fibrous links of the hair bundle in its cohesion, orientation and differential growth." Development **135**(8): 1427-37.

Li, G., C. Liu, J. Yuan, X. Xiao, N. Tang, J. Hao, H. Wang, X. Bian, Y. Deng and Y. Ding (2010). "CD133(+) single cell-derived progenies of colorectal cancer cell line SW480 with different invasive and metastatic potential." Clin Exp Metastasis **27**(7): 517-27.

Liao, H., R. J. Winkfein, G. Mack, J. B. Rattner and T. J. Yen (1995). "CENP-F is a protein of the nuclear matrix that assembles onto kinetochores at late G2 and is rapidly degraded after mitosis." J Cell Biol **130**(3): 507-18.

Liu, H., Z. S. Juo, A. H. Shim, P. J. Focia, X. Chen, K. C. Garcia and X. He (2010). "Structural basis of semaphorin-plexin recognition and viral mimicry from Sema7A and A39R complexes with PlexinC1." Cell **142**(5): 749-61.

Liu, J., J. Wang, Q. Huang, J. Higdon, S. Magdaleno, T. Curran and J. Zuo (2006). "Gene expression profiles of mouse retinas during the second and third postnatal weeks." Brain Res **1098**(1): 113-25.

Liu, Q., Q. Zhang and E. A. Pierce (2010). "Photoreceptor sensory cilia and inherited retinal degeneration." Adv Exp Med Biol **664**: 223-32.

Liu, X., O. V. Bulgakov, K. N. Darrow, B. Pawlyk, M. Adamian, M. C. Liberman and T. Li (2007). "Usherin is required for maintenance of retinal photoreceptors and normal development of cochlear hair cells." Proc Natl Acad Sci U S A **104**(11): 4413-8.

Liu, Y., Y. Shen, J. S. Rest, P. A. Raymond and D. J. Zack (2001). "Isolation and characterization of a zebrafish homologue of the cone rod homeobox gene." Invest Ophthalmol Vis Sci **42**(2): 481-7.

Lopez-Villar, E., L. Monteoliva, M. R. Larsen, E. Sachon, M. Shabaz, M. Pardo, J. Pla, C. Gil, P. Roepstorff and C. Nombela (2006). "Genetic and proteomic evidences support the localization of yeast enolase in the cell surface." Proteomics **6 Suppl 1**: S107-18.

Louvi, A. and E. A. Grove (2011). "Cilia in the CNS: the quiet organelle claims center stage." Neuron **69**(6): 1046-60.

MacLaren, R. E., R. A. Pearson, A. MacNeil, R. H. Douglas, T. E. Salt, M. Akimoto, A. Swaroop, J. C. Sowden and R. R. Ali (2006). "Retinal repair by transplantation of photoreceptor precursors." Nature **444**(7116): 203-7.

Maguire, A. M., F. Simonelli, E. A. Pierce, E. N. Pugh, Jr., F. Mingozzi, J. Bennicelli, S. Banfi, K. A. Marshall, F. Testa, E. M. Surace, S. Rossi, A. Lyubarsky, V. R. Arruda, B. Konkle, E. Stone, J. Sun, J. Jacobs, L. Dell'Osso, R. Hertle, J. X. Ma, T. M. Redmond, X. Zhu, B. Hauck, O. Zelenaia, K. S. Shindler, M. G. Maguire, J. F. Wright, N. J. Volpe, J. W. McDonnell, A. Auricchio, K. A. High and J. Bennett (2008). "Safety and efficacy of gene transfer for Leber's congenital amaurosis." N Engl J Med **358**(21): 2240-8.

Malm, E., V. Ponjavic, P. M. Nishina, J. K. Naggert, E. G. Hinman, S. Andreasson, J. D. Marshall and C. Moller (2008). "Full-field electroretinography and marked variability in clinical phenotype of Alstrom syndrome." Arch Ophthalmol **126**(1): 51-7.

Matsuoka, R. L., O. Chivatakarn, T. C. Badea, I. S. Samuels, H. Cahill, K. Katayama, S. R. Kumar, F. Suto, A. Chedotal, N. S. Peachey, J. Nathans, Y. Yoshida, R. J. Giger and A. L. Kolodkin (2011). "Class 5 transmembrane semaphorins control selective Mammalian retinal lamination and function." Neuron **71**(3): 460-73.

Matsuoka, R. L., K. T. Nguyen-Ba-Charvet, A. Parray, T. C. Badea, A. Chedotal and A. L. Kolodkin (2011). "Transmembrane semaphorin signalling controls laminar stratification in the mammalian retina." Nature **470**(7333): 259-63.

Maurus, D., C. Heligon, A. Burger-Schwarzler, A. W. Brandli and M. Kuhl (2005). "Noncanonical Wnt-4 signaling and EAF2 are required for eye development in Xenopus laevis." Embo J **24**(6): 1181-91.

Maw, M. A., D. Corbeil, J. Koch, A. Hellwig, J. C. Wilson-Wheeler, R. J. Bridges, G. Kumaramanickavel, S. John, D. Nancarrow, K. Roper, A. Weigmann, W. B. Huttner and M. J. Denton (2000). "A frameshift mutation in prominin (mouse)-like 1 causes human retinal degeneration." Hum Mol Genet **9**(1): 27-34.

Mears, A. J., M. Kondo, P. K. Swain, Y. Takada, R. A. Bush, T. L. Saunders, P. A. Sieving and A. Swaroop (2001). "Nrl is required for rod photoreceptor development." Nat Genet **29**(4): 447-52.

Messina, A., N. Ferraris, S. Wray, G. Cagnoni, D. E. Donohue, F. Casoni, P. R. Kramer, A. A. Derijck, Y. Adolfs, A. Fasolo, R. J. Pasterkamp and P. Giacobini (2011). "Dysregulation of Semaphorin7A/beta1-integrin signaling leads to defective GnRH-1 cell migration, abnormal gonadal development and altered fertility." Hum Mol Genet **20**(24): 4759-74.

Meyer, J. S., R. L. Shearer, E. E. Capowski, L. S. Wright, K. A. Wallace, E. L. McMillan, S. C. Zhang and D. M. Gamm (2009). "Modeling early retinal development with human embryonic and induced pluripotent stem cells." Proc Natl Acad Sci U S A **106**(39): 16698-703.

Meyer, M. R., A. Angele, E. Kremmer, U. B. Kaupp and F. Muller (2000). "A cGMP-signaling pathway in a subset of olfactory sensory neurons." Proc Natl Acad Sci U S A **97**(19): 10595-600.

Million, K., J. Larcher, J. Laoukili, D. Bourguignon, F. Marano and F. Tournier (1999). "Polyglutamylation and polyglycylation of alpha- and beta-tubulins during in vitro ciliated cell differentiation of human respiratory epithelial cells." J Cell Sci **112 (Pt 23)**: 4357-66.

Miraglia, S., W. Godfrey, A. H. Yin, K. Atkins, R. Warnke, J. T. Holden, R. A. Bray, E. K. Waller and D. W. Buck (1997). "A novel five-transmembrane hematopoietic stem cell antigen: isolation, characterization, and molecular cloning." Blood **90**(12): 5013-21.

Moore, K. B. and S. A. Moody (1999). "Animal-vegetal asymmetries influence the earliest steps in retina fate commitment in Xenopus." Dev Biol **212**(1): 25-41.

Morgans, C. W., P. Kensel-Hammes, J. B. Hurley, K. Burton, R. Idzerda, G. S. McKnight and S. M. Bajjalieh (2009). "Loss of the Synaptic Vesicle Protein SV2B results in reduced neurotransmission and altered synaptic vesicle protein expression in the retina." PLoS One **4**(4): e5230.

Morrow, E. M., M. J. Belliveau and C. L. Cepko (1998). "Two phases of rod photoreceptor differentiation during rat retinal development." J Neurosci **18**(10): 3738-48.

Morrow, E. M., T. Furukawa, E. Raviola and C. L. Cepko (2005). "Synaptogenesis and outer segment formation are perturbed in the neural retina of Crx mutant mice." BMC Neurosci **6**: 5.

Moynihan, K. L., R. Pooley, P. M. Miller, I. Kaverina and D. M. Bader (2009). "Murine CENP-F regulates centrosomal microtubule nucleation and interacts with Hook2 at the centrosome." Mol Biol Cell **20**(22): 4790-803.

Muranishi, Y., S. Sato, T. Inoue, S. Ueno, T. Koyasu, M. Kondo and T. Furukawa (2010). "Gene expression analysis of embryonic photoreceptor precursor cells using BAC-Crx-EGFP transgenic mouse." Biochem Biophys Res Commun **392**(3): 317-22.

Mustafi, D., A. H. Engel and K. Palczewski (2009). "Structure of cone photoreceptors." Prog Retin Eye Res **28**(4): 289-302.

Ng, L., J. B. Hurley, B. Dierks, M. Srinivas, C. Salto, B. Vennstrom, T. A. Reh and D. Forrest (2001). "A thyroid hormone receptor that is required for the development of green cone photoreceptors." Nat Genet **27**(1): 94-8.

Ng, L., A. Lyubarsky, S. S. Nikonov, M. Ma, M. Srinivas, B. Kefas, D. L. St Germain, A. Hernandez, E. N. Pugh, Jr. and D. Forrest (2010). "Type 3 deiodinase, a thyroid-hormone-

inactivating enzyme, controls survival and maturation of cone photoreceptors." J Neurosci **30**(9): 3347-57.
Nieoullon, V., R. Belvindrah, G. Rougon and G. Chazal (2007). "Mouse CD24 is required for homeostatic cell renewal." Cell Tissue Res **329**(3): 457-67.
Nishida, A., A. Furukawa, C. Koike, Y. Tano, S. Aizawa, I. Matsuo and T. Furukawa (2003). "Otx2 homeobox gene controls retinal photoreceptor cell fate and pineal gland development." Nat Neurosci **6**(12): 1255-63.
Nishida, S., Y. Hirohashi, T. Torigoe, H. Kitamura, A. Takahashi, N. Masumori, T. Tsukamoto and N. Sato (2012). "Gene expression profiles of prostate cancer stem cells isolated by aldehyde dehydrogenase activity assay." J Urol **188**(1): 294-9.
Oh, E. C., N. Khan, E. Novelli, H. Khanna, E. Strettoi and A. Swaroop (2007). "Transformation of cone precursors to functional rod photoreceptors by bZIP transcription factor NRL." Proc Natl Acad Sci U S A **104**(5): 1679-84.
Ohsawa, S., S. Hamada, H. Asou, K. Kuida, Y. Uchiyama, H. Yoshida and M. Miura (2009). "Caspase-9 activation revealed by semaphorin 7A cleavage is independent of apoptosis in the aged olfactory bulb." J Neurosci **29**(36): 11385-92.
Ohsawa, S., S. Hamada, K. Kuida, H. Yoshida, T. Igaki and M. Miura (2010). "Maturation of the olfactory sensory neurons by Apaf-1/caspase-9-mediated caspase activity." Proc Natl Acad Sci U S A **107**(30): 13366-71.
Okada, S. F., W. K. O'Neal, P. Huang, R. A. Nicholas, L. E. Ostrowski, W. J. Craigen, E. R. Lazarowski and R. C. Boucher (2004). "Voltage-dependent anion channel-1 (VDAC-1) contributes to ATP release and cell volume regulation in murine cells." J Gen Physiol **124**(5): 513-26.
Olney, J. W. (1968). "An electron microscopic study of synapse formation, receptor outer segment development, and other aspects of developing mouse retina." Invest Ophthalmol **7**(3): 250-68.
Osakada, F., H. Ikeda, M. Mandai, T. Wataya, K. Watanabe, N. Yoshimura, A. Akaike, Y. Sasai and M. Takahashi (2008). "Toward the generation of rod and cone photoreceptors from mouse, monkey and human embryonic stem cells." Nat Biotechnol **26**(2): 215-24.
Osakada, F., H. Ikeda, Y. Sasai and M. Takahashi (2009). "Stepwise differentiation of pluripotent stem cells into retinal cells." Nat Protoc **4**(6): 811-24.
Otto, E. A., T. W. Hurd, R. Airik, M. Chaki, W. Zhou, C. Stoetzel, S. B. Patil, S. Levy, A. K. Ghosh, C. A. Murga-Zamalloa, J. van Reeuwijk, S. J. Letteboer, L. Sang, R. H. Giles, Q. Liu, K. L. Coene, A. Estrada-Cuzcano, R. W. Collin, H. M. McLaughlin, S. Held, J. M. Kasanuki, G. Ramaswami, J. Conte, I. Lopez, J. Washburn, J. Macdonald, J. Hu, Y. Yamashita, E. R. Maher, L. M. Guay-Woodford, H. P. Neumann, N. Obermuller, R. K. Koenekoop, C. Bergmann, X. Bei, R. A. Lewis, N. Katsanis, V. Lopes, D. S. Williams, R. H. Lyons, C. V. Dang, D. A. Brito, M. B. Dias, X. Zhang, J. D. Cavalcoli, G. Nurnberg, P. Nurnberg, E. A. Pierce, P. K. Jackson, C. Antignac, S. Saunier, R. Roepman, H. Dollfus, H. Khanna and F. Hildebrandt (2010). "Candidate exome capture identifies mutation of SDCCAG8 as the cause of a retinal-renal ciliopathy." Nat Genet **42**(10): 840-50.
Pasterkamp, R. J. (2012). "Getting neural circuits into shape with semaphorins." Nat Rev Neurosci **13**(9): 605-18.
Pasterkamp, R. J., S. M. Kolk, A. J. Hellemons and A. L. Kolodkin (2007). "Expression patterns of semaphorin7A and plexinC1 during rat neural development suggest roles in axon guidance and neuronal migration." BMC Dev Biol **7**: 98.
Pasterkamp, R. J., J. J. Peschon, M. K. Spriggs and A. L. Kolodkin (2003). "Semaphorin 7A promotes axon outgrowth through integrins and MAPKs." Nature **424**(6947): 398-405.
Pearson, R. A., A. C. Barber, M. Rizzi, C. Hippert, T. Xue, E. L. West, Y. Duran, A. J. Smith, J. Z. Chuang, S. A. Azam, U. F. Luhmann, A. Benucci, C. H. Sung, J. W. Bainbridge, M. Carandini, K. W. Yau, J. C. Sowden and R. R. Ali (2012). "Restoration of vision after transplantation of photoreceptors." Nature **485**(7396): 99-103.

Pearson, R. A., A. C. Barber, M. Rizzi, C. Hippert, T. Xue, E. L. West, Y. Duran, A. J. Smith, J. Z. Chuang, S. A. Azam, U. F. Luhmann, A. Benucci, C. H. Sung, J. W. Bainbridge, M. Carandini, K. W. Yau, J. C. Sowden and R. R. Ali (2012). "Restoration of vision after transplantation of photoreceptors." Nature.

Pearson, R. A., A. C. Barber, E. L. West, R. E. MacLaren, Y. Duran, J. W. Bainbridge, J. C. Sowden and R. R. Ali (2010). "Targeted disruption of outer limiting membrane junctional proteins (Crb1 and ZO-1) increases integration of transplanted photoreceptor precursors into the adult wild-type and degenerating retina." Cell Transplant **19**(4): 487-503.

Pecho-Vrieseling, E., M. Sigrist, Y. Yoshida, T. M. Jessell and S. Arber (2009). "Specificity of sensory-motor connections encoded by Sema3e-Plxnd1 recognition." Nature **459**(7248): 842-6.

Perron, M. and W. A. Harris (2000). "Determination of vertebrate retinal progenitor cell fate by the Notch pathway and basic helix-loop-helix transcription factors." Cell Mol Life Sci **57**(2): 215-23.

Petrukhin, K., M. J. Koisti, B. Bakall, W. Li, G. Xie, T. Marknell, O. Sandgren, K. Forsman, G. Holmgren, S. Andreasson, M. Vujic, A. A. Bergen, V. McGarty-Dugan, D. Figueroa, C. P. Austin, M. L. Metzker, C. T. Caskey and C. Wadelius (1998). "Identification of the gene responsible for Best macular dystrophy." Nat Genet **19**(3): 241-7.

Pooley, R. D., K. L. Moynihan, V. Soukoulis, S. Reddy, R. Francis, C. Lo, L. J. Ma and D. M. Bader (2008). "Murine CENPF interacts with syntaxin 4 in the regulation of vesicular transport." J Cell Sci **121**(Pt 20): 3413-21.

Prada, C., J. Puga, L. Perez-Mendez, R. Lopez and G. Ramirez (1991). "Spatial and Temporal Patterns of Neurogenesis in the Chick Retina." Eur J Neurosci **3**(6): 559-569.

Prusky, G. T., P. W. West and R. M. Douglas (2000). "Behavioral assessment of visual acuity in mice and rats." Vision Res **40**(16): 2201-9.

Punzo, C., K. Kornacker and C. L. Cepko (2009). "Stimulation of the insulin/mTOR pathway delays cone death in a mouse model of retinitis pigmentosa." Nat Neurosci **12**(1): 44-52.

Rachel, R. A., T. Li and A. Swaroop (2012). "Photoreceptor sensory cilia and ciliopathies: focus on CEP290, RPGR and their interacting proteins." Cilia **1**(1): 22.

Rapaport, D. H., L. L. Wong, E. D. Wood, D. Yasumura and M. M. LaVail (2004). "Timing and topography of cell genesis in the rat retina." J Comp Neurol **474**(2): 304-24.

Raymond, P. A. (1991). "Retinal regeneration in teleost fish." Ciba Found Symp **160**: 171-86; discussion 186-91.

Reh, T. A. and E. M. Levine (1998). "Multipotential stem cells and progenitors in the vertebrate retina." J Neurobiol **36**(2): 206-20.

Reiners, J., T. Marker, K. Jurgens, B. Reidel and U. Wolfrum (2005). "Photoreceptor expression of the Usher syndrome type 1 protein protocadherin 15 (USH1F) and its interaction with the scaffold protein harmonin (USH1C)." Mol Vis **11**: 347-55.

Reiners, J., K. Nagel-Wolfrum, K. Jurgens, T. Marker and U. Wolfrum (2006). "Molecular basis of human Usher syndrome: deciphering the meshes of the Usher protein network provides insights into the pathomechanisms of the Usher disease." Exp Eye Res **83**(1): 97-119.

Rice, D. S., W. Huang, H. A. Jones, G. Hansen, G. L. Ye, N. Xu, E. A. Wilson, K. Troughton, K. Vaddi, R. C. Newton, B. P. Zambrowicz and A. T. Sands (2004). "Severe retinal degeneration associated with disruption of semaphorin 4A." Invest Ophthalmol Vis Sci **45**(8): 2767-77.

Rich, K. A., Y. Zhan and J. C. Blanks (1997). "Migration and synaptogenesis of cone photoreceptors in the developing mouse retina." J Comp Neurol **388**(1): 47-63.

Rivera, A., S. A. Fisher, L. G. Fritsche, C. N. Keilhauer, P. Lichtner, T. Meitinger and B. H. Weber (2005). "Hypothetical LOC387715 is a second major susceptibility gene for age-related

macular degeneration, contributing independently of complement factor H to disease risk." Hum Mol Genet **14**(21): 3227-36.
Robertis, D. (1960). "Some observations on the ultrastructure and morphogenesis of photoreceptors." J Gen Physiol. **43**(6): Suppl:1-13.
Roper, K., D. Corbeil and W. B. Huttner (2000). "Retention of prominin in microvilli reveals distinct cholesterol-based lipid micro-domains in the apical plasma membrane." Nat Cell Biol **2**(9): 582-92.
Ross, A. J., H. May-Simera, E. R. Eichers, M. Kai, J. Hill, D. J. Jagger, C. C. Leitch, J. P. Chapple, P. M. Munro, S. Fisher, P. L. Tan, H. M. Phillips, M. R. Leroux, D. J. Henderson, J. N. Murdoch, A. J. Copp, M. M. Eliot, J. R. Lupski, D. T. Kemp, H. Dollfus, M. Tada, N. Katsanis, A. Forge and P. L. Beales (2005). "Disruption of Bardet-Biedl syndrome ciliary proteins perturbs planar cell polarity in vertebrates." Nat Genet **37**(10): 1135-40.
Royo, P. E. and W. B. Quay (1959). "Retinal transplantation from fetal to maternal mammalian eye." Growth **23**: 313-36.
Sakaguchi, D. S., S. J. Van Hoffelen, E. Theusch, E. Parker, J. Orasky, M. M. Harper, A. Benediktsson and M. J. Young (2004). "Transplantation of neural progenitor cells into the developing retina of the Brazilian opossum: an in vivo system for studying stem/progenitor cell plasticity." Dev Neurosci **26**(5-6): 336-45.
Samson, M., M. M. Emerson and C. L. Cepko (2009). "Robust marking of photoreceptor cells and pinealocytes with several reporters under control of the Crx gene." Dev Dyn **238**(12): 3218-25.
Sato, T., T. Iwano, M. Kunii, S. Matsuda, R. Mizuguchi, Y. Jung, H. Hagiwara, Y. Yoshihara, M. Yuzaki, R. Harada and A. Harada (2013). "Rab8a and Rab8b are essential for multiple apical transport pathways but insufficient for ciliogenesis." J Cell Sci.
Schaumburg, J., O. Diekmann, P. Hagendorff, S. Bergmann, M. Rohde, S. Hammerschmidt, L. Jansch, J. Wehland and U. Karst (2004). "The cell wall subproteome of Listeria monocytogenes." Proteomics **4**(10): 2991-3006.
Schneider, L., M. Cammer, J. Lehman, S. K. Nielsen, C. F. Guerra, I. R. Veland, C. Stock, E. K. Hoffmann, B. K. Yoder, A. Schwab, P. Satir and S. T. Christensen (2010). "Directional cell migration and chemotaxis in wound healing response to PDGF-AA are coordinated by the primary cilium in fibroblasts." Cell Physiol Biochem **25**(2-3): 279-92.
Schneider, L., C. A. Clement, S. C. Teilmann, G. J. Pazour, E. K. Hoffmann, P. Satir and S. T. Christensen (2005). "PDGFRalphaalpha signaling is regulated through the primary cilium in fibroblasts." Curr Biol **15**(20): 1861-6.
Schubert, T., M. Hoon, T. Euler, P. D. Lukasiewicz and R. O. Wong (2013). "Developmental regulation and activity-dependent maintenance of GABAergic presynaptic inhibition onto rod bipolar cell axonal terminals." Neuron **78**(1): 124-37.
Schwartz, S. D., J. P. Hubschman, G. Heilwell, V. Franco-Cardenas, C. K. Pan, R. M. Ostrick, E. Mickunas, R. Gay, I. Klimanskaya and R. Lanza (2012). "Embryonic stem cell trials for macular degeneration: a preliminary report." Lancet **379**(9817): 713-20.
Scott, G. A., L. A. McClelland and A. F. Fricke (2008). "Semaphorin 7a promotes spreading and dendricity in human melanocytes through beta1-integrins." J Invest Dermatol **128**(1): 151-61.
Scott, G. A., L. A. McClelland, A. F. Fricke and A. Fender (2009). "Plexin C1, a receptor for semaphorin 7a, inactivates cofilin and is a potential tumor suppressor for melanoma progression." J Invest Dermatol **129**(4): 954-63.
Sedmak, T. and U. Wolfrum (2011). "Intraflagellar transport proteins in ciliogenesis of photoreceptor cells." Biol Cell **103**(10): 449-66.
Seiler, C., K. C. Finger-Baier, O. Rinner, Y. V. Makhankov, H. Schwarz, S. C. Neuhauss and T. Nicolson (2005). "Duplicated genes with split functions: independent roles of protocadherin15 orthologues in zebrafish hearing and vision." Development **132**(3): 615-23.

Semaphorin-Nomenclature-Committee (1999). "Unified nomenclature for the semaphorins/collapsins." Cell **97**(5): 551-2.

Serini, G., D. Valdembri, S. Zanivan, G. Morterra, C. Burkhardt, F. Caccavari, L. Zammataro, L. Primo, L. Tamagnone, M. Logan, M. Tessier-Lavigne, M. Taniguchi, A. W. Puschel and F. Bussolino (2003). "Class 3 semaphorins control vascular morphogenesis by inhibiting integrin function." Nature **424**(6947): 391-7.

Sernagor, E., S. Eglen, W. A. Harris and R. Wong (2006). Retinal Development. Cambridge, Cambridge University Press.

Sharma, M., S. S. Giridharan, J. Rahajeng, N. Naslavsky and S. Caplan (2009). "MICAL-L1 links EHD1 to tubular recycling endosomes and regulates receptor recycling." Mol Biol Cell **20**(24): 5181-94.

Sharom, F. J. and M. T. Lehto (2002). "Glycosylphosphatidylinositol-anchored proteins: structure, function, and cleavage by phosphatidylinositol-specific phospholipase C." Biochem Cell Biol **80**(5): 535-49.

Sharom, F. J. and G. Radeva (2004). "GPI-anchored protein cleavage in the regulation of transmembrane signals." Subcell Biochem **37**: 285-315.

Shirasawa, T., T. Akashi, K. Sakamoto, H. Takahashi, N. Maruyama and K. Hirokawa (1993). "Gene expression of CD24 core peptide molecule in developing brain and developing non-neural tissues." Dev Dyn **198**(1): 1-13.

Simonelli, F., A. M. Maguire, F. Testa, E. A. Pierce, F. Mingozzi, J. L. Bennicelli, S. Rossi, K. Marshall, S. Banfi, E. M. Surace, J. Sun, T. M. Redmond, X. Zhu, K. S. Shindler, G. S. Ying, C. Ziviello, C. Acerra, J. F. Wright, J. W. McDonnell, K. A. High, J. Bennett and A. Auricchio (2010). "Gene therapy for Leber's congenital amaurosis is safe and effective through 1.5 years after vector administration." Mol Ther **18**(3): 643-50.

Sivaprasad, S. and N. V. Chong (2006). "The complement system and age-related macular degeneration." Eye (Lond) **20**(8): 867-72.

Sonntag, S., G. Sohl, R. Dobrowolski, J. Zhang, M. Theis, E. Winterhager, F. F. Bukauskas and K. Willecke (2009). "Mouse lens connexin23 (Gje1) does not form functional gap junction channels but causes enhanced ATP release from HeLa cells." Eur J Cell Biol **88**(2): 65-77.

Srinivas, M., L. Ng, H. Liu, L. Jia and D. Forrest (2006). "Activation of the blue opsin gene in cone photoreceptor development by retinoid-related orphan receptor beta." Mol Endocrinol **20**(8): 1728-41.

Stone, E. M., A. V. Cideciyan, T. S. Aleman, T. E. Scheetz, A. Sumaroka, M. A. Ehlinger, S. B. Schwartz, G. A. Fishman, E. I. Traboulsi, B. L. Lam, A. B. Fulton, R. F. Mullins, V. C. Sheffield and S. G. Jacobson (2011). "Variations in NPHP5 in patients with nonsyndromic leber congenital amaurosis and Senior-Loken syndrome." Arch Ophthalmol **129**(1): 81-7.

Sturm, V., H. Leiba, M. N. Menke, E. M. Valente, A. Poretti, K. Landau and E. Boltshauser (2010). "Ophthalmological findings in Joubert syndrome." Eye (Lond) **24**(2): 222-5.

Sudo, H., H. A. Kodama, Y. Amagai, S. Yamamoto and S. Kasai (1983). "In vitro differentiation and calcification in a new clonal osteogenic cell line derived from newborn mouse calvaria." J Cell Biol **96**(1): 191-8.

Sui, G. Y., G. C. Liu, G. Y. Liu, Y. Y. Gao, Y. Deng, W. Y. Wang, S. H. Tong and L. Wang (2013). "Is sunlight exposure a risk factor for age-related macular degeneration? A systematic review and meta-analysis." Br J Ophthalmol **97**(4): 389-94.

Sundin, O. H., J. M. Yang, Y. Li, D. Zhu, J. N. Hurd, T. N. Mitchell, E. D. Silva and I. H. Maumenee (2000). "Genetic basis of total colourblindness among the Pingelapese islanders." Nat Genet **25**(3): 289-93.

Sung, C. H. and J. Z. Chuang (2010). "The cell biology of vision." J Cell Biol **190**(6): 953-63.

Suzuki, K., A. Kumanogoh and H. Kikutani (2008). "Semaphorins and their receptors in immune cell interactions." Nat Immunol **9**(1): 17-23.

Suzuki, K., T. Okuno, M. Yamamoto, R. J. Pasterkamp, N. Takegahara, H. Takamatsu, T. Kitao, J. Takagi, P. D. Rennert, A. L. Kolodkin, A. Kumanogoh and H. Kikutani (2007). "Semaphorin 7A initiates T-cell-mediated inflammatory responses through alpha1beta1 integrin." Nature **446**(7136): 680-4.

Swaroop, A., D. Kim and D. Forrest (2010). "Transcriptional regulation of photoreceptor development and homeostasis in the mammalian retina." Nat Rev Neurosci **11**(8): 563-76.

Szel, A., T. van Veen and P. Rohlich (1994). "Retinal cone differentiation." Nature **370**(6488): 336.

Takahashi, M., T. D. Palmer, J. Takahashi and F. H. Gage (1998). "Widespread integration and survival of adult-derived neural progenitor cells in the developing optic retina." Mol Cell Neurosci **12**(6): 340-8.

Takeuchi, H., K. Inokuchi, M. Aoki, F. Suto, A. Tsuboi, I. Matsuda, M. Suzuki, A. Aiba, S. Serizawa, Y. Yoshihara, H. Fujisawa and H. Sakano (2010). "Sequential arrival and graded secretion of Sema3F by olfactory neuron axons specify map topography at the bulb." Cell **141**(6): 1056-67.

Tamagnone, L., S. Artigiani, H. Chen, Z. He, G. I. Ming, H. Song, A. Chedotal, M. L. Winberg, C. S. Goodman, M. Poo, M. Tessier-Lavigne and P. M. Comoglio (1999). "Plexins are a large family of receptors for transmembrane, secreted, and GPI-anchored semaphorins in vertebrates." Cell **99**(1): 71-80.

Testa, F., A. M. Maguire, S. Rossi, E. A. Pierce, P. Melillo, K. Marshall, S. Banfi, E. M. Surace, J. Sun, C. Acerra, J. F. Wright, J. Wellman, K. A. High, A. Auricchio, J. Bennett and F. Simonelli (2013). "Three-year follow-up after unilateral subretinal delivery of adeno-associated virus in patients with Leber congenital Amaurosis type 2." Ophthalmology **120**(6): 1283-91.

Thiadens, A. A., A. I. den Hollander, S. Roosing, S. B. Nabuurs, R. C. Zekveld-Vroon, R. W. Collin, E. De Baere, R. K. Koenekoop, M. J. van Schooneveld, T. M. Strom, J. J. van Lith-Verhoeven, A. J. Lotery, N. van Moll-Ramirez, B. P. Leroy, L. I. van den Born, C. B. Hoyng, F. P. Cremers and C. C. Klaver (2009). "Homozygosity mapping reveals PDE6C mutations in patients with early-onset cone photoreceptor disorders." Am J Hum Genet **85**(2): 240-7.

Thornton, J., R. Edwards, P. Mitchell, R. A. Harrison, I. Buchan and S. P. Kelly (2005). "Smoking and age-related macular degeneration: a review of association." Eye (Lond) **19**(9): 935-44.

Thrasher, A. J., C. M. Casimir, C. Kinnon, G. Morgan, A. W. Segal and R. J. Levinsky (1995). "Gene transfer to primary chronic granulomatous disease monocytes." Lancet **346**(8967): 92-3.

Tomizawa, Y., Y. Sekido, M. Kondo, B. Gao, J. Yokota, J. Roche, H. Drabkin, M. I. Lerman, A. F. Gazdar and J. D. Minna (2001). "Inhibition of lung cancer cell growth and induction of apoptosis after reexpression of 3p21.3 candidate tumor suppressor gene SEMA3B." Proc Natl Acad Sci U S A **98**(24): 13954-9.

Tran, T. S., M. E. Rubio, R. L. Clem, D. Johnson, L. Case, M. Tessier-Lavigne, R. L. Huganir, D. D. Ginty and A. L. Kolodkin (2009). "Secreted semaphorins control spine distribution and morphogenesis in the postnatal CNS." Nature **462**(7276): 1065-9.

Tsujikawa, M. and J. Malicki (2004). "Intraflagellar transport genes are essential for differentiation and survival of vertebrate sensory neurons." Neuron **42**(5): 703-16.

Turner, D. L., E. Y. Snyder and C. L. Cepko (1990). "Lineage-independent determination of cell type in the embryonic mouse retina." Neuron **4**(6): 833-45.

Uchida, N., D. W. Buck, D. He, M. J. Reitsma, M. Masek, T. V. Phan, A. S. Tsukamoto, F. H. Gage and I. L. Weissman (2000). "Direct isolation of human central nervous system stem cells." Proc Natl Acad Sci U S A **97**(26): 14720-5.

Ugurlu, N., M. D. Asik, F. Yulek, S. Neselioglu and N. Cagil (2013). "Oxidative Stress and Anti-oxidative Defence in Patients with Age-related Macular Degeneration." Curr Eye Res **38**(4): 497-502.

Valente, E. M., J. L. Silhavy, F. Brancati, G. Barrano, S. R. Krishnaswami, M. Castori, M. A. Lancaster, E. Boltshauser, L. Boccone, L. Al-Gazali, E. Fazzi, S. Signorini, C. M. Louie, E. Bellacchio, E. Bertini, B. Dallapiccola and J. G. Gleeson (2006). "Mutations in CEP290, which encodes a centrosomal protein, cause pleiotropic forms of Joubert syndrome." Nat Genet **38**(6): 623-5.

Van Hoffelen, S. J., M. J. Young, M. A. Shatos and D. S. Sakaguchi (2003). "Incorporation of murine brain progenitor cells into the developing mammalian retina." Invest Ophthalmol Vis Sci **44**(1): 426-34.

Vasireddy, V., P. Wong and R. Ayyagari (2010). "Genetics and molecular pathology of Stargardt-like macular degeneration." Prog Retin Eye Res **29**(3): 191-207.

Walker, T. L., A. Wierick, A. M. Sykes, B. Waldau, D. Corbeil, P. Carmeliet and G. Kempermann (2013). "Prominin-1 allows prospective isolation of neural stem cells from the adult murine hippocampus." J Neurosci **33**(7): 3010-24.

Wang, J., M. A. O'Bara, S. U. Pol and F. J. Sim (2013). "CD133/CD140a-Based Isolation of Distinct Human Multipotent Neural Progenitor Cells and Oligodendrocyte Progenitor Cells." Stem Cells Dev.

Wang, M. M., R. Janz, R. Belizaire, L. J. Frishman and D. M. Sherry (2003). "Differential distribution and developmental expression of synaptic vesicle protein 2 isoforms in the mouse retina." J Comp Neurol **460**(1): 106-22.

Wang, R., K. Chadalavada, J. Wilshire, U. Kowalik, K. E. Hovinga, A. Geber, B. Fligelman, M. Leversha, C. Brennan and V. Tabar (2010). "Glioblastoma stem-like cells give rise to tumour endothelium." Nature **468**(7325): 829-33.

Wawersik, S. and R. L. Maas (2000). "Vertebrate eye development as modeled in Drosophila." Hum Mol Genet **9**(6): 917-25.

Weigmann, A., D. Corbeil, A. Hellwig and W. B. Huttner (1997). "Prominin, a novel microvilli-specific polytopic membrane protein of the apical surface of epithelial cells, is targeted to plasmalemmal protrusions of non-epithelial cells." Proc Natl Acad Sci U S A **94**(23): 12425-30.

West, E. L., A. Gonzalez-Cordero, C. Hippert, F. Osakada, J. P. Martinez-Barbera, R. A. Pearson, J. C. Sowden, M. Takahashi and R. R. Ali (2012). "Defining the integration capacity of embryonic stem cell-derived photoreceptor precursors." Stem Cells **30**(7): 1424-35.

West, E. L., R. A. Pearson, S. E. Barker, U. F. Luhmann, R. E. Maclaren, A. C. Barber, Y. Duran, A. J. Smith, J. C. Sowden and R. R. Ali (2010). "Long-term survival of photoreceptors transplanted into the adult murine neural retina requires immune modulation." Stem Cells **28**(11): 1997-2007.

West, E. L., R. A. Pearson, Y. Duran, A. Gonzalez-Cordero, R. E. MacLaren, A. J. Smith, J. C. Sowden and R. R. Ali (2012). "Manipulation of the recipient retinal environment by ectopic expression of neurotrophic growth factors can improve transplanted photoreceptor integration and survival." Cell Transplant **21**(5): 871-87.

West, E. L., R. A. Pearson, R. E. MacLaren, J. C. Sowden and R. R. Ali (2009). "Cell transplantation strategies for retinal repair." Prog Brain Res **175**: 3-21.

West, E. L., R. A. Pearson, M. Tschernutter, J. C. Sowden, R. E. Maclaren and R. R. Ali (2008). "Pharmacological disruption of the outer limiting membrane leads to increased retinal integration of transplanted photoreceptor precursors." Exp Eye Res **86**(4): 601-11.

Wetts, R. and S. E. Fraser (1988). "Multipotent precursors can give rise to all major cell types of the frog retina." Science **239**(4844): 1142-5.

Wolfrum, U. and A. Schmitt (2000). "Rhodopsin transport in the membrane of the connecting cilium of mammalian photoreceptor cells." Cell Motil Cytoskeleton **46**(2): 95-107.

Wollscheid, B., D. Bausch-Fluck, C. Henderson, R. O'Brien, M. Bibel, R. Schiess, R. Aebersold and J. D. Watts (2009). "Mass-spectrometric identification and relative quantification of N-linked cell surface glycoproteins." Nat Biotechnol **27**(4): 378-86.

Wong, L. L. and D. H. Rapaport (2009). "Defining retinal progenitor cell competence in Xenopus laevis by clonal analysis." Development **136**(10): 1707-15.

Xu, J., L. Morris, S. J. Fliesler, D. M. Sherry and X. Q. Ding (2011). "Early-onset, slow progression of cone photoreceptor dysfunction and degeneration in CNG channel subunit CNGB3 deficiency." Invest Ophthalmol Vis Sci **52**(6): 3557-66.

Yamagata, M. and J. R. Sanes (2008). "Dscam and Sidekick proteins direct lamina-specific synaptic connections in vertebrate retina." Nature **451**(7177): 465-9.

Yamagata, M., J. A. Weiner and J. R. Sanes (2002). "Sidekicks: synaptic adhesion molecules that promote lamina-specific connectivity in the retina." Cell **110**(5): 649-60.

Yanai, D., J. D. Weiland, M. Mahadevappa, R. J. Greenberg, I. Fine and M. S. Humayun (2007). "Visual performance using a retinal prosthesis in three subjects with retinitis pigmentosa." Am J Ophthalmol **143**(5): 820-827.

Yang, Z., N. J. Camp, H. Sun, Z. Tong, D. Gibbs, D. J. Cameron, H. Chen, Y. Zhao, E. Pearson, X. Li, J. Chien, A. Dewan, J. Harmon, P. S. Bernstein, V. Shridhar, N. A. Zabriskie, J. Hoh, K. Howes and K. Zhang (2006). "A variant of the HTRA1 gene increases susceptibility to age-related macular degeneration." Science **314**(5801): 992-3.

Yang, Z., Y. Chen, C. Lillo, J. Chien, Z. Yu, M. Michaelides, M. Klein, K. A. Howes, Y. Li, Y. Kaminoh, H. Chen, C. Zhao, Y. Chen, Y. T. Al-Sheikh, G. Karan, D. Corbeil, P. Escher, S. Kamaya, C. Li, S. Johnson, J. M. Frederick, Y. Zhao, C. Wang, D. J. Cameron, W. B. Huttner, D. F. Schorderet, F. L. Munier, A. T. Moore, D. G. Birch, W. Baehr, D. M. Hunt, D. S. Williams and K. Zhang (2008). "Mutant prominin 1 found in patients with macular degeneration disrupts photoreceptor disk morphogenesis in mice." J Clin Invest **118**(8): 2908-16.

Yang, Z. Y., J. Guo, N. Li, M. Qian, S. N. Wang and X. L. Zhu (2003). "Mitosin/CENP-F is a conserved kinetochore protein subjected to cytoplasmic dynein-mediated poleward transport." Cell Res **13**(4): 275-83.

Yasunaga, M., S. Tada, S. Torikai-Nishikawa, Y. Nakano, M. Okada, L. M. Jakt, S. Nishikawa, T. Chiba, T. Era and S. Nishikawa (2005). "Induction and monitoring of definitive and visceral endoderm differentiation of mouse ES cells." Nat Biotechnol **23**(12): 1542-50.

Yin, A. H., S. Miraglia, E. D. Zanjani, G. Almeida-Porada, M. Ogawa, A. G. Leary, J. Olweus, J. Kearney and D. W. Buck (1997). "AC133, a novel marker for human hematopoietic stem and progenitor cells." Blood **90**(12): 5002-12.

Young, R. W. (1985a). "Cell differentiation in the retina of the mouse." Anat Rec **212**(2): 199-205.

Zacchigna, S., H. Oh, M. Wilsch-Brauninger, E. Missol-Kolka, J. Jaszai, S. Jansen, N. Tanimoto, F. Tonagel, M. Seeliger, W. B. Huttner, D. Corbeil, M. Dewerchin, S. Vinckier, L. Moons and P. Carmeliet (2009). "Loss of the cholesterol-binding protein prominin-1/CD133 causes disk dysmorphogenesis and photoreceptor degeneration." J Neurosci **29**(7): 2297-308.

Zhang, B., Y. Hu and J. X. Ma (2009). "Anti-inflammatory and antioxidant effects of SERPINA3K in the retina." Invest Ophthalmol Vis Sci **50**(8): 3943-52.

Zhang, K., M. Kniazeva, M. Han, W. Li, Z. Yu, Z. Yang, Y. Li, M. L. Metzker, R. Allikmets, D. J. Zack, L. E. Kakuk, P. S. Lagali, P. W. Wong, I. M. MacDonald, P. A. Sieving, D. J. Figueroa, C. P. Austin, R. J. Gould, R. Ayyagari and K. Petrukhin (2001). "A 5-bp deletion in ELOVL4 is associated with two related forms of autosomal dominant macular dystrophy." Nat Genet **27**(1): 89-93.

Zhang, K., L. Zhang and R. N. Weinreb (2012). "Ophthalmic drug discovery: novel targets and mechanisms for retinal diseases and glaucoma." Nat Rev Drug Discov **11**(7): 541-59.

Zhang, Q., F. Zulfiqar, X. Xiao, S. A. Riazuddin, Z. Ahmad, R. Caruso, I. MacDonald, P. Sieving, S. Riazuddin and J. F. Hejtmancik (2007). "Severe retinitis pigmentosa mapped to 4p15 and associated with a novel mutation in the PROM1 gene." Hum Genet **122**(3-4): 293-9.

Zhang, S. S., X. Xu, J. Li, M. G. Liu, H. Zhao, M. B. Soares, C. J. Barnstable and X. Y. Fu (2005). "Comprehensive in silico functional specification of mouse retina transcripts." BMC Genomics **6**: 40.

Zhang, Y., K. Arner, B. Ehinger and M. T. Perez (2003). "Limitation of anatomical integration between subretinal transplants and the host retina." Invest Ophthalmol Vis Sci **44**(1): 324-31.

Zhao, Y., D. H. Hong, B. Pawlyk, G. Yue, M. Adamian, M. Grynberg, A. Godzik and T. Li (2003). "The retinitis pigmentosa GTPase regulator (RPGR)- interacting protein: subserving RPGR function and participating in disk morphogenesis." Proc Natl Acad Sci U S A **100**(7): 3965-70.

Zhou, K., C. Koike, T. Yoshida, M. Okabe, M. Fathy, S. Kyo, T. Kiyono, S. Saito and T. Nikaido (2013). "Establishment and characterization of immortalized human amniotic epithelial cells." Cell Reprogram **15**(1): 55-67.

Zhu, X., M. A. Mancini, K. H. Chang, C. Y. Liu, C. F. Chen, B. Shan, D. Jones, T. L. Yang-Feng and W. H. Lee (1995). "Characterization of a novel 350-kilodalton nuclear phosphoprotein that is specifically involved in mitotic-phase progression." Mol Cell Biol **15**(9): 5017-29.

Zola, H., B. Swart, I. Nicholson, B. Aasted, A. Bensussan, L. Boumsell, C. Buckley, G. Clark, K. Drbal, P. Engel, D. Hart, V. Horejsi, C. Isacke, P. Macardle, F. Malavasi, D. Mason, D. Olive, A. Saalmueller, S. F. Schlossman, R. Schwartz-Albiez, P. Simmons, T. F. Tedder, M. Uguccioni and H. Warren (2005). "CD molecules 2005: human cell differentiation molecules." Blood **106**(9): 3123-6.

Zuber, M. E., G. Gestri, A. S. Viczian, G. Barsacchi and W. A. Harris (2003). "Specification of the vertebrate eye by a network of eye field transcription factors." Development **130**(21): 5155-67.

11 Published materials

Published papers:

- Lakowski J, **Han YT**, Pearson RA, Gonzalez-Cordero A, West EL, Gualdoni S, Barber AC, Hubank M, Ali RR, Sowden JC. Effective Transplantation of Photoreceptor Precursor Cells Selected via Cell Surface Antigen Expression. Stem Cells. 2011 Sep;29(9):1391-404. doi: 10.1002/stem.694. PMID: 21774040

Meetings and presentations:

- **Ya-Ting Han**, Rachael Pearson, Jorn Lakowski, Robin Ali, Jane Sowden. Sema7a co-labels with PlexinC1, but not Itgb1, on the cell bodies of migrating photoreceptor cells in the retina.
  2012 July 11-13 UCL International conference for stem cells and regenerative medicine;
  2012 June 29 UCL neuroscience symposium (UCL) (Runner-up prize in the UCL-Zeiss poster competition);
  2012 June 1 Young Embryologist Meeting (UCL-ICH)
- Jorn Lakowski, **Yating Han**, Anai A. Gonzalez-Cordero, Emma West, Robin R. Ali, Rachael A. Pearson, and Jane C. Sowden. Towards Photoreceptor Replacement Therapy: Identifying The Cell Surface Marker Profile Of Photoreceptor Precursors.
  2012 March 26 ARVO Meeting Abstracts 53:2695
- **Ya-Ting Han**, Jorn Lakowski, Mike Baron, Rachael A. Pearson, Robin R. Ali, and Jane C. Sowden Transcriptome Analysis Of Crx-expressing Photoreceptor Precursor Cells For Photoreceptor Cell Replacement Therapy.
  2011 Nov 16 UCL-ICH open day;
  2011 April 22 ARVO Meeting Abstracts 52: 2229 (UCL graduate conference fund and ICH Dean's travel grant awarded)
- Jane C. Sowden, Michael Baron, Jorn Lakowski, **Ya-Ting Han**, James W. Bainbridge, Rachael A. Pearson, and Robin R. Ali The Adult Retinal Environment Favours New Rod Cell Integration And Limits Cone Cell Differentiation Following Transplantation Of Crx.gfp Precursor Cells
  2011 April 22 ARVO Meeting Abstracts 52
- Jorn Lakowski, **Yating Han**, Rachael A. Pearson, Robin R. Ali, and Jane C. Sowden Effective Transplantation Of Photoreceptor Precursor Cells Selected Via Cell Surface Antigen Expression
  2011 April 22 ARVO Meeting Abstracts 52:2225
- **Ya-Ting Han**, Jorn Lakowski, Michael Baron, Robin Ali, Jane Sowden. Transcriptome analysis and cell surface molecules of photoreceptor precursor cells.
  2011 Mar 1st UCL graduate poster competition (2nd prize in the poster competition);
  2010 Nov 17th UCL-ICH open day (1st prize in the poster competition)

12 Materials on CD

Single PDF copy of the full thesis

High resolution figures and Excel tables of thesis